Alma Mater Studiorum – Università di Bologna

DOTTORATO DI RICERCA IN

Ingegneria Civile, Chimica, Ambientale e dei Materiali

Ciclo XXXII

Settore Concorsuale: 09/D3 - IMPIANTI E PROCESSI INDUSTRIALI CHIMICI

Settore Scientifico Disciplinare: ING-IND/25 – IMPIANTI CHIMICI

DEVELOPMENT OF METHODOLOGIES SUPPORTING THE SUSTAINABLE AND SAFE INTEGRATION OF OFFSHORE CONVENTIONAL AND RENEWABLE ENERGY PRODUCTION

Presentata da: Anna Crivellari

Coordinatore Dottorato

Prof. Luca Vittuari

Supervisore

Prof. Valerio Cozzani

Co-Supervisore

Prof. Ibrahim Dincer

Esame finale anno 2020

Il mare insegna all'uomo l'umiltà…

Il mare insegna ancora una cosa importantissima
per la sopravvivenza dell'uomo stesso…

Gli insegna che dietro un orizzonte
ce n'è sempre un altro.

- Enzo Maiorca

All'apnea,
la quale, oltre alle indescrivibili emozioni che regala,
funge da canalizzatore di energia e passione,
contribuendo in questo caso
al completamento del mio Dottorato e
alla scrittura di questo lavoro.

Table of Contents

Abstract

Against a backdrop of rapidly increasing worldwide population and growing energy demand, the development of renewable energy technologies has become of primary importance in the effort to reduce greenhouse gas emissions. In addition, rapid increase in the oil prices coupled with concerns about the stability and security of fossil fuels extraction have led to emphasized interest in the exploitation of offshore renewable energy sources, such as offshore wind, sunlight, waves and tidal currents. However, it is often technically and economically infeasible to transport discontinuous renewable electricity for long distances to the shore. Another shortcoming of non-programmable renewable power is its integration into the onshore electrical network without affecting power quality, grid stability and the dispatching process.

On the other hand, the offshore oil & gas industry is striving to reduce overall carbon footprint from onsite power generators and limiting large expenses associated to carrying electric energy from the shore in case of remote facilities. Furthermore, the increased complexity and expansion towards challenging areas of offshore hydrocarbons operations call for higher attention to safety and environmental protection issues from potential major accident hazards. The rise of offshore oil & gas assets approaching the end of their useful life requires to deal with complex evaluation of the decommissioning options. Another multi-dimensional problem is the monetization of offshore natural gas reservoirs, particularly in case of stranded and depleted gas fields close to the shore.

Innovative hybrid energy systems, as Power-to-Gas (P2G), Power-to-Liquid (P2L) and Gas-to-Power (G2P) options, implemented at offshore locations, would offer the opportunity to overcome challenges of both renewable and oil & gas sectors by different strategies. The chemical conversion of renewable power into gas and liquid synthetic fuels (P2G and P2L) at offshore oil & gas facilities allows to ease storage and transportation of renewable energy from remote areas and to create new opportunities for aging offshore structures. On the other hand, gas turbine energy balancing systems coupled with renewable plants in G2P offshore projects offer the advantages of improving the dispatchability of renewable power injected into the grid and of valorising untapped gas resources. Despite the widespread experience of these concepts at the onshore context, no evidence has been found on offshore applications and existing literature studies are limited to feasibility assessments of the sole offshore P2G (hydrogen) option.

The present study aims at the development of systematic methodologies based on proper sustainability and safety performance indicators supporting the choice of P2G, P2L and G2P hybrid energy options for offshore green projects in early design phases. An in-depth analysis of the different offshore hybrid strategies was performed and key parameters for a preliminary screening of the alternatives were identified. The literature reviews on existing methods proposing metrics to assess sustainability of hybrid

energy systems, inherent safety of process routes in conceptual design stage and environmental protection of installations from oil and chemical accidental spills were carried out. To fill the gaps evidenced in the state of the art, a suite of specific decision-making methodologies was developed in the present study, based on representative multi-criteria indicators addressing technical, economic, environmental and societal aspects of alternative options. The integrated set of methods was specifically developed to capture different complex issues related to the offshore context, e.g. end-of-life oil & gas infrastructures, remote areas, stranded and depleted gas reservoirs, safety and environmental concerns of oil & gas operations. Sustainability assessment models are proposed for evaluation of alternative P2G/P2L strategies at remote off-grid areas and G2P options at depleted gas fields close to the grid. An inherent safety approach is defined to rank the hazard level of process units and overall facility of alternative designs of the offshore systems with respect to human, assets and environment targets of the offshore potential hazards. Finally, a process intensification screening methodology is proposed to investigate emerging chemical process routes for production of renewable fuels at low maturity level in view of further implementation in P2G/P2L offshore hybrid energy projects. A set of five case-studies was defined, covering different offshore scenarios of concern, to provide an assessment of the effectiveness and value of the suite of tools developed. The results of the case-studies show that the supporting tools and novel metrics developed are able to capture criticalities of the analysed offshore systems and to orient the choice of the best P2G/P2L/G2P hybrid energy option or design solution from the sustainability and/or safety perspectives. The results of sensitivity analysis based on the Monte Carlo simulation, applied to the outcome of some of the case-studies, confirm the ability of the methods to yield robust and meaningful results. The results obtained pave the way to consolidate informed strategies for the sustainable and safe development of offshore renewable energies.

Chapter 1.

Introduction

1.1. Renewable energy exploitation and challenges

Since the advent of the industrial revolution, fossil fuels have been the main source to supply the energy requirements of the human society. According to the International Energy Agency (EIA), in 2017 the global energy system continues to be dominated by fossil fuels, with oil accounting for 32% of energy supply worldwide, closely followed by natural gas and coal, at 22% and 27% respectively [1]. In the International Energy Outlook 2019 provided by the U.S. Department of Energy [2], the total world energy consumption has been projected to increase by 50% during the period 2018-2050. Despite the fastest growth of renewable energy worldwide, fossil fuels are expected to continue to meet most of the world's energy demand.

In the last years, concerns about pollution and climate change have raised public awareness confirming that carbon dioxide (CO_2) emissions associated with fossil fuels combustion represent the largest source of greenhouse gas (GHG) emissions [3]. On the other hand, energy security has become complex, due to the combination of rising political issue in major energy-producing countries, resource competition and record oil prices [4]. As a consequence, various internal frameworks and legally binding agreements have been released, emphasizing the urgent need for low carbon technologies, especially those from renewable energy sources [5]. In this framework, European Union became a worldwide pioneer in promoting renewable energy exploitation with the aim to improve supply security, competitiveness and environmental sustainability of renewable sources [6].

The deployment of sustainable emission-free renewables plays an important role for decarbonising the energy supply [7]. To date, a wide range of renewable energy resources located at onshore areas has been promoted for large-scale exploitation, e.g. hydro, solar, wind, geothermal, biofuels, biomass [8]. On the other hand, a huge quantity of clean power can be provided also from offshore renewable energy sources, such as offshore wind, solar energy, marine renewable energies in forms of surface waves and tidal streams [9].

Offshore wind energy can be defined as the energy generated from the wind at sea. Wind is produced by uneven heating of the earth's surface by the sun. A wind energy turbine can convert the kinetic energy of the wind into mechanical or electrical energy that can be harnessed for practical use: wind blows across the rotor blades, causing them to rotate and to drive a shaft which is connected to the rotor hub [10]. Over the last decade, offshore wind power has presented considerably high increase capacity worldwide reaching at the end of 2015 a quantity of 12.1 GW, from which 11 GW were developed in Europe [11]. Further growth led to a total installed offshore wind capacity in Europe of about 18 GW in 2018: UK gave the largest contribution, with 44% of all installations in MW, followed by Germany (34%), Denmark (7%), Belgium (6.4%) and Netherland (6%) [12]. The motivation for this development can be explained

by several benefits compared to its onshore counterpart [13]: high available area to harvest wind energy since there are no limitations relative to urban buildings and human activities, stronger and more uniform wind speed with less turbulence, limited visual and sound impact. However, these advantages are counterbalanced by some drawbacks [14,15]: higher costs of the permitting and engineering process, higher demand of raw materials, complex and expensive installation requiring specialized workers, need for adequate port infrastructure for the movement and assembly operation of the components, expensive subsea cables for farther systems from the shore, reduced reliability and availability with increasing distance of the system from the shore.

Offshore Wind Turbines (OWTs) show similarities to the onshore designs although several modifications must be applied to deal with aggressive marine environment specifically. Main components of an OWT are foundation, sub-structure, tower, blades-rotor-nacelle. Classification of OWTs can be made based on the number of blades (two- and three-blades), energy extraction mechanism (lift- and drag-based), axis orientation (horizontal and vertical axis), method at which the power is regulated at high wind speeds (stall-regulated and pitch-regulated) [16]. Typical OWTs in operation are characterized by three-bladed horizontal axis, pitch-regulated, upwind rotors whose diameter can range from 65 to 130 m and capacity between 1.5 MW and 5 MW. However, some vertical axis wind turbine prototypes (e.g. Aerogenerator X, Deepwind) have been proposed due its simple structure, rotation regardless of wind direction, low maintenance costs, potential for larger power production in deep waters [17]. Another classification of OWTs is based on the support structure, as illustrated in Figure 1.1. Fixed-grounded monopile foundations are predominant for 3-4 MW OWTs up to a water depth of 30 m. Different foundations (e.g. jacket, tripods and tripiles) are employed for large sizes and intermediate water depth (up to 50 m) [18]. In these years, the development of OWTs has succeeded in providing different floating designs (Tension Leg Platform or TLP, Semi-submersible, Spar Buoy), able to operate at higher distances from the shore and in deeper waters, thus allowing large energy potentials to be harnessed [19]. Several floating offshore projects have been fully commissioned and investigated all around the world (e.g. Hywind, Sway, WindFloat, PelaStar, Winflo, Hexicon Energy Design) [12,20,21].

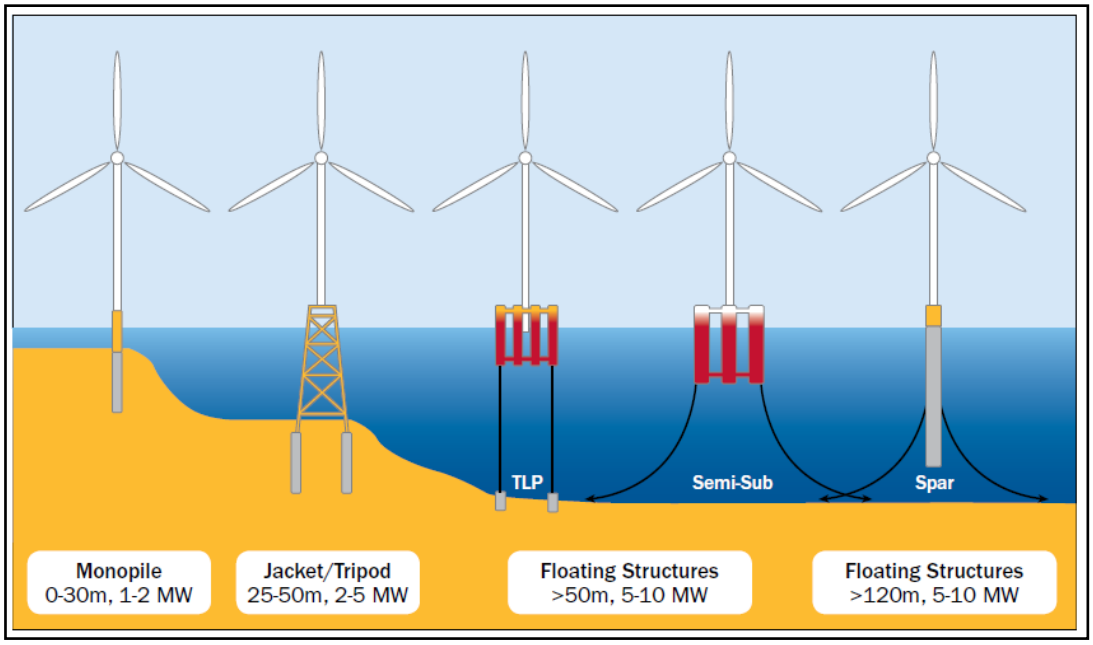

Figure 1.1. Classification of OWTs based on sub-structure [22].

Solar radiations, i.e. electromagnetic radiations emitted by the sun, represent the most abundant natural, easily exploitable, clean and reliable resource on earth, which can be exploited to produce solar power by means of solar Photovoltaics (PV) and Concentrating Solar Power (CSP) technologies [23]. Solar PV is one of the fastest growing renewable technologies reaching a global installed capacity of 481 GW in 2018, while CSP technology accounted for around 5 GW in the same year [24].

Solar CSP plants have increased in interest in the solar energy sector due to higher efficiency and lower costs [25]. Generally, CSP plants are composed of several components, i.e. solar concentrators, receiver, steam turbine and electrical generator and thermal storage: mirrors are used to concentrate solar rays and convert them into high-temperature heat; the heat is then channelled through a conventional generator to produce electricity [26]. As illustrated in Figure 1.2, CSP can be classified into four main technologies. Among them, the parabolic trough collectors show the most advanced operational experience up to 354 MW, operating temperature up to 500°C, high modularity and the best land-use factor [26]. They are used to concentrate sunlight into receiver tubes placed in the trough's focal line. A thermal transfer fluid as a synthetic thermal oil is delivered along these tubes. After heated to approximately 400°C by the solar radiation, the oil is pumped through heat exchangers to supply heat for vapour generation or other thermal applications. By installing the solar parabolic trough plant at offshore areas, the requirements for the concentrator systems can be simplified due to the sun's tracking along a vertical axis and the thermodynamic efficiency can increase due to the availability of huge quantity of cooling sea water [27].

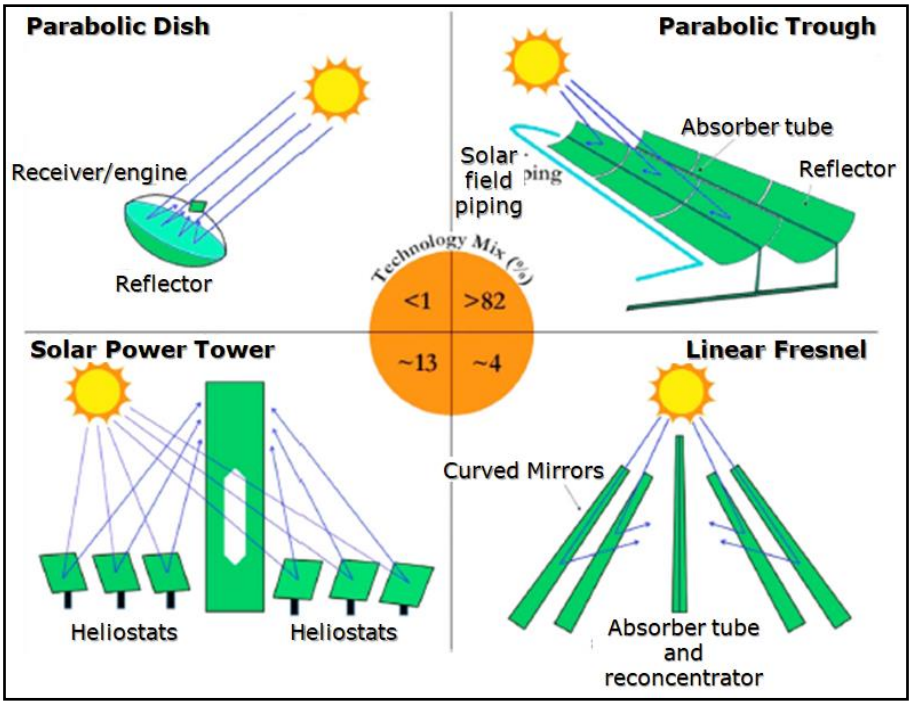

Figure 1.2. Classification of solar CSP technologies and related installed ratios in the technology mix, adapted from [26].

Solar PV plants consist of multiple cells, mechanical and electrical connections, which allow the direct conversion of solar rays into electricity without any heat engine [28]. Solar cells are the main components of the system which can be distinguished into three different generations based on the materials (crystalline silicon wafer-based cells, thin-film cells, organic materials-based cells) [29,30]. The classification of solar PV technologies is shown in Figure 1.3. Beside the common grounded mounted and roof top solar PV arrays, emerging applications are represented by offshore and floating PV plants due to the beneficial higher solar reflectance and low visual impact in open sea, availability of sea water for cooling [31,32]. Considering the same occupied area (e.g. at an offshore installation), it is reported that solar PV arrays at the commercial stage are more efficient in terms of electricity production compared to solar CSP technologies [23].

Figure 1.3. Classification of solar PV technologies, adapted from [33].

Wave energy is generated by blowing of wind on the sea surface, which is in turn created by the differential heating of the earth's surface induced by solar energy. There are several benefits supporting the emerging role of wave energy in the electricity mix compared to the other resources [34,35]: wave power density (2-3 kW/m^2) is greater than that of wind (0.4-0.6 kW/m^2) and solar (0.1-0.2 kW/m^2), wave energy offers smaller hourly and daily variability with greater predictability, waves can travel longer distances with minor energy losses and environmental interferences. On the other hand, the wave energy industry is a new and developing sector which requires research on basic components to overcome technological barriers, effective planning and consenting processes to deal with the non-technical issues and innovative instruments to support demonstration projects [36]. In 2016, 21 pre-commercial and first-of-a-kind demonstration projects have started production in marine environment, whose 15 projects were located within the European waters; maximum capacity has ranged from few kW to 10 MW. A few of them are grid-connected and have delivered electricity to the network [37].

The devices which capture the kinetic energy from waves and transform it into electricity are called Wave Energy Converters (WECs). WECs consist of four main components, i.e. structure and prime mover, foundation or mooring, the power take-off (PTO) system that converts mechanical energy into electrical energy, the control system [38]. Classification of WECs can be according to the installation location, i.e. shoreline, near shore (within 10-25 m water depth) and offshore (in water depth greater than 40 m) devices [39]. WECs can be also classified based on the conversion principle [39], as illustrated in Figure 1.4. According to a previous literature review [40], the following WECs were suggested to retain for offshore installation due to their higher technological status: Pelamis (based on the attenuator principle), Powerbuoy (based on the point absorber principle), Wave Dragon (based on the overtopping principle).

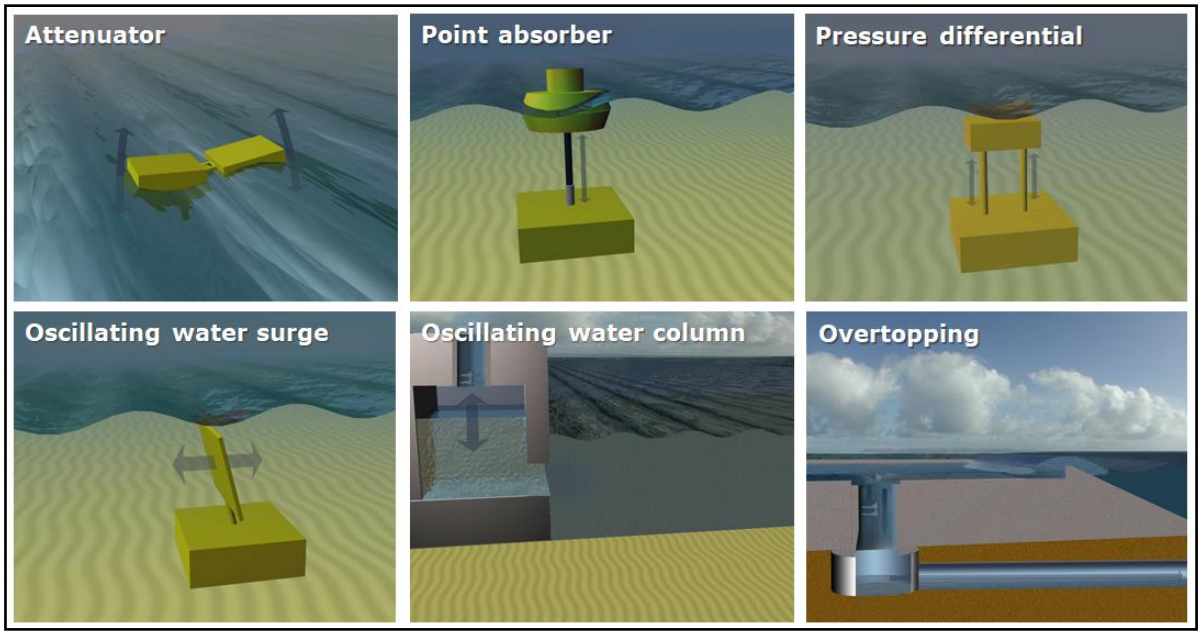

Figure 1.4. Classification of WEC technologies based on conversion principle, adapted from [41].

Tidal currents or tidal streams are water flows resulting from the rise and fall of the tides caused by the rotational and gravitational forces between earth, sun and moon [42]. Hence, tidal current energy is more regular and predictable over a longer time scale compared to wind, wave and solar energies and has the potential to provide a stable power output to the grid [43]. The tidal resource potential at a given site can be considered almost reliable in a short time span [44]. As the wave energy sector, the tidal energy industry has not yet reached the full commercial stage. However, significant progresses towards commercialization were established over the period 2014-2016: 14 tidal energy projects had been grid-connected and operated at the end of 2016 with capacity ranging from few MW to a maximum of 14 MW. Several devices in UK had delivered electricity to the network continuously for long periods [37].

Tidal Energy Converters (TECs) are turbines which utilize the energy of flowing water in tidal currents to generate electricity directly. Similar to OWT designs, TECs consist of a number of blades mounted on a hub, a gear box and a generator; these components are mounted on a support structure. Despite the similarities between the extraction methods of wind and tidal stream energies, rotor diameter of the tidal stream turbine is expected to be about half that of OWT of the same rated power since seawater is 800 times denser than air and water flow speed is generally smaller. As a result, power outputs are comparable. On the contrary, TECs must withstand greater water loading forces and effects of blockage and free surfaces [45]. As the conventional OWTs, TECs can be classified into horizontal and vertical axis technologies, which represent the first generation tidal devices for bottom-mounted installation [45]. Moreover, the European Marine Energy Centre (EMEC) includes other four types of technologies to the classification of TECs, as illustrated in Figure 1.5. thanks to the evolution towards second- and third-

generation devices. Another classification is made based on the TEC foundation, i.e. seabed mounted/gravity base, pile mounted, floating, hydrofoil inducing downforce, which evolves with increasing distance from the shore as in the case of OWTs sub-structure (Figure 1.1) [46].

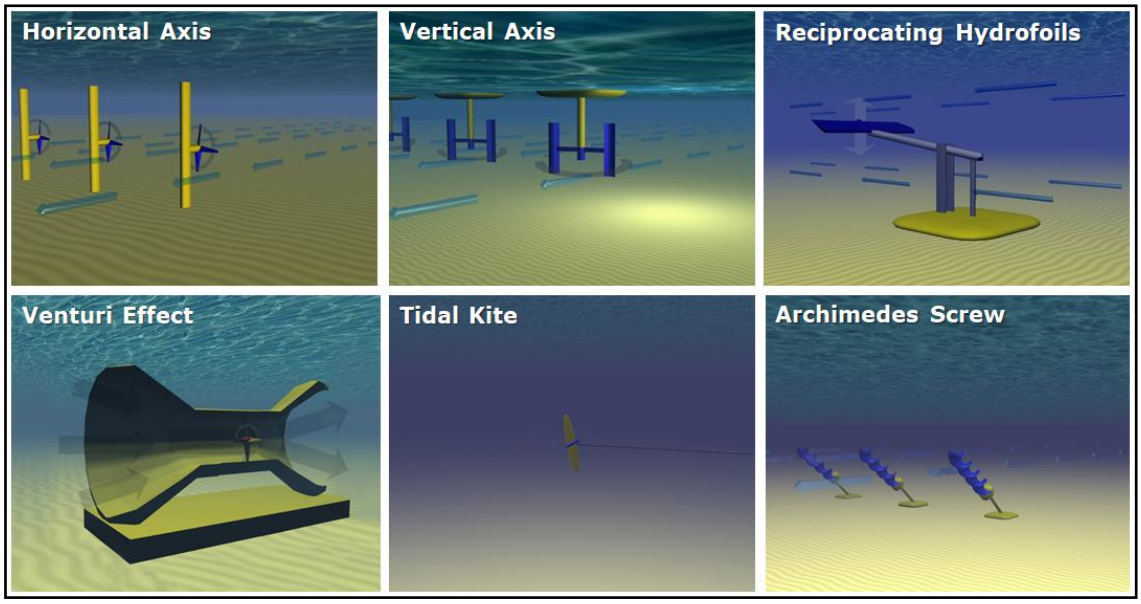

Figure 1.5. Classification of TEC technologies according to EMEC, adapted from [47].

Despite large potential and ongoing technological development of offshore renewable power generation, the main problem of all renewable energy sources, including offshore resources, is generally their dependency on daily or seasonal patterns and on environmental conditions which vary from place to place [48].

It is often considered technically and economically infeasible to transport discontinuous renewable power for long distances [49]. High voltage alternating current (HVAC) transmission lines are the preferred option to deliver large quantities of electricity from offshore areas due to the low cost of voltage transformation and more compact converter stations. However, HAVC cables have the disadvantage that energy losses become much larger with longer distances, in particular because of the capacitive phenomena concerning submarine cables which require dynamic-reactive power control. High voltage direct current (HVDC) cables can minimize the transmission losses and are suitable for long distances and large capacity of power transmission. Nevertheless, in DC systems the most important energy losses are due to the power conversion that is independent of the cable length. HVDC is capital intensive and requires costly converter stations at either end of the transmission line [50,51]. A critical transmission distance beyond which HVDC technology becomes convenient in terms of efficiency than HVAC is estimated as 55-80 km [16,52,53].

In addition, penetration of large amounts of intermittent renewable power may cause difficulties in the operation of the onshore electric grid [54]. Connecting intermittent and uncertain renewable sources to the electrical grid introduces challenges in various technical aspects, such as power quality, protection, generation dispatch control and reliability [55,56]. Usually grid operators evaluate the impact on the power quality of the local grid by means of dynamic models of the renewable power plant for use in the power system simulator. Such models should demonstrate that the actual power generation of the device and array of devices meet the specific grid code requirements (e.g. frequency stability, voltage, power factor, harmonics) in order to guarantee a safe grid connection [57]. Concerning the offshore wind power, currently there are different national codes and requirements, different power system simulators used by grid operators from one country to another, as well as scarce dialogue between wind farm developers/producers and grid operators [10]. Similarly, international standards provide discrepancies about the grid code and requirements for connecting solar PV plants to the grid [58]. However, a great effort was made by EWEA and DERLab and CENELEC to develop a harmonised grid code for wind and solar PV power integration in Europe [59,60]. From the perspective of wave and tidal current power, limited examples of the devices delivering electricity to the grid have been operating to date, and no specific grid code requirements have yet been issued at both national and European level [61,62].

1.2. Offshore oil & gas production and challenges

In such a transition perspective, the oil & gas industry is striving to become more energy efficient and sustainable [63]. Nowadays, offshore hydrocarbons installations often consist of energy consuming facilities and onsite electrical power is produced traditionally by low-efficiency polluting gas turbines (GTs) and synchronous diesel generators to drive directly compressors and pumps, power control systems and cathodic protection, supply heating for living and recreation areas, etc. [64]. Electrification by means of grid-connected subsea cables represents a possible option to reduce the consumption of fossil fuels, but the cost is high, particularly for remote installations [65].

Furthermore, several new offshore oil & gas projects have been developed in the Gulf of Mexico and in the North Sea, starting operations in challenging scenarios (e.g. increased technological and operational complexity, harsh environmental conditions, etc.), as well as implementing new design concepts (e.g. subsea production, advanced separation techniques, etc.) [66–69]. This requires a higher attention to the potential for safety and environmental impacts. Lessons learnt from past accidents [70,71], such as the Piper Alpha explosion (North Sea, 1988), the Bombay High fire (Arabian Sea, 2005) and the Macondo blowout (Gulf of Mexico, 2010), tragically evidence the potential for major accident hazards of offshore oil & gas operations. Such potential threats inevitably increase in view of the progress of the offshore sector. Directive 2013/30/EU on the safety of offshore oil & gas operations [72] introduced strict criteria

related to the safety and environmental performance of offshore facilities, also requiring companies to operate on the basis of a systematic risk management with respect to humans, assets and environment, and to demonstrate the ability of covering liabilities from major accidents.

On the other hand, offshore oil &gas production installations have a limited lifecycle and production decline of several mature offshore fields is expected due to resource depletion, thus the decommissioning of oil & gas assets is an unavoidable phase of offshore projects [73]. Among 6500 offshore oil & gas production installations worldwide, over 600 installations are designed to be decommissioned in the short-term, and a further 2000 structures by 2040 [74]. For example, in the North Sea 349 fields across the UK, Norwegian, Danish and Dutch continental shelves (2379 wells and 950000 tonnes of topsides) will enter the decommissioning phase over the period 2018-2027. In the UK continental shelf, including most of these infrastructures, about £15 billion are the forecasted costs of decommissioning by 2027 [75]. Moreover, in 80 gas production platforms installed in the Northern Adriatic Sea, most are at the moment approaching the end of their life or are completely disused [10]. Apart from the financial costs, decommissioning of an offshore production facility is a complex process, characterized by technical feasibility, environmental protection, safety, public opinion and legal challenges [74,76]. Fam et al. [77] reviewed the international and national regulations relevant for decommissioning, arguing that regulations in experienced countries should guide countries with less experience in that field. A typical offshore oil & gas installation can be composed of a topside, a jacket which supports the topside, and pipeline for export of hydrocarbons. Several options for decommissioning of an aging offshore installation can be distinguished [74,77–79], as illustrated in Figure 1.6. The selection among the alternatives should need the application of a systematic assessment accounting for multiple criteria (e.g. environmental, safety, etc.) [80,81].

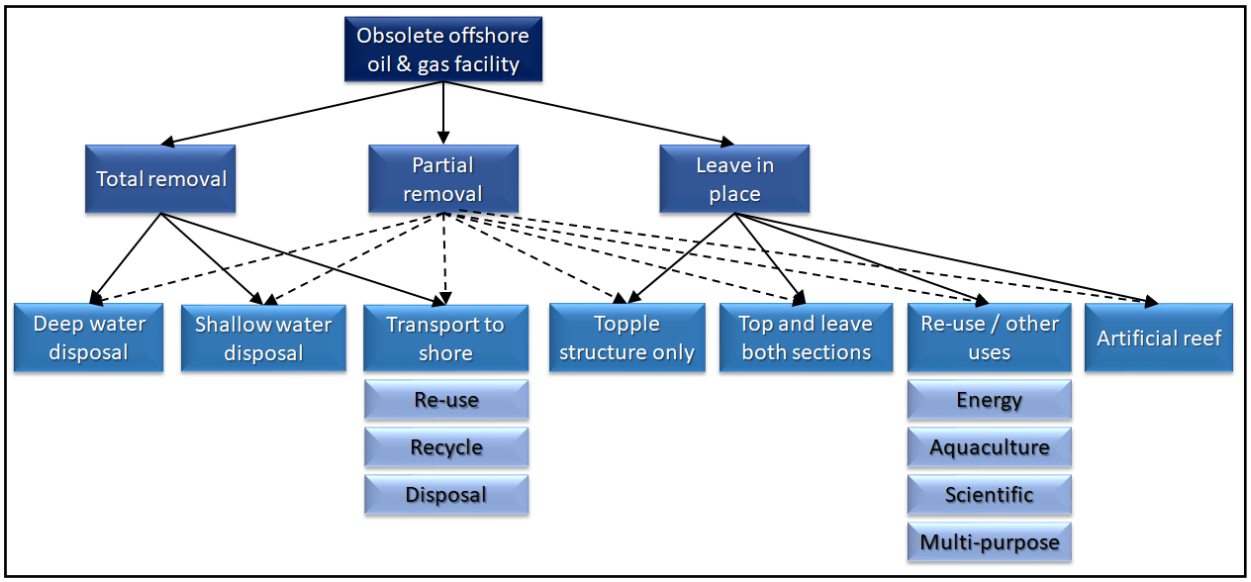

Figure 1.6. Classification of decommissioning options for offshore oil & gas production installation.

Natural gas is a versatile form of low polluting fuel, which is fast becoming the most promising of all the fossil resources since it is deposited more widely in the world than crude oil and coal [50]. It is estimated that the total proved reserves of natural gas at the end of 2018 are around 196.9 trillion m^3 [82]. Sources of natural gas may be not only non-associated gas reservoirs, but also associated gas from oil reservoirs, which is gas produced along with oil. Associated gas is generally considered as an undesirable by-product, which is either reinjected, flared, or vented [83]. To make natural gas and associated gas a major energy source coming after oil, infrastructure to transport and distribute gas to the power market should be developed.

Mokhatab et al. [50] reviewed the available technologies of gas transportation, such as compressed natural gas, natural gas hydrate, liquefied natural gas (LNG), pipeline natural gas, gas-to-liquid, with a wide range of possible products including clean fuels, plastic precursors, liquid hydrocarbons, and Gas-to-Power (G2P). This latter option consists in electrical power production at the producing field and transportation of the electricity by cable to the grid market. The evaluation of gas monetization options has become a multidimensional problem requiring a systematic approach to select the optimal option. Bearing in mind the technicalities of gas transportation, the economically attractive gas transmission mode depends on a number of parameters, i.e. reserve base, production capacity and distance between the gas source and the consumers [84], as illustrated in Figure 1.7.

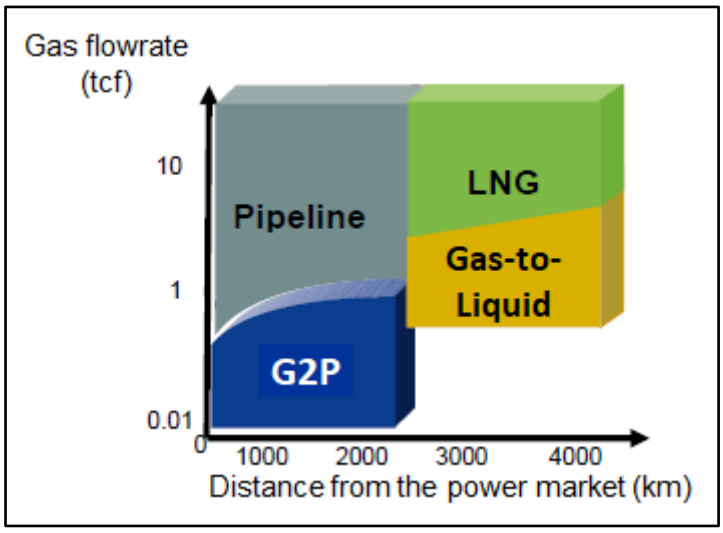

Figure 1.7. Gas valorisation options, adapted from [85].

1.3. Options for integration of renewable and conventional energy sources

In order to provide more reliable and steady power to the consumer, integration of more energy sources forming a hybrid power system has become very popular in recent years [86–88]. In general, the term hybrid energy system is used to define any power system which combines one or more renewable with

non-renewable energy sources, and can be grid-connected or off-grid, depending upon its purpose and production methods. A hybrid renewable energy system includes invariably an electricity storage system to meet the demand when either the demand is peak load demand or renewable energy source is not available for its intermittency. Therefore, the basic components of the hybrid energy system mainly comprise renewable energy generators (i.e. OWTs, solar PV arrays, WECs, etc.), non-renewable generators (i.e. GTs, diesel generators, etc.) to compensate for periods of non-productivity, power conditioning unit, storage device, load and sometimes may include grid [89]. Capitalizing on the strengths of both conventional and renewable energy sources, a suitable hybrid energy system could be able to achieve reduction in the costs associated to implementation and maintenance of the system, limited emission levels, improvement in reliability and performance of the overall system [49]. In addition, an appropriate electrical energy storage technology could enhance smoothing of the mismatch between time and occurrence of peak load and maximum power generated, increasing system flexibility, and reducing costs and losses for electricity transmission [57]. Some electrical energy storage devices using various physical principles are pumped hydro storage, compressed air energy storage, batteries, capacitors and flywheels. They vary broadly in terms of efficiency, storage capacity, cost, response time as well as technical maturity, but they provide limited storage capacity and durations [90,91].

Chemical energy conversion based on hydrogen (H_2) is commonly recognized as a promising solution to offer large storage capacity, with flexible storage durations from minutes to months, of surplus renewable electricity according to the peak-shaving technique [92]. Since it can be produced easily from water electrolysis and valorised in a full range of sectors, H_2 plays a fundamental role in the decarbonisation and security of the future energy system [93]. H_2 is also the first possible end-product of the "Power-to-Gas" (P2G) process chain [94]. To provide a practically unlimited injection into natural gas infrastructure or direct use as fuel, the second core block in the P2G technology consists of methanation, where the generated H_2 can further react with CO_2 to form synthetic natural gas (SNG) [95]. Another peak-shaving solution is represented by the "Power to Liquid" (P2L) pathway [96] aiming at the renewable production of synthetic liquid fuels as potential substitutes of liquid fossil fuels. In particular, methanol (CH_3OH) was identified as a more safe and easy-to-manage energy carrier than H_2 and SNG, due to its higher volumetric energy density, minor transport/handling issues and diverse applications [97]. On the other hand, according to the valley filling technique, during the last years several authors have proposed and modelled GTs as energy balancing system when the renewable energy is not enough than the required one in order to improve the dispatchability of renewable power into the grid [98–102].

The synergy of offshore renewable production with hydrocarbons exploitation at offshore facilities could avoid or limit long and less stable transmission power links, but also to make the oil & gas operations more sustainable [103,104]. With respect to the decommissioning issues, leaving aging oil & gas

infrastructure in place for alternative uses could offer great opportunities for prolonging their lifetime through energy, aquaculture, scientific and multi-purpose applications (Figure 1.5). In particular, the re-use of offshore structures for the exploitation of renewable energy sources would foster the "green decommissioning" or "blue economy", which plays an important role in the energy transition panorama [105,106]. In the last years, the concept of reconversion of aging offshore platforms for energetic uses (e.g. CO_2 sequestration for enhanced oil recovery, offshore wind and wave energies exploitation) has been largely addressed in the literature [107–110]. Moreover, as shown in Figure 1.6, G2P can be a more flexible, cheaper, less massive transport solution than pipeline or LNG technologies for stranded gas fields, i.e. marginal gas field and associated gas with a flowrate between about 380 billion Nm^3 and 38 trillion Nm^3 [84], and depleted gas fields, i.e. remaining gas in hydrocarbon reservoirs where the sale of its product no longer covers the production costs and production has been stopped due to the progressive decrease in reservoir pressure [111]. In addition, G2P appears the optimal option rather than gas-to-liquid if the gas field is located within a certain distance from the power market, e.g. 2500 km. In a G2P system, gas is processed and combusted at the offshore location and the produced electricity is sent either to the onshore grid or to other offshore platforms.

The implementation of P2G and P2L hybrid energy options at offshore oil & gas facilities, i.e. P2G/P2L offshore hybrid energy options, would overcome challenges of both renewable and oil & gas sectors, allowing an easier storage and transportation of energy and creating more valuable purposes for offshore structures approaching the decommissioning phase other than the lifetime extension [105]. GTs coupled with renewable plants in G2P offshore projects, i.e. G2P offshore hybrid energy options, would give dual advantages, compensating renewable power output fluctuations for grid integration as well as monetizing stranded and depleted gas resources.

1.4. Objectives and outline of the research project

In the last years, the P2G concept has claimed significant interest in the onshore context, with several pilot plants operating or under construction [112,113], while some P2L demonstration plants synthetizing CH_3OH from CO_2 hydrogenation have recently started production worldwide [114,115].

In the technical literature there are various examples of comprehensive techno-economic analyses investigating the feasibility and competitiveness of different onshore P2G business cases using well-known techno-economic and financial metrics [92,116,117]. Several scientific papers [118–128] analysed the performance of the P2G pathways for wind and solar energy conversion. Furthermore, during the last decade, many efforts have been made to evaluate the performance of renewable CH_3OH production. Almahdi et al. [129] investigated the catalytic hydrogenation of CO_2 using photocatalytic H_2 and carbon capture based on amine absorption. The same CH_3OH synthesis route was simulated and assessed

coupling with solar photovoltaic-based H_2 [130] and wind energy-based H_2 [131]. Finally, a new CH_3OH process based on water and thermochemical splitting of CO_2 linked to solar CSP technology was proposed by Kim et al. [132].

With respect to offshore applications, currently no real practical examples of P2G and P2L offshore hybrid energy systems can be found. As a part of the European H2ocean project [133], Serna et al. [134,135] demonstrated the feasibility of an offshore wave-H_2 platform for a specific location in the North Sea and then focused on the optimized control of H_2 production driven by co-located wind and wave power sources. Jepma et al. [136,137] evaluated the techno-economic feasibility of different offshore wind-based conversion options producing H_2 for different sectors. By applying an appropriate financial model, the results point out that a positive investment could be obtained if H_2 produced at offshore location is delivered to dedicated niche applications where green gas is valorised by means of a financial premium (chemical industry or the mobility sector). Similarly, a study by Meier [138] demonstrated that adoption of state-of-the-art technologies allows realizing large-scale offshore wind-H_2 platforms in the North Sea. Even though the project has appeared unprofitable due to high production costs of H_2, an economic improvement may be expected with the increase in fossil fuels prices and decrease in installation and operation costs of wind farms and electrolyzers. A recent study by Leporini et al. [78] pointed out that offshore H_2 production at a disused oil & gas structure for fuel shipping and automotive sectors is economically viable if powered by OWTs farm in case of the North Sea location and driven by floating solar PV panels in case of the Adriatic Sea site. On the contrary, offshore SNG synthesis driven by renewable sources was proposed as an interesting alternative to H_2 production at offshore oil & gas platforms by few authors [136,139]. However, no feasibility assessments addressing the performance analysis of this pathway has been carried to date. Similarly, no published work can be found in the literature evaluating CH_3OH process schemes for the valorisation of offshore renewable energy sources, as well as of the synergy between renewable and offshore oil & gas infrastructures.

Advantages of combining high solar shares and GTs into hybrid energy systems have been widely demonstrated in many projects worldwide [140–144]. In 2009, Aora Solar Energy Company, formerly known as EDIG Solar, launched start-up of the world's first hybrid solarized GT system to provide power to kibbutz Samar located in the southern desert of Israel [145]. Currently, combination of wind and solar power with gas generation technologies is commercially feasible through the modern FlexEfficiency* 50 combined-cycle power plant manufactured and tested by General Electric (GE) [146]. The core of such hybrid plant, the new F-class GT, shows higher efficiency and higher output resulting in less fuel consumption and lower emissions on a MWh basis. In addition, the ability to start up quickly, to change load rapidly and to run at low loads allows to compensate for the variable output of solar plants and wind farms [147–149]. In 2015, the first GE's FlexEfficiency* 50 plant started operation in Turkey, integrating

a 50 Hz 9FB GT, a steam turbine, a generator, 22 MW of GE wind turbines and 50 MW of eSolar's CSP tower technology [150]. However, to the best of the author's knowledge, no literature studies and practical applications exist on GTs technologies coupled with offshore renewable power plants for the valorisation of untapped fossil resources in G2P applications, as well as to increase renewable energy penetration for grid balancing.

The overall objective of this research project is to develop a suite of integrated, systematic methodologies supporting the choice of sustainable and safe hybrid energy systems integrating offshore renewable power generation with oil & gas production activities in challenging offshore scenarios, i.e. remote areas, stranded and depleted gas reservoirs, end-of-life oil & gas infrastructures, designs with high safety and environmental issues. To reach this goal, some sub-objectives were set, as summarized in the following.

- Analysis of the different offshore hybrid energy options

The analysis aims at gaining insights into the P2G, P2L and G2P strategies proposed for the synergetic exploitation of renewable sources at given offshore oil & gas sites, including the definition of the possible technology options and identification of strengths, weaknesses, opportunities and threats for their development. This analysis is intended to identify key parameters addressing the preliminary choice of the alternative strategies at different offshore contexts.

- Definition of indicator-based methodologies assessing sustainability and safety performance of alternative offshore hybrid energy options

The definition of quantitative assessment models aims to compare the performance of alternative P2G/P2L/G2P hybrid energy options by means of a set of multi-criteria indicators quantifying technical, economic, environmental and societal aspects. The methods are intended to be tools supporting decisions during the conceptual and front-end engineering design phases of offshore green projects and dealing with specific complex issues which may be experienced in the offshore context.

- Application of the assessment methodologies to case-studies

The introduction of specific case-studies aims to demonstrate the potential of the developed methodologies to capture the different issues related to the offshore context, to assess systematically and comprehensively the alternatives from sustainability and safety viewpoints and to orient the most suitable solution for each problem.

The present study is organized in six chapters. Chapter 1 introduces the background related to the renewable power production from offshore renewable energy sources, to the offshore oil & gas production

operations and possible options for synergy of these two sectors, in order to clearly define the motivation and objectives of the research project.

Chapter 2 contains the state of the art on P2G, P2L and G2P offshore hybrid energy options proposed for the exploitation of renewable sources at given offshore oil & gas sites and the definition of strengths, weaknesses, opportunities and threats for their development.

Chapter 3 reports the literature reviews on previous methods proposing metrics for the assessment of sustainability of hybrid energy systems, inherent safety of process routes in early design stages and environmental protection of installations from oil and chemical accidental spills. For each review, limits of the existing indicators are identified.

Chapter 4 describes a portfolio of methodologies based on multi-criteria indicators for the sustainability and safety performance comparison of alternative P2G, P2L and G2P offshore hybrid energy options in order to fill the research gaps emerged in the previous literature methods. Two sustainability assessment methodologies with a common framework and similar set of performance indicators are presented separately for the analysis of P2G/P2L strategies at remote oil & gas production facilities and for G2P systems at depleted gas fields closed to the shore, respectively, in order to address the specific peculiarities of such different systems. An inherent safety methodology based on the consequence analysis of accident scenarios with respect to personnel, structural assets and marine environment targets is defined to rank the hazard level of process units and overall facility of alternative designs of the offshore systems showing specific safety and environmental concerns. Finally, a methodology integrating sustainability and inherent safety performance analyses based on the concept of process intensification is described for screening the feasibility of emerging chemical process routes in view of suitable implementation in P2G/P2L offshore hybrid energy projects at remote oil & gas areas.

Chapter 5 defines a set of five case-studies showing specific peculiarities to provide a proof of the effectiveness and the value of the developed methodologies. Case-study 1 is introduced to demonstrate the applicability of the sustainability assessment methodology to alternative P2G and P2L strategies for the valorisation of offshore wind energy at a remote gas platform in the North Sea. Case-study 2 is defined to validate the proposed sustainability assessment methodology through the comparison of alternative offshore wind power-G2P options at a depleted gas field in the Adriatic Sea. Case-study 3 consisting of alternative designs with safety and environmental concerns at a gas production platform in the Adriatic Sea aims to prove the potential of the developed inherent safety assessment methodology. Case-study 4 concerning different releases from alternative offshore oil production installations is presented to investigate applicability of the novel indicators for environmental protection from oil accidental spills proposed within the inherent safety method. Case-study 5 is described to demonstrate the ability of the

process intensification screening methodology to assess comprehensively the sustainability and inherent safety performance of eleven emerging processes for renewable CH_3OH production and to address the most feasible designs to detailed assessment of alternative P2L hybrid energy options in a remote oil & gas site in the Atlantic Ocean.

Chapter 6 summarizes the conclusions of the research project and reports some recommendations for further work.

Chapter 2.

State of the art on P2G/P2L/G2P offshore hybrid energy options

2.1. Introduction

This chapter describes the state of the art on P2G/P2L/G2P offshore hybrid energy options proposed for the exploitation of offshore renewable energy sources in an energy transition framework. In the following paragraphs, each option considered is defined, including the assessment of different technology alternatives and the identification of strengths, weaknesses, opportunities and threats for their development at the offshore context.

2.2. State of the art on P2G and P2L hybrid energy options

Chemical energy carriers are considered as potential solutions to improve the penetration of fluctuating renewable power providing large-scale and long term capacity [151]. Converting electricity into gaseous and liquid fuels at the offshore facility and then delivering them to the onshore market can valorise more the resource exploitation thanks to the direct use of energy without storage and reconversion into electricity [105]. In the following, P2G and P2L options for offshore applications are presented separately.

2.2.1. Definition of P2G options

Renewable H_2 is mainly produced by water (H_2O) electrolysis which is the most important H_2O splitting method based on the generation of H_2 and oxygen (O_2) by means of direct electric current in an electrochemical device called electrolyzer [152]. The overall electrochemical reaction illustrated in Equation (2.1) can be segmented into two reactions. At the negatively charged cathode the reduction reaction occurs (Equation (2.2)), while oxidation reaction takes place at the positively charged anode (Equation (2.3)) [153].

$$H_2O \rightarrow H_2 + \frac{1}{2} O_2 \quad (2.1)$$

$$H_2O + 2\,e^- \rightarrow H_2 + O_2^- \quad (2.2)$$

$$O_2^- \rightarrow \frac{1}{2} O_2 + 2\,e^- \quad (2.3)$$

Electrolyzers can be classified preliminarily with respect to the state of electrolyte (solid, liquid), the type of electrolyte (acid, alkaline or ceramic) and the charge carrier (OH^-, H_3O^+, O^{2-}) into three main types: alkaline H_2O electrolysis with a liquid alkaline electrolyte, acidic proton exchange membrane electrolysis with a proton conducting polymer electrolyte membrane, and solid oxide electrolysis with oxygen ions conduction. The main techno-economic and environmental parameters of the H_2O electrolysis technologies investigated are summarized in Table 2.1.

Table 2.1. Comparative performance between H_2O electrolysis technologies.

	Alkaline electrolysis	Proton exchange membrane electrolysis	Solid oxide electrolysis cell
Technological status [92,152,154]	Commercial	Commercial	R&D
System size range [112,155]	0.25-760 Nm^3/h H_2 (1.8-5300 kW_{HHV})	0.01-240 Nm^3/h H_2 (0.2-1150 kW_{HHV})	-
Feed-in [138]	Potassium lye (KOH) – H_2O solution	Fresh H_2O	Steam
H_2O characteristics [156]	H_2O with an electrical conductivity of less than 5 µS/cm	Very pure H_2O with low conductivity (< 1 µS/cm)	Similar to proton exchange membrane electrolysis
Electrolyte [152]	Highly concentrated aqueous solution of KOH (25–30 wt%)	Acid polymer membrane (proton conducting)	Solid oxides ceramic membrane (oxygen ions conducting)
Current density (A/cm^2) [92,157]	0.3-0.5	0.6-2	0.3 - 0.6
Cell voltage (V) [154]	1.8-2.4	1.8-2.2	0.9 - 1.3
Operating temperature (°C) [158]	60-90	50-80	700 - 900
Operating pressure (bar) [158]	10-30	20-50	1 - 15
Electrical consumption (kWh/Nm^3 H_2) [155,157]	4.5 - 7.0	4.5-7.5	2.5 - 3.5
Electrical consumption including auxiliaries (kWh/Nm^3 H_2) [158]	5.0 - 5.9	5.0 - 6.5	3.7 - 3.9
System efficiency ($\%_{HHV}$) [112]	60-71	65-83%	-
System lifetime (y) [92]	10-20 years proven at 2-4% annual degradation rate	5 years proven at 2-4% annual degradation rate	1 year proven at 17% degradation rate
Stack lifetime (h) [116]	60000	40000	-
Product purity (%) [159]	99.5 (before purification); >99.999 (after deoxidiser and dryer)	99.95 (before purification); > 99.9998 (after deoxidiser and dryer)	-
Investment costs ($€_{2017}/kW_{HHV}$) [160]	873 - 2347	306 – 4748	-
Operational costs (% investment costs per year) [158]	2 – 3	3 - 5	-
Minimum load factor (%) [157]	20 – 40	0 - 10	-
Ramp-up time ($\%_{full\ load}/s$) [161]	0.13 – 10	10 - 100	-
Footprint (cell area, m^2) [157]	>4	<0.03	-
GHG emissions (kg_{CO2eq}/kg_{H2}) [162]		0.5995-2.9975	

It is remarkable that strict requirements in terms of the inlet H_2O are needed to guarantee long-term performance: ionic conductivity must be very low, with the number depending on the membrane characteristics [156]. Among sea H_2O desalination technologies, multi-stage flash distillation, multi-effect distillation, mechanical vapour compression, reverse osmosis, electrodialysis and membrane distillation can be evaluated [163]. A comparison of the techno-economic and environmental parameters of these technologies is illustrated in Table 2.2. In the present analysis, reverse osmosis was chosen as reference

technology for the sea H_2O desalination stage since it demonstrates high compatibility with renewable sources [164–166] and good ability to produce relatively pure H_2O required from proton exchange membrane electrolysis [167,168]. Moreover, reverse osmosis seems to be feasible for offshore applications due to modularity, minimum interruption time during maintenance and low electrical energy needs [169,170].

Table 2.2. Comparative performance between sea H_2O desalination technologies.

	Multi-Stage Flash Distillation	Multi-Effect Distillation	Mechanical Vapour Compression	Sea H2O Reverse Osmosis	Electrodialysis	Membrane Distillation
Technological status [164,171]	Commercial	Commercial	Commercial	Commercial	Commercial	R&D
System size range (m^3/d H_2O) [172]	50000 - 70000	5000 - 15000	100 - 3000	<128000	2 - 145000	-
Feed-in [164]	Sea H_2O (any)	Sea H_2O (any)	Sea H_2O (any)	Sea H_2O (35000)	Brackish H_2O (<5000)	Sea H_2O (any)
Product quality (ppm) [172]	10	10	10	400 - 500	150 - 500	-
Operating temperature (°C) [158]	90 - 110	70	<70	15 - 20	15-20	60 - 90
Energy use (kWh/m^3) [163,172]	Electrical: 2.5 - 5; Thermal: 15.8 - 23.5	Electrical: 2 - 2.5; Thermal: 12.2 - 19.1	Electrical: 7 - 12	Electrical: 3 - 8 (with energy recovery)	Electrical: 0.8-5.5	Total electrical and thermal: 628
Investment costs ($€_{2013}$/(m^3/d)) [163]	1596-3325	1197-2660	-	1197-3325	-	-
Operational costs (% investment costs per year) [164]	1.5 - 2.5					
GHG emissions (kg_{CO2eq}/m^3_{H2O}) [173]	14.4-24	7.7-19.2	10.6-11.5	4.8-8.6	2.5-5.3	-

Investment costs are estimated based on the assumption that 1$ = 0.75 € [174].

Besides the onsite uses as fuel for ships and GTs, another end-use can be represented by the onshore gas grid. The injection of the produced H_2 into existing gas pipeline leads to a H_2 enriched natural gas (HENG) blend which offers several benefits in terms of emissions and efficiency compared to natural gas [175]. However, transportation of HENG mixture depends firstly on the pipeline delivery pressure and on the maximum blending ratio tolerated by the existing infrastructure. Most transmission pipelines deliver natural gas along long distances at pressures from 60 bar to more than 125 bar, thus often requiring the operation of gas compressors at the offshore platform to ensure that the natural gas flowing through the pipeline maintains the desired pressure. On the other hand, the range of 5-20% by volume of H_2 in natural gas can be considered feasible by taking into account the general behaviour of the onshore gas grid and of specific gas devices [176]. Once arrived to the onshore terminal, the HENG blend may be injected into

the natural gas grid, provided that acceptability standards on heating value and Wobbe index required from the national gas-network regulation are fulfilled [177].

Other possible onshore end-uses for H_2 than gas grid injection can be the industry (refineries, chemical industry, light industry, etc.) and the mobility (fuel cell electric cars and buses) sectors. Thus, relatively pure H_2 can be delivered from the offshore facility to the onshore terminal avoiding limitations in the admixture injection in the existing gas grid. The development of an offshore H_2 transmission can be envisaged by adopting the existing experience gained in the onshore context. As investigated in the European Roads2HyCom project [178], there are several H_2 pipeline systems all around the world for industrial applications: these include networks in the Netherlands, Northern France, Belgium, Germany (Ruhr and Leipzig areas), UK (Teesside area), and North America (Gulf of Mexico, Texas-Louisiana, California). Overall, these pipelines transport pure and ultra-pure H_2 with an inner diameter of 100-300 mm and smaller extension compared to the lengths of existing natural gas networks (about 1500 km in Western Europe and 900 km in the USA). They are mostly realized using low to medium strength steels, with maximum operating pressures of 100 bar [179]. It should be noted that pipe diameters are expected to be smaller than pipeline delivering natural gas or admixture, due to the low density of pure H_2. An example of recommended diameters obtained from application of the general flow equation based on Bernoulli law for a range of volumetric flowrate of H_2 is reported in Table 2.3. These data derived from a recent study [180] consider an upstream pressure from about 30 to 75 bar, a downstream pressure of 24 bar (gauge) and pipeline length of 100 km. Once arrived at the onshore gas terminal, H_2 can be addressed to the mentioned end-uses, after passed the required gas quality control measurements and fulfilled the specific market requirements.

Table 2.3. Example of diameters of pipeline delivering pure H_2 for different throughputs [180].

H_2 volumetric flowrate (Nm^3/h)	Pipeline diameter (mm)
12000	100-150
40000	150-250
80000	200-300
120000	250-400

The combination of electrolysis and methanation allows to produce SNG, which can be easily delivered via existing gas pipeline without the need of new infrastructures or alternative systems [113]. The current processes available to produce SNG are based on catalytic or biological three-step methanation involving H_2 and CO_2. Catalytic methanation is a thermochemical exothermic process which typically operates at high temperature (200-700 °C) on a proper catalyst (usually based on nickel). SNG can be produced according to the Sabatier reaction [181]:

$$CO_2 + 4\ H_2 = CH_4 + 2\ H_2O \quad (2.4)$$

From the thermodynamic point of view, the reaction yield is promoted by high pressures (up to 100 bar), low temperatures, stoichiometric ratio of reactants (i.e. H_2 to CO_2 molar ratio equal to 4:1) and removing H_2O produced in the reactors [182]. Several steady-state reactor concepts were developed for the catalytic methanation, namely fixed-bed, fluidized-bed, three-phase and structured reactors. Whatever reactor design is chosen, the generated heat of the methanation reaction needs to be removed continuously: one possibility is to use at least two adiabatic beds and dilute the feed through recirculation of a part of the reactor's cooled gas outlet, while another one is the isothermal operation by transferring the reaction heat to a cooling medium [183]. In biological methanation, methanogenic archaea work in complex cooperation with co-enzymes as catalyst for the synthesis of H_2 and CO_2. Although the conversion occurs with the same reaction as in the chemical methanation, different temperature ranges for the reaction and response time are used [95]. The method is currently moving from research stage to demonstration phase based on in situ digester and separate reactor [154]. Some techno-economic and environmental parameters assessing the performance of methanation technologies are summarized in Table 2.4.

Table 2.4. Summary of comparative performance between methanation technologies.

	Catalytic methanation	Biological methanation
Technological status [92,95,154]	Commercial	Pre-commercial (pilot scale)
System size range [95]	Up to 1000 Nm^3/h SNG (< 500 MW_{HHV})	Up to 5.3 Nm^3/h (< 12 MW_{HHV})
Feed-in [92]	Any mixture of CO_2, H_2, CH_4, H_2O with low tolerance for sulphur, O_2 and vapour	Any mixture of CO_2, H_2, CH_4, H_2O with high tolerance for sulphur and vapour, but limited for O_2
Catalyst [95]	Ni, Ru, Rh, and Co	Methanogenic archaea
Product quality (conversion yield, %) [92]	92-96	98-99
Operating temperature (°C) [95]	200-750	20-60
Operating pressure (bar) [95]	4-80	1-3
Electrical consumption (kWh/kg_{SNG}) [184–186]	0.33	0.54
Efficiency excluding electrolysis ($\%_{HHV}$) [92,95,120,187,188]	70-85	75-98
Catalyst lifetime (h) [95]	24000	-
Investment costs ($€_{2013}/kW_{HHV}$) [95]	600-2750	100-800
Operational costs (% investment costs per year) [95]	10 (including replacement of the catalysts)	5 (heating requirements), 5 (miscellaneous)
Minimum load factor (%) [92,154,189]	0	0
Ramp-up time between 0-90% (min) [92]	30-60	0.02-3
Response time from standby mode (min) [95]	< 5	< 1
Footprint (gas hourly space velocity, h^{-1}) [154]	500-5000	< 100
GHG emissions ($kg_{CO2,eq}/kg_{SNG}$) [162,186]	0.3-1.8	0.85

It should be noted that, H_2 buffer storage is required to operate the methanation reactor continuously, even though the correlation between the optimum capacity of storage facility and methanation performance has

to be clearly determined yet [154]. An estimation of the pressurized H_2 storage can be based on the tank volume required to cover inoperability period of the electrolyzers [190].

Besides the onsite uses as fuel for ships and GTs, the main onshore end-use of SNG is the gas grid injection. Since CH_4 is the main component of conventional natural gas, SNG produced at the offshore facility can be delivered via existing natural gas without any limit in terms of maximum concentration, given the required compression to reach the desired delivery pressure. Once arrived to the onshore gas terminal, SNG can be directly injected into the onshore natural gas network, provided that constraints on heating value and Wobbe index imposed from the local grid code are met [177].

As described above, apart from H_2, CO_2 is the second reactant for methanation. CO_2 should be supplied with low costs and energy needs, ideally with high purity and suitable flowrate to balance the fluctuating demand [159]. Among the different CO_2 sources, CO_2 removal from raw natural gas or associated gas at the offshore facility represents a feasible option when the extracted hydrocarbons require to be purified to meet the requirements for transportation. CO_2 is a naturally occurring diluent in oil and gas reservoirs and can react with H_2S and H_2O to form corrosive compounds which threaten steel pipelines; no more than 2-3% concentration of CO_2 in natural gas pipeline is usually recommended [50]. Chemical absorption with amine solutions and membrane permeation are two of the most mature technologies which may be employed for this purpose [191,192]. A comparison based on relevant parameters between these separation techniques is reported in Table 2.5. A successful example of offshore carbon capture from natural gas by means of amine absorption is represented by the Sleipner Carbon Capture and Sequestration (CCS) project in the North Sea [193], where CO_2 is separated from natural gas containing up to 9% CO_2 at Sleipner T and transported to Sleipner A where it is injected into the Utsira formation.

Table 2.5. Comparative performance between CO_2 removal technologies from natural gas.

	Amine absorption	Membrane permeation
System size range [194]	Gas flowrate >20 MMscfd	Gas flowrate <20 MMscfd
Feed-in [194]	Low CO_2 conc. (2-15 %mol)	High CO_2 conc. (15-40 %mol)
CO_2 recovery % [195]	82-91	33-81
Operating pressure (bar) [191]	1-120	≤ 4
Electrical consumption (kWh/kg_{CO2}) [195]	0.84-0.89	0.13-0.28
Investment costs ($M€_{2008}$) [195]	2.1-12	1.2-9.6
Operational costs (% investment costs/y) [191]	15	18
GHG emissions ($kg_{CO2,eq}/kg_{CO2,recovered}$) [196]	0.0828	0.1957

Calculation of investment costs are based on the assumption that 1$ = 0.68€ [174].

It must be remarked that further gas treatment and significant compression may be required before supplying relatively pure CO_2 to the methanation reactor. The onshore CO_2 capture and transport to the offshore installation can be an alternative to deal with the problems issued by the onsite CO_2 separation

as well as to valorise offshore enhanced oil or gas recovery (EOR or EGR) activities [197,198]. Over 40 years, several projects worldwide have developed and applied successfully CO_2-EOR technology giving two major advantages: additional hydrocarbon recovery that extend the producing life of the depleted oil & gas fields and CO_2 storage to reduce GHG emissions [199,200]. Production from natural gas reservoirs can be also benefitted from CO_2-EGR applications, which is a recent technique providing pressure support in natural gas reservoirs to prevent subsidence and H_2O intrusion via both displacement and re-pressurization on the remaining natural gas [201].

Two main modes may be applied to transport CO_2 to the offshore site: offshore pipeline and shipping [202]. Shipping transport requires liquefaction, cryogenic buffer storage and on-ship conditioning [203]. Concerning the pipeline option, existing offshore transmissions can be re-used for CO_2 transportation under specific design constraints [204]. Carbon steel pipelines seem to be metallurgically suitable, provided that a proper verification of moisture content is performed. However, the main constraint of existing infrastructure is the design pressure which may be lower than the range 200-300 bar of optimal pressure rating required for new pipes delivering CO_2, thus CO_2 transportation capacity may be reduced. Another limitation is represented by the age of the existing pipeline, requiring that integrity analysis should be performed to evaluate its use during the remaining service life [205]. Examples of primary candidates of North Sea pipelines for re-use in CO_2 transportation can be found in the literature [204]. Knoope et al. [206] pointed out that gaseous CO_2 transportation in the range 15-30 bar is a cost-effective solution if the required pressure at the offshore facility is lower than 80 bar (i.e. the minimum allowable level for safe transportation of liquid phase CO_2) and the design pressure of existing infrastructure is between 90 and 150 bar. Moreover, gas phase transportation is recommended for relatively small CO_2 mass flowrates, e.g. less than 100 kg/s [206].

2.2.2. Definition of P2L options

P2L option aims at the renewable production of synthetic liquid fuels as potential substitutes of liquid fossil fuels in an energy transition panorama, e.g. CH_3OH, dimethyl ether, ammonia, Fischer-Tropsch fuel [207]. In particular, as first conceptualized by Olah in the so-called “Methanol Economy” [208], CH_3OH was proposed as more safe and easy-to-manage energy carrier than H_2 and SNG, due to its higher volumetric energy density, minor transport/handling issues and diverse applications [209]. Moreover, different green processes for CH_3OH production have been recently investigated instead of the traditional method via syngas [210], thus highlighting the promising role of this fuel for the global future energy transition. For this reason, CH_3OH has been selected as of P2L product to be investigated in this study.

Among the CO_2-to-CH_3OH production processes promoting the Carbon Capture and Utilization (CCU) concept, catalytic hydrogenation and electrochemical reduction of CO_2 were widely investigated in the literature [211–213]. Catalytic hydrogenation of CO_2 can occur by means of the following reaction [131]:

$$CO_2 + 3\ H_2 = CH_3OH + H_2O \quad (2.5)$$

As proved in the ICI, Lurgi, and Mitsubishi processes, typical ranges of temperature and pressure for this reaction are 250-300°C and 50-100 bar, respectively, over a Cu-based catalyst in a multi-tubular reactor requiring a strong need for H_2O and heat removal [214].

On the other hand, electrochemical conversion of CO_2 involves the reduction of CO_2 and oxidation of H_2O in an electrochemical cell at mild operating conditions, according to the overall global reaction [215]:

$$CO_2 + 2\ H_2O = CH_3OH + 1.5\ O_2 \quad (2.6)$$

A comparison based on some techno-economic and environmental parameters of these two production methods is reported in Table 2.6.

Table 2.6. Comparative performance between CH_3OH synthesis technologies using CO_2 source.

	Catalytic hydrogenation	Electrochemical reduction
Technological status	Commercial/Pre-commercial (pilot scale) [114]	Research & Development [211]
System size range [216]	0.05 – 3000 t/y	-
Feed-in	CO_2, H_2	CO_2, H_2O
Catalyst/Electrode [211,215]	Cu-based	Cu-based
Product quality (CH_3OH selectivity %) [212,215]	30-99.5	2-40 (faradic efficiency)
Operating temperature (°C)	250-300	15-25
Operating pressure (bar)	50-100	1-1.5
Energy efficiency excluding electrolysis (%) [92,215]	70-85	5-60
Investment costs ($M€_{2014}/(t_{CH3OH}/d)$) [131,217]	0.18-0.22	-
Operational costs (% investment costs per year) [218]	5	-
Greenhouse gas emissions (kg_{CO2eq}/kg_{CH3OH}) [216]	0.2-3.8	-

The investment costs are based on the assumption that 1$ = 0.75 € [174].

The same considerations reported above for CO_2 source supply to methanation are applied to the case of offshore CH_3OH synthesis. It is worth noting that catalytic hydrogenation of CO_2 may require that both H_2 and CO_2 are compressed to higher level than those required for catalytic methanation, thus adding further compression steps in the pathways producing CH_3OH. In particular, it would be convenient to pre-compress CO_2 to the same pressure of H_2 before being mixed and then compressed together to the reactor operating pressure [219].

Differently from H_2 and SNG, CH_3OH can be obtained in liquid phase at ambient conditions [131]. Therefore, it can be stored at the offshore platform in storage tanks commonly used for gasoline storage,

provided a proper protection from ignition sources in a dedicated location. Besides the onsite end-use as gas hydrate preventer, CH_3OH can be delivered to the onshore market using sealed cargo holds of tanker ships similar to those adopted for marine transportation of hydrocarbons [220]. Despite the several applications of CH_3OH as basic building block for a wide variety of chemical products, the most attractive end-use of renewable CH_3OH can be identified in the mobility sector due to its suitability for a flex-fuel mixture with gasoline in conventional internal combustion engines driven road vehicles [116,212].

2.3. State of the art on G2P hybrid energy options

The most common method to generate power from natural gas uses GT generators which are a type of internal combustion engine comprising of three sections, i.e. a compressor, combustion chamber and turbine, mounted on the same shaft. Compressed air is mixed with fuel injected through nozzles, the air-fuel mixture ignites under constant pressure conditions and the hot combustion gases are routed to spin a turbine driving a generator that converts the energy into electricity [221]. Therefore, the process of producing electricity involves combustion, compression, heat transfer and spinning, resulting in the need for equipment consuming a great deal of fuel, requiring considerable operation and maintenance efforts and inevitably producing GHG emissions.

The thermodynamic process used in GTs is the Brayton cycle, which is characterized by the firing temperature and pressure ratio. The pressure ratio is the compressor discharge pressure divided by the compressor inlet pressure, while the firing temperature is defined as the highest temperature in the cycle. The fuel to power efficiency and resulting emissions of the engine can be optimized by increasing these two parameters, which depends on the design of GTs [222]. Commercially, GTs are classified into industrial (heavy frame), aeroderivative designs, and micro GTs characterized by different capacity range and which can fulfil the high requirements of a wide spectrum of applications in terms of efficiency, reliability, flexibility and environmental compatibility [223,224]. Table 2.7 summarizes the comparison of these types of GTs technologies in simple cycle.

GTs can be either in simple-cycle or combined-cycle configurations. Simple-cycle power plants use GTs without heat recovery, while combined-cycle power plants use GTs and recover the waste heat from their exhaust-gas streams with heat-recovery steam generators to allow steam runs steam turbine generators, thus producing additional power. A typical simple-cycle GT can convert 30–40% of the fuel input into shaft output. Compared to simple-cycle installations, combined-cycle installations show higher power plant efficiency (55-60%) and thus less environmental emissions, but they are characterized by longer start-up time, purge needs and ramp-up to full load [221,222].

Table 2.7. Comparative performance between commercial GT technologies in simple cycle.

	Heavy frame GTs	Aeroderivative GTs	Micro GTs
Output power range	Up to 340 MW [222]	Up to 66 MW [222]	30-800 kW [225]
Nominal frequency	50/60 Hz	50/60 Hz	50/60 Hz [226]
Pressure ratio	18:1 [222]	30:1 [222]	3-4.5:1 [225]
Fuel-to-power efficiency	28-34% [227]	37-42% [227]	26-33% [225]
Internal design	Single shaft fixed to generator speed, multiple variable compressor vanes to control airflow [227]	Multiple independent shafts to run at optimal speed with secondary turbine matched to generator speed [227]	Air bearing technology, one moving part, no coolants, oils or grease [225]
Operational flexibility	Single high power unit [227]	Multiple lower power units [227]	Multiple lower power units [225]
Starting	No fast start capability without adverse impact to cyclic life, only about 350 kW required [227]	10 min depending upon configuration, without impact to cyclic life, helper motors required [227]	About 2 min, helper motors required [225]
Ramp-up time (acceleration to load)	Slow (10-15 min) [227]	Rapid (idle to full load in 2 min) [227]	-
Maintenance location	On-site maintenance requiring larger space [227]	Either on-site or at off-site facility[227]	-
Maintenance downtime	110-140 d (<99% availability) [227]	Up to 40 d (99% availability) [227]	-
Annual inspections	6-15 d [227]	30 h (heavy lift equipment not necessary) [227]	-
Combustion inspection	2-5 d [227]	Every 4000-8000 h [227]	8000-40000 h [225]
Skid dimension	50 m^2 [227]	37 m^2 [227]	22 m^2 [226]
Driver skid weight	120 tonnes [227]	60 tonnes [227]	12-14 tonnes [226]
Investment costs (€$_{2013}$/kW)	620 [228]	900 [228]	1158 [225]
Fixed operational costs	7 €$_{2013}$/kW-y [228]	11 €$_{2013}$/kW-y [228]	0.034-0.038 €$_{2013}$/kWh [225]
Greenhouse gas emissions (kg_{CO2eq}/kWh)	202 [229]	202 [229]	185 [230]

The investment costs are based on the assumption that 1$ = 0.75 € [174].

GTs are common technologies at offshore oil & gas platforms producing their own power. Due to weight and space constraints in offshore installations, GT simple-cycle configurations are the preferred method for power generation [53]. Aeroderivative GTs are typically the most prevalent in offshore facilities because of their compactness, lighter-weight designs and higher power density than comparable GTs [221]. Their high efficiency and fast-start capabilities mean that aeroderivative GTs also perform well in decentralized power generation applications [223,231]. Moreover, micro GTs allow to valorise associated gas with high tolerances on H_2S, CO_2, N_2, thus requiring minimal fuel pre-treatment and no exhaust after treatment [232]. Example of a large -scale offshore application of the G2P technology is represented by the advanced Sevan 700 MW power plant concept, developed by Sevan Marine in cooperation with Siemens Oil & Gas [233], which aims to serve as a power-supply hub for offshore oil & gas operations

and to transmit power from marginal or remote gas fields to shore over distances of 70-100 km. The concept consists of a cylindrical platform equipped by eight combined-cycle GTs fuelled by imported and re-gasified LNG or by gas from a local (stranded) gas field and an amine-based CO_2 capture system for injection into the sub-seabed reservoir facilitating EOR initiatives [234].

2.4. SWOT analysis of the alternative options

To raise full awareness about all the factors involving the feasibility of the innovative offshore hybrid energy options defined above, SWOT analysis, a tool frequently used in the field of business management [235], is performed for each pathway to highlight strengths, weaknesses, opportunities and threats. Figures 2.1, 2.2., 2.3 and 2.4 illustrate the results for the Power-to-H_2 option, Power-to-SNG option, Power-to-CH_3OH option, G2P option, respectively.

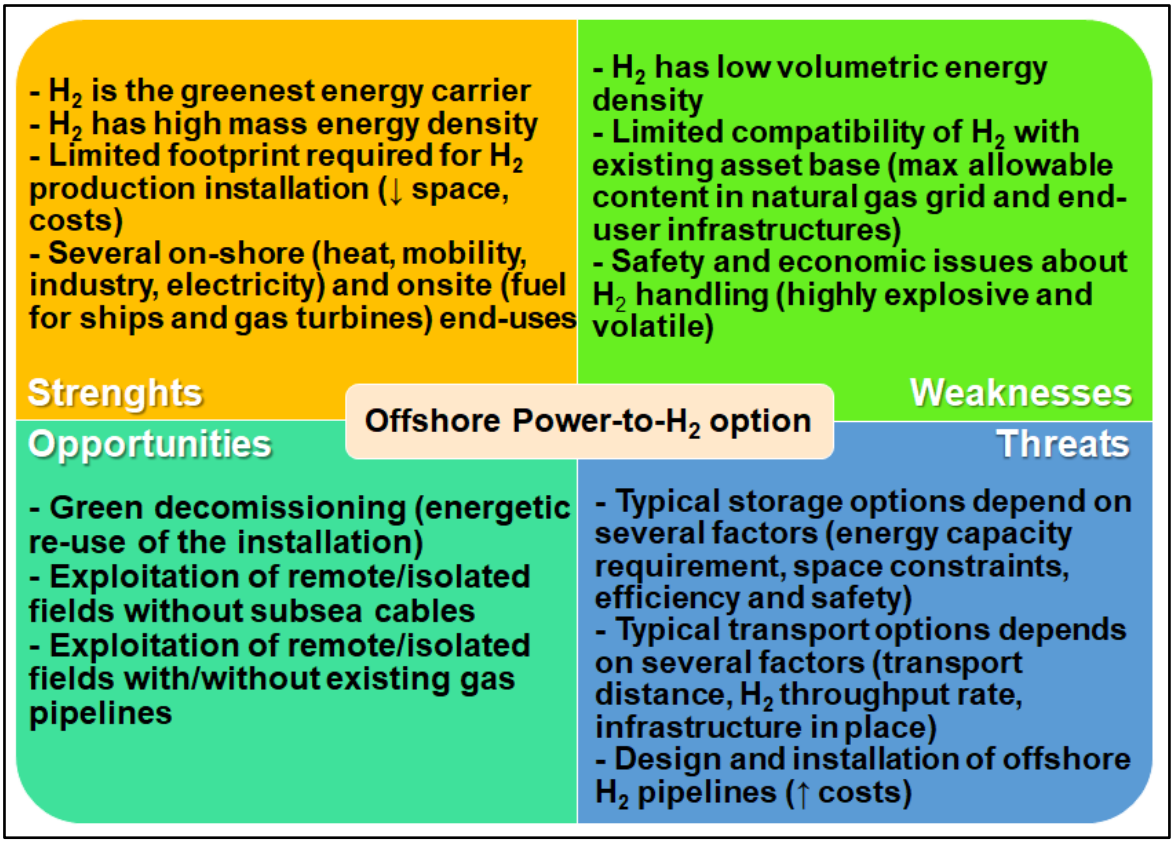

Figure 2.1. SWOT analysis for the P2G - H_2 offshore hybrid energy option.

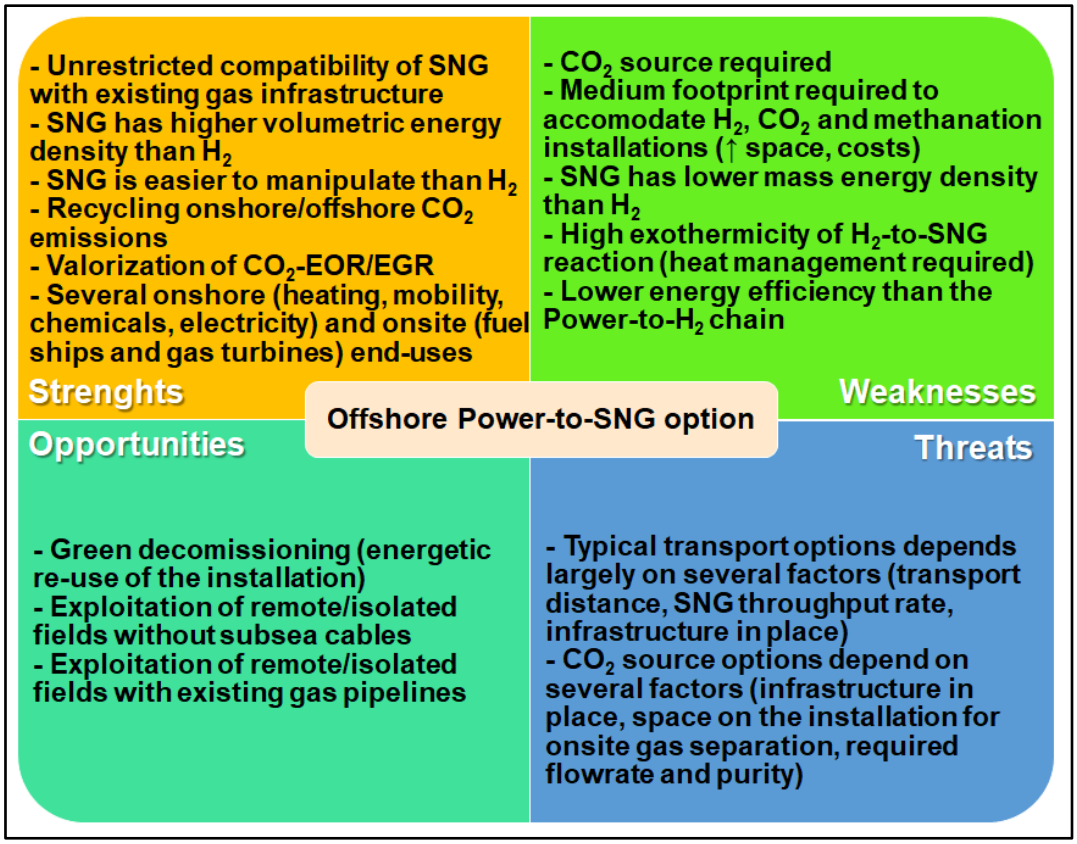

Figure 2.2. SWOT analysis for the P2G - SNG offshore hybrid energy option.

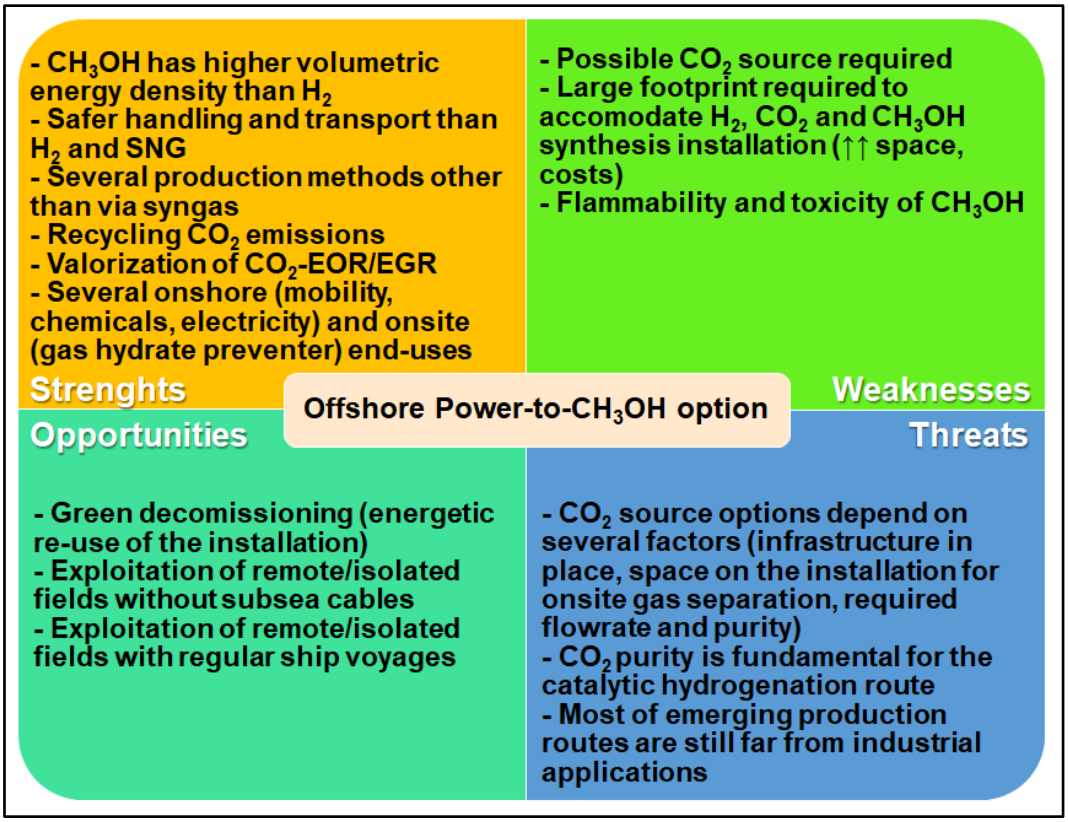

Figure 2.3. SWOT analysis for the P2L - CH_3OH offshore hybrid energy option.

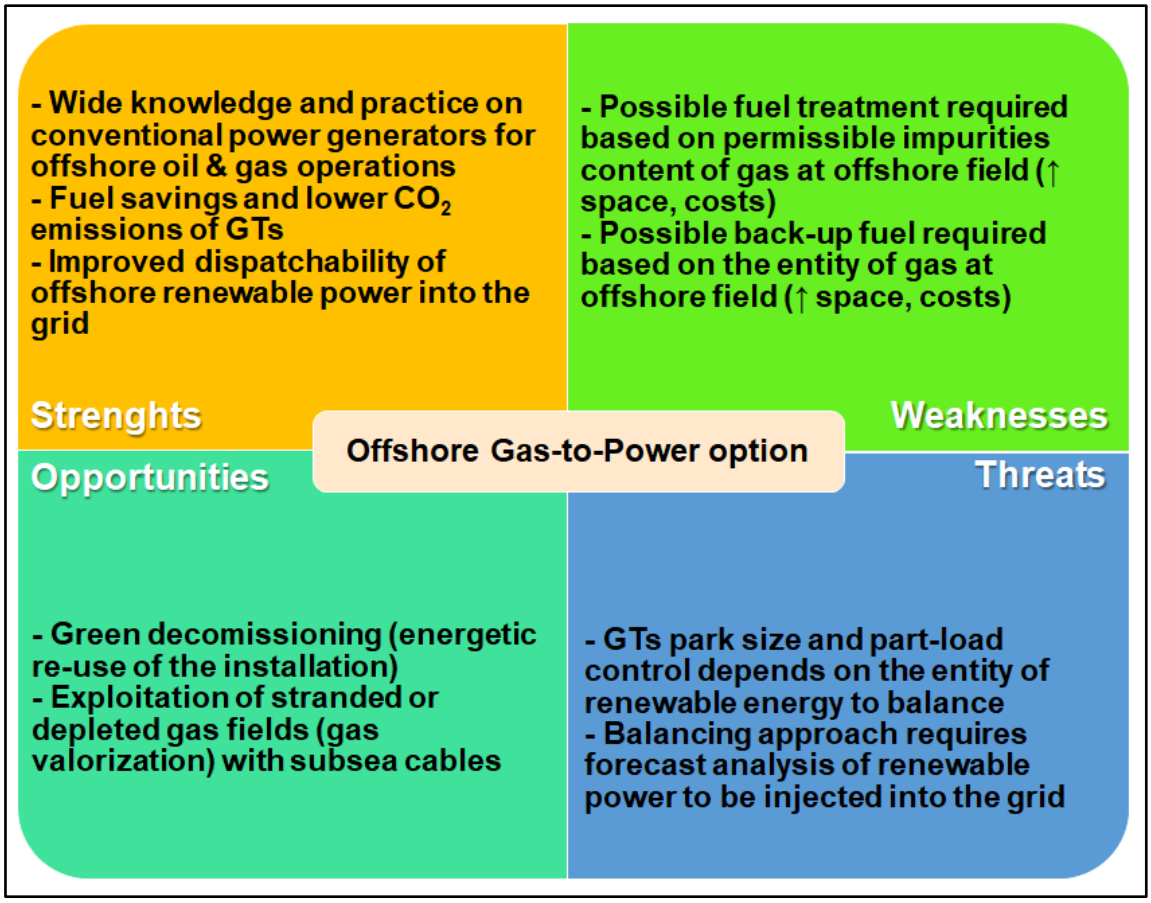

Figure 2.4. SWOT analysis for the G2P offshore hybrid energy option.

As a result of the opportunities highlighted in the SWOT analyses, a set of key parameters is identified addressing the preliminary choice of suitable P2G/P2L/G2P hybrid energy options which may be developed in a given site. The influencing parameters are listed in the following.

- Phase of the installation in its lifecycle, in order to evaluate the possibility for re-using the installation limiting technical, economic and environmental issues of decommissioning process.
- Distance to the onshore market of chemical products or of electrical power, in order to estimate the potential for conversion of renewable power into chemical carriers or for power dispatching into the grid.
- Type of field: to evaluate the monetization of stranded and depleted gas field.
- Onsite power generation and/or electrical cables to shore or to other platforms, in order to evaluate the use of existing conventional power generators and/or transmission of electricity directly via subsea cables.
- Presence of existing gas pipelines, in order to consider the transportation of gaseous chemicals.

- Presence of regular ship voyages, in order to consider the transportation of liquid chemicals in tankers or supply vessels;
- Presence of CO_2-EOR or CO_2-EGR activities, in order to assess the CO_2 supply to the chemical synthesis.

Table 2.8 summarizes the preliminary screening of the alternatives based on these factors. As emerged in this table, all the pathways may be considered for facilities at the end of their useful life for the energetic valorisation of the site. P2G and P2L may be more suitable options when the offshore facility is located at remote areas far from the product markets, and pipeline to shore and ship voyages exist. On the other hand, G2P may be adopted when the offshore facility is located in stranded or depleted gas fields, relatively close to the onshore electrical network and linked to it by means of subsea electrical cables. Finally, P2G - SNG and P2L options may be attractive solutions when CO_2-EOR or CO_2-EGR activities exist at the offshore site taking advantage of CO_2 supply for the chemical synthesis.

Table 2.8. Preliminary screening of P2G, P2L and G2P offshore hybrid energy options based on key parameters.

Key parameter		P2G (H_2)	P2G (SNG)	P2L (CH_3OH)	G2P
Lifecycle phase (decommissioning)		X	X	X	X
Distance to the onshore power/product market	High	X	X	X	
	Short				X
Type of field (stranded or depleted gas)					X
Onsite power generation/ subsea electrical cables					X
Existing gas pipeline		X	X	X	
Regular ship voyages				X	
CO_2-EOR/EGR activities			X	X	

Chapter 3.

State of the art of sustainability and safety assessment methods

3.1. Introduction

This chapter describes the literature methods based on sustainability indicators suitable for the analysis of hybrid energy systems. Moreover, the state of the art of indicators quantifying inherent safety and environmental protection from oil and chemical spills is described. The limits of the existing methods are identified.

3.2. Sustainability assessment methods

3.2.1. Generalities

Sustainability consists in a comprehensive concept presenting different interpretations based on the approaches and the goal of each work. No exact definition for sustainability exists [236]. However, the most frequently quoted definition is from "Our Common Future" (also known as the Brundtland Report) by the World Commission on Environment and Development [237]. This report introduced for the first time the concept of sustainable development as the "sustainability that satisfies the needs of the present without compromising the ability of future generations to meet their own needs", thus sustainability can be seen as the final goal of balancing social and economic activities and the environment. In 1998, the Encyclopedia of Life Support Systems [238] presented an enhanced definition of sustainable development as "the wise use of resources through critical attention to policy, social, economic, technological and ecological management of natural and human engineered capital so as to promote innovations that assure a higher degree of human needs fulfilment, or life support, across all regions of the world, while at the same time ensuring intergenerational equity". In the analysis of sustainability of a system three main pillars were commonly identified according to the triple bottom line framework [239]: environment, economy and society. On the contrary, Dincer and Rosen [240] proposed four key requirements to reach sustainable development, i.e. technological sustainability (e.g. providing efficient technologies), economic sustainability (e.g. providing affordable technologies), environmental sustainability (e.g. minimizing environmental impact), societal sustainability (e.g. satisfying societal, ethical and safety standards). Such four dimensions or aspects of sustainability are commonly addressed in the literature for the evaluation and comparison of alternative energy systems [241–243]: a sustainable technology should balance energy consumption and production with minimal negative impacts on economics and environment and meeting societal aspirations and needs.

Due to the multi-disciplinary concept of sustainability, the use of multi-criteria decision analysis (MCDA) methods were widely applied to perform a broad evaluation of the energy systems [244]. MCDA methodologies are popular techniques in sustainable energy management providing solutions to complex problems involving conflicting and multiple domains [245]. The selection of proper evaluation criteria or

indicators quantifying the different aspects of sustainability plays a key role in the MCDA process for the resolution of the problem and thus the identification of the best alternative [246]. Clearly enough, it is not helpful to use too many indicators for the sustainability performance assessment and decision-making. The indicators should cover all the aspects of sustainability without showing repeatability and overlap [247]. A set of desired properties of the indicators for an energy decision-making problem is defined in the following, as suggested in the literature [246–248].

- Exhaustivity: the criteria should reflect the essential characteristics and the whole performance of the system discriminating between the alternatives.
- Consistency: the indicators should be consistent with the decision-making objective.
- Independency: the indicators should not be functionally related at the same level.
- Measurability: the indicators should be measurable in quantitative value or qualitative terms.
- Simplicity: the indicators should be easily understandable and applicable.
- Limitation of measurement: the indicators should be small as enough in number at each level avoiding to communicate redundant and unneeded information.

During the last twenty years several authors have posed their attention on the sustainability assessment of energy systems and hybrid energy systems proposing indicator-based methodologies [242,246,249–251]. An in-depth investigation of existing indicators is crucial in order to identify a set of relevant indicators quantifying the sustainability performance of offshore hybrid energy options meeting the principles above listed. The review analysis of the state of the art on sustainability indicators is presented in the following.

3.2.2. Sustainability indicators for hybrid energy systems

The literature review has focused on MCDA evaluations for sustainability of energy systems and hybrid energy systems, involving a total of 110 studies published over the period 2000-2019. The indicators used are mainly divided into the aspects of sustainability mentioned above, i.e. technical, economic, environmental, societal. Tables 3.1 and 3.2 report the most frequently indicators applied in the literature, including the occurrence of each indicator in each dimension.

The reviewed articles analysed different energy systems, such as combined heat and power plants and natural gas systems (e.g. [252–255]), renewable energy systems involving wind farm, solar PV and CSP plants (e.g. [256–263]), hybrid systems with H_2 production and storage (e.g. [243,264–269]), SNG and biogas production (e.g. [120,124,270,271]), CH_3OH (e.g. [131,272]) and other biofuels and chemical commodities (e.g. [273–276]). Some studies focused on energy planning for given regions or countries

(e.g. [249,277–283]), while others dealt with energy policy and management issues (e.g. [250,259,284–287]).

Table 3.1. Technical and economic indicators found on the existing MCDA sustainability assessments of energy systems and hybrid energy systems.

Aspect	Indicator	Reference	Occurrence in related aspect
Technical	Energy efficiency	[120,243,252,253,255,256,258,259,261,264,266–268,288–310]	40.0%
	Exergy efficiency – Destruction	[243,255,261,264,268,278,311–313]	10.0%
	Primary energy ratio – Energy Pay Back Period/Return of Investment	[282,313–315]	4.4%
	Lifetime	[267,269,286,299,300,309,310,316–318]	11.1%
	Electricity/production rate	[258,262,280,289,308,319–321]	8.9%
	Installed capacity	[120,255,260,279,280,286,298,300,311,316–318,322,323]	15.6%
	Space requirement – Footprint	[243,252,262,264,265,267,277,280,286,290,298,311,313,317,324,325]	17.8%
	Energy use (fuel, renewables, electricity)	[131,268,273,283,285,288,294,301,320,326–329]	14.4%
	Material use (raw materials)	[131,273–275,330]	5.6%
	H_2O use	[249,263,278,279,282,301,302,320,323,330,331]	12.2%
	Resources availability	[256,266,276,286,302,311,317,318,327,332]	11.1%
	Diversity of energy supply mix	[120,249,250,266,268,283,287,290,301,333]	11.1%
	Operational flexibility	[120,263,266,268,277,287,298,310,311,318,325–327,334]	15.6%
	Technological maturity	[243,264,266,268,272,281,284,286,296,300,310,313,314,317,321,322,325,331,335–337]	22.2%
	Operational reliability	[131,255,300,308,318,321,322,325,338,256,258,266,268,271,277,284,297]	18.9%
	Compatibility of the technology	[258,266,276,286,317]	5.6%
	Security of supply	[131,276,281,284,286,289,296,298,311,317,327,333,334,339–343]	20.0%
	Cumulative energy demand	[271,289,311,326,333,344]	6.7%
Economic	Investment costs	[120,249–257,259,263,266,267,269,271,272,275–278,281,283,286–288,290,291,293–295,297,299,303,306–309,312,313,316–318,322–326,329,333,334,336,341,345–350]	64.0%
	Operation and maintenance (O&M) costs	[243,249–252,255,256,258,259,275,281,286,287,290,291,295,300,308,316–318,322–325,329,333,336,345,349,350]	34.8%
	Fuel/energy/raw materials costs	[252–254,258,266,267,269,275,288,293,294,303,306,307,318,323,326,334,340,349]	22.5%
	Levelized cost of product/energy	[124,243,249,250,279,283,290,298,302,304,308,312,315,318,321]	16.9%
	Value added	[274,278,330]	3.4%
	Net Present Value	[131,273,297,299,304,313,316,319,335,351,352]	12.4%
	Pay Back Period - Internal Rate of Return	[124,131,243,277,291,292,297,299,304,309,313,345,352]	14.6%
	Levelized value of product/energy- Incentive	[124,318,337]	3.4%
	Affordability	[264,266,277,296,301,341]	6.7%
	Competitiveness	[263,266,276,300,325,337]	6.7%
	Annual production costs	[120,249,250,261,278,280,282,283,302,311,312,327,348,353,354]	15.9%

Table 3.2. Environmental and societal indicators found on the existing MCDA sustainability assessments of energy systems and hybrid energy systems.

Aspect	Indicator	Reference	Occurrence in related aspect
Environmental	Global warming potential	[120,124,243,249,250,253,255,256,258,261,264,269,271,274,275,278,279,282,283,286,288,290,297,300,302,303,306–308,311,312,314,316–318,320–322,325,327,330,333–335,337,340,348–350,352–356]	51.9%
	GHG emissions	[131,266,276,277,284,285,296,302,315,320,341]	10.6%
	Direct CO_2 emissions	[252,263,266,267,272,288,293–295,304,313,323,329,331]	13.5%
	CO_2 emission avoided	[255,259,295,323,331,263,266,267,272,281,288,293,294]	12.5%
	NO_x emissions	[252,260,264,287,288,299,302,303,307,308,313,319,322,327,334,338,342,354]	17.3%
	SO_2 emissions	[254,264,288,303,308,334,354,355]	7.7%
	Acidification potential	[124,243,249,250,255,256,261,273–275,278,283,302,307,312,318,320,326,327,333,337,340,348,353,354,356]	25.0%
	Particulate matter emissions	[124,243,254,264,314,338,354]	6.7%
	Waste generation	[131,266,273,277,278,284,288,296,320,327,337,341,344,345]	13.5%
	Ozone layer depletion	[124,243,249,250,264,273–275,283,312,318,330,337]	12.5%
	Abiotic depletion potential	[243,249,250,264,271,278,297,312,318,329]	9.6%
	Biodiversity impact	[259,262,266,276,289,291,295,302,316,321,322,331,345,351]	13.5%
	Photochemical smog	[124,243,249,250,274,275,278,312,318,348,354]	10.6%
	Eutrophication potential	[124,243,264,273,275,278,283,312,337,339,348,354,357]	12.5%
	Aquatic/Terrestrial ecotoxicity potential	[243,250,254,264,273–275,302,330,337,339,354]	11.5%
	Land use	[243,252,253,256,258–260,272,273,279,282,287,288,295,296,298,306,309,311,313,314,323,326,327,338,340,346,348,349,354,357]	29.8%
	Air quality	[266,276,279,296,325]	4.8%
	Aggregated environmental indicator	[251,257,266,284,291,332,358]	6.7%
	Noise	[251,252,260,270,287,298,301,302,311,313,316,321,322,324,326,327,333,346]	17.3%
	Visual impact	[251,260,266,270,284,287,296,302,319,321,322,326,327,333,343]	14.4%
Societal	Job creation – Employment	[131,243,256,258–260,262,267,270,272,277–279,282–289,291,292,295,296,298,300,303,304,308,314,316,317,319,323,326,327,329,333,338,339,342,347,351,357,359]	61.3%
	Injury (workplace)	[250,278,283,284,293,294,339,344,357]	12.0%
	Fatalities (workplace)	[250,278,279,283,284,308,320,326,327,339,357]	14.7%
	Social acceptance	[250,256,259,266,277,281,284,286,295,298,300,301,308,309,317,321–323,329,336–338,340]	30.7%
	Chemical inherent safety	[273–275,330]	5.3%
	Process inherent safety	[273–275,330]	5.3%
	Occupational health	[124,243,250,252,273–275,278,287,297,298,312,313,326,327,329,330,334,337,339,343,348,354,357]	30.7%
	Labour	[256,271,291,309,311,327,344,347]	10.7%

From Table 3.1, it is observed that “energy efficiency” arises as the most common technical indicator. Few authors proposed exergy measures (“exergy efficiency” and “exergy destruction rate”) in addition to energy efficiency [243,255,261,264] or preferred the sole exergy metrics [268,278,311–313] to address

the technical dimension of sustainability. Energy efficiency based on the first-law of thermodynamics represents how well an energy conversion or transfer process is accomplished, i.e. the quantity of energy, while exergy efficiency based on the second law of thermodynamics provides a measure of approximation to reversible or ideal operation, i.e. the quality of energy [360].

With respect to the economic dimension in Table 3.1, the "investment costs" and "O&M costs" appear as the most used indicators. It is worth noting that some studies (e.g. [124,279,298,302,304,315,321]) preferred "levelized cost of energy/product" as alternative to these two indicators, while other works (e.g. [243,250,283,308,312,339,357,359]) selected all the three metrics for the economic assessment. Levelized costs are the total present costs of the system/technology (including both investment and O&M costs) divided by the electricity or chemical production over the economic lifecycle. Only one article among the mentioned ones [124] took into account a further indicator quantifying the levelized revenue/value of product in addition to the cost metrics. On the other hand, some authors proposed the "net present value" indicator accounting for the difference between cash inflows and cash outflows in a given period [361] instead of separated "investment costs", "O&M costs", "levelized cost of product/energy", "levelized value of product/energy" indicators [131,273,319,335,351,352], while others used different indicators for the assessment [297,304,313,316,362].

Focusing on the environmental aspect of sustainability in Table 3.2, "global warming potential" (i.e. how much energy can be absorbed when 1 ton of a specific gas is released into the atmosphere over a given period relative to the emission of 1 ton of CO_2) is the preferred indicator in the reviewed literature; it was used with other indicators commonly employed in Life Cycle Analysis (LCA) method for estimating the environmental impacts associated to the life cycle of a system/technology (e.g. "acidification potential", ozone layer depletion", etc.). After the definition of goal and scope, LCA requires inventory analysis by collecting materials and energy used in the system and related to the environment and impact assessment by applying midpoint and endpoint approaches [363]. As alternative to the life cycle "global warming potential" indicator, "greenhouse gas emissions" or "direct CO_2 emissions" were proposed by some authors.

Finally, the most adopted societal indicator in the reviewed literature (Table 3.2) is represented by "job creation-employment". It is worth mentioning that several authors considered the impact of harmful emissions into air on humans by means of "occupational health" indicators including human toxicity potential (as LCA indicator) and workplace impacts due to fugitive emissions, but only a few addressed chemical and process inherent safety issues by means of quantitative metrics.

Another finding from the review analysis is that none of the indicator-based methods were applied to hybrid energy systems installed or projected to be implemented at offshore oil & gas facilities.

3.2.3. Limits of the existing methods

From the analysis reported above, it can be found that several indicators addressing technical, economic, environmental and societal dimensions were proposed in the literature for the MCDA assessment of sustainability performance of energy systems and hybrid energy systems. However, some limitations exist in the most used metrics as summarized in the following.

The technical dimension is mainly addressed through the "energy efficiency" indicator by most of the reviewed methods. However, traditional energy analysis based on the first law of thermodynamics should be augmented by an exergy approach based on the second law of thermodynamics [364]. Thus, both energy and exergy metrics should be accounted for a clear understanding of the efficient use of resources within offshore hybrid energy production options.

In case of economic indicators, double counting problems arise if "investment costs" and "O&M costs" are used with "levelized cost of product/energy", thus violating the principle of independency described above. Similar issues emerge when "net present value" is included in the economic indicators since it depends on "investment costs", "O&M costs" or "levelized cost of product/energy". Furthermore, the concept of market prices and revenues which may influence highly the economic feasibility of the system/feasibility are not clearly investigated by the reviewed methods through specific indicators but considered indirectly in the "net present value" indicator. Despite "net present value" may be adopted as the sole metric for economic performance assessment in the sustainability model, it can be concluded that separated metrics addressing costs and revenues can be considered advantageous in order to pinpoint the expected performance of alternatives offshore hybrid energy options with respect to two different aspects separately.

LCA for environmental impact assessments is a systematic framework widely employed in the reviewed studies. However, it is worth mentioning that double-counting is a common issue in such a type of analysis, particularly when different products and processes are overlapped in the overall system [365]. Another double-counting issue when applying LCA may occur when both midpoint indicators focussing on single environmental problems (e.g. climate change or acidifications) and endpoint indicators (e.g. human health) are used in the assessment [366]. Furthermore, the independency principle may be not fulfilled adopting different environmental LCA indicators, e.g. "global warming potential" seems to depend partially upon "stratospheric ozone depletion potential" since ozone-depleting substances cause inevitably an increase in GHG emissions.

The reviewed methods do not explore largely chemical and process safety indicators within the societal dimension of sustainability. Nevertheless, safety is a paramount factor in the selection of suitable technologies for greener use of offshore oil & gas facilities. Specific indicators accounting for the potential

hazards and targets of offshore operations should be included for a thorough sustainability assessment of offshore hybrid energy systems.

A lack of applications to energy systems installed at the offshore oil & gas facilities represents another limitation of the reviewed sustainability metrics.

3.3. Inherent safety assessment methods

3.3.1. Generalities

Several new offshore projects have been developed in the Gulf of Mexico and in the North Sea, starting operations in challenging areas (increased technological and operational complexity, harsh environmental conditions, etc.) as well as implementing new design concepts [66–69]. This requires a higher attention to the potential for safety and environmental impacts. Lessons learnt from past accidents [70,71], such as the Piper Alpha explosion (North Sea, 1988), the Bombay High fire (Arabian Sea, 2005) and the Macondo blowout (Gulf of Mexico, 2010), tragically evidence the potential for major accident hazards of offshore oil & gas operations affecting human, assets, environment and reputation. Such potential threats inevitably increase in view of the progress of the offshore sector. In particular, the adoption of innovative solutions, e.g. hybrid power systems involving hazardous chemical energy carriers (H_2, SNG, CH_3OH), may add further criticalities to the profile of the offshore facility, thus requiring to improve safety records adequately and to be more aware of environmental issues.

The safety performance of an offshore oil & gas installation originates from decisions taken in the different stages of the project lifecycle (i.e. conceptual study, front-end engineering and design, detailed design, construction, commissioning, operation, decommissioning) [367,368]. Addressing the underlying hazards in the early phases of a project, where the degrees of freedom for system change are higher, was widely proven as a cost-effective strategy in the process and chemical industry [369–371] and suggested also for offshore installations [372–374]. Procedural, passive and active risk reduction strategies are often relied upon, but these have yet to achieve optimal risk reduction due to inadequacies in procedures or to the degradation of physical safety systems. A more robust way of achieving hazard management in offshore oil & gas activities, thus meeting high safety and environmental standards on an offshore facility, may be to take advantage of the inherent safety approach.

Professor Kletz [375–377] was the first to propose the inherent safety concept consisting in eliminating, where possible, or in drastically reducing hazards at source rather than controlling the risk during process design and operation. A well-known set of principles or guidewords was formalized to orient technology design toward inherent safety [378], as listed in the following.

- Intensification: it identifies the actions aimed at the minimization of the plant and equipment inventory, thus reducing the hazard level associated to the possible loss of containment.
- Moderation: it consists in the promotion of actions aimed to the reduction of the hazards due to operating conditions.
- Substitution: it classifies the actions aimed to the development of substances, process schemes and equipment characterized by a higher inherent safety.
- Simplification: it concerns the design actions aimed to reduce the complexity of the process and/or of the plant, thus reducing the possibility of errors and likelihood of loss of containment.
- Limitation of effects: it consists in actions aimed to the design of a process and/or of a plant where the consequences of the possible loss of containment are effectively reduced and possibility of escalation is minimized.

Benefits of implementing inherent safety philosophy throughout the whole plant lifecycle have been clearly highlighted by several studies [379–382]. Moreover, it has been proven that an inherently safer design has a positive effect on all three spheres of sustainability [383–386]. The implementation of inherent safety strategies in the conceptual and front-end engineering design of an offshore project can reduce design and management costs, simplify the requirement for engineered safety devices and related procedures [387].

However, the sole inherent safety principles do not yield a quantitative picture of the achieved safety performance of design alternatives [388]. Applying inherent safety strategies in the early design of offshore facilities, traditionally dominated by economic considerations, requires objective metrics, able to pinpoint the fundamental differences in the hazard profile among the alternative options and reduce time and efforts when fewer expensive modifications are needed later [389–391].

In the process and petrochemical industry, the use of metrics specifically developed for supporting design activities in the implementation of inherent safety strategies widely emerged in the last two decades as a result of an effort to overcome the difficulties in judging inherent safety only on the basis of conceptual principles [392,393]. However, a recent literature search by Tang et al. 2018 [394] reveals that no inherent safety indicators specific to the offshore sector have been proposed so far: offshore oil and gas installations present distinctive features in terms of layouts and interaction with the environment which are not accounted in the indicators developed for onshore applications. The analysis of the state of the art of indicators related to inherent safety assessment of alternative process and design options in early design activities is presented in the following.

3.3.2. Inherent safety indicators for early design activities

In order to rank the process routes in the early design phase, Edwards and Lawrence [395] developed a metric called Prototype Index for Inherent Safety (PIIS), which takes into account reaction conditions such as temperature and pressure, properties of materials such as explosiveness, flammability and toxicity, process inventory and reaction yield. One drawback of PIIS is to concentrate on reactions and do not consider other process aspects. Another approach proposed later by Cave & Edwards [396] was the Environmental Hazard Index (EHI) intended to be used in conjunction with PIIS since it allows to rank the chemical process route by the estimated environmental impact of a chemical release.

In 1999, Heikkilä [397] developed an index, called the Inherent Safety Index (ISI), which considers a wider range of factors, such as process safety structure, safety of equipment, side reactions, chemical reactions, etc. by means of chemical and process ISIs. These sub-indicators are based on Boolean mathematics, and each sub-range can be seen as a set with proper boundaries. This behaviour may produce two significant effects, i.e. excessive sensitivity in regions close to the limits of each sub-range and insufficient sensitivity within each sub-range.

In order to overcome these problems, Gentile et al. [398] improved some factors in the ISI indicator by using fuzzy set theory and thus developing the Fuzzy Logic-based inherent Safety Index (FLSI), which considers chemical properties and plant layout as main factors and uses hierarchical fuzzy if-then rules to combine qualitative information (expert judgment) and quantitative data (numerical modelling).

Furthermore, within the European INSIDE project, a paper-based toolkit called INSET [399] was developed to provide an aid process engineers to choose and optimize inherently safer and environmentally friendly plants. However, similarly to ISI and FLSI, this tool relies on the evaluation of inherent safety scores and requires much time and efforts.

A more systematic and automated expert system for the design of inherently safer processes in route selection and flowsheet development stages was proposed by Palaniappan et al. [400,401], presenting a new Inherent Safety Index (the i-Safe index) for ranking process routes and a graphical method for analysing reaction networks. Compared to the pioneering PIIS [402], i-Safe includes direct reaction hazard evaluation through heat of reaction and reactivity rating but it does not have direct inventory or process equipment related metrics.

A different approach for assessing environment, health and safety (EHS) aspects in early phases of design was considered by Koller et al. [403] in their EHS method, which incorporates all available information with the help of different priority levels and is applicable when some substance data are missing. The EHS method do not yet propose an aggregation algorithm addressing different effects.

The Dow Fire & Explosion Index (F&EI) [404], the Dow Chemical Exposure Index (CEI) [405], and the Mond Fire, Explosion and Toxicity Index (FETI) [406] were developed as possible tools for quantitative inherent safety assessment, even though they require information which is not always available in the early design stages of the project.

The Hazard Identification and Ranking (HIRA) method was developed by Khan and Abbasi [407] to overcome some drawbacks of Dow's methods. It allows to rank the chemical processes units mainly in terms of the hazardous substances and operating conditions associated with them based in two metrics, i.e. the Fire and Explosion Index and the Toxicity Index. An attempt to incorporate into the HIRA the contribution of safety measures needed to minimize the unit hazards was made later by Khan et al. [408] through an indicator called Safety Weighted Hazard Index (SWeHI). Successively, Khan and Amyotte [409,410] proposed an Integrated Inherent Safety Index (I2SI) which integrates the hazard potential and safety costs and is intended to be applicable throughout the life cycle of process design. In order to produce a method driving inherently safer choices in the early phases of the layout design, some modifications were introduced to the original version of I2SI [411,412]. In particular, reference indicators were added to the indexing system in order to reduce the expertise used in the definition of inherent safety principles applicability. Among which, the Domino Hazard Index (DHI) allows to assess the actual consequences of potential domino accident escalation and rank the domino hazards of all units considering also the effect of active and passive protection measures.

Following the approach of the Integrated Risk Estimation Tool (iRET) for explosion consequences studies [413], Leong and Shariff proposed the Inherent Safety Index Module (ISIM) [414] to overcome issues of previous indicators (in particular ISI by Heikkilä [415]) related to the need for manual data transfer of process information and parameters for inherent safety level calculation. ISIM developed in Microsoft Excel spreadsheet was integrated with Aspen HYSYS for simplicity of data transfer. However, ISIM suffers from the shortcomings highlighted above for ISI. Moreover, ISIM quantifies the inherent safety level with respect to specific aspects (temperature, pressure, explosiveness) without propose an overall indicator. An enhancement of ISIM with respect to the level of explosiveness was represented by the Process Route Index (PRI) [416]. It allows to quantify the inherent safety level of the overall process route considering single contributions of components in the mixture. PRI was developed based on process parameters which influence the outcome of explosion incident (mass, energy, combustibility) taking into account the average values. Moreover, in order to further improve the selected route, the process streams can be ranked to identify and prioritize streams requiring modifications by means of the Process Stream Index (PSI) [417]. Instead of considering the average values of the properties of the process route as for PRI, the ratio of the specific parameter for the selected stream to the average of that parameter for the

whole simulation was used. Similar to PRI, expert judgement cannot be used since the scaling scoring approach was eliminated from the analysis.

In 2011, the Enhanced Inherent Safety Index (EISI) [418] was proposed to overcome some limitations of ISI [415], i.e. consideration of the sole maximum value of parameters, unconcern about the material quantity, number of equipment in the plant and complexity of the process. By this way, similar processes which would normally obtain the same score in Heikkilä method [415] can be compared even though additional input data concerning material balances are necessary. An improvement of this approach was proposed by Gangadharan and co-workers through the Comprehensive Inherent Safety Index (CISI) [419], which accounts also for the reactivity hazard due to particular mixture in the calculation of equipment index and the complexity due to connections between single units for the calculation of the total inherent safety index. However, differently from EISI, CISI relies on expert judgement for the scoring and weighting of indicators for the overall metrics, as proposed in the ISI method.

An alternative approach proposed by Srinivasan & Nhan [420] concerns the calculation of an Inherent Benign-ness Indicator (IBI) based on safety, health and environment factors. Avoiding any expert judgement, parameters are first scaled through an objective scaling mechanism and then assessed by means of a multivariate statistical approach based on principal component analysis. The scores and loadings on the first two principal components lead to the IBI. IBI allows to identify the similarities and differences between alternative chemical routes and points out the most hazardous property in a process route. However, as the methods mentioned above, the IBI approach does not provide an assessment based on accident scenarios and their consequences.

To reduce the disadvantage of subjectivity in indicators values and weighting, Jiao & Xiang [421] proposed a metrics integrating fuzzy inference and Analytic Hierarchy Process (AHP), called Inherent Preference Index (IPI). The method comprises safety and health aspects proposing seven sub-indicators.

Another alternative to the discrete subjective scoring index-based method was given by Ahmad et al. [422] who proposed an inherent safety assessment method for the petrochemical industry called Numerical Descriptive Inherent Safety Technique (NuDIST). NuDIST incorporates logistic functions in the score assignments to chemical and process safety parameters and then adds together all the scores to obtain the final NuDIST score for each route. The NuDIST technique was extended through the addition of root-cause analysis to identify the largest hazards in a process by means of a technique called Graphical Descriptive Technique for Inherent Safety Assessment (GRAND) [423]. Later, a new method called Inherent Safety Assessment for Preliminary Engineering Design Stage (ISAPEDS) was proposed by the same co-authors [424] involving five main safety parameters which are operating temperature, operating pressure, flammability, explosiveness and toxicity, assessed in relations to each other.

Inherent Safety Key Performance Indicators (IS-KPIs) was proposed as a consequence-based approach addressing separately humans and process equipment targets due to domino accident escalations [425,426]. The KPIs are based on damage distances estimated through consequence simulation tools and equipment safety scores to account for the credibility of equipment releases. Domino hazard indicators, i.e. Unit Domino Hazard Index (UDI) and Target Domino Hazard Index (TDI), were proposed by Cozzani et al. [16] for a simplified and straightforward layout screening with respect to escalation hazard. The set was based on the assessment of inherent safety distances calculated using specific escalation thresholds. Simple rules of thumb were presented, without the need for running models for consequences analysis.

Rusli et al. [427] proposed a risk-based method aiming at the calculation of the Inherent Risk of Design Index (IRDI) to rank the process options considering the severity and potential of hazard transfer to other parts of the process after the introduction of inherently safer modifications. IRDI was derived from the combination of DI indicator proposed in the I2SI method [410] and the Likelihood Index of Hazard Conflicts (LIHCs) after the evaluation of inherent safety design options.

Another risk-based approach was developed by Rathnayaka et al. [428] called Risk-based Inherent Safety Index (RISI) to orient decisions on the optimum design with maximum inherent safety addressing hazard likelihood reduction. RISI can be calculated by first estimating the Risk for Base Design, RiskBD, and then the Inherent Safety Risk for alternative design, ISRisk, which is the quantitative representation of the residual risk of the alternative design after implementing inherent safety strategies into the system. No aggregation of effects was defined in this method since the damage radius of each accident scenario is multiplied for the probability of occurrence of the considered scenario.

Table 3.3 summarizes the comparison of indicator-based methods for inherent safety implementation in early design stages. It can be observed that most of the methods require in input information about chemicals, reactions, operating conditions, inventory, process flow diagrams. On the other hand, site characteristics, meteo-marine conditions and preliminary layout are needed for calculation of few indicators (e.g. Dow's methods, HIRA-FEDI, HIRA-TDI, SWeHI, IS-KPIs, RISI, DHI, I2SI). It is emerged that a number of studies rely on elements of expert judgment to define the safety scores (e.g. PIIS, EHI, ISI, ISIM) or have embed scoring tables that were defined with reference to processes in onshore chemical plants (e.g. INSET, i-Safe, Dow F&EI). More sophisticated indicators rely on consequence simulation models for the objective quantification of the hazard level from expected scenarios. However, the requirements for application in early phases of the project lead to customization of such models for situations typical of the onshore plants. For example, some methods (e.g. Dow CEI, HIRA-FEDI, HIRA-TDI, SWeHI, I2SI, DHI, RISI) embed consequence models in their calculation formula, but provide fixed equations with adjustable parameters. Other metrics (e.g. IS-KPIs) allow for user-defined consequence modelling, thus being customizable to different contexts than the onshore one.

While all the proposed indicators consider hazards for human targets in the assessment, only a few include the evaluation of potential damage to the environmental aquatic targets (EHI, INSET, EHS, IBI, I2SI). The potential damage to assets is considered only by a few dedicated indicators (IS-KPIs, DHI, UDI/TDI), even though referring to process equipment in the onshore context. Finally, aggregation of results can be performed through specific functions (e.g. IS-KPIs, SWeHI, DHI, I2SI, UDI/TDI) or can be implicit derived from the combination of different effects with penalties (e.g. Dow F&EI, Mond FETI, HIRA-FEDI).

Table 3.3. Comparison of the existing inherent safety indicator-based methods.

	PIIS[395], EHI [396]	ISI [397], FLSI [429], EISI [418], CISI [419], IPI [421]	INSET (I,J tools) [399]	i-Safe [400,401]	EHS [403]	ISIM [414], PRI [416], PSI [417]	IBI [420]	NuDIST [422], GRAND [423], ISAPEDS [424]	Dow F&EI [404], Dow CEI [405] Mond FETI [430]	HIRA-FEDI and TDI [407], SWeHI [408], I2SI [409,410]	IS-KPIs [425,426]	IRDI [427]	RISI [428]	DHI + I2SI [411,412]	UDI/TDI [431]
Input data															
Chemicals	X	X	X	X	X	X	X	X	X	X	X	X	X	X	X
Reactions	X	X	X	X	X	X	X	X	X	X	X	X	X	X	
Operating conditions	X	X	X	X	X	X	X	X	X	X	X	X	X	X	X
Equipment inventory	X	X	X		X	X		X	X	X	X	X	X	X	X
Flowrates		X							X	X	X	X	X	X	
PFD	X	X	X	X	X	X	X	X	X	X	X	X	X	X	X
Preliminary layout									X	X			X	X	X
Site and weather data									X	X	X		X	X	
Accident consequence evaluation															
None / Expert judgement	X	X				X			X	X		X	X		
Fixed formula (non customizable)									X	X			X	X	
Customizable models											X				
Considered targets															
Humans	X	X	X	X	X	X	X	X	X	X	X	X	X	X	
Process equipment											X			X	X
Structural elements															
Aquatic environment	X		X		X		X			X				X	
Aggregation of the results		X		X					X	X	X	X		X	X

Indicators with similar features (e.g. progressive versions based on the same indexing system) are grouped together.

3.3.3. Limits of the existing methods

From the analysis reported above, it can be found that several indicator-based approaches were proposed in the literature for the assessment of inherent safety performance of alternative chemical process alternatives in early design stages related to the onshore context. However, some limitations exist in such metrics as summarized in the following.

The methods which rely on consequence simulations models with a fixed formula (e.g. Dow CEI, HIRA-FEDI, HIRA-TDI, SWeHI, I2SI, DHI, RISI) do not take into consideration features relevant for offshore applications, such as high congestion, possibility of structural damage, and weather conditions typical of the marine environment. The IS-KPIs method allowing a customizable consequence modelling is potentially tailorable to the case of offshore installations. However, no specific guidance is provided on the application to this context. Hence, specific expertise is required for the application and results are potentially inconsistent among different assessments. Furthermore, no method from the literature review focuses explicitly on damage on the marine environment and structural elements of the assets, both critical aspects for the offshore oil & gas industry. Overall, it can be concluded that offshore oil & gas installations present distinctive features in terms of layouts and interaction with the environment which are not accounted in the indicators developed for onshore applications.

As a result of the limitations described above, examples of application of inherent safety indicators to the design of offshore oil & gas facilities are currently limited: the study by Xin et al. [432] applies I2SI and DHI to the layout optimization of topside deck of a FLNG facility, while Crivellari et al. [433,434] applied a customized version of IS-KPIs method to the process selection. In both cases, the study presented is specific to the case assessed and lacks of a detailed methodology description to support the generalized application to widespread multi-target analysis of offshore projects.

3.4. Assessment of environmental damage caused by the spill of oil or chemicals in sea water

3.4.1. Generalities

The offshore oil & gas industry recognizes an extreme importance to the management of the risk related to the spill of oil or hydrosoluble chemicals into the sea deriving from its activities. Directive 2013/30/EU on the safety of offshore oil & gas operations [72] introduced strict criteria related to the environmental performance of offshore facilities, also requiring operators to demonstrate the ability of covering liabilities from major accidents. However, it is worth noting that the Directive does not propose or require the application of any specific methodological tool to assess the environmental consequences associated with

potential oil and chemical spills causing severe marine pollution with serious impacts to wildlife and their habitats.

Oil releases are a form of marine pollution which can result in both immediate and long-term environmental damage to different environmental compartments, i.e. sea surface, water column, sea bottom, shoreline, as proved by some relevant past oil accidents reviewed in the following.

The 2010 BP Deepwater Horizon accident in the Gulf of Mexico caused the largest offshore spill in the USA history, with extensive contamination of surface water, water column, deep-sea corals and benthos, nearshore and coastal ecosystems [435]. Despite massive clean-up efforts following major oil spills, historical evidence showed that long-term effects of embryonic exposure to hydrocarbons may be expected for several years in fish along the water column, in addition to the immediate mortality of seabirds and benthic invertebrates on oiled shores [436–438].

In 1989, the oil tanker Exxon Valdez slammed into Bligh Reef and spilled more than 42 million L of crude oil into the cold, clear waters of Alaska's Prince William Sound [439]. The spill caused acute mortality of seabirds, sea otters and harbour seals as well as macroalgae and benthic invertebrates on oiled shores. Long-term effects of embryonic exposure in fish along the water column were also reported [440].

In 1969, the barge Florida went aground near West Falmouth and spilled between 650 000 and 700 000 L of No. 2 fuel oil into Buzzards Bay [441]. Animals were highly impacted by the spilled oil, and massive mortality of marine life including fish, worms, crustaceans, and molluscs occurred in a few days. Oil-covered marsh grasses died within a few weeks after the spill [442]. It was found that petroleum-derived hydrocarbons persist in sediments and that detectable sub-lethal biological impacts in fiddler crabs, salt marsh grasses and ribbed mussels are still evident 40 years after the original spill [443–445].

Other past accidents from oil tankers, e.g. Sea Empress (1996), Erika (1999), Prestige (2002), MSC Napoli (2007), revealed that birds approaching the sea surface, fish and benthos along the water column, and shellfishes living in shallow seafloor close to the shoreline were the most damaged environmental targets [446].

On the other hand, completely hydrosoluble chemicals used in offshore oil & gas operations, such as glycol and CH_3OH for gas dehydration, are classified as hazardous and noxious substances, i.e. any substance other than oil likely to induce harm to living resources and human health or that has harmful impact on marine environment if released into the sea, which dissolve rapidly and completely after their spill [447]. As a consequence, spills from such substances have the potential to cause only acute damage compared to oil spills which can produce both short- and long-term effects. Overall, water column can be

considered as the most impacted environmental compartment by chemical accidental spills, as demonstrated by some relevant past accidents described in the following.

In 2000, the Ievoli Sun, a chemical tanker in route from Fawley to Barcelona with 6000 t of chemicals sank to a depth of 70 m in the English Channel leading to spill into the sea of 3998 t styrene, 1027 t of methylethylketone, 996 t isopropyl alcohol. It is reported that styrene spill led to a slight contamination of recovered shellfish [448].

Overloading of the tanker Crystal Rubino at Port of Harmina in 2000 resulted in a spill of 2 t of nonylphenol ethoxylate. Mortal consequences on fishes and reproduction problems on seagulls which ate the dead fishes were noticed from this maritime accident [449].

It must be remarked that according to ISO 31000:2018 [450], risk can be defined as the combination of the likelihood of occurrence of an event and the entity of consequences (i.e. severity) associated to that event. Severity of environmental accidents can be considered as combination of hazard and vulnerability if wildlife in the area factors. The hazard of environmental damages caused by oil and hydrosoluble chemicals depends on multi-faceted aspects related not only to the quantity spilled, but also to the ambient conditions during and after the accident [451,452]. The identification of the hazard associated to the offshore oil and chemicals spills is thus fundamental in order to reduce or mitigate their impact on the different environmental compartments of the sea.

The use of indicators represents a widespread approach in offshore risk management to capture and effectively communicate complex issues, as the hazards due to accidental events [394]. During the last decade several quantitative oil spill risk/hazard models were proposed in literature taking advantage of recent progress in comprehensive oil spill fate and trajectory models. Moreover, some metrics were developed to evaluate the risk/hazard associated to chemical spills. The analysis of the state of the art of indicators related to oil spills and hydrosoluble chemical spills is presented in the following.

3.4.2. Indicators for environmental damage caused by oil spills

Kleissen et al. [453] proposed an environmental risk assessment tool for oil spills due to shipping accidents based on risk maps derived from the combination of oil presence vulnerability, average spill size per year reported for given spill class and ecological vulnerability in each grid cell.

Astiaso Garcia et al. [454] developed the Oil Spills Hazard Index associated to the discharge of crude oil from tankers in a given port of the Italian coasts within a 50 km distance between the release and the shoreline.

A marine oil spill risk mapping tool was defined by Dongdong et al. [455] using a hierarchical system based on technical characteristics, environmental conditions, emergency plan and vulnerability of risk receptor of the coastal area. This model does not take into account meteo-marine information and oil fate modelling for the calculation of the indicators, as the methods above described.

In 2012, Olita et al. [456] combined hazard maps of oil mass stranded on the shoreline per unit of surface and vulnerability maps of coastal environment into severity maps based on a 3D finite element model simulating hydrodynamics and waves of the Strait of Bonifacio and oil weathering process.

A severity mapping method to assess the risk posed by operational oil discharges from ships using the deterministic-stochastic MEDSLIK-II model was provided by Liubartseva et al. [457] for Southern Adriatic and Northern Ionian seas. They proposed the estimation of hazard based on distribution of hourly oil concentration at given threshold values of mass oil per unit of surface (i.e. thickness) for oil slick and mass oil per unit of coastline length for beached oil. The same model was used by Al-Shami et al. [458] to produce an oil spill risk map by combining the Environmental Sensitivity Index for shoreline with the Weighted Assessment of Shoreline Hazard index (WASH) based on oiling probability of being hit at each beach segment, average concentration of oil stranding on the shore, average time needed for oil to beach on a coastline. Similarly, Marignani et al. [459] proposed the Oil Spill Risk Index for based on Shoreline Exposure Index adapted from WASH, Biodiversity Vulnerability Index and Environmental Sensitivity Index for the coastal site. The concept of oil stranded mass per unit of coastal length combined with vulnerability of the shoreline was adopted also in the deterministic risk model by Sepp Neves et al. [460].

Melaku Canu et al. [461] developed a 3D finite element hydrodynamic model (SHYFEM) method to evaluate the risk for a given coastal segment by oil spills generated in open sea from offshore facilities and reached the coastal site within a given period of 10 days.

A statistical oil spill risk model for port areas based on probability of slick occurrence, volume of oil in the thick slick over the entire slick lifetime (i.e. volume exposure) and vulnerability of the area was presented by Guo [462]. A 0.1 mm thickness was reported as threshold for eco-toxicity of the slick.

Finally, a quantitative oil risk management system using 2D/3D oil spill VOILS (Vela-OIL-Selfe) model for estuarine-to-oceanic spaces was described in Azevedo et al. [463] as combination of vulnerability and severity maps in coastal areas.

Table 3.4 summarizes the comparison of the indicator-based methods for environmental damage from oil spills. It can be observed that some methodologies are risk evaluations, while other models provide severity indicators as combination of hazard and vulnerability factors. Moreover, it should be noted that most of the approaches assess accidental releases from ships in coastal sites with shoreline as main

environmental target. The severity indicator by Melaku Canu et al. [461] is based on oil spills from offshore oil & gas facilities, but this model still focuses on shoreline marine organisms as the unique target damaged by oil. A specific oil hazard indicator is provided in the method by Astiaso Garcia et al. [454], but its use is limited to hydrocarbon maritime traffic along the coastlines, as all the methods mentioned above. The sea surface compartment is considered exclusively in Guo et al. [462], but this method shows the same characteristics of most of other models related to spills from ships in port areas.

Table 3.4. Comparison of the existing indicator-based methods for environmental protection from oil spills.

Reference of the model	Evaluation type	Release type	Location	Sector	Environmental compartment target
Kleissen et al. [453]	Risk	Accidental	Open sea	Shipping	Sea surface, shoreline
Astiaso Garcia et al. [454]	Severity (Hazard)	Accidental	Coast	Shipping	Sea surface
Dongdong et al. [455]	Severity	Accidental	Coast	Shipping	Shoreline
Olita et al. [456]	Severity	Accidental	Coast	Shipping	Shoreline
Liubartseva et al. [457]	Severity	Operational	Coast	Shipping	Sea surface, shoreline
Al-Shami et al. [458]	Risk	Accidental	Coast	Shipping	Shoreline
Marignani et al. [459]	Risk	Accidental	Coast	Coastal tourism, industry	Shoreline
Sepp Neves et al. [460]	Severity	Accidental	Coast	Coastal oil storage	Shoreline
Melaku Canu et al. [461]	Severity	Accidental	Coast	Offshore oil & gas operations, Shipping	Shoreline
Guo [462]	Risk	Accidental	Coast	Shipping	Sea surface
Azevedo et al. [463]	Risk	Accidental	Coast	Shipping	Shoreline

3.4.3. Indicators for environmental damage from chemical spills

Edwards and co-workers [396,464] proposed EHI metrics as combination of released inventory of a given chemical and summation of Specific Water Hazard Index (SWHI) and Specific Terrestrial Hazard Index, related to loss of containment from onshore plants. SWHI was defined as the ratio of the predicted environmental concentration (PEC) of chemical into aquatic environment to LC_{5O} limit (i.e. concentration of chemical in water which kills 50% of a test population over a given period).

Similarly, the Environmental Harm Index was defined by the English Department of Environment, Transport and the Regions (DETR) [465,466] to estimate the hazard associated to the aquatic environment (river, estuaries, lakes) from accidental chemical releases. In addition to the ratio of PEC to LC_{50}, the ratio associated to length at which the release exceeds the threshold concentration in water and the ratio associated to recovery time were considered.

In 1998, Wilday et al. [467] proposed the Environmental Severity Index by revising the metrics by DETR including the short-term and long-term DoE criteria for definition of reference values in the ratios of

parameters. This model does not take into account meteo-marine information and spatial variation of PEC for the calculation of the indicators, as the methods above described.

Successively, the Environmental Impact Factor (EIF) by SINTEF [468,469] was developed based on the Dose related Risk and Effect Assessment Model (DREAM) for risk of operational produced water and drilling cuttings discharges. For release of single chemical compound, EIF can be defined as the number of cells of the water column (with volume of 100000 m^3) where the ratio of PEC to Predicted No Effect Concentration (PNEC) (i.e. the concentration of a chemical at which below no adverse effects of exposure in an ecosystem are measured) is equal or greater to 1 which corresponds to a risk equal or greater than 5%. Whereas, for release of mixture, EIF is the number of cells of the water column (with volume of 100000 m^3) where the sum of the risk calculated for each compound in the mixture is equal or greater to 5%. According to the DREAM model, PEC is 3D and time variable.

The ratio of PEC to PNEC was proposed as measure of hazard also in the PROTEUS multi-models system by the UK Natural Environment Research Council (NERC) and Engineering and Physical Sciences Research Council (EPSRC) [470,471] and in the MIKE hydrodynamic tool by the Danish Hydraulic Institute (DHI) [472]. 3D and temporal variable simulations are carried out to support environmental risk assessments of discharges of produced water and drilling wastes from offshore exploration and production activities.

Finally, the Chemical Hazard Unit (CHU) method was suggested by IMARES [473] to mathematically simplify the EIF, PROTEUS and MIKE models for hazard estimation from produced water discharges. CHU can be defined as combination of chemical discharged load and the hazard quotient related to the ratio of PEC at a given distance of 500 m from the reference platform to PNEC.

Table 3.5 summarizes the comparison of the indicator-based methods for environmental protection from chemical spills reviewed above. It clearly appears that some methodologies are risk evaluations, while other models provide directly hazard measurements. However, all the methods are consistent in estimating the damage due to chemical spills as ratio of the actual concentration derived from the release and a given threshold value. Moreover, they consider the water column as main environmental target. The approaches by SINTEF [468,469], NERC and EPSRC [470,471], DHI [472] and IMARES [473] are based on spills in open sea from offshore oil & gas facilities, but these models are intended for operational discharges of produced water and drilling cuttings. The other methods assess accidental releases into aquatic environment, but they are limited to the shipping and chemical industry sectors and to onshore locations.

Table 3.5. Comparison of the existing indicator-based methods for environmental protection from hydrosoluble chemical spills.

Reference of the model	Evaluation type	Release type	Location	Sector	Environmental compartment target
Edwards and co-workers [396,464]	Severity (Hazard)	Accidental	Onshore plant	Chemical industry	Water column
DETR [465,466]	Severity (Hazard)	Accidental	Rivers/estuaries/lakes	Shipping	Water column
Wilday et al. [467]	Severity (Hazard)	Accidental	Rivers/estuaries/lakes	Shipping	Water column
SINTEF [468,469]	Risk	Operational	Open sea	Offshore oil & gas operations	Water column, Seafloor
NERC and EPSRC [470,471]	Risk	Operational	Open sea	Offshore oil & gas operations	Water column
DHI [472]	Risk	Operational	Open sea	Offshore oil & gas operations	Water column
IMARES [473]	Risk	Operational	Open sea	Offshore oil & gas operations	Water column

3.4.4. Limits of the existing methods

From the analysis reported above, it can be concluded that several indicator-based approaches were proposed in the literature for the environmental damage due to oil spills, while only few metrics were proposed with respect to hydrosoluble chemical spills. Some limitations exist for both type of indicators, as summarized in the following.

Most of the indicators related to oil accidental releases consider mainly the shipping sector, thus neglecting the offshore oil & gas activities. Moreover, they focus mainly on the shoreline, thus ignoring the other environmental marine compartments which may be polluted in case of oil spills, as emerged from the analysis of oil past accidents. Finally, they are mostly intended for risk evaluation without specifying proper hazard metrics.

Concerning the indicators available for chemical spills releases, all of them consider the water column as environmental target thus confirming the findings from the analysis of past accidents. A few are related to offshore oil & gas operations, even though providing risk evaluations of operational discharges of produced water.

Chapter 4.

Assessment methodologies for P2G, P2L and G2P offshore hybrid energy options

4.1. Introduction

This chapter presents the methodologies developed within the present research project for the assessment of the offshore hybrid energy options described in Chapter 2. Four methods were developed, showing a similar schematic procedure (displayed at the end of Chapter 3) but presenting specific features associated to the analyzed hybrid energy options and/or the performance aspects.

The novel aspect of such methodologies is presented on a general basis in Section 4.2, and are discussed in the light of the state of the art presented in Chapter 3.

The different characteristics of P2G/P2L systems and G2P systems highlighted in the SWOT analysis in Chapter 2 ask for the development of separate methodologies able to capture peculiarities of the hybrid energy options even though presenting the same model framework and similar set of sustainability indicators. Therefore, two assessment methodologies for the comparison of the sustainability performance are defined for P2G and P2L options in Section 4.3 and for G2P options in Section 4.4, respectively.

The complexity of the threats of concern in the offshore context requires the development of an array of inherent safety indicators to completely address the different targets of the potential hazards (people, environment, assets, etc.). A multi-target methodology assessing the inherent safety profile of alternative offshore design options at early design stages is thus described in Section 4.5.

In order to provide an integrated analysis of sustainability and safety performance, a systematic multi-criteria methodology is presented in Section 4.6 based on the idea of process intensification for the conceptual design of emerging chemical production processes.

Finally, Section 4.7 describes some sensitivity analysis techniques to be used in the proposed methodologies.

4.2. Novelty of the methodologies developed in the present study

To deal with the shortcomings of the existing assessment methods highlighted in Chapter 3, in the present research project an effort was made to propose novel systematic indicator-based methodologies, which are based on a common MCDA scheme but are tailored to capture specific sustainability and safety issues of offshore P2G/P2L and G2P hybrid energy projects. These quantitative methodologies represent detailed decision-making support tools in problems regarding the choice of the optimal offshore system in decommissioning projects and the valorization of depleted reservoirs.

Figure 4.1 displays the general assessment procedure based on the systematic MCDA approach which is adopted in the development of the methodologies proposed in the present study. As shown in the figure,

different alternatives are first formulated, defining a common reference basis and boundaries for the analysis and collection of the required input data. After that, proper indicators are defined to evaluate the performance of the alternatives. Optionally, indicators scales are transformed into commensurable units in the normalized step, then weights are assigned to the indicators to reflect their importance in the weights elicitation step. Next, a mathematical algorithm (MCDA method) is applied for the aggregation of the indicators. Finally, alternatives are ranked based on the single and aggregated indicators. Sensitivity analysis may be performed to test the robustness of the results.

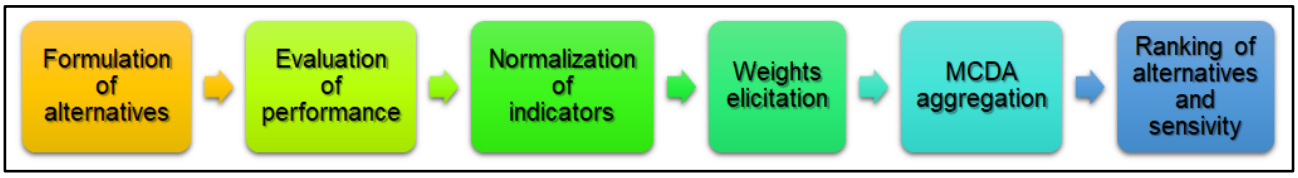

Figure 4.1. Scheme of the general model used for the assessment of offshore hybrid energy options.

A novel aspect of the present study consists in the introduction of specific peculiarities in the general procedure presented above, which are related to the type of offshore hybrid energy options under analysis (P2G/P2L and G2P systems) and the type of performance evaluation (sustainability and/or inherent safety analyses).

Other novelties of in the developed methodologies regard the definition of multi-criteria performance indicators addressing sustainability and safety aspects of the alternative offshore systems in order to fill the gaps in the existing literature.

A concise yet representative set of technical, economic, environmental and societal indicators was developed and is proposed to evaluate the sustainability performance of the offshore hybrid energy options, thus avoiding double-counting problems and quantifying separately important aspects for innovative systems design (e.g. energy and exergy, costs and revenues).

Moreover, a new array of inherent safety indicators is defined addressing all the potential targets of the hazards in offshore oil & gas production facilities (e.g. humans, structural elements of the assets, marine environment) and accounting for the characteristic layout of the offshore installations. For instance, in the perspective of defining indicators addressing the environmental target, new metrics are specifically developed to quantify the hazard level associated to accidental oil and hydrosoluble chemical spills in the open sea from offshore oil & gas operations.

Finally, a comprehensive integration of such inherent safety indicators into the proposed set of sustainability indicators is provided in order to cover the safety issues of the societal dimension.

4.3. Sustainability assessment methodology for P2G and P2L options

In this section, the sustainability assessment methodology proposed for P2G and P2L offshore hybrid energy options is described. An overview of the method including the details of the steps and proposed performance indicators is presented in the following paragraphs.

4.3.1. Overview of the method

As per literature review reported in Chapter 3 (Section 3.2), a sustainability assessment model is proposed to provide a systematic comparison of alternative P2G and P2L options for offshore renewable energy conversion at given offshore oil & gas sites. A limited yet exhaustive number of indicators addressing technical, economic, environmental and societal dimensions of sustainability is defined to capture specific features of the strategies including production at the offshore oil & gas installations, transportation to the land and end-use at the onshore market. Moreover, a profitability metrics is proposed to compare the effective viability of the green offshore projects, providing a further important measure of the performance of the strategies, besides the four aspects mentioned above.

The methodology is intended to be a decision-making tool to assess the feasibility of P2G and P2L projects at offshore oil & gas production facilities located at remote areas from the onshore electrical grid, which may be at the end of their useful life thus projects on renewable power exploitation have been initiated or are under investigation for the energetic valorisation of the site. The approach has a general applicability to every type of renewable energy source, even though resources for which technology development has succeeded in providing renewable generators able to operate at higher distances from shore and in deeper waters (e.g. offshore wind power) are currently the most reasonable for the analysis. Moreover, different P2G and P2L strategies may be compared, even though pathways producing H_2, SNG, CH_3OH for multiple applications in the onshore market are specifically considered in the description of the model.

The flow chart of the methodology is illustrated in Figure 4.2. As shown in this figure, a preliminary step (step 0) is necessary divided into two stages. The first stage (step 0.1) concerns the definition of the offshore oil & gas site providing input data about the field and infrastructures. Table 4.1 summarizes this information. In the second stage (step 0.2), the offshore renewable energy to be exploited is preliminarily evaluated by taking into account existing projects and/or feasibility studies on resource potential assessment in the selected area. After that, the procedure is divided into five main steps, which are described in detail in the following paragraphs.

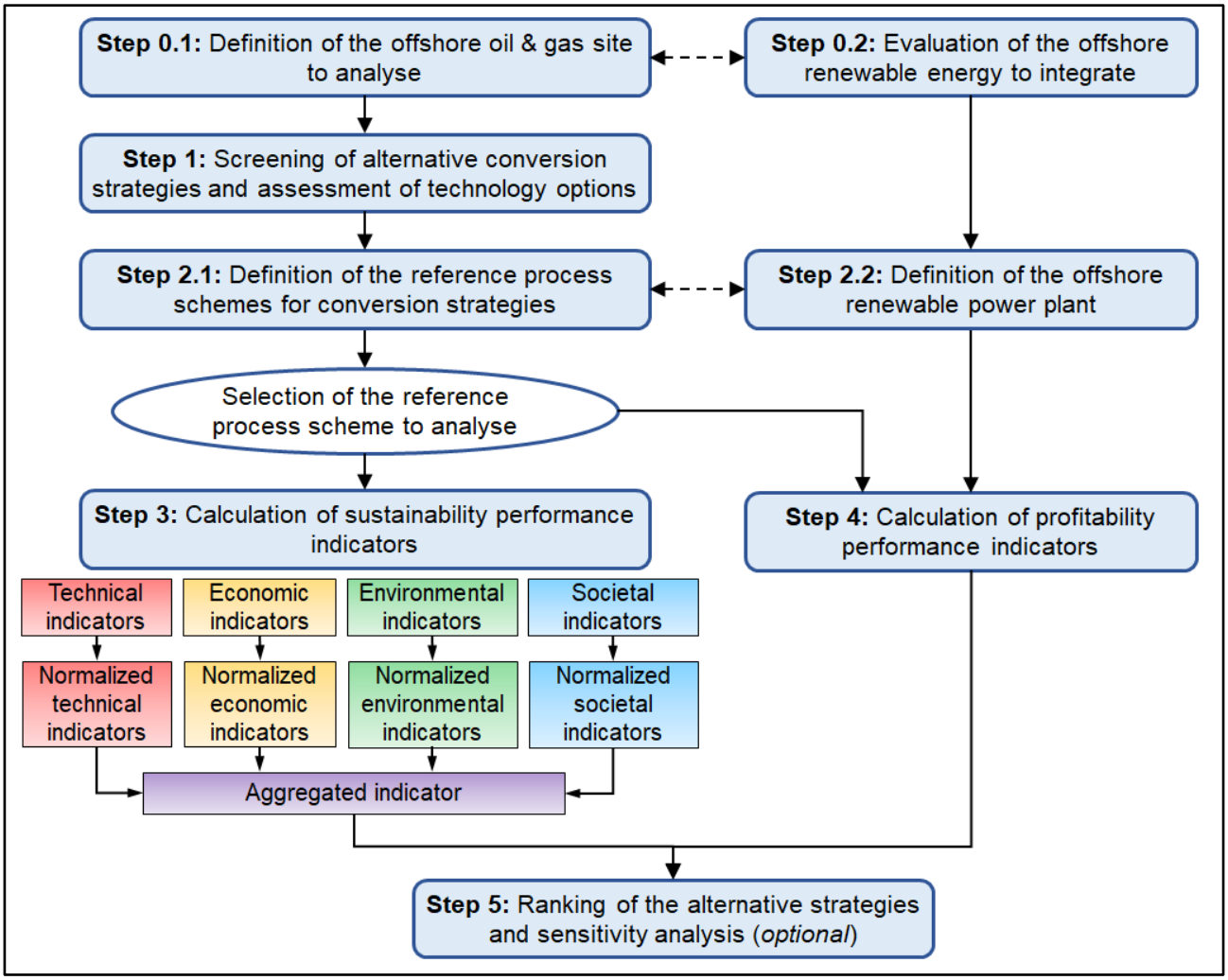

Figure 4.2. Flow chart of the sustainability assessment model for P2G and P2L offshore hybrid energy options.

Table 4.1. Details of the offshore site required in input to the sustainability assessment methodology.

Data about the field	
a)	Entity of gas reservoirs (type, production, CO_2 presence and concentration)
b)	Water depth
c)	Distance from site to the closest onshore grid, to onshore shipyard, to port
Data about the infrastructures	
d)	Characteristics of the offshore structures (type, remaining lifetime)
e)	Preliminary dimensions and estimated free space of the offshore structure, if available
f)	Features of gas pipelines to the grid and/or other platforms, if present (delivery pressure, length, capacity)
g)	Features of electrical subsea cables to the grid and/or other platforms, if present (voltage, length, diameter)
h)	Number of regular voyages of supply vessels every year, if present

4.3.2. Step 1: Evaluation of alternative strategies and assessment of technology options

In the first step of the procedure, a preliminary evaluation of the possible P2G and P2L strategies which may be considered for application of the present methodology to the selected site is performed based on the information collected in step 0.1 about the field and infrastructures.

Strategies to be considered need to first identified and characterized in terms of process stages from input supply to end-use. Process stages can be input supply, first conversion, first conditioning (including storage and compression), second conversion, second conditioning (including storage and compression), etc., transportation. A further specification should be made about the location of the process stage, i.e. onshore or offshore.

As described in Chapter 2, different strategies can be conceptualized as potential pathways for conversion of offshore renewable energy in remote areas. Figure 4.3 shows an example of schemes of six P2G and P2L strategies involving H_2, SNG, CH_3OH, including the main process stages. Clearly enough, alternative strategies and/or different process stages may be considered to carry out this step of the procedure. As shown in Figure 4.3, all the pathways start with H_2 production (first conversion step) by means of H_2O electrolysis after seawater desalination. Conditioning step (including storage and compression) and second conversion step can then be added based on the final product of the pathway. Options 1 and 2 produce H_2, Options 3a and 3b have SNG as final product, Options 4a and 4b aim at CH_3OH production. All these steps are supposed to take place at the offshore oil & gas platform defined in step 0.1 and completely supplied by the electricity produced from the renewable plant linked to it. The final product can then be transported onshore by means of pipeline (in case of H_2 and SNG) or ships (in case of CH_3OH) and sold to the market for specific end-uses, i.e. gas grid (in case of H_2 and SNG), industry and mobility (in case of H_2), mobility (in case of CH_3OH). In Option 1, the produced H_2 is transported via existing gas pipeline in admixture with natural gas flow, while pure H_2 is delivered by means of new pipeline in Option 2. Two different CO_2 inputs can be supplied to options producing SNG and CH_3OH, i.e. CO_2 separation from raw gas at the offshore facility or CO_2 purchase from the onshore market and delivery to the offshore site. As a matter of fact, if gas pipelines from the offshore platform to the onshore gas terminal and/or to other platforms are not present at the site under analysis, Options 1 and 2 should be excluded from the analysis, as well as Option 3b and Option 4b. If CO_2 is present in relatively small composition in the raw gas, onsite separation of CO_2 may be unfeasible, thus Options 3a and 4a should not be taken into account in the comparative assessment.

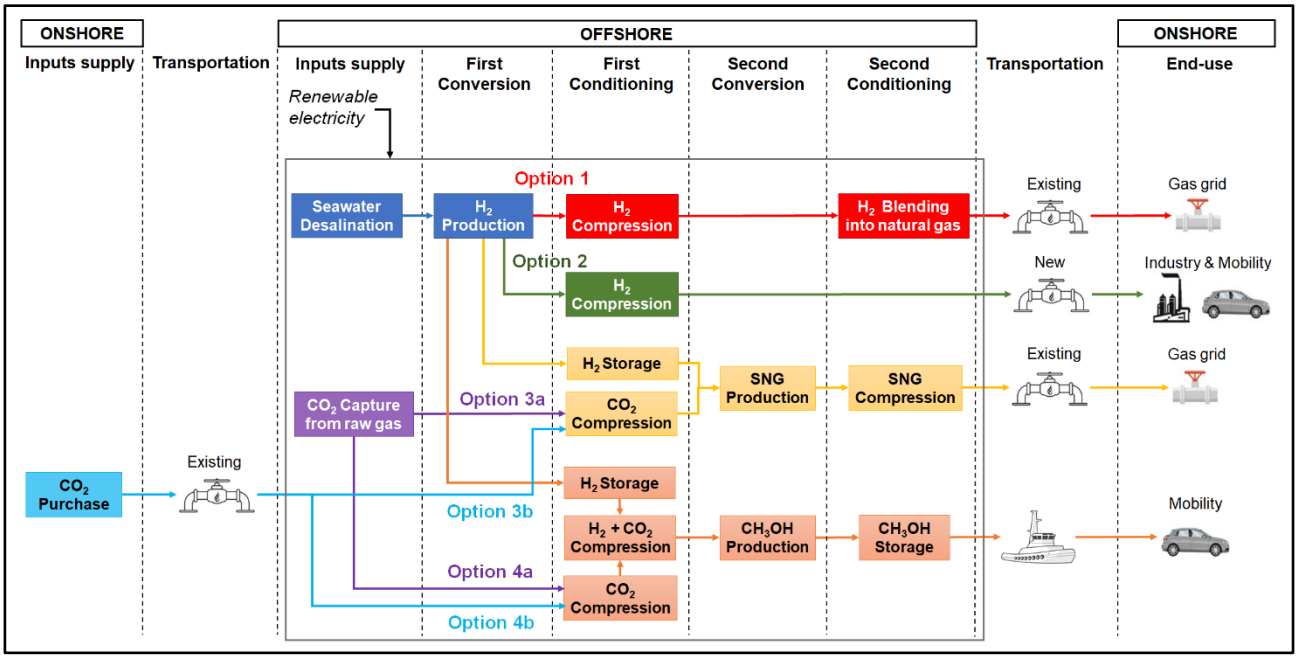

Figure 4.3. Simplified block diagram of the proposed P2G and P2L strategies for offshore renewable energy conversion.

Once evaluated the strategies and associated process stages, a given technology option needs to be selected for each process stage. A review of alternative technologies for the process stages illustrated in Figure 4.3 is reported in Chapter 2. Table 4.2 summarizes some recommendations which may be used to address the choice in this step of the procedure, including the technology proposed as the most suitable according to them. There is no doubt that other options may be chosen based on the knowledge status and data availability about the technologies selected for the analysis.

Table 4.2. Recommendations for the assessment of technology options of some process stages of P2G and P2L strategies.

Process stage	Technology options	Recommendations for the choice	Proposed suitable technology
H_2 production	Alkaline electrolysis, Proton exchange membrane electrolysis, Solid oxide electrolysis cell	For P2G and P2L applications, it is recommended that electrolyzers operate with high efficiency to avoid unnecessary energy losses, with highly dynamic behaviour (small ramp-up time) to follow the fluctuant power input of renewables and with very low minimal load for flexible operation. Pressurized operation is advantageous to reduce or eliminate the cost of an external compressor and its associated additional equipment. A simple and compact layout is highly desired in offshore context. A reliable and modular system may facilitate marine transportation and reduce installation and maintenance time at offshore platform.	Proton exchange membrane electrolysis [156,157,165]
Sea H_2O desalination	Multi-stage flash distillation, Multi-effect distillation, Mechanical vapour compression, Reverse osmosis, Electrodialysis, Membrane distillation	For sea H_2O desalination driven by renewable energies, it is suggested that the technology option demonstrates high compatibility with renewable sources and good ability to produce water at a suitable purity required in input from the electrolysis technology. A technology with high modularity, minimum interruption time during maintenance and low electrical energy needs is more suitable for offshore applications.	Reverse osmosis [164–170]
H_2, SNG, CO_2 compression	Centrifugal compressor, Reciprocating compressor	Smooth operation, high reliability and suitability for process fluctuations may be better features.	Centrifugal compressor [474]
H_2 new pipeline	Low to medium strength steels, with maximum operating pressures of 100 bar	The design of new offshore pipeline is strictly related to the pipeline flow capacity which depends upon several factors, such as the desired mass flowrate at the destination and required delivery pressure, as well as the pipe diameter, allowable pressure drops, viscosity and molecular weight of the gas. The steady-state isothermal flow may be a good approximation for relatively long pipeline operating in stable conditions [475].	Use of Weymouth equation applicable to compressible fluid in turbulent flow, long pipelines and pressure drop greater than 40% of the upstream pressure [476]
SNG production	Catalytic methanation, Biological methanation	Offshore methanation may take advantages from higher maturity technology, smaller reactor size per equal feed gas (i.e. higher gas hourly space velocity), lower power input and maintenance time.	Catalytic methanation [154]
CO_2 capture from raw gas	Amine absorption, Membrane permeation	Given the strict constraints of offshore oil & gas platform, modularity, footprint and equipment weight may be the more important criteria. Relatively higher concentration of CO_2 in moderate gas flowrates may require a simpler process scheme.	Membrane permeation [194]
CO_2 delivery	Liquid transportation, Gas transportation in pipeline	Gaseous CO_2 transportation in the range 15-30 bar may be a cost-effective solution if the required pressure at the offshore facility is lower than 80 bar (i.e. the minimum allowable level for safe transportation of liquid phase CO_2) and design pressure of existing infrastructure is between 90 and 150 bar. For P2G and P2L application at offshore platform, it is expected the need for relatively small CO_2 flowrate (i.e. below 10 kg/s).	Gas transportation [206]
CH_3OH production	Catalytic hydrogenation, Electrochemical reduction	Higher maturity, higher conversion of CO_2, higher selectivity of CH_3OH are better characteristics.	Catalytic hydrogenation [114]
CH_3OH delivery	Time charter or voyage charter party contract for ship hire	A contract method mostly used for supply vessels in oil & gas operations and based on daily hire rate is more suitable.	Time charter party contract [477]

4.3.3. Step 2: Definition of the reference process schemes for conversion strategies and of the offshore renewable power plant

Step 2 of the methodology consists in the definition, characterization and collection of quantitative data for the comparison of the strategies identified in step 1. The comparison of different options requires to define first common reference basis and common boundaries to be considered in the analysis.

When different strategies are characterized by the same starting process stage e.g. H_2 production in Figure 4.3, a common reference basis may be introduced by considering equal production capacity of the electrolyzers. Such a capacity can be expressed in terms of ratio of the rated size of electrolyzers to the size of the renewable energy plant which is assumed to supply power to electrolyzers. Therefore, the choice of the optimal ratio may be based on the typical actual energy production of the renewable plant with respect to its theoretical maximum at the site (i.e. capacity factor). Moreover, the capacity of electrolyzers may be chosen by considering their designs features (i.e. dimensions, distance between stacks, weight), provided that space and weight requirements of the offshore platform are met. An example of such analyses is reported in the literature [137]. Clearly enough, the final decision may be addressed by taking into account the impact of such a capacity on the economics of the conversion processes.

The boundaries of the alternative strategies need to be defined consistently among the options. The goal of the assessment is to analyse the performance of pathways converting energy supplied by the same renewable power plant into chemicals at a given offshore location and delivering it to the onshore market for a given end-use. Thus, boundaries should limit to the process stages identified in step 1 leaving outside on-site utilities (e.g. boilers for steam production, nitrogen separation facilities, wastewater treatments, etc.) since they may be already in place or may be designed independently for other uses at the offshore platform. The performance and costs of the renewable plant and its connection with the oil & gas platform are important to assess the overall profitability of P2G and P2L strategies, but are neutral with respect to the selection of the technological alternatives for electric energy conversion if powered by renewable electricity. Therefore, the boundaries for calculation of the technical, economic, environmental and societal indicators as well as of the aggregated indicators for each alternative should be limited to the conversion process, thus excluding the renewable energy conversion and transmission to the offshore platform. These steps should be included in the analysis only for the profitability assessment in order to investigate effectively the viability of the offshore projects.

As a consequence, step 2 is divided into two stages, as illustrated in Figure 4.2: the first one (step 2.1) is dedicated to the definition of the reference process schemes and the second one (step 2.2) is the definition of the renewable power plant.

In step 2.1, for each reference process scheme, components should be selected for the technology option identified in step 1. Example of quantitative data which should be collected for each component is summarized in Table 4.3. If the electrolyzers capacity is set as reference basis, H_2 production in the scheme can be first calculated and then inputs (e.g. sea H_2O and CO_2) and further outputs (e.g. SNG and CH_3OH) of the process schemes can be estimated based on the collected technical features of components.

Table 4.3. Input data for the definition of reference process schemes in the sustainability assessment methodology.

Technical data	
a)	Unit capacity, electrical and mechanical efficiency and pressure ratio per stage in case of machinery, reaction conversion and stochiometric molar ratio in case of reactor
b)	Materials (substances, composition, properties, e.g. enthalpy and entropy), operating conditions (pressure, temperature), nominal flowrates, inventories
c)	Specific electrical power required, specific heat duty (in kWh/kg or kWh/Nm^3)
Economic data	
d)	Capital expenditure (CAPEX) in units of currency
e)	Operational expenditure (OPEX) in units of currency per year
f)	Cost price of input material, e.g. CO_2 supply from onshore market, if present (in units of currency per mass)
g)	Grey market price (excluding financial incentive), green market price (including financial incentive) of the final products (in units of currency per mass)
Environmental data	
h)	GHG emission factor (in $kg_{CO2,eq}$/kWh or $kg_{CO2,eq}$/kg or $kg_{CO2,eq}$/Nm^3)

Regarding the economic analysis, the required information is preliminary estimates of capital expenditure (CAPEX) and operational expenditure (OPEX). Typically, CAPEX includes development and project management costs (i.e. development and consenting services, environmental surveys, resource and met-ocean assessment, geological and hydrographical surveys, engineering and consulting), all equipment costs, balance of plant costs (including electronics, instrumentation and controls), installation and commissioning costs (including installation of equipment and balance of plant, site work, logistics, development insurance, construction project management and spent contingency), and sometimes decommissioning costs. Whereas, OPEX commonly comprises fixed and variable operation and maintenance (O&M) costs including costs associated to operations related to management of the assets in terms of health and safety, logistics, monitoring, and to maintenance and service activities for equipment and balance of plant [361]. It should be noted that in case of use of existing gas pipeline in the field, CAPEX associated to transportation of gas in the strategy may be disregarded. Concerning transportation via ship, service speed of the supply vessel may be defined in order to estimate the number of days required for total round trip and total OPEX associated to ship hire based on the distance between the closest harbour and the offshore platform and number of ship voyages (collected in step 0.1). Decommissioning costs may be excluded from the analysis if the site can be energetically re-used in the future, taking advantage of the groundwork and construction already carried out.

For a consistent economic comparison of different strategies, a reference currency and year should be set Therefore, if required, cost data retrieved from the literature can be adjusted by applying an annualized average conversion rate from actual currency of the cost data retrieved in the literature to refence currency as well as a price index to account for inflation from a past year to reference year may be applied [478]:

$$Cost_{curr_{ref},y_{ref}} = Cost_{curr_{act},y_{act}} \cdot Exc_{curr_{act},y_{act} \rightarrow curr_{ref},y_{act}} \cdot (Pr_{y_{ref}}/Pr_{y_{act}}) \quad (4.1)$$

where Exc is the annual average exchange rate from actual currency to reference currency at the actual year [174], Pr is the price index at reference and actual years, e.g. Chemical Engineering Plant Cost Index (CEPCI) [479] or the total industrial Producer Price Index (PPI) [480], "$curr$" and "y" in the pedix refer to the currency and year of cost data respectively, "act" and "ref" in the pedix refer to actual and reference cost data, respectively.

Market prices of the final products of the pathways strictly depend upon the end-use defined for the strategy and the economic scenario where the strategy is going to operate. In order to investigate the economic feasibility of renewable P2G and P2L products from a possible investor's view, two different prices can be considered for the use of the present methodology, as illustrated in Table 4.3: grey price and green market prices. Grey prices represent the conventional prices of the products without any consideration of their renewable energy content; they may be estimated based on the statistical data of local market for gas grid, industry and/or mobility sectors. Based on the policy support instruments implemented in the Regulation for promotion of renewable energy use, green prices can be defined as the prices of the products generated by 100% renewable energy, which include specific green premium in addition to grey prices or are directly green tariffs established by local Governments. Possible extensions of current incentives for biogas and biofuels as well as introduction of carbon emissions allowances and/or tax at national level may be considered for the estimation of these green prices of the strategies.

In step 2.2, the renewable power plant intended to be linked to the offshore oil & gas platform hosting the P2G or P2L conversion processes is characterized by means of preliminary technical and economic data summarized in Table 4.4. The size may be chosen based on information about the capacity of existing offshore plants operating at full scale in distant zones and/or availability of techno-economic investigations in the literature. If needed, Equation (4.1) can be applied to adjust the economic data.

Table 4.4. Input data for the definition of the renewable plant in the sustainability assessment methodology.

Technical data	
a)	Size, preliminary layout, net energy production
b)	Distance to the offshore platform, to the closest port
Economic data	
c)	CAPEX including electrical transmission (in units of currency)
d)	OPEX including electrical transmission (in units of currency per year)
f)	Market price for renewable electricity into the onshore grid (in units of currency per kWh)

It should be noted that access (i.e. the percentage of time that a device can be accessed for O&M operations) and availability (i.e. the time that the device is able to produce power) levels play an important role in the associated OPEX calculation of the renewable plant [481,482]. Furthermore, total CAPEX usually includes CAPEX associated offshore substation (i.e. alternating current switchgear, transformers, converter electronics and filter and used to increase the voltage prior to its use) and electrical connection to shore and onshore substation. Therefore, costs data related to offshore substation may be disregarded if the substation is assumed to be located at the offshore oil & gas platform linked to the renewable plant, taking advantage of infrastructures sharing of the hybrid energy system. Moreover, the cost associated to export cable to shore and onshore substation may be included in the analysis if further business scenarios are considered, e.g. zero integration of wind energy into the offshore oil & gas operations and the sole selling of renewable electricity to the grid, P2G and P2L conversion of the excess wind power otherwise curtailed according to grid agreements. In these latter situations, market price associated to selling of renewable electricity to the grid needs to be estimated (as shown in Table 4.4), taking into account the incentive mechanism implemented at national level for renewable power integration (e.g. feed-in tariff, feed-in-premiums, quota-based tradable green certificates, investment subsidies or tax cuts). Clearly enough, eligibility requirements to receive support should be verified case-by-case based on the local Regulation.

It is worth mentioning that the present methodology does not pose any restriction in the approach used to obtain the required input data, as well as on databases and tools to support their collection. The uncertainty of input data may be verified in the last step of the procedure through sensitivity analysis.

4.3.4. Step 3: Calculation of sustainability performance indicators

In the third step of the methodology, the sustainability assessment of the defined reference process schemes for P2G and P2L strategies is performed by applying the battery limits and using information described in step 2. A set of indicators addressing technical, economic, environmental and societal aspects of sustainability is calculated for each reference process scheme. It must be remarked that the proposed set is a result of an optimization aimed to capture specific features of P2G and P2L offshore hybrid energy

options. Clearly enough, the set is open to the addition of further indicators in view of an improved assessment.

4.3.4.1. Technical performance assessment

In order to address both quantity and quality of energy, two metrics are proposed to evaluate the technical performance of the P2G and P2L strategies, namely global energy efficiency based on the first law of thermodynamics and the global exergy efficiency based on second law of thermodynamics. For steady-state processes in systems, the energy and exergy efficiencies are defined as ratio of energy or exergy in product outputs with respect to energy or exergy in inputs [240].

In the present methodology, the energy efficiency or first-law efficiency of each reference process scheme associated to the strategy can be defined as:

$$\eta = \frac{LHV \cdot \dot{m}}{\sum_{k=1}^{N}(\dot{W}_k + \dot{Q}_k)} \tag{4.2}$$

where η is the global energy efficiency indicator for the strategy , $\dot{m}$ is the mass flowrate of the useful product (i.e. H_2, SNG, CH_3OH) in outlet from the reference process scheme, LHV is the lower heating value on mass basis of the useful product, $\dot{W}$ and $\dot{Q}$ are the electrical power required and heat duty, respectively, of the k-th component of the reference process scheme, N is the total number of process stages in the reference process scheme. Note that the higher heating value (HHV) may be used in Equation (4.2) as alternative to LHV. $\dot{W}$ and $\dot{Q}$ can be calculated by combining the specific electrical power required and heat duty of the component with information about the unit capacity. Values of HHV and LHV of the final products of the P2G and P2L strategies analysed in this work are summarized in Table 4.5.

Similarly, the exergy efficiency or second-law efficiency of each reference process scheme associated to the strategy is:

$$\psi = \frac{ex \cdot \dot{m}}{\sum_{k=1}^{N}(\dot{Ex}_k^{\dot{W}} + \dot{Ex}_k^{\dot{Q}})} \tag{4.3}$$

where ψ is the global exergy efficiency indicator for the P2G and P2L strategy, ṁ is the mass flowrate of the useful product (i.e. H_2, SNG, CH_3OH) in outlet from the reference process scheme, ex is the specific total exergy on mass basis of the useful product, $\dot{Ex}^{\dot{W}}$ and $\dot{Ex}^{\dot{Q}}$ are the exergy rate due to electrical work and heat duty, respectively, of the k-th component of the reference process scheme, N is the total number of process stages in the reference process scheme.

$\dot{Ex}^{\dot{W}}$ illustrated in Equation (4.3) can be evaluated as follows:

$$\dot{Ex}^{\dot{W}} = \dot{W} \tag{4.4}$$

where $\dot{W}$ is the electrical power required associated to the component defined in Equation (4.2). On the other hand, $\dot{Ex}^{\dot{Q}}$ expressed in Equation (4.3) is calculated as follows:

$$\dot{Ex}^{\dot{Q}} = \dot{Q}\ (|1- T_0/T_s|) \tag{4.5}$$

where $\dot{Q}$ is the heat duty associated to the component defined in Equation (4.2), T_s is the absolute temperature of the boundary where heat rate crosses and T_0 is the reference environment temperature. Reference conditions can be taken as ambient temperature T_0 of 298 K and ambient pressure P_0 of 1.01 bar [240].

The exergy associated to the outlet stream of the final product in Equation (4.3) is defined as sum of two main parts:

$$ex = ex_{ph} + ex_{ch} \tag{4.6}$$

where ex_{ph} is the physical exergy rate per mass flow, i.e. the maximum work obtainable from the system as it reaches the thermal and mechanical equilibrium with the environment. The physical exergy ex_{ph} is calculated as:

$$ex_{ph} = h - h_0 - T_0\ (s - s_0) \tag{4.7}$$

where h and s are the specific enthalpy and entropy of the stream, respectively, at operating conditions of the stream and at reference environment conditions, T_0 is the reference environment temperature. Reference conditions may be taken as ambient temperature T_0 of 298 K and ambient pressure P_0 of 1.01 bar [240]. On the other hand, the chemical exergy ex_{ch} is the chemical exergy rate per mass flow, i.e. the maximum work obtainable from the system as it moves from the environmental state to the reference state, which is defined as [240]:

$$ex_{ch} = \frac{1}{mw} \cdot (\sum_c x_c\ ex^0_{ch,c} + R\ T_0 \sum x_c \ln(x_c)) \tag{4.8}$$

where x_c is the molar fraction of compound c in the stream, ex^0_{ch} is the standard specific chemical exergy of compound at T_0 and P_0 in kJ/mol units, R is the universal gas constant (in kJ/mol-K), T_0 is the reference environment temperature, mw is the molecular weight of the stream. Clearly enough, ex_{ch} is the same as ex^0_{ch} of the final product if the outlet stream from the reference process scheme can be considered as relatively pure. Values of ex^0_{ch} of the final products of P2G and P2L strategies analysed in this work are summarized in Table 4.5.

Given the definition of η and ψ, the higher their values, the higher technical performance of the strategy.

Table 4.5. Heating values and standard chemical exergies of some final products of P2G and P2L strategies.

Chemical energy carrier	LHV (kJ/kg) [360]	HHV (kJ/kg) [360]	ex_{ch}^{0} (kJ/kmol) [483]
H_2	120000	141800	236090
SNG	50050	55530	831200
CH_3OH	19920	22660	720000

4.3.4.2. Economic performance assessment

To assess the economic performance of the different alternatives and identify the most suitable solution from a possible investor's perspective, two metrics are proposed in this methodology, namely levelized cost of product (LCOP) and levelized value of product (LVOP), in order to account for the effect of costs and revenues associated to each strategy separately. All these parameters are expressed in units of currency per MWh of energy content in the final product of the strategy.

LCOP represents a measure of the present costs (discounted to present value) divided by the production of the final product in terms of energy content throughout the economic lifetime of the project [124] and can be calculated for each strategy as follows:

$$LCOP = \frac{\sum_{k=1}^{N} CAPEX_k + \sum_{t=1}^{T}\sum_{k=1}^{N}\left(\frac{OPEX_{k,t}}{(1+r)^t}\right)}{\sum_{t=1}^{T}\left(\frac{B_t}{(1+r)^t}\right)} \quad (4.9)$$

where LCOP is the proposed levelized cost of product indicator, CAPEX in units of currency is the capital expenditure associated to the k-th component of the reference scheme, OPEX in units of currency per year is the operating expenditure associated to the k-th component of the reference scheme at the th-year of the lifecycle, N is the total number of the process stages considered in the reference scheme, T is the total number of years in the economic lifetime of the strategy, B is the annual production of the final product at the t-th year of the economic lifetime, r is the discount rate referred to the th-year used to discount OPEX and B values. B in Equation (4.9) can be estimated by multiplying the annual mass flowrate of the final product of each reference scheme for the corresponding heating value.

In accordance with the levelized cost concept, LVOP is proposed as economic parameter quantifying the annualized total revenue (discounted to present value) derived from selling the final product to a given market with regard to the production in terms of energy content (discounted to present value) during the economic lifetime of the project [124]. LVOP can be calculated for each strategy as follows:

$$LVOP = \frac{\sum_{t=1}^{T}\left(\frac{R_{sell,t}}{(1+r)^t}\right)}{\sum_{t=1}^{T}\left(\frac{B_t}{(1+r)^t}\right)} \quad (4.10)$$

where LVOP is the proposed levelized value of product indicator, R_{sell} is the revenue gained at the t-th year from the product selling to the corresponding market in units of currency per year, T is the total number of years in the project lifespan of the strategy, B is the annual production of the final product at the t-th year of the economic lifetime defined in Equation (4.9), r is the discount rate referred to the th-year used to discount R_{sell} and B values. R_{sell} in Equation (4.10) can be calculated by multiplying the produced flowrate of the final product of each pathway for the corresponding market price. It is worth noting that two different LVOP can be calculated based on the input data used: the first one is evaluated by using in Equation (4.10) grey and green market prices of the products, respectively: one LVOP does not consider any financial incentive for selling of renewable chemicals, while the second one accounts for support schemes for promotion of renewable-based P2G and P2L products into the market.

Given the definitions of the proposed indicators, the lower LCOP and the higher LVOP, the higher economic performance of the alternative.

4.3.4.3. Environmental performance assessment

Total GHG emissions from the components of the reference process schemes can be considered as a measure of the environmental impact of the proposed strategies. An indicator called levelized GHG emissions (LGHG) is proposed in the present methodology in accordance with the LCOP and LVOP indicators described above, regardless the application of LCA method for environmental impact assessment. LGHG can be defined as the emissions from relevant components of the scheme divided by the production of the final product in terms of energy content:

$$LGHG = \frac{\sum_{k=1}^{N} e_{GHG,k}}{LHV \cdot \dot{m}} \tag{4.11}$$

where LGHG in $kg_{CO2,eq}$/MWh is the proposed environmental performance indicator for the P2G and P2L strategy, e_{GHG} is the mass flowrate of GHG emissions from the k-th component of the scheme, N is the total number of process stages considered in the scheme, ṁ is the mass flowrate of the useful product in outlet from the reference process scheme, LHV is the lower heating value on mass basis of the useful product. e_{GHG} can be calculated by combining the specific emission factor of the component with information about the unit capacity. Note that HHV may be used in Equation (4.11) as alternative to LHV. Given this definition, the lower LGHG, the higher environmental performance of the alternative.

4.3.4.4. Societal performance assessment

The societal dimension of sustainability is preliminarily disregarded in the description of this methodology. Throughout the present chapter (Section 4.5), some safety-related indicators which may be used to address this aspect of sustainability are defined.

4.3.4.5. Aggregated performance assessment

The calculation of indicators described above allows to assess the expected performance of each reference process scheme with respect to specific issues. For the purpose of an easy and clear communication of the overall sustainability profile of the alternative strategies, a procedure is required to compare and combine the indicators addressing different aspects into a single-value indicator. The construction of a composite indicator commonly requires the application of normalization, weighting and aggregation steps, even though the approach to adopt in each step is based on the type of multi-criteria assessment.

In MCDA method, normalization or scaling refers to any procedure where diverse-unit cardinal scores are converted into a dimensionless numerical value with a common direction [247]. Normalization appears a necessary precursor to weighting and aggregation procedures when applying compensatory MCDA methodologies, while it is not essential in non-compensatory MCDA techniques which usually rank the alternatives based on their relative performance. Compensability refers to the possibility of offsetting a bad performance of an alternative on one indicator by a sufficiently good performance of the same alternative on another indicator [244]. Moreover, in compensatory approaches, weights are substitution rates representing the capacity for trade-off between the indicators, thus variation in one of them lead to a change in the others accordingly. On the other hand, weights used in non-compensatory methods are considered as importance coefficients indicating the voting power of the indicators [484]. Coming to decision context involving sustainability, a "weak" sustainability perspective enables the substitution of different forms of capital (e.g. financial, ecological, human), while "strong" sustainability perspective believes that some natural capitals are highly important and cannot be substituted by man-made capital [244]. According to these concepts, non-compensatory MCDA methods allows the adoption of the strong sustainability perspective by eliminating or limiting the need for compensation between aspects of sustainability, whereas compensatory approaches only make sense from the weak sustainability concept [236].

In the following, a partial compensatory aggregation approach is described for use in the present methodology by revising a consolidated procedure from the existing literature [243,264]. As shown in Figure 4.1, the approach is composed of three main steps: the technical, economic, environmental and societal indicators calculated for each reference process scheme are first normalized and then combined into an overall aggregated indicator by means of proper weighting and aggregation techniques.

Concerning normalization, a non-dimensional indicator can be determined between zero (undesired) and 1 (desired) by comparing the actual indicator (I_{act}) with respect to a given target values (I_{target}). When the aim is to minimize the value of the indicator to increase the performance (e.g. minimizing the

environmental emissions, minimizing levelized costs, minimizing the hazard level for society) the non-dimensional indicator (X_I) is calculated for each option as follows:

$$X_I = \frac{I_{target}}{I_{act}} \qquad I_{act} > I_{target} \tag{4.12}$$

If I_{act} is lower than I_{target}, X_I in Equation (4.12) is set equal to 1. On the other hand, when the goal is to maximize the indicator to increase the performance (e.g. maximizing efficiencies, maximizing levelized revenues), the following equation is applied to calculate X_I:

$$X_I = \frac{1 - I_{target}}{1 - I_{act}} \qquad I_{act} < I_{target} \tag{4.13}$$

If I_{act} is greater than I_{target}, X_I in Equation (4.13) is set equal to 1.

The selection of I_{target} is an important yet critical phase which may strongly influence the results of the assessment. In this methodology, an external normalization is proposed consisting in the use of reference values representing performance of the best available process for the considered alternative. When technology options are selected as the most suitable for the process stages of the strategy, the target performance may be referred to these technologies and considered as the expected performance in the near future due to improvement in the process. It must be remarked that complete flexibility is given to data sources from the literature used to collect the target values, despite proper selection of data is fundamental to obtain significant results.

The normalized indicator associated to η and ψ, i.e. X_η and X_ψ , can be calculated by means of Equation (4.13). The final technical normalized indicator (X_{tech}) should be obtained as suitable aggregation of X_η and X_ψ.

Concerning the economic aspect, since LCOP and LVOP have an opposing direction, the normalized indicator associated to LCOP, i.e. X_{LCOP}, is calculated by applying Equation (4.12), while the normalized indicator associated to LVOP is derived through Equation (4.13). It is reasonable to expect a decrease in LCOP due to cost reductions related to technology improvement and/or supply chain improvement, while an increase in LVOP because of higher incentives promoted by Regulations for production of renewable chemicals. The final economic normalized indicator (X_{econ}) should be calculated by means of proper aggregation of X_{LCOP} and X_{LVOP}.

From the environmental perspective, like for LCOP, the normalized indicator associated to LGHG, i.e. X_{LGHG}, can be calculated by applying Equation (4.12). Since one sole indicator is proposed within the

environmental dimension in the present methodology, X_{LGHG} corresponds to the final environmental normalized indicator (X_{env}).

Weighting is a relatively controversial issue of the entire aggregation approach, which can imply intrinsic subjectivity and application of social, environmental or economic policy objectives, and may strongly influence the outcomes [485]. Trade-offs weights are needed to obtain a composite indicator by combining normalized indicators. A common method to extract trade-offs between indicators is the AHP method [486] which makes use of pair-wise comparisons to evaluate performance of the alternatives on indicators (scoring) and indicators among themselves (weighting) [484]. To limit the intrinsic subjectivity of this process, the application of a literature procedure for deriving importance coefficients between indicators based on proper criteria and perspectives of decision makers [487] is proposed in this work for elicitation of trade-offs weights, as described in the following.

The evaluation of relative importance of indicators is performed based on three main criteria, i.e. time, space and receptor. Time and space aspects of an indicator are related to the inter-generational and intra-generational equity, respectively, of sustainability, while receptor criterion is associated to the level of impact of an indicator on human and ecosystem targets. The assessment is performed by using a Likert rating scale on five levels (i.e. 1: very unimportant, 2: unimportant, 3: neutral, 4: important, 5: very important) as a function of the perspective of decision makers [487]. Three different archetypes are defined to categorize abstractly the possible decision makers, i.e. the individualist, egalitarian and hierarchist schemes. Equal weighting is further added to these schemes.

The individualist perspective is self-centred and unconcerned about inter- and intra-generational equity. Moreover, its viewpoint can be considered resilient focussing on human rather than ecosystem targets. Thus, according to individualist scheme, indicators are evaluated on a short-term horizon, local perception and based on concerns with respect to human receptors. The egalitarian archetype is interested in inter- and intra-generational equity and shows a precautionary thinking characterized by long-term and global viewpoint. In addition, its perspective is susceptible which can be translated into concerns addressing ecosystem rather than human receptors. The hierarchist scheme has more tolerant approach of decision making based on negotiation and compromise. It exhibits a medium-term horizon and regional perspective, as well as gives importance to both the receptors impartially [488]. To take an example of the procedure, Table 4.6 is used as support material. For each perspective, a score 1-5 is attributed to each of three indicators X, Y and Z with respect to a given criteria. X, Y, Z may be sub-indicators in a category (e.g. energy efficiency and exergy efficiency) or category indicators to aggregated in the overall indicator (e.g. technical, economic and environmental aspects). The overall score associated to each indicator is the sum of the scores given for three criteria. The relative importance of X, Y and Z is determined as the ratio of the associated overall score to the sum of overall scores, i.e. 0.22, 0.38 and 0.41, respectively.

Table 4.6. Example of scoring indicators based on time, space, receptor criteria for a given perspective.

Criteria	Indicator X	Indicator Y	Indicator Z
Time	3	5	5
Space	3	4	5
Receptor	2	5	5
Overall score (sum)	8	14	15
Relative importance weight	0.22	0.38	0.41

After that, overall scores identified in Table 4.6 are used to derive trade-offs between indicators by means of a series of pair-wise comparisons. The score associated to the pair-wise comparison X-Y is the overall score associated to X (i.e. 8 in Table 4.6) minus the overall score associated to Y (i.e. 14 in Table 4.6), i.e. -6. Similarly, the score associated to the pair-wise comparison Y-Z is -1 and X-Z is -7. Thus, the trade-offs associated to these scores can be derived by using Table 4.7 which shows results for pair-wise comparison between two general indicators A e B.

Table 4.7. Trade-off of indicator A with respect to indicator B associated to pair-wise comparison A-B.

Pair-wise comparison A-B	Trade-off	Pair-wise comparison A-B	Trade-off
-12	0.077	+1	2.000
-11	0.083	+2	3.000
-10	0.091	+3	4.000
-9	0.100	+4	5.000
-8	0.111	+5	6.000
-7	0.125	+6	7.000
-6	0.143	+7	8.000
-5	0.167	+8	9.000
-4	0.200	+9	10.000
-3	0.250	+10	11.000
-2	0.330	+11	12.000
-1	0.500	+12	13.000
0	1.000		

Once determined the trade-off for each pair-wise comparison, a pair-wise comparison matrix can be drawn for a given perspective to summarize the estimated trade-offs. Table 4.8 illustrates the comparison matrix associated to data in Table 4.6 by using Table 4.7. Also, the sum of the entries in column are reported in this table for each indicator. It should be noted that for a group of three indicators only three comparisons are needed to complete the matrix since values on the diagonal cells are always 1 and values in the remaining cells are equal to the reciprocal of their counterpart.

Table 4.8. Example of pair-wise comparison matrix built by using scores in Table 4.6 and data in Table 4.7.

Criteria	Indicator X	Indicator Y	Indicator Z
Indicator X	1.000	0.143	0.125
Indicator Y	6.993	1.000	0.500
Indicator Z	8.000	2.000	1.000
Sum	15.993	3.143	1.625

Finally, an evaluation matrix can be created (Table 4.9): values in the columns associated to X, Y and Z are first obtained by dividing each entry in Table 4.8 by the sum of the entries in column, then the trade-offs weights between indicators are estimated through the common maximal eigenvector method (i.e. averaging values across the rows). As shown in Table 4.9, the trade-off weights associated to X, Y and Z are 0.062, 0.354 and 0.584.

Table 4.9. Example of evaluation matrix associated to the pair-wise comparison matrix in Table 4.8 and trade-off weights.

Criteria	Indicator X	Indicator Y	Indicator Z	Trade-off weight
Indicator X	0.063	0.045	0.077	0.062
Indicator Y	0.437	0.318	0.308	0.354
Indicator Z	0.500	0.636	0.615	0.584

To check consistency of the evaluations, a consistency index is estimated by the following equation [486]:

$$CI = (\lambda_{max} - m_I)/(m_I - 1) \quad (4.14)$$

where CI is the consistency index, λ_{max} is the principal eigen value, m_I is the number of indicators in the evaluation (i.e. the size of the evaluation matrix). λ_{max} can be estimated by multiplying each row of the pair-wise comparison matrix in Table 4.7 for the trade-off vector, thus obtaining a vector of three elements (0.185, 1.077, 1.786). Then, such latter vector is divided by the corresponding element in the trade-off vector and then assuming the mean value, i.e. 3.035 in the example described. A CI value of 0.0175 is then derived by applying Equation (4.14). A perfectly consistent decision maker should always obtain CI equal to 0. However, small inconsistencies may be tolerated. Therefore, a random index (RI) is estimated by using Table 4.10 (if number of indicators is less than 11) and then a consistency ratio is calculated as follows [486]:

$$CR = CI/RI \quad (4.15)$$

where CR is the consistency ratio, CI is the consistency index and RI is the random index. A value of CR lower than 0.1 is suggested for tolerable inconsistencies and thus reliable results from the process, otherwise the judgements are untrustworthy [486]. For the example illustrated, RI of 0.58 is applied from Table 4.10 and CR is estimated as 0.030, thus verifying the consistency of the evaluations.

Table 4.10. Values of random index for small problems to check consistency of pair-wise comparisons [486].

Size of comparison m	2	3	4	5	6	7	8	9	10
RI	0	0.58	0.90	1.12	1.24	1.32	1.41	1.45	1.51

Once identified the weights between sub-indicators within each category and weights between category indicators, a two-stage aggregation process is performed to obtain a single-value composite indicator. Among the different aggregation rules, the weighted arithmetic mean (WAM) or weighted geometric mean (WGM) are proposed in this study for each category indicator and then for the overall indicator.

Next, normalized sub-indicators (e.g. X_{η}, X_{ψ}, X_{LCOP}, X_{LVOP}, X_{LGHG}) are aggregated into a category indicator associated to each aspect of sustainability (e.g. X_{tech}, X_{econ}, X_{env}) by means of Equation (4.16) in case of WAM and of Equation (4.17) in case of WGM:

$$X_c = \sum_{f=1}^{F} w_{f,c} \cdot X_{f,c} \qquad \sum_{f=1}^{F} w_{f,c} = 1 \tag{4.16}$$

$$X_c = \prod_{f=1}^{F} (X_{f,c})^{w_{f,c}} \qquad \sum_{f=1}^{F} w_{f,c} = 1 \tag{4.17}$$

where, pedix "c" refers to the aspect of sustainability, pedix "f" refers to the sub-indicator in the category c, F is the total number of sub-indicators in category c, w is the weight associated to sub-indicator f in category c. The sum of the intra-category weights is equal to one irrespective of the aggregation procedure.

Overall indicator aggregating the category indicators of sustainability is called in this work Aggregated Sustainability Index (ASI), which is determined by using WAM in Equation (4.18) or WGM in Equation (4.19):

$$ASI = \sum_{c=1}^{C} w_c \cdot X_c \qquad \sum_{c=1}^{C} w_c = 1 \tag{4.18}$$

$$ASI = \prod_{c=1}^{C} (X_c)^{w_c} \qquad \sum_{c=1}^{C} w_c = 1 \tag{4.19}$$

where pedix "c" refers to the aspect of sustainability, C is the total number of aspects (categories) considered in the sustainability assessment, w is the weight associated to category c. The sum of the category weights is equal to one irrespective of the aggregation procedure.

It should be noted that WAM is characterized by full substitutability and compensability, thus implying that the overall aggregated indicator may be indifferent to extreme values of indicators. On the other hand, WGM can assume only partial compensability and substitutability [489] reflecting appropriately bad performance in any category or indicator in the overall aggregated indicator As a consequence, larger difference between indicators is penalized through a lower aggregated indicator [490]. Moreover, despite

the larger adoption of WAM to obtain comprehensive metrics, it is more susceptible to double counting when indicators are not independent [485]. Thus, in this latter case, WGM is the most preferred method.

It must be remarked that the MCDA method described above should be applied when the process alternatives producing the same final product are compared in order to use consistent process-related target values among the options. In case of a comparison of process schemes producing different products, a non-compensatory method which is able to deal with heterogeneous scales of indicators and to maintain their original concrete verbal meaning seems to be more suitable. In this case, the calculated technical, economic, environmental and societal indicators are aggregated into a single-value metrics without the need for the normalization stage.

Some examples of non-compensatory MCDA methods are preference-based or outranking methods, e.g. ELECTRE (ELimination and Et Choice Translating REality) [491] and PROMETHEE (Preference Ranking Organization METHod for Enrichment Evaluation) [492] which are widely used to assess sustainability-related problems [246]. The basic principle of these methods is the construction of outranking relations, i.e. a binary relation (S) defined on a set of alternatives such that, for each pair a and b, alternative a is at least as good as (i.e. it outranks) alternative b (aSb), and then the exploitation of the relations to allow the ranking of alternatives [493]. Both ELECTRE and PROMETHEE perform pair-wise comparison of alternatives in order to rank them with respect to a number of criteria (i.e. indicators). To analyse the outranking relations, they make use of threshold values accounting for indifference and preference when two alternatives are compared (three types required with ELECTRE and two types with PROMETHEE), as well as weights between indicators in terms of importance coefficients. Among the different methods in the ELECTRE and PROMETHEE families, ELETRE II, III, IV and PROMETHEE II allow to obtain a final ranking of alternatives, particularly based on a dimensionless indicator with PROMETHEE II (i.e. the net outranking flow) [494,495]. Different approaches may be applied to determine proper threshold values and criteria weights [496–498]. The approach based on time-space-receptor criteria and individualist-egalitarian-hierarchist archetypes proposed in this work can be useful for weights elicitation. For example, weights illustrated in Table 4.7 may be adopted for ranking of alternatives based on indicators X, Y and Z with ELECTRE and PROMETHEE methods.

4.3.5. Step 4: Calculation of profitability performance indicators

In step 4 of the procedure illustrated in Figure 4.2, a profitability analysis among the alternative strategies is performed in order to check the effective viability of the alternative projects. This can provide another important measure of the performance of the strategies, in addition to the technical, economic and environmental and societal performance assessments carried out in the previous step. To be a worthwhile investment, a venture for a new energy conversion process must be profitable; it is not enough that the

venture makes a large net profit, but that profit over the lifetime must be greater than the original capital investment for the venture.

Among the possible profitability measures [361], the widely used net present value (NPV) is proposed in the present methodology separately from LCOP and LVOP in order to avoid any possible double-counting problems and aggregation issues into an overall sustainability indicator requiring the definition of common battery limits for calculation of the indicators. NPV is defined as follows:

$$NPV = \sum_{t=1}^{T}\left(\frac{R_{sell,t}}{(1+r)^t} - \frac{\sum_{k=1}^{N} OPEX_{k,t} + OPEX_{renew,t}}{(1+r)^t}\right) - \sum_{k=1}^{N} CAPEX_k - CAPEX_{renew} \quad (4.20)$$

where R_{sell} is the revenue at th-year defined in Equation (4.10), CAPEX and OPEX are the costs parameters associated to the k-th unit and to the renewable power plant, N is the total number of the process stages considered in the reference scheme, T is the total number of years in the economic lifetime of the strategy, r is the discount rate referred to the th-year used to discount R_{sell} and OPEX values. A positive value of NPV implies that the revenues are greater than the total costs over the analysed period, thus the investor can make a profit. Otherwise, the project is not still feasible. NPV equal to 0 means no loss or gain.

As discussed in the description of step 2, NPV may be calculated for different business scenarios, besides the situation considered in Equation (4.20), in order to investigate the attractiveness of the projects by adding or changing the revenues gained from the onshore market. Examples can be the baseline situation of zero integration of renewable power into the chemical processes, thus only electrical grid connection between the offshore wind farm and onshore substation, as well as revenues from the electricity selling to suppliers may be conceptualized. Another situation may be the inclusion of an electrical export cable to shore in addition to the connection to the platform, thus a part of offshore renewable power may be directly routed to the land and a double revenue may be obtained coming from the selling of both electricity and final product of the pathway. In case of these latter business scenarios, market price associated to the selling of renewable electricity to the grid needs to be included as well as costs for electrical cables and onshore substation.

4.3.6. Step 5: Ranking of alternatives and sensitivity analysis

The calculation of the sustainability performance indicators in step 3 of the procedure allows to compare and rank the reference process schemes of the strategies from the viewpoint of different aspects and overall fingerprinting of sustainability. However, the construction of aggregated indicators may result in various issues of uncertainty associated to erroneous input data, normalization, weighting and aggregation methods.

Use of sensitivity analysis can assist in identifying gaps and verify the robustness of the ranking of the process schemes based on the aggregated indicator. In particular, if the compensatory aggregation approach proposed in the present methodology is adopted, normalized approach based on target values defined in the normalization of the indicators are unavoidably affected by a level of uncertainty, since they are derived from estimates about future projections. On the other hand, it is recognized that a number of parameters, e.g. preference functions and thresholds values, should be determined for use of outranking methods, thus resulting in a potential source of uncertainty which needs to be taken into account. Concerning weights elicitation, the adoption of the approach based on time-space-receptor criteria and individualist-egalitarian-hierarchist perspectives may be a way to reduce uncertainty associated to this stage. However, no matter the application of sensitivity analysis to check the influence of variation in weight factors on the aggregated indicators.

The calculation of the profitability indicator proposed in step 4 of the procedure provides a ranking of the strategies under different business scenarios as well as identification of viable projects. This can be considered as a further important measure, besides the integrated performance assessment performed in the previous step. In this case, NPV values may be affected by uncertainty related to the estimation of input data, which are economic parameters associated to the renewable power plants and reference process schemes. Therefore, in the final step of the procedure, sensitivity analysis may be applied to assess the robustness of the relative ranking of the alternatives based on NPV by identifying the most critical (uncertain) input parameters and varying them in given ranges.

Some sensitivity analysis techniques which may be used for the sake of these verifications are described in Section 4.7 of this chapter.

4.4. Sustainability assessment methodology for G2P options

This section describes the methodology proposed for the sustainability performance assessment of alternative G2P offshore hybrid energy options conceptualized in Chapter 2. An overview of the method including the details of the steps and proposed performance indicators is presented in the following paragraphs.

4.4.1. Overview of the method

From the limits of existing sustainability assessment methods highlighted in Chapter 3 (Section 3.2), a straightforward methodology is developed in this work to compare the sustainability performance of offshore renewable plant coupled with GT energy balancing system installed at existing offshore oil & gas installations for G2P applications. The set of sustainability indicators defined in the assessment model

described in Section 4.3 is properly adapted to capture the peculiarities of concern. Renewable-based target values are introduced for normalization of the proposed indicators in view of single-value metrics which eases the ranking of the alternative systems.

The methodology is intended to be a support tool to evaluate the feasibility of offshore G2P projects at offshore oil & gas production facilities in non-associated gas reserves classified as stranded or depleted fields, which are located relatively close to the onshore electrical grid and for which projects on renewable power exploitation have been initiated or are under investigation for the energetic valorisation of the site. The approach has a general applicability to every type of offshore renewable energy source for which technology development and incentive schemes have promoted the integration into the onshore network, even though offshore wind and wave energy sources are specifically considered for the description of the methodology. Finally, the method can be adopted to both assess alternative G2P offshore hybrid energy system at a specific offshore site and compare different offshore sites for the same type of hybrid solution.

The flow chart of the methodology is illustrated in Figure 4.4. As shown in this figure, a preliminary step (step 0) is necessary divided into two stages. The first stage (step 0.1) concerns the definition of the offshore oil & gas sites providing input data about the field and infrastructures, as summarized in Table 4.11. In the second stage (step 0.2), the offshore renewable energy to be exploited is evaluated by taking into account existing projects and/or feasibility studies on renewable potential assessment and power integration into the grid in the selected areas. It should be noted that in case of more than one offshore site to analyse, the same type of renewable source should be considered for a consistent comparison. After that, the procedure is divided into seven main steps, described in detail in the following paragraphs.

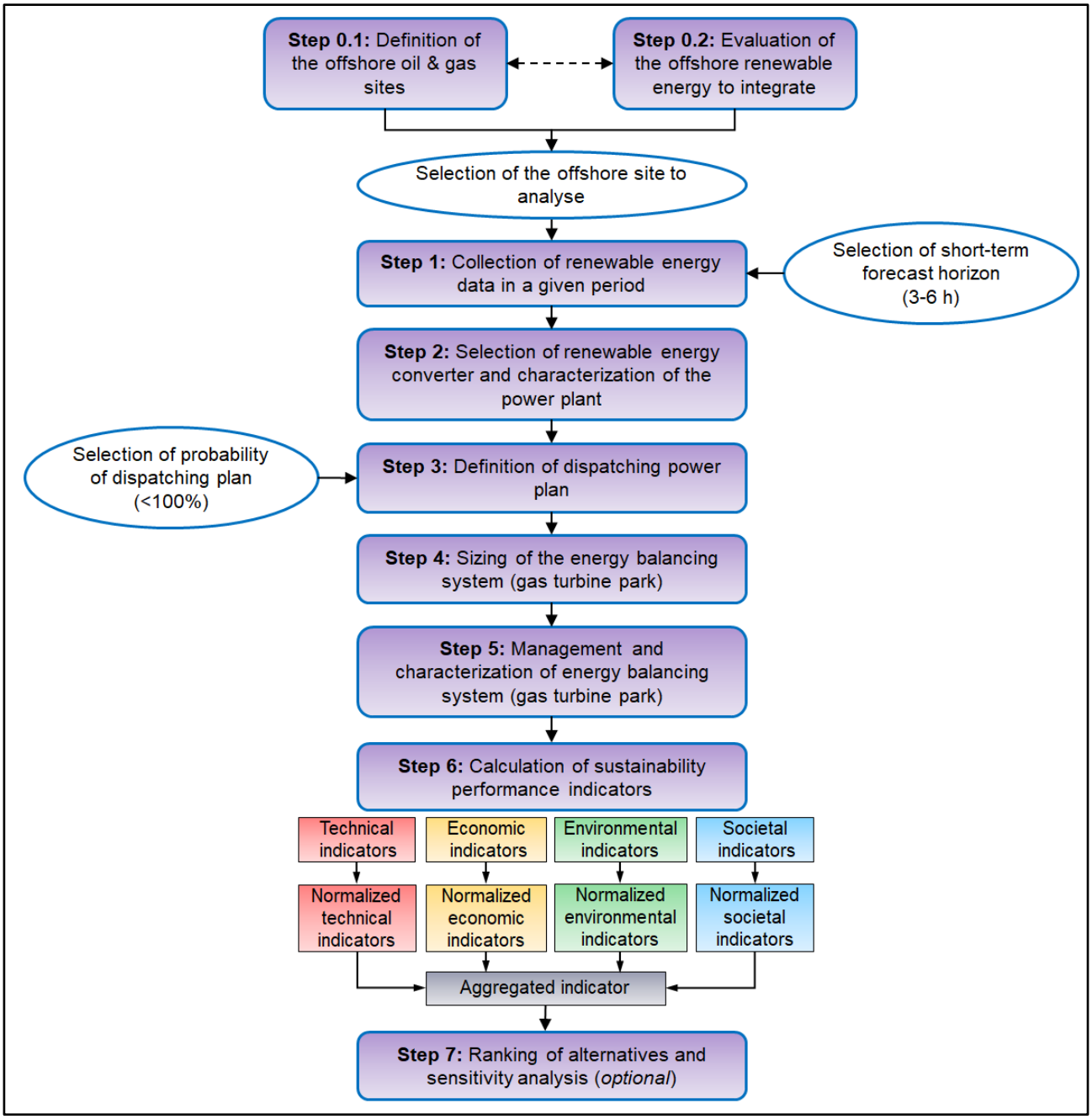

Figure 4.4. Flow chart of the sustainability assessment model for G2P offshore hybrid energy options.

Table 4.11. Details of the offshore site required in input to the sustainability assessment methodology.

Data about the field	
a)	Entity gas reserves (type, production, properties, e.g. heating value)
b)	Water depth, bathymetry
c)	Distance from site to the closest onshore grid, to onshore shipyard, to port
Data about the infrastructures	
d)	Characteristics of the offshore structures (type, remaining lifetime)
e)	Preliminary dimensions, elevation of decks, estimated free space of the offshore structure
f)	Features of electrical subsea cables to the grid and/or other platforms, if present (voltage, length, diameter)

4.4.2. Step 1: Collection of renewable energy data

In the first step of the procedure illustrated in Figure 4.4, specific data about renewable energy potential need to be collected for each offshore site. This consists of characteristic meteo-marine parameters associated to each type of renewable source and needed for the estimation of available theoretical renewable power at a given site.

In case of offshore wind energy, the wind force is converted into a turning force by acting on the rotor blades of a wind turbine; theoretically power of an air mass that the wind can transfer to the rotor is [10]:

$$P_{wind,avail}(v_{wind}) = \frac{1}{2} \cdot \rho_{air} \cdot A_{rot} \cdot v_{wind}^3(z) \quad (4.21)$$

where $P_{wind,avail}$ is the available kinetic wind power, ρ_{air} is the density of air (assumed equal to 1.225 kg/m^3 at normal atmospheric pressure and 15°C), A_{rot} is the swept area of the wind turbine, v_{wind} is the mean wind speed at turbine hub height z. However, the power which van be extracted by the rotor is not equal to the kinetic power of flow; according to the Betz's limit, the mechanical energy which theoretically is extractable from the wind is the maximum power coefficient $C_{p,Betz}$ equal to 0.593 [16]. Therefore, average hourly wind speed is the environmental parameter required for the application of the proposed methodology when offshore wind energy is selected as renewable source.

In case of irregular waves propagating in deep waters, the wave energy flux corresponding to the power content per unit of surface of the crest length is [499]:

$$P_{wave,avail} = \frac{1}{64\,\pi} \cdot \rho_{water} \cdot {a_g}^2 \cdot H_s^2 \cdot T_m \quad (4.22)$$

where $P_{wave,avail}$ is the available wave power, ρ_{water} is the density of seawater (generally 1025 kg/m^3), a_g is the gravitational acceleration, H_s is the significant wave height which is the average height of the highest third of waves during a certain period (typically 30 minutes), and T_m denotes the mean spectral wave period which is the average time between consecutive crossings of the mean sea level line in an upwards direction. Note that the peak wave period (T_p) representing the wave period with the highest energy can also be used in Equation (4.22), instead of T_m. Therefore, average hourly values of significant wave height, peak and mean wave periods are considered as input data to the present methodology in case of selection of wave energy source.

For the purpose of G2P hybrid energy options integrated into the electrical network, two different types of parameters need to be retrieved independently from the considered renewable source in a given period: real data and forecast data. The choice of the period may be based on the time interval during which this

information is available. It is worth noting that in case of more than one offshore site to analyse, the same period should be considered for a consistent comparison.

Real data are in-situ measurements derived from specific devices located at the offshore site or near it. An anemometer is the device for measuring wind speed (and often wind direction and air temperature), which can be classified into cup anemometer, hot wire anemometer, laser doppler anemometer and sonic anemometer [10]. If wind measurements are not available at the height at which the turbine is to be installed, wind speed values can be adjusted to the turbine hub height z by means the following wind shear logarithmic law [500]

$$v_{wind}(z) = v_{wind,r} \cdot \frac{\ln\left(\frac{z}{z_0}\right)}{\ln\left(\frac{z_r}{z_0}\right)} \tag{4.23}$$

where $v_{wind}(z)$ is the wind speed at hub height z, $v_{wind,r}$ is the wind speed at generic height z_r (e.g. measured wind from anemometer), z is the turbine hub height, z_r is the generic height at which $v_{wind,r}$ is obtained (e.g. anemometer height), z_0 is the roughness length in the current wind direction (commonly 0.0002 m for water areas in open sea [501]). The available wind speed profile at the site can be assessed by taking into account the minimum threshold value of 6 m/s at hub height for the exploitation of offshore wind at a given site, as established by the Orecca FP7 project [502]. After collected, wind data are usually modelled by means of a distribution describing the frequency of various wind speeds over the selected period. Different statistical distributions can be used to represent the nature of the wind [503], among them the most widely used is the Weibull probability density function:

$$p(v_{wind}, k, c) = \frac{k}{c}\left(\frac{v_{wind}}{c}\right)^{k-1} e^{-\left(\frac{v_{wind}}{c}\right)^{k}} \tag{4.24}$$

where v_{wind} is the random wind speed, k is the shape factor, c is the scale factor. Calculation of these latter parameters can be performed according to literature methods [504].

In-situ recording of wave data can be performed by means of different devices: wavestaff, pressure recorder, accelerometer buoy or waverider buoy, shipborne wave recorder [505]. Based on the type of instrument and recording technique used, there are different ways to obtain statistics of wave climate. Among them, average values of wave parameters described above (and also mean wave direction) are commonly provided for short-term statistics. Bivariate distributions of occurrences corresponding to different combinations of H_s and T_m (or T_p) can be derived, i.e. scatter diagrams. A more condensed way to describe the way conditions than a scatter diagram is to group some bins of scatter diagram into a limited number of zones, referred to as sea states, according to the recommendations given in [506]. The monthly and annual available power per unit front can be also calculated by means of Equation (4.22); a value of 10 kW/m is suggested as possible minimum threshold for wave exploitation at a given site [106].

It should be noted that records from measuring devices may be provided at fixed interval which can vary from few minutes to 10 minutes or 30 minutes, and in some cases, they may be missing over the desired period. Therefore, a proper approach should be applied to convert the available values of parameters into hourly averages for the application of this methodology, e.g. arithmetic mean. In case of the lack of entire months data, missing hourly values may be created using linear interpolation using the same month from previous or subsequent years. It is worth noting that the use of times series as much complete as possible is recommended in order to achieve consistent results, particularly in the comparison of different offshore sites.

On the other hand, forecast data can be obtained by means of a proper forecasting approach which depends first on the renewable source considered and forecast horizon.

Wind speed forecasting techniques can be divided into four main groups according to the time horizon required [507]: ultra-low short term forecasting (from few minutes to 1 ahead), e.g. the persistence method; short-term forecasting (from one hour to six hours ahead) e.g. the statistical methods including auto regressive (AR), auto regressive moving average (ARMA) and auto regressive integrated moving average (ARIMA); medium-term forecasting (from several hours to 1 day ahead) and long-term forecasting (from one day to one week or more ahead), e.g. the physical approach based on numerical weather prediction (NWP) using weather forecast data. Around 6 h forecast horizon can be identified as limit between the use of statistical and physical methods [508].

Concerning wave forecasting, two major groups can be distinguished: physics-based and time series models [509]. Physics models, such as the WAVEWATCH III, the Wave Model (WAM) of European Commission for Medium-range Weather Forecasts (ECMWF) and Simulating WAves Near shore (SWAN), use energy balance equation which solves the wave action balance as a function of source and sink terms. They can include wind-induced forces, nonlinear wave–wave interactions, and dissipation by white capping in deep water, while they can consider shoaling and bottom friction in shallow water. On the other hand, time series methods include regressions, neural networks, even though newer techniques such as genetic programming algorithms and artificial intelligence are used. From comparison between physics and time series model in the literature [510], it emerged that statistical methods are more accurate than physic models over horizon 1-4 h, while for longer forecasts physic-based methods tend to have better forecasting features, provided that the convergence point between the two groups of techniques at which comparable accurate results may be achieved is around 6 h forecast horizon [511], similar to the findings retrieved for wind forecasting.

In order to provide an optimal integration of renewable energy generation into the electrical network through energy balancing systems, it is important to forecast renewable data over a time horizon consistent

with the operation of electricity grids and markets. The requirements regarding renewable power predictions rely on the specific market and usually driven by market operation constraints rather than technical or physical issues [16]. These horizons can be about 6 h in the USA, Canada and UK [512], while in Europe forecasts of 4-5 h in advance are required for real-time unit commitments (e.g. time required for switching on alternate sources) and forecasts in the order of 2-3 days ahead are used to determine the available reserves for the day-ahead market [509]. Overall, a time horizon of up to 6 h ahead allows to react to a varying production and regulating capacity at the system operators' disposal, thus a selection of a given value of forecast horizon between 3 and 6 h is proposed in the present methodology, as shown in Figure 4.4.

In accordance with the retrieved real data, forecast renewable parameters should be collected on an hourly basis over the same period. Based on the forecast dataset used, some information may be missing within the interval, thus averages between the available hourly values may be performed to fill the gaps for the sake of simplicity.

4.4.3. Step 2: Selection of renewable energy converter and characterization of the power plant

In step 2 of the proposed approach, the renewable energy converter needs to be selected based on the parameters collected in step 1 and features of the offshore site in order to calculate real and forecast power curves. After that, the renewable power plant is characterized by calculating the power curves and economic data. The procedures to apply are detailed in the following.

4.4.3.1. Selection of renewable energy converter

The procedure for the selection of the suitable renewable energy converter is different depending on the type of renewable source considered. The choice of the OWT can be based on the water depth of the considered offshore site, according to the classification of the types of structures and foundations reported in Chapter 1. Moreover, wind turbine class defined in the International Electrotechnical Commission (IEC) design standard 61400-1 3rd Edition: Design Requirements [513] based on annual average wind speed, extreme 50-year gust and turbulence intensity can be determined according to the wind conditions at the offshore site and used as a criterion for the converter selection [514]. In order to gain more accurate results, a turbine with a height as much equal as possible to the height of the anemometer can be also considered in the turbine choice. Furthermore, power curve of the wind turbine representing the relationship between the produced output power and hub height wind speed as well associated trend of power coefficient C_p (also called efficiency of aerogenerator) are given by the manufacturers and can be

used to model the performance of the OWT. Figure 4.5 illustrates an example of power curve for a constant speed and pitch regulated turbine.

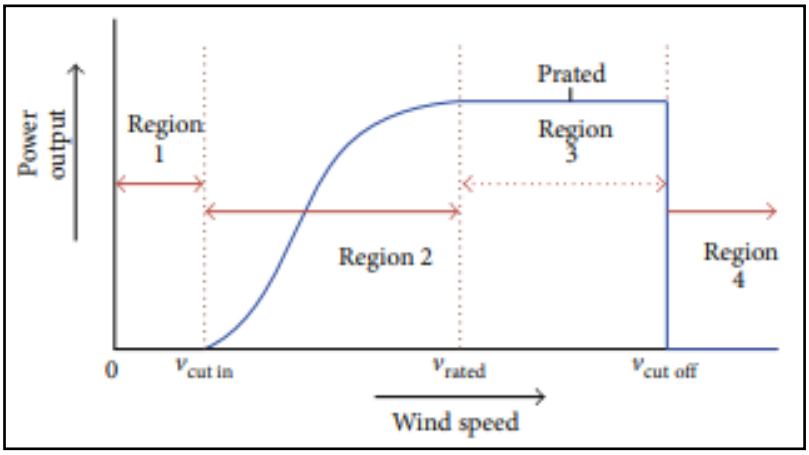

Figure 4.5. Example of power curve of a pitch-regulated wind turbine [515].

As shown in Figure 4.5, a first region can be identified below the lower wind speed limit, the cut-in speed, where the output power is 0. Then, a rapid increase in the power appears between the cut-in speed at which the wind turbine starts to operate and the rated speed at which the turbine produced the rated power (i.e. its nameplate capacity). Finally, in the third region, the output power is constant equal to the rated power up to the upper speed limit, the cut-off speed, beyond which the wind turbine stops production and turns out of the main wind direction (i.e. output power is zero). The selection of a wind turbine characterized by a power curve which matches more largely the wind regime of the site allows to optimize the efficiency of the wind energy plant. The gross annual energy production (AEP) can be estimated as key factor of the selected offshore wind turbine [516]:

$$AEP_{wind} = \int_{v_{cut-in}}^{v_{cut-off}} p_{wind}(v) \cdot P_{OWT}(v) \cdot n_{year} \cdot AV_{OWT}\ dv \tag{4.25}$$

where AEP_{wind} is the predicted amount of wind power produced over a year (in kWh/year or MWh/year) based on the turbine power curve excluding losses (e.g. downtime, wake, electrical and other losses), p_{wind} is the wind speed frequency distribution calculated e.g. by means of Equation (4.24), P_{OWT} is the electrical power for each wind speed derived from the power curve, n_{year} is the number of hours per year, AV is the OWT availability, i.e. the amount of time the device is able to produce power based on device reliability and access level for maintenance (typically 90-97% [482]). Another parameter which can be used to evaluate the chosen offshore wind turbine is the capacity factor (CF) representing the ratio of annual energy production to maximum energy production if the turbine runs at rated power all the year [516]. Therefore, the higher AEP and CF, the higher suitability of the turbine for the offshore site in terms

of production. Once selected the proper OWT device, the actual electrical power produced by OWT can be calculated for each wind speed over the period under analysis as follows:

$$P_{OWT}(v_{wind}) = P_{wind,avail}(v_{wind}) \cdot C_p(v_{wind}) \quad (4.26)$$

where P_{OWT} is the produced power from the OWT, $P_{wind,avail}$ is the available wind power illustrated in Equation (4.21), C_p is the power coefficient of the OWT which usually accounts for the aerodynamic efficiency (describing blades performance), mechanical efficiency (i.e. efficiency of the drivetrain and electrical efficiency (i.e. efficiency of generator and power electronics), v_{wind} is the average wind speed within the operating limits of the turbine (cut-in and cut-off). It should be noted that C_p varies with wind speed and commonly provided by manufacturer in addition to the power curve. Useful computer program to estimate the performance of commercial wind turbines is provided by PelaFlow Consulting [517].

On the other hand, the selection of the suitable WEC can be first based on the sea characteristics at the site of interest, i.e. the water depth and the distance from shore, as described in the classification of wave energy devices reported in Chapter 1. Also, the technological development level, i.e. the availability of real tests performed at different scales in terms of reliability, power production and designs, as well as connection to electrical network, can be considered. In particular, a conversion matrix relating the produced power P_{wave} to H_s and T_m (or T_p) for a characteristic length of WEC installed at a given water depth is useful way to model performance of the device and evaluate suitability of the wave climate at the selected area. An example of conversion matrix associated to Pelamis P2 device is illustrated in Figure 4.6. As shown in this figure, the matrix is available at a resolution of 0.5 m for H_s and 0.5 s for T_m. The maximum output power is 750 kW at H_s greater or equal to 5.5 m. At H_s of 5.5 m, the maximum power is for T_m between 6.5 and 9.5 s, while at greater values of H_s the maximum is reached for values of T_m up to 12 s. Conversion matrices for other devices are available in the literature, with different bin resolution [509,518,519]. Note that power matrix may refer to WEC electrical power: otherwise it corresponds to the absorbed power and power-take-off and generator efficiencies should be considered for electrical power generation.

$T_m(s)$ / $H_s(m)$	Power matrix (in kW)																
	5	5.5	6	6.5	7	7.5	8	8.5	9	9.5	10	10.5	11	11.5	12	12.5	13
0.5	0	0	0	0	0	0	0	0	0	0	0	0	0	0	0	0	0
1	0	22	29	34	37	38	38	37	35	32	29	26	23	21	0	0	0
1.5	32	50	65	76	83	86	86	83	78	72	65	59	53	47	42	37	33
2	57	88	115	136	148	153	152	147	138	127	116	104	93	83	74	66	59
2.5	89	138	180	212	231	238	238	230	216	199	181	163	146	130	116	103	92
3	129	198	260	305	332	340	332	315	292	266	240	219	210	188	167	149	132
3.5	0	270	354	415	438	440	424	404	377	362	326	292	260	230	215	202	180
4	0	0	462	502	540	546	530	499	475	429	384	366	339	301	267	237	213
4.5	0	0	544	635	642	648	628	590	562	528	473	432	382	356	338	300	266
5	0	0	0	739	726	731	707	687	670	607	557	521	472	417	369	348	328
5.5	0	0	0	750	750	750	750	750	737	667	658	586	530	496	446	395	355
6	0	0	0	0	750	750	750	750	750	750	711	633	619	558	512	470	415
6.5	0	0	0	0	750	750	750	750	750	750	750	743	658	621	579	512	481
7	0	0	0	0	0	750	750	750	750	750	750	750	750	676	613	584	525
7.5	0	0	0	0	0	0	750	750	750	750	750	750	750	750	686	622	593
8	0	0	0	0	0	0	0	750	750	750	750	750	750	750	750	690	625

Figure 4.6. Example of conversion matrix for Pelamis P2 device (power values are reported in kW and refers to electrical power) [519].

Similar to the offshore wind energy, AEP by means of the WEC can be estimated as follows [506]:

$$AEP_{wave} = \sum_s P_{wave,avail,s} \cdot p_{wave,s} \cdot L \cdot \eta_{WEC,s} \cdot en_{wave,s} \cdot \eta_{PTO} \cdot \eta_{gen} \cdot n_{year} \cdot AV_{WEC} \quad (4.27)$$

where s is the sea state over the period of interest characterized by proper combination of H_s and T_e (or T_p) [506], $P_{wave,avail}$ is the available wave power following Equation (4.22), p_{wave} and en_{wave} are the probability of occurrence and wave energy contribution of the sea state defined by proper combinations of H_s and T_e (or T_p) as suggested in [506], L is the characteristic or active length of the device along which the machine absorbs the incoming wave energy (e.g. width of the ramp for an overtopping floating WEC, floater diameter in case of point absorber fixed WEC, length of WEC in case of attenuator, chamber width in case of oscillating water column [520]), η_{WEC} is the WEC efficiency accounting for the primary conversion in the device and representing the ratio between the relative amount of energy absorbed and available wave energy to the device (or capture width ratio), η_{PTO} is the power take-off efficiency used for conversion of absorbed power into rotating mechanical power, η_{gen} is the efficiency of generator used for conversion of rotating mechanical power into electrical power (e.g. frequency converters and filters). η_{WEC} values are often determined based on experimental tests or numerical simulations as a function of H_s and T_e (or T_p) for given operating ranges based on the working principle of the device [506,521], while η_{PTO} and η_{gen} have typical values based on the type of PTO [520], n_{year} is the number of hours per year, AV is the WEC availability i.e. the amount of time the device is able to produce power based on device reliability and access level for maintenance (typically lower than 90% [482]).

In case of lack of sea trials data for calculation of η_{WEC}, WEC conversion matrix provided in the literature can be used to convert the wave height and period series into power series (P_{wave}) by means of interpolations in computer programming codes. In case of power matrix referring to the absorbed power, AEP by means of WEC can be calculated as follows:

$$AEP_{wave} = \sum_s P_{wave,s} \cdot p_{wave,s} \cdot \eta_{PTO} \cdot \eta_{gen} \cdot AV_{WEC} \cdot n_{year} \quad (4.28)$$

Otherwise, if the power refers to electrical power, η_{PTO} and η_{gen} can be excluded from Equation (4.28). Similar to the case of offshore wind power, CF associated to wave energy production from WEC can be calculated. Higher values of AEP and CF at a given site can address the selection of the suitable WEC.

The simple way to estimate the electricity production of a WEC at a specific site over the desired time interval is to convert the wave data into power data by using the power matrix associated to the WEC as described above. Therefore, the electrical power produced from WEC for each sea state is:

$$P_{WEC}(s) = P_{wave}(s) \cdot \eta_{PTO} \cdot \eta_{gen} \quad (4.29)$$

where P_{WEC} is the WEC electrical power, s is the sea state over the selected period characterized by combination of H_s and T_e (or T_p), P_{wave} is the power derived from the conversion of wave data at s-th state by using the power matrix of WEC, η_{PTO} and η_{gen} are the power-take-off and generator efficiencies, respectively, defined in Equation (4.27).

Equations (4.26) and (4.29) can be applied by using both the real and forecast data collected for the offshore site in step 1, thus real and forecast power curves on an hourly basis are obtained accordingly for use in the following step of the procedure. It should be noted that selection of different forecast horizon in step 1 results in different forecast power curves.

4.4.3.2. Characterization of renewable power plant

Once selected the renewable energy device for the analysis, the size of the renewable power system needs to be defined in this step of the procedure. Information about the capacity of existing plants already connected to the network or previously studied for future grid integration should be taken into account for a proper decision-making. It is worth noting that the same type of renewable energy device and same size of the plant should be adopted to ensure a consistent comparison between different offshore sites, provided that suitability to environmental conditions (e.g. water depth, average wind speed, wave energy flux per unit of crest length, etc.) of both the locations is verified.

In case of offshore sites characterized by different energy potential for use of the same energy converter design, the site with better environmental features which lead to the adoption of more productive and mature device should be assumed as reference and proper similarity laws should be applied in order to

scale down the devices at the other sites. This could be verified more likely in case of marine energy sector since it is not at as advanced stage of development as the wind energy and solar energy industry.

Various simplified scaling laws for wind turbine are available in the technical literature [522], which use expression of P_{OWT} in Equation (4.26) and incorporate variation of rotational speed, variation of rotor radius and variation of the incidence of the blades (pitch setting) with respect to the rotor plane in case of a stall-regulated rotor. In wind turbine dimensional analysis, examples of dimensionless parameters are power coefficient C_p, thrust coefficient, moment coefficient, etc. If the scaling factor λ is based on the rotor diameter (*D*), the theory of geometric similarity between model and prototype devices can be achieved by keeping constant the tip speed ratio (i.e. the ratio of circumferential speed at the blade tip and wind speed upstream the rotor), by maintaining the same blade profile, number of blades and materials, as well as by adjusting proportionally all other dimensions (radius, profile chord, etc.) [523]. Main rules are summarized in Table 4.12. Therefore, by varying D with respect to the value selected for the reference OWT, P_{wind} varies and thus power curve may match better the wind speed distribution of the less productive sites leading to an increase in the associated AEP and CF. Note that these relations are approximations which are valid under specific assumptions [524], among which weight does not represent an issue for wind turbine blades and design parameters do not lead to Reynolds number, i.e. the ratio between inertial force and viscous force, less than 200000 [523].

In case of primary conversion in WEC, gravity and inertial forces are dominant and the effect of remaining forces such as kinematic viscosity is small, thus mechanical similarity is achieved by the Froude's scaling law between model and prototype devices [525]. The scaling factor λ based on Froude similitude can be defined as the ratio between characteristic length L of the device along which the machine absorbs the incoming wave energy (e.g. width of the ramp for an overtopping floating WEC, floater diameter in case of point absorber fixed WEC, length of WEC in case of attenuator, chamber width in case of oscillating water column [520]) which derives from the fact that by varying the capture width the output power changes, but the device's response keeps constant with the spread over the frequency range similar [526]. Then, P_{wave}, H_s, T_m and T_p parameters change according to the scale dependence illustrated in Table 4.12. By using these rules, original conversion matrix of the WEC design selected for the reference site can be scaled down according to the procedure described by O'Connor et al. [527] to assess the different ratings of the device at different wave climates.

Table 4.12. Example of main scaling rules based on scaling factor λ for OWTs and WECs at different sites [523,526].

		OWT ($\lambda = D_1/D_2$)	WEC ($\lambda = L_1/L_2$)
Parameter	Relation	Scale dependence	Scale dependence
Wind power P_{wind}	$P_{wind,1}/P_{wind,2}$	λ^2	
Rotational speed Ω	Ω_1/Ω_2	λ^{-1}	
Weight W	W_1/W_2	λ^3	
Wave power P_{wave}	$P_{wave,1}/P_{wave,2}$		$\lambda^{7/2}$
Significant wave height H_s	$H_{s,1}/H_{s,2}$		λ
Wave period T_m or T_p	$T_{m,1}/T_{m,2}$ or $T_{p,1}/T_{p,2}$		$\lambda^{1/2}$

Once identified the nominal power of the down-scaled devices, it is important to determine the number of converters needed to produce the benchmark nameplate capacity of the renewable plant assumed for the reference site.

Having calculated the real power and forecast power on an hourly basis, the curves can be matched over the selected period. It should be noted that the matching is specific for each offshore site, as well as for each forecast horizon selected in step 1. An example of combination of monthly P_r and P_f (estimated with forecast horizon of 6 h) for WEC at a given offshore site is illustrated in Figure 4.7. As evident from this figure, in several hours of the month there is a deviation between the real and forecast powers, which is important to quantify for the application of the following step of the procedure.

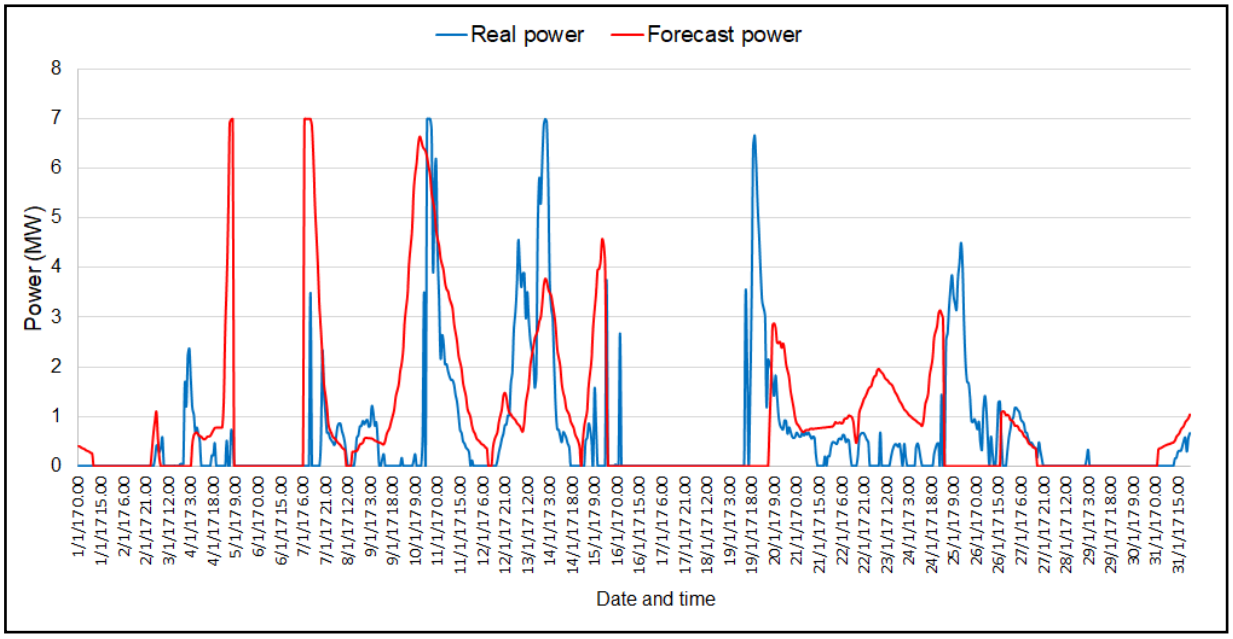

Figure 4.7. Example of monthly real power and forecast power (6 h horizon) from WEC at a given offshore site.

Having characterized the renewable plant from the technical point of view (power production), some economic parameters need to be collected for the sake of the economic performance assessment in this methodology. The required information is preliminary estimates of CAPEX and OPEX to the renewable plant, as described in Section 4.3. It should be noted that CAPEX and OPEX costs for grid connection of the renewable plant are usually shared in a different way among producer and Transmission System Operator (TSO) based on the cost approach applied at transmission grid level in a given country: according to the shallow cost approach Producer bears the cost to connect the plant to the closest connection point of the onshore grid, while he/she bears costs of all connections and grid reinforcement due to integration in the deep cost approach [18]. For a consistent economic comparison of different strategies, a reference currency and year should be set Therefore, if required, cost data retrieved from the literature can be adjusted by applying an annualized average conversion rate from actual currency to refence currency as well as a price index to account for inflation from a past year to reference year in Equation (4.1). Another important economic parameter to be collected for the application of this methodology is the electricity market price for renewable power depending on the pull mechanism adopted at national level for promotion of renewable energy integration, as described in Section 4.3.

For the purpose of the integration of non-programmable renewable power into the electrical grid, the producer is usually asked by local Energy Authorities, e.g. TSO, to declare the forecast power to be injected into the grid before the real injection. Thus, local TSO can perform some activities for good dispatching, e.g. planning reserve power generation required to offset unforeseen deviations between supply and demand, as well as quantifying balancing capacity reserves needed from utilities when supply is variable in order to cover unforeseen deficits (i.e. forecasting lower than injection) and surpluses (i.e. forecasting greater than injection) [528]. Based on the local regulations put in place to deal with grid integration and unbalances of renewable power, the producer may receive some incentives for participating on the market (i.e. when power injection is greater than the declared one), but he/she may pay economic penalties in case of negative power unbalances (i.e. when power injection is lower than the declared one) [229]. Therefore, for the purpose of the present methodology, prices established by local TSO for positive and negative power unbalances need to be collected. Such prices, commonly expressed in units of currency per MWh of power unbalance, are based on the local legislative framework on renewable integration into the grid and power unbalance mechanism. Clearly enough, eligibility requirements to these schemes should be verified case-by-case based on the local Regulation.

4.4.4. Step 3: Definition of dispatching power plan

In step 3 of the methodology, power prediction errors are analysed and used for definition of the dispatching plan to declare in view of the integration of renewable power into the grid. In order to limit

possible penalties imposed by TSO associated to incorrect declarations, the prediction error between the real injected power and forecast power should be estimated and minimized as much accurately as possible. To reduce the risk related to randomness of renewable energy source and foster the improvement of power predictions, a common principle is imposing to Producers a certain probability of being able to correctly produce the declared power (i.e. probability of correct dispatching, $Prob_d$), thus penalizing them only for injections which incur into an error higher than the allowable one with respect to forecast injections.

It is worth mentioning that power injections into the grid do not correspond to real power production at the offshore site due to different energy losses, among which inter-array losses (i.e. losses related to wake effects) and electrical losses (i.e. ohmic losses dissipated as heat in inter-array cables, export cables to shore and HVAC substation). Whereas, electrical losses vary with power plant layout, voltage levels, cable length and type of sub-station, as well as can fall under the responsibility of TSO or Producer based on the country's policy [20]. However, array losses can be generally reduced by optimizing the layout of the renewable plant, e.g. by means spacing between the devices. Moreover, HVAC cables (with maximum rating of about 200 MW per three-phase cable at voltage level of 150-170 kV and maximum distance of around 200 km) for which power losses increase significantly with cable length give relatively small losses if the distance between the offshore site and injection point is relatively small, i.e. 20-50 km, as in the case of G2P offshore hybrid energy solutions. Therefore, in the present methodology, a simplified assumption is made, i.e. produced power derived from real weather data in step 2 is approximated to the power injected into the grid. Under this hypothesis, the prediction error is calculated in step 3 of the procedure as follows:

$$\xi = P_r - P_f \tag{4.30}$$

where ξ is the absolute error between the real power and forecast power corresponding to the same hour over the period under analysis, P_r and P_f are the real and forecast powers, respectively, calculated in step 2 of the procedure for the renewable plant at a given site. As a matter of fact, ξ has negative value in case of production lower than the forecast quantity, otherwise it shows a positive value. It is worth noting that every set of ξ values is estimated for a given forecast horizon, given the definition of forecast power.

Once estimated, prediction errors are statistically analysed in order to quantify the power corresponding to a $Prob_d$ lower than 100%, i.e. the dispatched power (P_d), and match it with the corresponding P_r and P_f curves in a dispatching plan. A proper distribution can be selected to approximate the sample of ξ values for different intervals over the analysed period, i.e. for each month if the period of the analysis is one year. Commercial statistical tools can be used for the approximation, e.g. EasyFit software [529] allows to analyse easily errors data, provide the histogram of the errors and fit a large number of distributions. The choice of the best fitting is based on the analysis of specific accuracy parameters

provided from the tool for the different distributions. Moreover, probability density function (PFD) and cumulative distribution function (CDF) of the sample of data can be obtained from the statistical analysis for each distribution. Figure 4.8 and Figure 4.9 show examples of PDF and CDF, respectively, for the Cauchy distribution which fits the monthly ξ data referred to a forecast horizon of 6 h.

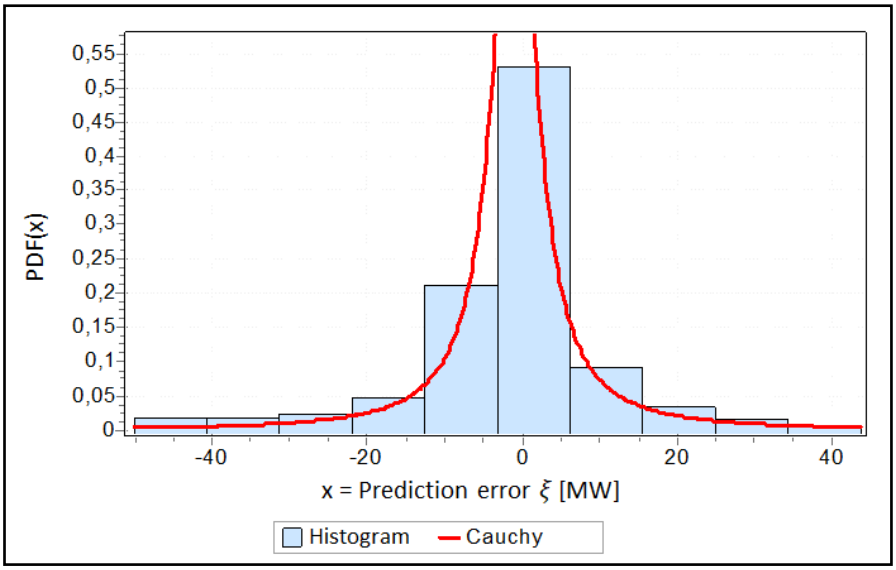

Figure 4.8. Example of PDF of monthly prediction errors (6 h forecast horizon) provided from EasyFit tool.

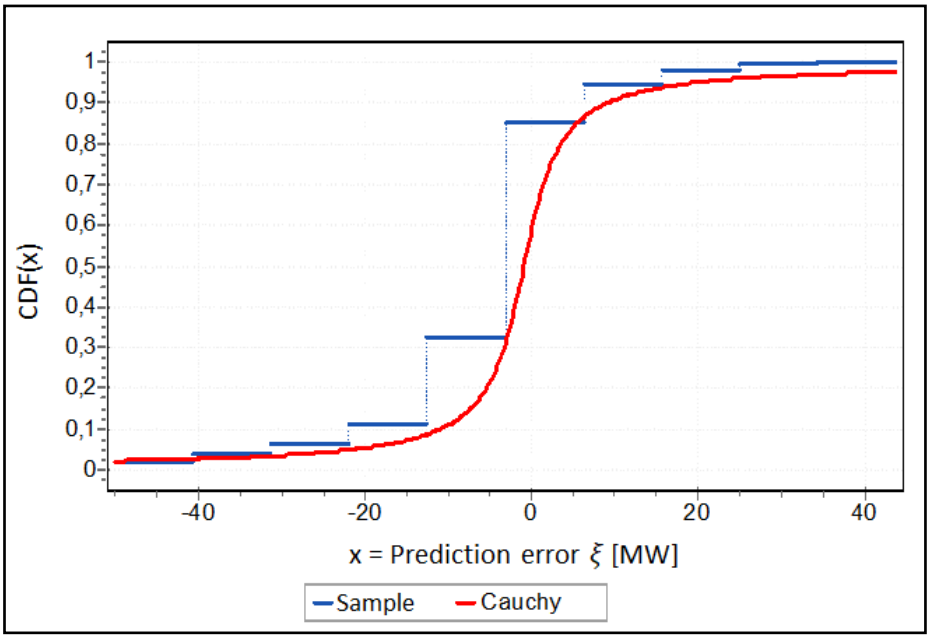

Figure 4.9. Example of CDF of monthly prediction errors (6 h forecast horizon) provided from EasyFit tool.

In order to define the dispatching plan, a given value of $Prob_d$ lower than 100% needs to be selected, as shown in Figure 4.4. Assuming a $Prob_d$ of 80% means that for 20% of the time the renewable energy source is not enough to produce the forecast power for injection into the grid [229]. Thus, P_d declared for injection into the grid is necessarily lower than the forecast power P_f and the available power between P_d and P_f is considered to be lost. The reduction of P_d with respect to P_f is called in the present methodology dispatching error and defined as follows:

$$\xi_d = P_d - P_f \tag{4.31}$$

where ξ_d is the dispatching absolute error between P_d and P_f at the same hour over the selected interval whose value should be negative, P_d and P_f are the dispatched and forecast powers, respectively. In the proposed method, ξ_d is calculated as the error corresponding to a cumulative probability of incorrect dispatching equal to 100% minus $Prob_d$, i.e. the probability that ξ is lower than or equal to the allowable ξ_d. Thus, the best CDF curve selected by means of the statistical tool for each sample of ξ is used to determine ξ_d for a given $Prob_d$. For example, if $Prob_d$ is considered as 80% and Cauchy CDF in Figure 4.9 is adopted for ξ data, the allowable ξ_d corresponding to a cumulative probability of incorrect dispatching of 20% (i.e. CDF equal to 20%) is equal to about -5.4 MW. Thus, the hourly P_d values can be estimated as a quantity of 5.4 MW lower than P_f values at the same hour by applying Equation (4.31), provided that the smallest possible value for P_d is 0.

It is worth noting that a given value of ξ_d is obtained for CDF curve of ξ values in a given time interval (e.g. one month) thus different ξ_d values correspond to different intervals of the period under analysis. Moreover, ξ_d strictly depends on the assumed $Prob_d$, thus P_d changes by varying $Prob_d$ while keeping the same forecast power P_f. An example of combination of monthly P_r, P_f (estimated with 3 h forecast horizon) and P_d (estimated with $Prob_d$ of 80%) for OWT at a given site is illustrated in Figure 4.10.

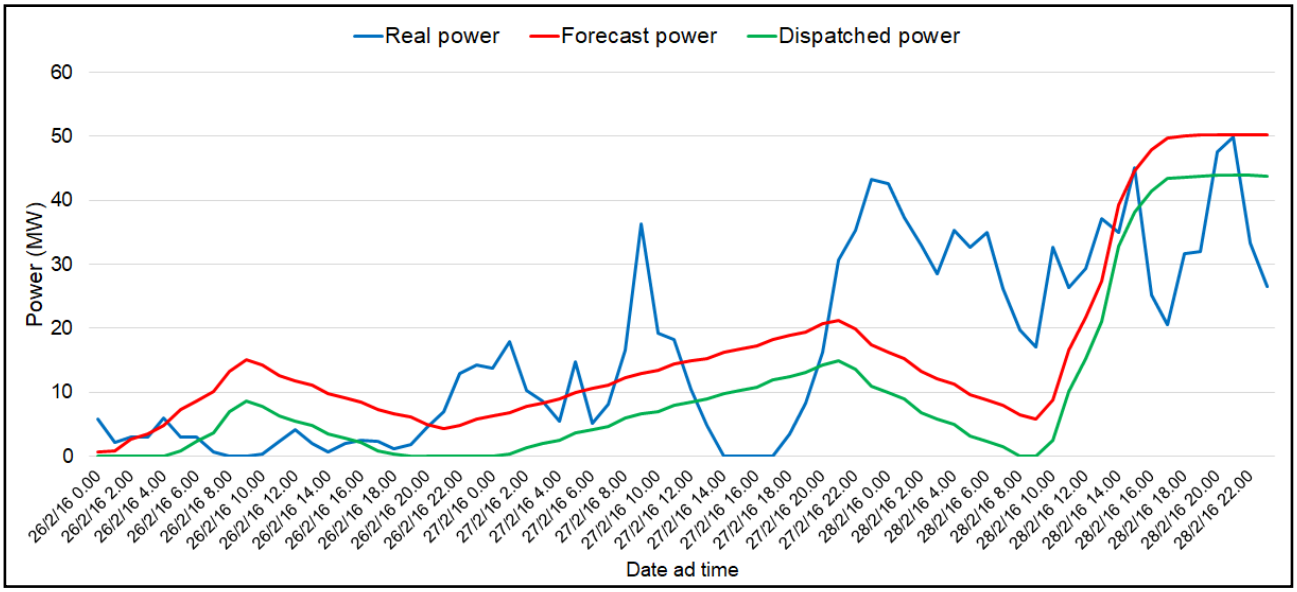

Figure 4.10. Example of monthly P_r, P_f (3 h horizon) and P_d (80% probability) from OWT at a given offshore site.

4.4.5. Step 4: Definition of the gas turbine park

GT introduced in Chapter 2 is the technology chosen in the present methodology as energy balancing system to apply the valley filling technique when P_r is not enough to satisfy the declared dispatching power plan, i.e. P_r is lower than P_d. The choice can be motivated due to simple installation, good ability to work at partial load, as well as suitability to be fuelled by raw natural gas without the need for gas conditioning and purification (dehydration, sweetening, removal of impurities) of GTs compared to other turbomachines. The purpose of the GT park in the G2P offshore hybrid energy system is dual: on one hand it allows to reduce the economic penalties which may be paid by producer to TSO for negative power unbalances; on the other hand, it provides extra power with respect to the renewable energy, which can be sold to the electric grid increasing the revenue for producer. In addition, the GT park allows the monetization of the stranded and depleted gas fields located relatively close to the shore. However, it is worth mentioning that this conventional energy technology produces GHG emissions into the atmosphere and associated economic penalties. Due to the coupling with the offshore renewable power plant, the GT park is unavoidably characterized by lower energy efficiency than the nominal one due to its operation at partial load and during some hours of the considered time interval.

In step 4 of the procedure, the size of the GT park is estimated by considering the maximum power which could be provided from the turbomachines ($P_{GT,max}$) in the analysed period, i.e. when $Prob_d$ is equal to 100% and thus P_f corresponds to P_d at each hour. Given the function of GTs, $P_{GT,max}$ can be evaluated only during the hours at which P_r is lower than P_f as the difference between the hourly P_f and P_r at the

same hour. Figure 4.11 shows an example of matching between the real power and forecast power from WEC calculated for an interval of few days in a month: hourly $P_{GT,max}$ is represented by means of the yellow bars in the figure, while greys bars in the figure are the hourly power surpluses when P_r is greater than P_f and GTs are not intended to work.

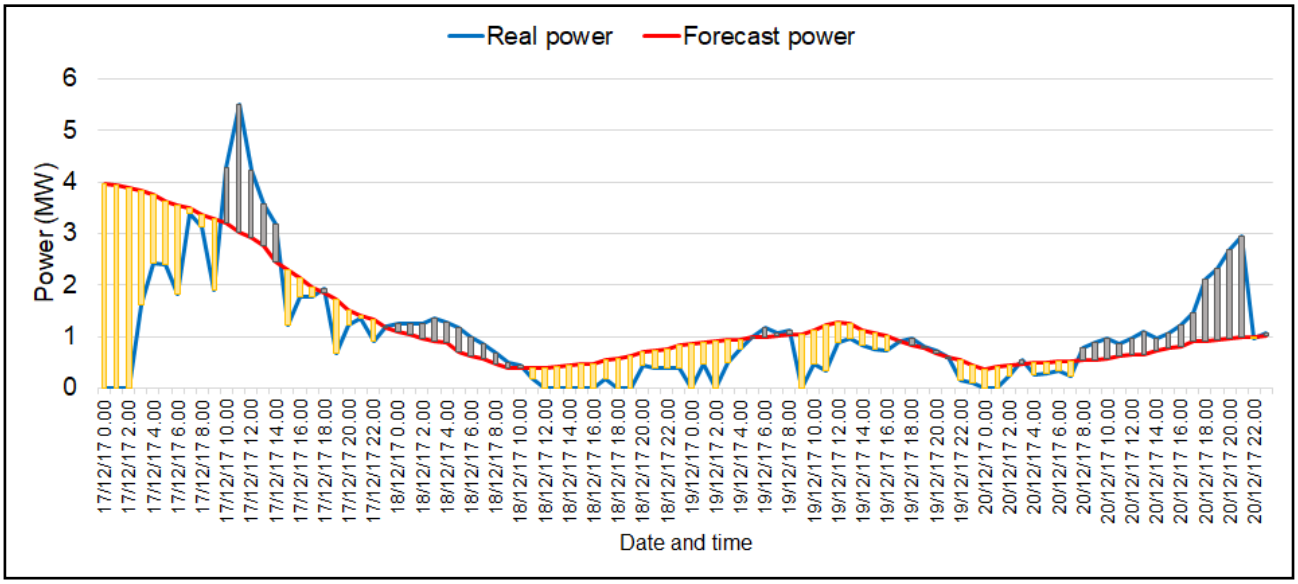

Figure 4.11. Example of estimation of maximum power which could be provided from GTs coupled with WEC for a given interval.

It is recommended to calculate $P_{GT,max}$ for the same intervals at which ξ_d values are estimated in step 3. Then, the final size of the GT park is conservatively assumed in the present methodology as the highest $P_{GT,max}$ occurred among the values calculated for different intervals, i.e. the maximum $P_{GT,max}$ over the entire period of the analysis. It is worth noting that the size of the GT park is strictly related to the forecast horizon selected for P_f, thus different capacities may be derived by varying the horizon. Moreover, when different offshore sites are evaluated at the same the interval, different sizes of the GT park are obtained correspondingly due to different trend of both real and forecast power curves.

As the size of the GT park has been identified, it is necessary to select the equipment model to install at the offshore site by taking into account the nominal power and footprint of single machines. When different offshore sites are evaluated, the same GT model should be selected for a consistent comparison. Among the GTs typologies described in Chapter 2, compact and light-weight aeroderivative GTs are ideally suited for power generation at offshore platform in the low-medium range (4-66 MW), while micro GTs are the common option for small capacity (lower than 1 MW). After the selection, the nominal power at full load ($P_{GT,nom}$), nominal efficiency at full load ($\eta_{GT,nom}$) and dimensions of the machine are noted. The total number of GTs ($N_{GT,tot}$) needed to reach with their single nominal capacity the identified size

of the park is calculated and then total footprint of the park is derived. This latter parameter can be compared with the available free space in the offshore structure (Table 4.11).

4.4.6. Step 5: Management and characterization of gas turbine park

In step 5 of the methodology, the suitable part-load control strategy for the GT park designed in the previous step needs to be defined. When there is a certain number of machines operating at part-load, the electrical efficiency of the park tends to decrease with respect to the efficiency at full load ($\eta_{GT,nom}$) leading to the so-called part-load efficiency (η_{GT}). The efficiency reduction at part-load can be expressed as function of the part-load ratio depending on the category of GT. For aeroderivative GTs, the following correlation proposed in the literature [229] is used in the present methodology:

$$\frac{\eta_{GT}}{\eta_{GT,nom}} = 0.7035 \cdot \left(\frac{P_{GT}}{P_{GT,nom}}\right)^3 - 1.91151 \cdot \left(\frac{P_{GT}}{P_{GT,nom}}\right)^2 + 2.0642 \cdot \left(\frac{P_{GT}}{P_{GT,nom}}\right) + 0.1481 \quad (4.32)$$

For micro GTs, a proper correlation is derived in the present work by regressing the part load efficiency curve of commercial micro GTs by Capstone Turbine Corporation (C800 and C330 models) [225,530], expressed as follows:

$$\frac{\eta_{GT}}{\eta_{GT,nom}} = 2.1812 \cdot \left(\frac{P_{GT}}{P_{GT,nom}}\right)^3 - 4.6655 \cdot \left(\frac{P_{GT}}{P_{GT,nom}}\right)^2 + 3.4475 \cdot \left(\frac{P_{GT}}{P_{GT,nom}}\right) + 0.0584 \quad (4.33)$$

In both Equations (4.32) and (4.33), η_{GT} is the part-load efficiency, $\eta_{GT,nom}$ is the efficiency of at full load (i.e. the nominal efficiency), P_{GT} is the power produced at part-load, $P_{GT,nom}$ is the power produced at full load (i.e. the nominal power).

The average efficiency of the entire park at part-load relies on the number of GTs in operation and their part-load, provided that keeping in operation the minimum number of turbines to produce the required power may lead the highest average load (i.e. highest average efficiency) and the lowest number of maintenance hours and costs. Among possible control strategies proposed in the literature for GTs [531–535], the approach suggested by Guandalini et al. [229] is adopted in the present work, which consists in managing each GT of the park in parallel at the same part-load. Starting from the full-load condition of the park, i.e. when every machine is operating at its nominal power ($P_{GT,1,nom}$), if the load decreases all the machines reduce equally their load up to the condition at which one machine can be switched-off and all remaining machines return to operate with their $P_{GT,1,nom}$. After a further decrease of the load, these machines reduce again their load up to the condition at which a second machine can be switched-off and the remaining machines return to operate at full load. This procedure proceeds until one sole machine works in the system before reaching its minimum technical load. It is worth noting that a minimum allowable load is set for GTs, i.e. 50% of the nominal load in order to meet the environmental limits on

CO and NO_x commonly imposed in the technical specifications. In the following, an example of the application of such an approach to some hours of a day is described by using Table 4.13 as support.

Table 4.13. Example of estimation of hourly part-load efficiency of the GT park.

Hour	P_r (MW)	P_f - 6 h horizon (MW)	$P_{GT,max}$ (MW)	P_d – 80% $Prob_d$ (MW)	$P_{GT,eff}$ (MW)	N_{GT}	P_{GT} (MW)	$P_{GT}/P_{GT,nom}$	$\eta_{GT}/\eta_{GT,nom}$	η_{GT}
16:00	8.3	47.2	38.9	36.8	28.5	5	28.5	55%	82%	26%
17:00	16.2	49.3	33.0	38.8	22.6	4	22.6	43%	74%	24%
18:00	30.6	49.8	19.2	39.3	8.7	2	8.7	17%	44%	14%
19:00	35.4	50.0	14.6	39.5	4.1	1	4.1	8%	30%	10%
20:00	43.3	50.2	6.9	39.8	-	-	-	-	-	-
21:00	42.7	50.3	7.6	39.8	-	-	-	-	-	-
22:00	37.3	50.2	12.9	39.5	2.5	-	-	-	-	-

Since a $Prob_d$ less than 100% has been defined in step 2, the effective power which should be provided by the GT park to satisfy the defined dispatching plan ($P_{GT,eff}$) for a given hour is lower than the corresponding $P_{GT,max}$ identified in step 4. $P_{GT,eff}$ can be estimated only during the hours at which P_r is less than P_d as the difference between the hourly P_d and P_r at the same hour. As shown in Table 4.13, $P_{GT,max}$ is required at all the hours displayed because P_r is lower than P_f, while $P_{GT,eff}$ shows a value only in case of 5 out of 7 hours (i.e. when P_r is lower than P_d).

Having estimated the need for a GT park with total capacity of 52.2 MW and $N_{GT,tot}$ equal to 9 aeroderivative turbines (each one with single nominal capacity $P_{GT,1,nom}$ of 5.8 MW and nominal efficiency $\eta_{GT,nom}$ of 32.2%), it is possible to define the power corresponding to the switch-off point including the number of remaining turbines in operation and their part-load power range, according to the approach described above. Table 4.14 summarizes these data.

Table 4.14. Example of power ranges for operating GTs in the part-load control strategy.

Number of operating turbines N_{GT}	Power for turbine switch-off (MW)	Power range for operating turbines before the next switch-off (MW)
9	52.2	$46.4 < P_{GT} \leq 52.2$
8	46.4	$40.6 < P_{GT} \leq 46.4$
7	40.6	$34.8 < P_{GT} \leq 40.6$
6	34.8	$29.0 < P_{GT} \leq 34.8$
5	29.0	$23.2 < P_{GT} \leq 29.0$
4	23.2	$17.4 < P_{GT} \leq 23.2$
3	17.4	$11.6 < P_{GT} \leq 17.4$
2	11.6	$5.8 < P_{GT} \leq 11.6$
1	5.8	$2.9 < P_{GT} \leq 5.8$
0	2.9	-

As shown in Table 4.14, the GT park can operate from its nominal capacity $P_{GT,nom}$ of 52.2 MW to the minimum allowable load limit equal to 50% of $P_{GT,1,nom}$ (i.e. 2.9 MW). At 52.2 MW all nine machines operate at full load. For power lower than 52.2 MW, the nine machines operate in parallel at the same part-load until switching-off one of them and operating the other eight machines at full load for a total power of 46.4 MW, which is the power corresponding to the first switch-off. Thus, the power range for operation of 9 machines at the same part-load before the switch-off is 46.4-52.2 MW. This procedure is applied to determine other P_{GT} ranges of operating turbines, whose values are illustrated in the table. From these data, the number of operating turbines N_{GT} required to supply $P_{GT,eff}$ at the hours of interest can be estimated, as shown in Table 4.13. The hourly powers supplied by the operating turbines (P_{GT}) are then reported. No turbine operates in case of hour 22:00 since $P_{GT,eff}$ is below the minimum load limit for the park of 2.9 MW, thus P_{GT} is zero at this hour and the quantity corresponds to the negative unbalance power for which Producer may pay an economic penalty to TSO. After that, the hourly ratio $P_{GT}/P_{GT,nom}$ can be calculated and corresponding hourly ratio $\eta_{GT}/\eta_{GT,nom}$ can be derived by application of Equation (4.32). Given $\eta_{GT,nom}$, hourly η_{GT} values of the GT park are then evaluated.

In view of the technical performance assessment in step 6 of the procedure, in addition to the power produced from the GT park during the operating hours, the hourly fuel input power (P_{fuel}) is required resulting from the fuel (natural gas) combustion in GTs. P_{fuel} can be calculated based on the hourly P_{GT} and η_{GT} values. Table 4.15 summarizes the results based on the example above reported. Hourly P_{fuel} can be obtained as ratio of P_{GT} to η_{GT} at each hour, thus fuel input power occurs only during the hours at which GTs effectively operate under the defined control strategy.

Table 4.15. Example of estimation of hourly fuel consumption and CO_2 emissions of the GT park.

Hour	P_{GT} (MW)	η_{GT} (%)	P_{fuel} (MW)	$e_{GHG,GT}$ (kg_{CO2eq})
16:00	28.5	26%	107.9	21796
17:00	22.6	24%	94.7	19130
18:00	8.7	14%	61.1	12350
19:00	4.1	10%	42.8	8639
20:00	-	-	-	-
21:00	-	-	-	-
22:00	-	-	-	-

Moreover, for the sake of the environmental assessment, GHG emissions from the GT park are required, provided that emissions from the renewable power plant can be neglected as mentioned in the description of step 2. Hourly emissions ($e_{GHG,GT}$), commonly expressed in units of CO_2eq for a given period can be evaluated from P_{fuel} values estimated at the same hours by assuming a typical emission factor per unit of fuel (natural gas) power. For example, typical emission factor values are 202 kg/MWh_{fuel} in case of

aeroderivative GTs [229] and 185 kg/MWh_{fuel} in case of micro GTs [230,536]. Referring to the example above mentioned, $e_{GHG,GT}$ values from aeroderivative turbines in the considered period are reported in Table 4.15.

For the economic evaluation in the following step of the procedure, CAPEX and OPEX associated to the GT plant. Example of costs data for aeroderivative and micro GTs which may be used for application of the present methodology is available in the literature [230,474,537]. Equation (4.1) may be applied to adjust the economic data. Furthermore, in view of the integration of hybrid energy system into the grid, price associated to the selling of conventional electricity to the grid is needed for the analysis. It should be noted that they rely upon the time interval and local market considered in the analysis. The wholesale market electricity prices, commonly expressed in units of currency per MWh, may be retrieved from available statistical trends at national level over the desired period and associated to conventional electrical power produced from the GT park.

Finally, the last information required for economic analysis is the price associated to GHG emissions from the GT plant, which may be a carbon allowance total direct GHG emissions from specific sectors in a cap-and-trade system (e.g. emission trading scheme or ETS) or a pre-defined carbon tax on GHG emissions based on the policy adopted by local Government to reduce carbon emissions [538]. Information about the regional, national and subnational carbon pricing initiatives implemented, scheduled and under considerations, including the associated prices, is published every year by World Bank [539].

4.4.7. Step 6: Calculation of sustainability indicators for the hybrid energy system

In the final step of the methodology (step 6), the sustainability performance of the G2P hybrid energy system at the offshore site are assessed by using the information derived from the previous steps and calculating a set of indicators addressing technical, economic, environmental and societal aspects. The set is adapted from the indicators defined in the sustainability assessment model for P2G and P2L hybrid energy option in Section 4.3, with the aims to capture in a concise yet representative way specific features of G2P offshore hybrid energy systems. Clearly enough, the set is open to the addition of further indicators in view of an improved assessment.

4.4.7.1. Technical performance assessment

Compared to the technical indicators defined in the sustainability model in Section 4.3, one sole indicator is proposed in this methodology for assessing the technical performance of the G2P hybrid energy system:

$$\eta_{el} = \frac{\sum_{t=1}^{T}(P_{r,t} + P_{GT,t})}{\sum_{t=1}^{T}(P_{renew,avail,t} + P_{fuel,t})} \tag{4.34}$$

where η_{el} is the electrical efficiency of the offshore hybrid energy system, P_r is the hourly real power produced from the renewable plant estimated in step 2, P_{GT} is the hourly power supplied by the GT park estimated in step 5, $P_{renew,avail}$ is the hourly available renewable power estimated in step 1, P_{fuel} is the hourly fuel consumption of the GT park calculated in step 5, "*t*" in pedix is the hour at which parameters are evaluated over the entire period of the analysis T. It is worth mentioning that energy losses occurring inter-array cables and export cable are neglected for calculation of Equation (4.34). P_{GT} and P_{fuel} give a contribution only during the hours at which the GT park operates under the control strategy defined in step 5. Given the definition of the proposed indicator, the higher η_{el}, the higher technical performance of the hybrid energy system.

4.4.7.2. Economic performance assessment

Similar to the economic indicators defined in the sustainability model in Section 4.3, two indicators are proposed in the present methodology, i.e. the levelized cost of energy (LCOE) and the levelized value of energy (LVOE), by revising the definition of such standard economic metrics for power generation systems given in the literature [540]. All these parameters are expressed in units of currency per MWh of total electrical power produced from the hybrid energy system and intended for grid injection.

LCOE is defined for the hybrid energy system as follows:

$$LCOE = \frac{CAPEX_{renew} + CAPEX_{GT} + \sum_{t=1}^{T}\left(\frac{OPEX_{renew,t} + OPEX_{GT,t}}{(1+\frac{r}{m})^{m}}\right)}{\sum_{t=1}^{T}\left(\frac{P_{r,t} + P_{GT,t}}{(1+\frac{r}{m})^{m}}\right)} \tag{4.35}$$

where CAPEX in units of currency is the capital expenditure associated to the renewable plant and GT park, OPEX is the operational expenditure in units of currency per hour evaluated at t-th hour over the analysed interval for the renewable plant and GT park, P_r and P_{GT} are the hourly powers defined in Equation (4.34), "*t*" in pedix is the hour at which parameters are evaluated over the entire period of the analysis, T is the total number of the hours in the period of the analysis, r is the discount rate referred to the period T and m is the number of hours in this period. As opposed to η_{el}, the lower LCOE, the higher economic performance of the hybrid energy system from the costs viewpoint.

On the other hand, LVOE is calculated as follows:

$$LVOE = \frac{\sum_{t=1}^{T}\left(\frac{R_{sell,t} + R_{unb+,t} - C_{unb-,t} - Ce_{GHG}}{(1+\frac{r}{m})^{m}}\right)}{\sum_{t=1}^{T}\left(\frac{P_{r,t} + P_{GT,t}}{(1+\frac{r}{m})^{m}}\right)} \tag{4.36}$$

where R_{sell} is the revenue gained at t-th hour of the analysed period from electrical power selling to the grid, R_{unb+} is the revenue gained at t-th hour of the analysed period due to positive unbalance of the produced power P_r with respect to declared P_d in the dispatching plan, C_{unb-} is the cost paid at t-th hour of the analysed period due to negative unbalance of the produced power P_r with respect to declared P_d which are not covered by the GT plant, $C_{e_{GHG}}$ is the hourly cost associated to GHG emissions from the GT park, P_r and P_{GT} are the hourly powers defined in Equation (4.34), "t" in pedix is the hour at which parameters are evaluated over the entire period of the analysis T, r is the discount rate referred to the period T and m is the number of hours in that period.

R_{sell} at t-th hour in Equation (4.36) can be defined as follows:

$$R_{sell,t} = Price_{el,conv} \cdot P_{GT,t} + Price_{el,renew} \cdot P_{r,t} \quad (4.37)$$

where $Price_{el,conv}$ is the price in units of currency per MWh of conventional electrical power, P_r and P_{GT} are the hourly powers defined in Equation (4.34), $Price_{el,renew}$ is the price in units of currency per MWh of renewable electrical power based on the national pull mechanism.

Hourly R_{unb+} and C_{unb-} in Equation (4.36) are calculated as:

$$R_{unb+,t} = Price_{unb+} \cdot P_{unb+,t} \quad (4.38)$$

$$C_{unb-,t} = Price_{unb-} \cdot P_{unb-,t} \quad (4.39)$$

where $Price_{unb+}$ and $Price_{unb-}$ are the prices in units of currency per MWh of positive and negative unbalances, respectively, collected in step 2, P_{unb+} is the hourly positive unbalance occurring when P_r is greater than P_d estimated once defined the dispatching plan in step 3 , P_{unb-} is hourly negative unbalance occurring when P_r is lower than P_d and GTs cannot operate due to technical minimum load limit which can be estimated once defined the management of the GT park in step 5.

C_{GHG} at t-th hour in Equation (4.36) is estimated as:

$$C_{GHG} = Price_{GHG} \cdot e_{GHG,GT,t} \quad (4.40)$$

where $Price_{GHG}$ is the price in units of currency per mass of CO_2eq emissions, $e_{GHG,GT}$ are the hourly GHG emissions from the GT park.

4.4.7.3. Environmental performance assessment

Similar to the environmental indicator defined in sustainability model in Section 4.3, LGHG quantifying GHG emissions from the GT park divided by the total energy production over the analysed period is proposed in this methodology:

$$LGHG = \frac{\sum_{t=1}^{T} e_{GHG,GT,t}}{\sum_{t=1}^{T}(P_{r,t} + P_{GT,t})} \quad (4.41)$$

where $e_{GHG,GT}$ are the hourly GHG emissions from the GT park calculated in step 5, P_r and P_{GT} are the hourly powers defined in Equation (4.34), "t" in pedix is the hour at which parameters are evaluated over the entire period of the analysis, T is the total number of hours in the analysed period. Similar to LCOE, the lower LGHG, the higher environmental performance of the hybrid energy system.

4.4.7.4. Societal performance assessment

As discussed in the sustainability model in Section 4.3, the societal dimension of sustainability is preliminarily disregarded also in the description of this methodology. Throughout the present chapter (Section 4.5), some safety-related indicators which may be used to address this aspect of sustainability are defined.

4.4.7.5. Aggregated performance assessment

The indicators defined above allow the assessment of different aspects of sustainability. In order to quantify and communicate the overall performance of the system, aggregation of the indicators into a single-value metrics is recommended.

The compensatory aggregation approach presented in the sustainability assessment methodology in Section 4.3 is proposed in the present method, since alternative G2P offshore hybrid energy systems producing the same product, i.e. renewable and conventional electricity for grid applications, are compared. Therefore, normalization based on proper references target values, weighting based time-space-receptor criteria and individualist-egalitarian-hierarchist perspectives, and aggregation based on WAM and WGM methods are applied in order to calculate ASI indicator defined in Equation (4.18) or Equation (4.19) for each system under analysis. The details of these stages and related considerations are described in sub-Section 4.3.4.5. For the sake of the present model, target values for normalization of disaggregated indicators are intended to be reference values for the power generation technology, e.g. measures of the expected performance of the renewable energy plant in the near- or long-term future provided from projections available in the relevant literature.

4.4.8. Step 7: Ranking of alternatives and sensitivity analysis

The calculation of the indicators in the previous step allows to compare and rank different G2P offshore hybrid energy systems at a given site or the same G2P offshore hybrid energy system at different locations. The ranking can be performed from the viewpoint of different aspects (e.g. technical, economic,

environmental) and overall profile of sustainability. The considerations presented for sensitivity analysis in the sustainability model of Section 4.3 can be applied also in this method.

4.5. Inherent safety assessment methodology

In this section, the inherent safety assessment methodology proposed for P2G/P2L/G2P offshore hybrid energy options is described. An overview of the method, including details of the steps and proposed performance indicators are presented in the following paragraphs.

4.5.1. Overview of the method

Given the literature review reported in Chapter 3 (Sections 3.3 and 3.4), a systematic methodology is defined in this study assessing the inherent safety performance of offshore facilities where hazardous materials (chemicals, oil, natural gas) are present. A specific set of inherent safety and environmental protection KPIs is proposed based on consequences of potential accident scenarios with respect to different targets of concern in offshore oil & gas production installations, i.e. humans, assets and the marine environment. The method evaluates and ranks the different hazard sources, also considering the specific features of offshore facilities (multi-layer layout, high congestion, etc.). Moreover, it provides a database of references (e.g. specific classification of oil & gas process units, generic event trees of surface and subsea releases, typical credit factors of equipment releases), which ease its application in the early phase of the design.

The proposed multi-target methodology can be used to compare the inherent safety performance of alternative designs of P2G/P2L/G2P offshore hybrid energy options at offshore oil & gas production sites. It is intended to be an efficient support tool to orient inherent safety-oriented choices by ranking units of the option and entire scheme for further detailed assessment (risk assessment and management of change). The method is suitable to complement with its safety focus the technical, economic and environmental considerations of sustainability, thus providing some metrics to address the societal aspect of the assessment models described in Sections 4.3 and 4.4.

The flow chart of the methodology is illustrated in Figure 4.12. The first step of the method (step 0) encompasses the definition of the design options and characterization of the potential targets of interest. In the following steps (from 1 to 7), each design option is assessed separately. The single equipment units are classified and match with suitable release modes and credit factors. Next, event trees are associated to each release mode and damage parameters are estimated for each accident scenario by using well-known consequence simulation models. Finally, a set of inherent safety indicators is calculated for each unit and for the overall facility addressing specific targets of concern. Aggregated multi-target indicators are

obtained by means of normalization and weighting strategies. All these steps are described in detail in the following paragraphs.

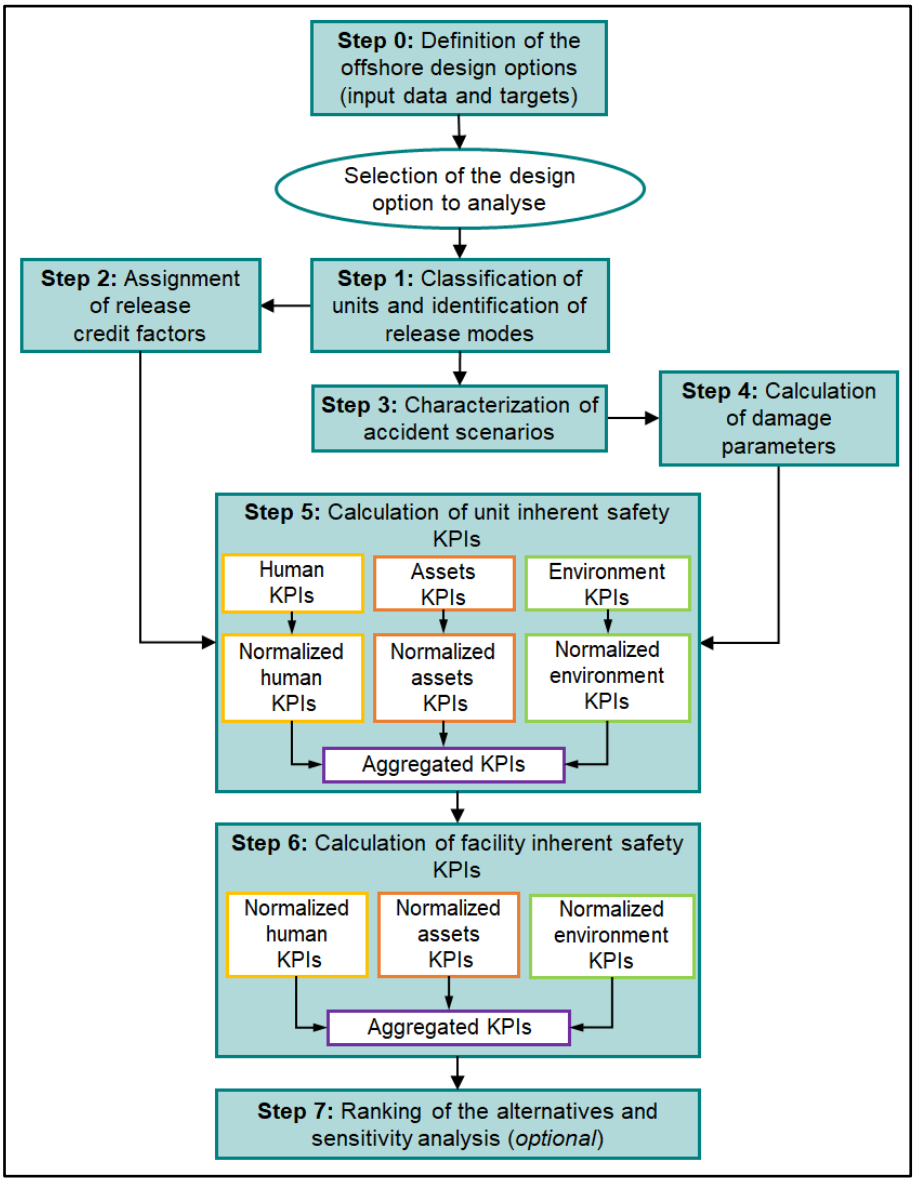

Figure 4.12. Flow chart of the inherent safety assessment model for P2G and P2L offshore hybrid energy options.

4.5.2. Step 0: Definition of design options and characterization of targets

The definition of process design options to be analysed is performed in step 0 by collecting specific input data summarized in Table 4.16. They consist of preliminary information about process and utilities, general layout and dimensions of the installation, equipment units and environmental conditions at the offshore location.

Table 4.16. Input data required for the inherent safety assessment methodology.

Data about the process, utilities and equipment	
a)	Materials (substances, composition, dangerous properties, physical properties, i.e. °API in case of oil), operating conditions (pressure, temperature), nominal flowrates, inventories
b)	General plant specifications (pipework diameter, main dimensions of the equipment units)
c)	Piping and Instrumentation Diagram (P&ID), if present
Data about the installation	
d)	Characteristics of the offshore structure (fixed/floating, manned/unmanned)
e)	Preliminary layout, dimensions, elevation (deck) of each equipment unit
Data about the environment	
f)	Meteo-marine parameters (water depth, average values of air temperature, sea surface temperature, wind speed, currents speed)
g)	Ships approaching the installation (supply vessel, shuttle tanker, work vessel, authority ship)

Since a multi-target approach is developed, in step 0 potential targets should be identified based on the input data collected, and then characterized. In the present methodology, three categories of potential targets from a major accident are identified for offshore installations: humans, assets and the marine environment.

Human targets in offshore context are found both on the decks of the installation (e.g. personnel involved in processing and/or maintenance operations) and on board of marine vessels approaching the facility.

Asset targets can be divided into three main sub-categories. The first includes process and utility equipment containing hazardous material, whose damage may trigger secondary scenarios with potential accident escalation (i.e. domino accidents) [541,542]. The second asset sub-category contains all structural elements of the installation (e.g. legs, columns, beams and other critical component) whose damage may result in partial or total collapse of the structure, while the third sub-category groups the hulls of supply vessels.

Environmental targets includes marine organisms which may be damaged in the different environmental compartments (sea surface, water column, seafloor, shoreline) based on the type of fluid released (oil, diesel, and chemicals such as glycol and CH_3OH). The air compartment of the environment is typically not of concern in the assessment of offshore accidental releases, due to the rapid dilution of vapour and gas phases into the atmosphere [543].

Oil spills can cause a damage to all four compartments, as proved by the review analysis of past accidents. However, in case of loss of containment events occurring at open sea, the sea surface and the water column are the first to be affected by oil [544]. As soon as oil is released, it starts immediately to spread over the sea surface creating a slick which causes damage to the organisms living in the proximity of the sea surface, particularly in case of high viscosity and low volatile oils (i.e. persistent slicks). In the water column, oil enters the upper layers of the sea in the form of suspended droplets, as well as dissolved oil

compounds. The environmental damage of this compartment tends to be attributed only to the dissolved oil fraction and is usually limited to a small extent due to the positive effect of the currents on the dilution of the extremely small fraction of hydrosoluble oil molecules which dissolve in water. The contamination of the seafloor occurs when oil droplets dispersed in the water column interact with the particles suspended in water, thus leading to aggregates which sink slowly down to the seabed. Sedimentation mainly occurs along coastal zones with shallow waters where particulate is abundant, and water is subjected to intense mixing [545]. As the oil slick and droplets in the contaminated water column are moved simultaneously by wind and currents, spilled oil has the potential to reach the shore and the low-depth seabed in front of it [546]. Therefore, seafloor and shoreline pollution can be considered as secondary processes in case of open sea spills. Overall, sea surface is considered in the present methodology as the main environmental compartment for the quantification of the consequences of oil spills, because this is the first compartment to be impacted by the oil and the one from which the contamination of the other compartments begins.

On the other hand, as demonstrated by the review analysis of past chemical spills, water column is considered as the sole environmental compartment which may be polluted by spills of completely hydrosoluble chemicals.

As a result, two sub-categories of targets are considered in this study as the environmental targets, i.e. sea surface compartment polluted by oil spills and water column compartment damaged by releases of soluble chemicals.

Once the targets have been defined, a reference damage threshold should be assumed for each critical target in order to characterize the extent of the effects of potential accident scenarios in the following step of the procedure. Table 4.17 shows an example of threshold values proposed for the application of the present approach. Clearly enough, different thresholds may be considered depending on the framework of application and on the presence of specific requirements deriving e.g. from applicable technical standards or legislation.

Table 4.17. Threshold values of accident scenarios proposed in the inherent safety assessment model for each target.

Accident scenario and related effect	Target					
	Humans	Assets (Process and utility equipment)	Assets (Facility structures)	Assets (Marine structures)	Marine environment (sea surface)	Marine environment (water column)
Flash fire - transient radiation	½ Lower Flammability Limit (LFL), %vol	*n.c.*	*n.c.*	*n.c.*	-	-
Fireball - transient radiation	7 kW/m^2	15^a – 50^b kW/m^2	100 kW/m^2	100 kW/m^2	-	-
Jet fire - stationary radiation	7 kW/m^2	15^a – 50^b kW/m^2	100 kW/m^2	100 kW/m^2	-	-
Pool fire - stationary radiation	7 kW/m^2	15^a – 50^b kW/m^2	100 kW/m^2	100 kW/m^2	-	-
Vapour Cloud Explosion (VCE) - overpressure	0.14 barg	0.16^b – 0.22^a barg	0.50 barg	0.30 barg	-	-
Physical/mechanical explosion - overpressure	0.14 barg	0.16^b – 0.22^a barg	0.50 barg	0.30 barg	-	-
Toxic cloud in atmosphere - toxic concentration	Immediately Dangerous to Life and Health (IDLH), ppm	-	-	-	-	-
Ecotoxic dissolved volume (hydrosoluble chemicals) - ecotoxic concentration	-	-	-	-	-	Predicted No Effect Concentration (PNEC) in marine water, mg/L
Ecotoxic floating slick (oil) – slick thickness	-	-	-	-	Thickness for lethal dose to organisms, μm	

Apex “a”: atmospheric target equipment; apex “b” pressurized target equipment. *n.c.* stands for not applicable.

Thresholds for human targets are based on technical documents as representing 1% probability of irreversible effects on individuals exposed to fire, explosion and toxic release [547–550].

Domino escalation thresholds for offshore process and utility equipment are based on previous work by Cozzani et al. [551,552]. For other assets categories, heat load and blast overpressure proposed for design of offshore structures are selected on the basis of relevant technical report and standards [547,553]. Toxic effects are not of concern for this target category.

With respect to the pollution of marine environment, the damage to the ecosystems may be caused by different environmental stress mechanisms (e.g. chemical stress, physical stress, particulate stress of droplets, burial stress, etc.) on the relevant environmental compartment [554]. The present methodology focuses on the chemical stressor (eco-toxicity), as it is closely related to the accidental releases and can affect all the considered compartments. In case of pollution of sea surface due to oil spills, the thickness of the floating slick causing lethal damage of seabirds, dolphins, sea otters, sea bears and other mammals living on the sea surface [555] is assumed as the threshold value. The most obvious impact of oil on these organisms is the fouling of their plumage or fur or skin, causing the loss of the insulation properties of their outer protective layer and thus their death by hypothermia [451]. On the other hand, PNEC of the chemical compound on sea birds, fishes, sea plants during long term or short term exposure [469,554,556,557] is conservatively assumed as the limit value for environmental pollution of water column due to chemicals dissolution.

As the different targets can be present in different spatial zones around the facility, it is not possible to directly compare the KPIs related to different target categories. Thus, a normalization based on the characterization of the spatial zones where the targets are present (i.e. vulnerability zones for a target) will be used in steps 5 and 6 of the procedure illustrated in Figure 4.12. The plan view area of the vulnerability zone will be used as normalization factor, which is the "yardstick" for defining the relative magnitude of the potential accident scenarios in the normalization process. Table 4.18 reports examples of these area for each target of concern.

Table 4.18. Reference vulnerability areas proposed in the inherent safety assessment model for each target of concern.

Target	Humans	Assets (Process and utility equipment)	Assets (Facility structures)	Assets (Marine structures)	Marine environment
Vulnerability area (m^2)	Plan view area of the topside (*case-specific*)	Plan view area of the topside (*case-specific*)	Plan view area of the topside (*case-specific*)	Circle area of the safety zone (500 m radius)	Circle area of the safety zone (500 m radius)

As shown in Table 4.18, the plan view area of the topside is proposed for human targets, process and utility equipment and facility structures. On the other hand, for marine assets structures and marine environment targets, the 500 m radius safety zone around the installation established by European Authorities for ship/installation collision avoidance [72,558–560] is suggested as impact area. It must be remarked that in case of sea surface compartment polluted by oil spills, the impact area may be covered several orders of magnitudes. As a consequence, the estimation of normalization factor seems to be more complex than the other targets and cannot ignore the definition of case studies. Nevertheless, the circle area of the safety zone (or at most multiples of it) can be preliminarily assumed as first try for the purpose of normalization.

4.5.3. Step 1: Classification of units and identification of release modes

As shown in Figure 4.12, the starting point for the application of the procedure is the identification of equipment units and assignment of release modes for each offshore design option selected for the analysis. A classification of equipment based on its function was developed. A suitable scheme of eight general categories is proposed in Table 4.19 based on an in-depth analysis of the most common process and utility equipment used in offshore oil & gas facilities. From each main category, one or more sub-categories are derived specifying some equipment features.

Table 4.19. Functional categorization proposed for equipment of offshore production oil & gas facilities.

General categories	Sub-categories	Code
Process/storage vessel	Atmospheric vessel (storage tank, degasser, column, cryogenic tank, etc.)	EQ1.1
	Pressurized vessel (separator, column, knock-out drum, scrubber, etc.)	EQ1.2
	Filter (cartridge, basket, plate screen, etc.)	EQ1.3
Heat exchanger	Shell & Tube, plate, air-cooler	EQ2.1
Flare/vent system	HP/LP vent, HP/LP flare	EQ3.1
Pipe	Sealine	EQ4.1
	Riser (steel fixed, flexible), umbilical	EQ4.2
	Process piping, manifold, header	EQ4.3
Pressure change equipment	Pump (centrifugal, reciprocating)	EQ5.1
	Compressor (centrifugal, reciprocating)	EQ5.2
Wellhead	Surface, subsea	EQ6.1
Pig trap	Launchers, receivers	EQ7.1
Others	Purge burner, reactor, etc.	EQ8.1

HP: high pressure, LP: low pressure

Reference release modes for the possible offshore critical events are associated to each category of equipment. Critical events in offshore production oil & gas facilities are linked to the loss of containment of hydrocarbons and chemicals from process equipment and pipework [71,561–565]. The definition of reference release modes is used to characterize loss of containment events in terms of release geometry, duration, entity or conditions [566–569]. On the other hand, the wide availability and variability of techniques for the identification of appropriate release categories may create inconsistencies when applied to different types of equipment. For this reason, in the current methodology a set of four reference release modes is applied (Table 4.20). Table 4.21 matches the proposed release modes with the equipment categories proposed in Table 4.19.

Table 4.20. Proposed set of reference release modes associated to equipment units.

Reference release mode		Code
Small leak, continuous release from a 10 mm equivalent diameter hole		R1
Medium leak, continuous release from a 50 mm equivalent diameter hole		R2
Catastrophic rupture	Instantaneous release of the inventory	R3a
	Continuous release from a full-bore rupture of the main pip connected to the equipment	R3b

Table 4.21. Association of reference event tree codes to release modes of equipment units.

Equipment EQ	Post-release substance state	R1	R2	R3a	R3b
EQ1.1 Atmospheric vessel	Liquid	a)	a)	b)	a)
	Gas	d)	d)	e)	d)
	Liquid-Gas	g)	g)	h)	g)
EQ1.2 Pressurized vessel	Liquid	a)	a)	c)	a)
	Gas	d)	d)	f)	d)
	Liquid-Gas	g)	g)	i)	g)
EQ1.3 Filter	Liquid	a)	a)	b)	a)
	Gas	d)	d)	f)	d)
	Liquid-Gas	g)	g)	i)	g)
EQ2.1 Heat exchanger	Liquid	a)	a)	b)	a)
	Gas	d)	d)	f)	d)
	Liquid-Gas	g)	g)	i)	g)
EQ3.1 Flare/vent system	Gas	d)	d)	f)	d)
EQ4.1 Sealine	Liquid	l)*	l)*	-	l)*
	Gas	m)*	m)*	-	m)*
	Liquid-Gas	n)*	n)*	-	n)*
EQ4.2 Riser, umbilical	Liquid	a) / l)*	a) / l)*	-	a) / l)*
	Gas	d) / m)*	d) / m)*	-	d) / m)*
	Liquid-Gas	g) / n)*	g) / n)*	-	g) / n)*
EQ4.3 Manifold, header	Gas	d) / m)*	d) / m)*	-	d) / m)*
	Liquid-Gas	f) / n)*	f) / n)*	-	f) / n)*
EQ5.1 Pump	Liquid	a)	a)	-	a)
	Liquid-Gas	g)	g)	-	g)
EQ5.2 Compressor	Gas	d)	d)	-	d)
EQ6.1 Wellhead	Gas	d) / m)*	d) / m)*	-	d) / m)*
	Liquid-Gas	g) / n)*	g) / n)*	-	g) / n)*
EQ7.1 Pig trap	Liquid	a)	a)	c)	a)
	Gas	d)	d)	f)	d)
	Liquid-Gas	g)	g)	i)	g)

R1, R2, R3a and R3b are the reference release modes defined in Table 4.20. Letters a to l identify the reference event tree corresponding to the release, as reported in Appendix C. The codes marked with star (*) refer to a release below the water level.

4.5.4. Step 2: Assignment of credit factors to release modes

Credit factors are used in the present methodology in order to provide different weight to the credibility of the possible loss of containment events of concern for an equipment. As a matter of facts, equipment units, due to the inherent characteristics of their design and operation mode (multiple connections, moving

parts, safety margins, pressure cycles, etc.) have different likelihood to occur in a given release mode. Credit factors are based on expected equipment leak frequency data.

In step 2 of the proposed approach, credit factors are calculated as the frequency of the reference release modes defined in Table 4.20 to occur for the equipment unit of interest. In the methodology, it is advised to use as credit factors the specific release frequencies reported in the technical literature for offshore oil & gas equipment [570–575].

If the P&IDs of the facility are available as input data, a detailed analysis is also possible, based on parts count of the items and release frequencies obtained from past data repositories [576–579].

Otherwise, generic data can be selected from a reference table of credit factors for different equipment classes illustrated in Table 4.22, which is developed in this study from a survey of several P&IDs of offshore oil & gas facilities. The specific value to be used in the proposed ranges in Table 4.22 should be selected depending on the level of complexity of the equipment (e.g. many flanged connections, instruments and valves correspond to the upper bound of the range) and age/maintenance status of the plant. Furthermore, modifications of the adopted credit factors may be applied to equipment not in permanent service (e.g. test separators). In this case the credit factor may be scaled by a utilization factor equal to the ratio of the working hours of the equipment to the yearly service hours of the plant.

Table 4.22. Example of ranges of credit factors proposed for releases from offshore oil & gas equipment.

Equipment EQ		R1	R2	R3a	R3b
EQ1.1	Storage vessels (chemicals, diesel tanks)	$2.2 \cdot 10^{-3} \div 1.1 \cdot 10^{-2}$	$7.6 \cdot 10^{-4} \div 3.7 \cdot 10^{-3}$	$2.7 \cdot 10^{-5} \div 2.4 \cdot 10^{-4}$	*n.a.*
	Process vessels (oily drains tanks, oil-water degasser/separators)	$4.0 \cdot 10^{-3} \div 1.2 \cdot 10^{-2}$	$1.1 \cdot 10^{-3} \div 2.3 \cdot 10^{-3}$	$1.1 \cdot 10^{-3} \div 1.6 \cdot 10^{-3}$	$1.1 \cdot 10^{-3} \div 1.6 \cdot 10^{-3}$
EQ1.2	Production separators	$7.1 \cdot 10^{-3} \div 2.0 \cdot 10^{-2}$	$1.3 \cdot 10^{-3} \div 1.7 \cdot 10^{-2}$	$3.0 \cdot 10^{-4} \div 1.0 \cdot 10^{-3}$	$3.0 \cdot 10^{-4} \div 1.0 \cdot 10^{-3}$
	Other vessels (knock-out drum, coalescer, scrubber)	$6.8 \cdot 10^{-3} \div 1.8 \cdot 10^{-2}$	$1.1 \cdot 10^{-3} \div 9.7 \cdot 10^{-3}$	$2.5 \cdot 10^{-4} \div 4.8 \cdot 10^{-4}$	$2.5 \cdot 10^{-4} \div 4.8 \cdot 10^{-4}$
EQ1.3	Filter	$3.7 \cdot 10^{-3} \div 1.6 \cdot 10^{-2}$	$6.7 \cdot 10^{-4} \div 2.8 \cdot 10^{-3}$	$2.3 \cdot 10^{-4} \div 3.9 \cdot 10^{-4}$	$2.3 \cdot 10^{-4} \div 3.9 \cdot 10^{-4}$
EQ2.1	Shell & Tube (HC shell/tube side)	$4.4 \cdot 10^{-3} \div 2.3 \cdot 10^{-2}$	$6.2 \cdot 10^{-4} \div 3.2 \cdot 10^{-3}$	$3.0 \cdot 10^{-4} \div 1.5 \cdot 10^{-3}$	$3.0 \cdot 10^{-4} \div 1.5 \cdot 10^{-3}$
EQ3.1	Flare/vent system	*Case-specific*			
EQ4.1	Sealine	$4.9 \cdot 10^{-4} \div 1.2 \cdot 10^{-3}$	$7.6 \cdot 10^{-5} \div 2.2 \cdot 10^{-4}$	*n.a.*	$3.9 \cdot 10^{-5} \div 1.0 \cdot 10^{-4}$
EQ4.2	Steel riser, umbilical	$4.3 \cdot 10^{-4} \div 1.1 \cdot 10^{-3}$	$7.5 \cdot 10^{-5} \div 3.4 \cdot 10^{-4}$	*n.a.*	$3.9 \cdot 10^{-5} \div 1.6 \cdot 10^{-4}$
EQ4.3	Manifold, header	$1.0 \cdot 10^{-3} \div 4.1 \cdot 10^{-3}$	$1.5 \cdot 10^{-4} \div 6.9 \cdot 10^{-4}$	*n.a.*	$1.4 \cdot 10^{-5} \div 2.8 \cdot 10^{-4}$
EQ5.1	Reciprocating pump	$5.1 \cdot 10^{-3} \div 1.4 \cdot 10^{-2}$	$1.2 \cdot 10^{-3} \div 3.1 \cdot 10^{-3}$	*n.a.*	$8.0 \cdot 10^{-4}$
	Centrifugal pump	$6.9 \cdot 10^{-3} \div 1.7 \cdot 10^{-2}$	$7.2 \cdot 10^{-4} \div 2.3 \cdot 10^{-3}$	*n.a.*	$1.3 \cdot 10^{-4} \div 5.1 \cdot 10^{-4}$
EQ5.2	Reciprocating compressor	$5.0 \cdot 10^{-2} \div 8.0 \cdot 10^{-2}$	$6.0 \cdot 10^{-3} \div 9.0 \cdot 10^{-3}$	*n.a.*	$1.0 \cdot 10^{-3} \div 3.0 \cdot 10^{-3}$
	Centrifugal compressor	$1.2 \cdot 10^{-2} \div 1.6 \cdot 10^{-2}$	$1.4 \cdot 10^{-3} \div 1.9 \cdot 10^{-3}$	*n.a.*	$3.1 \cdot 10^{-4} \div 3.9 \cdot 10^{-4}$
EQ6.1	Surface wellhead	$7.5 \cdot 10^{-6} \div 1.3 \cdot 10^{-5}$	$7.2 \cdot 10^{-6} \div 1.3 \cdot 10^{-5}$	*n.a.*	$4.4 \cdot 10^{-6} \div 3.1 \cdot 10^{-5}$
	Subsea wellhead	$1.1 \cdot 10^{-6} \div 1.9 \cdot 10^{-5}$	$1.0 \cdot 10^{-6} \div 1.8 \cdot 10^{-6}$	*n.a.*	$6.3 \cdot 10^{-7} \div 2.3 \cdot 10^{-5}$
EQ7.1	Launchers	$7.2 \cdot 10^{-3} \div 1.2 \cdot 10^{-2}$	$1.6 \cdot 10^{-3} \div 2.4 \cdot 10^{-3}$	$8.1 \cdot 10^{-4} \div 1.1 \cdot 10^{-3}$	$8.1 \cdot 10^{-4} \div 1.1 \cdot 10^{-3}$
EQ8.1	Others	*Case-specific*			

n.a. stands for not applicable. R1, R2, R3a and R3b are the reference release modes defined in Table 4.20.

4.5.5. Step 3: Characterization of accident scenarios

Step 3 of the proposed methodology links the release modes to major accident scenarios associated to each unit, e.g. pool fire, fireball, toxic dispersion, etc. Coherently with established consequence analysis methods, post-release event trees are used for this task. While case-specific event trees can be built with a number of consolidated techniques [567–569], the standardized characteristics of the equipment and

operations in the offshore oil & gas industry allowed developing a customized set of reference event trees applicable to the present assessment.

Appendix C reports the proposed set of generic event trees. Event trees are associated to each release mode on the basis of the equipment category (Table 4.19) and physical state of substance after the release (liquid phase, gas phase, gas/liquid mixture) according to the scheme reported in Table 4.21. Since in the offshore context a unit or part of it may be located below the sea level, specific event trees are proposed to account for the cases of subsea release in addition to those developed for surface releases. The reference event trees from Appendix C must be pruned accounting for the specific characteristics of the released material (e.g. if non-toxic materials are released, the branches related to "toxic cloud" are neglected). The event trees may be customized to include specific results of HazOp, bow-tie analysis or of other hazard identification techniques, and, in particular, to include the action of safety systems for the mitigation of release consequences.

4.5.6. Step 4: Calculation of damage parameters

In step 4 of the procedure illustrated in Figure 4.12, the consequence analysis of each accident scenario following the release mode of each unit is carried out, in order to calculate the damage parameter addressing each of the targets of concern (human, assets, sea surface, water column)

The damage parameter for humans and assets targets are defined in this study as the maximum horizontal distance from the unit where the effect associated to fire/explosion/toxic scenarios reaches the threshold value defined in Table 4.17 and the target may be present. The calculation of the physical effects of a scenario is performed by using suitable consequence models [569,580–591]. Several models and commercial software tools are available in the literature and may be used for the purpose, e.g. Process hazard analysis software (PHAST) by DNV GL [592] and ALOHA hazard modelling program for the CAMEO software suite by EPA [593], commonly adopted for consequence analysis of atmospheric releases.

Concerning the sea surface compartment impacted by possible surface oil spills, different damage parameters may be estimated in this methodology with different levels of detail, based on the desired complexity of the analysis as well as availability of simulation tools for predicting fates and effects of oil spills into the sea, e.g. the freeware software by NOAA, i.e. Automated Data Inquiry for Oil Spills (ADIOS) [594] and General NOAA Operational Modeling Environment (GNOME) [595], and the licensed software by SINTEF, i.e. Oil Spill Contingency and Response (OSCAR) [596] and Oil Weathering Model (OWM) [597]. The proposed damage parameters are briefly described in the following including some features for their estimation.

The simplest damage parameter for sea surface pollution (i.e. level 1 of detail) is considered in this study as the oil mass spilled into the sea, which can be estimated by using release categories in Table 4.20 and release source models available in the literature, without the need for any simulation tool and threshold value.

Higher-level damage parameters quantifying the impact of oil spills on the sea surface (i.e. level 2 of detail) are the trend over time of the oil mass in the slick or the trend over time of the oil mass in the thick slick (i.e. with a thickness equal or greater than the threshold value in Table 4.17), and the persistence of the oil mass in the slick over a given time. The calculation of these parameters depends on the simulation tool adopted for consequence analysis and, in particular, on the ability to represent the slick as much realistically as possible, the simulation time, the ability to consider oil release temperature (estimated with the spilled mass using release source models), air and sea surface temperatures (collected in input data in Table 4.16), the ability to account for the wind and currents fields in the site.

With respect to the oil fate simulation tools mentioned above, GNOME is not able to take into account any value of mentioned temperatures, ADIOS and OWM tools consider thermal equilibrium between air, water and release, thus requiring to specify only one value. OSCAR distinguishes between the three temperatures, thus all three values are needed in input. Concerning the environmental data, ADIOS, OWM and GNOME evaluates only the wind speed for modelling, while OSCAR also the currents speed. Except for ADIOS which has a limit in the released mass in input (between 320 kg e 79415 t), the tools are able to simulate all the possible values of oil mass. For accidental spills with a relatively short duration (instantaneous or continuous spills with a duration of about 10 minutes), it is advised to simulate the releases as instantaneous with ADIOS, GNOME and OWM, while setting a minimum duration time with OSCAR (e.g. 1 hour) since it requires this parameter in addition to the released mass without allowing the instantaneous spill simulation.

Furthermore, all the softwares can provide the oil budget (i.e. oil mass balance) over the time; GNOME, ADIOS and OWM tools have a limit time for simulation (three days for GNOME, while five days for others), OSCAR does not pose limits on simulation time (i.e. a limit time cannot be identified).

It is worth mentioning that an oil spill on the sea surface leads to a slick characterized by a first expansion phase until a maximum condition is reached and then a reduction phase until exhausting at the end of its lifetime. Only OSCAR tool allows to simulate both the phases, while ADIOS, GNOME and OWM consider the sole expansion phase and provide in outputs results until the end of this phase (if the expansion phase duration is lower than the limit time imposed by the software) or until their limit time (if the expansion phase duration is greater than the limit time imposed by the software). Moreover, ADIOS, GNOME and OWM model the slick as homogeneous entity, i.e. with variable thickness over time but

spatially uniform in each point of the slick; whereas, OSCAR considers a variable slick thickness over space and time, i.e. a realistic representation of the slick. As a result, ADIOS, GNOME and OWM allow to estimate the oil mass in the slick over the simulation time limit; OSCAR provides the oil mass in the eco-toxic thick slick over the entire lifetime of the thick slick (i.e. time where the slick show a thickness equal or greater to the threshold value somewhere).

The most sophisticated damage parameters for environmental targets over the sea surface (i.e. level 3 of detail) are considered related to the geometric features of the oil slick, i.e. surface area of the slick or of the thick slick (with a thickness equal or greater than the threshold value in Table 4.17) and its persistence over a given time. These parameters can be estimated by means of a limited number of tools, e.g. OSCAR and ADIOS with differences imposed by the characteristics (and limits) of the software, as described in the considerations above.

Lastly, in this research project one sole damage parameter is considered to quantify the water column pollution due to possible surface spills of completely soluble chemicals: this is the polluted volume of water derived from the ratio of the spilled mass of the chemical compound to the corresponding threshold value reported in Table 4.17. For the sake of simplicity and scares availability of suitable simulation tools, in this study such a parameter is estimated as radius of a hypothetical cylinder with volume equal to the calculated polluted volume and height equal to a water depth of 50 m. The latter value is assumed as the maximum limit in depth for water column contamination, also based on the results of simulations involving different chemical compounds in Oil Spill Contingency and Response (OSCAR) [596].

Offshore installations are characterized by a multi-level layout. The basic features of the preliminary layout (e.g. release point location, congested volumes) should be taken into account in the accident scenario simulation. Particular attention should be given to the simulation of liquid releases and sub-sea releases. The typical use of grated surfaces in offshore facilities results in liquid pools formed at sea level rather than at the elevation of the unit originating the release. Simulation of releases from equipment which are partially or totally submerged, e.g. risers or subsea items, must take into account the dispersion phenomena both below and above the sea surface. In order to obtain worst case consequences (maximum values of damage parameters), release orientation, target elevation, atmospheric conditions and marine conditions shall be appropriately selected among credible values in order to obtain the worst credible cases.

4.5.7. Step 5: Calculation of unit inherent safety KPIs

For each unit of the design option, in step 5 of the procedure, a set of two inherent safety KPIs is calculated addressing each target of interest: both indicators provide a quantification of the inherent safety performance of the units but focus on specific aspects of interest for early design stages.

The first KPIs is called potential hazard index (PI), which captures the worst-case accident scenario in terms of highest damage parameters within the release categories of the unit. Being independent from the credit factors, they rely upon design choices, e.g. operative conditions, unit inventories and equipment locations. Whereas, the second KPI, named inherent hazard index (HI), is calculated by weighting the damage parameters with credit factors associated to releases of the unit [426]. Therefore, this latter metric introduces the role of the safety score of the equipment unit used in the operation, anticipating the safety performance assessment typically defined only in the later detailed design stages of a project. By ranking the hazard level of potentially and credibly critical units, the proposed KPIs allow to limit time and costs for the offshore project and thus to address inherently safer solutions during the early design phase. It is worth noting that the proposed indicators both show lower values as the inherent safety performance of the unit increases. The procedure for the calculation of these KPIs is described in the following for each target of concern.

4.5.7.1. Performance assessment for humans

For humans, the unit inherent safety KPIs are defined as follows:

$$HPI_k = \pi \max_i (\max_j d_{i,j,k}^2) \tag{4.42}$$

$$HHI_k = \pi \sum_i (cf_{i,k} \cdot \max_j d_{i,j,k}^2) \tag{4.43}$$

where HPI is the potential hazard index addressing the human target for the k-th unit (in m^2), HHI is the inherent hazard index addressing the human target for the k-th unit (in m^2/y), d is the damage parameter for the human target (in m) associated to the j-th accident scenario following the i-th release mode of the k-th unit, cf is the credit factor (in 1/y) assigned to the i-th release mode of the k-th unit. The distance d is estimated by means of consequence analysis as described in step 4, while cf is attributed to equipment release as described in step 3. As a matter of facts, HPI represents the maximum impact area derived from the worst-case accident scenario affecting humans among those originated from the unit reference release modes, while HHI is the credible damage area from the unit releases.

4.5.7.2. Performance assessment for assets

Concerning the assets, the unit inherent safety KPIs are defined for each category (process and utility equipment, facility structures, marine structures) as follows:

$$API_{l,k} = \pi \max_i (\max_j e_{i,j,k,l}^2) \tag{4.44}$$

$$AHI_{l,k} = \pi \sum_i (cf_{i,k} \cdot \max_j e_{i,j,k,l}^2) \tag{4.45}$$

where API is the potential hazard index addressing the l-th assets category for the k-th unit (in m^2), AHI is the inherent hazard index addressing the l-th assets category for the k-th unit (in m^2/y), e is the damage parameter addressing l-th assets category (in m) defined in step 5 for the j-th accident scenario following the i-th release mode of the k-th unit, cf is the credit factor defined in Equation (4.43). The distance e is estimated by means of consequence analysis as described in step 4, while cf is attributed to equipment release as described in step 3. Given similar equations, API and AHI have the same meaning and unit of measure reported above for KPIs addressing human targets. A set of three potential KPIs and of three inherent KPIs may be at the most obtained for the assets target.

4.5.7.3. Performance assessment for environmental targets

For the environmental damage of sea surface and water column compartments, a different calculation of the unit inherent safety KPIs is proposed with respect to human and assets targets. As explained above, different types of damage parameters are considered addressing the vulnerable targets living along water column impacted by chemical spills and the vulnerable targets on the sea surface polluted by oil spills. Therefore, a different definition of KPIs associated to chemical releases and oil spills into the sea is provided in this study, as described in the following.

The potential and inherent KPIs associated to chemical releases are defined as follows:

$$EPI_{chem,k} = \pi \max_i g_{i,k}^2 \tag{4.46}$$

$$EHI_{chem,k} = \pi \sum_i (cf_{i,k} \cdot g_{i,k}^2) \tag{4.47}$$

where EPI_{chem} (in m^2) and EHI_{chem} (in m^2/y) are the potential hazard index and inherent hazard index, respectively, addressing the water column target due to chemical spills derived from the k-th unit, g is the damage parameter for water column target (in m) following the i-th release mode of the k-th unit, cf is the credit factor defined in Equation (4.43). The distance g is estimated from the polluted water column as described in step 4, while cf is attributed to equipment release as described in step 3.

Concerning the KPIs related to oil spills, three levels KPIs are defined in this research project with an increasing level of detail from the first to the third, corresponding to three levels of damage parameters described in step 4 of the method. It should be noted that such KPIs are alternative for quantification of the hazard level of oil leakages; the selection of suitable KPI is dependent upon the availability of data for the analysis and simulation tools for oil fate modelling.

The level 1 KPIs for oil spill hazard quantification are associated to the oil mass spilled into the sea and can be calculated as follows:

$$EPI_{oil1.1,k} = \max_i m_{oil-rel,i,k} \quad (4.48)$$

$$EHI_{oil1.1,k} = \sum_i (cf_{i,k} \cdot m_{oil-rel,i,k}) \quad (4.49)$$

where $EPI_{oil1.1}$ is the potential hazard indicator of level 1 addressing the environment target on the sea surface due to oil spills derived from the k-th unit (in units of tons), $EHI_{oil1.1}$ is the inherent hazard indicator of level 1 addressing the environment target on the sea surface due to oil spills derived from the k-th unit (in tons/y), $m_{oil-rel}$ is the oil mass spill following the i-th release mode from the k-th unit (in units of tons), cf is the credit factor defined in Equation (4.43). $m_{oil-rel}$ is estimated as described in step 4, while cf is attributed to equipment release as described in step 3. Clearly enough, avoiding the use of simulation tools for consequences of oil fate, the proposed two KPIs represent a preliminary estimation of the potential and credible hazard associated to the oil spill from the unit.

The level 2 KPIs for quantification of oil leak hazard can be divided into two sub-level indicators: level 2.1 KPIs are based on the sole oil mass in slick, while level 2.2 KPIs are based on both oil mass in the slick (or thick slick) and its persistence over a limit time (or thick slick lifetime). It must be remarked that the expressions of these KPIs may be different according to the simulation software used, given unavoidable differences (and limits) of the tools. KPIs of level 2.1 can be calculated as follows:

$$EPI_{oil2.1,k} = \min_{t=0 \div t_{lim}} (\max_i m_{oil-sl,i,k}(t)) \quad (4.50)$$

$$EHI_{oil2.1,k} = \min_{t=0 \div t_{lim}} (\sum_i (cf_{i,k} \cdot m_{oil-sl,i,k}(t))) \quad (4.51)$$

where $EPI_{oil2.1}$ is the potential hazard indicator of level 2.1 addressing the environment target on the sea surface due to oil spills derived from the k-th unit (in units of tons), $EHI_{oil2.1}$ is the inherent hazard indicator of level 2.1 addressing the environment target on the sea surface due to oil spills derived from the k-th unit (in units of tons/y), m_{oil-sl} is the oil mass in the slick following the i-th release mode from the k-th unit as function of time t (in units of tons), t_{lim} is the limit time imposed by the simulation software (e.g. ADIOS, GNOME, OWM), cf is the credit factor defined in Equation (4.43). m_{oil-sl} and t_{lim} are estimated as described in step 5 for given simulation tools. Given the considerations reported above in the estimation of damage parameters (step 4), it is worth mentioning that Equations (4.50) and (4.51) can be calculated only by using ADIOS, GNOME and OWM tools. In case of OSCAR software, as the thick slick extinguishes at a given time, the oil mass in the thick slick becomes null, thus level 2.1 KPI would lose its content.

KPIs of level 2.2 are defined as follows:

$$EPI_{oil2.2,k} = \int_0^{t_{lim}} (\max_i m_{oil-sl,i,k}(t))\, dt \quad (4.52)$$

$$EHI_{oil2.2,k} = \int_0^{t_{lim}} (\sum_i (cf_{i,k} \cdot m_{oil-sl,i,k}(t)))\, dt \quad (4.53)$$

where $EPI_{oil2.2}$ is the potential hazard indicator of level 2.2 addressing the environment target on the sea surface due to oil spills derived from the k-th unit (in units of tons · d), $EHI_{oil2.2}$ is the inherent hazard indicator of level 2.2 addressing the environment target on the sea surface due to oil spills derived from the k-th unit (in units of tons · d /y), m_{oil-sl} is the oil mass in the slick defined in Equation (4.50), t_{lim} is the limit time imposed by the simulation software (e.g. ADIOS, GNOME, OWM), cf is the credit factor defined in Equation (4.43). Given the considerations reported above in the estimation of damage parameters (step 4), it is worth noting that Equations (4.52) and (4.53) can be calculated by using ADIOS, GNOME and OWM tools. In case of adoption of OSCAR software, the equations to be applied are:

$$EPI_{oil2.2,k} = \int_0^{\infty} (\max_i m_{oil-th,i,k}(t))\, dt \quad (4.54)$$

$$EHI_{oil2.2,k} = \int_0^{\infty} (\sum_i (cf_{i,k} \cdot m_{oil-th,i,k}(t)))\, dt \quad (4.55)$$

where m_{oil-th} is the oil mass of the thick slick with a thickness equal or greater a threshold value in Table 4.17 following the i-th release mode from the k-th unit as function of time (in tons), ∞ represents the concept that OSCAR does not pose limits on simulation time, thus the calculation can be made over the lifetime of the thick slick. Clearly enough, KPIs of level 2.2 represent the potential and credible oil mass slick exposure.

The level 3 KPIs consider the geometric features of the thick slick, i.e. the surface of the slick, thus they are based on the most accurate modelling approach, since the thick area is the key parameter causing sea surface pollution. At this level, two sub-level indicators are defined: KPIs of level 3.1 are a function of the sole area of the slick (or thick slick), while level 3.2 KPIs represent the slick surface exposure, mentioned above. Similarly to level 2 KPIs, expressions of these KPIs may be different according to the simulation software used. Level 3.1 KPIs are calculated as follows:

$$EPI_{oil3.1,k} = \max_{t=0 \div t_{lim}} (\max_i A_{oil-sl,i,k}(t)) \quad (4.56)$$

$$EHI_{oil3.1,k} = \max_{t=0 \div t_{lim}} (\sum_i (cf_{i,k} \cdot A_{oil-sl,i,k}(t))) \quad (4.57)$$

where $EPI_{oil3.1}$ is the potential hazard indicator of level 3.1 addressing the environment target on the sea surface due to oil spills derived from the k-th unit (in units of km^2), $EHI_{oil3.1}$ is the inherent hazard indicator of level 3.1 addressing the environment target on the sea surface due to oil spills derived from the k-th unit (in units of km^2/y), A_{oil-sl} is the oil surface area of the slick following the i-th release mode from the k-th unit as function of time t (in km^2), t_{lim} is the limit time defined in Equation (4.50), cf is the credit factor defined in Equation (4.43). It should be noted that Equations (4.56) and (4.57) should be

applied only in case of simulations with ADIOS among the tools mentioned above because of the considerations reported in the description of damage parameters (step 4). For modelling in OSCAR tool, the following expressions can be used:

$$EPI_{oil3.1,k} = \max_{t=0\div\infty} (\max_{i} A_{oil-th,i,k}(t)) \tag{4.58}$$

$$EHI_{oil3.1,k} = \max_{t=0\div\infty} (\sum_i (cf_{i,k} \cdot A_{oil-th,i,k}(t))) \tag{4.59}$$

where A_{oil-th} is the surface of the thick slick with a thickness equal or greater a threshold value in Table 4.17 following the i-th release mode from the k-th unit as function of time (in km^2), ∞ represents the concept that OSCAR does not pose limits on simulation time, thus the calculation can be made over the lifetime of the thick slick.

KPIs of level 3.2 calculated with tools imposing limit simulation time and dismissing the slick thickness concept, e.g. ADIOS, are defined as follows:

$$EPI_{oil3.2,k} = \int_0^{t_{lim}} (\max_{i} A_{oil-sl,i,k}(t))\, dt \tag{4.60}$$

$$EHI_{oil3.2,k} = \int_0^{t_{lim}} (\sum_i (cf_{i,k} \cdot A_{oil-sl,i,k}(t)))\, dt \tag{4.61}$$

where $EPI_{oil3.2}$ is the potential hazard indicator of level 3.2 addressing the environment target on the sea surface due to oil spills derived from the k-th unit (in units of km$^2 \cdot$ d), $EHI_{oil3.2}$ is the inherent hazard indicator of level 3.2 addressing the environment target on the sea surface due to oil spills derived from the k-th unit (in units of km$^2 \cdot$ d/y), A_{oil-sl} is the oil surface area of the slick defined in Equation (4.56), t_{lim} is the limit time defined in Equation (4.50), cf is the credit factor defined in Equation (4.43). Otherwise, for sophisticated software (e.g. OSCAR), the following equations can be applied for calculation of level 3.2 KPIs:

$$EPI_{oil3.2,k} = \int_0^{\infty} (\max_{i} A_{oil-th,i,k}(t))\, dt \tag{4.62}$$

$$EHI_{oil3.2,k} = \int_0^{\infty} (\sum_i (cf_{i,k} \cdot A_{oil-th,i,k}(t)))\, dt \tag{4.63}$$

where A_{oil-th} is the surface of the thick slick with a thickness equal or greater a threshold value in Table 4.17 following the i-th release mode from the k-th unit as function of time t (in km^2), ∞ represents the concept that OSCAR does not pose limits on simulation time, thus the calculation can be made over the lifetime of the thick slick.

4.5.7.4. Multi-target performance assessment

For a concise yet representative inherent safety performance comparison between different units of the design option under analysis, an aggregated indicator addressing all the targets of the potential hazards in a single value is more suitable than an array of single indicators. In the present methodology, the KPIs calculated for single targets are combined in a two-stage compensatory MCDA approach, which comprises normalization of the indicators calculated for each category of targets and then aggregation into one multi-target indicator by applying proper trade-off weights.

A site-specific external normalization approach based on spatial dimensions influenced by the impacts associated to each category [273] is adapted in the present methodology to obtained normalized indicators within each category of targets for further aggregation. The characteristic impact area in units of square meters defined for each target of concern in step 0 is proposed as normalization factor for the corresponding indicator. By this way, the normalization factor is independent from the considered process designs, but depends on the specific offshore facility where alternative design options are evaluated. Each normalized indicator can be obtained by applying the following general formula:

$$X_I = \frac{I_{act}}{A_{vuln}} \tag{4.64}$$

where X_I is the normalized indicator associated to I_{act}, I_{act} is the actual indicator addressing a specific target of concern among humans, assets and environment, A_{vuln} is the vulnerability area defined for the specific target in step 0 of the procedure. In case of the sea surface environment polluted by oil spills, different level KPIs are defined in terms of meaning and units of measure. Thus, normalization illustrated in Equation (4.64) and further aggregation can be applied only whether KPI level 3.1 based on the oil slick surface, defined in Equations (4.58) and (4.59), are used as KPIs addressing this sub-category of the environment target. For all the other KPIs defined above, no issues about the direct application of Equation (4.64).

It should be noted that in case of assets and environment targets, more than one sub-category of targets may exist, i.e. process and utility equipment, facility structures, marine structures. The maximum normalized indicator among those addressing the sub-categories of the target is considered conservatively for further aggregation steps. The same procedure can be applied in the case of KPIs addressing environmental targets, considering the maximum normalized value among those addressing sea surface compartment due to oil spills and water column compartment due to chemical spills. It is worth noting that only one KPI among those of different levels defined for the sea surface pollution due to oil leaks should be selected for the aggregation.

The application of such normalization procedure is performed for both potential and inherent KPIs separately, thus leading to two sets of normalized indicators addressing three main categories of targets for each unit of the design option: the first set includes the potential KPIs, i.e. PI_{hum}, PI_{ass}, PI_{env} for humans, assets and environment respectively, the second one comprises the inherent KPIs, i.e. HI_{hum}, HI_{ass}, HI_{env}.

Finally, WAM or WGM method is used to obtain single-value multi-target indicators for each unit of the design option, as described in the sustainability assessment methodology in Section 4.3. Equation (4.18) can be adapted to apply WAM method to this model:

$$PI_{ov,k} = w_{hum} \cdot PI_{hum,k} + w_{ass} \cdot PI_{ass,k} + w_{env} \cdot PI_{env,k} \tag{4.65}$$

$$HI_{ov,k} = w_{hum} \cdot HI_{hum,k} + w_{ass} \cdot HI_{ass,k} + w_{env} \cdot HI_{env,k} \tag{4.66}$$

where PI_{ov} and HI_{ov} are the overall potential and inherent KPIs addressing multiple targets for the k-th unit, PI_{hum}, PI_{ass} and PI_{env} are the normalized potential KPIs addressing humans, assets, environment targets, respectively, for the k-th unit, HI_{hum}, HI_{ass} and HI_{env} are the normalized inherent KPIs addressing humans, assets, environment targets, respectively, for the k-th unit, w_{hum}, w_{ass} and w_{env} are the weights associated to humans, assets and environment targets categories, respectively, reflecting the trade-offs or substitution rates which can be accepted among the categories of targets (their summation closes to one) [236].

The unit aggregated KPIs using WGM technique are obtained adapting Equation (4.19):

$$PI_{ov,k} = {PI_{hum,k}}^{w_{hum}} \cdot {PI_{ass,k}}^{w_{ass}} \cdot {PI_{env,k}}^{w_{env}} \tag{4.67}$$

$$HI_{ov,k} = {HI_{hum,k}}^{w_{hum}} \cdot {HI_{ass,k}}^{w_{ass}} \cdot {HI_{env,k}}^{w_{env}} \tag{4.68}$$

where the nomenclature is defined in Equations (4.65) and (4.66).

The selection of weight factors may be controversial in the context of inherent safety of offshore oil & gas facilities: they should be independent from the assessed alternatives, but may depend on the local conditions and policy implemented by the oil & gas company. Equal priority can be assigned, i.e. weight factors equal to 1/3 if the categories of the targets considered for the analysis are three, at least in a preliminary step, provided that proper sensitivity analysis is performed to investigate the influence of weights on the KPIs results.

4.5.8. Step 6: Calculation of facility inherent safety KPIs

Having calculated the single-target and multi-target KPIs for the units, the inherent safety performance for each facility design option is estimated in step 6 of the procedure. As shown in Figure 4.11, the

normalized single-target indicators are first calculated and then combined to obtain the aggregated multi-target KPIs for the facility. Clearly enough, this procedure is applied to both potential and inherent KPIs, as performed for the single units.

The normalized single-target indicators are derived by summation of indicators estimated for the units of the design option in step 6. For example, for human target, the facility KPIs can be calculated as follows:

$$PI_{hum,fac} = \sum_{k=1}^{N} PI_{hum,k} \tag{4.69}$$

$$HI_{hum,fac} = \sum_{k=1}^{N} HI_{hum,k} \tag{4.70}$$

where $PI_{hum,fac}$ and $HI_{hum,fac}$ are the potential and inherent hazard KPIs addressing humans, respectively, for the facility design option, k is the unit of the option, N is the total number of units analysed for the option. Similar expressions can be applied to the other categories of targets.

From these indicators, the multi-target KPIs indicating the overall hazard level of the entire facility are derived, applying similar equations for the single units according to the method adopted for aggregation. In these equations, weights among the KPIs addressing single targets categories are the same considered for the single units.

4.5.9. Step 7: Ranking of alternatives and sensitivity analysis

The aggregated KPIs calculated in step 6 allow the assessment and ranking of the expected inherent safety performance of the units of each design option, based either on a direct assessment of potential worst-credible-case accident scenarios (potential KPIs) or on likely safety performance of the unit by accounting for fragility of equipment (inherent KPIs), with respect to both specific categories of targets and as a whole. It is worth noting that the higher the values of the indicators, the higher the criticality of the unit.

From the calculation of facility KPIs in step 6, the global inherent safety performance of alternative design options can be compared and ranked in terms of either hazard level of process operations (potential KPIs) or hazard level weighted by credit factors of equipment (inherent KPIs), addressing specific categories of targets and as a whole. It should be remarked that the lower values of indicators, the higher inherent safety profile of the option.

For both units and facility, the ranking based on single-target indicators allows highlighting the different contributors to the safety profile, while ranking based on multi-target indicators provides information about overall inherent safety fingerprinting of the design options.

Quite obviously, the results obtained are influenced by the weights used in the aggregation procedure, which may be considered as less accurate measures than other parameters used in the assessment.

Therefore, sensitivity analysis is worth to perform in order to check the influence of variation in the values of weights on the aggregated KPIs and rankings of the alternatives. Some sensitivity analysis techniques which may be used for the sake of these verifications are described in Section 4.7 of this chapter.

4.6. Process intensification screening methodology

This section describes the methodology developed to integrate sustainability and safety performance analysis, based on the idea of process intensification in view of the screening of chemical production processes characterized by low maturity level and potentially adopted in P2G and P2L offshore hybrid energy options. An overview of the method is presented in the following paragraphs.

4.6.1. Overview of the method

The goal of this methodology is to provide a systematic approach for analysing the feasibility of chemical production processes at early maturity level (i.e. experimental proof of concept, technology validated in lab, technology validated/demonstrated in industrial site, pilot plant) based on the concept of process intensification (PrI). The desired chemical product may be one of the promising chemical energy carriers to be used in P2G or P2L offshore hybrid energy options described in Chapter 2 (i.e. H_2, SNG, CH_3OH). The process routes may be novel production methods classified in the existing literature as alternative to the conventional production process in order to make the synthesis more renewable-based and sustainable. A set of screening indicators addressing technical, economic, environmental and societal dimensions is proposed to rank the process intensification level of the proposed process schemes. Therefore, this method represents an attempt to cover all the dimensions of the sustainability assessment model presented in Section 4.3.

The methodology is intended to be a support tool orienting the choice of relatively new yet promising chemical processes for their implementation in P2G and P2L offshore hybrid energy projects. By this way, the proposed approach represents a precursor for further detailed site-specific assessment of the renewable-based integrated systems at a given offshore oil & gas site.

The flow chart of the methodology is illustrated in Figure 4.13. As shown in this figure, a preliminary step (step 0) is necessary, consisting in the definition of the reference process schemes for the alternative production routes of the chemical compound intended to be used as energy carrier in P2G or P2L offshore hybrid energy options. This requires a review on the state-of-the-art technologies for each alternative production route and then the selection of the most suitable one based on operating conditions and operating mode, as well as product yield. It is noteworthy that milder conditions, continuous operation

mode, as well higher yield of the desired product are preferable factors. For each technology selected from the technical literature, some input data related to the process are required, summarized in Table 4.23.

To perform a consistent assessment between different processes, a common reference basis should be defined. The production rate and purity of the desired product may be selected as a basis based on given criteria, e.g. the output of the most mature existing plant, purity specification for the marketplace, available capacity of raw materials, specific site restraints related to the maximum allowable space. Moreover, the boundaries for the analysis of the alternative process schemes need to be defined consistently among the options. Given the goal of the assessment, boundaries should limit to the main process (i.e. the core process from raw material to the desired product at the reference basis) as well as the main on-site utilities necessary for the main process tom operate (e.g. boilers for steam production, refrigeration cycles, etc.). However, in the analysis of the utilities, only the fraction of the utility stream employed by the process under analysis should be accounted for. The battery limits do not include upstream operations and/or downstream operations which are realized in another location than that of the considered plant. After the reference process schemes have been defined, the assessment can be performed through five main steps, described in the following paragraphs.

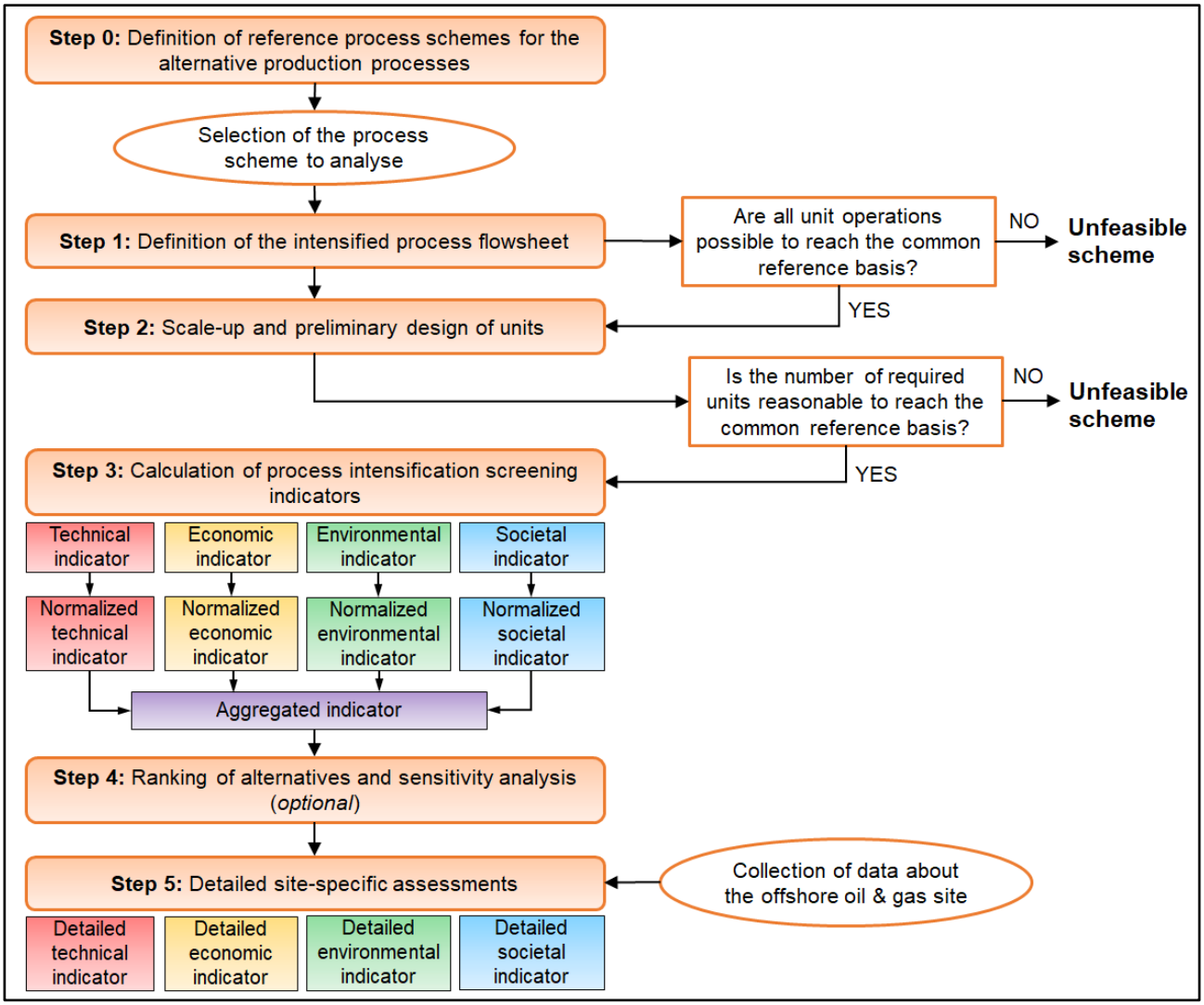

Figure 4.13. Flow chart of the PrI screening methodology for novel chemical process routes in P2G and P2L offshore hybrid energy options.

Table 4.23. Input data required for the PrI screening methodology.

a)	Stoichiometry of all reactions, range of temperatures and pressures, phase
b)	Molar conversion of reactants, selectivity or yield of products
c)	Physical state and method of regeneration of catalyst, if present
d)	Physical state, purity, flowrate of raw materials
e)	Physical state, purity, flowrate of the desired product
f)	Operating mode (continuous, batch, semi-continuous)
g)	Preliminary technology readiness level (TRL) [598]
h)	Process constraints, if present (e.g. processing conditions where some material can decompose or become unstable, or substrate can be damaged, or liquid medium can be inactive)

4.6.2. Step 1: Definition of the intensified process flowsheet

The overall transformation from raw materials into the final product at desired flowrate and purity may require a series of intermediate steps carried out through reaction, separation of chemical mixtures, phase

separation, change of temperature, pressure and phase, mixing or splitting [478]. For example, if the outlet stream from the reactor does not have the desired temperature, composition and phase, additional unit operations should be introduced. Therefore, in step 1 of the methodology, for each defined reference scheme, a flowsheet representing the diagrammatic representation of the process steps with their interconnections should be created by selecting suitable basic unit operations to include and evaluating their combination properly [599].

Separation operations are introduced in the process flowsheet when raw materials need to be purified before the reaction and/or products, by-products and unreacted raw materials are mixed in the reactor effluent. The typology of separation depends on the phase of the stream and differences in physical properties of compounds in the stream. To give some examples, vapour-liquid separation in distillation column is commonly used for liquid mixtures when differences in vapour pressure are large, while membrane separation can be employed for gas mixtures when permeabilities and/or solubilities of the compounds through a membrane differ. Optionally, change in temperature in heat exchangers and/or change in pressure in pumps, compressors, expanders and valves may be added to the process flowsheet in order to adjust temperature and pressure levels to reach the desired reaction conversions and separation factors. Much more extensive presentations, including comparisons, of the different unit operations to insert into the flowsheet are given in the literature [478,600,601].

In the view of a sustainable and efficient process design, the PrI concept should be applied to the process flowsheet. PrI can be defined as any chemical engineering development which leads to a substantially smaller, cleaner, safer and more energy efficient technology [602]. Different definitions of the PrI activities can be found in the literature [603]. One of them consists in the process integration in terms of material and/or energy recovery.

Concerning the integration of material flows into the flowsheet, it is recommended to recover and recycle more than 99% of unreacted reactants of the desired reactions, except for non-valuable unconverted compounds (e.g. air and water compared to organics) [604]. Considering a light component as one boiling at a temperature lower than propylene (- 48 °C), when a light reactant or a light feed impurity or a light by-product from the reaction are present, it would be a good practice to introduce gas recycle and purge stream, i.e. recycling reactants to the reaction operation and purging one or more undesirable compounds from the process [604]. While keeping the information about stoichiometry of the reactions and local conversion of limiting reagent at the reactor, gas recycling with a recycle ratio as higher as possible leads not only to raw material minimization, but also to an increase in the overall conversion of limiting reagent and overall yield of the desired product with respect to local conversion and local yield. Moreover, if possible, recovering material streams containing a certain amount of the product is further suggested to

minimize wastes. Once recycle operations have been inserted in the process flowsheet, mixing operation is added to combine two or more streams in case of recycle [478].

On the other hand, focusing on the heat and power integration, it is desirable to maximize energy recovery looking forward minimum use of utilities: high-temperature streams may be cooled and/or condensed in order to heat and/or vaporize cold streams in the process, as well power produced by turbines and heat engines may be supplied to compressors and pumps. Also, heat produced from exothermic reaction can be removed by using cooling jacket or coils through which a cold process stream or cold utility is circulated. First, the heat available in hot streams and cold streams should be calculated as well as the available and the required electrical power in the process. According to the first law of thermodynamics, the duties which cannot be satisfied by heat and power recovery within the process dictate the need for external utilities, i.e. steam, cooling water, thermal oil, air-cooling, refrigeration, electricity. It should be noted that a physically realizable heat exchanger network requires that also a positive driving force exist between hot and cold streams, thus satisfying the second-law of thermodynamics [604]. The temperature interval method based on the minimum approach temperature of 10 -15 °C between hot and cold streams may be used for calculation of minimum energy recovery [478]. The, preliminary estimates of exit temperatures of streams flowing through a heat exchanger, assumed as an external shell-and-tube exchanger using counter-current flow, are made applying the following near-optimal minimum approach temperature [478]: 10 °C or less for temperatures below ambient, 20 °C for temperatures at or above ambient up to 150 °C, 50 °C for higher temperatures.

Another PrI activity for an intensified process flowsheet relies on the task integration, i.e. combining multiple unit operations into single process units in order increase the unit performance in terms of product quality, compactness, environmental impact and energy use [603]. Some of the proposed PrI equipment can be advanced separation technologies assisted by membrane, i.e. reverse osmosis for seawater desalination or pervaporation to remove low concentration of organics from liquid mixtures. Others suggested in the literature are combined reaction/separation technologies, i.e. reactive distillation, selective/catalytic membrane reactive separation.

To facilitate the definition of the intensified process flowsheet, process simulators, e.g. Aspen PLUS and Aspen HYSYS by Aspen Technology [605], CHEMCAD by Chemstations [606], and PRO/II PRO/II Process Engineering by Aveva [607], may be used for simulation of steady-state processes. By solving mass and energy balances coupled with phase equilibria, and transport and chemical kinetics equations, these tools allow to predict flowrates, compositions, operating conditions and physical properties of all the streams as well as required electrical power and heat duty associated to the equipment units. Simplified models and shortcut procedures offered by process simulators are useful in this step of the procedure to approximate reaction and separation operations with relatively little available information in order to

obtain an estimate of their performance. PrI activities above described may be simply simulated by using recycle operator and heat exchanger models.

Given the intensified process flowsheets for each scheme, a preliminary screening of alternative production processes under analysis is performed based on operating parameters of unit operations in the flowsheet. As shown in Figure 4.13, a reference process scheme may not proceed to the following step of the procedure if one or more unit operations are not suitable, e.g. when the concentration of the product in the output stream from the synthesis section is not feasible for a given separation technique.

4.6.3. Step 2: Scale-up and preliminary design of equipment units

If the reference process scheme has passed step 2, conceptual scale-up and design of all simulated equipment is carried out in step 3 of the procedure based on the material and energy output data provided from the process simulator for each unit of the flowsheet. This allows to quantify the effective number of components required for each operation in the scheme and perform further preliminary screening of the alternative process schemes.

Standard approaches for a preliminary design of process and utility equipment for heat and material transfer [608–610] can be adopted in order to estimate main geometric data of the components and evaluate the required units for a given unit operation. Common heuristics or rules of thumb available in the literature [361,611] may be applied to address proper design choices.

The conceptual design of process routes at low maturity level implies dealing with scale-up issues of specific equipment used for the synthesis at the laboratory scale, electrochemical cells, catalytic tubular reactors, etc. The philosophy of scaling-up chemical process units consists that values of corresponding dimensionless groups of the two units (prototype and full-scale) are similar [612]. The criteria normally employed in thermochemical reactors scale-up are those of geometric, kinematic and thermal similarity between the reactors [613]. In the case of electrochemical reactors, an additional criterion needed for scaling-up is the current/potential similarity [614]. For reactor using non-thermal plasma to produce highly energetic species, e.g. dielectric barrier discharge (DBD) reactors, similarity may be based on the energy characteristics, i.e. the discharge power with respect to frequency, voltage and capacitance of the reactor [615]. Scale-up of photocatalytic reactors may be applied by comparing the efficiency to install activated immobilized catalyst per unit of reaction liquid volume in the reactor [616]. Table 4.24 summarizes examples of scale-up approaches proposed in the literature for some reactor concepts which may be applied to the conceptual design of novel chemical production processes.

Table 4.24. Example of scale-up approaches for different concepts of reactors employed in alternative chemical production processes.

Equipment unit	Scale-up approach	Source for scale-up approach	Example of full-scale parameter
Isothermal tubular reactor	i) Increasing the tube diameter (up to a given diameter $d_{t,full-scale}$) while keeping constant tube length (up to a given length $L_{t,full-scale}$) ii) Increasing the number of tubes (up to a given number $n_{t,full-scale}$ per reactor) while keeping constant inlet flowrate per unit of tube area	[613]	$d_{t,full-scale}$= 60 mm $L_{t,full-scale}$ = 6 m $n_{t,full-scale}$ = 6000
Electrochemical cell	i) Fixing the inter-electrode gap while increasing the superficial area of individual cells (up to a given area $A_{c,full-scale}$) ii) Stacking individual cells in multi-cell reactors (up to a given number of cells $n_{c,full-scale}$ per reactor)	[614]	$A_{c,full-scale}$ = 16 m^2, $n_{c,full-scale}$= 200
Non-thermal plasma DBD reactor	i) Fixing the specific input energy while increasing discharge power (up to a given value $P_{dbd,full-scale}$) ii) Stacking individual reactors based on the related power supplied by generator (up to a given $P_{gen,dbd,full-scale}$ per stack)	[615]	$P_{dbd,full-scale}$ = 28 W (frequency 50 Hz, voltage 20 kV) $P_{gen,dbd,full-scale}$ = 300 W
Photocatalytic reactor (immersion-type with lamp)	i) Increasing the outside diameter of the lamp (up to a given diameter $d_{lamp,full-scale}$) and working volume in reactive lamp (up to a given ratio $\varepsilon_{lamp,full-scale}$ while keeping constant reaction performance ii) Increasing the volume of reactor (up to a given volume $V_{imm,full-scale}$) while keeping constant produced flowrate per unit of internal volume	[616]	$d_{lamp,full-scale}$ = 10 mm $\varepsilon_{lamp,full-scale}$ = 90% $V_{imm,full-scale}$ = 1000 m^3

As shown in Figure 4.13, a reference process scheme may not proceed to the following step of the procedure (step 3) if the number of units derived from the scale-up and design approach for at least one unit operation of the intensified process flowsheet is unrealistic with respect to installation in large-scale chemical process plant, e.g. more than 20 distillation units, more than 40 heat exchangers.

4.6.4. Step 3: Calculation of process intensification screening indicators

The effect on the design of the gradual intensification of the process scheme is assessed in step 3 of the procedure through the evaluation of screening indicators addressing different objectives of PrI concept. As discussed above, only the feasible intensified process flowsheets succeeding in the preliminary screening in the previous steps are considered for the indicator-based assessment in this step.

The original objective of PrI is to propose a sustainable process design aiming to be efficient (large reduction of energy consumption), economical (large reduction of processing costs), and environmental-friendly (reduction of carbon emissions and waste) [617]. The extension of the motivations of PrI to safety-related societal issues, i.e. reduction of the size of equipment units [603], offers the opportunity to significantly reduce the inventory of dangerous substances in the process and limit the consequences of potential hazards, thus realizing one of the principles of the inherent safety conceptualized by Kletz [369], i.e. minimization. Therefore, in the present methodology, some of the technical, economic and environmental indicators defined in the sustainability performance assessment model in Section 4.3 are complemented with some safety metrics addressing specific targets of potential hazards presented in the inherent safety assessment method in Section 4.5.

Among the technical indicators introduced in sub-Section 4.3.4.1, global energy efficiency of the reference process scheme, η, defined in Equation (4.2) is selected to address the energetic objective of the PrI concept in the present methodology. To cover the economic aspect of PrI, levelized cost of product indicator, LCOP, defined in Equation (4.9) is suggested for application of this method. LGHG indicator defined in Equation (4.11) is proposed to assess the environmental performance of the intensified process scheme in this methodology. Table 4.3 summarizes the input data required for the calculation of these indicators. Most of this information can be easily collected by using the outputs of the process simulator adopted in step 2. Since the goal of this step is to perform a screening analysis of the alternatives production routes independently from the location of the plant, simplified approaches may be adopted to estimate costs data associated to the process scheme, i.e. applying general assumptions commonly recommended in the literature for estimation of total capital investment and annual costs of a new onshore chemical process plant [478].

Concerning the inherent safety metrics, the most relevant target among humans, assets and environment should be selected for the purpose of the present screening analysis based on the hazard properties of the desired product of the production processes. For example, humans can be considered as the critical targets when H_2, SNG and CH_3OH are evaluated in the process schemes due to their flammability (and toxicity in case of CH_3OH) properties. Among the potential and inherent KPIs described in the performance assessment for human target (sub-Section 4.5.7.1), HHI defined in Equation (4.43) for each unit of the process scheme is selected in this methodology because it represents a more effective measure of the unit hazard level weighting damage area of accident scenarios and safety scores of equipment. The HHI associated to the entire process scheme can be obtained by summing up the single units HHI. The required input data for calculation of this indicator are reported in Table 4.16. By applying the same considerations made above for the other metrics, only information about the process and utility equipment should be collected disregarding the facility and environment conditions. Assumptions proposed for consequence

analysis of accident scenarios in onshore plants e.g. conservative environmental conditions and/or height of release with respect to humans [425], may be applied for estimation of damage distances required in HHI.

In order to provide a more concise assessment of PrI level of the intensified process designs, an overall indicator can be calculated from aggregation of the technical, economic, environmental and societal metrics evaluated above. The compensatory MCDA approach presented in the sustainability assessment methodology in Section 4.3 is proposed in the present method, since alternative process schemes producing the same final chemical product are compared. Therefore, normalization based on process-target values, weighting based time-space-receptor criteria and individualist-egalitarian-individualist perspectives, and aggregation based on arithmetic or geometric mean are applied in order to obtain a single-value indicator for the intensified process design, called in the present methodology Process Intensification Screening (PrIS) indicator. The details of these stages and related considerations are described in sub-section 4.3.4.5. Specific differences applied in this methodology are described in the following.

In the present model, only one indicator is defined for each category of the PrI concept, thus a single-step aggregation procedure is needed after the normalization of the indicators. Moreover, since different production schemes which have not already reached the commercial status are compared, target values for normalization of disaggregated indicators may be considered as performance measures associated to the actual large-scale production process of the chemical compound under analysis. Once collected the target values from the technical literature, X_{η} can be calculated by means of Equation (4.13), while X_{LCOP}, X_{LGHG} and X_{HHI} through Equation (4.12), given the consideration described in sub-Section 4.3.4.5. Finally, PrIS indicator can be calculated for each intensified process scheme by applying WAM method or WGM method, as described in the sustainability assessment methodology in Section 4.3:

$$PrIS = w_{\eta} \cdot X_{\eta} + w_{LCOP} \cdot X_{LCOP} + w_{LGHG} \cdot X_{LGHG} + w_{HHI} \cdot X_{HHI} \tag{4.71}$$

$$PrIS = {X_{\eta}}^{w_{\eta}} \cdot {X_{LCOP}}^{w_{LCOP}} \cdot {X_{LGHG}}^{w_{LGHG}} \cdot {X_{HHI}}^{w_{HHI}} \tag{4.72}$$

where PrIS is the process intensification screening indicator proposed as aggregated indicator for each scheme, X_{η}, X_{LCOP}, X_{LGHG}, X_{HHI} are the normalized indicators associated to η, LCOP, LGHG, HHI indicators, respectively, w_{η}, w_{LCOP}, w_{LGHG}, w_{HHI} are the weights attributed to η, LCOP, LGHG, HHI indicators, respectively, estimated based on the time-space- criteria and individualist-egalitarian-hierarchist perspectives of decision makers.

4.6.5. Step 4: Ranking of alternatives and sensitivity analysis

The calculation of the screening indicators in step 3 of the procedure allows comparing and ranking feasible designs of the process schemes which have passed the preliminary screenings based on operating features of unit operations and number of units in the scheme. The ranking can be performed from different viewpoints (i.e. technical, economic, environmental, inherent safety) and overall fingerprinting of the PrI concept.

As described in Section 4.3, the adoption of the proposed compensatory aggregation approach can introduce some uncertainties related to target vales used in the normalization of indicators and weights for the final aggregation. Sensitivity analysis is worth to perform in order to check the influence of variation in the values of target values on the PrIS indicator of the process scheme and rankings of the alternatives. Techniques described in Section 4.7 of this chapter may be applied to test the stability of the results.

4.6.6. Step 5: Application of detailed site-specific assessments

In the last step of the procedure, P2G and P2L offshore hybrid energy options can be conceptualized and properly simulated integrating the best intensified process schemes emerged in step 4 with renewable plants at a given offshore oil & gas site. Detailed site-specific assessments are then carried out to analyse and compare the assessment of such advanced integrated systems.

As shown in Figure 4.13, the application of detailed assessment methods requires to input not only the information related to the process scheme from the previous steps of the procedure, but also that associated to the oil & gas site considered for the analysis in terms of offshore oil & gas infrastructures to host the conversion process and meteo-marine conditions to evaluate renewable energy exploitation. Data that may be needed are summarized in Table 4.1. Similarly to the approach described above, sustainability and safety aspects of the alternative system designs can then be evaluated based on a detailed set of technical, economic, environmental and inherent safety indicators.

The inherent safety methodology described in Section 4.5 can be applied for a thorough assessment of the inherent safety fingerprinting of the offshore alternative design options based on multi-target potential and inherent KPIs. On the other hand, exergy has several qualities which makes it suitable as the confluence of energy, economic viability and environment, thus exergy-based methods can be identified as promising tools to quantify and improve sustainability performance of innovative system designs [240]. Exergy analysis allows to quantify the exergy efficiencies of the integrated system and its component as true measure of approach to the ideality, as well as the thermodynamic imperfections of the integrated system and its component in terms of exergy destructions representing losses in energy quality [130,618].

Therefore, it gives more illuminating insight into process performance than energy analysis. Moreover, the connection between exergy and economics appears fundamental for a thorough feasibility evaluation of emerging integrated systems at early design stage. Exergoeconomics, combining exergy-based thermodynamic assessment and economic principles at the level of system components provides useful information about the cost-effectiveness of the analysed system and its component [619,620]. By combining exergy analysis with a comprehensive environmental assessment method (e.g. LCA method), exergoenvironmental analysis reveals the environmental impact assigned to the exergy streams, identifying the system components with highest environmental impact and the options for possible improvements [621,622]. A new ranking of alternatives can be produced from the detailed site-specific evaluation. A further sensitivity analysis investigating the effect of varying some key parameters on the final results may then be applied.

4.7. Sensitivity analysis techniques

Different techniques are available in the literature to perform sensitivity analysis based on the purpose of the investigation [623], i.e. to determine which parameters require further investigation to reduce output uncertainty, or which parameters are insignificant for the analysis under consideration, or which input data contribute more to the output variability, or which consequences are generated in the outputs by changing the input parameters. They can range from the simplest one-at-a-time sensitivity measures to more complex standardized regression coefficients and statistical tests based on partitioning of empirical input distributions. In practical applications regarding comparison of different alternatives based on aggregated performance indicators, it is important to understand how the uncertainty may affect the ranking of the alternatives and test how robust such a ranking may be considered. A sound and auditable approach is to verify the effect of variation in influential parameters on the relative performance of the output indicators among couples of the alternatives rather than on their absolute values. This is called discernibility analysis, generated from the combination of comparative analysis and uncertainty analysis [624].

Based on the idea of discernibility analysis, in the present study a general approach is proposed for verification of the ranking of the alternatives in the assessment methodologies described above. It consists first in identifying a confidence interval for each uncertain parameter by evaluating the uncertainty associated to data sources used to define such a variable or assuming fixed variation. Then, propagation of uncertainties in the parameters is investigated through the common Monte Carlo simulation method [625], attributing a proper distribution of probabilities of the values of the parameters in the selected range (e.g. uniform distribution, beta distribution, triangular distribution, etc.). By Monte Carlo runs, cumulative

probability distributions of differences between selected couples of alternative options are provided. The analysis of such distributions highlights possible inversion in the ranking of the alternatives as well as the probability corresponding to such an inversion for a given number of simulations. Clearly enough, the lower probability for possible inversion in the ranking, the higher the robustness of these results. When several input parameters are considered in the analysis, a simple one-at-a-time sensitivity can ease the identification of the most influential variables for further stochastic variation by means of the Monte Carlo approach.

Chapter 5.

Case-studies

5.1. Introduction

In this chapter, the assessment methodologies presented in Chapter 4 are applied to five case-studies. Some case-studies introduce different challenging situations, from offshore remote fields to depleted gas reservoirs and aging installations, thus offering opportunities for the development of P2G/P2L/G2P offshore hybrid energy options. Others are representative of specific safety and environmental issues, which may be experienced during early design activities of the offshore systems or serve as examples of emerging chemical process routes requiring a preliminary investigation for further application in P2G/P2L offshore hybrid energy options. The analysis of the case-studies aims to demonstrate the ability of the developed portfolio of assessment models to capture in a flexible way the different issues related to the offshore context, to assess the alternatives by means of a comprehensive MCDA approach and to orient the most suitable solution for each problem. The case-studies described in this chapter are briefly presented in the following in order to better motivate the application of the methodologies developed in the present research project.

Case-study 1 consists of a gas production platform located in a remote area of the North Sea where exploitation of offshore wind energy is considered for the energetic valorisation of the site. Therefore, such a case-study provides the opportunity for the conversion of renewable electricity produced from an OWT farm into alternative chemical energy carriers at the offshore facility, i.e. H_2, SNG and CH_3OH. The goal of the analysis of this case-study is to demonstrate the potential of the sustainable assessment methodology presented in Section 4.3 to compare and rank alternative P2G and P2L hybrid energy strategies at the defined offshore site.

Case-study 2 concerns a gas production installation located in a depleted field in the Adriatic Sea relatively close to the shore, where the feasibility of an OWT farm is investigated for the integration of renewable power into the onshore electrical network. As a result, this case-study provides the opportunity to improve the dispatchability of offshore wind energy and valorize the untapped gas resources using GT technologies at the offshore facility. The aim of the analysis of this case-study is to prove the capacity of the sustainability assessment methodology presented in Section 4.4 to compare and rank alternative G2P hybrid energy options at the defined offshore site.

Case-study 3 represents the design of alternative production and separation schemes of an offshore facility exploiting natural gas in the Adriatic Sea, which shows safety criticalities. The goal of the analysis is to demonstrate the ability of the inherent safety assessment methodology described in Section 4.5 to rank critical design solutions based on the developed multi-target KPIs and capture the different contributors to the safety profile of the offshore system during early design activities. The analysis of the

P2G/P2L/G2P hybrid energy options which may be adopted at the offshore site is thus disregarded in this case-study.

A novel set of KPIs for environmental protection from oil accidental spills with three different levels is defined within the inherent safety methodology in Section 4.5. Different tools for consequence analysis of oil fate are proposed for calculation of environmental KPIs of levels 2 and 3. Thus, case-study 4, consisting of different oil releases from four offshore oil production facilities, was carried out with the aim to specifically test the capacity of the developed set of environmental KPIs to rank the hazard level of different oil spills. As for case-study 3, the implementation of P2G/P2L/G2P hybrid energy options at the offshore sites is preliminarily ignored in the analysis of this case-study.

Case-study 5 consists of alternative process routes for renewable CH_3OH production at low maturity level which need to be investigated comprehensively, based on different performance aspects, for a suitable adoption in P2L offshore hybrid energy options. Thus, the PrI screening methodology described in Section 4.6 is applied to this case-study in order to check the viability of the alternative processes integrating both sustainable and safety analyses demonstrated in the previous case-studies and to address the most feasible schemes to detailed assessment of P2L hybrid energy systems in the Atlantic Ocean.

In the following sections, each case-study is presented and discussed in detail, including proper assumptions made for the analysis, results and discussion.

5.2. Case-study 1: Application of the sustainability assessment methodology to OWT farm and P2G/P2L options

The sustainability assessment methodology described in Section 4.3 is applied to a case-study located in a remote area in the North Sea in order to demonstrate the ability of the method to rank alternative P2G and P2L offshore hybrid energy options based on the proposed sustainability and profitability performance indicators.

5.2.1. Definition of the offshore oil & gas site and evaluation of the strategies

A remote area located in the North Sea is considered as a location of the offshore oil & gas platform hosting the process units of the alternative P2G and P2L options for conversion of renewable energy. Offshore wind energy is considered as renewable source to be exploited at the offshore site and converted into chemical energy carriers at the offshore facility, given previous feasibility analyses on large scale offshore wind-H_2 platforms in the North Sea [136–138].

As required from step 0 of the procedure illustrated in Figure 4.2, the offshore oil & gas site is defined providing input data about the field and infrastructures. The platform is supposed to be an off-grid gas production platform in the central part of the North Sea, where gas fields are actually exploited and linked to the gas market in UK, Norway, Germany, France and Belgium by means of sealines (Langeled, Zeepipe, Statpipe, Zeepipe, Franpipe) [626]. Most of these gas pipelines are considered for re-use in CO_2 transportation in a previous investigation [204]. The Sleipner Vest field in the Sleipner area (blocks 15/6 and 15/9 in the North Sea) is taken as a reference, where water depth is 100 m and natural gas with 4-9% CO_2 is extracted and treated by using amine absorption in order to remove CO_2 [193].

The UK is selected as reference market for the end-uses of the final products of the conversion processes, as well as for the possible supply of required input materials. A gas sealine linking the gas platform to a UK gas terminal is considered, with a length of 500 km, a delivery pressure of 155 bar, a capacity of $72 \cdot 10^6$ Sm^3/d, which are features similar to those of the existing Langeled pipeline from Sleipner to Easington (UK) [627]. Furthermore, another sealine 400 km long is considered for transportation of other gases than natural gas from the shore, inspired by the Central Area Transmission System (known as CATS) natural gas transportation and processing system delivering gas from the Central North Sea to Teesside terminal (North East of UK) [204]. Moreover. an onshore harbour located at a distance of 200 km from the offshore area, which is approximately the distance of the Aberdeen port from the Sleipner area, is considered for the docking of supply vessels to and from the offshore platform. About 12 voyages per year are reasonably estimated for supply vessels.

Having collected the input data summarized in Table 4.1, possible conversion strategies are evaluated according to step 1 of the procedure. Given the characteristics of the selected oil & gas site, the six pathways and associated process stages illustrated in Figure 4.3 are considered for the analysis in this case-study, thus H_2, SNG and CH_3OH are evaluated as chemical energy carriers and final products for the onshore market. The electrical power required for the process operations at the offshore facility is considered to be completely supplied by an OWT farm located in proximity to the gas platform and linked to it by means of an electrical grid connection.

The 500 km-pipeline can be adopted to deliver H_2-natural gas mixture and SNG, while the 400 km-pipeline can be used to supply gaseous CO_2 from the shore. Regarding the transportation of pure H_2, the maximum operating pressure is set as 100 bar, bearing in mind the experience gained from H_2 pipelines mostly realized around the world [179]. For each alternative, the details of the technologies adopted for the process stages, components and their operating conditions are reported in Appendix A of the present study.

5.2.2. Definition of the OWT farm and reference process schemes

According to step 2 of the procedure in Figure 4.2, the OWT farm and reference process schemes of the alternative strategies are defined. Given the water depth of the Sleipner area, an offshore floating wind farm is considered for renewable power conversion. Among the possible floating concepts, the Hywind II technology by Equinor [628], consisting of a Spar-Buoy foundation moored with a three catenary mooring lines to the seabed, stabilised using ballast, designed to carry one upwind turbine in the region 2.3-6 MW in water depths greater than 100 m, is considered. A previous work by Myhr et al. [629] investigating the levelized cost of energy of different floating concepts at a generic Northern European site is used in this case-study as main literature source to retrieve technical and economic data of the renewable plant. The OWT farm is assumed to be composed of 100 wind turbines of 5 MW nominal capacity each one, thus leading to total size of 500 MW. The main technical data associated to the plant are summarized in Table 5.1. Table 5.2 reports economic information of the plant, as obtained from Myhr et al. [629].

Table 5.1. Case-study 1: Technical data of the OWT farm considered in the analysis [629].

	Value/properties
Size of offshore wind farm	500 MW (100 turbines of 5 MW capacity)
Layout	Square formation (10 x 10) with inner distance between each turbine of 1 km
Distance offshore-onshore substations	200 km
Distance to construction and operations port	200 km
Offshore converter substation	500 MW Voltage Source Converter
Inter-array cable	Alternating current, 33 kV voltage, copper, 300 mm^2 area, 191.6 km total length, 224 MW average power transmitted within the farm, 0.3% average power loss
Export cable	Direct current, 320 kV voltage, extruded, 1500 mm^2 area, 200 km length, 0.5% average power loss
Theoretical production	360 MWh/MW/y
Capacity factor	45.8%
Wind farm availability	94%
Aerodynamic array losses	7%
Electrical array losses	1.8% (inter-array, offshore substation, export cable), 1.3% (inter-array, offshore substation)
Other losses	3%
Net load factor	38.1% (inter-array, offshore substation, export cable), 38.3% (inter-array, offshore substation)
Net energy production	3340.9 MWh/MW/y (inter-array, offshore substation, export cable), 3357.9 MWh/MW/y (inter-array, offshore substation)

Table 5.2. Case-study 1: Economic data of the OWT farm considered in the analysis [629].

Cost	Cost segment	Value
CAPEX Production and acquisition	Turbine (excluding tower)	$6.41 \cdot 10^6$ €
	Substructure and tower	$3.74 \cdot 10^6$ €
	Mooring system	$4.61 \cdot 10^5$ €
	Inter-array cable	$5.38 \cdot 10^7$ €
	Offshore substation (excluding platform)	$1.27 \cdot 10^5$ €
	Export cable	$8.86 \cdot 10^7$ €
	Onshore substation	$7.15 \cdot 10^5$ €
CAPEX Installation and commissioning	Turbine	$7.86 \cdot 10^5$ €
	Mooring system	$1.67 \cdot 10^7$ €
	Inter-array cable	$3.77 \cdot 10^7$ €
	Export cable	$1.18 \cdot 10^8$ €
OPEX O&M	Material	$7.10 \cdot 10^6$ €/y
	Labour	$4.80 \cdot 10^6$ €/y
	Equipment (mother vessel, port facilities, 2 maintenance vessels)	$4.01 \cdot 10^6$ €/y
	Other equipment	$4.04 \cdot 10^7$ €/y
OPEX Operation phase insurance		$1.75 \cdot 10^4$ €/y

All values in the table are referred to year 2013.

Given the size of the OWT farm, a common reference basis for the analysis of the alternative strategies is set as maximum power feed fraction of the wind farm output to the electrolyzers, i.e. 10% in this study. Therefore, the total electrolyzers capacity is 50 MW for all the alternatives, which corresponds to 753.8 kg/h of H_2 production based on features of the technology considered in this process stage and detailed in Appendix A.

Specific battery limits are considered in the assessment. The performance and costs of the OWT farm and its connection with the oil & gas platform are considered in the overall profitability of P2G and P2L strategies, but excluded in the sustainability assessment due to neutrality with respect to the selection of the technological alternatives for electricity conversion. Thus, the boundaries for calculation of the sustainability indicators for each alternative are limited to process stages.

Technical, economic and environmental dimensions of sustainability are investigated in this case-study, thus leaving the societal aspect out of the scope of the analysis. The parameters required in input for each reference process scheme are estimated based on data and assumptions detailed in Appendix A.

The grey prices for H_2 and SNG intended for the grid (Options 1, 3a and 3b) are based on the UK 2018 wholesale price of natural gas (non-households consumers) equal to 30 €/MWh [630] by applying the corresponding higher heating values (i.e. 39.4 kWh/kg for H_2, 14.5 kWh/kg for SNG). For Option 2, the H_2 selling price is obtained as average value between European selling prices for light industry (3.8-9.4 €/kg) and for car and buses (4-7 €/kg) [631]. In the case of CH_3OH, market price for Options 4a/4b is

estimated based on the Methanex European posted contract price referred to December 2018 [632]. The values used in this study are summarized in Table 5.3.

The non-domestic renewable heat incentive (RHI) established by the UK Office of Gas and Electricity Markets (OfGem) for the first 40000 MWh of injected biomethane into the grid between 22 May and 31 December 2018 [633], i.e. of 57.2 £/MWh, is considered to calculate the equivalent green prices of H_2 in the natural gas mixture in case of Option 1 and of SNG in case of Options 3a and 3b. Conversion from £/MWh to €/kg is performed by using the 2018 currency conversion rate in Table A.5 in Appendix A and HHV value of 39.4 kWh/kg for H_2 and of 14.5 kWh/kg for SNG. The UK ETS price of 16.37 $/$t_{CO2}$ referred to year 2018 [634] (i.e. 13.91 €/t_{CO2} by applying the 2018 currency conversion rate in Table A.5 in Appendix A) is assumed to calculate the cost savings of CO_2 emissions allowance thanks to the production of renewable H_2 and CH_3OH with respect to the fossil ones. Considering GHG emissions for H_2 produced by means of steam reforming (with CH_4 in input) equal to 72.4 g_{CO2eq}/MJ (i.e. about 10.3 kg_{CO2eq}/kg_{H2}) and for H_2 produced from electrolysis equal to 0 g_{CO2eq}/MJ (i.e. 0 kg_{CO2eq}/kg_{H2}) [635], the green premium in Option 2 is estimated as the difference between these two GHG emissions multiplied for the considered ETS price, i.e. 0.14 €/kg. The same approach is applied to estimate the savings in case of Options 4a and 4b by assuming GHG emissions for diesel equal to 95.10 g_{CO2eq}/MJ (i.e. about 3.80 kg_{CO2eq}/kg_{diesel}) and for Sunflower biodiesel equal to 32 g_{CO2eq}/MJ (i.e. about 1.28 kg_{CO2eq}/kg_{diesel}). The added value for CH_3OH as fuel in the mobility sector is 0.035 €/kg. The financial incentive calculated for Options 2, 4a and 4b are then added to the grey prices in order to obtain the green selling prices of the products. Table 5.3 summarizes the values of the green selling prices adopted for the alternative strategies.

Table 5.3. Case-study 1: Grey and green market prices of the final products considered for the alternative strategies.

	Option 1	Option 2 (H_2)	Option 3a/3b	Option 4a/4b
Final product and end-use	H_2 admixture for grid injection	H_2 for industry and mobility sectors	SNG for grid injection	CH_3OH for mobility sector
Grey market price (€/kg)	1.18	6.00	0.44	0.43
Green market price (€/kg)	2.55	6.14	0.94	0.46

5.2.3. Assumptions made for the sustainability assessment

To quantify the technical aspect of sustainability performance of the alternative process schemes, among the indicators defined in Section 4.3, the energy efficiency indicator, η, is selected in this case-study, disregarding the calculation of the exergy efficiency indicator, ψ. HHV values summarized in Table 4.5 are assumed to apply Equation (4.2). The mass flowrate $\dot{m}$ of the final product and electrical power required $\dot{W}$ associated to the components of each strategy are estimated based on the data detailed in Appendix A. $\dot{W}$ values are summarized in Table 5.4.

Regarding the economic performance assessment, both LCOP and LVOP proposed in the assessment model in Section 4.3 are calculated for the reference process schemes. CAPEX and OPEX required in Equation (4.9) are calculated as detailed in Appendix A. The reference currency and year for the cost analysis are € referred to 2018. Thus, if required, cost adjustments based on Equation (4.1) are performed by considering conversion rates and total industrial PPI summarized in Table A.5 in Appendix A. Final CAPEX and OPEX values considered for calculation of the economic indicators are summarized in Table 5.4 for the different process stages of the alternatives. Each revenue required in Equation (4.10) is calculated by multiplying the produced flowrate of the final product of each pathway by the corresponding market price (Table 5.3).

Moreover, an economic lifetime of 10 years is conservatively assumed for all the alternatives, without any further investment, considering the lifetime of the electrolyzers [636], which are expected to be the most expensive components of the conversion processes. CAPEX of each component of the process stage occurs at the beginning of the project, while OPEX, production and revenues are discounted at each year of the project lifespan. The discount rate r is considered constant along the economic lifetime period and equal to 8%, in agreement with previous studies [116,119,124,159]. Neither income taxes nor depreciation are considered, for the sake of simplicity. These assumptions are applied also for calculation of NPV defined in Equation (4.20) in the profitability assessment.

LGHG indicator defined in Equation (4.11) is used to quantify the environmental performance of the alternatives. GHG emissions associated to each reference process scheme are calculated as detailed in Appendix A. The values obtained for the relevant process stages of the six pathways are summarized in Table 5.4.

Table 5.4. Case-study 1: Technical, economic and environmental data of process stages of the alternatives.

Process stage	Option	$\dot{W}$ (kW)	CAPEX (€)	Annual OPEX (€/y)	GHG emissions (kg_{CO2eq}/y)
Desalination	1, 2, 3a, 3b, 4a, 4b	$9.05 \cdot 10$	$3.31 \cdot 10^5$	$6.62 \cdot 10^3$	$1.90 \cdot 10^4$
H_2 production	1, 2, 3a, 3b, 4a, 4b	$5.27 \cdot 10^4$	$4.35 \cdot 10^7$	$4.56 \cdot 10^6$	$3.96 \cdot 10^6$
H_2 compression	1	$9.01 \cdot 10^2$	$7.94 \cdot 10^5$	$3.17 \cdot 10^4$	-
H_2 transportation	1	-	-	$8.79 \cdot 10^5$	-
H_2 compression	2	$6.17 \cdot 10^2$	$5.64 \cdot 10^5$	$2.26 \cdot 10^4$	-
H_2 transportation	2	-	$2.48 \cdot 10^8$	$5.68 \cdot 10^6$	-
CO_2 capture	3a	$1.02 \cdot 10^3$	$6.89 \cdot 10^5$	$1.24 \cdot 10^5$	$1.73 \cdot 10^7$
CO_2 compression	3a	$3.06 \cdot 10^2$	$1.58 \cdot 10^6$	$7.91 \cdot 10^4$	-
H_2 storage	3a, 3b, 4a, 4b	-	$1.10 \cdot 10^7$	$2.20 \cdot 10^5$	-
SNG production	3a, 3b	$4.99 \cdot 10^2$	$1.35 \cdot 10^7$	$1.31 \cdot 10^6$	$3.97 \cdot 10^6$
CO_2 purchase	3b	-	-	$8.60 \cdot 10^4$	-
CO_2 transportation	3b	-	-	$6.87 \cdot 10^6$	-
CO_2 compression	3b	$1.04 \cdot 10$	$1.64 \cdot 10^5$	$8.21 \cdot 10^3$	-
SNG compression	3a, 3b	$3.22 \cdot 10^2$	$2.17 \cdot 10^5$	$1.30 \cdot 10^4$	-
SNG transportation	3a, 3b	-	-	$2.21 \cdot 10^5$	-
CO_2 capture	4a	$1.36 \cdot 10^3$	$9.19 \cdot 10^5$	$1.65 \cdot 10^5$	$2.31 \cdot 10^7$
CO_2 compression	4a	$4.08 \cdot 10^2$	$1.92 \cdot 10^6$	$9.59 \cdot 10^4$	-
H_2 + CO_2 compression	4a	$5.67 \cdot 10^2$	$2.03 \cdot 10^6$	$1.02 \cdot 10^5$	-
CH_3OH production	4a, 4b	$1.55 \cdot 10^3$	$3.65 \cdot 10^6$	$3.80 \cdot 10^4$	$9.10 \cdot 10^6$
CO_2 purchase	4b	-	-	$3.15 \cdot 10^5$	-
CO_2 transportation	4b	-	-	$6.87 \cdot 10^6$	-
CO_2 compression	4b	$1.39 \cdot 10$	$1.99 \cdot 10^5$	$9.95 \cdot 10^3$	-
H_2 + CO_2 compression	4b	$5.14 \cdot 10^2$	$1.90 \cdot 10^6$	$9.52 \cdot 10^4$	-
CH_3OH storage	4a, 4b	-	$4.11 \cdot 10^5$	$8.23 \cdot 10^3$	-
CH_3OH transportation	4a, 4b	-	-	$2.07 \cdot 10^5$	-

In order to provide a concise yet representative comparison between the overall performance of the alternatives based on different aspects, the above defined indicators are aggregated into a global indicator. Among the approaches for aggregated performance assessment described in Section 4.3, a non-compensatory MCDA method is applied in this case-study since alternatives producing different products (H_2, SNG, CH_3OH) are compared, thus avoiding the need for normalization of indicators based on process-related target values. The PROMETHEE II method [494] is selected in order to obtain a complete ranking of the alternatives based on the net outranking flow (Φ) ranging between -1 and 1.

In the present study, the calculation of the aggregated scores of the six alternative conversion technologies is performed by using Visual Promethee 1.4 Academic Edition software [497], where PROMETHEE II is implemented. The values of the indicators estimated by applying Equations (4.2), (4.9), (4.10) and (4.11) are provided as an input, using an evaluation performance matrix. The maximization is then selected for η and LVOP, while the other two indicators are minimized. Based on the performance data

provided in input to the software, the recommendations provided from the tool about the most suitable preference function and related preference thresholds are applied.

The evaluation of relative importance weights among indicators is performed by applying the approach described in Section 4.3 based on time-space-receptor criteria and individualist-egalitarian-hierarchist perspectives. Equal weighting is further added to the archetypes of decision makers. Before scoring and weighting, the indicators selected for the assessment of the case-study are classified in terms of time, space and receptor based on their definition.

Being a measure of resource use, η is considered important for a long-term perspective where resource scarcity may require more efficient methods. It is relevant on a global scale since improvements may lead to better and resource utilization and lower emissions, reduced costs. Ecosystem is evaluated as main receptor by this indicator, but also humans may be influenced since resource use and costs are human-related areas.

LCOP exhibits mainly short-term, local/regional and anthropocentric perspectives. However, it can be considered unimportant over time since externalities (e.g. available resources, socio-political variations and other local/regional factors) are internalized into the cost assessment.

As opposed to LCOP, LVOP can influence both humans and ecosystem receptors at a regional scale because financial incentives on market prices of the products may be implemented due to policy adopted by the local Government as a response to environmental issues and resource depletion. With respect to time it shows the same features of LCOP.

Finally, LGHG is considered a very important long-term and global-scale concern, even though its effect may be short-term and at local scale based on the incidence of weather. Thus, it is evaluated as neutral on time and space criteria. Both humans and ecosystems are sensitive receptors.

For each archetype, given scores are assigned to indicators based on the three criteria. The overall score to each indicator is estimated as the sum of the scores given with respect to each criterion. The relative importance of the indicators is determined as the ratio of the associated overall score to the sum of overall scores. All the values of assigned scores and weights are reported in Table 5.5. Figure 5.1 illustrates the comparison of weights based on the different perspectives mentioned above to be used in the aggregated sustainability assessment. As shown in this figure, the individualist archetype prioritized LCOP, LGHG and LVOP because of its selfish and resilient viewpoint, while the egalitarian method gave higher priority to η besides LGHG. On the other hand, slight variations in prioritizing the indicators appeared in case of the hierarchist perspective, thus leading to similar findings than the weighting scheme.

Table 5.5. Case-study 1: Scores and weights assigned for aggregation of indicators based on different perspectives.

Schemes	Criteria	Indicators for sustainability performance assessment			
		η	LCOP	LVOP	LGHG
		Score 1-5	Score 1-5	Score 1-5	Score 1-5
Individualist	Time	2	3	3	3
	Space	3	4	2	3
	Receptor	2	4	5	5
	Sum	7	11	10	11
	Relative importance weight	0.179	0.282	0.256	0.282
Egalitarian	Time	5	3	3	5
	Space	5	3	4	5
	Receptor	4	1	5	5
	Sum	14	7	12	15
	Relative importance weight	0.292	0.146	0.250	0.313
Hierarchist	Time	3.5	3	3	4
	Space	4	3.5	3	4
	Receptor	3	2.5	5	5
	Sum	10.5	9	11	13
	Relative importance weight	0.273	0.260	0.234	0.234
Equal weighting	Relative importance weight	0.250	0.250	0.250	0.250

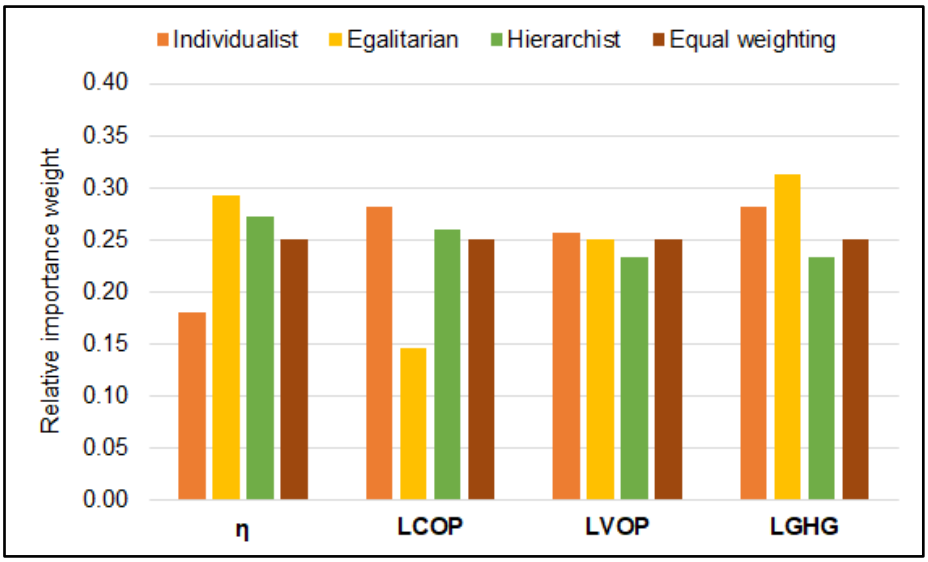

Figure 5.1. Case-study 1: Weights among the indicators based on different perspectives for the aggregated sustainability assessment.

5.2.4. Assumptions made for the profitability assessment

For the purpose of profitability assessment based on NPV in Equation (4.20), three business cases (BCs) are analysed and compared each other: BC1, BC2 and BC3. BC1 represents the baseline situation of zero integration of wind energy into the offshore oil & gas operations, thus only electrical grid connection

between the offshore wind farm and onshore substation, as well as revenues from the electricity selling to suppliers are conceptualized.

BC2 represents the situation described in Figure 4.3, which considers the electrical connection between the wind farm and the platform but only gas grid or ship travel to shore, thus the entire offshore wind power is used for the processes at the platform and only revenues coming from the selling of final products to the onshore markets can be gained.

Finally, BC3 aims to conceptualize the situation of an offshore hybrid energy system integrated into the electrical network which uses electrolysis as energy balancing system in order to limit wind curtailments according to grid connection agreements, handle large electrical power fluctuations of the wind power plant and absorbing the unpredicted excess of power production, otherwise curtailed, for synthesis of valuable chemicals [229]. As a result, an electrical export cable to shore is present in addition to the connection mentioned in BC2, thus a part of offshore wind power is directly routed to the land and the other part is converted into the chemical energy carrier at the offshore platform. In such a situation, a double revenue can be obtained coming from the selling of both electricity and final product of the pathway.

In order to perform the profitability analysis for the different BCs described above, economic data related to the offshore wind farm in Table 5.2 are adjusted by applying cost indices in Table A.5 of Appendix A. Moreover, the following further specific assumptions are made.

The offshore substation including AC switchgear, transformers, converter electronics and filter and used to increase the voltage prior to its use, is supposed to be located at the offshore gas platform considered in the analysis; thus, the platform costs of offshore substation proposed by Myhr et al. [629] are disregarded in the calculation of CAPEX, as illustrated in Table 5.2.

The electrical connection between the OWT farm and the gas platform (where the offshore substation is located) is considered for all BCs, while the export subsea cable between the offshore substation and onshore substations is evaluated only in case of BC1 and BC3. According to these two situations, different values for electrical losses, load factor and net energy production are reported in Table 5.2. Moreover, CAPEX associated to export cable and its installation, as well as CAPEX associated to onshore substation reported in Table 5.2 are excluded from the profitability analysis of BC2, but included in the assessment of BC1 and BC3.

For the assessment of BC1 and BC3, market prices of renewable electricity delivered to the grid are estimated based on the current policy implemented in the reference country. UK supports large-scale renewable electricity projects, including offshore wind farms, under the Renewables Obligation (RO)

mechanism [637]. According to RO, once the generating plant has been accredited, generators can be issued Renewables Obligation Certificates (ROCs) by the UK Office of Gas and Electricity Markets (OfGem) based on the net renewable electricity generated each month by the plant and then sell them directly or indirectly to electricity suppliers, providing an additional income on top the selling of electricity wholesale price. Suppliers are asked to purchase ROCs amounting to a "headroom" figure set by the Department of Energy and Climate Change (DECC) for each financial year, involving a forecasting renewable generation and adding 10%. Suppliers can then redeem the purchased ROCs in order to show their compliance with the obligation, paying a penalty in the form of the buy-out price for every MWh below the obligation. The buy-out payments made are put into a buy-out fund which is redistributed among the suppliers who presented correct number of ROCs at the end of the period.

In this case-study, it is supposed that eligibility requirements for full accreditation under RO scheme are met by the OWT farm, being an offshore wind generating station, already been commissioned, located within the territorial waters of the UK and connected to a transmission network in Great Britain, and then accreditation is granted after the application approval. As a consequence, revenues derived from the electricity market (at the wholesale market price) and ROCs market (at ROCs recycle value reported each year by OfGem) awarded for eligible output are included in the NPV calculation of BC1 and BC3. According to the guidance for generators about RO scheme [638], for installed capacity after 2016 the level of support for OWT farm is established as 1.8 ROCs per MWh of eligible electricity produced each month. The UK wholesale electricity market of 64.3 £/MWh referred to December 2018 [639] and recycle rate per ROC of 5.85 £/ROC referred to year 2018 [640] are assumed for the calculations. To convert these prices into €, the corresponding exchange rate reported in Table A.5 of Appendix A is applied. The net energy production from OWT farm reported in Table 5.1 is used to calculate the eligible monthly renewable output for the analysis of BC1 and BC3, assuming for the sake of simplicity 500 MW and 440 MW capacities, respectively. Therefore, in BC3, about 60 MW of the available wind power is considered for conversion into H_2, SNG, CH_3OH at the offshore platform, avoiding curtailments. The final annual revenues from renewable electricity selling to the UK market are calculated equal to $1.41 \cdot 10^8$ €/y for BC1 and $1.08 \cdot 10^8$ €/y for BC3.

5.2.5. Sustainability and profitability assessment results

Table 5.6 summarizes the results obtained for the technical, economic and environmental performance indicators calculated for the case-study, based on the data summarized in Table 5.4. The ranking of the alternatives with respect to each indicator is also reported.

Table 5.6. Case-study 1: Technical, economic and environmental indicators for the alternatives and associated ranking.

	η		LCOP		LVOP (no incentive)		LVOP (with incentive)		LGHG	
	Value (%)	Rank	Value (€/MWh)	Rank	Value (€/MWh)	Rank	Value (€/MWh)	Rank	Value (kg_{CO2eq}/MWh)	Rank
Option 1	59.39	2	43.4	1	28.0	4	60.2	4	14.3	1
Option 2	59.71	1	212.0	6	142	1	145.0	1	14.3	1
Option 3a	39.92	6	89.0	2	30	3	64.6	3	132.0	5
Option 3b	40.90	5	125.0	4	30	3	64.6	3	41.4	3
Option 4a	43.39	4	123.0	3	120	2	129.0	2	299.0	6
Option 4b	44.82	3	177.0	5	120	2	129.0	2	108.0	4

As shown in Table 5.6, when the energy efficiency indicator is considered, Options 1 and 2 are the most efficient, with values of η around 60%. Option 2 appears slightly more efficient than Option 1 due to lower delivery pressure assumed for the H_2 pipeline, leading to lower electrical power required for compression (Table 5.4). In the other options, the additional process stages of conversion and conditioning needed to produce SNG and CH_3OH implies a decrease in the expected technical performance. For these processes, η results lower for Options 3a and 3b (around 40%) than for Options 4a and 4b (around 44%).

Concerning the ranking of the alternatives based on LCOP, Option 1 shows the best economic performance (i.e. lowest LCOP value) in addition to the best technical performance based on η, while Options 2 demonstrates the highest value of LCOP. This can be attributed to higher transportation costs associated to this option, as shown in Table 5.4.

The two sets of LVOP values calculated, based respectively on grey and green market prices of the final products, are both summarized in Table 5.6 in order to evaluate the impact of the financial incentives on the levelized revenues. In both cases, the highest LVOP is associated to H_2 intended for use in industry and mobility (Option 2), followed by CH_3OH for mobility (Options 4a/4b). As a consequence, industry and mobility sectors are the most advantageous end-markets for P2G and P2L products. Another finding gained in the case-study is that the upgrading from grey to green market prices appears highly beneficial in case of Options 1, 3a and 3b, for which gas grid injection is the end-use of the product. These options show approximately a doubling of the LVOP values when incentives are considered.

On the other hand, the highest environmental performance, corresponding to the lowest LGHG value, is obtained for Options 1 and 2, thus confirming the ranking based on η and LCOP. The highest values calculated for Options 3b and 4b are attributed to larger environmental impact associated to onsite CO_2 capture, as reported in Table 5.4.

Table 5.7 summarizes the values of the overall aggregated indicators, Φ, derived from the application of the PROMETHEE II method to the technical, economic and environmental indicators of the six

conversion processes considered in the case-study. The table also reports the ranking of the alternatives based on different sets of weight coefficients, corresponding to different archetypes of decision makers illustrated in Figure 5.1. When analysing the results, Option 1 showed the best aggregated performance according to the individualist, hierarchist and equal weighting perspectives. Whereas, Option 2 is the most performant based on the egalitarian scheme. This confirms the ranking previously identified based on indicators addressing single aspects of sustainability.

Table 5.7. Case-study 1: Comparison of ranking of the pathways based on the overall aggregated sustainability indicator for different weighting schemes.

	Individualist scheme		Egalitarian scheme		Hierarchist scheme		Equal weighting	
	Φ value	Rank	Φ value	Rank	Φ value	Rank	Φ value	Rank
Option 1	0.317	1	0.313	2	0.358	1	0.335	1
Option 2	0.213	2	0.410	1	-0.262	2	0.273	2
Option 3a	-0.161	4	-0.273	3	-0.195	3	-0.200	3
Option 3b	-0.123	5	-0.167	5	-0.170	5	-0.163	5
Option 4a	-0.184	3	-0.258	4	-0.176	4	-0.181	4
Option 4b	-0.063	6	-0.26	6	-0.080	6	-0.064	6

The NPV indicator of the alternatives is calculated for the different BCs described above by applying Equation (4.20). The results are displayed in Figure 5.2. As appears evident in this figure, the baseline situation considered in BC1 results in the most profitable investment with NPV of about 226 M€. Whereas, all the P2G and P2L pathways in BC2 show negative values of NPV, thus indicating that the sole revenues from the products selling are not sufficient to cover the total costs under the assumed input data. In this case, the break-even market prices of the products to reach NPV equal to 0 are estimated as 13.3 €/kg, 20.4 €/kg, 6.8 €/kg, 7.5 €/kg, 2.4 €/kg, 2.9 €/kg for Options 1, 2, 3a, 3b, 4a, 4b respectively. Therefore, with respect to the market prices in Table 5.3, to reach the break-even point, prices should increase about three times for Option 2, five times for Options 1 and 4a, six times for Option 4b, seven times for Option 3a and eight times for Option 3b. When additional revenues deriving from the electricity selling to suppliers are considered in BC3, more favourable results are obtained: NPV values of all the alternatives increased proportionally than BC2, becoming less negative as in Options 2, 3a, 3b, 4b, and even positive in case of Option 1 (37 M€) and Option 4a (10 M€).

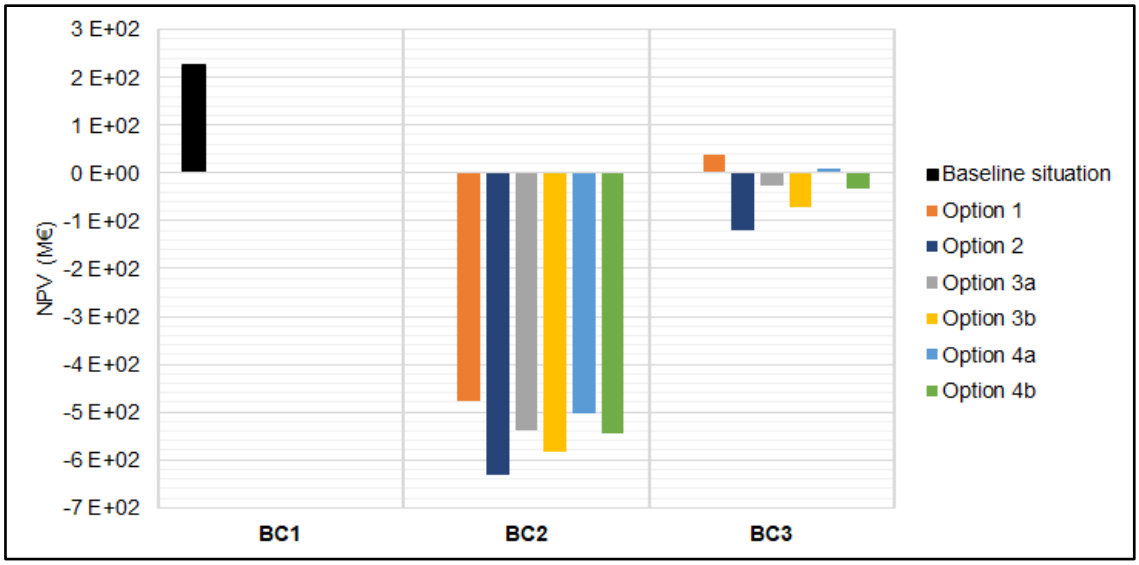

Figure 5.2. Case-study 1: Comparison of NPV of the alternatives in the BCs considered for profitability analysis.

5.2.6. Results of sensitivity analysis

In this case-study, the adoption of the approach based on time-space-receptor criteria and different archetypes of decision makers for weights elicitation in the integrated sustainability assessment is considered as an alternative way to reduce uncertainty associated to this stage, thus sensitivity analysis is not applied to verify the robustness of aggregated sustainability indicators obtained for the alternatives.

In case of profitability analysis, sensitivity analysis is applied to the most profitable P2G and P2L alternatives emerged in the NPV assessment in Figure 5.2, i.e. Option 1 and Option 4a of BC3. As described in Section 4.7, a one-at-a-time fixed variation with respect to the baseline value of cost factors involving in the NPV calculation is first performed to identify the most influential parameters. The effects on NPV of CAPEX and OPEX associated to the technologies of the process stages, CAPEX and OPEX of the wind farm, green market prices of the product, wholesale electricity price and discount rate are investigated by varying their base value within ± 20% range, one at a time. Figure 5.3 shows the tornado charts obtained for the selected alternatives.

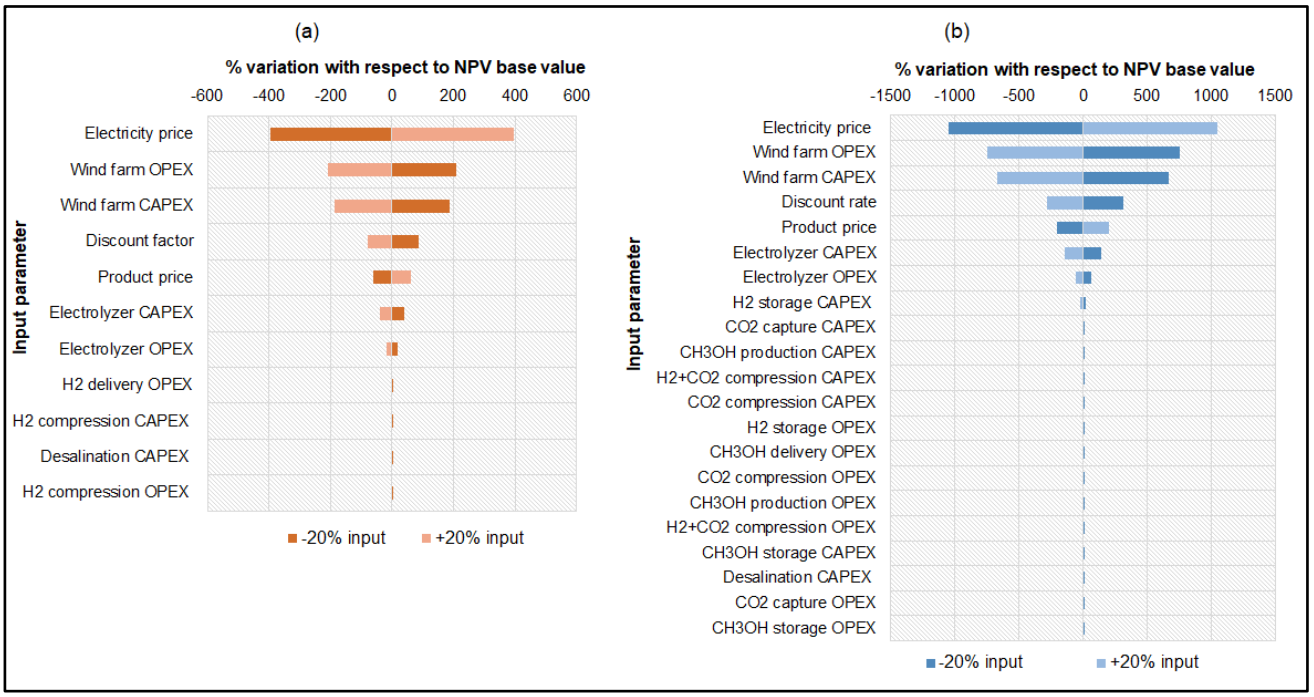

Figure 5.3. Case-study 1: Tornado charts from sensitivity analysis on NPV of (a) Option 1 and (b) Option 4a of BC3.

As shown in Figure 5.3, all the input factors drive a linear direct variation in NPV, except for the market prices of the products and wholesale electricity price which varied inversely. For both Options 1 and Option 4a, the wholesale electricity price is identified as the most critical parameter, followed by OPEX and CAPEX of the wind farm. The next ones are the discount rate and market prices of the products. Finally, CAPEX and OPEX associated to electrolyzers are other relevant factors derived from the analysis of both the alternatives. These eight input parameters are thus considered as the most uncertain factors in the analysis.

In order to study uncertainty propagation from the dataset to the results, the Monte Carlo simulation approach implemented in MATLAB programming software [641] is adopted, by assuming a probability distribution for each uncertain parameter and then repeating the calculation for a reasonably high number of times, randomly varying it within proper ranges of values [642]. Triangular distribution is adopted in this case-study for all the key parameters, since it is often used in estimating cost risks because the math is simple and it nearly approximated a lognormal distribution [643]. The uncertainty ranges are determined based on specific considerations discussed in the following. Table 5.8 summarizes the minimum and maximum value of the ranges adopted for the Monte Carlo simulations.

Table 5.8. Case-study 1: Ranges assumed for the key uncertain parameters in the Monte Carlo simulation approach.

	Wind farm CAPEX (€)	Wind farm OPEX (€)	Electrolysis CAPEX (€)	Electrolysis OPEX including O&M and stack replacement (% CAPEX/y)	H_2 price in Option 1 (€/kg)	CH_3OH price in Option 4a (€/kg)	Electricity price (€/MWh)	Discount rate (%)
Minimum value of the range	$3.21 \cdot 10^8$	$5.20 \cdot 10^7$	$3.50 \cdot 10^7$	7	1.400	0.428	59.9	2
Maximum value of the range	$1.94 \cdot 10^9$	$6.47 \cdot 10^7$	$7.50 \cdot 10^7$	12	3.129	0.499	75.2	14

The maximum values of the ranges for CAPEX and annual OPEX of the wind farm are derived from CAPEX and annual OPEX estimates reported for commercial floating wind deployments by Carbon Trust [644], i.e. $2.7 \cdot 10^6$ £ and $0.09 \cdot 10^6$ £/y referred to year 2015, respectively. On the other hand, the minimum values of the ranges associated to these parameters are evaluated based on the cost prospects for offshore wind farm in the North Sea after 2030 [645]: a value of $2.84 \cdot 10^8$ £ referred to year 2018 is obtained for CAPEX by summation of the contributions of its components (i.e. $1.4 \cdot 10^7$ £ for wind turbine, $1.0 \cdot 10^7$ £ for substructure, $4.0 \cdot 10^7$ £ for intra-array cables, $6.0 \cdot 10^7$ £ for project development, $1.6 \cdot 10^8$ £ for installation), while a value of $4.6 \cdot 10^7$ £/y referred to year 2018 is estimated for annual OPEX. To convert the cost values into € referred to year 2018, the average exchange rate and price indices reported in Table A.5 of Appendix A are used for application of Equation (4.1).

The limits for CAPEX and annual OPEX of the electrolyzers are derived from statistical data published in the technical literature [631]. Information about proton exchange membrane electrolyzer operating at 30 bar and 1 MW at year 2017 is used for maximum values of the ranges: CAPEX of 1500 €/kW and, O&M costs equal to 4% of CAPEX/y and stack replacement costs of 600 €/kW every 40000 h of operation (i.e. 40% of CAPEX/y). On the other hand, for minimum values of the ranges, data about proton exchange membrane electrolyzer operating at 60 bar and 20 MW capacity at year 2025 is considered, i.e. CAPEX of 700 €/kW and, O&M costs equal to 2% of CAPEX/y and stack replacement costs of 210 €/kW every 50000 h of operation (i.e. 30% of CAPEX/y). By multiplying for the 50 MW capacity considered for electrolyzers in the case-study, final values of the limits can be obtained.

The minimum value of the range for the H_2 market price in Option 1 is considered equal to the H_2 injection price forecast in 2025 in UK by Tractebel and Hinicio [631], under the assumptions that injection tariffs will decrease as a carbon tax emerges in the near future, leading to an increase in the wholesale natural gas price. On the contrary, the maximum value of the range associated to this variable is estimated by

assuming the non-domestic RHI established by OfGem for the first 40000 MWh of injected biomethane first published before 2018 [646], i.e. 65.1 £/MWh between 1 January to 31 March 2016. From this information, the price in €/kg is obtained by applying the 2016 currency conversion rate in Table A.5 of Appendix A and HHV value of 39.4 kWh/kg for H_2.

Concerning the market price of CH_3OH in Option 4a, minimum value of the range is assumed equal to the grey market price (Table 5.3). Whereas, maximum limit of the range is estimated by considering the forecast ETS price of CO_2 emissions allowance in 2025 [631], equal to 28.1 €/t_{CO2}, and calculating the added value of renewable CH_3OH due to cost savings according to the procedure described for green market price estimation in the main text.

The UK wholesale electricity price attributed to wind electrical power sold to the grid is varied within the range in €/MWh proposed in the technical literature [631] for year 2017, in case of the minimum limit, and for year 2025, in case of the maximum limit.

Discount rate is instead varied as suggested in a previous study [647].

The results of the analysis are presented as distribution of NPV differences between selected couples of the alternatives, as commonly proposed in the discernibility analysis [624]. Figure 5.4 reports the cumulative probability of the values of the differences among NPV of different couples of the selective alternatives with respect to the baseline situation BC1 calculated by 10^6 Monte Carlo runs.

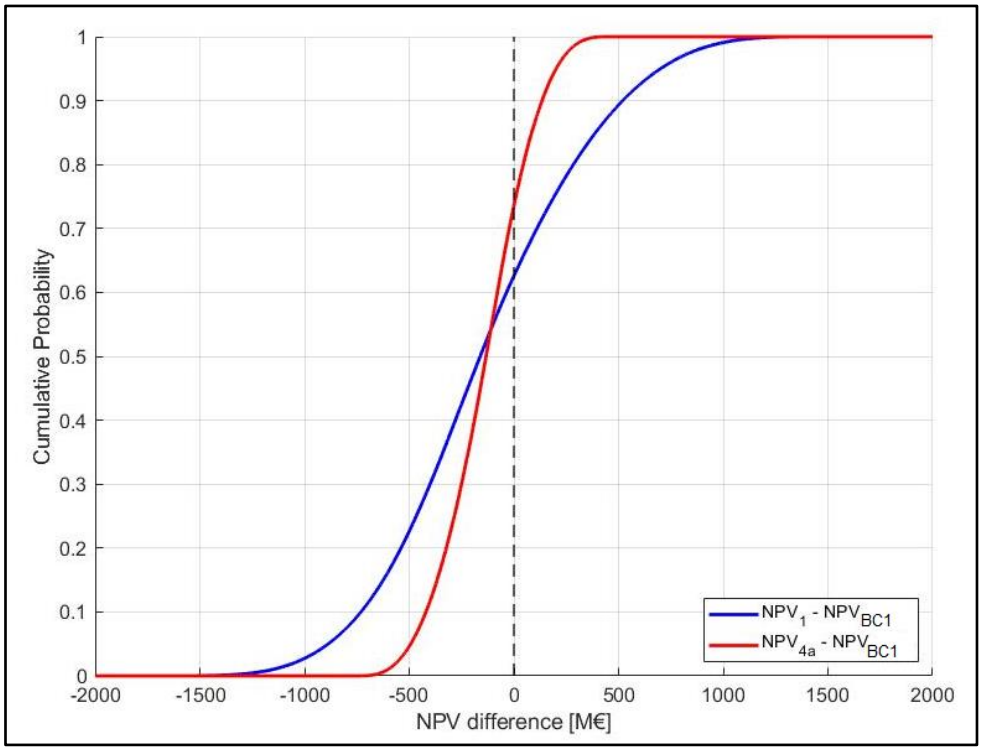

Figure 5.4. Case-study 1: Cumulative probability of the NPV differences of Options 1 and 4a in BC3 with respect to BC1.

As evidenced in Figure 5.4, both Options 1 and 4a demonstrate very similar profitability performance with respect to BC1, thus the ranking between them is affected by the variability in the input parameters. In particular, Option 1 has about 40% probability of being more profitable than BC1, while Option 4a shows higher NPV for approximately 30% probability. Therefore, the results of the analysis confirm the profitability ranking illustrated in Figure 5.3 over a moderate number of simulations. It is verified that the increase in the number of runs up to 10^7 simulations does not affect the findings illustrated in Figure 5.4.

5.2.7. Conclusions

The case-study was considered to demonstrate the potential of the proposed sustainability assessment methodology for P2G and P2L offshore hybrid energy options described in Section 4.3 for the conversion of offshore wind energy at the facility and the selling of the products to the onshore market.

Options 1 and 2 show the best performance based on both technical, economic and environmental indicators and the aggregated sustainability indicator. This is also confirmed by applying different criteria and perspectives of decision makers to elicitation of weights among indicators.

A situation where P2G and P2L conversion processes are used to limit wind power curtailments due to grid integration appears more favourable in NPV assessment than the sole chemical production. Selling pure H_2 and CH_3OH to industry and mobility sectors, besides electricity to the network, give positive NPV values. Sensitivity analysis through Monte Carlo simulations proves the robustness of these findings.

5.3. Case-study 2: Application of the sustainability assessment methodology to OWT farm and G2P options

The methodology described in Section 4.4 is applied to a case-study consisting of a gas production platform in a depleted gas field in the Adriatic Sea close to the onshore electrical grid, in order to rank the sustainability performance of alternative G2P offshore hybrid energy options composed of an OWT farm coupled with GTs at the offshore facility.

5.3.1. Definition of the offshore oil & gas site and renewable power plant

An offshore depleted gas field located in the Adriatic Sea and relatively close to the onshore grid is considered as the location for the development of the G2P offshore hybrid energy options. Offshore wind energy is selected as renewable source to be exploited for energetic valorisation of the site and integrated into the onshore electrical network, given a previous study investigating the feasibility of an offshore wind farm in the northern Adriatic Sea, off coast of Rimini (Italy) [110].

As required from step 0 of the procedure illustrated in Figure 4.4, the offshore oil & gas site is defined providing input data about the field and infrastructures. The oil & gas platform is supposed to be one of the gas production platforms in the A.C 1.AG. block in the northern Adriatic Sea, in water depth of about 25 m. Natural gas is actually extracted by means of 18 wells out of total 58 drilled wells at relatively low pressure and sent via pipeline to the onshore gathering and treatment Casalborsetti plant (Ravenna). Average gas production at the field is estimated at the end of 2016 as 54809296 Sm^3/y. The platform at the field is a multi-leg fixed structure with topside area of 48 x 26 m^2, ageing about 25 years and located around 20 km from the coast [648]. No subsea cables to the grid or other platforms are installed in the area. The closest onshore transmission grid (alternating current, 380 kV voltage) operated by the Italian TSO TERNA [649] is located in Ravenna, about 25 km far from the gas field.

According to step 1 of the methodology, data about wind speed and frequencies are retrieved from an experimental campaign launched in the area between November 2013 and November 2016 through an anemometer installed at Garibaldi A platform at 50 m above the sea level (a.s.l.) height. The average 10-minute wind speeds collected in the year 2015-2016 are used to assess the wind energy potential in this case-study.

The observed probability density function of the wind speed at 50 m a.s.l. is shown in Figure 5.5. The average observed wind speed yields 3.79 m/s. Different methods suggested in the literature [504,650] are used to determine the parameters of the Weibull fitted distribution, i.e. the shape factor k and the scale factor c in Equation (4.24). The parameters identified with the empirical method (k and c equal to 1.54 and 4.21, respectively) are found to best fit with a coefficient of determination R^2 of 0.949, as shown in Figure 5.5. Arithmetic mean is used for sake of simplicity to convert measured wind speeds into series of hourly values in the analysed period.

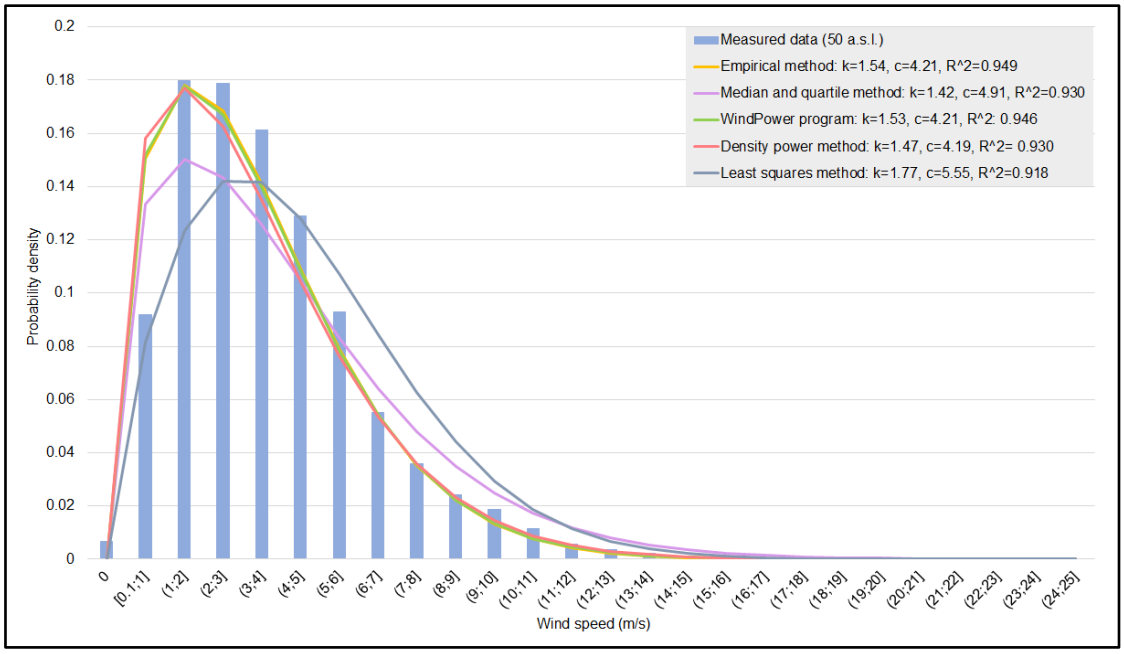

Figure 5.5. Case-study 2: Data about the wind speed at the selected offshore site (experimental probability density and Weibull distribution fitted with different methods).

ERA5 reanalysis dataset for global climate and weather by ECMWF [651] is adopted in this case study to retrieve short-term forecast data about wind speed in the selected site. ERA5, with free access, is developed by means of the Copernicus Climate Change Service and provides hourly values of several terrestrial and oceanic weather variables from 1979 to 2-3 months before the present, with a global horizontal coverage and horizontal resolution 0.25° x 0.25°. Among the available parameters, the reduced resolution ten member ensemble (EDA) sub-daily data related to horizontal and vertical wind speeds at 10 m a.s.l. are downloaded for the analysis. The forecast can be downloaded at two different initialization times in the day (06:00 and 18:00) for four different forecast horizons or steps (3 h, 6 h, 9 h, 12 h). Therefore, in case of instantaneous parameters, the horizontal and vertical wind speeds from the forecast at time 06:00 and step 3 h represent the wind speeds at 06:00 + 3 h, i.e. at 09:00. Similarly, the horizontal and vertical wind speeds from the forecast at time 06:00 and step 6 h represent the wind speeds at 06:00 + 6 h, i.e. at 12:00 [652]. Data from ERA5 for forecast step 3 h and 6 h are considered in this case-study: data related to forecast 3 h represents wind speeds at 09:00 and 21:00 in the day, while data related to forecast 6 h represents wind speeds at 12:00 and 0:00 of the next day. Having downloaded the data for the period of interest, the resulting hourly wind speed to be used for wind power calculation is obtained by combining the horizontal and vertical components of wind speeds from ERA5. Figures 5.6 and 5.7 illustrate the trend of the resulting wind speeds at 09:00 and 21:00, respectively, related to forecast horizon 3 h over the analysed period. Figures 5.8 and 5.9 show the trend of the resulting wind speeds at 12:00 and 00:00 (next day), respectively, related to forecast horizon 6 h over the analysed period.

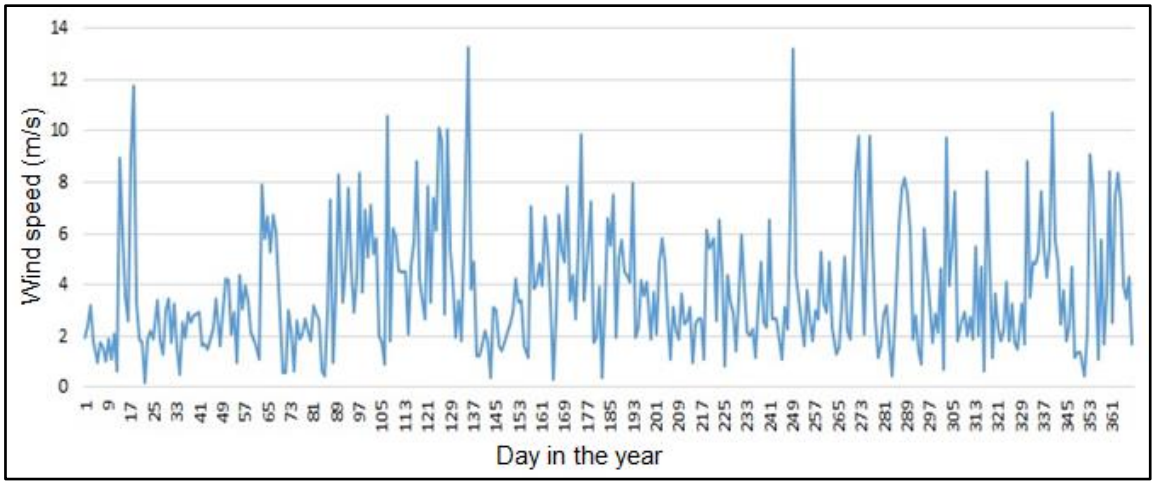

Figure 5.6. Case-study 2: Forecast wind speeds (horizon 3 h) at time 09:00.

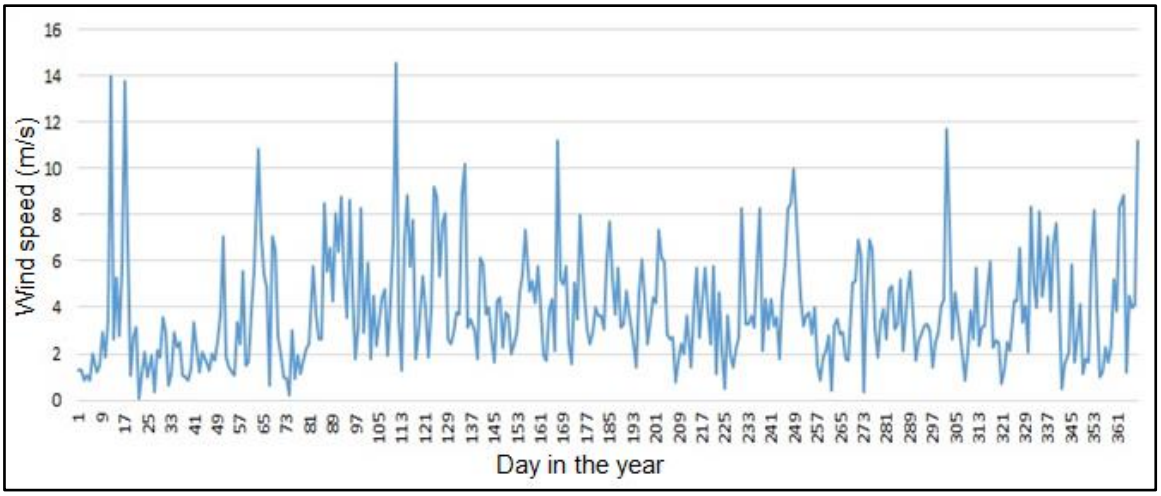

Figure 5.7. Case-study 2: Forecast wind speeds (horizon 3 h) at time 21:00.

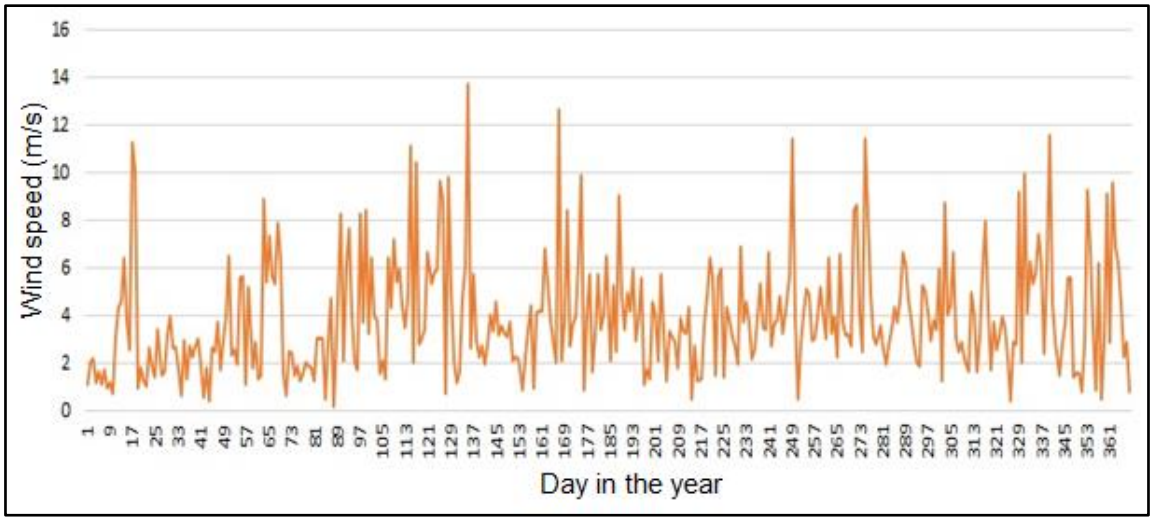

Figure 5.8. Case-study 2: Forecast wind speeds (horizon 6 h) at time 12:00.

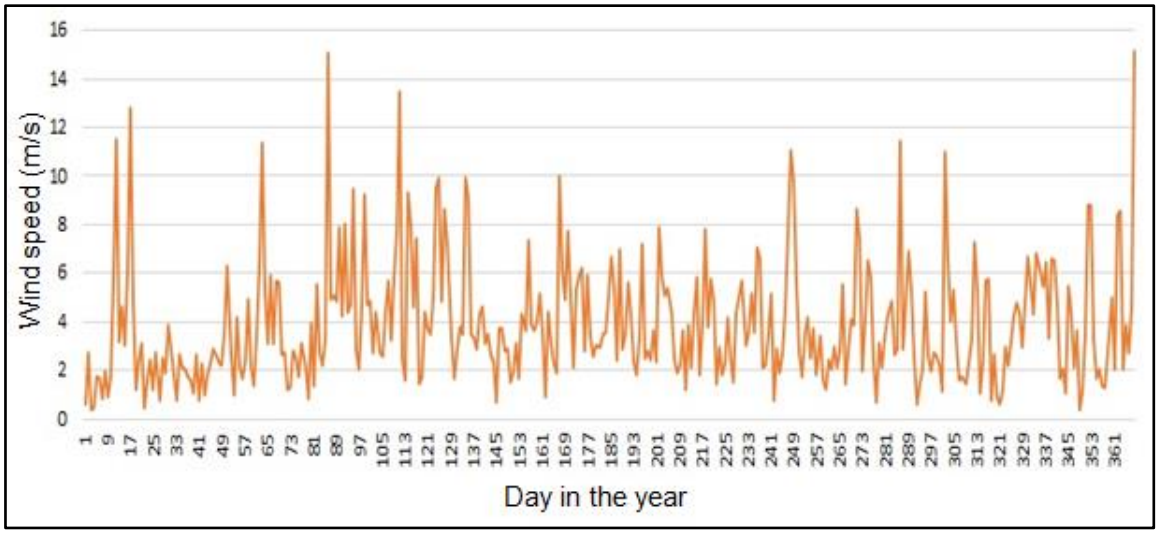

Figure 5.9. Case-study 2: Forecast wind speeds (horizon 6 h) at time 00:00 of next day.

In order to obtain the wind speeds for each hour of the day in the period of interest for a given forecast horizon, a simplified approach based on arithmetic mean between the available values is applied, thus filling the gaps in wind speed series related to the two forecast steps from ERA5. To take an example, with reference to forecast horizon 3 h, wind speed value at 15:00 is first calculated as arithmetic mean between the available values from ERA5 at 09:00 and 21:00, then the wind speed values at 12:00 is the arithmetic mean between the value at 09:00 (available in ERA5) and value at 15:00 (previously calculated), and so forth to obtain the hourly values in the year. The same approach is applied to the series related to forecast horizon 6 h.

According to step 2 of the procedure in Figure 4.4, the OWT model is chosen in order to calculate the real and forecast wind power curves from the wind speed data. Given the average wind speed of 3.8 m/s and water depth of 25 m at the offshore site, the commercially available Nordex N90/2500 Offshore by the German Nordex SE characterized by cut-in speed of 3 m/s and monopile steel sub-structure is considered in this case-study. Technical data of the OWT is summarized in Table 5.9. The power curve of Nordex N90/2500 Offshore and related power coefficient C_p trend are illustrated in Figure 5.10.

Table 5.9. Case-study 2: Main technical data of Nordex N90/2500 Offshore wind turbine [653].

Parameter	Value
Nameplate capacity	2500 kW
Rotor diameter	90 m
Swept area	6.362 m^2
Hub height	104 m
Cut-in speed	3.5 m/s
Rated speed	12 m/s
Cut-off speed	25 m/s
Wind class	IEC IIa

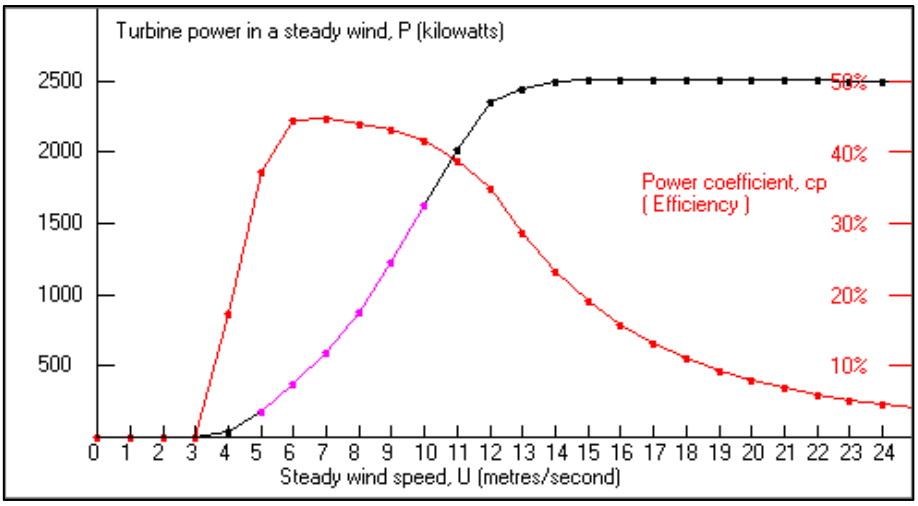

Figure 5.10. Case-study 2: Power curve and Cp trend for NORDEX N90/2500 Offshore [517].

The AEP at the offshore site by means of the selected offshore wind turbine is estimated as described in Section 4.4. Before this calculation, the wind speeds measured from anemometer are adjusted to the hub height of the turbine (Table 5.9) according to Equation (4.23). Average wind speed in the adjusted sample of data is 4.04 m/s. The parameters of Weibull fitted distribution based on empirical method are k and c equal to 1.54 and 4.46, respectively, with coefficient of determination R^2 of 0.960. Power values are derived by using the power curve in Figure 5.10. Number of hours in the year is considered as 8784, while availability of OWT as 0.97. By applying Equation (4.25), AEP is obtained equal to 2052 MWh/y. Capacity factor CF of the selected OWT over the analysed period is derived as 9.35%.

The nominal size of the OWT farm is fixed in this case-study as 50 MW, as similarly considered in the previous feasibility study in the northern Adriatic Sea [110], thus composed of 20 NORDEX N90/2500 Offshore turbines. The farm is supposed to be placed in proximity of the gas production platform, linked via subsea cables to the platform where offshore substation increasing the voltage (e.g. up to 132 kV) is installed. An export HVAC transmission line of about 20 km is assumed between the platform and the coast.

The available wind power from OWT farm, $P_{wind,avail}$, on an hourly basis is calculated by using real wind speed data and A_{rot} of the selected turbine in Equation (4.21) and then multiplying for the number of turbines in the farm. The actual electrical power produced by the OWT farm on an hourly basis is determined by using the real and forecast wind speeds data and the power curve in Figure 5.10 for a single OWT and then multiplying for the number of turbines in the farm. Adjustments of measured and forecast wind speeds to the hub height are applied by means of Equation (4.23).

For a renewable non-programmable power plant with size greater than 10 MVA linked to the electrical grid, the Italian dispatching system operates under the single pricing mechanism, thus the economic

penalization or gain associated to the plant depends only on the global sign of the zonal unbalance (i.e. unbalance associated to the macro-area where the dispatching point under analysis is located) [654]. According to this model, the producer should pay TERNA, in case of negative unbalance and obtain a remuneration by TERNA in case of positive unbalance from the power plant: if the power unbalance of the plant has an opposite sign than the zonal unbalance during the same relevant period in the macro-area where the dispatching point is located, such an unbalance is not fully penalized but may receive some benefits, e.g. producer may gain more than the actual electricity market price for the positive unbalance or pay TSO a lower price than the actual electricity market price for the negative unbalance). Table 5.10 summarizes the principles of the single pricing mechanism. In this table, $Price_{MGP}$ represents the price of the accepted supply offers in the day-ahead market, while $Price_{MB\downarrow}$ and $Price_{MB\uparrow}$ are the average prices of the bids and supply offers, respectively, accepted in the market of ancillary services in real-time balance, weighted by volume.

Table 5.10. Case-study 2: Summary of the single pricing mechanism for unbalance remuneration or penalization.

	Positive unbalance of power plant	Negative unbalance of power plant
Positive zonal unbalance	Producer receives by TSO $\min(\text{Price}_{\text{MGP}}, \text{Price}_{\text{MB}\downarrow})$	Producer pays TSO $\min(\text{Price}_{\text{MGP}}, \text{Price}_{\text{MB}\downarrow})$
Negative zonal unbalance	Producer receives by TSO $\max(\text{Price}_{\text{MGP}}, \text{Price}_{\text{MB}\uparrow})$	Producer pays TSO $\max(\text{Price}_{\text{MGP}}, \text{Price}_{\text{MB}\uparrow})$

MGP stands for "Mercato del giorno prima" (day-ahead market), MB stands for "Mercato del bilanciamento" (balancing market).

Considering the incentive scheme for promotion of renewable energy sources different than solar PV, the Italian legislation [655] establishes that a new renewable plant or hybrid energy plant is eligible to ask "Gestore Servizi Energetici" (GSE) [656] for a feed-in tariff (FIT) based on the renewable type and size of the plant. In case of offshore wind power, small-scale plants ranging between 1 and 60 kW of nominal power can directly request the permission for FIT after starting the production, while large-scale plant (nominal power greater than 5 MW) should participate in public unique bid auction in order to determine the incentive level for the produced power and, if entered in useful position, asks for the FIT after realizing the plant and starting the production. For plant with nominal power greater than 500 kW, FIT is an incentive for the net renewable power injected into the grid defined as follows:

$$In_{OWT} = T_{b,red} + T_{prem} - Price_{MGP} \tag{5.1}$$

where In_{OWT} in €/MWh is the incentive for offshore wind power produced from the plant and injected into the grid available for a maximum of 25 years, $T_{b,red}$ is the base tariff (165 €/MWh) reduced by a given percentage assigned during the auction (between 2% and 40%), $Price_{MGP}$ is the zonal electricity market price in the day-ahead market, T_{prem} is the premium tariff (40 €/MWh) when Producer covers the costs for connection of the plant to the grid.

5.3.2. Definition of the dispatching power plan and sizing of the gas turbine park

EasyFit software [529] is adopted in the case-study to perform the statistical analysis of the prediction errors (ξ) calculated on an hourly basis by means of Equation (4.30) for the forecast horizons 3 h and 6 h. For each month of the analysed year, a histogram of errors is obtained and the best fitted distribution is properly selected. Tables 5.11 and 5.12 summarize the distributions and related parameters adopted for each monthly error sample based on forecast horizon 3 h and 6 h, respectively.

Table 5.11. Case-study 2: Probability distributions of prediction error based on forecast horizon 3 h and dispatching error corresponding to 80% and 90% probability of correct dispatching.

Month of the period	Fitted distribution of the prediction errors ξ (and related parameters)	Dispatching error ξ_d (MW) corresponding to $Prob_d$ of 80% or CDF = 20%	Dispatching error ξ_d (MW) corresponding to $Prob_d$ of 90% or CDF = 10%
1	Cauchy (σ=0.55, μ=0)	-0.757	-1.693
2	Log-Logistic 3P (σ=11.6, β=27.4, γ = -26.5)	-2.158	-3.800
3	Cauchy (σ=1.733, μ=0)	-2.386	-5.335
4	Cauchy (σ=4.655, μ=0)	-6.407	-14.327
5	Cauchy (σ=1.620, μ=-0.249)	-2.479	-5.235
6	Cauchy (σ=3.014, μ=-0.695)	-4.484	-9.971
7	Laplace (λ=0.148, σ=-0.823)	-7.024	-11.716
8	Cauchy (σ=1.428, μ=0)	-1.967	-4.395
9	Cauchy (σ=1.341, μ=0)	-1.845	-4.126
10	Log-Logistic 3P (σ=6.47·10^8, β=3.32·10^9, γ=-3.32·10^9)	-7.123	-11.295
11	Cauchy (σ=1.537, μ=0)	-2.115	-4.730
12	Cauchy (σ=3.066, μ=0)	-4.220	-9.436

Table 5.12. Case-study 2: Probability distributions of prediction error based on forecast horizon 6 h and dispatching error corresponding to 80% and 90% probability of correct dispatching.

Month of the period	Fitted distribution of the prediction errors ξ (and related parameters)	Dispatching error ξ_d (MW) corresponding to $Prob_d$ of 80% or CDF = 20%	Dispatching error ξ_d (MW) corresponding to $Prob_d$ of 90% or CDF = 10%
1	Cauchy (σ=0.90, μ=0)	-1.245	-2.784
2	Cauchy (σ=0.34, μ=0)	-0.470	-1.050
3	Cauchy (σ=2.17, μ=0)	-2.984	-6.672
4	Laplace (λ=0.09, σ=-0.44)	-10.477	-18.067
5	Cauchy (σ=1.786, μ=-0.271)	-2.723	-5.766
6	Cauchy (σ=3.247, μ=-0.946)	-5.415	-10.939
7	Cauchy (σ=2.429, μ=-0.682)	-4.025	-8.157
8	Cauchy (σ=2.329, μ=-0.609)	-3.814	-7.775
9	Cauchy (σ=2.464, μ=-0.868)	-4.259	-8.450
10	Cauchy (σ=2.086, μ=-0.550)	-3.422	-6.971
11	Cauchy (σ=2.547, μ=0)	-3.501	-7.839
12	Cauchy (σ=4.097, μ=0)	-5.640	-12.611

Two different probabilities of correct dispatching, $Prob_d$, are considered in this case-study, i.e. 80% and 90%. Dispatching error, ξ_d, corresponding to these two probabilities is calculated for each monthly error sample based on forecast horizons 3 h and 6 h as described in Section 4.4. CDF of the fitted distribution of prediction errors is set equal to 20% to estimate ξ_d values corresponding to $Prob_d$ of 80%, while a CDF of 10% is used to estimate ξ_d values corresponding to $Prob_d$ of 90%. ξ_d findings for the monthly data based on forecast horizon 3 h are reported in Table 5.11, while Table 5.12 summarizes the results of ξ_d for monthly data based on forecast horizon 6 h. By applying Equation (4.31), hourly dispatched power series (P_d) series are derived for the different forecast horizons and $Prob_d$, bearing in mind that the smallest possible value for P_d is 0.

As described in Section 4.4, the size of the GT park coupled with the OWT farm is estimated based on the differences between the hourly P_f and P_r values during the hours at which P_r is lower than P_f, also indicated as $P_{GT,max}$. Table 5.13 summarizes the monthly $P_{GT,max}$ values obtained for the two different forecast horizons considered in the analysis.

Table 5.13. Case-study 2: Maximum power which could be provided from GTs for the two forecast horizons.

Month of the period	$P_{GT,max}$ (MW) for forecast horizon 3 h	$P_{GT,max}$ (MW) for forecast horizon 6 h
1	49.1	49.9
2	22.1	38.1
3	48.9	50.3
4	39.7	47.1
5	49.2	48.7
6	41.1	50.0
7	27.8	40.4
8	31.8	21.9
9	48.5	48.7
10	47.2	49.7
11	25.3	41.7
12	49.0	49.9

From Table 5.13, the highest $P_{GT,max}$ for forecast horizon 3 h is 49.2 MW associated to month 5, while 50.0 MW in month 6 is the greatest $P_{GT,max}$ for forecast horizon 6 h. As a matter of facts, the nameplate size of the GT park is approximated to 50 MW in this case-study. Given this capacity, aeroderivative GTs are evaluated suitable for the park. The SGT-A05 KB7HE model by Siemens [657] is selected for the analysis. Technical data of this turbomachine is nominal power at full-load ($P_{GT,1,nom}$) of 5.8 MW, electrical efficiency at full-load ($\eta_{GT,nom}$) of 32.2%, footprint 9 x 27 m^2. Therefore, the GT park in this case-study is considered to be composed 9 machines for a total nominal power ($P_{GT,nom}$) of 52.2 MW, total electrical efficiency at full-load ($\eta_{GT,nom}$) of 32.2%, total footprint 219 m^2. This latter value is

considered reasonable, given the topside dimensions of the offshore gas platform where the GT is supposed to be installed.

GHG emissions from conventional power plant are legislated in Italy by the EU ETS scheme based on the cap and trade principle [538]. The EU ETS legislation creates allowances which represent essentially rights to emit GHG emissions. Each year, some allowances are given for free to certain participants, while the remaining is sold via auctions. At the end of the year, participants return allowances based on the actual emissions in that years. If a participant has insufficient allowances, he/she either reduces the emissions or buys more allowances on the market.

5.3.3. Assumptions made for the assessment

Four different scenarios (SCs) are compared in this case-study in order to evaluate the influence of different forecast horizon (3 h and 6 h) and different probability of correct dispatching (80% and 90%) on the sustainability performance of alternative G2P offshore hybrid energy options at the defined offshore site.

A reference SC (SC1) is considered consisting of forecast power data based on time horizon 3 h and dispatched power data defined with $Prob_d$ equal to 80%. From SC1, other three SCs are then introduced with respect to this reference scenario: SC2 is derived by increasing $Prob_d$ to 90% and considering the same forecast horizon than SC1, SC3 considers an increased forecast horizon of 6 h but the same $\mathrm{Prob_d}$ than SC1, SC4 is based on both higher forecast horizon and $Prob_d$ than SC1 (6 h and 90%, respectively).

Given the definition of the OWT farm (50 MW nominal size) and the GT park (52.2 MW nominal size), in this case-study the comparative assessment of the defined SCs based on sustainability indicators is focussed on a more restricted yet representative interval than the entire analysed year in order to better demonstrate the potential of the approach. Three days between 26th and 28th February 2016 (month 4 of the period under analysis) are selected.

To quantify the technical aspect of sustainability performance of the G2P hybrid energy system in the different SCs, the electrical efficiency indicator, η_{el}, defined in Equation (4.34) is adopted. $P_{wind,avail}$ values are estimated by using measured wind speeds and swept area of the rotor in Equation (4.21). P_{GT} and P_{fuel} are calculated by applying the control strategy according to step 5 of the methodology. The estimation of the part-load efficiency is performed by applying Equation (4.32) for aeroderivative GTs. The part-load power ranges illustrated in Table 4.14 are used to determine the number of operating turbines before the next switch-off.

In order to compare the environmental performance of the G2P offshore hybrid energy options, LGHG defined in Equation (4.37) is used. Emission factor of 202 kg/MWh_{fuel} suggested for aeroderivative GTs [229] is assumed to estimate the hourly GHG emissions from the operating machines of the park.

Regarding the economic performance assessment, both LCOE and LVOE proposed in the model of Section 4.4 are calculated for the different SCs. CAPEX and OPEX of the GTs required in Equation (4.35) are derived from the literature costs of aeroderivative GTs in 50 MW power plant [658]. The reference currency and year for the cost analysis are € referred to 2016. Thus, cost adjustments based on Equation (4.1) are performed by considering conversion rates from $ to € and PPI values from year 2013 to 2016, summarized in Table A.5 of Appendix A. The investment and O&M costs estimated in a previous study [110] for a 54 MW OWT farm composed of 15 turbines (3.6 MW single nominal power) in the Northern Adriatic Sea are approximated to CAPEX and OPEX of the renewable plant in Equation (4.35), due to the similarity in features of the plant and location. No costs adjustments are applied to these data. Moreover, decommissioning costs are disregarded in the analysis. CAPEX and OPEX assumptions and values for OWT farm and GTs in the case-study are summarized in Table 5.14. It is worth noting that OPEX associated to GTs is the only parameter varying among the SCs since it relies on the number of operating turbines employed every hour to fulfil the defined dispatching power plan.

Table 5.14. Case-study 2*:* Economic data of the OWT farm and GTs considered in the hybrid energy system.

Cost	Cost segment	Assumption	Value
CAPEX of OWT farm	Onshore yard	Estimate of the activity cost at the port of Ravenna [110]	$4.59 \cdot 10^6$ €
	Wind turbine structure (nacelle, tower, generator)	$4.32 \cdot 10^3$ k€ per turbine [110]	$8.64 \cdot 10^7$ €
	Transition piece and foundation	$1.4 \cdot 10^3$ €/t of steel, 467.682 t per support structure (monopile) [110]	$1.31 \cdot 10^7$ €
	Export cable to shore	$1.3 \cdot 10^3$ €/m [110]	$2.60 \cdot 10^4$ €
	Transformer and intra-array cables	$2.39 \cdot 10^2$ €/kW [110]	$1.20 \cdot 10^7$ €
	Wind turbine installation	6 days/turbine [110]	$6.48 \cdot 10^6$ €
	Foundation installation	6 days/support structure [110]	$8.30 \cdot 10^5$ €
	Contingency	$2.45 \cdot 10^2$ €/kW [110]	$1.22 \cdot 10^7$ €
	Preoject authorization	$3.17 \cdot 10^2$ €/kW [110]	$1.59 \cdot 10^7$ €
OPEX of OWT farm	O&M	$1.44 \cdot 10^2$ €/kW-y [110]	$8.22 \cdot 10^2$ €/h
CAPEX of GTs	Capital cost	$1.51 \cdot 10^3$ $\$_{2013}$/kW [658]	$6.83 \cdot 10^7$ €
OPEX of GTs	Fixed O&M	$2.9 \cdot 10$ $\$_{2013}$/kW-y [658]	$2.68 \cdot 10^{-3}$ €/kW-h

Concerning the revenues and costs for the positive and negative unbalances required for calculation of LVOE in Equation (4.36), the single pricing model is supposed to be applied to energy unbalances

generated by the difference between the dispatched power P_d declared to grid operator and the total produced from OWT farm and GTs intended for grid injection. The dispatching point is considered to be located in Ravenna, thus the macro-area for unbalance prices estimation is assumed North Italy. Moreover, in this case-study, it is supposed that eligibility requirements for access to unique bid auction for renewable incentive are met by the OWT farm, being a new offshore wind generating station with nominal capacity greater than 5 MW connected to the Italian electrical grid, and then accreditation of the incentive is granted after the request approval. In_{OWT} in Equation (5.1) is calculated by making the following assumptions: the net energy is equal to the produced renewable electricity disregarding the losses along the transmission and utility services due to unavailability of data, $T_{b,red}$ is the base tariff reduced by the average value between the minimum and maximum percentages (i.e. 21%), the costs for the transmissions are covered by producer according to the shallow cost approach, thus T_{prem} of 40 €/MWh is considered. Regarding costs for GHG emissions required in Equation (4.36), the Producer of the hybrid energy plant is assumed to participate in the EU ETS cap and trade system buying allowances from auctions or other participants for GHG emissions from the GT park. Carbon allowance price is fixed in this case-study equal to 15 €/t_{CO2eq}, as suggested in a previous work [229].

CAPEX values are supposed to occur at the beginning of the project, while OPEX, power production revenues and costs are discounted at each hour of the selected interval. Referring to Equation (4.35) and Equation (4.36), the discount rate r is considered constant over the selected interval and equal to 7%, in agreement with a previous literature study [229], while m is set as 72 h. Neither income taxes nor depreciation are considered, for the sake of simplicity.

In order to rank the SCs based on the aggregated sustainability performance, ASI indicator defined in is calculated by applying the compensatory aggregation approach described in Section 4.3. Table 5.15 reports the target values used in this case-study for normalization of disaggregated indicators related to technical upper limits of wind energy conversion and performance of offshore wind power in the near future. For each target value, brief description and assumption are included.

Table 5.15. Case-study 2: Target values assumed for normalization of disaggregated indicators.

	Value	Description and assumption	Literature source
$\eta_{el,target}$	52.9%	Betz limit for wind energy conversion through a turbine	[16]
$LCOE_{target}$	92.4 €$_{2016}$/MWh	Estimated LCOE for new generation technologies (offshore wind) entering in services in 2022/2023. The literature value of 108 \$$_{2018}$/MWh is converted into €$_{2016}$/MWh by means of Equation (4.1) using PPI values of 99.1 (for 2016) and 104.2 (for 2018) [659] and exchange rate from \$$_{2016}$ to €$_{2016}$ of 0.90 [174].	[660,661]
$LVOE_{target}$	34.2 €$_{2016}$/MWh	Estimated levelized avoided cost of electricity (i.e. proxy measure for potential revenues from sales of electricity generated from the plant) for new generation technologies (offshore wind) entering in service in 2023. The literature value of 40 \$$_{2018}$/MWh is converted into €$_{2016}$/MWh by means of Equation (4.1) using PPI values of 99.1 (for 2016) and 104.2 (for 2018) [659] and exchange rate from \$$_{2016}$ to €$_{2016}$ of 0.90 [174].	[661]
$LGHG_{target}$	12 kg$_{CO2eq}$/MWh	Harmonized mean of published CO_{2eq} emissions estimates for offshore wind power.	[662]

The evaluation of relative importance weights among indicators is performed by applying the approach described in Section 4.3 based on time-space-receptor criteria and individualist-egalitarian-hierarchist perspectives. Equal weighting is further added to the archetypes of decision makers. Before scoring and weighting, the indicators selected for the assessment of the case-study are classified in terms of time, space and receptor based on their definition. The same considerations introduced for η, LCOP, LVOP and LGHG in case-study 1 are applied to the corresponding performance indicators in this case-study. Since the economic aspect is quantified by LCOE and LVOE, the relative importance weights among the two indicators are first identified (Table 5.16) and then used to derive evaluation matrix and the trade-off weights associated to them (Table 5.17).

Table 5.16. Case-study 2: Scores and weights assigned for aggregation of sub-indicators quantifying the technical aspects based on different perspectives.

Schemes	Criteria	Indicators for economic aspect	
		LCOE	LVOE
		Score 1-5	Score 1-5
Individualist	Time	3	3
	Space	4	2
	Receptor	4	5
	Sum	11	10
	Relative importance weight	0.524	0.476
Egalitarian	Time	3	3
	Space	3	4
	Receptor	1	5
	Sum	7	12
	Relative importance weight	0.368	0.632
Hierarchist	Time	3	3
	Space	3.5	3
	Receptor	2.5	5
	Sum	9	11
	Relative importance weight	0.450	0.550

Table 5.17. Case-study 2: Evaluation matrix and trade-off weights among economic indicators based on different perspectives.

		LCOE	LVOE	Trade-off weight
Individualist	LCOE	0.667	0.667	0.667
	LVOE	0.333	0.333	0.333
Egalitarian	LCOE	0.143	0.143	0.143
	LVOE	0.857	0.857	0.857
Hierarchist	LCOE	0.248	0.248	0.248
	LVOE	0.752	0.752	0.752
Equal weighting	LCOE	-	-	0.500
	LVOE			0.500

The same procedure is then applied to determine the trade-offs weights among the category indicators. Relative importance weights are determined by using scores attributed to η and LGHG in Table 5.5 and assuming averages of the scores assigned to LCOE and LVOE in Table 5.16 for the different archetypes of decision-makers. Table 5.18 summarizes these values, while Figure 5.11 illustrates the comparison of trade-off weights based on the different perspectives. It is verified that all the evaluations are consistent according to CR index in Equation (4.15).

Table 5.18. Case-study 2: Scores and weights assigned for aggregation of category indicators based on different perspectives.

Schemes	Criteria	Technical aspect	Economic aspect	Environmental aspect
		η_{el}	LCOE, LVOE	LGHG
		Score 1-5	Score 1-5	Score 1-5
Individualist	Time	2	3	3
	Space	3	3	3
	Receptor	2	5	5
	Sum	7	10.5	11
	Relative importance weight	0.246	0.368	0.386
Egalitarian	Time	5	3	5
	Space	5	4	5
	Receptor	4	3	5
	Sum	14	9.5	15
	Relative importance weight	0.364	0.247	0.390
Hierarchist	Time	3.5	3	4
	Space	4	3	4
	Receptor	3	4	5
	Sum	10.5	10	13
	Relative importance weight	0.313	0.299	0.388

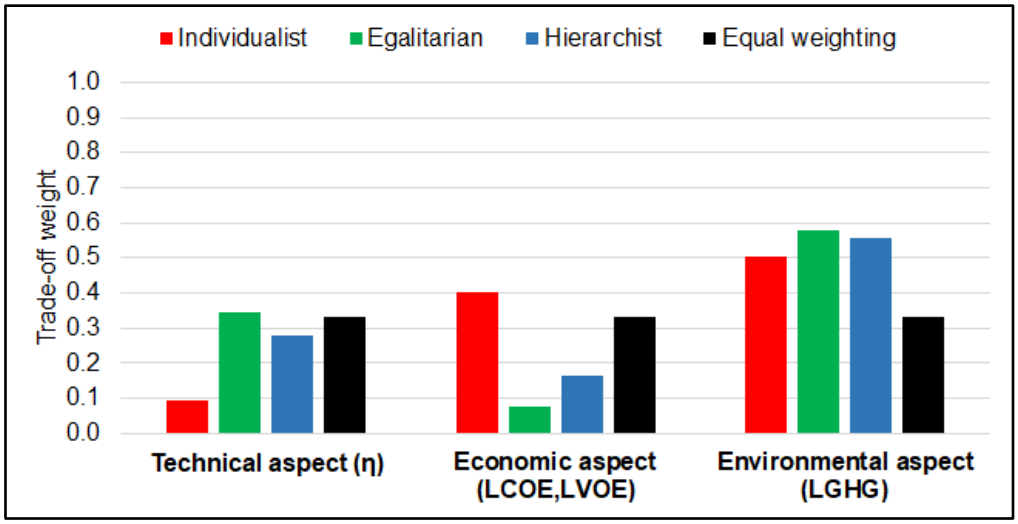

Figure 5.11. Case-study 2: Weights among the category indicators based on different perspectives for the sustainability assessment.

From Figure 5.11, it clearly appears that there are variations between the different archetypes in prioritizing specific indicators over the others. The individualist archetype gives higher priority to LGHG with a trade-off weight of about 50%, followed by the economic aspect indicators (40%). Similarly, the egalitarian method prioritizes LGHG (60%), but prefers more η_{el} (35%) than economic indicators. The hierarchist method exhibits similar priority to all the indicators than the egalitarian archetype. No archetype approximates the equal weighting scheme.

5.3.4. Preliminary comparison of the matching of power curves

A preliminary investigation of the expected performance of the G2P hybrid energy system in the different SCs is carried out by comparing the matching of real power (P_r), forecast power (P_f) and dispatched power (P_d) curves over the selected interval. Figures 5.12, 5.13, 5.14 and 5.15 illustrate the matching of the power curves calculated for SC1, SC2, SC3, SC4, respectively. In all these figures, P_r curves are the same, yellows bars represent the hourly effective power which should be provided by the GT park to satisfy the defined dispatching plan ($P_{GT,eff}$), while grey bars consist in the positive unbalance power during the hours where the operation of GT park is not required.

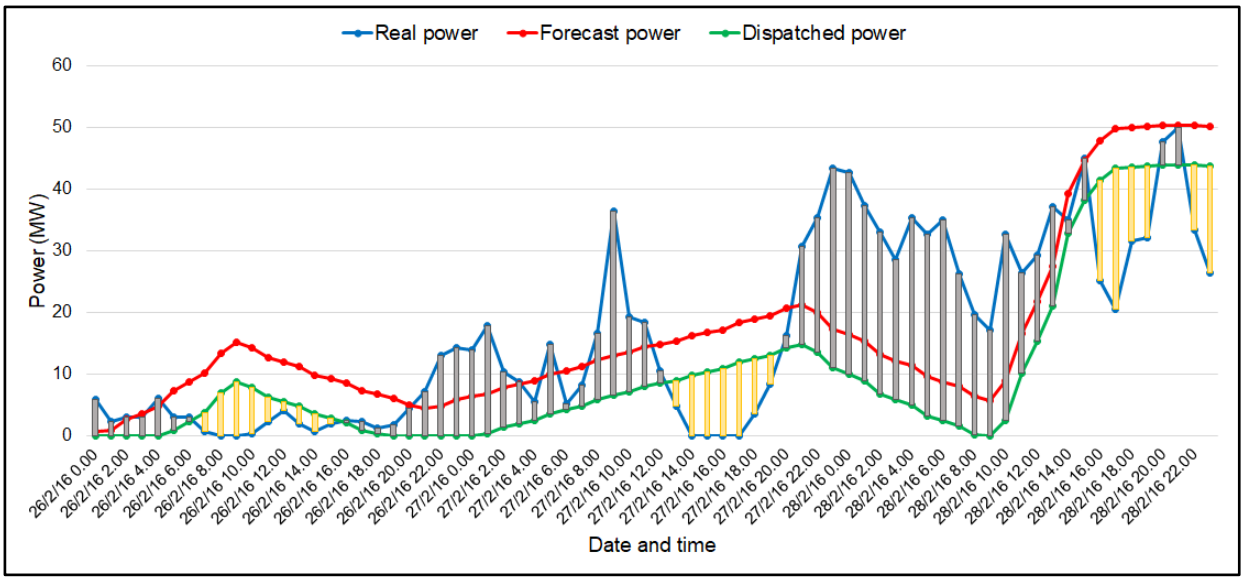

Figure 5.12. Case-study 2: Matching of P_r, P_f and P_d curves over the selected interval for SC1.

As shown in Figure 5.12, P_d is lower than P_f for a quantity which represents the dispatching error ξ_d estimated in month 4 of the period for forecast horizon of 3 h and $Prob_d$ equal to 80%, i.e. -6.4 MW (Table 5.11), provided that the smallest possible P_d is 0. By summing up the yellow bars illustrated in the figure, the total $P_{GT,eff}$ over the selected interval is 189.2 MW. Quite obviously, this value is lower than the maximum power which could be provided from the turbomachines ($P_{GT,max}$), which is estimated in this SC as 389.9 MW. Therefore, considering the defined dispatching plan based on $Prob_d$ of 80%, it is emerged a decrease of 51.5% in $P_{GT,eff}$ with respect to $P_{GT,max}$. By summing up the grey contributions in the figure, the total positive unbalance power results equal to 627.8 MW.

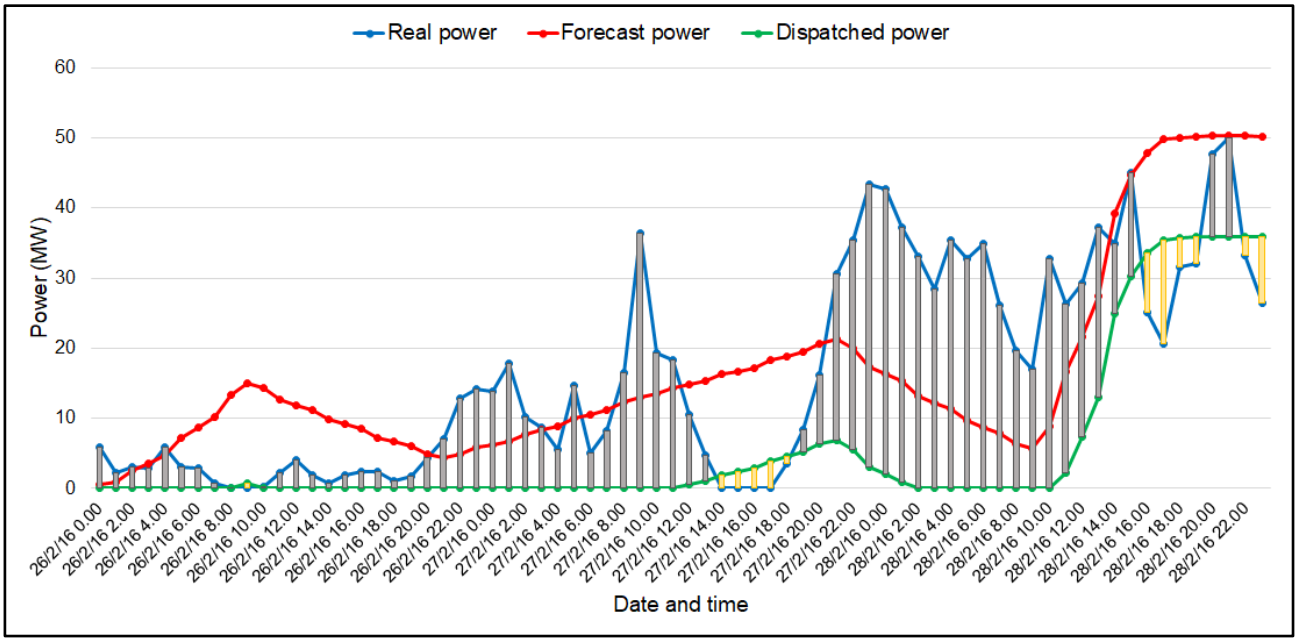

Figure 5.13. Case-study 2: Matching of P_r, P_f and P_d curves over the selected interval for SC2.

From Figure 5.13, it appears evident that P_f curve is the same than SC1, given the equal forecast horizon assumed in SC2. Therefore, $P_{GT,max}$ is estimated equal to the value reported in SC1 (389.9 MW). Whereas, a different P_d curve is displayed compared to SC1, given the increased $Prob_d$. As shown in Table 5.11, the dispatching error ξ_d of month 4 is identified in this case as -14.3 MW, i.e. more than double of ξ_d in SC1. As a result, the total $P_{GT,eff}$ over the selected interval is estimated as 56 MW against 189.2 MW of SC1 and the reduction in $P_{GT,eff}$ compared to $P_{GT,max}$ is 85.6%. Therefore, the higher Prob_d, the lower power which could be provided from GTs with respect to maximum power. Furthermore, the number of hours related to positive unbalance power (grey bars) is clearly larger than that in Figure 5.12. The total positive unbalance power for SC2 is calculated as 836.8 MW which is higher than that obtained in SC1.

From the preliminary comparison of SC2 with respect to SC1, the performance of the hybrid energy system is expected to be characterized by lower costs for negative unbalances due to higher $Prob_d$, higher revenues for positive unbalances due to higher total positive unbalance power, lower fuel consumption of GTs as well as lower GHG emissions and related costs due to lower $P_{GT,eff}$. On the other hand, lower revenues from electricity selling to the grid may be derived because of lower $P_{GT,eff}$.

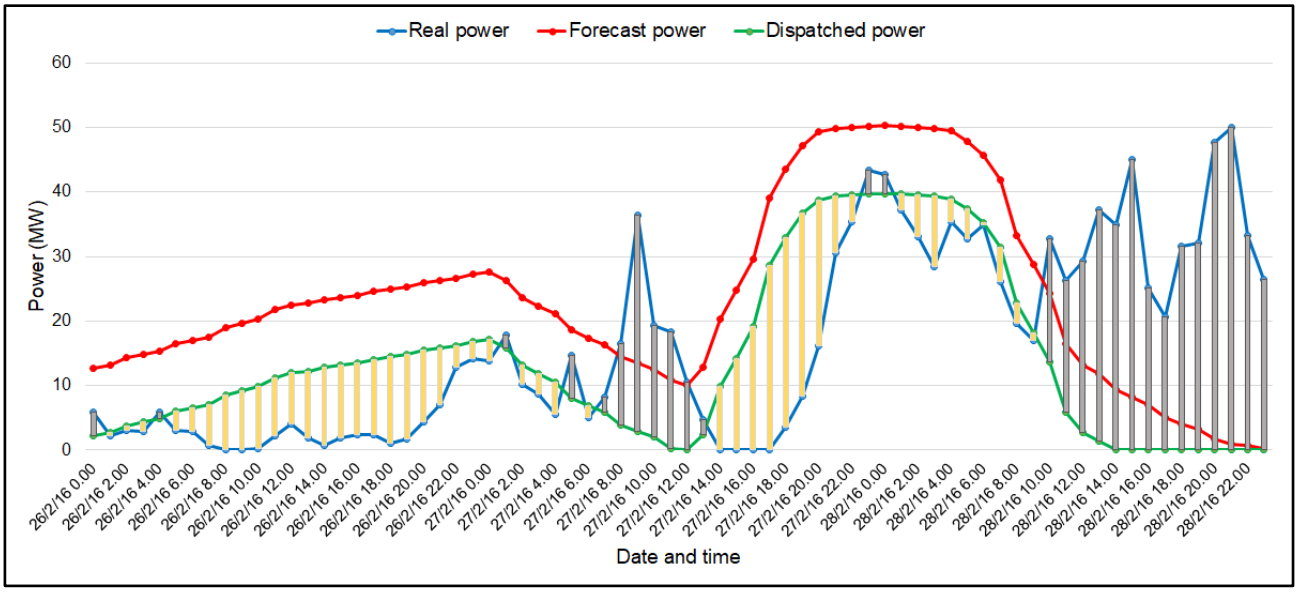

Figure 5.14. Case-study 2: Matching of P_r, P_f and P_d curves over the selected interval for SC3.

Figure 5.14 exhibits a different trend in P_f curve compared to Figure 5.12 due to higher forecast horizon considered in SC3 than the reference scenario. By summing up the yellow bars illustrated in the figure, the total $P_{GT,max}$ over the selected interval is 918.5 MW, which is significantly higher than that in SC1 (389.9 MW). As a result, a slightly higher dispatching error ξ_d of month 4 is obtained in this case, i.e. -10.5 MW (Table 5.12), compared to SC1 (-6.4 MW). By summing up the yellow bars in Figure 5.14, $P_{GT,eff}$ is estimated as 387.6 MW, i.e. larger value than SC1. However, the decrease in $P_{GT,eff}$ with respect to $P_{GT,max}$ is 57.8%, which is barely greater than that in SC1, as for ξ_d finding. On the other hand, a lower total positive unbalance power is calculated, i.e. 564.6 MW, compared to SC1.

Overall, compared to the reference scenario, for SC2, it is expected higher costs for negative unbalances due to higher $P_{GT,max}$ and $P_{GT,eff}$, lower revenues from positive unbalances due to lower total positive unbalance power, higher fuel consumption of GTs as well as GHG emissions and related costs. For the revenues due to electricity selling, it is not possible to predict an increase or decrease due to the different trend in P_f which implies a different number of hours where the GT park could be operative.

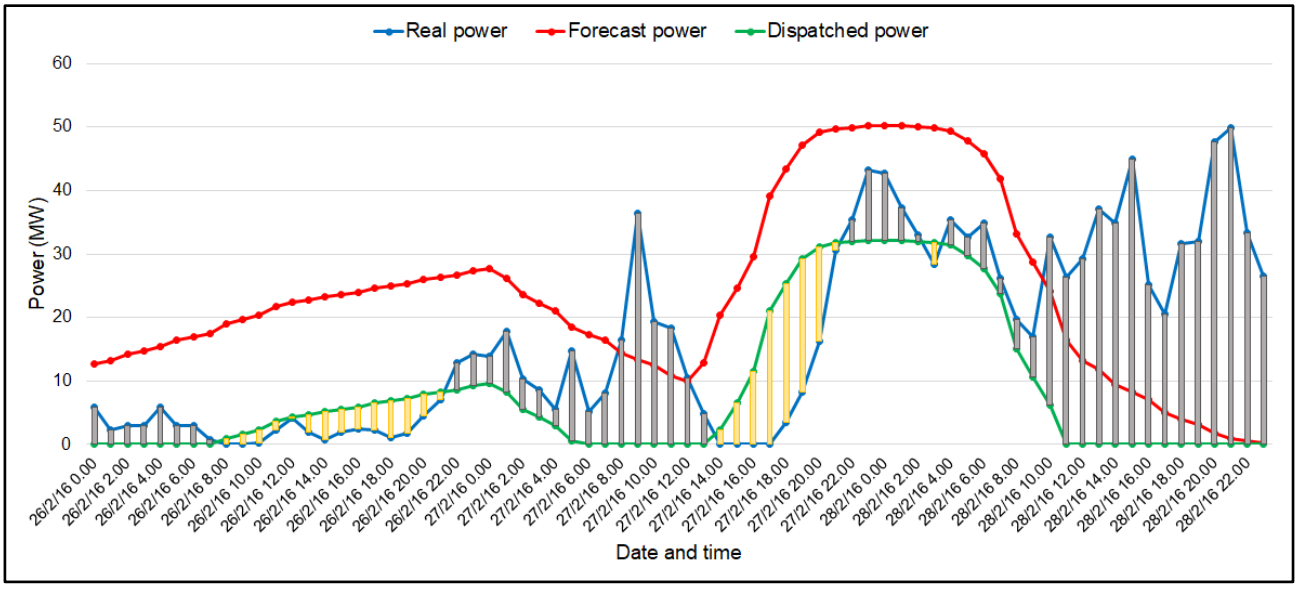

Figure 5.15. Case-study 2: Matching of P_r, P_f and P_d curves over the selected interval for SC4.

As expected from the adoption of both higher forecast horizon and $Prob_d$, a different P_f curve (as in SC3) as well as higher ξ_d (as in SC2) emerge in Figure 5.15 compared to Figure 5.12. Quite obviously, the total $P_{GT,max}$ in SC4 over the selected interval is the same than that estimated in SC3, i.e. 918.5 MW. Given a ξ_d value for month 4 of -18.1 MW (Table 5.12), $P_{GT,eff}$ in SC4 is calculated as 144.2 MW, which is slightly lower than that in SC1 (189.2 MW), but higher than SC2 (56 MW) where $Prob_d$ is the same. However, the decrease in $P_{GT,eff}$ than $P_{GT,max}$ results 84.3%, i.e. higher than that in SC1 but about the same than that in SC2. Concerning the positive unbalance power (grey bars in Figure 5.15), a total value of 719.6 MW is obtained, which is greater than that of SC1 (627.8 MW) but lower than SC2 (836.8 MW) where $Prob_d$ is the same. Compared to the other SCs, in case of SC4 it appears difficult to predict the performance of the hybrid energy system due to the combined effects of higher forecast horizon and $Prob_d$.

5.3.5. Results of sustainability assessment

Table 5.19 summarizes the technical, economic and environmental parameters calculated for the four SCs related to the entire interval selected for the analysis. The hourly data calculations are detailed for each scenario in Appendix B. As shown in Table 5.19, the GT park in SC2 operates for the lowest number of hours among the considered scenarios, requires the smallest amount of fuel (P_{fuel}) and OPEX, and produces the smallest power to satisfy the defined dispatching plan (P_{GT}) and GHG emissions ($e_{GHG,GT}$). Moreover, the hybrid energy system in SC2 shows the highest revenues due to positive power unbalance (R_{unb+}) and the lowest costs associated to GHG emissions (C_{GHG}) and negative power unbalance (C_{unb-}). Clearly enough, the higher $\mathrm{Prob_d}$ and lower forecast horizon, the better performance on these parameters,

thus confirming the findings obtained in the preliminary comparison of the power curves matching. On the other hand, the largest revenues due to electricity selling to the grid (R_{sell}) is obtained when lower $Prob_d$ and higher forecast horizon are considered (SC3) because of greater P_{GT} produced over many operating hours of the GT park.

Table 5.19. Case-study 2: Technical, economic, environmental parameters of the hybrid energy system in the four SCs.

Parameter	SC1	SC2	SC3	SC4
Number of operating hours for GT park	18	6	36	14
Total $P_{wind,avail}$ (MWh)	2881.86	2881.86	2881.86	2881.86
Total P_{fuel} (MWh)	1134.39	325.53	2256.20	819.36
Total P_r (MWh)	1190.92	1190.92	1190.92	1190.92
Total P_{GT} (MWh)	181.42	44.41	373.69	130.69
Total $e_{GHG,GT}$ (kg_{CO2eq})	229146.24	65757.83	455752.80	165510.35
Discounted total power (MWh)	1279.66	1151.90	1458.96	1232.35
$CAPEX_{OWT}$ (€)	151472096	151472096	151472096	151472096
$CAPEX_{GT}$ (€)	68253730	68253730	68253730	68253730
Discounted total $OPEX_{OWT}$ (€)	55165.43	55165.43	55165.43	55165.43
Discounted total $OPEX_{GT}$ (€)	483.63	118.38	996.19	348.38
Total R_{sell} (€)	209032.78	204262.25	216711.28	207922.76
Total R_{unb+} (€)	10404.10	34373.76	20163.94	26609.79
Total C_{unb-} (€)	227.32	333.00	714.10	468.52
Total C_{GHG} (€)	3437.19	986.37	6836.29	2482.66

From the data in Table 5.19, the technical, economic and environmental indicators defined in Section 4.3 are calculated for each SC. Figure 5.16 illustrates the comparison of these indicators.

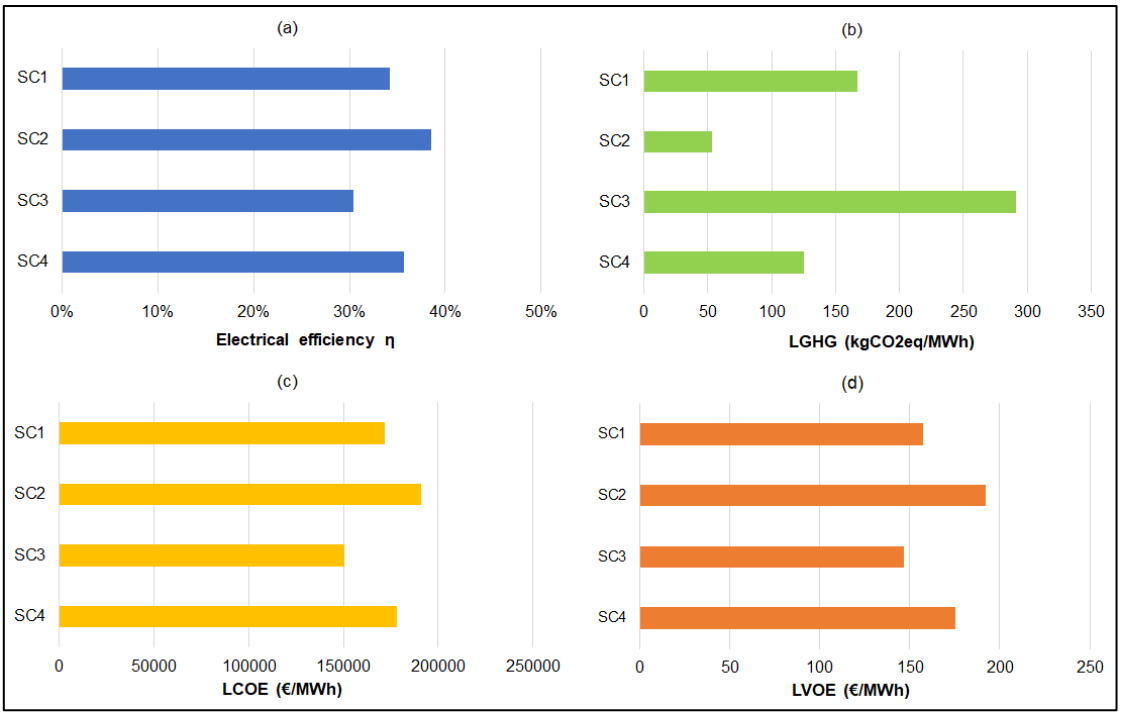

Figure 5.16. Case-study 2: Comparison of technical, economic and environmental indicators among the four SCs.

With respect to the technical performance in Figure 5.16a, the highest electrical efficiency, η_{el}, of the hybrid energy system is obtained in SC2, as a result of the lower number of operating hours of the GT park and fuel consumption shown in Table 5.19. It is worth noting that the ranking of SCs based on η_{el} is inversely proportional to these two parameters. As a consequence, it can be concluded that the higher $Prob_d$ and lower forecast horizon selected for the analysis, the better technical performance of the hybrid energy system.

Looking at the environmental indicator results (Figure 5.16b), SCs are ranked on LGHG with the same order than emerged in η_{el}, i.e. SC2 provides the best performance (i.e. the lowest LGHG value) followed by SC4, SC1 and finally SC3 with the highest LGHG. This is a direct consequence of diminishing $e_{GHG,GT}$ while decreasing the number of operating hours of the GT park, as illustrated in Table 5.19. The same conclusions described above about the influence of $Prob_d$ and forecast horizon on η_{el} can be drawn in case of LGHG.

Concerning the LCOE findings in Figure 5.16c, the lowest value of this indicator is calculated for SC3 while the highest one for SC2. Therefore, referring to Equation (4.35), the effect of the discounted total power produced from the hybrid system prevails on LCOE rather than total costs: the highest power generated in SC3 leads to the best economic performance even though the greatest $OPEX_{GT}$ associated to the GT park, as shown in Table 5.19. As a matter of facts, the lower $Prob_d$ and higher forecast horizon selected for the analysis, the better LCOE indicator, differently from η_{el} and LGHG conclusions.

From Figure 5.16d, SC2 appears the scenario characterized by the highest LVOE value while SC3 is the worst performant, thus confirming the ranking based on η_{el} and LGHG. This highlights that the results on R_{unb+}, C_{GHG} and C_{unb-} parameters play an important role on the estimation of LVOE rather than R_{sell} values. Therefore, it can be concluded that the higher $Prob_d$ and lower forecast horizon selected for the analysis, the better economic performance on LVOE of the hybrid energy system.

By using target values in Table 5.19 for normalization of indicators and applying weights trade-offs in Tables 5.17 and 5.18 to the normalized indicators, ASI values for four SCs are calculated based on different perspectives of decision makers and weighted mean method. Figure 5.17 displays the results.

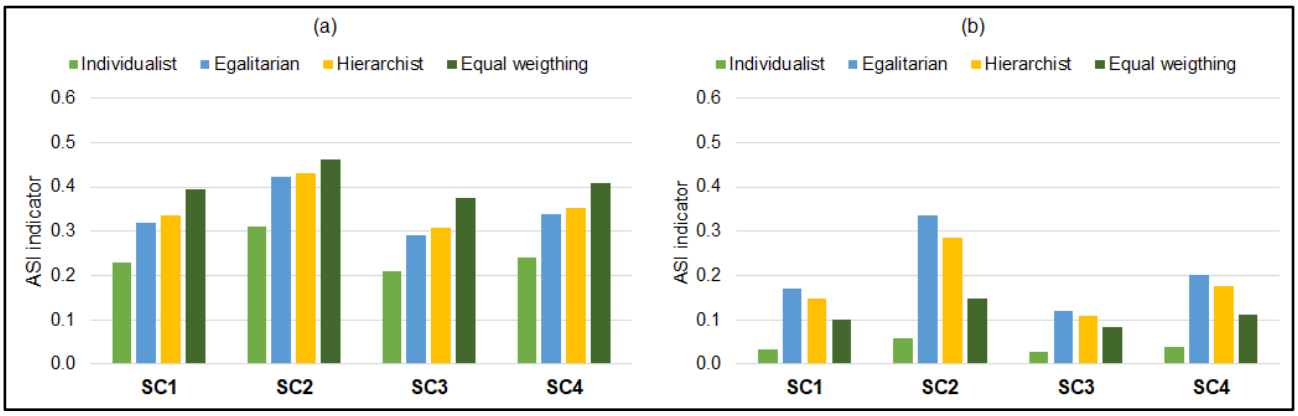

Figure 5.17. Case-study 2: Comparison of ASI indicators for the four SCs based on different perspectives and (a) WAM and (b) WGM methods for aggregation.

Looking at the results obtained through the weighted arithmetic mean (Figure 5.17a), SC2 is identified as the scenario with the best performance (i.e. highest ASI) based on all the schemes of decision makers, thus confirming the findings obtained from η_{el}, LGHG and LVOE comparison. For this SC, comparable ASI values are obtained according to egalitarian, hierarchist and equal weighting methods, ranging from 0.42 to 0.46, while individualist approach yields lower ASI (i.e. 0.3). SC4 and SC1 are the second and third ranked with similar values of ASI based on the same perspective of decision makers. On the other hand, SC3 results in the most penalized scenario with respect to all perspectives. Therefore, forecast data based on lower time horizon and dispatching power plan defined on higher $Prob_d$ can be considered optimal parameters to enhance the overall sustainability fingerprinting of the offshore hybrid energy system.

The same ranking of the SCs appears focussing on Figure 5.17b when the weighted geometric mean is used for calculation of ASI. However, it should be noted that, being equal archetype, the egalitarian method provides the highest ASI values than the other schemes. Moreover, lower values of ASI are

obtained for all the SCs compared to Figure 5.17a, as a consequence of large differences between normalized indicators.

A further investigation is performed with the aim to evaluate in each of the four defined SCs. the potential benefits of the G2P offshore hybrid energy system compared to the sole offshore renewable plant linked to the onshore electrical grid (i.e. without the energy balancing GTs). In this latter case, costs associated to the negative unbalance (C_{unb-}) are quantified based on all the hourly negative differences between P_r and P_d, GHG emissions and related costs are not considered, are attributed only to the renewable power receiving the financial incentive (In_{OWT}), η_{el} and R_{sell} are evaluated with the sole terms associated to the wind power, CAPEX and OPEX of GTs are not estimated. Table 5.20 summarizes the main results obtained for the different SCs excluding the energy balancing system ($SC_{no\text{-}G2P}$). Figure 5.18 illustrates the relative difference in the technical and economic performance indicators of the G2P hybrid energy system with respect to the sole renewable plant in the four SCs. Quite obviously, LGHG comparison is neglected due to assumption of zero emissions from the OWT farm.

Table 5.20. Case-study 2: Technical and economic parameters calculated for the four SCs excluding the GT energy balancing systems.

Parameter	$SC1_{no\text{-}G2P}$	$SC2_{no\text{-}G2P}$	$SC3_{no\text{-}G2P}$	$SC4_{no\text{-}G2P}$
Total $P_{wind,avail}$ (MWh)	2881.86	2881.86	2881.86	2881.86
Total P_r (MWh)	1190.92	1190.92	1190.92	1190.92
Discounted total power (MWh)	1279.66	1151.90	1458.96	1232.35
$CAPEX_{OWT}$ (€)	151472096	151472096	151472096	151472096
Discounted total $OPEX_{OWT}$ (€)	55165.43	55165.43	55165.43	55165.43
Total R_{sell} (€)	20287	202873.65	202873.65	202873.65
Total R_{unb+} (€)	10404.10	34373.76	20163.94	26609.79
Total C_{unb-} (€)	7867.82	3157.05	16924.58	6142.36

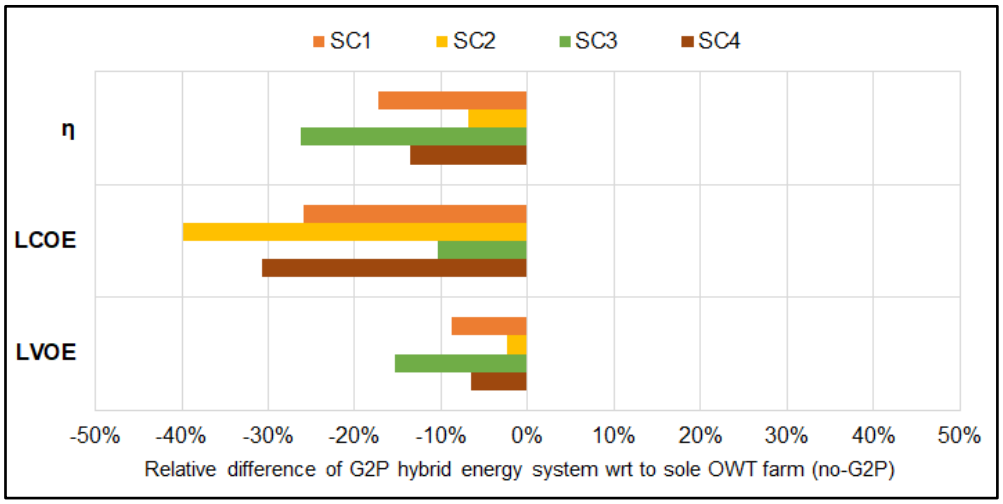

Figure 5.18. Case-study 2: Relative difference in the performance of G2P hybrid energy system with respect to the sole OWT farm for the four SCs.

As shown in Table 5.20, all the parameters remain unchanged compared to the SCs evaluated in the hybrid energy system (Table 5.19), except for the C_{unb-} which are significantly higher due to lack of GT park. Among the scenarios, the greatest C_{unb-} is identified in $SC3_{no\text{-}G2P}$ (about 17 k€), while the largest increase of C_{unb-} with respect to the data in Table 5.19 is attributed to $SC1_{no\text{-}G2P}$ (almost 33%).

Despite these results, from Figure 5.18, it appears evident that the adoption of the G2P hybrid energy system with respect to the sole renewable plant is not advantageous over the selected time interval. Negative percentages illustrated in the figure mean that the hybrid energy option produces worse indicators than the OWT farm in each SC, i.e. lower η_{el}, higher LCOP and lower LVOE. However, it should be noted that SC2 shows greater potential for enhancement in η and LVOE of compared to other scenarios, with relative differences between the hybrid energy system and the sole OWT farm lower than 7%. This confirms the outcomes from the previous analyses on single and aggregated indicators about the beneficial effect of lower forecast horizon and higher $Prob_d$ on the sustainability performance.

5.3.6. Results of sensitivity analysis

The stability of the ranking of the four SCs based on ASI indicators is investigated by applying sensitivity analysis technique described in Section 4.7. The Monte Carlo method implemented in MATLAB programming software [641] is adopted to investigate the influence of random variation of target values used for normalization of disaggregated indicators on the relative differences of ASIs of SC2, SC3 and SC4 with respect to the reference SC1. The analysis of the effect of varying weights among indicators is reasonably disregarded due to the approach adopted for weights elicitation, as discussed in case-study 1.

All the target values are equally varied between $\pm$20% the baseline value reported in Table 5.15. The uniform distribution is conservatively adopted for all the indicators to ensure more conservative results and avoid assumptions about the distributions of the reference indicators. 10^6 runs are performed in all the simulations. The results of the analysis are illustrated in Figure 5.19 based on different perspectives of decision makers and weighted mean methods.

Figure 5.19 clearly shows that SC2 and SC4 are always the best options with respect to SC1 for all the perspectives of decision makers and for both the aggregation methods, because of the positive ASI differences obtained with 10^6 simulations. On the other hand, a negative difference appears in case of SC3 in all the situations and runs. Therefore, it can be concluded that the ranking of the scenarios depicted in Figure 5.17 is completely proved. Equal findings are obtained by increasing the variation range of target values up to $\pm$50%, as well as the Monte Carlo runs up to 10^7 simulations.

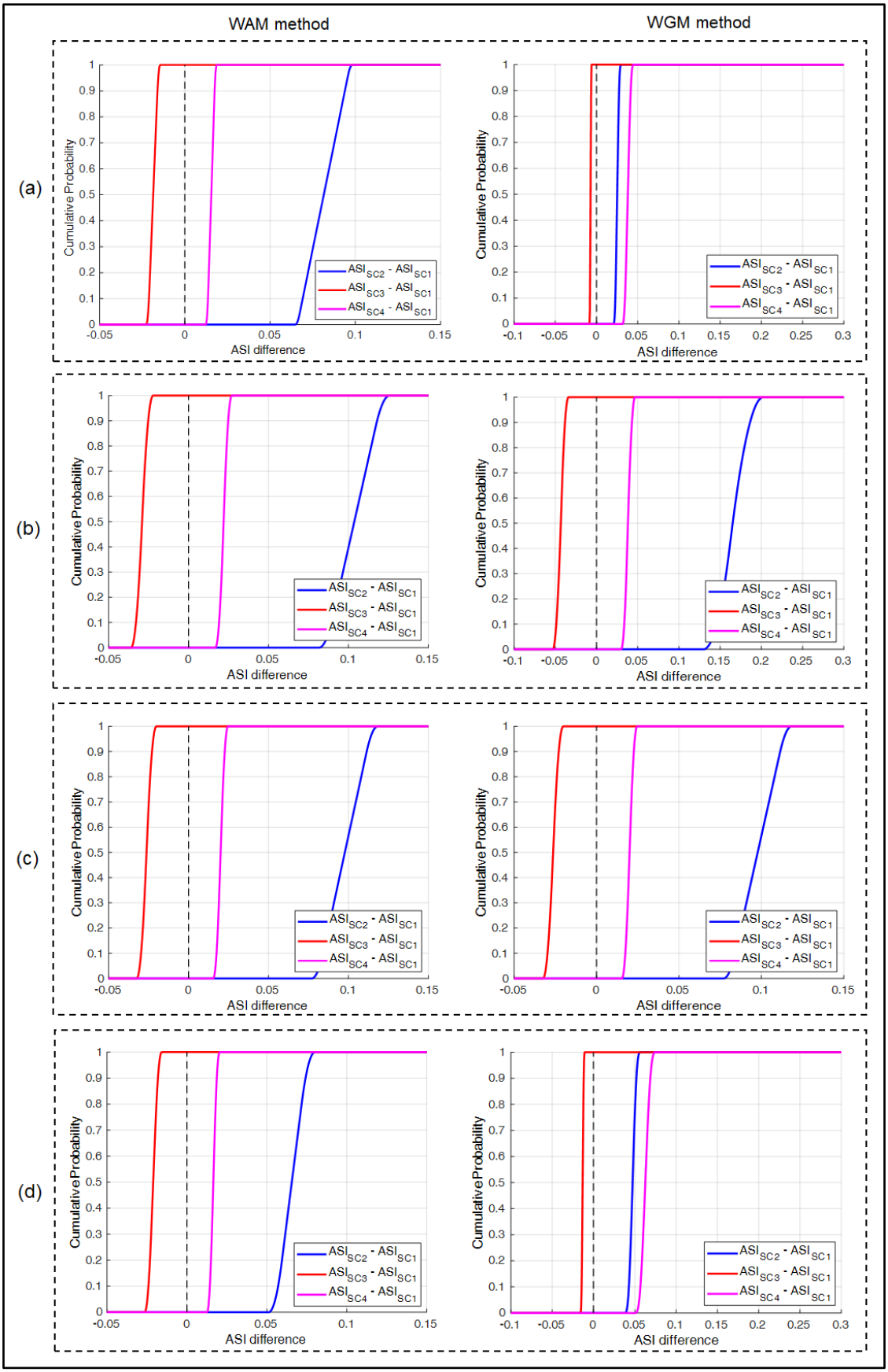

Figure 5.19. Case-study 2: Cumulative probability of the ASI differences of SC2, SC3 and SC4 with respect to SC1 using (a) individualist, (b) egalitarian, (c) hierarchist, (d) equal weighting schemes.

5.3.7. Conclusions

An offshore hybrid energy system located in a gas depleted field in the Adriatic Sea and composed of an OWT farm coupled with aeroderivative GTs at a gas facility is considered to demonstrate the potential of the sustainability assessment methodology described in Section 4.4 for alternative G2P hybrid energy options defined on different short-term forecast horizons and $Prob_d$.

In the selected time interval (three days), the hybrid energy system in SC2 characterized by lower forecast horizon (3 h) and higher $Prob_d$ (90%) shows the best performance based on η_{el}, LVOE and LGHG indicators, as well as aggregated indicator ASI. Despite the hybrid energy system in SC3 based on higher forecast horizon (6 h) and lower $Prob_d$ (80%) exhibits the lowest LCOP indicator among the alternatives, such a system gives the worst ASI value. This is also confirmed by applying different criteria and perspectives of decision makers to elicitation of weights among indicators, as well as using WAM and WGM methods for aggregation. Sensitivity analysis performed by varying randomly the target values used in the normalization of indicators reveals a high degree of confidence in the ranking of the scenarios based on ASI indicators.

Even though the G2P offshore hybrid energy system allows to significantly reduce the negative unbalance costs of the offshore wind power production with respect to the declared dispatching plan, the sustainability performance of the OWT farm excluding the GT energy balancing technologies appears more favourable over the analysed period.

5.4. Case-study 3: Application of the inherent safety assessment methodology to alternative designs of an offshore gas production installation

The methodology described in Section 4.5 is applied to a case-study consisting of different design options of a gas production platform in the Adriatic Sea, in order to specifically demonstrate the ability of the method to address safety criticalities of early design solutions in offshore structures disregarding preliminarily the implementation of P2G/P2L/G2P offshore hybrid energy options.

5.4.1. Overview of the alternative design options

The case-study concerns the design of an offshore facility exploiting natural gas from five wells of a gas field located in shallow water (average depth 70 m). The gas is processed (free water separation) and then exported onshore by a sealine. Three alternative options are proposed for the process layout of the facility. The simplified flow diagrams are shown in Figure 5.20. Option 1 (reference design) consists of five surface wellheads and dedicated separators on the topside. Option 2 considers the use of two manifolds

connecting the wells to one production separator and one test separator. Option 3 comprises 5 subsea wellheads with related subsea manifolds and risers, connected to single topside production separator and test separator.

The inherent safety assessment methodology described in Section 4.5 is applied to preliminary assess the inherent safety benefits expected by the alternative configurations. Actually, the case-study is representative of a common conflict that may be experienced when applying inherent safety principles in design of offshore systems: the use of a single production separator (Option 2) is expected to result in a better safety performance as a consequence of the inherent safety principles addressing minimization of the overall system inventory and process simplification [375–377,663,664]. However, also Option 3 (implementation of subsea wellheads) applies the inherent safety principles of segregation and reduction of the effects [375–377,431,664].

All the design options require a topside structure. A multi-level four-legged jacket structure with similar dimensions (approximately 35 m long by 18 m wide) is considered for all the cases. A side view of the installation with indication of main decks and relative elevation above the sea level is illustrated in Figure 5.20. Process and utility equipment are located on the cellar and mezzanine deck levels and confined within solid deck plating above and below even though the wellhead module is located on a grated surface.

Besides the process equipment described in Figure 5.20, the topside also hosts some utilities, common to all the options: the chemicals system for gas hydrates prevention (diethylene glycol and CH_3OH), a pig launcher for cleaning and inspection of the gas export sealine, the treatment system for produced oily-waters, the fuel gas system for main electrical power generation and the recovery tank for oily drains. Other designed modules typically present (e.g. vent unit, purge burner system, compressed air module) are not considered in the present analysis due to their irrelevance in terms of dangerous substances and/or discontinuous operation.

The platform has no living quarters and is remotely controlled, but potential human targets are periodically present on all decks of the installation for inspection and maintenance. The platform is regularly approached by supply vessels which constitute a potential assets target and that carry on board further potential human targets. As for environment targets, only the contamination of the water column is considered, due to the materials present on the natural gas topside platform (i.e. oily-water, soluble chemicals). Therefore, as required from step 0 of the procedure illustrated in Figure 4.12, the targets identified are humans, all three categories of assets (process and utility equipment, facility structure, marine structures), and one category of environment target (i.e. water column polluted due to soluble chemical spills and dissolved oil molecules).

The hypothetical location of the facility (Adriatic sea) has a mean annual wind speed between 1.6 and 5.4 m/s, air temperature that ranges between -5°C and 32°C with 80% relative humidity and seasonal sea surface temperature between 11°C and 23°C [665,666].

Required input information for the units is obtained by preliminary design data of the process and equipment. Table 5.22 summarizes these data. The normalization values for the KPIs are defined according to the guidelines provided in Table 4.18, given the facility dimension and the safety zone of 500 m radius, and summarized Table 5.23.

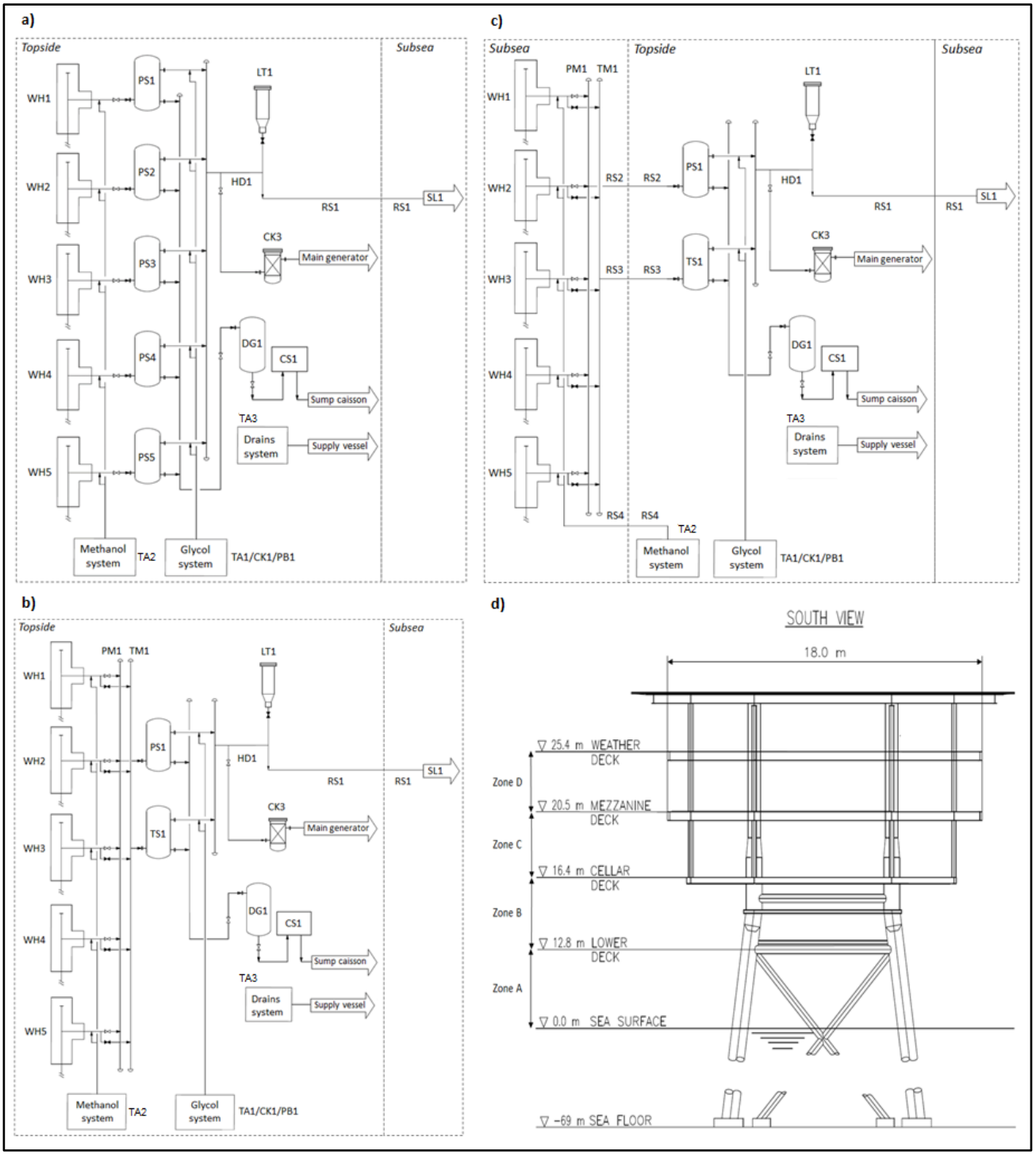

Figure 5.20. Case-study 3: Simplified process flow diagrams of design options and side view of the installation. WH: Wellhead; RS: Riser/Umbilical; PM: Production manifold, TM: Test manifold: PS: Production separator; TS: Test separator; HD: Header; LT: Launching trap; SL: Sealine; TA: Atmospheric tank; PA: Distribution pump; PB: Injection pump; CK: Cartridge filter; DG: Degasser; CS: Coalescence separator.

Table 5.21. Case-study 3: Main input data for equipment considered in the three alternative design options.

Equipment and design option	Key substance	Pressure (barg)	Temp. (°C)	Inlet flowrate (kg/s)	Diameter (mm)	Height or Length (m)	Auxiliary items	Topside zone	EQ code
WH1 (1&2)	CH_4	94	51	0.34	62	2090	-	D	EQ6.1
WH2 (1&2)	CH_4	106	53	1.28	62	2090	-	D	EQ6.1
WH3 (1&2)	CH_4	96	53	1.53	62	2090	-	D	EQ6.1
WH4 (1&2)	CH_4	106	52	1.55	62	2090	-	D	EQ6.1
WH5 (1&2)	CH_4	94	54	0.43	62	2090	-	D	EQ6.1
WH1 (3)	CH_4	94	51	0.34	62	2000	-	A	EQ6.1
WH2 (3)	CH_4	106	53	1.28	62	2000	-	A	EQ6.1
WH3 (3)	CH_4	96	53	1.53	62	2000	-	A	EQ6.1
WH4 (3)	CH_4	106	52	1.55	62	2000	-	A	EQ6.1
WH5 (3)	CH_4	94	54	0.43	62	2000	-	A	EQ6.1
PS1 (1)	CH_4	62	13	0.34	500	2.15	I: 6, V:12	C	EQ1.2
PS2 (1) / TS1 (2 & 3)	CH_4	73	15	1.28	500	2.15	I: 6, V:12	C	EQ1.2
PS3 (1)	CH_4	73	14	1.53	500	2.15	I: 6, V:12	C	EQ1.2
PS4 (1)	CH_4	70	14	1.55	500	2.15	I: 6, V:12	C	EQ1.2
PS5 (1)	CH_4	79	16	0.43	500	2.15	I: 6, V:12	C	EQ1.2
PS1 (2&3)	CH_4	46	2	5.13	1400	2.8	I: 6, V:12	C	EQ1.2
PM1 (2)	CH_4	46	2	5.13	203.2	10	I: 2, V: 5	D	EQ4.3
PM1 (3)	CH_4	46	2	5.13	203.2	10	I: 2, V: 5	A	EQ4.3
RS2 (3)	CH_4	46	2	5.13	152.4	200	V: 1	A & B	EQ4.2
TM1 (2)	CH_4	73	15	1.28	152.4	10	I: 2, V: 5	D	EQ4.3
TM1 (3)	CH_4	73	15	1.28	152.4	10	I: 2, V: 5	A	EQ4.3
RS3 (3)	CH_4	73	15	1.28	101.6	200	V: 1	A & B	EQ4.2
HD1 (1&2&3)	CH_4	46	2	5.13	203.2	15	I: 6, V: 4	B	EQ4.3
RS1 (1&2&3)	CH_4	46	2	5.13	355.6	200	V: 1	A	EQ4.2
SL1 (1&2&3)	CH_4	46	2	5.13	355.6	18000	V: 1	A	EQ4.2
LT1 (1&2&3)	CH_4	46	2	5.13	355.6	4.5	I: 2, V: 7	D	EQ7.1
CK3 (1&2&3)	CH_4	2	49	0.01	219	1.03	I: 6, V: 6	C	EQ1.3
TA1/CK1/PB1 (1&2&3)	Glycol	0	20	-	1300	2.4	I: 6, V: 12, F:1, G: 1	C	EQ1.1
TA2/CK2/PA2 (1&2&3)	CH_3OH	0	20	-	500	1.2	I: 6, V: 12, F:1, G: 1	C	EQ1.1
RS4 (3)	CH_3OH	*n.r.*	20	0	50.8	200	V: 1	A & B	EQ4.2
DG1 (1&2&3)	100 ppm oil in water	0	20	0.002	800	2.4	I: 3, V:6	B	EQ1.1
CS1 (1&2&3)	100 ppm oil in water	0	20	0.002	1000	4.6	I:3, V:5	B	EQ1.1
TA3 (1&2&3)	100 ppm oil in water	0	20	-	1250	3.5	I: 4; V:12	B	EQ1.1

Equipment labels and congestion zones refer to Figure 5.20. In the auxiliary item column the codes report the number of items considered for each unit. I: instrument connection, V: valve, F: filter, G: pump.

Table 5.22. Case-study 3: Vulnerability area used as normalization factor for each identified target.

	Humans	Process and utility equipment	Facility structures	Marine structures	Water column
Reference vulnerability area (m^2)	630	630	630	785 000	785 000

5.4.2. Assumptions made for the assessment

Step 4 of the procedure requires to estimate damage parameters by using well-known consequence simulation models. The calculation of damage parameters for accident scenarios following releases above water surface is performed using the consequences analysis models reported in the TNO's Yellow Book [582] and in other relevant publications [583], implemented in PHAST software tool [667]. Atmospheric stability class E and a wind speed of 3 m/s are considered [668], as these conditions lead to the worst-case damage distances for most scenarios. For modelling VCEs, the TNO Multi-Energy model is used considering the inter-desk volumes shown in Figure 5.20. The process decks are reasonably congested with large items of equipment and pipework: the approach suggested by Kinsella [669] and Raman et al. [670] is used for the selection of charge strength.

In the case of gas releases below the sea surface, the empirical cone model described in the HSE's Offshore Technology Report [585] is adopted. The model is coupled, where relevant, with atmospheric gas dispersion models.

Finally, the PNEC value of marine water reported in the technical literature for glycol and CH_3OH [671] (i.e. 1 ppm and 15.4 ppm, respectively) and the PNEC of marine water proposed in the DREAM model for aliphatic hydrocarbons [468] (i.e. 0.0404 ppm) are conservatively assumed to estimate the contaminated volume of water column due to spills of soluble chemicals and oily-water and the associated damage distances.

5.4.3. Results of inherent safety analysis for the single units

According to step 1 of the procedure illustrated in Figure 4.12, the equipment of the three alternative design options are classified according to the functional equipment categories in Table 4.19, as shown in Table 5.22. This categorization allows identifying the reference release modes, by using the matrix in Table 4.21. Credit factors are assigned to each release mode considering the failure frequencies published by International Association of Oil & Gas Producers (IOGP) [576–579] and Det Norske Veritas (DNV) [573]. The credit factor for each release mode accounts for both the main equipment body (e.g. process vessel) and the expected number of auxiliary items and connections (valves, instruments, etc.) belonging to the unit, as summarized in Table 5.22.

For the test separator in Options 2 and 3, as well as for the subsea test manifold and test riser in Option 3, a utilization factor of 6.6% is applied to the credit factors (estimated service time of 576 hours per year). Table 4.21 and Appendix C are used for the selection of specific offshore event trees for all the release modes. As discussed in Section 4.5, the reference event trees are pruned considering the hazard properties of the released materials. Since the produced natural gas is classified as non-toxic and non-ecotoxic (low levels of hydrogen sulphide), only fire and explosion scenarios are considered, as shown in Table 5.23.

By applying step 4 of the procedure in Figure 4.12, the resulting damage distances calculated for human and assets targets extend beyond the deck sizes (e.g. values up to 150 m), especially in the case of surface designs (Options 1 and 2), while water column pollution show maximum values lower than 130 m in all the options, due to the small inventories of liquid hazardous materials in the system. Table 5.23 compares the results obtained for some units belonging to different options.

As expected, units processing pressurized natural gas and located in a highly congested deck (e.g. separators PS2 of Option 1 and PS1 of Option 2, wellhead WH2 of Option 1) can originate VCE scenarios with high damage distances for human and assets targets. Other severe scenarios for humans result from fireball and flash fires in specific units that can release high quantities of flammable material (e.g. separator PS1 of Option 2, riser RS1). For the subsea wellhead (e.g. WH2 of Option 3), flash fire emerges the most critical scenario, as low congestion in splash zone is not expected to result in relevant VCE effects. Resulting damage distances in this case are smaller than the ones calculated for the topside unit. The glycol storage tank (e.g. TA1) appears as the most dangerous unit for the water column target (i.e. with the highest damage distance due to environmental dispersion) in all the three options.

Table 5.23. Case-study 3: Credit factors, event trees and damage distances for some surface and subsea units.

Unit and option	Credit factor (1/y)	Reference release mode	Event tree	Final accident scenarios	Damage distance (m)				
					Humans	Process and utility	Facility structures	Floating structures	Water column
WH2 (Op.1)	$1.0 \quad 10^{-5}$	R1	d)	Jet fire	24	18	5	5	-
				VCE	86	78	20	43	-
				Flash fire	21	-	-	-	-
	$1.0 \quad 10^{-5}$	R2	d)	Jet fire	35	27	5	5	-
				VCE	86	78	20	43	-
				Flash fire	32	-	-	-	-
	$1.9\ 10^{-5}$	R3b	d)	Jet fire	35	27	5	5	-
				VCE	86	78	20	43	-
				Flash fire	32	-	-	-	-
WH2 (Op.3)	$1.4 \cdot 10^{-6}$	R1	m)*	VCE	0	0	0	0	-
				Flash fire	10	-	-	-	-
	$1.4 \cdot 10^{-6}$	R2	m)*	VCE	0	0	0	0	-
				Flash fire	24	-	-	-	-
	$1.2 \cdot 10^{-5}$	R3b	m)*	VCE	0	0	0	0	-
				Flash fire	28	-	-	-	-
PS2 (Op.1)	$7.9 \cdot 10^{-3}$	R1	d)	Jet fire	21	16	5	5	-
				VCE	86	78	36	50	-
				Flash fire	18	-	-	-	-
	$1.5 \cdot 10^{-3}$	R2	d)	Jet fire	38	5	5	5	-
				VCE	86	78	36	50	-
				Flash fire	26	-	-	-	-
	$4.2 \cdot 10^{-4}$	R3a	f)	BLEVE	12	11	6	8	-
				Fireball	54	–	–	–	-
				VCE	53	48	22	31	-
				Flash fire	12	-	-	-	-
	$4.2 \cdot 10^{-4}$	R3b	d)	Jet fire	38	5	5	5	-
				VCE	86	78	36	50	-
				Flash fire	26	-	-	-	-
PS1 (Op.2)	$7.9\ 10^{-3}$	R1	d)	Jet fire	17	13	5	5	-
				VCE	86	78	36	50	-
				Flash fire	15	-	-	-	-
	$1.5\ 10^{-3}$	R2	d)	Jet fire	60	5	5	5	-
				VCE	86	78	36	50	-
				Flash fire	36	-	-	-	-
	$4.2\ 10^{-4}$	R3a	f)	BLEVE	22	20	10	14	-
				Fireball	97	-	-	-	-
				VCE	86	78	36	50	-
				Flash fire	14	-	-	-	-
	$4.2\ 10^{-4}$	R3b	d)	Jet fire	60	5	5	5	-
				VCE	86	78	36	50	-
				Flash fire	36	-	-	-	-
RS1 (Op. 1,2,3)	$9.9\ 10^{-4}$	R1	d)	Jet fire	17	13	5	5	-
				VCE	33	29	0	0	-
				Flash fire	15	-	-	-	-
	$3.1\ 10^{-4}$	R2	d)	Jet fire	97	73	5	5	-
				VCE	46	41	0	0	-
				Flash fire	103	-	-	-	-
	$1.4\ 10^{-4}$	R3b	d)	Jet fire	97	73	5	5	-
				VCE	46	41	0	0	-
				Flash fire	103	-	-	-	-
TA1 (Op. 1,2,3)	$1.8\ 10^{-2}$	R1	a)	Pool Fire	36	19	5	5	-
				Envir. Dissol.	-	-	-	-	129
	$2.7\ 10^{-3}$	R2	a)	Pool Fire	36	19	5	5	-
				Envir. Dissol.	-	-	-	-	129
	$1.1\ 10^{-3}$	R3a	b)	Pool Fire	36	19	5	5	-
				Envir. Dissol.	-	-	-	-	129

Equipment labels refer to Figure 5.20. Event tree codes refer to Table 4.21 and Appendix C.

The estimation of damage distances for each target of concern allows the calculation of potential and inherent KPIs (PI and HI, respectively) for each unit of the design options addressing single targets, according to step 6 of the procedure in Figure 4.12. From application of Equations (4.42) and (4.43), KPIs addressing human target are calculated. Couples of KPIs are derived for the three categories of assets by means of Equations (4.44) and (4.45). Finally, the potential and inherent KPIs associated to releases of soluble chemicals and oily-water are obtained by applying Equations (4.46) and (4.47). The KPIs results for the units of the three options of the case-study are illustrated in Figure 5.21.

From Figure 5.21, it appears that the potential KPIs clearly show a different pattern of hazard profile among the units of every considered options. Topside equipment handling large flowrates of gas (e.g. separators, surface wellheads, launching trap, gas header, manifolds) are generally identified as critical units for both human and asset targets. As observed before, this can be tracked back mainly to the possibility of the releases to originate gas clouds in congested sections of the topside. Differences in unit PIs among the different targets originate from the consequences of these gas cloud scenarios. The export riser is recognized for all three design options as the most potentially critical unit for human target (i.e. with the highest HPI value) due to possibility of a large flash fire from a full-bore rupture close to the sea surface. Separators, traps, surface wellheads and manifolds score high unit API values for assets, due to possibility of severe VCE scenarios. It should be noted that, while for units in the cellar deck (e.g. process separators in zone C) every sub-category of assets target has high API score, units in less congested zones (e.g. wellheads in zone D) score lower API values for targets characterized by higher damage thresholds (e.g. facility structures, as for Table 4.17); this is due to the lower strength expected for the VCE scenario when the release occurs in a less congested zone.

Equipment like storage tanks, auxiliary pumps and filters operating at low pressure with liquid materials have minor hazard potential for most target categories. Only when the released material has marine toxicity effects, they become the most relevant units for water column target, e.g. glycol tank which has large inventory of eco-toxic material if compared to other units handling liquid phases in the considered facility.

An appreciable reduction of unit potential KPIs is obtained for all cases in which subsea units can be compared with a topside counterpart (e.g. wellheads and manifolds of Option 3 compared to Option 2). This demonstrates subsea equipment to actually be inherently safer units for this case-study, since a more limited number of scenarios and smaller damage distances are expected, as discussed above for WH1 of Option 3.

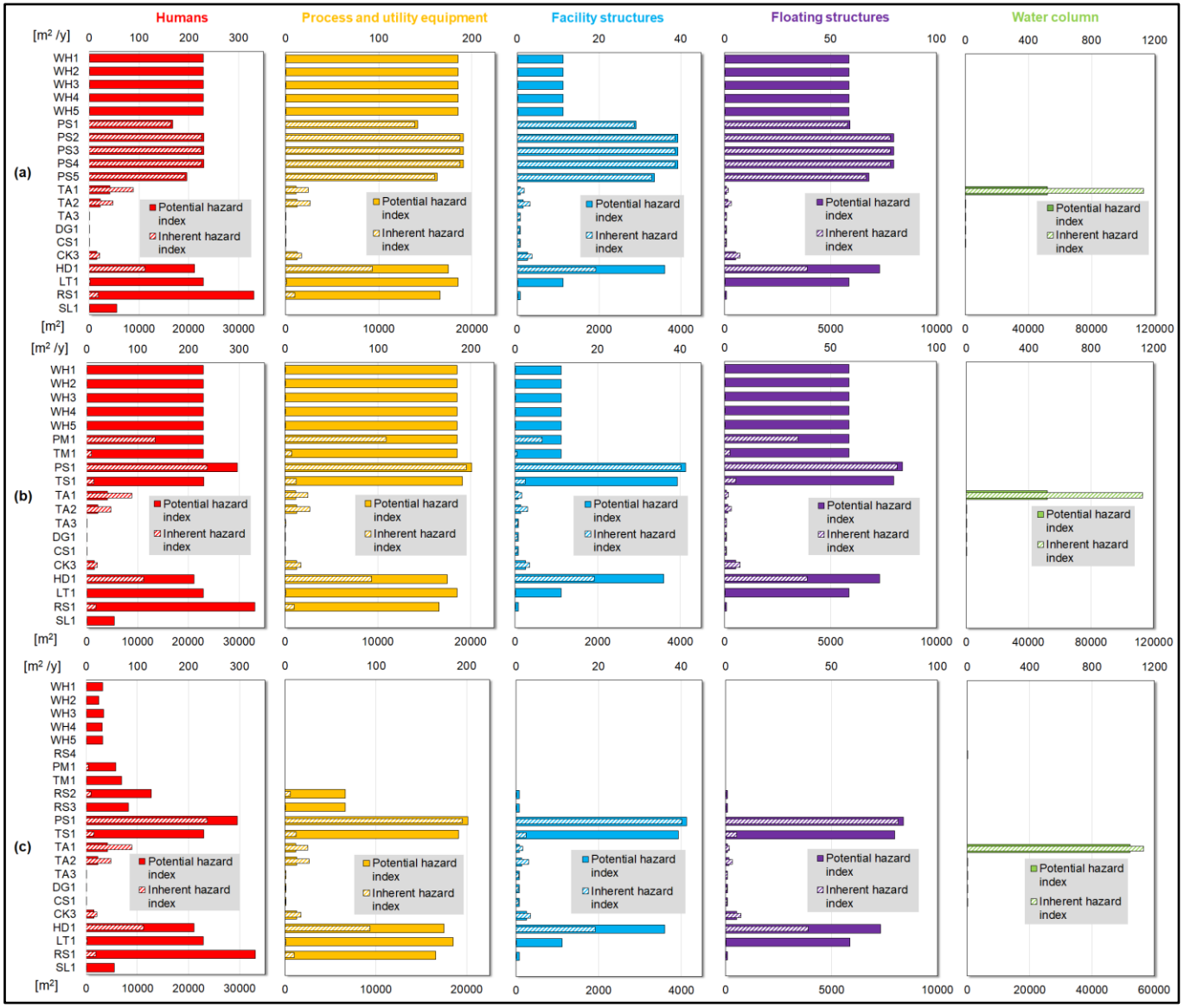

Figure 5.21. Case-study 3: Comparison of unit KPIs addressing single targets among (a) Option 1, (b) Option 2 and (c) Option 3.

The introduction of credit factors for the release modes by means of the unit inherent KPIs provides a further insight on the role of the equipment safety score on the inherent safety performance, and allows a better understanding of how the combination of different aspects (e.g. damage area and equipment safety score) affect the ranking of the critical units.

From Figure 5.21, it appears that the units scoring the greater values of the unit inherent KPIs for both human and asset targets in the considered case-study are the process separators. This confirms the ranking of these units, previously identified by the unit potential KPIs. However other pipe-like equipment (wellheads, manifolds, headers) characterized by high unit PI shows lower values of the unit HI than the separators. The score is affected by the value of the credit factors, which is strongly influenced by the expected number of potential leakage points (nozzles, instrument connections, valves, etc.) present on the unit.

The inherent KPIs for environmental targets identify once again the glycol system as the most critical unit. This is due to the large inventory of eco-toxic material combined with the high likelihood of release (i.e. high credit factors) typical of atmospheric storages.

5.4.4. Results of inherent safety analysis for the facility

In order to evaluate the facility-level inherent safety performance of the alternative process options (step 6 of the procedure in Figure 4.12), Figure 5.22 shows the facility KPIs addressing single targets obtained by summing up the normalized single-target indicators of the units, as indicated in Equations (4.69) and (4.70).

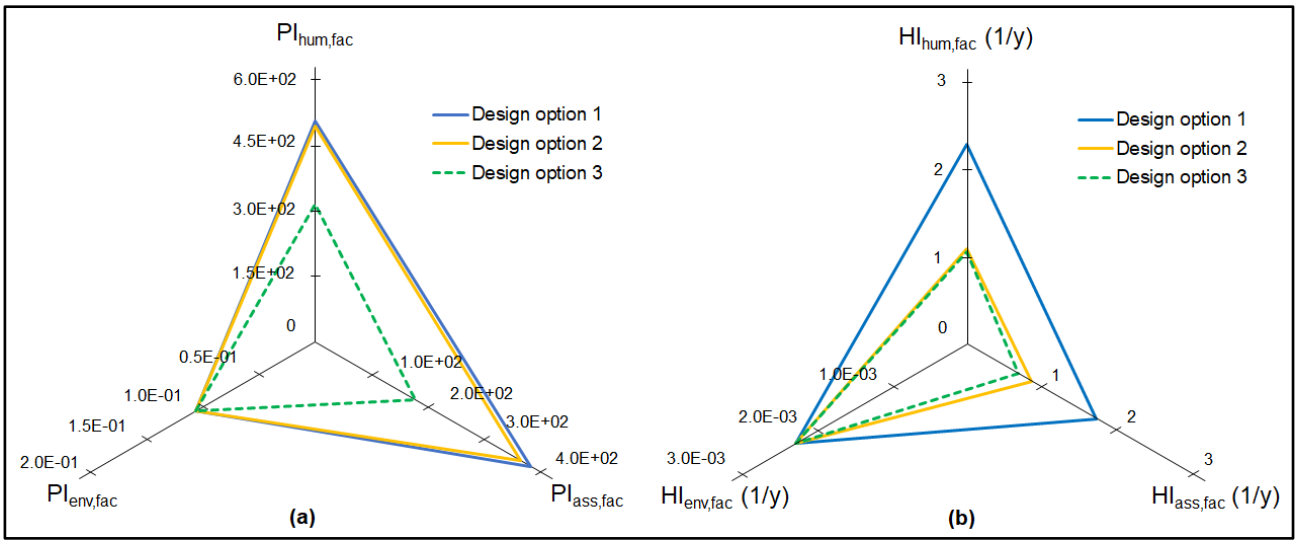

Figure 5.22. Case-study 3: Comparison of (a) facility potential KPIs and (b) facility inherent KPIs addressing single targets among the three design options.

As illustrated in the top panel (Figure 5.22a), Option 2 results in very similar facility potential KPIs in comparison to Option 1 for all the targets categories considered. This means that the benefits introduced by the reduction of the number of separators are actually balanced by the higher potential hazard resulting from the higher inventory when a single production separator is used. Thus, a balance is identified in this case between the inherent safety guidewords of simplification and minimization. Option 3 demonstrates the best safety performance compared to the other options, due to lower potential KPIs both for human and assets targets. This is the result of the use of subsea equipment, characterized by moderate severity scenarios. The environmental aspects are identified as non-discriminating in the comparison, since the key units in the definition of the KPIs addressing water column targets are the same for all the options.

When facility inherent KPIs (Figure 5.22b) are considered, a higher safety performance of Option 2 to Option 1 is identified. This is mainly due to the lower credibility of the releases from wellheads and manifolds, discussed earlier when analysing the corresponding KPIs for the single units. Option 3 demonstrates the best safety performance compared to other options. This is true not only from the point of view of severity of accident scenarios for human and assets targets, but also considering their likelihood with respect to the equipment categories used. Actually, despite the plots of Options 2 and 3 in Figure 5.22b are very similar, a careful examination of the results obtained for single units and for the potential KPIs proves that the coupling between subsea manifold and riser in Option 3 is inherently safer than the sole surface manifold in Option 2.

The conclusions above are further underlined by the facility multi-target KPIs calculated in this case-study by applying the WAM method to facility single-target KPIs (with weights factors equal to 1/3). Figure 5.23 illustrates the values of these indicators as well as the contribution of each target category. As expected for a gas production platform, the highest contribution to both potential and inherent KPIs is obtained for human and assets targets for all the design options, while environmental targets are almost unaffected. The contributions associated to humans and targets are comparable, with a slightly higher score deriving from human targets. Given these findings, sensitivity analysis on the weight factors among the single-target indicators would appear trivial, thus is disregarded in the present case-study.

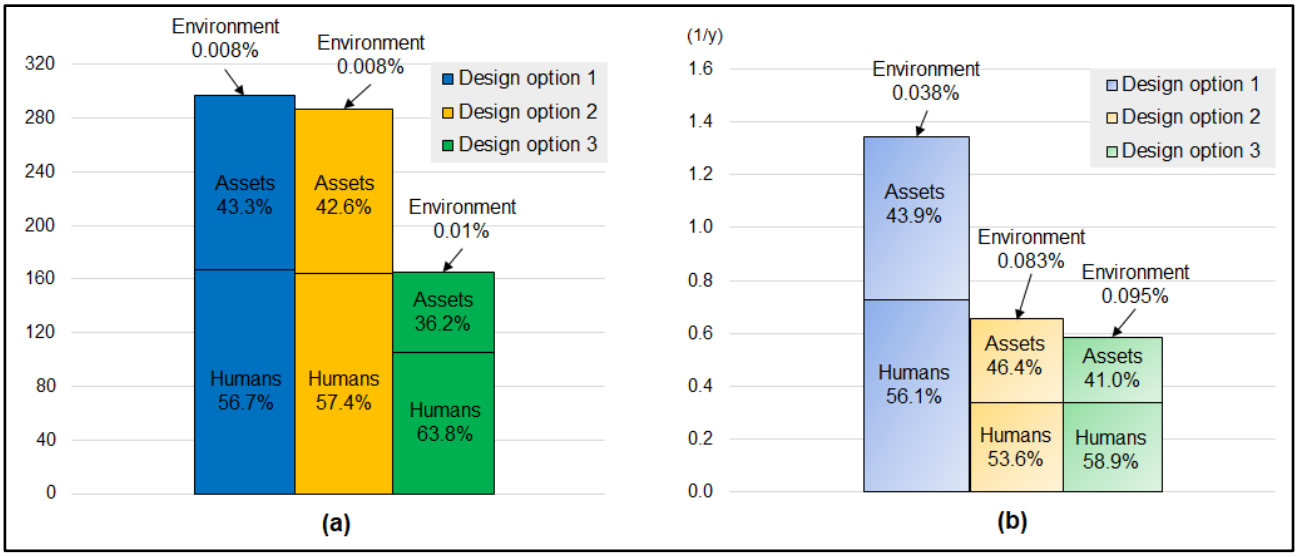

Figure 5.23. Case-study 3: Comparison of (a) facility multi-target potential KPIs and (b) facility multi-target inherent KPIs among the three design options.

5.4.5. Conclusions

Alternative designs for an offshore gas production platform in the Adriatic Sea are considered, to prove the ability of the proposed inherent safety KPIs methodology proposed in Section 4.4 to capture safety criticalities of different extraction and processing solutions of the offshore system with respect to human, assets and environment targets.

Critical equipment are identified for each deign option by unit potential and inherent KPIs, also providing details on specific impacts on the different target categories. Process separators show the worst inherent safety performance for human and assets targets, while the glycol tank is the most hazardous unit with respect to the water column target.

The integrated safety profile of the entire facility is also communicated by means of multi-target KPIs, including the contribution of the different targets to the overall fingerprinting. Subsea systems are identified as inherently safer than surface designs based on both potential and inherent KPIs. As expected for a gas production platform, humans and process equipment are the targets exposed to higher hazards.

5.5. Case-study 4: Application of the environmental protection indicators to oil spills from alternative offshore oil production installations

A case-study consisting of different oil spills from different oil production platforms is introduced with the aim to specifically evaluate the potential of the novel set of environmental KPIs developed within the

inherent safety KPIs methodology in Section 4.5. In this case study, no reference is given to the implementation of P2G/P2L/G2P offshore hybrid energy options at the offshore sites.

Four specific problems are addressed in this case-study. The first concerns the potential of the different KPIs to provide the same severity ranking of oil releases. The second consists in establishing if the different KPIs could be considered equivalent in expressing the environmental severity of the spills. The third verification is made to check if different tools are interchangeable in the calculation of KPIs of levels 2 and 3. Finally, the last issue is to verify the equivalence between the highest level KPIs. Given different features of the tools and different calculations proposed for the same KPI, it is worth mentioning that equal values of KPIs are not likely to be obtained for the same release when using different software. Their values may be similar, or at most of the same order of magnitude. It is thus out of the scope of the present study to compare the tools that may be used to simulate an oil release in water.

5.5.1. Definition of the oil spill scenarios

The oil spills considered in this case-study are potential releases derived from four different offshore facilities for oil/gas production located in different areas.

The first facility, indicated as RM in the study, is a fixed oil production installation and a Floating Storage and Offloading (FSO) unit, which are distant a few kilometres and are connected by a sealine. Both structures were supposed to be located in the southern part of the Adriatic Sea (Italy), off coast of Abruzzo in 80 m of water depth. The installation produces crude oil with 11.5 °API through 12 topside wellheads as well as gathers the same type oil from two nearby platforms (9 wells and 8 wells, respectively) delivered by dedicated sealines. In order to meet the requirements for transportation to the FSO, at the main platform oil collected in the production manifold is first heated in two heat exchangers and then routed to two gas-liquid separators in order to separate the associated gas from the liquid stream. The separated oil is then pumped and delivered via one sealine to the FSO. After being received by the FSO, oil is stored in 7 tanks until transportation by oil tankers to an onshore refinery plant.

The second facility, called VG in this study, consists of an oil production platform and an FSO unit, distant a few kilometres and connected by two sealines, i.e. one for oil delivery from the platform to FSO and the other one for diluent from FSO to the platform. Both structures are supposed to be located in the Mediterranean Sea, off coast Sicily at about 120 m water depth. Crude oil with 15.4 °API is extracted from about 20 wells through topside wellheads located on the platform. In the production manifold, the oil is mixed with a diluent in order to reduce its viscosity and prevent solidification. The diluent is stored in the FSO, delivered to the platform through one of the two sealines and pumped into the manifold mentioned above. The blend produced from the mixing of the oil and the diluent is then routed to a first separation vessel for eliminating the gas from the liquid phase. The blend derived from this first separation

is heated and further sent to a second separation unit. Finally, after gas separation, the blend is pumped and transferred via the second sealine to the FSO unit for storage. From the FSO, the blend is transported by oil tankers to onshore refinery plants.

The third platform, named MA in the analysis, is a gas production platform, supposed to be located in the northern Adriatic Sea (Croatian area) in water depth of about 69 m. At the platform, power generation is provided by means of a diesel fuel system composed of tank, pump, filter.

The fourth facility, called AP in the study, is an offshore oil production installation supposed to be located off the coast of the Republic of Congo in water depth of 80 m, where light crude oil (around 28-32 °API) with a water-to-oil ratio of 0.3 is extracted from wells. At the platform, oil is first separated by means of one two-phase production separator and then pumped to one header for the transportation via sealine to shore.

In total, sixteen spills from continuous release and catastrophic rupture of equipment units of the four facilities are considered in the analysis. For each facility, Table 5.24 reports the releases, the substance considered, oil density (in °API), oil temperature, mass of the spill, duration of the spill. Moreover, air temperature and sea surface temperature are tabulated for each facility. It can be noticed that the considered releases show significant differences in both oil properties, characteristics of the release and environmental conditions at the site. With respect to the release duration, no values are reported in case of catastrophic rupture, while about 10 minutes are considered for continuous releases.

Table 5.24. Case-study 4: Input data considered for the oil spills from the four offshore facilities.

Facility	Release	Substance	Density (°API)	Oil release temperature (°C)	Release duration (s)	Released oil mass into sea (kg)	Order of magnitude for mass	Air temperature (°C)	Sea surface temperature (°C)
RM	RM1	Crude oil	11.5	65	600	117	0.1	15	15
	RM2	Crude oil	11.5	65	600	1053	1	15	15
	RM3	Crude oil	11.5	80	600	1697	1	15	15
	RM4	Crude oil	11.5	65	600	3394	1	15	15
	RM5	Crude oil	11.5	20	-	12857143	10000	15	15
VG	VG1	Crude oil	11.5	101	600	121	0.1	19	19
	VG2	Diluent	62.3	20	600	438	0.1	19	19
	VG3	Blend	22.9	85	600	2744	1	19	19
	VG4	Diluent	62.3	20	-	10224200	10000	19	19
	VG5	Blend	22.9	30	-	13485364	10000	19	19
MA	MA1	Diesel	35.0	15	-	918	1	15	15
	MA2	Diesel	35.0	20	-	1020	1	15	15
AP	AP1	Crude oil	30.0	36	600	938	1	25	25
	AP2	Crude oil	30.0	32	180	2127	1	25	25
	AP3	Crude oil	30.0	36	-	6048	7	25	25
	AP4	Crude oil	30.0	36	205	8018	7	25	25

5.5.2. Assumptions made for the assessment

Four different software are adopted for the calculation of the higher level KPIs, i.e. ADIOS [594], GNOME [595], OSCAR [596] and OWM [597]. Main features of the tools are described in Section 4.4.

With respect to the input data summarized in Table 5.24, some small releases cannot be simulated by using ADIOS software due to limits of the tool on the mass of the spill (lower than 320 kg and higher 79415 t), i.e. RM1, VG1 and VG2. All the spills are simulated with the other tools.

Due the relatively short duration of the releases shown in Table 5.24, the releases are assumed instantaneous in the modelling with ADIOS, GNOME and OWM. Since the instantaneous release in ADIOS corresponds to a spill of 1 h, such a relatively small value is assumed in the simulations with OSCAR which is unable to simulate instantaneous spills requiring in input both mass and release duration.

Concerning the three temperatures listed in Table 5.24, GNOME is not able to take into account any value of mentioned temperatures, ADIOS and OWM tools consider thermal equilibrium between air, water and release, thus requiring to specify only one value. In this study, simulations with ADIOS and OWM are carried out by assuming the sea surface temperature. Since OSCAR distinguishes oil, air and sea surface temperatures among them, thus all three values are provided in input.

Each tool provides a given oil database: it is limited to four oils in GNOME, at least ten oils in the other software. The common oil between all the databases of the tools are rare, thus in the modelling with each tool, different assumptions are made concerning the selection of the oils for simulations of releases of the case-study. However, the choice and attribution of the suitable oil is performed based on the similarity in the densities between oils illustrated in Table 5.24 and available oils in the databases.

As described in Section 4.5, the fate of the spill strongly depends upon the wind and currents conditions. In this case-study, for the sake of simplicity, values constant in time and uniform in space are assumed for both the wind (6 m/s) and the currents (0.13 m/s) with all the tools. Moreover, in the case of OSCAR which considers both these two parameters, their vectors are considered as orthogonal. Since the proposed KPIs are addressed to the sea surface compartment, the wind and current directions are assumed in order to avoid sedimentation and beaching, thus keeping the oil slick in open sea.

Table 5.25 summarizes the assumptions for simulations of the releases in Table 5.24 with the different tools.

Table 5.25. Case-study 4: Assumptions made for the simulations of the oil spills with the four oil fate modelling tools.

Release	Substance in ADIOS	Density (°API) in ADIOS	Substance in GNOME	Density (°API) in GNOME	Substance in OWM	Density (°API) in OWM	Substance in OSCAR	Density (°API) in OSCAR
RM1	WEST DELTA BLOCK 30	11.4	FUEL OIL #6	8 - 15	GRANE	18.7	GRANE	18.7
RM2	WEST DELTA BLOCK 30	11.4	FUEL OIL #6	8 - 15	GRANE	18.7	GRANE	18.7
RM3	WEST DELTA BLOCK 30	11.4	FUEL OIL #6	8 - 15	GRANE	18.7	GRANE	18.7
RM4	WEST DELTA BLOCK 30	11.4	FUEL OIL #6	8 - 15	GRANE	18.7	GRANE	18.7
RM5	WEST DELTA BLOCK 30	11.4	FUEL OIL #6	8 - 15	GRANE	18.7	GRANE	18.7
VG1	WEST DELTA BLOCK 30	11.4	FUEL OIL #6	8 - 15	GRANE	18.7	GRANE	18.7
VG2	NAPHTHA N+A, MAPCO	63.3	GASOLINE	50 – 70.6	SLEIPNER (IKU)	58.4	KEROSENE (JET A1)	45.4
VG3	CARPINTERIA	22.9	FUEL OIL #4	20 - 24	MANDALAY BATTELLE	20.3	FORSETI 2001	23.0
VG4	NAPHTHA N+A, MAPCO	63.3	GASOLINE	50 – 70.6	SLEIPNER (IKU)	58.4	KEROSENE (JET A1)	45.4
VG5	CARPINTERIA	22.9	FUEL OIL #4	20 - 24	MANDALAY BATTELLE	20.3	FORSETI 2001	23.0
MA1	EUGENE ISLAND BLOCK 276	35	DIESEL	27.5 – 41.1	Marine Diesel	36.4	Marine Diesel	36.4
MA2	EUGENE ISLAND BLOCK 276	35	DIESEL	27.5 – 41.1	Marine Diesel	36.4	Marine Diesel	36.4
AP1	ABU SAFAH, ARAMCO	28.4	MEDIUM CRUDE OIL	22.3 – 31.1	NORNE (1998-5)	32.7	Eldfisk2000	28.9
AP2	ABU SAFAH, ARAMCO	28.4	MEDIUM CRUDE OIL	22.3 – 31.1	NORNE (1998-5)	32.7	Eldfisk2000	28.9
AP3	ABU SAFAH, ARAMCO	28.4	MEDIUM CRUDE OIL	22.3 – 31.1	NORNE (1998-5)	32.7	Eldfisk2000	28.9
AP4	ABU SAFAH, ARAMCO	28.4	MEDIUM CRUDE OIL	22.3 – 31.1	NORNE (1998-5)	32.7	Eldfisk2000	28.9

5.5.3. Calculated values of environmental KPIs

Data collected in Tale 5.24 and assumptions above discussed allow the calculation of the three levels KPIs defined in Section 4.5 for each oil release. For the sake of this analysis, only the potential hazard index is estimated for each type of the proposed KPIs, thus disregarding the evaluation of inherent hazard index. It must be remarked that $EPI_{1.1}$ (indicated as KPI 1.1 in this case-study) is calculated through Equation (4.48), $EPI_{oil2.1}$ (i.e. KPI 2.1 in this case-study) is obtained by applying Equation (4.50) with ADIOS, GNOME and OWM, thus neglecting simulation with OSCAR. For $EPI_{oil2.2}$ (i.e. KPI 2.2 in this case-study), Equation (4.52) is used with ADIOS, GNOME and OWM, while Equation (4.54) is applied with OSCAR. KPIs of level 3 are evaluated by applying Equations (4.56) and (4.60) with ADIOS, and through Equations (4.58) and (4.62) with OSCAR. Table 5.26 summarizes the environmental KPIs results for each of the analysed releases of the case-study based on data in Table 5.24 and the outputs from the different tools.

Table 5.26. Case-study 4: KPIs calculated for the oil spills with the four simulation tools.

		ADIOS		GNOME		OWM		OSCAR	ADIOS		OSCAR	
Release	KPI 1.1 (ton)	KPI 2.1 (ton)	KPI 2.2 (ton·d)	KPI 2.1 (ton)	KPI 2.2 (ton·d)	KPI 2.1 (ton)	KPI 2.2 (ton·d)	KPI 2.2 (ton·d)	KPI 3.1 (km^2)	KPI 2.2 (km^2·d)	KPI 2.1 (km^2)	KPI 2.2 (km^2·d)
RM1	$1.2 \cdot 10^{-1}$	-	-	$8.3 \cdot 10^{-2}$	$2.8 \cdot 10^{-1}$	$1.0 \cdot 10^{-1}$	$5.2 \cdot 10^{-1}$	$4.1 \cdot 10^{-3}$	-	-	$4.4 \cdot 10^{-3}$	$1.9 \cdot 10^{-4}$
RM2	1.1	$9.6 \cdot 10^{-1}$	$4.2 \cdot 10^{-2}$	$7.4 \cdot 10^{-1}$	2.5	$9.1 \cdot 10^{-1}$	4.7	$6.0 \cdot 10^{-2}$	$1.1 \cdot 10^{-2}$	$2.2 \cdot 10^{-4}$	$3.4 \cdot 10^{-2}$	$1.8 \cdot 10^{-3}$
RM3	1.7	1.5	$4.8 \cdot 10^{-1}$	1.2	4.1	1.5	7.5	$3.4 \cdot 10^{-1}$	$1.7 \cdot 10^{-2}$	$5.4 \cdot 10^{-3}$	$2.4 \cdot 10^{-2}$	$6.0 \cdot 10^{-3}$
RM4	3.4	2.7	$9.7 \cdot 10^{-1}$	2.4	8.1	2.9	$1.5 \cdot 10$	$8.5 \cdot 10^{-1}$	$3.4 \cdot 10^{-2}$	$9.6 \cdot 10^{-3}$	$4.4 \cdot 10^{-2}$	$1.5 \cdot 10^{-2}$
RM5	$1.3 \cdot 10^{4}$	$1.1 \cdot 10^{4}$	$4.2 \cdot 10^{3}$	$9.1 \cdot 10^{3}$	$3.1 \cdot 10^{4}$	$1.1 \cdot 10^{4}$	$5.7 \cdot 10^{4}$	$4.8 \cdot 10^{4}$	$1.3 \cdot 10^{2}$	1.1	$1.0 \cdot 10$	$3.7 \cdot 10$
VG1	$1.2 \cdot 10^{-1}$	-	-	$8.5 \cdot 10^{-2}$	$2.9 \cdot 10^{-1}$	$1.0 \cdot 10^{-1}$	$5.3 \cdot 10^{-1}$	$3.7 \cdot 10^{-4}$	-	-	$9.1 \cdot 10^{-5}$	$3.8 \cdot 10^{-6}$
VG2	$4.4 \cdot 10^{-1}$	-	-	$1.0 \cdot 10^{-2}$	$2.8 \cdot 10^{-1}$	$2.5 \cdot 10^{-2}$	$1.7 \cdot 10^{-1}$	$7.0 \cdot 10^{-3}$	-	-	$6.2 \cdot 10^{-3}$	$4.1 \cdot 10^{-4}$
VG3	2.7	1.4	$5.1 \cdot 10^{-1}$	1.4	5.6	2.1	$1.1 \cdot 10$	$6.3 \cdot 10^{-1}$	$3.0 \cdot 10^{-2}$	$8.5 \cdot 10^{-3}$	$2.9 \cdot 10^{-4}$	$7.4 \cdot 10^{-3}$
VG4	$1.0 \cdot 10^{4}$	$1.7 \cdot 10^{3}$	$1.2 \cdot 10^{3}$	$6.1 \cdot 10$	$1.8 \cdot 10^{3}$	$6.4 \cdot 10^{2}$	$5.4 \cdot 10^{3}$	$1.4 \cdot 10^{4}$	5.9	$5.4 \cdot 10^{-1}$	1.5	4.7
VG5	$1.4 \cdot 10^{4}$	$1.0 \cdot 10^{4}$	$1.7 \cdot 10^{4}$	$6.8 \cdot 10^{3}$	$2.7 \cdot 10^{4}$	$1.0 \cdot 10^{4}$	$5.2 \cdot 10^{4}$	$4.4 \cdot 10^{4}$	$1.4 \cdot 10^{2}$	$8.2 \cdot 10$	$1.6 \cdot 10^{2}$	$2.3 \cdot 10^{2}$
MA1	$9.2 \cdot 10^{-1}$	$5.6 \cdot 10^{-1}$	$3.1 \cdot 10^{-2}$	$3.2 \cdot 10^{-1}$	1.6	$2.1 \cdot 10^{-1}$	1.6	$1.6 \cdot 10^{-2}$	$1.1 \cdot 10^{-2}$	$2.3 \cdot 10^{-4}$	$5.6 \cdot 10^{-3}$	$2.7 \cdot 10^{-4}$
MA2	1.0	$6.2 \cdot 10^{-1}$	$3.4 \cdot 10^{-2}$	$3.5 \cdot 10^{-1}$	1.8	$2.4 \cdot 10^{-1}$	1.8	$2.7 \cdot 10^{-2}$	$1.2 \cdot 10^{-2}$	$2.5 \cdot 10^{-4}$	$6.0 \cdot 10^{-3}$	$3.7 \cdot 10^{-4}$
AP1	$9.4 \cdot 10^{-1}$	$6.3 \cdot 10^{-1}$	$3.3 \cdot 10^{-2}$	$5.8 \cdot 10^{-1}$	2.1	$6.5 \cdot 10^{-1}$	3.5	$6.2 \cdot 10^{-3}$	$1.1 \cdot 10^{-2}$	$2.2 \cdot 10^{-4}$	$3.2 \cdot 10^{-3}$	$2.2 \cdot 10^{-4}$
AP2	2.1	1.2	$4.5 \cdot 10^{-1}$	1.3	4.7	1.5	7.8	$3.3 \cdot 10^{-1}$	$2.4 \cdot 10^{-2}$	$7.1 \cdot 10^{-3}$	$1.8 \cdot 10^{-2}$	$6.5 \cdot 10^{-3}$
AP3	6.1	3.5	1.3	3.7	$1.4 \cdot 10$	4.2	$2.2 \cdot 10$	1.3	$6.8 \cdot 10^{-2}$	$1.8 \cdot 10^{-2}$	$7.0 \cdot 10^{-2}$	$2.5 \cdot 10^{-2}$
AP4	8.0	4.7	1.7	5.0	$1.8 \cdot 10$	5.5	$3.0 \cdot 10$	1.9	$9.0 \cdot 10^{-2}$	$2.3 \cdot 10^{-2}$	$1.1 \cdot 10^{-1}$	$3.8 \cdot 10^{-2}$

5.5.4. Analysis of the ranking of the spills based on different KPIs

The KPIs summarized in Table 5.26 have different definitions and unit of measures, depend upon different damage parameters, different variability range. Thus, they cannot be immediately compared. In order to verify if the different KPIs give equal ranking of the oil spills, i.e. KPIs of level 2 and 3 calculated with different tools lead the same order of magnitude. of the releases than the simplest KPI 1.1, an internal normalization based on a linear scale transformation (max-min method) [672] is performed for each KPI calculated with a given tool. By this way, normalized values of KPIs are obtained ranging between 0 and 1. Quite obviously, for each type of KPI (calculated with a tool in case of KPIs of levels 2 and 3), a value of 0 corresponds to the minimum KPI in the set of releases evaluated, while a value of 1 corresponds to the maximum one. Clearly enough, such a normalization has no meaning for facilities characterized by only two oil spills, e.g. facility MA. Figure 5.24 illustrates the normalized KPIs for the releases of facilities RM, VG and AP.

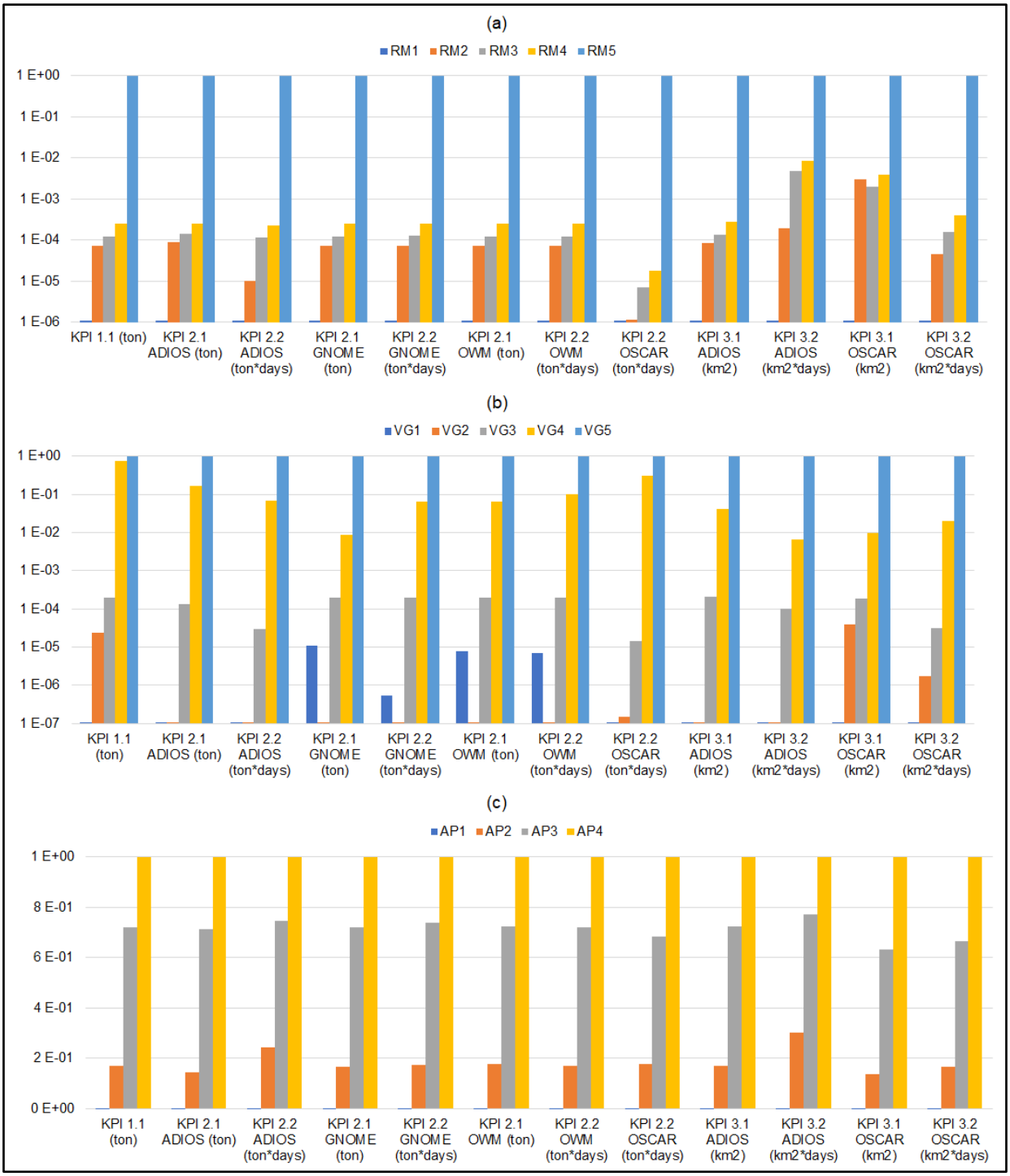

Figure 5.24. Case-study 4: Normalized values of the three levels environmental KPIs calculated for the oil spills of (a) facility RM, (b) facility VG, (c) facility AP.

From the results displayed in Figure 5.24, some conclusions can be drawn based on the mass of releases, type of oil (density), oil temperature.

On the one hand, when releases with different mass are considered, having the same oil and similar oil temperature, it appears that all the KPIs produce the same ranking of the environmental severity of the

spills, with an increased criticality corresponding to an increase in the mass of the spills, as in the case of the facility AP (Figure 5.24c). Therefore, for a preliminary ranking of the releases it is sufficient to refer to KPI 1.1, avoiding to calculate higher level KPIs and use a simulation tool.

On the other hand, when releases with different mass and oil temperature are evaluated, even in the case of the same type of oil (as in the case of the facility RM illustrated in Figure 5.24a), different KPIs can give different rankings of the releases. Similar conclusions emerge when the spills are characterized by different mass, temperature and oil type, as in the case of the facility VG (Figure 5.24b). Since OSCAR is the only code considering all the three temperature of concern (oil, air, sea surface), KPIs results obtained through this tool should be considered the most reliable when the temperatures are different, compared to the findings with the other tools.

In the case of the facility RM (Figure 5.24a), KPI 1.1 indicates an increased criticality of the spills, from RM1 to RM5. All the KPIs of levels 2 and 3 confirm this order, except for KPI 3.1 based on the slick surface, which gives a reverse ranking in case of RM2 and RM3 compared to the other metrics. This is mainly due to the higher temperature of RM3 with respect to RM2 even though the large spill mass associated to RM2, as shown in Table 5.24. A greater spill temperature ensures the evaporation of oil (i.e. its transition from the slick to the atmosphere), as well as determines a lower oil viscosity allowing the dispersion of oil into the sea (i.e. its transition from the slick to the water column). As a matter of facts, the higher mass of the spill, the more hazardous release, and the lower spill temperature, the less critical release. The contributions of spill mass and oil temperature can get along with each other with different and unpredictable effects: the mass contribution prevails in case of OSCAR KPI 3.2, while the temperature contribution is prevalent when OSCAR KPI 3.1 is considered. However, such a prevalence is limited since the values of OSCAR KPI 3.1 for the releases RM2 and RM3 are not only of the same order of magnitude, but also differ of a factor lower than two.

In the case of the facility VG in Figure 5.24b, KPI 1.1 shows the following ranking of the spills: VG1, VG2, VG3, VG4, VG5. It is worth noting that KPI 2.1 with GNOME, KPI 2.2 with GNOME, KPI 2.1 with OWM and KPI 2.2 with OWM invert the ranking of VG1 and VG2 compared to KPI 1.1 and the other KPIs. Clearly enough, VG1 has smaller spill mass, higher temperature and higher density (i.e. lower °API) than VG2, as illustrated in Table 5.24. It is worth noting that oil density is not the only important parameter affecting the oil fate; the oil viscosity is also influencing, and other physic-chemical parameters can play a role though at a smaller extent. Therefore, the presence of the suitable oil in the tool database is crucial for simulations, and when the desired oil is missing it is essential to select an oil with physico-chemical properties as much similar as possible. GNOME with only four oils available in its database is thus the worst tool for an appropriate choice of the oil. As a matter of facts, the higher mass of the spill, the more hazardous release, and the lower spill temperature, the less critical release, and the severity of

the spill should increase by increasing the oil density. The contributions of spill mass, oil temperature and oil type can get along with each other with different and unpredictable effects. GNOME and OWM codes neglecting the release temperature consider VG1 and VG2 at the same temperature, thus the oil type contribution prevails on the mass contribution and VG2 is more hazardous than VG1 based on GNOME KPI 2.1 and GNOME KPI 2.2., OWM 2.1 and OWM 2.2.

The considerations described above highlight that when spills with different mass and different oil and/or temperatures are evaluated, the sole released mass (KPI 1.1) does not represent a reliable indicator of the severity of the environmental consequences of the spills. Given these conclusions, it is certainly that GNOME is not the optimal tool because of its drawbacks about the availability of oils in the database and impossibility to account for the release temperature. If the releases show different mass and oil density even though similar temperature, ADIOS and OWM can be adopted, provided that only mass higher than 320 kg are simulated with ADIOS. On the other hand, OSCAR should be considered the most suitable tool when the spills have different properties in mass, density and temperature.

5.5.5. Equivalence of the different KPIs

In addition to the verification of the ranking, a further investigation is performed to establish if the different KPIs could be considered equivalent in expressing the environmental severity of the spills. To answer this question, the non-normalized KPI values of spills characterized by similar mass are compared.

Thus, the releases listed in Table 5.24 are classified based on order of magnitude of the spill mass in three groups: releases of order of magnitude 10000 t (i.e. VG4, RM5, VG5 which show different oil type but similar temperature), releases of order of magnitude 1 t (i.e. MA1, MA2, AP1, AP2, RM2, RM3, RM4, VG3 which are different in oil type and temperature), and releases of order of magnitude 0.1 t (i.e. RM1, VG1 and VG2 which are different in oil type and temperature). AP3 and AP4 are excluded from this classification, being the unique with a spilled mass of about 7 t, same oil type and temperature; another group of releases with 7 t spill mass is thus considered composed of AP3 and AP4. The order of magnitude of the different releases is shown in the Table 5.24.

For each of the mentioned release classes, different KPIs are compared with the aim to verify if KPIs of levels 2 and 3 calculated with different tools show values of the same order of magnitude within each group, as in the case of KPI 1.1 values which correspond to the spill mass and thus are similar within each group. Figures 5.25, 5.26, 5.27 and 5.28 illustrate the results for the group of releases of order of magnitude 10000 t, 7 t, 1 t and 0.1 t, respectively. In each figure, the results are displayed based on the level of KPIs and related to each couple (KPI, tool).

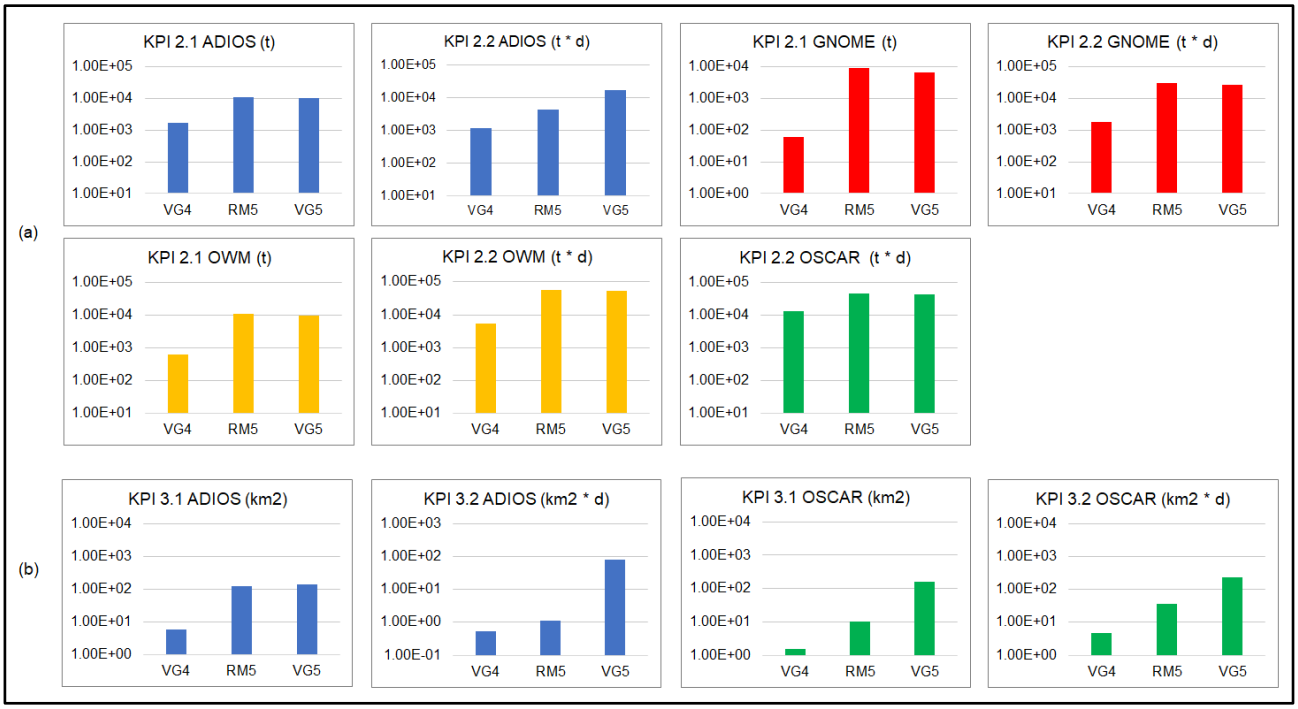

Figure 5.25. Case-study 4: KPIs results of (a) level 2 and (b) level 3, for releases of order of magnitude 10000 t.

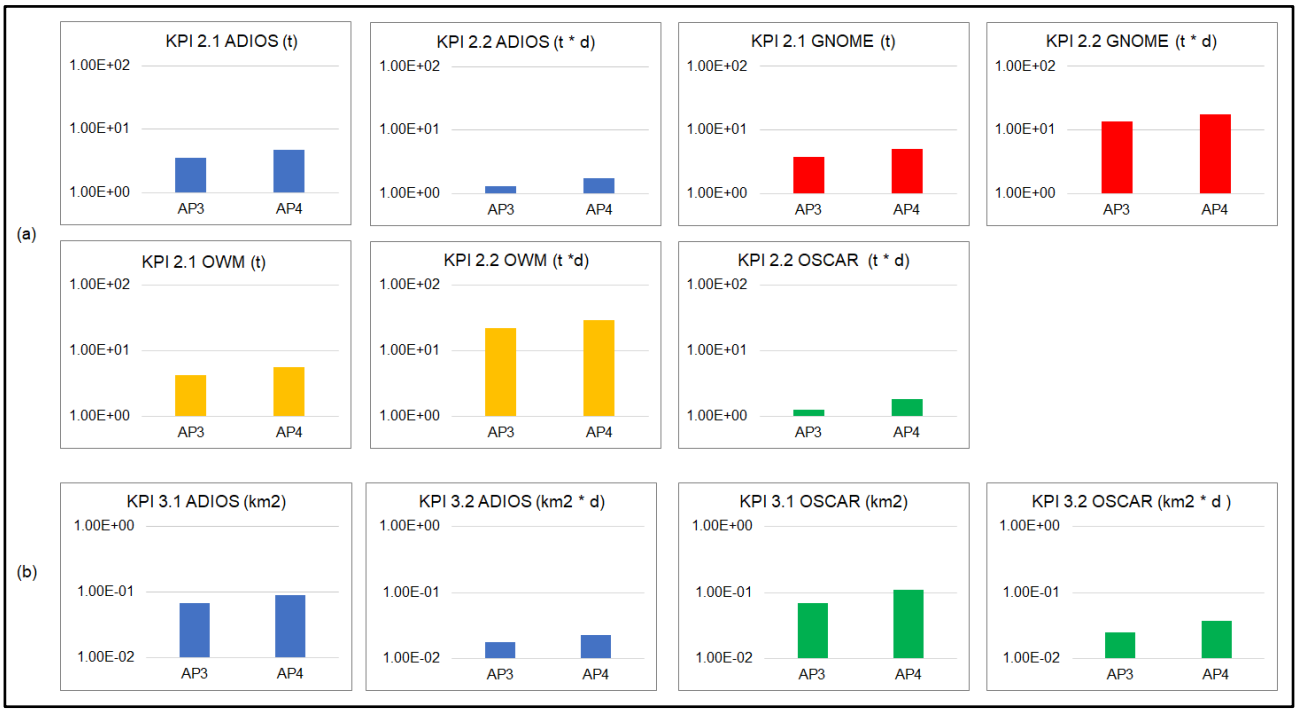

Figure 5.26. Case-study 4: KPIs results of (a) level 2 and (b) level 3, for releases of 7 t.

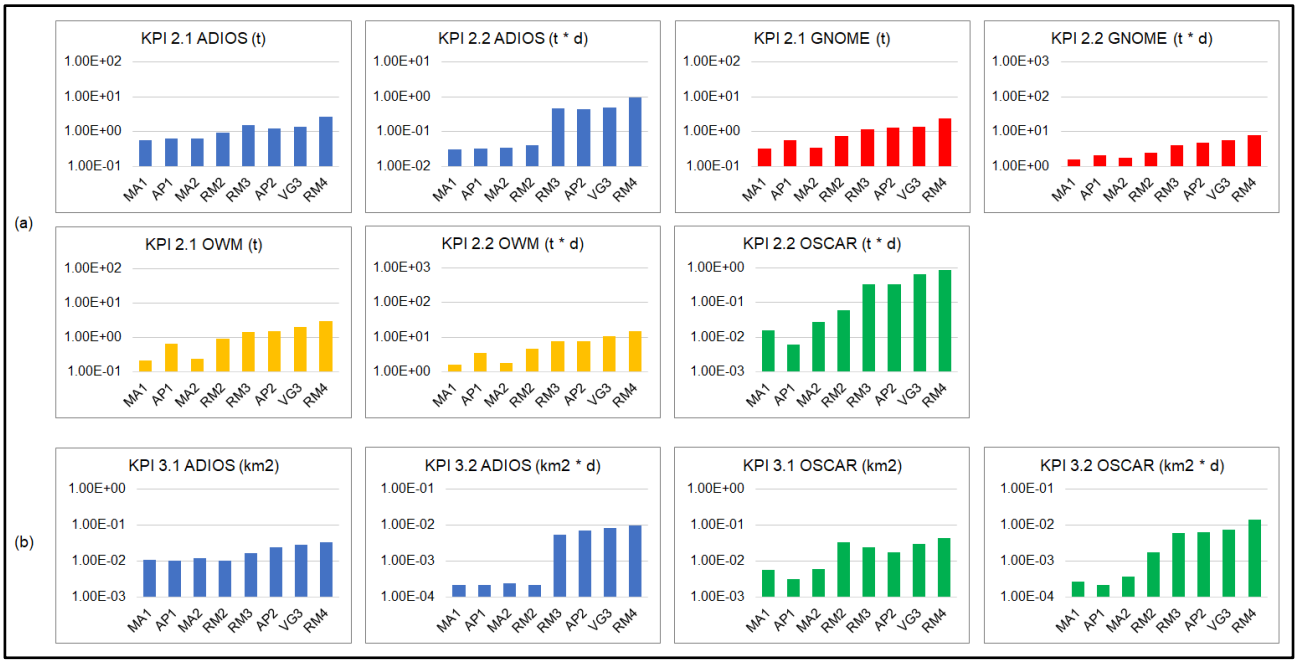

Figure 5.27. Case-study 4: KPIs results of (a) level 2 and (b) level 3, for releases having an order of magnitude 1 t.

Figure 5.28. Case-study 4: KPIs of (a) level 2 and (b) level 3, for releases having an order of magnitude 0.1 t.

Looking at the releases of about 7 t spill mass (Figure 5.26), given the same oil type and temperatures, all the KPIs indicate that AP4 is slightly more hazardous than AP3 due to higher mass of the release. It should be concluded that the proposed three level KPIs are equivalent in representing the environmental hazard

of the releases with equal oil and temperatures, and thus KPI 1.1 is sufficient to quantify the severity of the environmental consequences of the spills, as previously evidenced in the ranking analysis.

However, for the other groups of releases (order of magnitude 1000 t, 1 t, 0.1 t), it appears that the KPIs of levels 2 and 3 differ of at least an order of magnitude. From Figure 5.25, differences in the values of KPIs of level 2 can be null (e.g. KPI 2.1 with ADIOS and KPI 2.2 with OSCAR), moderate (e.g. ADIOS KPI 2.2, GNOME KPI 2.2, OWM KPI 2.1 and KPI 2.2), or substantial (e.g. GNOME KPI 2.1); whereas, KPIs of level 3 differs moderately in case of KPI 3.1 with ADIOS or hugely in case of ADIOS KPI 3.2, OSCAR KPI 3.1 and KPI 3.2. Similar findings emerge for the group of releases of order of magnitude 1 t (Figure 5.27): differences in the values of KPIs of level 2 can be null (e.g. KPI 2.1 with ADIOS, GNOME KPI 2.1 and KPI 2.2), moderate (e.g. ADIOS KPI 2.2, OWM KPI 2.1 and KPI 2.2), or substantial (e.g. OSCAR KPI 2.2); KPIs of level 3 show the same order of magnitude in case of ADIOS KPI 3.1, but differs rather well in case of KPI 3.2 with ADIOS and OSCAR KPI 3.1 or considerably in case of OSCAR KPI 3.2. Figure 5.28 shows that notable differences in the values of the KPIs of level 2 (e.g. GNOME KPI 2.1 and OSCAR KPI 2.2) and of level 3 (e.g. OSCAR KPI 3.1 and 3.2) are present also for releases of order of magnitude 0.1 t. Overall, the differences among the KPI values inside each group of spills are due to the different fate of the spilled oil, which depends not only on the mass, but also on the oil density and the spill temperature: low density and high temperature spills are less hazardous than high density and low temperature releases. KPIs of level 3 differ more than KPIs of level 2.

Therefore, it can be concluded that in case of different oil types and/or spill temperatures, the proposed KPIs are not equivalent in representing the environmental hazard of the releases and the sole released mass (KPI 1.1) cannot be used to indicate the severity of the environmental consequences of the spills. It is certainly true that higher level KPIs (i.e. KPI 3.1 and KPI 3.2) should be considered more suitable than the other KPIs in measuring the environmental hazard, since they are based on the slick surface, which is the actual damage factor for the sea surface compartment.

5.5.6. Analysis of interchangeability of the different tools

In addition to the ranking and equivalence analyses performed above, another investigation is performed to verify if the different tools are interchangeable in calculating the proposed KPIs. For this reason, the non-normalized KPIs of levels 2 and 3 calculated with different software tools are compared within each group of releases defined above. Figure 5.29 illustrates the KPIs grouped by the order of magnitude of the spill mass.

Figure 5.29. Case-study 4: KPIs of levels 2 and 3 for group of releases of order of magnitude (a) 10000 t, (b) 7 t, (c) 1 t, (d) 0.1 t.

From Figure 5.29a, when releases of 100000 t are compared, it appears that different tools produce KPIs values with similar order of magnitude in some cases (e.g. values of KPI 2.1 for RM5 and VG5, values of KPI 3.1 and KPI 3.2 for RM5) and different up to one order of magnitude in other cases (e.g. values of KPI 2.1 for VG4, values of KPI 2.2 for VG4 and RM5). ADIOS and OWM give similar results about KPI 2.1, but different from GNOME; values of KPI 2.2 with ADIOS and OWM differ up to one order of magnitude. In the cases of KPIs of level 3, ADIOS and OSCAR show similar KPIs for VG5, different for VG4 and highly different for RM5.

Looking at the releases of about 7 t (Figure 5.29b), different tools produce values of KPIs of the same order of magnitude in case of KPI 2.1, KPI 3.1 and KPI 3.2. For KPI 2.2, GNOME and OWM produce values of the same order of magnitude, but greater until one order of magnitude than those calculated with ADIOS and OSCAR.

Focussing on releases of 1 t in Figure 5.29c, in case of KPI 2.1, KPI 3.1 and KPI 3.2, different tools give results of the same order of magnitude, except for RM2 in case of KPI 3.2. For KPI 2.2, GNOME and OWM produce values of the same order of magnitude and similar among them, but greater until two orders of magnitude than those calculated with ADIOS and OSCAR which are similar among them.

For group of releases of 0.1 t illustrated in Figure 5.29d, GNOME and OWM give values of the same order of magnitude in case of KPI 2.1. For KPI 2.2, GNOME and OWM produce values of the same order of magnitude and similar among them, but until two orders of magnitude greater than those calculated with OSCAR.

Overall, it can be concluded that, in each group of releases, the different tools produce differences of at least an order of magnitude in the values of KPIs. As a consequence, for the sake of KPIs calculation, there is no doubt that the proposed tools are not interchangeable. Clearly enough, if available, OSCAR code should be considered more suitable compared to the other tools, due to the ability to provide a sophisticated and thus more realistic simulation of the oil slick fate.

5.5.7. Equivalence of third level of KPIs

Given the previous verifications, KPI 3.1 and KPI 3.2 should be considered more suitable than the other KPIs in measuring the environmental hazard and, if available, the OSCAR tool is the most accurate tool for their calculations. The results illustrated in Figure 5.29 are used to verify if the two mentioned KPIs are equivalent in quantifying the severity of the releases.

It should be noted that in each group of release, KPIs calculated with OSCAR differ of two orders of magnitude (e.g. in the cases of releases of 10000 t in Figure 5.29a and 0.1 t in Figure 5.29d). Moreover, KPI 3.1 and KPI 3.2 with OSCAR rank similarly the spills: in the group of releases of 10000 t the ranking

of increasing criticality is VG4, RM5, VG5 for both KPIs, in the group of releases of 0.1 t the ranking is VG2, VG1, RM1 for both KPIs; in the group of releases of order of magnitude 1 t some inversions appear in the ranking even though negligible. Therefore, these KPIs can be considered equivalent in expressing the environmental severity of the spills. In addition, it is worth mentioning that in the group of releases of 10000 t (Figure 5.29a), values of OSCAR KPI 3.1 and KPI 3.2 show the same differences when moving from VG4 to RM5 and from RM5 to VG5. Similarly, in the group of releases of 0.1 t (Figure 5.29d) values of OSCAR KPI 3.1 and KPI 3.2 indicate the same difference of one order of magnitude moving from VG2 to VG1 and one order of magnitude from VG1 to RM1. In the group of release of 1 t, both KPI 3.1 and KPI 3.2 exhibit differences of two orders of magnitude moving from RM4 to MA1: the spills RM2, RM3, AP2, VG3, RM4 give KPI 3.1 values one order of magnitude greater than the releases MA1, AP1, MA2; the release RM4 has KPI 3.2 one order of magnitude higher than RM2, and the release RM2 shows KPI 3.2 one order of magnitude higher than M1, AP1 and MA2. Therefore, KPI 3.1 and KPI 3.2 are not only equivalent but also show differences of the same order of magnitude with each group of spills.

In conclusion, KPI 3.1, i.e. the maximum area of the thick surface of the slick can be considered a good estimate of KPI 3.2, i.e. the thick slick surface exposure: KPI 3.1 can be used instead of the more complex KPI 3.2. However, KPI 3.2 remains the best choice for representing the environmental hazard of spills.

In case of unavailability of OSCAR, ADIOS may be the other tool to estimate the KPIs of level 3, provided the concerns discussed above about the use of tools different from OSCAR. In this case, KPI 3.1 and KPI 3.2 calculated with ADIOS are not equivalent. Looking at Figure 5.29a, ADIOS KPI 3.1 has about the same order of magnitude for RM5 and VG5, which are one order of magnitude higher than VG4; whereas, ADIOS KPI 3.2 differs of one order of magnitude moving from VG4 to RM5 and another one order of magnitude from RM5 to VG5. Therefore, as opposed to OSCAR, levels 3 KPIs with ADIOS cannot be considered equivalent in indicating the severity of the spills.

5.5.8. Conclusions

In this case-study, the novel set of environmental KPIs related to oil accidental spills developed within the inherent safety methodology in Section 4.5 is applied to different oil releases derived from four offshore oil platforms, in order to investigate the ability of such indicators to assess the hazard level associated to oil spills with the use of different tools for higher level KPIs.

The different level KPIs do not provide the same ranking of the environmental severity of the releases. The selection of the suitable KPIs to rank the oil spills makes no difference in case of releases with different mass, but equal oil type (i.e. oil density) and temperature.

Only when the releases have the same temperature and oil composition KPI 1.1 based on the spilled mass is a useful metrics for a rough ranking of the environmental severity of the spills, without requiring the need for simulation tools.

For releases with similar mass and different oil and/or temperature, some KPIs show values with the same order of magnitude, while others differ up to two orders of magnitude. Therefore, the different KPIs are not equivalent in expressing the environmental severity of the spills and the spilled quantity cannot be used to establish with greater detail the hazard of the spills

The oil fate consequence simulation tools adopted for calculation of KPIs of level 2 and 3 do not provide equivalent results, since different software produce differences up to two orders of magnitude in the values of the indicators for the same KPI.

KPIs of level 3 based on the slick surface should be preferred when compared to KPIs of level 2 based on the oil mass in the slick, due to the more sophisticated definition and thus more reliable evaluation of the environmental damage caused by oil spills. Being the most sophisticated tool to model the fate of the oil slick, OSCAR code is more suitable than the other software. Between OSCAR KPI 3.1 and OSCAR KI 3.2, the optimal choice is KPI 3.2 corresponding to the thick slick exposure and thus to the real environmental damage. However, given higher simplicity in the calculation, OSCAR KPI 3.1 based on the thick slick surface represents a good estimate of OSCAR KPI 3.2.

5.6. Case-study 5: Application of the process intensification screening methodology to alternative production processes for renewable CH_3OH

The PrI screening methodology described in Section 4.6 was applied to the investigation of eleven novel process routes for CH_3OH production, integrating the sustainability and safety performance analyses presented in the previous case-studies and in Chapter 4, to identify the safer and more sustainable production process, in the perspective of P2L applications. The better design options identified were selected for a further detailed assessment of their application to a P2L offshore hybrid energy systems at a remote oil & gas field in the Atlantic Ocean.

5.6.1. Overview of the alternative CH_3OH production processes

As firstly conceptualized by the Nobel Prize Laureate George A. Olah [208], among synthetic fuels, CH_3OH can be recognized as one of the most promising medium for storing, transporting and using energy because of its high volumetric energy density, easy handling and logistics, and multiple end-uses from the chemical industry to the transport sector [96]. The conventional method to produce CH_3OH industrially

is a well-known and simple process, comprising the production of synthesis gas, conversion of the synthesis gas into CH_3OH and distillation of the output from the reactor. Other than conventional route, potentially more efficient and green pathways for the CH_3OH production have been proposed according to the Olah's concept of the "Methanol Economy": these routes can be based on the direct partial oxidation of CH_4 valorising the exploitation of natural gas or can use CO_2 as input source in order to promote the "Carbon Capture and Utilization (CCU)" schemes [210]. Zakaria and Kamarudin [673] reported an overview of recent literature focussing on direct conversion of CH_4 to CH_3OH. Nine different production technologies can be distinguished for this type of process: three conventional catalytic processes (i.e. homogeneous radical gas-phase reactions, low temperature heterogenous catalysis, homogeneous catalysis in solution), membrane-based biocatalysis, plasma technology, photocatalysis, supercritical water technology, fuel cell technology and electrosynthesis. On the other hand, Ganesh [211] performed a comprehensive review on available methods for the conversion of CO_2 into CH_3OH. Two different routes can be identified: the thermo-chemical catalytic hydrogenation of CO_2 and the electrochemical reduction of CO_2 in water.

As required from step 0 of the procedure in Figure 4.13, reference process schemes of the eleven routes are defined based on given technology proposed in the technical literature. For each scheme, the details of the process, reactions, main components and material balance are reported in Appendix D of the present study. Information required as an input for the analysis of the process schemes is summarized in Table 5.27.

As shown in Table 5.27, the most mature process results in the catalytic hydrogenation of CO_2 which shows the highest TRL [217], given the operational CRI George Olah's pilot plant where about 4000 t/y (i.e. 500 kg/h) of renewable CH_3OH is produced by recycling flue CO_2 [114]. Whereas, other ten processes are only validated at a laboratory scale. Moreover, most of the processes operate in continuous mode, except for biocatalysis (batch mode), photocatalysis and electrosynthesis (semi-continuous mode). Some processes produce CH_3OH in liquid phase, others in gas phase. However, only catalytic hydrogenation of CO_2 gives relatively high yield, flowrate and purity of CH_3OH. In case of homogeneous catalysis in solution, no information is reported about CH_3OH production, since the process selected from the literature source produces a CH_3OH derivative compound, CF_3COOCH_3(MTFA), from which CH_3OH may be derived by adding further operations in the process.

Table 5.27. Case-study 5: Main input data of eleven routes for alternative CH_3OH production required for the PrI methodology.

Process scheme	Reference source	TRL (Horizon 2020)	Operating conditions	Operating mode	Molar conversion of CO_2 or CH_4	Molar yield of CH_3OH	CH_3OH flowrate (t/h)	CH_3OH phase	CH_3OH fraction in the outlet stream
CO_2 catalytic hydrogenation	[216]	6-7	235°C, 50 bar, Gas	Continuous	47.00%	98.90%	4.15	Liquid (25°C, 1 bar)	99.5%mol (99.7%wt)
CO_2 electroreduction	[674]	4	25°C, 1 bar, Gas-Liquid	Continuous	0.25%	0.25%	$3.66 \cdot 10^{-9}$	Liquid	0.00017%mol (0.00030%wt)
Homogeneous radical gas-phase reaction	[675]	4	451°C, 50 bar, Gas	Continuous	9.5%	72.20%	$1.62 \cdot 10^{-7}$	Gas	6.57%mol (11.51%wt)
Low temperature heterogeneous catalysis	[676]	4	50°C, 20 bar, Gas-Liquid	Continuous	0.50%	46.10%	$6.81 \cdot 10^{-8}$	Liquid	0.26%mol (0.46%wt)
Homogeneous catalysis in solution	[677]	4	85°C, 83 bar, Gas-Liquid	Continuous	0.18%	-	-	-	-
Membrane-based biocatalysis	[678]	4	28°C, 1 bar, Gas-Liquid	Batch (2 batches per day)	10.36%	10.36%	$8.50 \cdot 10^{-8}$	Liquid	0.09%mol (0.16%wt)
Plasma technology	[679]	4	25°C, 1 bar, Gas	Continuous	23.00%	8.28%	$3.36 \cdot 10^{-8}$	Gas	0.69%mol (0.58%wt)
Photocatalysis	[680]	4	55°C, 1 bar, Gas	Semi-continuous (4 batches per day)	0.348%	0.20%	$2.16 \cdot 10^{-10}$	Gas	0.00025%mol (0.00041%wt)
Supercritical water technology	[681]	4	410°C, 250 bar, Gas-Liquid	Continuous	4.50%	1.30%	$1.94 \cdot 10^{-7}$	Gas	0.009%mol (0.016%wt)
Fuel cell technology	[682]	4	100°C, 1 bar, Gas	Continuous	0.69%	0.61%	$1.22 \cdot 10^{-9}$	Gas	0.06%mol (0.05%wt)
Electrosynthesis	[683]	4	25°C, 1 bar, Gas-Liquid	Semi-continuous (4 batches per day)	62.19%	60.66%	$7.43 \cdot 10^{-9}$	Liquid	0.017%mol (0.030%wt)

Given the data summarized in Table 5.27, some features of CH_3OH final product from the most mature process (i.e. catalytic hydrogenation of CO_2) are assumed in this case-study as a common reference basis for the analysis of the eleven alternative process routes. Moreover, the actual scale of the largest plant for renewable CH_3OH based on this process (George Olah facility) is considered for the common production flowrate. Thus, relatively pure CH_3OH in the liquid state, with a mass flowrate of 500 kg/h (15.64 kmol/h), is fixed as benchmark in this case-study. The boundary limits described in Section 4.5 are assumed in this study. To perform a consistent assessment, common physical state and conditions of input materials to the different processes are considered based on the technical information about typical gas storage in the market: gaseous CH_4 at 25°C and 138 bar, gaseous O_2, N_2, He and Ar at 25°C and 156 bar, gaseous CO_2 at 25°C and 57 bar, air at 25°C and 8 bar. Liquid solutions are considered to be supplied at ambient conditions.

5.6.2. Intensified process flowsheets of the alternative schemes

According to step 1 of the procedure illustrated in Figure 4.13, an intensified process flowsheet is defined for each reference process scheme by applying the described PrI activities. In particular, for all the schemes, gas recycle and purge are applied to gaseous streams after the reaction and pre-heating of the inlet streams to the reactor to the reaction temperature is included by recovering, if possible, the energy from other material streams within the process. Separation of gas mixtures is applied through stages of cooling and adiabatic flash. Separation by means of distillation is considered for concentrations of CH_3OH in the liquid stream higher than 3%wt. Organophilic pervaporation of CH_3OH from aqueous solution is introduced for concentration of CH_3OH in the range 0.05%-20%wt until suitable composition for distillation is obtained. Below the concentration of 0.05%wt, no separation operation is assumed to be feasible, due to techno-economic limitations. Reactive distillation is considered in case of homogeneous catalysis in solution, to derive CH_3OH from CF_3COOCH_3(MTFA).

Aspen HYSYS v10 [684] is used as process simulator to facilitate the simulation of the intensified process flowsheets. For most of unit operations Aspen components are used: Aspen shell & tubes exchanger for heat transfer, Aspen pump, compressor and control valve for pressure change, Aspen two-phase separator and distillation column for separation, Aspen conversion reactor for CH_3OH synthesis reaction, Aspen continuous stirred tank reactor followed by distillation column for reactive distillation.

The main boundary conditions and assumptions made for simulation of these components are: pumps and compressors have adiabatic efficiency of 75%, maximum outlet temperature of fluid in compressor is 250 °C, minimum difference between the outlet temperatures of the fluids in shell & tubes exchanger is 15-30 °C, filling factor of separators is 50%, valve operating characteristics is linear with 50% opening, distillate rate is fixed in distillation column equal to the benchmark CH_3OH flowrate while reflux ratio

and number of stages are set based on conventional column design procedure [601], stoichiometric reactions and associated conversion of main reactant are set in conversion reactor, kinetic information about the reaction of CF_3COOCH_3(MTFA) into CH_3OH is fixed in continuous stirred tank reactor.

Moreover, Aspen recycle operator is used to recycle streams by setting the tolerance multipliers for vapour fraction, temperature, pressure, flow, enthalpy, and composition between 1 and 10 (forward transfer direction). Lastly, Aspen component splitter is adopted to simply model the membrane unit of the pervaporation plant by assuming experimental data provided in the literature for PERVAP 4060 membrane at 70°C [685]. The Peng Robinson package available in Aspen HYSIS is used for thermodynamic properties of the compounds involving in the processes, except for aqueous solutions for which UNIQUAC package for liquid is adopted.

5.6.3. Preliminary screenings results

The intensified process flowsheets simulated in Aspen HYSYS are reported for each process scheme in Appendix D, with associated details about the material streams, energy streams of the components and improved performance of the plant because of the applied PrI activities. As discussed in the methodology section, a preliminary screening of alternative process routes can be carried out as a result of step 1 of the method based on features of outlet streams after the synthesis section (including reactor and possible heat exchangers and/or flash drums). Table 5.28 summarizes the main findings.

Table 5.28. Case-study 5: Preliminary screening results of the alternative CH_3OH process routes from the definition of the process intensified flowsheets.

Process scheme	Mass fraction of CH_3OH in the post-synthesis liquid stream	Separation by means of pervaporation	Separation by means of distillation
CO_2 catalytic hydrogenation	60.65%	-	X
CO_2 electroreduction	0.00032%	-	-
Homogeneous radical gas-phase reaction	18.76%	-	X
Low temperature heterogeneous catalysis	0.46%	X	X
Homogeneous catalysis in solution	0.14%	-	X
Membrane-based biocatalysis	0.016%	X	X
Plasma technology	94.47%	-	X
Photocatalysis	0.00058%	-	-
Supercritical water technology	0.02%	-	-
Fuel cell technology	10.08%	-	X
Electrosynthesis	0.05%	X	X

As shown in Table 5.28, mass fractions of CH_3OH in the liquid stream after the synthesis section is lower than the lower limit of 0.05%wt imposed for further separation in case of CO_2 electroreduction,

photocatalysis, and supercritical water technology. These three process schemes are thus excluded from the following equipment scale-up and design analyses. For low temperature heterogeneous catalysis, biocatalysis and electrosynthesis, two or more stages of pervaporation are first applied to provide a suitable CH_3OH concentration in the stream and thus allow further separation of the mixture by means of distillation. For the remaining process schemes, distillation without any pervaporation stage appears suitable. It is worth noting that, in case of homogeneous catalysis in solution, pervaporation cannot be applied due to the significant amount of trifluoroacetic acid (TFA) in addition to H_2O and CH_3OH in the post-synthesis stream.

To perform the further screening of the eight intensified process schemes, step 2 of the procedure in Figure 4.13 is applied. First, the number of units required for pervaporation and distillation operations is estimated. Then, the number of reactors needed in the synthesis section is determined. Finally, the number of heat transfer equipment in the scheme is evaluated.

An industrial pervaporation stack in general has an effective superficial area of 18 m^2, section area of 540 x 540 mm^2 and length of 1600 mm. The pervaporation unit can include up to 50 stacks for a total superficial area of 900 m^2, 15000 mm length, 2900 mm height, 2500 mm width [686]. Therefore, given the technical data of the experimental pervaporation membrane considered in this case-study (i.e. 28 cm^2 for feed flowrate of 182 L/h [685]) and the feed flowrate of each pervaporation unit simulated in the intensified process flowsheet (Appendix D), the required total number of industrial units and related footprint can be estimated. The results for low temperature heterogenous catalysis, biocatalysis and electrosynthesis are reported in Table 5.29. Quite obviously, excessive area is needed for pervaporation plants, thus indicating the unfeasibility of these schemes for the following step of the procedure.

Concerning the distillation, the approach proposed in standard handbooks for chemical engineering design [601,610] is applied to determine diameter and height of columns, provided the limits on these parameters indicated in the literature for calculation of capital cost of commercial vertical sieve trays columns (e.g. 0.6- 4.5 m diameter, 8-50 m height) [361]. Number of distillation columns obtained for the process schemes is illustrated in Table 5.29. As appears evident, homogeneous catalysis in solution is the only scheme requiring significant columns, thus demonstrating its unsuitability for proceeding the analysis.

For the remaining four intensified process schemes (catalytic hydrogenation of CO_2, homogeneous radical gas-phase reaction, plasma technology, fuel cell technology), number of required reactors is estimated by applying the scale-up approaches proposed in Section 4.6 for different types of reactors. The results are summarized in Table 5.29. As shown in this table, a relatively high amount of dielectric barrier discharge reactors are needed in case of plasma technology, corresponding to a total 2100 MW of high voltage power supply (300 W single generator [687]). Considering that a conventional plant for large-scale

CH_3OH production (5000 t/d) from natural gas requires about 463 MW, it is clear that the intensified process scheme based on plasma technology is unfeasible and thus excluded from the following assessment.

With respect to the heat transfer unit such as heater, coolers, vaporizers and condensers, a preliminary estimation of the heat transfer area is first made based on heat duties derived from simulations in Aspen HYSYS, on tabulated design overall heat transfer coefficient appropriate to the fluids and equipment, and on logarithmic mean temperature differences (and driving force correction factor, where applicable) by applying standard design procedures [600,610]. Ranges of geometrical area provided in the literature for capital costs of commercial shell & tubes heat exchangers are considered to evaluate the number of equipment for each intensified process scheme. Table 5.29 reports the results from this investigation. It is notable that the process based on fuel cell technology requires a considerable number of heat transfer equipment items, which is reasonably inappropriate for a chemical process plant.

As a matter of facts, catalytic hydrogenation of CO_2 and homogeneous radical gas-phase reaction are the more feasible intensified process schemes, succeeding in the preliminary screening analyses.

Table 5.29. Case-study 5: Preliminary screening results of the alternative CH_3OH process routes from the scale-up and design of equipment.

Process scheme	Number of pervaporation units	Number of distillation columns	Number of reactors	Number of heat transfer equipment
CO_2 catalytic hydrogenation	-	1	1	4
Homogeneous radical gas-phase reaction	-	1	1	16
Low temperature heterogeneous catalysis	51537 (193 ha)	1	*n.c.*	*n.c.*
Homogeneous catalysis in solution	-	53	*n.c.*	*n.c.*
Membrane-based biocatalysis	105211 (395 ha)	1	*n.c.*	*n.c.*
Plasma technology	-	1	6641584 (2100 MW)	*n.c.*
Fuel cell technology	-	1	10 (0.21 ha)	64
Electrosynthesis	1685147841 (6319304 ha)	1	*n.c.*	*n.c.*

ha: hectare (1 ha=10000 m^2), *n.c.*: not considered.

5.6.4. Assumptions made for the assessment

The final intensified process flowsheets of catalytic hydrogenation of CO_2 (scheme A) and radical gas-reaction phase reaction (scheme B) are illustrated in Figure 5.30 and Figure 5.31, respectively, including the effective number of equipment derived from application of step 2. Details of material and energy streams illustrated in these figures are reported in Appendix D.

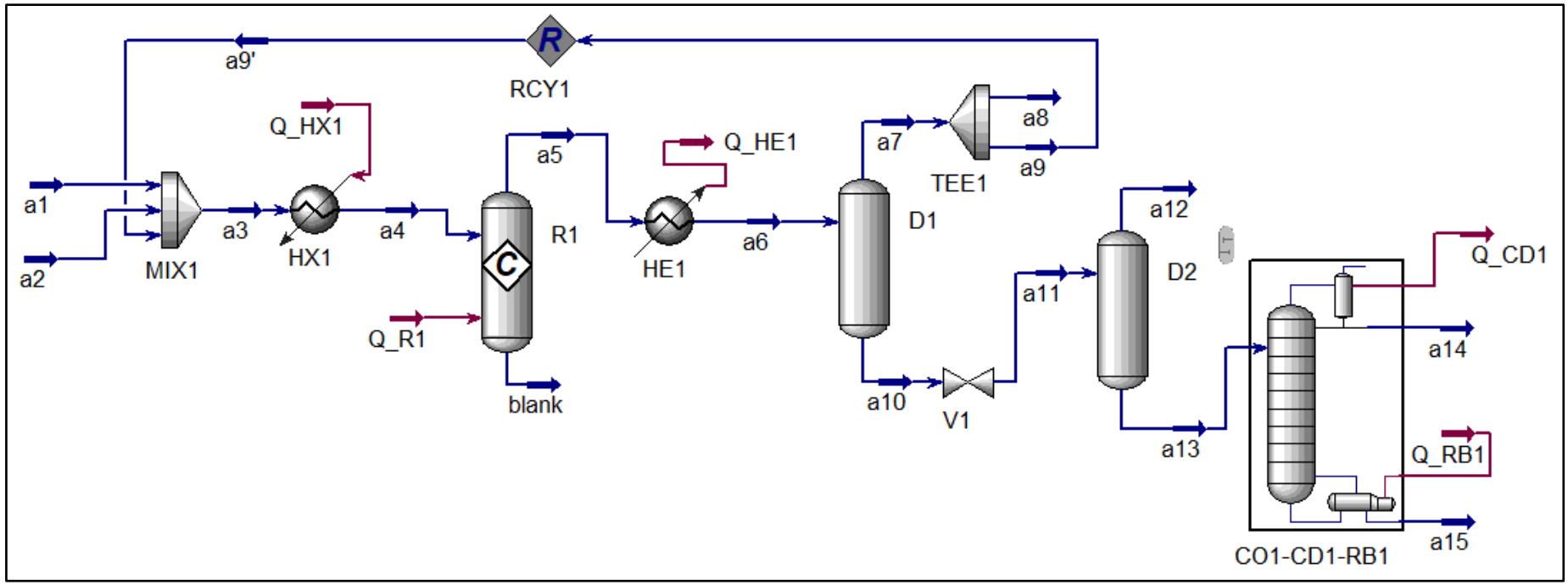

Figure 5.30. Case-study 5: Final intensified process flowsheet for catalytic hydrogenation of CO_2 (scheme A).

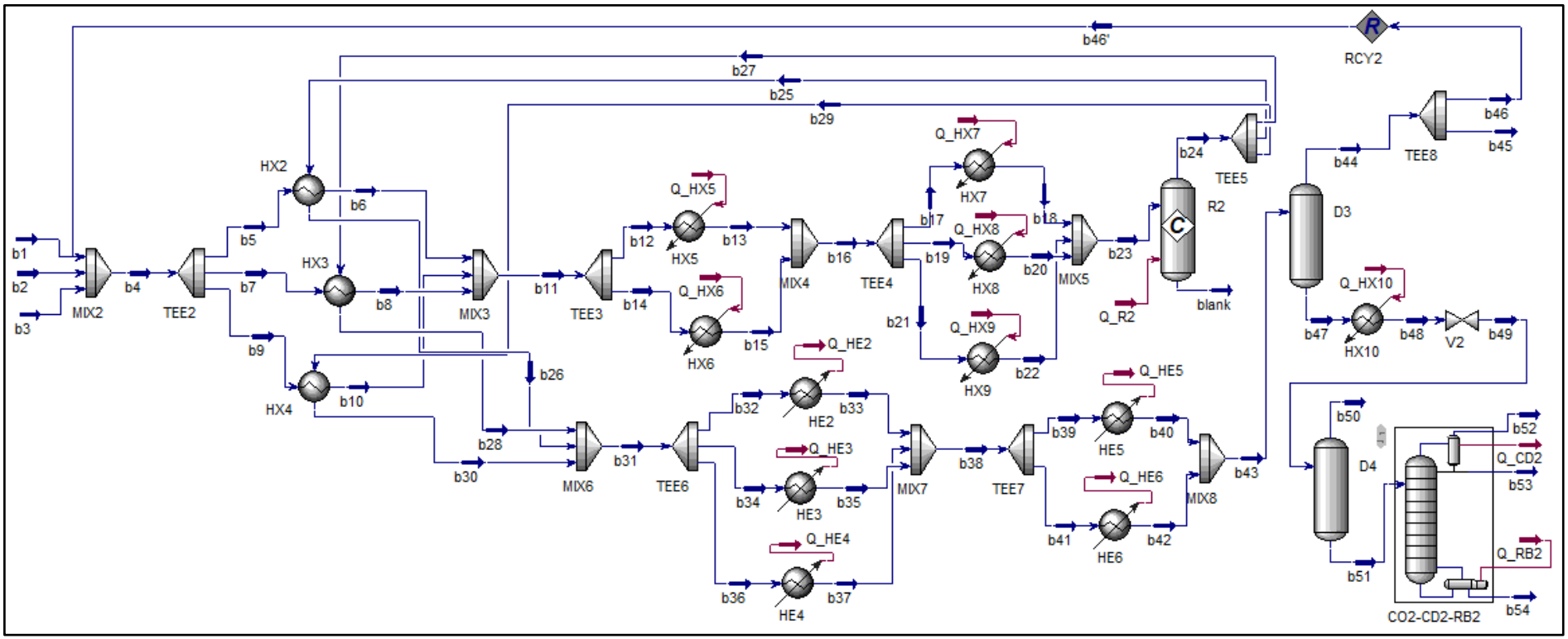

Figure 5.31. Case-study 5: Final intensified process flowsheet for homogeneous radical gas-phase reaction (scheme B).

To quantify the technical performance of the alternative process schemes, the energy efficiency indicator, η, defined din Equation (4.2) is calculated using LHV values summarized in Table 4.5. From the material and energy streams information obtained with Aspen HYSYS simulation reported in Appendix D, global input and output energies of the plant are evaluated for η calculation and summarized in Table 5.30.

Regarding the economic performance assessment, LCOP associated to the plant during a given economic lifetime is calculated by adapting Equation (4.9). In this case-study, CAPEX of single equipment are estimated in terms of equipment bare-module cost (C_{bm}) based on the Guthrie method and then added to site costs, building costs, offsite facilities costs, royalties and start-up costs in order to calculate to total capital investment cost (C_{tci}), as described by Seider et al. [361]. On the other hand, annual OPEX of the process plant in this case-study is estimated in terms of total production costs (C_{prod}), including feedstock, utilities, operations, maintenance, operating overhead, property and taxes, depreciation, sales, general expenses, as presented in Seider et al. [361]. Geometric and economic data estimated for the units of the final intensified process flowsheets of the two schemes are reported in Appendix D. This appendix contains also the details of the calculations, assumptions and values for the cost segments of C_{tci} and C_{prod} of the two schemes. The reference currency and year for the cost analysis are € referred to 2019; cost adjustments by means of Equation (4.1) are performed by considering conversion rates and CEPCI values [688]; the plant operating factor of 0.9 (i.e. 328.5 days over the year) is assumed. Final C_{tci} and C_{prod} values are summarized in Table 5.30 for the two schemes. For the sake of LCOP calculation, an economic lifetime of 25 years is considered as typically considered for a new onshore chemical process plant [361]; the discount rate r is taken constant over the economic lifetime period and equal to 8%, in agreement with previous studies [116,119,124,159].

For calculation of environmental indicator LGHG defined in Equation (4.11), GHG emissions associated to outlet gas streams from the plant are estimated by using the direct generation of GHG emissions within the process calculated in Aspen HYSYS based on EU 2007/589/EC carbon emission factor for natural gas fuel (56.1 kg CO_2e/GJ). Table 5.30 summarizes the data for the two designs.

Table 5.30. Case-study 5: Technical, economic and environmental data of schemes A and B.

Parameter	Scheme A	Scheme B
Input energy	a2 (LHV): 5376.0 kW Q_HX1: 317.6 kW	b1 (LHV): 13382.4 kW Q_HX7: 1785.2 kW, Q_HX8: 1785.2 kW, Q_HX9: 1785.2 kW, Q_HX10: 411.0 kW, Q_RB2: 1078.9 kW
Output energy	a14 (LHV): 2773.3 kW	a14 (LHV): 2775.6 kW
GHG emissions (IFPP 2007)	a8: 1.3 kg_{CO2eq}/h a12: 53.5 kg_{CO2eq}/h	b45: 708.7 kg_{CO2eq}/h, b50: 611.0 kg_{CO2eq}/h, b52: 0.5 kg_{CO2eq}/h
Total capital investment cost C_{tci}	$4.45 \cdot 10^7$ €	$2.25 \cdot 10^9$ €
Total annual production cost C_{prod}	$7.49 \cdot 10^7$ €/y	$1.39 \cdot 10^{10}$ €/y

Material and energy streams labels refer to names of components and states in Figure 5.30 for scheme A and Figure 5.31 for scheme B.

The unit inherent KPI addressing human target of the potential hazard, HHI, defined in Equation (4.43) is calculated for each relevant component (i.e. containing dangerous substances) of the process scheme adopting the methodology described in Section 4.5. Input data are the material streams from Aspen HYSYS and the equipment data from the preliminary design performed in step 2 of the PrI screening methodology, which are both detailed in Appendix D. General atmospheric conditions for an onshore industrial site are assumed for consequence simulation analysis: 2 m/s wind speed and Pasquill class F (conservative parameters), 25°C ambient temperature, 70% relative humidity, 0.17 surface roughness, -9.85°C surface temperature. For estimation of damage distance for human target, consequences analysis models reported in the TNO's Yellow Book [582] and in other relevant publications [583], both implemented in PHAST tool [667], are used. Threshold values of accident scenarios reported in Table 4.17, are adopted. Damage distance for flash fire and toxic cloud are evaluated at 1 m height above the ground. Moreover, due to lack of information about the layout of the plant, charge strength of 5 and obstructed volume of 2500 m^3 are assumed for TNO Multi-Energy model.

Because of unavailability of equipment P&IDs, the ranges of credit factors proposed in Table 4.22 are conservatively adopted in this case-study, bearing in mind that the goal of this analysis is a screening of the alternatives. For most of units, average values in the credit factors range is selected, except for distillation column for which the upper limit in the range reported for atmospheric vessel is chosen due to more items in the parts count than flash drum. In case of heat exchangers using ammonia as refrigerant fluid (i.e. HE2-HE3-HE4 in scheme B), credit factors are conservatively approximated to the highest values among those assigned to process heat exchanger and ammonia (reciprocating) compressor in the refrigeration cycle. Safety scores of releases from chemical reactors from the technical literature [572] are instead used for R1 and R2 in the two designs. Table 5.31 summarizes credit factors, even trees, damage distances of the final accident scenarios and HHI values for each unit of the two designs.

Table 5.31. Case-study 5: Credit factors, event trees, damage distances and HHI for each unit of the schemes A and B.

Equipment unit (scheme)	EQ code	Key Substance/mixture	Release mode	Credit factor (1/y)	Event tree	Final accident scenario	Damage distance (m)	HHI (m^2/y)
HX1 (scheme A)	EQ2.1	H_2+CO_2 (gas)	R1	$9.8 \cdot 10^{-3}$	d)	VCE	13.0	5.71
			R2	$1.4 \cdot 10^{-3}$	d)	VCE	9.3	
			R3a/R3b	$5.6 \cdot 10^{-4}$	f)+d)	VCE	9.3	
R1 (scheme A)	EQ8.1	H_2+CO_2 (gas), H_2+CH_3OH (gas)	R1	$1.0 \cdot 10^{-5}$	d)	VCE	23.9	$5.02 \cdot 10^{-2}$
			R2	$5.0 \cdot 10^{-6}$	d)	VCE	23.9	
			R3a/R3b	$1.3 \cdot 10^{-5}$	f)+d)	VCE	23.9	
HE1 (scheme A)	EQ2.1	H_2+CH_3OH (gas)	R1	$9.8 \cdot 10^{-3}$	d)	VCE	23.9	$2.11 \cdot 10$
			R2	$1.4 \cdot 10^{-3}$	d)	VCE	23.9	
			R3a/R3b	$5.6 \cdot 10^{-4}$	f)+d)	VCE	23.9	
D1 (scheme A)	EQ1.2	H_2+CO_2 (gas), CH_3OH (liquid)	R1	$9.6 \cdot 10^{-3}$	a)/d)	VCE	14.4	$1.12 \cdot 10$
			R2	$2.2 \cdot 10^{-3}$	a)/d)	VCE	14.4	
			R3a/R3b	$3.7 \cdot 10^{-4}$	c)/f)+a)/d)	Toxic cloud	54.8	
D2 (scheme A)	EQ1.1	CH_3OH (gas), CH_3OH (liquid)	R1	$5.8 \cdot 10^{-3}$	a)/d)	Pool fire	6.1	1.03
			R2	$1.6 \cdot 10^{-3}$	a)/d)	Jet fire	8.1	
			R3a/R3b	$6.5 \cdot 10^{-5}$	b)/e)+a)/d)	Toxic cloud	9.8	
CO1-CD1 (scheme A)	EQ1.1	CH_3OH (gas), CH_3OH (liquid)	R1	$1.1 \cdot 10^{-2}$	a)/d)	Pool fire	10.9	5.86
			R2	$3.7 \cdot 10^{-3}$	a)/d)	Pool fire	10.9	
			R3a/R3b	$2.4 \cdot 10^{-4}$	b)/e)+a)/d)	VCE	15.6	
HX2-HX3-HX4 (scheme B)	EQ2.1	CO+CH_4 (gas)	R1	$9.8 \cdot 10^{-3}$	d)	Toxic cloud	74.9	$4.05 \cdot 10^{2}$
			R2	$1.4 \cdot 10^{-3}$	d)	Toxic cloud	194.6	
			R3a/R3b	$5.6 \cdot 10^{-4}$	f)+d)	Toxic cloud	190.0	
HX5-HX6 (scheme B)	EQ2.1	CO+CH_4 (gas)	R1	$9.8 \cdot 10^{-3}$	d)	Toxic cloud	66.1	$3.02 \cdot 10^{2}$
			R2	$1.4 \cdot 10^{-3}$	d)	Toxic cloud	161.4	
			R3a/R3b	$5.6 \cdot 10^{-4}$	f)+d)	Jet fire	168.6	
HX7-HX8-HX9 (scheme B)	EQ2.1	CO+CH_4 (gas)	R1	$9.8 \cdot 10^{-3}$	d)	Toxic cloud	42.4	$1.29 \cdot 10^{2}$
			R2	$1.4 \cdot 10^{-3}$	d)	Toxic cloud	93.5	
			R3a/R3b	$5.6 \cdot 10^{-4}$	f)+d)	Jet fire	141.3	
R2 (scheme B)	EQ8.1	CO+CH_4 (gas)	R1	$1.0 \cdot 10^{-5}$	d)	Toxic cloud	42.4	2.32
			R2	$5.0 \cdot 10^{-6}$	d)	Toxic cloud	94.0	
			R3a/R3b	$1.3 \cdot 10^{-5}$	f)+d)	Jet fire	227.9	
HE2-HE3-HE4 (scheme B)	EQ2.1	CO+CH_4 (gas), Ammonia (gas)	R1	$9.8 \cdot 10^{-3}$	d)	Toxic cloud	69.0	$3.38 \cdot 10^{2}$
			R2	$1.4 \cdot 10^{-3}$	d)	Toxic cloud	186.8	
			R3a/R3b	$5.6 \cdot 10^{-4}$	f)+d)	Jet fire	141.0	
HE5-HE6 (scheme B)	EQ2.1	CO+CH_4 (gas)	R1	$6.7 \cdot 10^{-2}$	d)	Toxic cloud	136.5	$1.85 \cdot 10^{4}$
			R2	$7.4 \cdot 10^{-3}$	d)	Toxic cloud	789.2	
			R3a/R3b	$2.1 \cdot 10^{-3}$	f)+d)	Jet fire	168.4	
D3 (scheme B)	EQ1.2	CO+CH_4 (gas), CH_3OH (liquid)	R1	$9.6 \cdot 10^{-3}$	a)/d)	Toxic cloud	127.5	$6.72 \cdot 10^{3}$
			R2	$2.2 \cdot 10^{-3}$	a)/d)	Toxic cloud	843.0	
			R3a/R3b	$3.7 \cdot 10^{-4}$	c)/f)+a)/d)	Toxic cloud	1070.7	
HX10 (scheme B)	EQ2.1	CH_3OH (liquid)	R1	$9.8 \cdot 10^{-3}$	a)	VCE	7.3	1.98
			R2	$1.4 \cdot 10^{-3}$	a)	VCE	7.3	
			R3a/R3b	$5.6 \cdot 10^{-4}$	b)+a)	VCE	7.3	
D4 (scheme B)	EQ1.1	CO_2 (gas), CH_3OH (liquid)	R1	$5.8 \cdot 10^{-3}$	a)/d)	Pool fire	5.6	$7.34 \cdot 10^{-1}$
			R2	$1.6 \cdot 10^{-3}$	a)/d)	Pool fire	5.6	
			R3a/R3b	$6.5 \cdot 10^{-5}$	b)/e)+a)/d)	Pool fire	5.6	
CO2-CD2 (scheme B)	EQ1.1	CH_3OH (gas), CH_3OH (liquid)	R1	$1.1 \cdot 10^{-2}$	a)/d)	Pool fire	12.3	7.69
			R2	$3.7 \cdot 10^{-3}$	a)/d)	Pool fire	12.3	
			R3a/R3b	$2.4 \cdot 10^{-4}$	b)/e)+a)/d)	Jet fire	26.1	

Labels refer to names of components in Figure 5.30 for scheme A and Figure 5.31 for scheme B. EQ codes refer to Table 4.19. Release modes refer to Table 4.20. Event tree codes refer to Table 4.21 and Appendix C.

In order to rank the overall PrI level of the process schemes, the process intensification screening indicator, PrIS, defined in Equation (4.71) or Equation (4.72) is calculated by applying the compensatory MCDA approach described in Section 4.6. Table 5.32 reports the target values used in this case-study for normalization of disaggregated indicators related to the performance of the actual reference process for large-scale CH_3OH production (i.e. steam reforming from natural gas). For each target value, brief description and assumption are included.

Table 5.32. Case-study 5: Target values assumed for the normalization of disaggregated indicators.

	Value	Description/Assumption	Literature source
η_{target}	52.3%	Ratio of total energy in CH_3OH based on LHV (1163 MW) to total energy in input (1760 MW) for the conventional large-scale plant (5000 t/d) without CO_2 capture source	[689]
$LCOP_{target}$	62.9 €$_{2019}$/MWh	LCOP in 25 y economic lifetime and 8% interest rate for the conventional large-scale plant (5000 t/d) without CO_2 capture source. The literature value of 275.1 \$$_{2014}$/t is converted into €$_{2019}$/MWh by means of Equation (4.1) using CEPCI values of 576.1 (for 2014) and 613.3 (for 2019) [690] and exchange rate from \$$_{2019}$ to €$_{2019}$ of 0.8935 [174].	[689]
$LGHG_{target}$	63.3 kg_{CO2eq}/MWh	GHG emissions for the conventional large-scale plant (5000 t/d) without CO_2 capture source. The literature value of 0.3533 t_{CO2eq}/t is converted into kg_{CO2eq}/MWh by using LHV of CH_3OH	[689]
HHI_{target}	6 m^2/y	Average risk to human life from major chemical industrial accidents	[273]

The evaluation of relative importance weights among indicators is performed by applying the approach described in Section 4.3 based on time-space-receptor criteria and individualist-egalitarian-hierarchist perspectives. Equal weighting is further added to the archetypes of decision makers. Before scoring and weighting, the indicators selected for the assessment of the case-study are classified in terms of time, space and receptor based on their definition. The same considerations introduced for η, LCOP ang LGHG in case-study 1 are applied to this case-study. HHI is an indicator quantifying the likelihood of severe accident scenarios for human target. It is short-term with respect to the time horizon. Moreover, it is local in terms of space perspective as it quantifies the inherent hazard within the area containing the chemical plant. This indicator is consistent with respect to association with humans as opposed to ecosystem.

For each archetype, given scores are assigned to indicators based on the three criteria. The overall score to each indicator is estimated as the sum of the scores given with respect to each criterion. The relative importance of the indicators is determined as the ratio of the associated overall score to the sum of overall scores. All the values of assigned scores and weights are reported in Table 5.33. These weights are used

to derive pair-wise comparison matrix, evaluation matrix and the trade-off weights among indicators. Figure 5.32 illustrates the comparison of trade-off weights based on the different perspectives mentioned above. It is verified that all the evaluations are consistent according to CR index in Equation (4.15).

Table 5.33. Case-study 5: Scores and weights assigned for aggregation of indicators based on different perspectives.

Schemes	Criteria	Indicators for PrI assessment			
		η	LCOP	LGHG	HHI
		Score 1-5	Score 1-5	Score 1-5	Score 1-5
Individualist	Time	2	3	3	5
	Space	3	4	3	5
	Receptor	2	4	5	5
	Sum	7	11	11	15
	Relative importance (weight)	0.159	0.250	0.250	0.341
Egalitarian	Time	5	3	5	1
	Space	5	3	5	1
	Receptor	4	1	5	1
	Sum	14	7	15	3
	Relative importance (weight)	0.359	0.179	0.385	0.077
Hierarchist	Time	3.5	3	4	3
	Space	4	3.5	4	3
	Receptor	3	2.5	5	3
	Sum	10.5	10	13	9
	Relative importance (weight)	0.253	0.217	0.313	0.217

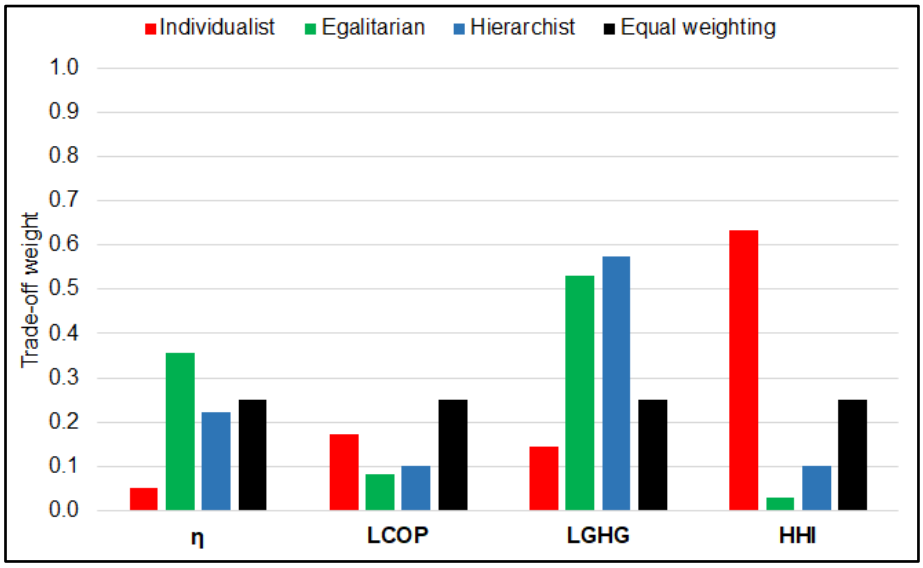

Figure 5.32. Case-study 5: Weights among the indicators based on different perspectives for the PrI assessment.

From Figure 5.32, it appears evident that there are variations between the different archetypes in prioritizing specific indicators over the others. The individualist archetype prioritizes HHI indicator with a trade-off weight of almost 63% and neglects the energy efficiency indicator (trade-off of 5%). On the

other hand, the egalitarian method gives the highest importance to LGHG (53%) followed by energy efficiency (36%) and the least priority to HHI (a merely 3% of weight). Similarly, the hierarchist method exhibits similar preference than egalitarian method with the highest trade-off to LGHG (58%). No archetype approximates the equal weighting scheme.

5.6.5. Process intensification screening results

Figure 5.33 displays the comparison of the technical, economic, environmental and inherent safety indicators between the two schemes based on the data summarized in Tables 5.30 and 5.31.

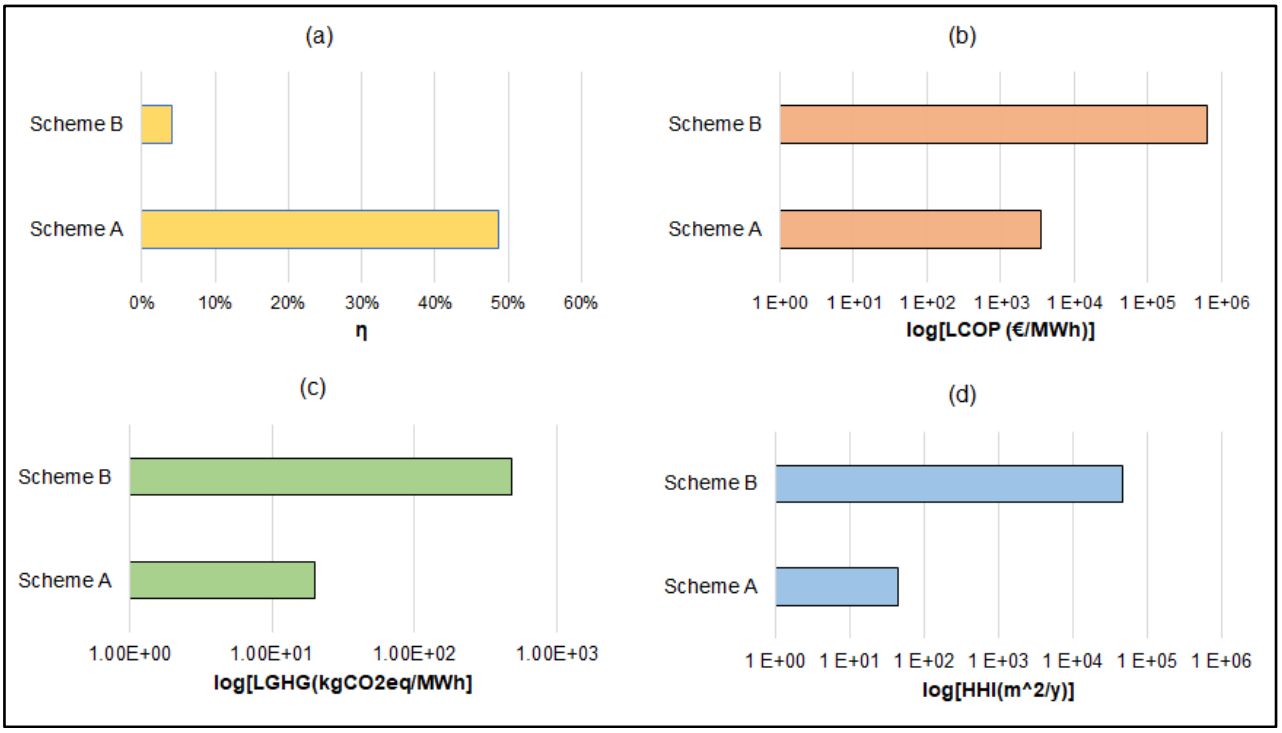

Figure 5.33. Case-study 5: Comparison of disaggregated (a) technical, (b) economic, (c) environmental and (d) inherent safety indicators between the two schemes.

As shown in Figure 5.33a, when the energy efficiency indicator is considered, scheme A is the most efficient, with values of η around 48%. Whereas, a mere 4% is obtained for scheme B due to significant input energy required to pre-heat the gas mixture for CH_3OH synthesis, as illustrated in Table 5.30.

Concerning the LCOP results (Figure 5.33b), scheme A gives the best economic performance showing a LCOP value which is around two orders of magnitude lower than that of the other scheme. The higher number of process equipment and larger entity of specific utilities required (e.g. refrigeration, molten salt) detailed in Tables D.14 and D.15 in Appendix D, are the main cause for considerable C_{tci} and C_{prod} costs in scheme B, thus penalizing the resulting LCOP indicator compared to scheme A.

From Figure 5.33c, the highest environmental performance, corresponding to the lowest LGHG value, is obtained for scheme A, thus confirming the ranking based on η and LCOP. The worst LGHG estimated for scheme B is attributed to larger environmental impact of the gas streams (purge and vapor phase of atmospheric flash drum) in outlet from the plant, as reported in Table 5.30.

When inherent KPIs addressing human target are compared (Figure 5.33d), a higher safety performance of scheme A (i.e. lower value of HHI) is evident with respect to scheme B. The most critical units in both the designs are identified as coolers and pressurized flash drums after the synthesis reactors, as shown in Table 5.31. Thus, severity of accident scenarios following the releases in such equipment contribute more to the inherent safety performance of the scheme rather than the credibility of the releases. Toxic clouds due to CO releases result in more severe consequences than VCE due to H_2 releases (Table 5.31), thus penalizing the performance of scheme B compared to scheme A.

The PrIS indicators calculated with different perspectives of decision makers and weighted mean methods are illustrated in Figure 5.34 for the two schemes.

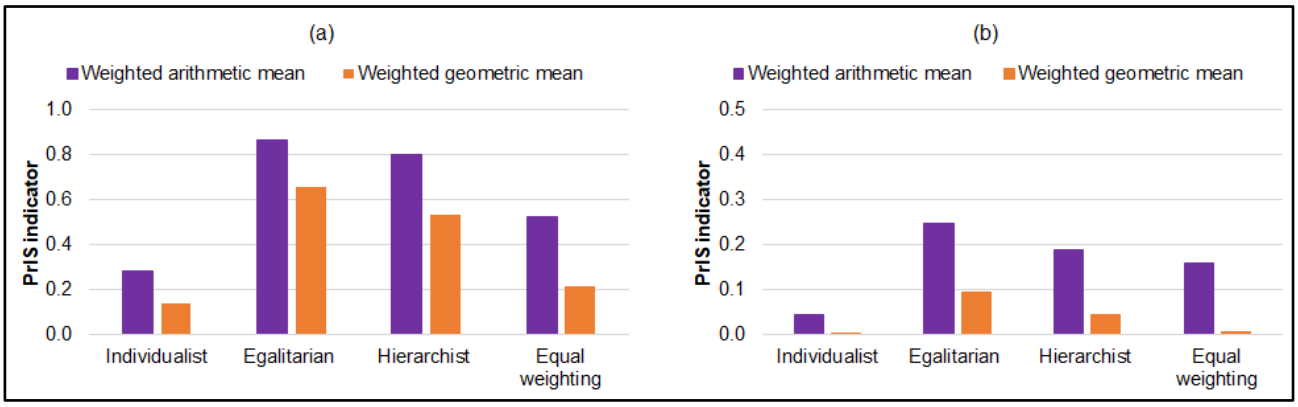

Figure 5.34. Case-study 5: PrIS indicator based on different perspectives and weighted mean method for (a) scheme A and (b) scheme B.

Looking at the results obtained for scheme A (Figure 5.34a), the egalitarian method gives the highest values of PrIS calculated with both arithmetic mean (0.867 and geometric mean (0.654) compared to the other archetypes. On the other hand, the individualist method shows the lowest values of the aggregated indicator, i.e. 0.28 in case of WAM method and 0.14 in case of WGM method.

Similar results are present when focussing on scheme B in Figure 5.34b: PrIS is favourable when the egalitarian perspective is adopted, while it is penalized by the individualist method. However, it should be noted that, being equal archetype and weighting method, relatively lower values of the PrIS and thus worse performance are obtained compared to scheme A, as a direct consequence of disaggregated indicators in Figure 5.33. Another finding from these graphs is that PrIS indicators calculated with the

arithmetic mean decrease more largely than values derived with geometric mean in case of scheme B than the other one. Therefore, WGM method tends to further penalize the least performant scheme.

5.6.6. Results of sensitivity analysis

Sensitivity analysis is applied to assess the robustness of the relative ranking of the two schemes based on the PrIS indicator. In this case-study, the analysis is performed by varying randomly the target values selected for normalization of disaggregated metrics according to the Monte Carlo method described in Section 4.6 and implemented in MATLAB software [641]. The adoption of the approach, based on time-space-receptor criteria and different archetypes of decision makers for weights elicitation in the integrated assessment is considered as an alternative way to reduce uncertainty associated to this stage, thus sensitivity analysis is not applied to verify the effect of stochastic variation in weights on the PrIS indicators.

All the target values are equally varied between $\pm$30% the baseline value reported in Table 5.32. The uniform distribution is conservatively adopted for all the indicators, thus avoiding any assumption about the distributions of the reference indicators. Due to the relatively simple problem in this case-study, 10^6 simulations were found to be sufficient to reach the convergence and independence from the number of simulations. The cumulative probability distributions of the differences of PrIS of scheme B with respect to scheme A based on different perspectives of decision makers and weighted mean methods are shown in Figure 5.35. From this figure, it clearly appears that scheme B always shows a lower performance with respect to scheme A with the assumed uncertainty ranges of the target values, independently from the perspective and aggregation method used, since the PrIS differences are always negative. This also confirms the high robustness of the ranking illustrated in Figure 5.34. Furthermore, it was verified that the increase in the variation range of target values up to $\pm$50% does not influence the results.

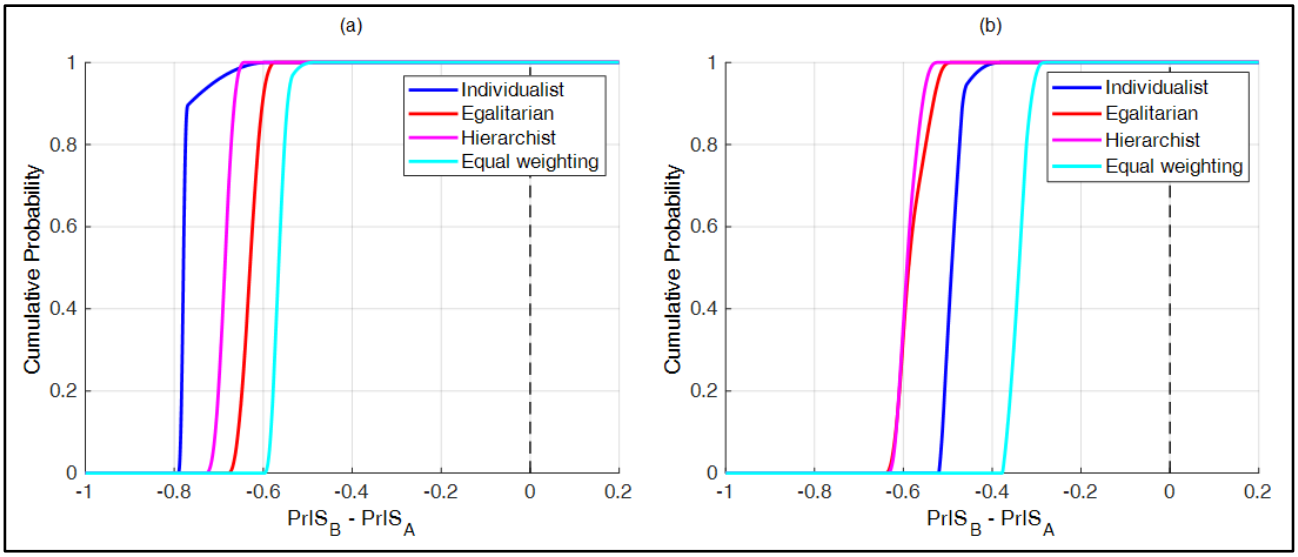

Figure 5.35. Case-study 5: Cumulative probability of the PrIS differences of scheme B with respect to scheme A using (a) WAM method and (b) WGM method for aggregation.

5.6.7. Results of detailed site-specific assessment

A detailed site-specific assessment is carried out to further analyse the performance of the P2L offshore hybrid energy options composed of the intensified process schemes A and B driven by offshore wind and solar thermal energies at a remote offshore oil & gas location. Both process schemes (A and B) are assumed to be installed at an offshore gas production platform located in the Thebaud gas field of the Offshore Energy Sable Project [691], which has started the first activity of the decommissioning phase since 2017. The field is approximately 225 km offshore Nova Scotia (Canada), in the Atlantic Ocean, in water depths ranging between 20 m and 80 m. The Thebaud facility consists of two main platforms connected by a walkway; a compression platform with associated equipment is installed on a standalone structure connected to the main platforms by a bridge. Hydrocarbons produced at the satellite platforms in the field are transported to the Thebaud facility and mixed with wellstreams extracted from the Thebaud wellheads. The resulting mixture is separated and dehydrated onsite using triethylene glycol (TEG) solvent. The produced H_2O is treated and discharged into sea, while gas and condensate are recombined and delivered to an onshore gas plant in Nova Scotia.

In this detailed assessment, scheme A makes use only of infrastructures of the offshore facility without any integration with its oil & gas operations. H_2 is produced by means of desalination and electrolysis of sea H_2O, while CO_2 is delivered from the onshore market via ship. The block diagrams of the P2L offshore hybrid energy options based on scheme A (option 1) are shown in Figure 5.36, where five sub-systems are indicated with different colors: H_2 production (in red color), CH_3OH synthesis (in green color), CH_3OH separation (in light-blue color), solar-thermal plant (in orange color), wind-diesel plant (in blue

color). The useful product is relatively pure liquid CH_3OH to be used as a fuel for onshore energy production, industrial and mobile applications. On the other hand, since CH_4 is required as a raw material in scheme B, a coupling of the process with the oil & gas operations occurring at the selected offshore facility is considered. Figure 5.37 shows the schematics of the P2L offshore hybrid energy option based on scheme B (option 2), where eleven sub-systems are represented with different colors: hydrocarbons separation (in magenta color), gas dehydration (in dark green color), gas treatment (in ochre color), O_2 production (in red color), CH_3OH synthesis (in green color), CH_3OH separation (in light-blue color), solar-thermal plant (in orange color), wind-diesel plant (in blue color), ammonia refrigeration cycles (in brown color), propane refrigeration cycle (in grey color). In addition to main product (liquid CH_3OH), oil and export gas to be delivered to onshore treatment plants, as well as H_2 to be employed as fuel at the offshore facility are secondary useful products. The description of the two integrated systems, including the details of process states, components and sub-systems is reported in Supplementary Material of [692].

In both options, offshore wind farm and solar parabolic solar collectors are considered to supply electrical and heat power, respectively, meeting the energy demand of the process schemes for CH_3OH production. Even though these resources have several advantages, wind or solar generators in a stand-alone system cannot supply continuously the load due to their fluctuating nature. Therefore, diesel generators are integrated with the wind farm, while solar thermal energy storage are combined with the parabolic trough technology, as shown in Figures 5.36 and 5.37.

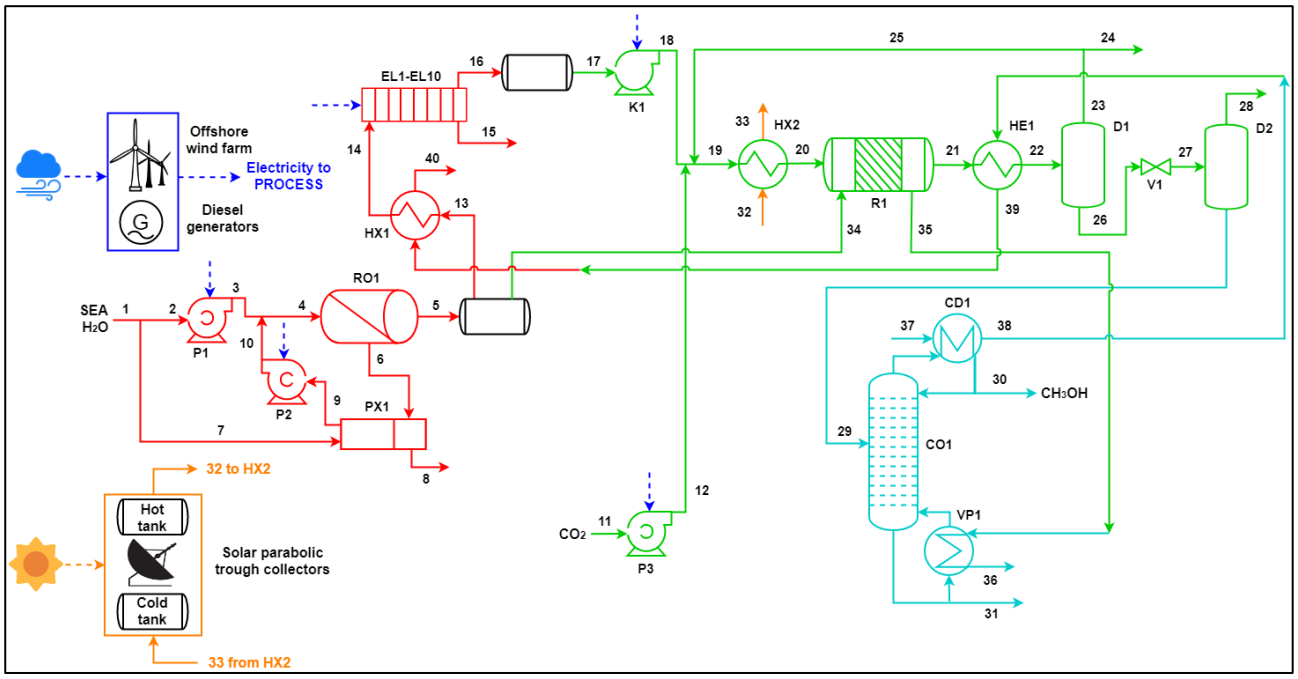

Figure 5.36. Case-study 5: Block diagram of P2L offshore hybrid energy option based the intensified process scheme A for CH_3OH production (option 1) [692].

The renewable power plants integrated with schemes A and B are designed adopting two commercial tools based on environmental conditions at the given offshore location and energy needs of the process. The Hybrid Optimization Model for Multiple Energy Resources (Homer) Pro version 3.12.3 (Academic) [693] by HOMER Energy is used as design and simulation tool for hybrid system composed of offshore wind farm, diesel generators, converter linked to a given electrical load. The wind resource input for Homer are monthly average wind speed data at the selected offshore site retrieved from the NASA Surface meteorology and Solar Energy database. Obtained the total electrical consumptions required in input to each process scheme from simulation with Aspen HYSYS, this amount is set as capacity of the primary load in the hybrid renewable system. The design of solar-thermal plant is performed by means of the open source System Advisor Model (SAM) version 2017.9.5 [694] developed by National Renewable Energy Laboratory. A modified version of the physical trough model described in Wagner et al. [695] is used to simulate the solar parabolic trough system for thermal applications. The solar resource data at the considered offshore field retrieved from the NREL National Solar Radiation Database (NSRDB) are given in input to SAM, including a design value of direct normal irradiance (DNI). Obtained from Aspen HYSYS the heat rates required in HX2 of option 1 (Figure 5.36), HX9, HX10-HX11 and VP4 of option 2 (Figure 5.37), their values are considered as design heat sink power in SAM modelling. The key parameter and assumptions applied to the design of the wind-diesel plant in Homer tool and solar-thermal plant in SAM software are summarized in Supplementary Material of [692].

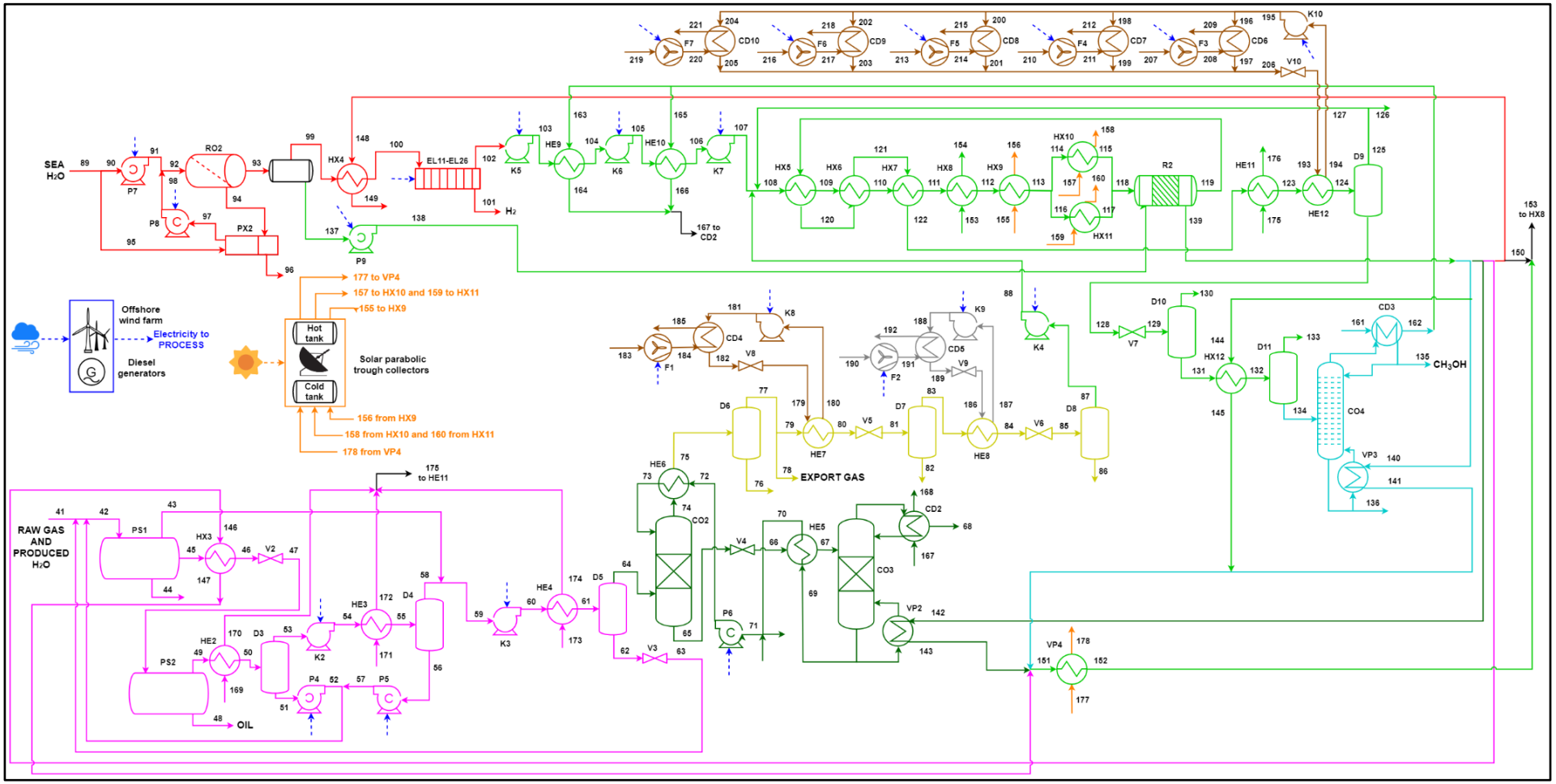

Figure 5.37. Case-study 5: Block diagram of P2L offshore hybrid energy option based the intensified process scheme B for CH_3OH production (option 2) [692]

Exergy analysis based on second law of thermodynamics is performed in this case-study to assess and compare exergy efficiencies (ψ) and exergy destruction rates due to irreversibility ($\dot{E}x_d$) of the integrated systems and associated sub-systems. Details and assumptions of the thermodynamic assessment, as well as equations used for calculation of ψ and $\dot{E}x_d$ of single units, sub-systems and overall system of options 1 and 2 are reported in main text and Supplementary Material of [692].

Besides, the specific exergy costing (SPECO) method [696] is selected as exergoeconomic approach to determine and compare the economic performance of the two options by using results from the exergy analysis. Exergoeconomic parameters for the evaluation are the total cost rate ($\dot{C}_{total}$), i.e. cost rate associated to capital investment and O&M expenses ($\dot{Z}$) plus cost rate associated to $\dot{E}x_d$ ($\dot{C}_d$), and exergoeconomic factor (f), i.e. the share of non-exergy related costs to the overall costs which is useful to address the improvement of the component performance. Details and assumptions of the exergoeconomic analysis, as well as equations adopted for the calculation of exergoeconomic parameters of single units, sub-systems and overall system of options 1 and 2 are reported in main text and Supplementary Material of [692].

The detailed results of $\dot{E}x_d$ and ψ obtained for single components of the two options are reported in the Supplementary Material of [692]. The highest $\dot{E}x_d$ for option 1 is attributed to EL1-EL10 which is about 6216 kW, while in case of option 2, electrolyzers EL11-EL26 with $\dot{E}x_d$ of 9857 kW follow the most critical components of this option, which are the flash drums D7 and D8 showing $\dot{E}x_d$ of around 23385 kW and 16757 kW, respectively. From ψ results for option 1, values close to 100% are obtained for most of components, except for HX1 and D1 whose ψ range from approximately 60% to 75%, for EL1-EL10 and PX1 whose ψ are almost 50%, and for the distillation unit CD1-CO1-VP1 which has the lowest value among the components (34%). Concerning option 2, similar findings to those obtained for $\dot{E}x_d$ emerge, i.e. the components with higher $\dot{E}x_d$ give lower ψ (between 12 and 50%).

Figure 5.38 dispalys the findings on $\dot{E}x_d$ of the sub-systems of the two options. By examining this figure, the wind-diesel plant sub-system has the highest $\dot{E}x_d$ in both options, even though with a difference of one order of magnitude among them due to the different size of these plants in the two options. The second critical sub-system in the irreversibility contribution analysis is H_2 production in option 1 (Figure 5.38a) and gas treatment in option 2 (Figure 5.38b), in full accordance with the results described for $\dot{E}x_d$ of single components.

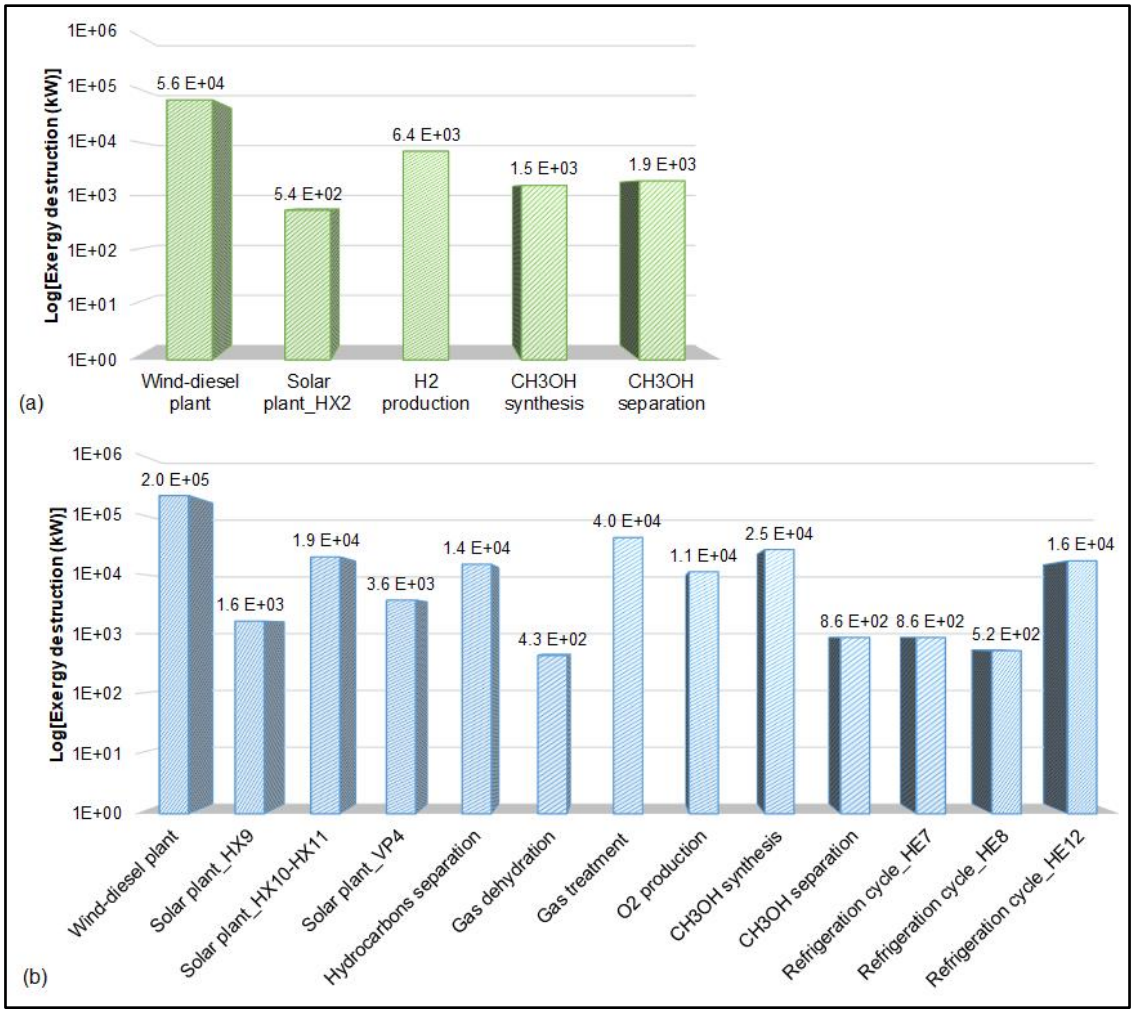

Figure 5.38. Case-study 5: Exergy destruction rate of sub-systems of (a) option 1 and (b) option 2 [692].

Figure 5.39 shows ψ values of different sub-systems in the two options, except for the refrigeration cycles for which exergetic coefficient of performance (COP) is illustrated. According to Figure 5.39a, CH_3OH synthesis sub-system with ψ of 60% is the most efficient sub-system in option 1, while the hydrocarbons separation and gas dehydration sub-systems give the highest ψ in option 2 (Figure 5.39b) with values close to 100%. On the other hand, for the both options, the wind-diesel plant shows the worst ψ (almost 20%), in full accordance with $\dot{E}x_d$ sub-systems analysis.

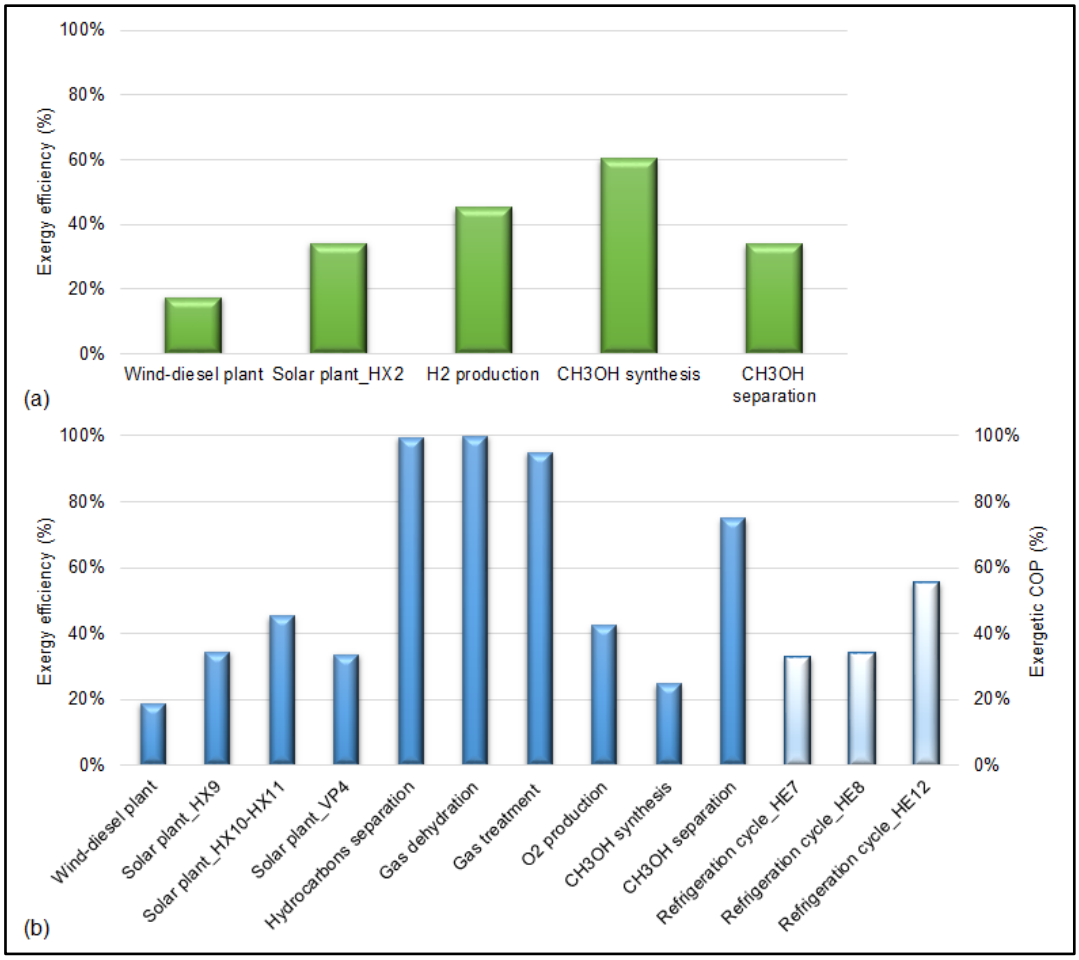

Figure 5.39. Case-study 5: Exergy efficiency of sub-systems of (a) option 1 and (b) option 2 [692].

Focusing on the exergoeconomic analysis results, $\dot{Z}$ and $\dot{C}_d$ values estimated for each component of the two options are detailed in the Supplementary Material of [692]. The highest Ż of process components in option 1 (i.e. excluding the wind-diesel and solar-thermal plants) is observed for electrolyzers EL1-EL10 which give a value of $5.24 \cdot 10^2$ \$/h. These components are penalized also by $\dot{C}_d$, which results in the highest value among the components of option 1 ($5.64 \cdot 10^3$ \$/h). In addition, f calculated for these components has relatively low value (8.5%), thus indicating that exergy-related costs prevail on non-exergy-related costs and improvement in the component performance could be achieved by selecting higher quality electrolyzers. In option 2, the most expensive process components result in electrolyzers EL11-EL26 with a slightly higher $\dot{Z}$ value than that obtained in option 1, followed by compressor K10 of the refrigeration cycle linked to cooler HE12. On the other hand, heater HX5, reactor R2 and cooler HE11 appear as the more critical components with respect to $\dot{C}_d$ values and $\dot{C}_{total}$ values. The f values associated to these units suggest employing more expensive components (i.e. increasing geometrical area of thermal equipment and increasing CH_3OH throughput of reactor) in order to reduce $\dot{E}x_d$ and enhance their exergoeconomic viability.

Figure 5.40 illustrates the contribution of each sub-system to overall cost rate $\dot{C}_{total}$ of the two options. In case of option 1 (Figure 5.40a), the largest percentage (44.5%) is represented by the wind-diesel plant, followed by the H_2 production sub-system with 27% portion. However, as shown in Figure 5.40b, the CH_3OH synthesis sub-system gives the highest share of $\dot{C}_{total}$ in option 2, showing a percentage of about 47%, while the wind-diesel plant contributes for a 30%.

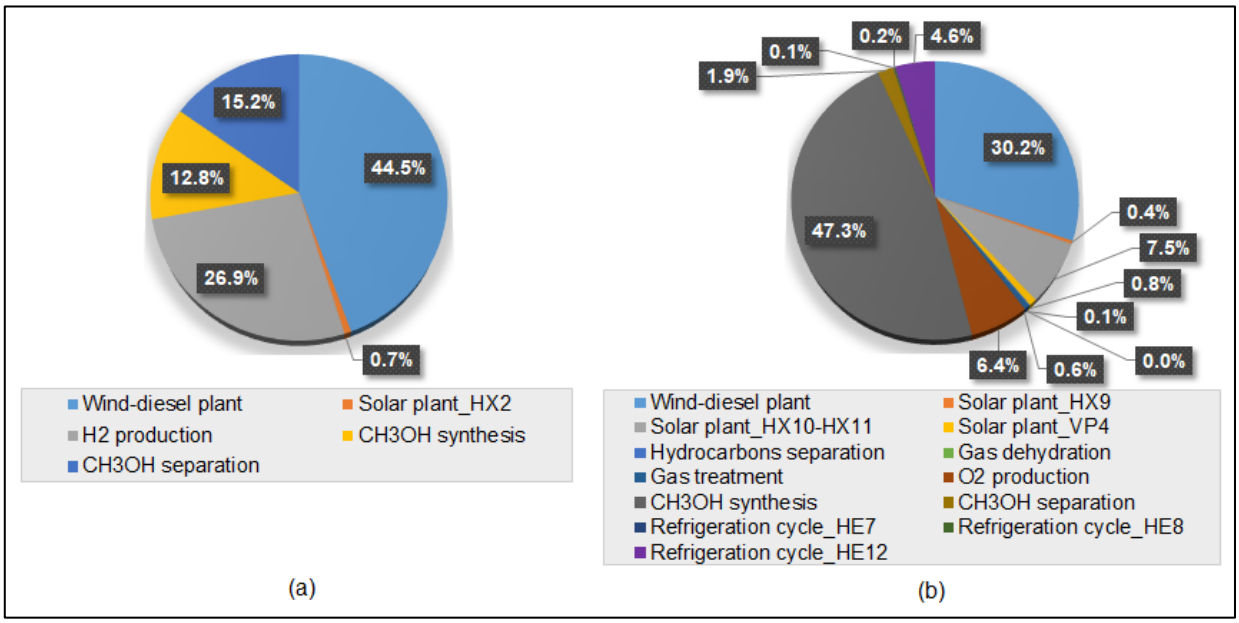

Figure 5.40. Case-study 5: Percentage of total cost rate calculated for the sub-systems of (a) option 1 and (b) option 2 [692].

The exergoeconomic factors calculated for the sub-systems of each option are shown in Figure 5.41. As appears evident, the wind-diesel plant is identified in both options as the sub-system with the maximum f, i.e. 100% in case of option 1 (Figure 5.41a) and 91% in case of option 2 (Figure 5.41b), thus indicating that the non-exergy costs associated to capital investment and O&M expenses are dominant and replacing the wind turbines and diesel generators with more affordable ones is suggested to improve the sub-system economic performance. Conversely, for the other critical sub-systems emerged in the total cost rate analysis, f values lower than 10% are obtained, thus highlighting that the exergy-related costs, i.e. costs associated with $\dot{E}x_d$, are much higher than non-exergy related costs. It is thus recommended to reduce irreversibility increasing capital investment and O&M costs by changing inefficient components with ones having a better exergetic performance, as highlighted in the f analysis performed for single components.

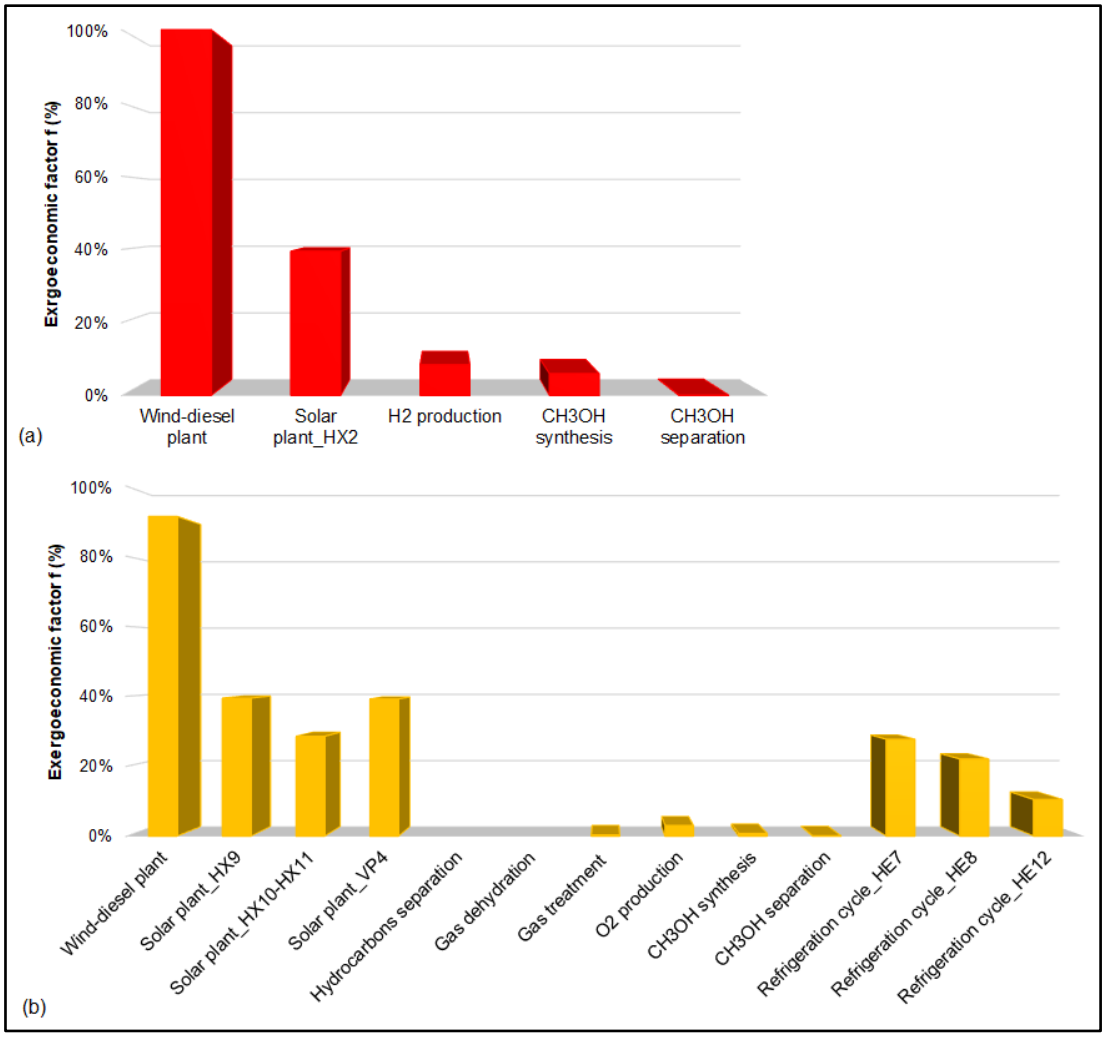

Figure 5.41. Case-study 5: Exergoeconomic factor calculated for the sub-systems of (a) option 1 and (b) option 2 [692].

Figure 5.42 illustrates the comparison of overall exergy and exergoeconomic parameters among the two options. From Figure 5.42a, the highest amount of $\dot{E}x_d$ belongs to option 2 with a value of $3.2 \cdot 10^5$ kW, which is an order of magnitude higher than that calculated for option 1. This is due to the higher number of offshore wind turbines considered in the wind-diesel sub-system, which is responsible for the highest fraction of the total exergy destruction rate in both options (Figure 5.40). From the ψ point of view, option 2 gives the best performance with a value of 87%, which is significantly greater than that of option 1 (a mere 2%). This satisfactory outcome is attributed to the integration of the process scheme for CH_3OH production with oil & gas operations, which provides as input hydrocarbons and yields to multiple co-products with relatively higher chemical exergy in addition to CH_3OH. As a matter of fact, the highest ψ are calculated for the hydrocarbons separation, gas dehydration and gas treatment sub-systems in option 2 (Figure 5.39b).

As emerged in Figure 5.42b, option 2 results in the most expensive scheme with $\dot{C}_{total}$ equal to $1.4 \cdot 10^5$ \$/h, because of higher number of expensive components for the CH_3OH synthesis in addition to larger

offshore wind farm size compared to option 1. On the other hand, option 2 is characterized by lower f, i.e. about 31% against 48% of option 1, thus indicating that about 70% of total costs of option 2 are related to $\dot{E}x_d$. Consequently, in general, greater opportunity for improving exergoeconomic performance could be offered by option 2 by means of choosing more expensive components, while in option 1 non-exergy-related and exergy-related costs should be optimized simultaneously through appropriate trade-offs.

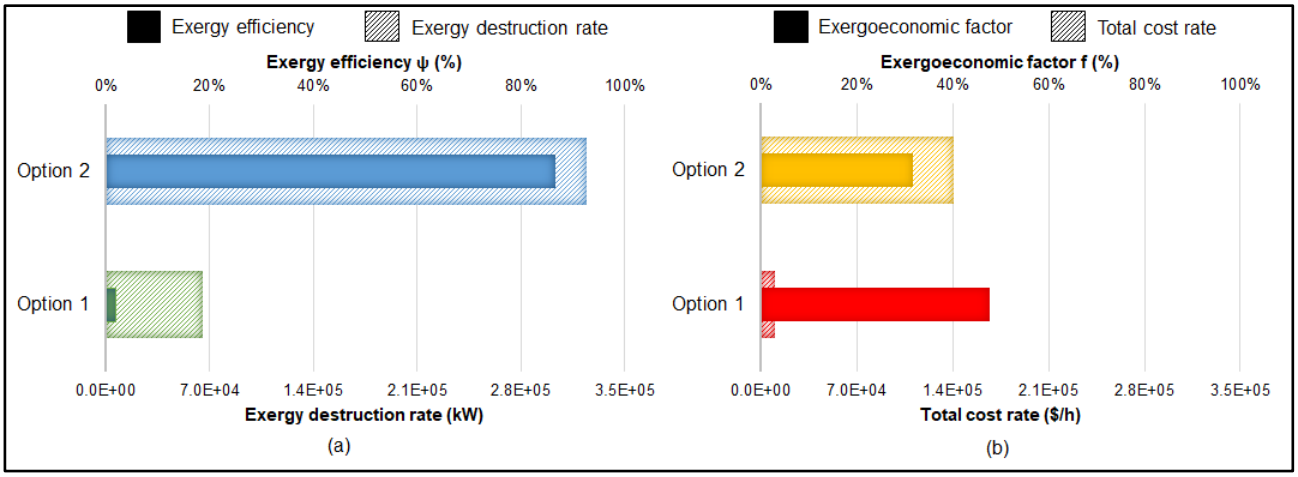

Figure 5.42. Case-study 5: Comparison of overall (a) exergy destruction rate and exergy efficiency, (b) total cost rate and exergoeconomic factor, between the two options [692].

5.6.8. Conclusions

In this case-study, eleven novel process routes producing CH_3OH are considered to demonstrate the potential of the PrI screening methodology described in Section 4.6 to investigate comprehensively the sustainability and safety performance of the process schemes and address the feasible ones to detailed exergy and exergoeconomic performance assessment.

For a given CH_3OH productivity of 500 kg/h, catalytic hydrogenation of CO_2 (scheme A) and homogeneous radical gas-phase reaction of CH_4 (scheme B) result in feasible intensified process schemes, succeeding in the preliminary screenings based on proper features of separation operations and reasonable number of equipment items in the plant. The other nine schemes, still immature for the selected CH_3OH benchmark, are thus excluded from the PrI detailed assessment.

Scheme A shows the best performance based on disaggregated technical, economic, environmental and inherent safety indicators, as well as on the aggregated PrIS indicator. This is also confirmed by the application of different criteria and perspectives of decision makers to elicitation of weights among indicators, as well as different weighting techniques. The results of the sensitivity analysis investigating the effect of random variations in target values used for normalization of indicators on the PrIS of the two

schemes confirm that the overall higher PrI level of intensified scheme A over scheme B is not affected by data uncertainty.

The exergy and exergoeconomic site-specific analysis of the two schemes integrated with offshore renewable energy sources into P2L offshore hybrid energy options at a remote gas production platform in the Atlantic Ocean allow identifying that option 2 based on process scheme B is the most expensive system with the highest portion of thermodynamic irreversibility. However, these drawbacks are compensated by the use of CH_4 from offshore oil & gas operations at the facility, which yields to multiple fuels, thus leading to improved exergy efficiency and cost savings compared to option 1 based on process scheme A.

Chapter 6.

Conclusions

6.1. Concluding remarks

In this research project, novel quantitative assessment methodologies are developed to support the choice of suitable P2G, P2L and G2P offshore hybrid energy production options from the sustainability and safety viewpoints, also considering challenging situations that may arise in the future, i.e. end-of-life oil & gas infrastructures, operations in harsh environment and remote areas, depleted gas reservoirs. These approaches are useful for the analysis of conceptual and front-end engineering design phases of offshore green projects when modifications and/or improvements arising from sustainability and safety drivers are considered. The proposed methods are based on a common systematic MCDA procedure, but present specific peculiarities related to the type of the offshore hybrid energy system analyzed and the type of evaluation. Multi-criteria performance indicators addressing sustainability and/or inherent safety aspects are defined within the methodologies in order to fill the gaps in the existing literature methods and to provide a clear yet comprehensive communication of the performance of innovative offshore systems. The developed supporting tools are applied to case-studies to ensure proof of effectiveness and value of the methodologies.

The main concluding remarks are the following.

- Definition of two novel methodologies for the analysis of the sustainability performance of alternative P2G/P2L and G2P offshore hybrid energy options

The sustainability assessment methodology developed for P2G and P2L offshore hybrid energy options allows a comparison of alternative strategies at remote oil & gas production facilities in phase of decommissioning, including renewable production of H_2, SNG, CH_3OH at the offshore installation, transportation to the shore and multiple end-uses at the onshore market. The sustainability assessment methodology developed for G2P offshore hybrid energy options allows assessing alternative systems composed of offshore renewable plants coupled with GT technologies exploiting untapped gas resources at the offshore facility and producing electricity for injection into the close onshore grid. Both these two methods provide a similar concise yet representative set of indicators capturing the technical, economic, environmental and societal aspects of sustainability, selected as the most relevant from the existing literature sustainability metrics for hybrid energy systems, if suitable, or developed within the present work. The aggregated indicator (ASI) communicating the overall sustainability profile of the strategies is defined based on process-related or renewable source-related target values for normalization of indicators (if the compensatory approach is adopted), time-space-receptor criteria and individualist-egalitarian-hierarchist perspectives of decision makers for weights elicitation, and two weighted mean methods for the aggregation.

- Development of a novel supporting methodology for the analysis of the inherent safety performance of alternative designs of P2G/P2L/G2P offshore hybrid energy options

The inherent safety assessment methodology allows the ranking of hazard level of process units and of the overall facility, showing specific safety and environmental concerns of alternative design options. Overcoming the limits of the existing metrics on inherent safety and environmental protection from accidental releases, the methodology consists of a systematic procedure which introduces innovative criteria concerning the damage assessment to three main target categories of potential offshore hazards (i.e. personnel, structural assets and marine environment polluted by oil and chemical spills) and accounts for specific peculiarities of the offshore structures in the accident modelling (i.e. high congestion, multi-level layout) and for the credibility of loss of containment from oil & gas equipment. Aggregated multi-target KPIs quantifying the overall safety fingerprinting of the alternatives are defined based on vulnerability zones of the target of concern for the normalization of indicators and two weighted mean methods for the aggregation. Some of the output KPIs can be used for both the stand-alone inherent safety performance analysis and integration into the sustainability model developed for P2G, P2L and G2P offshore hybrid energy options to address the societal dimension.

- Definition of a supporting methodology integrating sustainability and inherent safety analyses for the screening of emerging chemical process routes of P2G/P2L hybrid energy options

The PrI screening methodology provides an integrated sustainability and inherent safety analysis based on the idea of process intensification in order to investigate comprehensively the feasibility of chemical emerging process routes for the synthesis of P2G/P2L products and to orient the choice of suitable processes into P2G and P2L projects at remote oil & gas areas. The method consists of a detailed procedure to test the feasibility of intensified process flowsheets and designs through preliminary screenings and to rank the PrI level of the most feasible ones based on a set of technical, economic, environmental and inherent safety metrics selected from the indicators defined in the sustainability and inherent safety methodologies developed in this work. The aggregated indicator (PrIS) quantifying the overall performance of the options is calculated according to the approach described in the sustainability assessment models in the thesis. The analysis based on these metrics is precursor to detailed site-specific assessment of the integrated systems driven by renewable energy sources at remote offshore oil & gas sites.

- Demonstration of the developed methodologies by the application to case-studies

The proof of effectiveness and value of the four supporting methods developed in the thesis are demonstrated through the application to five case-studies, which offer opportunities for valorization of offshore wind power at remote oil & gas field (case-study 1) and at depleted gas field close to the shore

(case-study 2), present safety and environmental critical designs at offshore oil & gas facilities (case-studies 3 and 4), introduce emerging chemical production routes to be investigated for implementation in oil & gas processes at remote areas (case-study 5). For all the cases, the methods are able to meet the expectations depicted "a priori" in the description of the methodologies. They succeed in identifying critical alternatives from sustainable and/or safety perspectives and orienting the choice of the optimal system given the situation under analysis. Furthermore, applicability and flexibility of the methods are proved since the proposed tools allow to guarantee a sound and auditable assessment of all the different systems analyzed capturing the peculiarities of concern and requiring an input information available at early design stages of innovative projects. When applied, sensitivity analysis based on the Monte Carlo simulation approach confirms the ability of the methods to yield robust and meaningful results. In conclusion, the results obtained pave the way to consolidate informed strategies for the safe and sustainable deployment of offshore renewable energies at oil & gas fields.

6.2. Recommendations

Despite the methodologies developed in this research project provide systematic decision support tools based on sustainability and inherent safety indicators, the following recommendations are suggested for further work.

A limited yet relevant number of indicators is defined for the sustainability assessment of alternative offshore hybrid energy options derived from an extensive review of the more used metrics in the literature. However, the set is actually open to the addition of further indicators in view of an improved assessment. In particular, some indicators such "job creation" and "social acceptance" should be investigated for their inclusion into the societal aspect, in addition to the safety-related metrics developed in this thesis. Furthermore, the adoption of environmental impact LCA indicators using a commercial software should be evaluated as alternative to LGHG indicator proposed in the present thesis, being careful about the possible double-counting issues.

The panel method composed of academic and industrial experts in the field of sustainability should be incorporated for weights elicitation in the MCDA aggregation approach to provide a more realistic perspective of decision-makers. Equal recommendations should be applied in case of weights among inherent safety multi-target KPIs.

The sustainability assessment model for G2P hybrid energy options should be further validated by considering other offshore renewable energy sources (e.g. waves, tidal currents, solar radiations) and/or a combination of them, as well as comparing a given hybrid energy system at different locations to investigate the influence of case-specific parameters.

Further application of the inherent safety multi-target KPIs methodology to alternative P2G/P2L/G2P hybrid energy options at different offshore oil & gas sites should be performed.

Process modelling using commercial simulators in the process intensification screening methodology should be further improved by reducing the simplified assumptions made and improving the reaction/separation models adopted.

Optimization procedure should be further applied to the case-studies to determine the optimal values of the parameters which can maximize the overall aggregated performance metrics of the system, e.g. maximizing ASI in case of the sustainability models, minimizing inherent safety multi-target KPIs of the entire design option, maximizing PrIS in case of the process intensification screening methodology.

Acknowledgements

The PhD is a unique yet challenging experience which requires great determination and continuous willingness to get involved. Without the support of some people I would not have been able to reach the end of this journey successfully.

I would like to express my earnest gratitude to my Supervisor Prof. Valerio Cozzani. His expertise and guidance were significant to develop this work and to address my future career.

I am extremely pleased to express my sincere appreciation to my co-Supervisor Prof. Ibrahim Dincer for giving me the opportunity to conduct my research period in his team at the Ontario Tech University. Attending his interactive lectures and receiving his precious advises during and after my period in Canada contributed to extend my knowledge on exergy and sustainable development concepts and to perform important performance analyses of hybrid energy systems for this work. In addition, I am especially grateful to the help given by the hard-working PhD students of ACE 3030B lab.

I would like to express my special thanks to Dr. Sarah Bonvicini for her encouragement to start the PhD after my Master's Degree, continuous support during these years and essential collaboration to the activity regarding KPIs for environmental protection from accidental oil and chemical spills. I would extend my thanks to Dr. Valeria Casson Moreno for her constructive contribution to the investigation and analysis of the alternative CH_3OH production routes. A kind gratefulness goes to all my colleagues, PhD students and fellows, of my research group at DICAM. Being surrounded by brilliant and valuable persons was meaningful to succeed in my PhD.

Last but not at least, my utmost gratitude goes to my wonderful parents for their loving support and blessings from a distance. Also, my deep thankfulness goes to my closest friends and companions on adventures on the" deep blue sea" who constantly encouraged me throughout this work and enriched the quality of my free time.

References

[1] International Energy Agency (IEA). Key world energy statistics 2019.

[2] U.S. Energy Information Administration (EIA). International Energy Outlook 2019 with projections to 2050 2019:85. doi:10.1080/01636609609550217.

[3] Intergovernmental Panel on Climate Change (IPCC). Climate Change 2014: Synthesis Report. 2014. doi:10.1017/CBO9781107415324.

[4] Escribano Francés G, Marín-Quemada JM, San Martín González E. RES and risk: Renewable energy's contribution to energy security. A portfolio-based approach. Renew Sustain Energy Rev 2013;26:549–59. doi:10.1016/j.rser.2013.06.015.

[5] Panwar NL, Kaushik SC, Kothari S. Role of renewable energy sources in environmental protection: A review. Renew Sustain Energy Rev 2011;15:1513–24. doi:10.1016/j.rser.2010.11.037.

[6] European Parliament. Promotion of renewable energy sources in the European Union 2016. doi:10.2861/062931.

[7] Edenhofer O, Seyboth K, Creutzig F, Schlömer S. On the Sustainability of Renewable Energy Sources. Annu Rev Environ Resour 2013;38:169–200. doi:10.1146/annurev-environ-051012-145344.

[8] Hussain A, Arif SM, Aslam M. Emerging renewable and sustainable energy technologies: State of the art. Renew Sustain Energy Rev 2017;71:12–28. doi:10.1016/j.rser.2016.12.033.

[9] Oliveira MF, Saidel M a., Queiroz ARS, Filho EN. Renewable sources at offshore petroleum and gas production platforms. 2012 Pet Chem Ind Conf 2012:1–6. doi:10.1109/PCICON.2012.6549652.

[10] Adriatic IPA. Offshore Wind Energy: Research, Experimentation, Development - Technoogical state of the art. 2012.

[11] GWEC. Global status of Wind Power in 2015 2016.

[12] Wind Europe. Offshore wind in Europe: Key trends and statistics 2018 2019:1–37. doi:10.1016/S1471-0846(02)80021-X.

[13] Esteban MD, Diez JJ, López JS, Negro V. Why offshore wind energy? Renew Energy 2011;36:444–50. doi:10.1016/j.renene.2010.07.009.

[14] Kaldellis JK, Apostolou D. Life cycle energy and carbon footprint of offshore wind energy. Comparison with onshore counterpart. Renew Energy 2017;108:72–84. doi:10.1016/j.renene.2017.02.039.

[15] Bilgili M, Yasar A, Simsek E. Offshore wind power development in Europe and its comparison with onshore counterpart. Renew Sustain Energy Rev 2011;15:905–15. doi:10.1016/j.rser.2010.11.006.

[16] Ackermann T. Wind Power in Power Systems. John Wiley & Sons, Ltd; 2005. doi:10.1002/0470012684.

[17] Sun X, Huang D, Wu G. The current state of offshore wind energy technology development. Energy 2012;41:298–312. doi:10.1016/j.energy.2012.02.054.

[18] Vázquec Hernández C, Telsnig T, Villalba Pradas A. JRC Wind Energy Status Report 2016 Edition. 2017. doi:10.2760/332535.

[19] Wang X, Zeng X, Li J, Yang X, Wang H. A review on recent advancements of substructures for offshore wind turbines. Energy Convers Manag 2018;158:103–19. doi:10.1016/j.enconman.2017.12.061.

[20] Nilsson D, Westin A. Floating wind power in Norway: Analysis of opportunities and challenges 2014.

[21] International Renewable Energy Agency (IRENA). Innovation Outlook: Offshore Wind. Abu Dhabi, UAE: 2016.

[22] European Wind Energy Association (EWEA). Deep water - The next step for offshore wind energy. 2013.

[23] Khan J, Arsalan MH. Solar power technologies for sustainable electricity generation - A review. Renew Sustain Energy Rev 2016;55:414–25. doi:10.1016/j.rser.2015.10.135.

[24] International Renewable Energy Agency (IRENA). Renewable Energy Statistics 2019 2019.

[25] Zhang HL, Baeyens J, Degrève J, Cacères G. Concentrated solar power plants: Review and design methodology. Renew Sustain Energy Rev 2013;22:466–81. doi:10.1016/j.rser.2013.01.032.

[26] Islam MT, Huda N, Abdullah AB, Saidur R. A comprehensive review of state-of-the-art concentrating solar power (CSP) technologies: Current status and research trends. Renew Sustain Energy Rev 2018;91:987–1018. doi:10.1016/j.rser.2018.04.097.

[27] Diendorfer C, Haider M, Lauermann M. Performance Analysis of Offshore Solar Power Plants. Energy Procedia 2014;49:2462–71. doi:10.1016/j.egypro.2014.03.261.

[28] Singh GK. Solar power generation by PV (photovoltaic) technology: A review. Energy 2013;53:1–13. doi:10.1016/j.energy.2013.02.057.

[29] Shubbak MH. Advances in solar photovoltaics: Technology review and patent trends. Renew Sustain Energy Rev 2019;115:109383. doi:10.1016/j.rser.2019.109383.

[30] Husain AAF, Hasan WZW, Shafie S, Hamidon MN, Pandey SS. A review of transparent solar photovoltaic technologies. Renew Sustain Energy Rev 2018;94:779–91. doi:10.1016/j.rser.2018.06.031.

[31] Ranjbaran P, Yousefi H, Gharehpetian GB, Astaraei FR. A review on floating photovoltaic (FPV)power generation units. Renew Sustain Energy Rev 2019;110:332–47. doi:10.1016/j.rser.2019.05.015.

[32] Kumar V, Shrivastava RL, Untawale SP. Solar Energy: Review of Potential Green & Clean Energy for Coastal and Offshore Applications. Aquat Procedia 2015;4:473–80. doi:10.1016/j.aqpro.2015.02.062.

[33] Sahu A, Yadav N, Sudhakar K. Floating photovoltaic power plant: A review. Renew Sustain Energy Rev 2016;66:815–24. doi:10.1016/j.rser.2016.08.051.

[34] Drew B, Plummer A., Sahinkaya MN. A review of wave energy converter technology. J Power Energy 2009;223:887–902. doi:10.1243/09576509JPE782.

[35] Falcão AF de O. Wave energy utilization: A review of the technologies. Renew Sustain Energy Rev 2010;14:899–918. doi:10.1016/j.rser.2009.11.003.

[36] O'Hagan AM, Huertas C, O'Callaghan J, Greaves D. Wave energy in Europe: Views on experiences and progress to date. Int J Mar Energy 2016;14:180–97. doi:10.1016/j.ijome.2015.09.001.

[37] Magagna D, Monfardini R, Uihlein A. JRC Ocean Energy Status Report 2016 Edition. 2016. doi:10.2790/866387.

[38] International Renewable Energy Agency (IRENA). Wave Energy. 2014.

[39] Titah-Benbouzid H, Benbouzid M. An up-to-date technologies review and evaluation of wave energy converters. Int Rev Electr Eng 2015;10.

[40] Koca K, Kortenhaus A, Oumeraci H, Zanuttigh B, Angelelli E, Cantu M, et al. Recent Advances in the Development of Wave Energy Converters. Proc. Tenth Eur. Wave Tidal Energy Conf. 2-5 Sept. 2013, Aalborg, Denmark: 2013.

[41] EMEC. Classification of Wave Energy devices n.d. http://www.emec.org.uk/marine-energy/wave-devices/ (accessed October 10, 2019).

[42] Rourke FO, Boyle F, Reynolds A. Tidal energy update 2009. Appl Energy 2010;87:398–409. doi:10.1016/j.apenergy.2009.08.014.

[43] Magagna D, Uihlein A. 2014 JRC Ocean Energy Status Report: Technology, Market and Economic Aspects of Ocean Energy in Europe. 2015. doi:10.2790/866387.

[44] Kaufmann N, Carolus T, Starzmann R. Turbines for modular tidal current energy converters. Renew Energy 2019;142:451–60. doi:10.1016/j.renene.2019.04.120.

[45] Roberts A, Thomas B, Sewell P, Khan Z, Balmain S, Gillman J. Current tidal power technologies and their suitability for applications in coastal and marine areas. J Ocean Eng Mar Energy 2016;2:227–45. doi:10.1007/s40722-016-0044-8.

[46] International Renewable Energy Agency (IRENA). Tidal energy. Abu Dhabi, UAE: 2014. doi:10.1006/rwos.2001.0032.

[47] EMEC. Classification of Tidal Energy devices 2019. http://www.emec.org.uk/marine-energy/tidal-devices/ (accessed October 10, 2019).

[48] Sovacool BK. The intermittency of wind, solar, and renewable electricity generators: Technical barrier or rhetorical excuse? Util Policy 2009;17:288–96. doi:10.1016/j.jup.2008.07.001.

[49] Zahedi A. A review of drivers, benefits, and challenges in integrating renewable energy sources into electricity grid. Renew Sustain Energy Rev 2011;15:4775–9. doi:10.1016/j.rser.2011.07.074.

[50] Mokhatab S, Poe WA, Mak JY. Handbook of Natural Gas Transmission and Processing - Principles and Practices. 3rd ed. Waltham, USA: Elsevier Inc.; 2015.

[51] Chozas JF, Soerensen HC, Korpås M. Integration of wave and offshore wind energy in a european offshore grid. Proc Int Offshore Polar Eng Conf 2010;1:926–33.

[52] Siemens AG. Offshore Installations powered from shore - Safe, reliable, economic and environmentally friendly 2015. http://www.ospar.org/work-areas/oic/installations.

[53] Chokhawala R. Powering platforms. ABB Rev 2008:52–6.

[54] Bird L, Milligan M, Lew D. Integrating Variable Renewable Energy: Challenges and Solutions. 2013. doi:NREL/TP-6A20-60451.

[55] Leavey S. Mitigating Power Fluctuations from Renewable Energy Sources. School of Physics and Astronomy, University of Glasgow, 2012.

[56] Shivashankar S, Mekhilef S, Mokhlis H, Karimi M. Mitigating methods of power fluctuation of photovoltaic (PV) sources - A review. Renew Sustain Energy Rev 2016;59:1170–84. doi:10.1016/j.rser.2016.01.059.

[57] International Energy Agency (IEA). Variability of Wind Power and Other Renewables - Management options and strategies. Paris, France: International Energy Agency (IEA); 2005.

[58] Khairy H, EL-Shimy M, Hashem G. Overview of Grid Code and Operational Requirements of Grid-connected Solar PV Power Plants. Ind. Acad. Collab. Conf. Energy Sustain. Dev. Track, Cairo, Egypt: 2015. doi:10.13140/RG.2.2.28137.08809.

[59] EWEA. Powering Europe: wind energy and the electricity grid. 2010.

[60] Degner T, Arnold G, Braun M. Utility-scale PV systems: Grid connection requirements, test procedures and European harmonization 2016:132–6.

[61] Blavette A, Lewis A, Egan M, Sullivan DO, Blavette A, Lewis A, et al. Grid integration of wave and tidal energy. Procedings ASME 30th Int. Conf. Ocean. Offshore Arct. Eng., Rotterdam, The Nerherlands: 2011, p. 749–58. doi:10.1115/OMAE2011-49953.

[62] Uihlein A, Magagna D. Wave and tidal current energy - A review of the current state of research beyond technology. Renew Sustain Energy Rev 2016;58:1070–81. doi:10.1016/j.rser.2015.12.284.

[63] IFC, IPIECA, UNDP. Mapping the Oil and Gas Industry To the Sustainable Development Goals: an Atlas 2017.

[64] Absi Halabi M, Al-Qattan A, Al-Otaibi A. Application of solar energy in the oil industry - Current status and future prospects. Renew Sustain Energy Rev 2015;43:296–314. doi:10.1016/j.rser.2014.11.030.

[65] Cheng X, Korpas M, Farahmand H. The impact of electrification on power system in Northern Europe. Int. Conf. Eur. Energy Mark. EEM, June 6-9, Dresden, Germany: IEEE; 2017. doi:10.1109/EEM.2017.7981866.

[66] Dalane K, Dai Z, Mogseth G, Hillestad M, Deng L. Potential applications of membrane separation for subsea natural gas processing: A review. J Nat Gas Sci Eng 2017;39:101–17. doi:10.1016/j.jngse.2017.01.023.

[67] Nmegbu CGJ, Ohazuruike L V. Subsea Technology: a Wholistic View on Existing Technologies and Operations. Int J Appl or Innov Eng Manag 2014;3:81–7.

[68] Tay WH, Lau KK, Lai LS, Shariff AM, Wang T. Current development and challenges in the intensified absorption technology for natural gas purification at offshore condition. J Nat Gas Sci Eng 2019;71:102977. doi:10.1016/j.jngse.2019.102977.

[69] de Andrade Cruz M, de Queiroz Fernandes Araújo O, de Medeiros JL. Deep seawater intake for primary cooling in tropical offshore processing of natural gas with high carbon dioxide content: Energy, emissions and economic assessments. J Nat Gas Sci Eng 2018;56:193–211. doi:10.1016/j.jngse.2018.06.011.

[70] Christou M, Konstantinidou M. Safety of offshore oil and gas operations: Lessons from past accident analysis. 2012. doi:10.2790/73321.

[71] Vinnem JE. Offshore risk assessment vol 1 - Principles, modelling and application of QRA

studies. 3rd ed. London, United Kingdom: Springer Series in Reliability Engineering; 2014. doi:10.1007/978-1-4471-5207-1.

[72] Directive 2013/30/UE. Directive 2013/30/EU of the European Parliament and of the Council of 12 June 2013 on safety of offshore oil and gas operations and amending Directive 2004/35/EC. Official Journal of the European Union; 2013.

[73] Speight JG. Handbook of Offshore Oil and Gas Operations. Laramie, Wyoming, USA: Elsevier Gulf Professional Publishing; 2015. doi:10.1016/B978-1-85617-558-6/00001-5.

[74] Sommer B, Fowler AM, Macreadie PI, Palandro DA, Aziz AC, Booth DJ. Decommissioning of offshore oil and gas structures – Environmental opportunities and challenges. Sci Total Environ 2019;658:973–81. doi:10.1016/j.scitotenv.2018.12.193.

[75] Oil & Gas UK. Decommissioning Insight 2018 2018.

[76] Lakhal SY, Khan MI, Islam MR. An "Olympic" framework for a green decommissioning of an offshore oil platform. Ocean Coast Manag 2009;52:113–23. doi:10.1016/j.ocecoaman.2008.10.007.

[77] Fam ML, Konovessis D, Ong LS, Tan HK. A review of offshore decommissioning regulations in five countries - Strengths and weaknesses. Ocean Eng 2018;160:244–63. doi:10.1016/j.oceaneng.2018.04.001.

[78] Leporini M, Marchetti B, Corvaro F, Polonara F. Reconversion of offshore oil and gas platforms into renewable energy sites production: Assessment of different scenarios. Renew Energy 2019;135:1121–32. doi:10.1016/j.renene.2018.12.073.

[79] Bernstein BB, Bressler A, Cantle P, Henrion M, DeWitt J, Kruse S, et al. Evaluating Alternatives for Decommissioning California's Offshore Oil and Gas Platforms: A technical analysis to inform state policy. Calif Ocean Sci Trust 2015.

[80] Fowler AM, Macreadie PI, Jones DOB, Booth DJ. A multi-criteria decision approach to decommissioning of offshore oil and gas infrastructure. Ocean Coast Manag 2014;87:20–9. doi:10.1016/j.ocecoaman.2013.10.019.

[81] Burdon D, Barnard S, Boyes SJ, Elliott M. Oil and gas infrastructure decommissioning in marine protected areas: System complexity, analysis and challenges. Mar Pollut Bull 2018;135:739–58. doi:10.1016/j.marpolbul.2018.07.077.

[82] BP. BP Statistical Review of World Energy 2019.

[83] PetroWiki. Associated and nonassociated gas. SPE Int 2015. http://petrowiki.org/Associated_and_nonassociated_gas (accessed September 30, 2019).

[84] PetroWiki. Monetizing Stranded Natural Gas. SPE Int 2015. http://petrowiki.org/Monetizing_stranded_gas (accessed September 30, 2019).

[85] Watanabe T, Inoue H, Horitsugi M, Oya S. Gas to Wire (GTW) system for developing "small gas field" and exploiting "associated gas." SPE Int. Oil Gas Conf. Exhib., Beijing, China: 2006.

[86] Deshmukh MK, Deshmukh SS. Modeling of hybrid renewable energy systems. Renew Sustain Energy Rev 2008;12:235–49. doi:10.1016/j.rser.2006.07.011.

[87] Paska J, Biczel P, Kłos M. Hybrid power systems - An effective way of utilising primary energy sources. Renew Energy 2009;34:2414–21. doi:10.1016/j.renene.2009.02.018.

[88] Goodbody C, Walsh E, Mcdonnell K, Owende P. Regional integration of renewable energy

systems in Ireland - The role of hybrid energy systems for small communities. Int J Electr Power Energy Syst 2013;44:713–20. doi:10.1016/j.ijepes.2012.08.012.

[89] Shivarama Krishna K, Sathish Kumar K. A review on hybrid renewable energy systems. Renew Sustain Energy Rev 2015;52:907–16. doi:10.1016/j.rser.2015.07.187.

[90] Beaudin M, Zareipour H, Schellenberglabe A, Rosehart W. Energy storage for mitigating the variability of renewable electricity sources: An updated review. Energy Sustain Dev 2010;14:302–14. doi:10.1016/j.esd.2010.09.007.

[91] Díaz-González F, Sumper A, Gomis-Bellmunt O, Villafáfila-Robles R. A review of energy storage technologies for wind power applications. Renew Sustain Energy Rev 2012;16:2154–71. doi:10.1016/j.rser.2012.01.029.

[92] Decourt B, Lajoie B, Debarre R, Soupa O. Leading the energy transition Factbook: Hydrogen-based energy conversion 2014.

[93] de Valladares M-R. Global Trends and Outlook for Hydrogen. 2017.

[94] Lehner M, Tichler R, Steinmuller H, Koppe M. The Power-to-Gas Concept. Power-to-Gas Technol. Bus. Model., Heidelberg, New York, Dordrecht, London: Springer Cham; 2014. doi:10.1007/978-3-319-03995-4.

[95] DNV KEMA. Systems Analyses Power to Gas - Technology Review. 2013.

[96] Varone A, Ferrari M. Power to liquid and power to gas: An option for the German Energiewende. Renew Sustain Energy Rev 2015;45:207–18. doi:10.1016/j.rser.2015.01.049.

[97] Olah GA, Goeppert A, Surya Prakash GK. Beyond Oil and Gas: The Methanol Economy. 2nd ed. Weinheim: WILEY-VCH Verlag GmbH & Co; 2009. doi:10.1016/S1351-4180(06)71901-8.

[98] Guandalini G, Campanari S, Romano MC. Power-to-gas plants and gas turbines for improved wind energy dispatchability: Energy and economic assessment. Appl Energy 2015;147:117–30. doi:10.1016/j.apenergy.2015.02.055.

[99] Rist JF, Dias MF, Palman M, Zelazo D, Cukurel B. Economic dispatch of a single micro-gas turbine under CHP operation. Appl Energy 2017;200:1–18. doi:10.1016/j.apenergy.2017.05.064.

[100] Alomoush MI. Microgrid combined power-heat economic-emission dispatch considering stochastic renewable energy resources , power purchase and emission tax. Energy Convers Manag 2019;200:112090. doi:10.1016/j.enconman.2019.112090.

[101] Pourghasem P, Sohrabi F, Abapour M, Mohammadi-Ivatloo B. Stochastic multi-objective dynamic dispatch of renewable and CHP-based islanded microgrids. Electr Power Syst Res 2019;173:193–201. doi:10.1016/j.epsr.2019.04.021.

[102] Abdel-Geliel M, Zidane IF, Anany M, Rezeka SF. Modeling and simulation of a hybrid power generation system of wind turbine, micro-turbine and solar heater cells. IEEE Int Conf Control Autom ICCA 2014:1304–9. doi:10.1109/ICCA.2014.6871112.

[103] Oliveira MF, Saidel M a., Queiroz ARS, Filho EN. Renewable sources at offshore petroleum and gas production platforms. 2012 Pet. Chem. Ind. Conf., 2012. doi:10.1109/PCICON.2012.6549652.

[104] Kolstad ML, Årdal AR, Sharifabadi K, Undeland TM. Integrating Offshore Wind Power and Multiple Oil and Gas Platforms to the Onshore Power Grid Using VSC-HVDC Technology.

Mar Technol Soc J 2014;48:31–44. doi:10.4031/MTSJ.48.2.5.

[105] Oudman BL. Green Decommissioning: Re-Use of North Sea Offshore Assets in a Sustainable Energy Future. Proc. 13th Offshore Mediterr. Conf. Exhib. March 29-31, Ravenna, Italy: 2017.

[106] Zanuttigh B, Angelelli E, Kortenhaus A, Koca K, Krontira Y, Koundouri P. A methodology for multi-criteria design of multi-use offshore platforms for marine renewable energy harvesting. Renew Energy 2016;85:1271–89. doi:10.1016/j.renene.2015.07.080.

[107] Kolian SR, Godec M, Sammarco PW. Alternate uses of retired oil and gas platforms in the Gulf of Mexico. Ocean Coast Manag 2019;167:52–9. doi:10.1016/j.ocecoaman.2018.10.002.

[108] Azzarone D, Monti C. Renewable Power Generation in a Traditional Hydrocarbon Asset: The Value of a Synergy. Proc. 13th Offshore Mediterr. Conf. Exhib., Ravenna, Italy: 2017, p. 1–12.

[109] Azimov U, Birkett M. Feasibility study and design of an ocean wave power generation station integrated with a decommissioned offshore oil platform in UK waters. Int J Energy Environ 2017;8:161–74.

[110] Schweizer J, Antonini A, Govoni L, Gottardi G, Archetti R, Supino E, et al. Investigating the potential and feasibility of an offshore wind farm in the Northern Adriatic Sea. Appl Energy 2016;177:449–63. doi:10.1016/j.apenergy.2016.05.114.

[111] Altieri G. The decision to abandon a field. Encycl. Hydrocarb., vol. 1, Roma, Italy: Istituto della Enciclopedia Italiana fondata da Giovanni Treccani S.p.A.; 2005, p. 761–8.

[112] Gahleitner G. Hydrogen from renewable electricity: An international review of power-to-gas pilot plants for stationary applications. Int J Hydrogen Energy 2013;38:2039–61. doi:10.1016/j.ijhydene.2012.12.010.

[113] Bailera M, Lisbona P, Romeo LM, Espatolero S. Power to Gas projects review: Lab, pilot and demo plants for storing renewable energy and CO2. Renew Sustain Energy Rev 2017;69:292–312. doi:10.1016/j.rser.2016.11.130.

[114] CRI. The George Olah Plant - World's Largest CO2 Methanol Plant 2011. http://carbonrecycling.is/george-olah/ (accessed September 30, 2019).

[115] MCI. Mitsui Chemicals to Establish a Pilot Facility to Study a Methanol Synthesis Process from CO2 2008. https://www.mitsuichem.com/en/release/2008/080825e.htm (accessed September 30, 2019).

[116] Enea Consulting. The potential of power-to-gas. 2016.

[117] Thomas D, Mertens D, Meeus M, Van der Laak W, Francois I. Power-to-Gas Roadmap for Flanders 2016.

[118] Ferrero D, Gamba M, Lanzini A, Santarelli M. Power-to-Gas Hydrogen: Techno-economic Assessment of Processes towards a Multi-purpose Energy Carrier. Energy Procedia 2016;101:50–7. doi:10.1016/j.egypro.2016.11.007.

[119] Parra D, Patel MK. Techno-economic implications of the electrolyser technology and size for power-to-gas systems. Int J Hydrogen Energy 2016;41:3748–61. doi:10.1016/j.ijhydene.2015.12.160.

[120] Vo TTQ, Xia A, Rogan F, Wall DM, Murphy JD. Sustainability assessment of large-scale storage technologies for surplus electricity using group multi-criteria decision analysis. Clean Technol Environ Policy 2017;19:689–703. doi:10.1007/s10098-016-1250-8.

[121] Walker SB, Van Lanen D, Fowler M, Mukherjee U. Economic analysis with respect to Power-to-Gas energy storage with consideration of various market mechanisms. Int J Hydrogen Energy 2016;41:7754–65. doi:10.1016/j.ijhydene.2015.12.214.

[122] Balan OM, Buga MR, Brunot A, Badea A, Froelich D. Technical and economic evaluation of Power-to-Gas in link with a 50 MW wind park. J Energy Storage 2016;8:111–8. doi:10.1016/j.est.2016.10.002.

[123] Bartela Ł, Kotowicz J, Dubiel K. Technical – economic comparative analysis of energy storage systems equipped with a hydrogen generation installation. J J Power Technol 2016;96:92–100.

[124] Parra D, Zhang X, Bauer C, Patel MK. An integrated techno-economic and life cycle environmental assessment of power-to-gas systems. Appl Energy 2017;193:440–54. doi:10.1016/j.apenergy.2017.02.063.

[125] Mathur J, Agarwal N, Swaroop R, Shah N. Economics of producing hydrogen as transportation fuel using offshore wind energy systems. Energy Policy 2008;36:1212–22. doi:10.1016/j.enpol.2007.11.031.

[126] Loisel R, Baranger L, Chemouri N, Spinu S, Pardo S. Economic evaluation of hybrid off-shore wind power and hydrogen storage system. Int J Hydrogen Energy 2015;40:6727–39. doi:10.1016/j.ijhydene.2015.03.117.

[127] Hou P, Enevoldsen P, Eichman J, Hu W, Jacobson MZ, Chen Z. Optimizing investments in coupled offshore wind -electrolytic hydrogen storage systems in Denmark. J Power Sources 2017;359:186–97. doi:10.1016/j.jpowsour.2017.05.048.

[128] Chiuta S, Engelbrecht N, Human G, Bessarabov DG. Techno-economic assessment of power-to-methane and power-to-syngas business models for sustainable carbon dioxide utilization in coal-to-liquid facilities. J CO2 Util 2016;16:399–411. doi:10.1016/j.jcou.2016.10.001.

[129] Almahdi M, Dincer I, Rosen MA. Analysis and assessment of methanol production by integration of carbon capture and photocatalytic hydrogen production. Int J Greenh Gas Control 2016;51:56–70. doi:10.1016/j.ijggc.2016.04.015.

[130] Esmaili P, Dincer I, Naterer GF. Development and analysis of an integrated photovoltaic system for hydrogen and methanol production. Int J Hydrogen Energy 2014;40:11140–53. doi:10.1016/j.ijhydene.2015.04.077.

[131] Matzen M, Alhajji M, Demirel Y. Chemical storage of wind energy by renewable methanol production: Feasibility analysis using a multi-criteria decision matrix. Energy 2015;93:343–53. doi:10.1016/j.energy.2015.09.043.

[132] Kim J, Henao CA, Johnson TA, Dedrick DE, Miller JE, Stechel EB, et al. Methanol production from CO2 using solar-thermal energy: Process development and techno-economic analysis. Energy Environ Sci 2011;4:3122–32. doi:10.1039/c1ee01311d.

[133] H2ocean project. 2016 n.d. http://www.h2ocean-project.eu/ (accessed April 4, 2018).

[134] Serna Cantero A, Tadeo F. Offshore hydrogen production using wave energy. Universidad de Valladolid, 2013.

[135] Serna Á, Yahyaoui I, Normey-Rico JE, de Prada C, Tadeo F. Predictive control for hydrogen production by electrolysis in an offshore platform using renewable energies. Int J Hydrogen Energy 2017;42:12865–76. doi:10.1016/j.ijhydene.2016.11.077.

[136] Jepma CJ, Noujeim JP, Hofman E, von Schot M, Schulze P, Florission O. Smart sustainable

combinations in the North Sea Area (NSA) - Make the energy transition work efficiently and effectively. 2015.

[137] Jepma C, Schot M van. On the economics of offshore energy conversion: smart combinations Converting offshore wind energy into green hydrogen on existing oil and gas platforms in the North Sea. 2017.

[138] Meier K. Hydrogen production with sea water electrolysis using Norwegian offshore wind energy potentials. Int J Energy Environ Eng 2014;5:1–12. doi:10.1007/s40095-014-0104-6.

[139] Sedlar DK, Vulin D, Krajačić G, Jukić L. Offshore gas production infrastructure reutilisation for blue energy production. Renew Sustain Energy Rev 2019;108:159–74. doi:10.1016/j.rser.2019.03.052.

[140] Barigozzi G, Bonetti G, Franchini G, Perdichizzi A, Ravelli S. Thermal performance prediction of a solar hybrid gas turbine. Sol Energy 2012;86:2116–27. doi:10.1016/j.solener.2012.04.014.

[141] Schwarzbözl P, Buck R, Sugarmen C, Ring A, Marcos Crespo MJ, Altwegg P, et al. Solar gas turbine systems: Design, cost and perspectives. Sol Energy 2006;80:1231–40. doi:10.1016/j.solener.2005.09.007.

[142] Grange B, Dalet C, Falcoz Q, Siros F, Ferrière A. Simulation of a hybrid solar gas-turbine cycle with storage integration. Energy Procedia 2014;49:1147–56. doi:10.1016/j.egypro.2014.03.124.

[143] Turchi CS, Ma Z, Erbes M. Gas Turbine / Solar Parabolic Trough Hybrid Designs. ASME Turbo Expo 2011 June 6-10, Vancouver, Canada: 2011. doi:10.1115/GT2011-45184.

[144] Spelling J. Hybrid Solar Gas-Turbine Power Plants - A Thermoeconomic Analysis. 2013.

[145] De Morsella C. World' s First Solar Gas Hybrid Power Plant Launched in Israel. Green Econ Post 2009. http://greeneconomypost.com/solar-gas-hybrid-power-plant-3368.htm (accessed January 3, 2017).

[146] General Electric. FlexEfficiency* 50 combined cycle power plant 2011.

[147] Brown N. Gas Turbine to Help Grow Renewable Energy. Clean Tech Publ 2011. https://cleantechnica.com/2011/05/29/gas?turbine?to?help?grow?renewable?energy/ (accessed January 3, 2017).

[148] Bullis K. GE Combines Natural Gas, Wind, and Solar. MIT Technol Rev 2011. https://www.technologyreview.com/s/424223/ge?combines?natural?gas?wind?and?solar/ (accessed January 3, 2017).

[149] Perry TS. GE's New Gas Turbines Play Nicely With Renewables. IEEE Spectr 2012. http://spectrum.ieee.org/energywise/energy/fossil-fuels/ges-new-gas-turbines-play-nicely-with-renewables (accessed January 3, 2017).

[150] Wang U. GE Adds eSolar and Wind to Natural Power Plant Design in Turkey. Renew Energy World 2011. http://www.renewableenergyworld.com/articles/2011/06/ge?adds?esolar?and?wind?to?natural?power?plant?design?in?turkey.html (accessed September 30, 2019).

[151] Zhang X, Bauer C, Mutel CL, Volkart K. Life Cycle Assessment of Power-to-Gas : Approaches , system variations and their environmental implications. Appl Energy 2017;190:326–38. doi:10.1016/j.apenergy.2016.12.098.

[152] Dincer I, Zamfirescu C. Sustainable Hydrogen Production. 1st ed. Amsterdam, Netherlands:

Elsevier Inc.; 2016.

[153] Koponen J, Kosonen A, Ahola J. Review of water electrolysis technologies and design of renewable hydrogen production systems. 2015.

[154] Götz M, Lefebvre J, Mörs F, McDaniel Koch A, Graf F, Bajohr S, et al. Renewable Power-to-Gas: A technological and economic review. Renew Energy 2016;85:1371–90. doi:10.1016/j.renene.2015.07.066.

[155] Bhandari R, Trudewind CA, Zapp P. Life cycle assessment of hydrogen production via electrolysis - A review. vol. 85. 2014. doi:10.1016/j.jclepro.2013.07.048.

[156] Kotowicz J, Jurczyk M, Ecel DW¸, Ogulewicz W. Analysis of Hydrogen Production in Alkaline Electrolyzers. Open Access J J Power Technol 2016;96:149–56.

[157] Carmo M, Fritz DL, Mergel J, Stolten D. A comprehensive review on PEM water electrolysis. Int J Hydrogen Energy 2013;38:4901–34. doi:10.1016/j.ijhydene.2013.01.151.

[158] Buttler A, Spliethoff H. Current status of water electrolysis for energy storage, grid balancing and sector coupling via power-to-gas and power-to-liquids: A review. Renew Sustain Energy Rev 2018;82:2440–54. doi:10.1016/j.rser.2017.09.003.

[159] Schiebahn S, Grube T, Robinius M, Tietze V, Kumar B, Stolten D. Power to gas: Technological overview, systems analysis and economic assessment for a case study in Germany. Int J Hydrogen Energy 2015;40:4285–94. doi:10.1016/j.ijhydene.2015.01.123.

[160] Saba SM, Müller M, Robinius M, Stolten D. The investment costs of electrolysis – A comparison of cost studies from the past 30 years. Int J Hydrogen Energy 2018;43:1209–23. doi:10.1016/j.ijhydene.2017.11.115.

[161] Bertuccioli L, Chan A, Hart D, Lehner F, Madden B, Standen E. Study on development of water electrolysis in the EU. 2014.

[162] Reiter G, Lindorfer J. Global warming potential of hydrogen and methane production from renewable electricity via power-to-gas technology. Int J Life Cycle Assess 2015;20:477–89. doi:10.1007/s11367-015-0848-0.

[163] Ghaffour N, Missimer TM, Amy GL. Technical review and evaluation of the economics of water desalination: Current and future challenges for better water supply sustainability. Desalination 2013;309:197–207. doi:10.1016/j.desal.2012.10.015.

[164] IEA, IRENA. Water Desalination Using Renewable Energy. 2012.

[165] Greenlee LF, Lawler DF, Freeman BD, Marrot B, Moulin P. Reverse osmosis desalination: Water sources, technology, and today's challenges. Water Res 2009;43:2317–48. doi:10.1016/j.watres.2009.03.010.

[166] Al-Karaghouli A, Kazmerski L. Renewable energy opportunities in water desalination, Desalination trends and technologies. In: Michael Schorr, editor. Desalination, Trends Technol., InTech; 2011, p. 149–84. doi:10.5772/583.

[167] Serna Á, Tadeo F. Offshore hydrogen production from wave energy. Int J Hydrogen Energy 2014;39:1549–57. doi:10.1016/j.ijhydene.2013.04.113.

[168] Di Blasi A, Andaloro L, Siracusano S, Briguglio N, Brunaccini G, Stassi A, et al. Evaluation of materials and components degradation of a PEM electrolyzer for marine applications. Int J Hydrogen Energy 2013;38:7612–5. doi:10.1016/j.ijhydene.2012.10.062.

[169] Charcosset C. A review of membrane processes and renewable energies for desalination. Desalination 2009;245:214–31. doi:10.1016/j.desal.2008.06.020.

[170] Gilau AM, Small MJ. Designing cost-effective seawater reverse osmosis system under optimal energy options. Renew Energy 2008;33:617–30. doi:10.1016/j.renene.2007.03.019.

[171] Wang P, Chung TS. Recent advances in membrane distillation processes: Membrane development, configuration design and application exploring. J Memb Sci 2015;474:39–56. doi:10.1016/j.memsci.2014.09.016.

[172] Al-Karaghouli A, Kazmerski LL. Energy consumption and water production cost of conventional and renewable-energy-powered desalination processes. Renew Sustain Energy Rev 2013;24:343–56. doi:10.1016/j.rser.2012.12.064.

[173] Lai W, Ma Q, Lu H, Weng S, Fan J, Fang H. Effects of wind intermittence and fluctuation on reverse osmosis desalination process and solution strategies. Desalination 2016;395:17–27. doi:10.1016/j.desal.2016.05.019.

[174] OFX. Yearly Average Rates 2019. https://www.ofx.com/en-au/forex-news/historical-exchange-rates/yearly-average-rates/ (accessed March 16, 2019).

[175] Garmsiri S, Rosen MA, Smith GR. Integration of Wind Energy, Hydrogen and Natural Gas Pipeline Systems to Meet Community and Transportation Energy Needs: A Parametric Study. Sustainability 2014;6:2506–26.

[176] Altfeld K, Pinchbeck D. Admissible hydrogen concentrations in natural gas systems. 2013. doi:ISSN 2192-158X.

[177] Guandalini G, Campanari S. Wind Power Plant and Power-to-Gas System Coupled With Natural Gas Grid Infrastructure: Techno-Economic Optimization of Operation. Vol 9 Oil Gas Appl Supercrit CO2 Power Cycles; Wind Energy 2015:V009T46A004. doi:10.1115/GT2015-42229.

[178] Perrin J, Steinberger-Wilckens R. Roads2HyCom project - “European Hydrogen Infrastructure Atlas” and “Industrial Excess Hydrogen Analysis.” 2007.

[179] Takahashi K. Hydrogen transportation. In: Ohta T, Veziroglu TN, editors. Energy carriers Convers. Syst., vol. II, Encyclopedia of Life Support Systems (EOLSS); 2009.

[180] Kuczynski S, Łaciak M, Olijnyk A, Szurlej A, Włodek T. Thermodynamic and Technical Issues of Hydrogen and Methane-Hydrogen Mixtures Pipeline Transmission. Energies 2019;12:1–21. doi:10.3390/en12030569.

[181] Schaaf T, Grünig J, Schuster MR, Rothenfluh T, Orth A. Methanation of CO2 - storage of renewable energy in a gas distribution system. Energy Sustain Soc 2014;4:1–14. doi:10.1186/s13705-014-0029-1.

[182] Benjaminsson G, Benjaminsson J, Rudberg R. Power-to-Gas – A technical review. SGC Rapp 2013;284:67. doi:SGC Rapport 2013:284.

[183] Gutiérrez-Martín F, Rodríguez-Antón LM. Power-to-SNG technology for energy storage at large scales. Int J Hydrogen Energy 2016;41:19290–303. doi:10.1016/j.ijhydene.2016.07.097.

[184] Reiter G, Lindorfer J. Global warming potential of hydrogen and methane production from renewable electricity via power-to-gas technology. Int J Life Cycle Assess 2015;20:477–89. doi:10.1007/s11367-015-0848-0.

[185] Sternberg A, Bardow A. Life Cycle Assessment of Power-to-Gas : Syngas vs Methane. ACS

Sustain Chem Eng 2016;4:4156–65. doi:10.1021/acssuschemeng.6b00644.

[186] Electrochaea.dk ApS. Final report Power-to-Gas via Biological Catalysis (P2G-Biocat). 2014.

[187] Fritt-Rasmussen J, Linnebjerg JF, Sørensen MX, Brogaard NL, Rigét FF, Kristensen P, et al. Effects of oil and oil burn residues on seabird feathers. Mar Pollut Bull 2016;109:446–52. doi:10.1016/j.marpolbul.2016.05.029.

[188] Burkhardt M, Koschack T, Busch G. Biocatalytic methanation of hydrogen and carbon dioxide in an anaerobic three-phase system. Bioresour Technol 2015;178:330–3. doi:10.1016/j.biortech.2014.08.023.

[189] DNV GL. Power-to-Gas project in Rozenburg, The Netherlands. 2015.

[190] Greiner CJ, KorpÅs M, Holen AT. A Norwegian case study on the production of hydrogen from wind power. Int J Hydrogen Energy 2007;32:1500–7. doi:10.1016/j.ijhydene.2006.10.030.

[191] Araújo OQF, Reis A de C, de Medeiros JL, do Nascimento JF, Grava WM, Musse APS. Comparative analysis of separation technologies for processing carbon dioxide rich natural gas in ultra-deepwater oil fields. J Clean Prod 2017;155:12–22. doi:10.1016/j.jclepro.2016.06.073.

[192] Gadelha TS, Guimarães ARS, Nakao A, Araújo O de QF, de Medeiros JL. A comparative economical analysis of technologies for CO2 removal from offshore natural gas. In: Karimi IA, Srinivasan R, editors. 11th Eur. Symp. Process Syst. Eng. July 15-19, Elsevier B.V; 2012.

[193] Norwegian Petroleum. Sleipner Vest Field 2019. https://www.norskpetroleum.no/en/facts/field/sleipner-vest/ (accessed April 20, 2019).

[194] Baker RW, Lokhandwala K. Natural gas processing with membranes: An overview. Ind Eng Chem Res 2008;47:2109–21. doi:10.1021/ie071083w.

[195] Peters L, Hussain A, Follmann M, Melin T, Hägg MB. CO2 removal from natural gas by employing amine absorption and membrane technology - A technical and economical analysis. Chem Eng J 2011;172:952–60. doi:10.1016/j.cej.2011.07.007.

[196] Khoo HH, Tan RBH. Life cycle investigation of CO2 recovery and sequestration. Environ Sci Technol 2006;40:4016–24. doi:10.1021/es051882a.

[197] Verma MK. Fundamentals of Carbon Dioxide-Enhanced Oil Recovery (CO2-EOR) - A Supporting Document of the Assessment Methodology for Hydrocarbon Recovery Using CO2-EOR Associated with Carbon Sequestration. 2015.

[198] Quintella C, Dino R, Santana Musse AP. CO2 Enhanced Oil Recovery and Geologic Storage: An Overview with Technology Assessment Based on Patents and Articles. Proc SPE Int Conf Heal Saf Environ Oil Gas Explor Prod 2010. doi:10.2118/126122-MS.

[199] Sweatman RE, Crookshank S, Edman S. Outlook and Technologies for Offshore CO2 EOR/CCS Projects. Offshore Technol. Conf., vol. OTC 21984, Houston, TX, USA: 2011. doi:10.4043/21984-MS.

[200] Leung DYC, Caramanna G, Maroto-Valer MM. An overview of current status of carbon dioxide capture and storage technologies. Renew Sustain Energy Rev 2014;39:426–43. doi:10.1016/j.rser.2014.07.093.

[201] International Energy Agency (IEA) Greenhouse Gas Emissions (GHG). CO2 Storage in Depleted Gas Fields. 2009.

[202] Roussanaly S, Brunsvold AL, Hognes ES. Benchmarking of CO2 transport technologies: Part II - Offshore pipeline and shipping to an offshore site. Int J Greenh Gas Control 2014;28:283–99. doi:10.1016/j.ijggc.2014.06.019.

[203] European Technology Platform for Zero Emission Fossil Fuel Power Plants (ZEP). The Costs of CO2 Transport: Post-demonstration CCS in the EU 2011:1–53.

[204] BERR. Development of a CO2 transport and storage network in the North Sea 2007.

[205] EU CO2Europipe Consortium. D2.1.1 Existing infrastructure for the transport of CO2. 2011.

[206] Knoope MMJ, Guijt W, Ramírez A, Faaij APC. Improved cost models for optimizing CO2 pipeline configuration for point-to-point pipelines and simple networks. Int J Greenh Gas Control 2014;22:25–46. doi:10.1016/j.ijggc.2013.12.016.

[207] Tremel A, Wasserscheid P, Baldauf M, Hammer T. Techno-economic analysis for the synthesis of liquid and gaseous fuels based on hydrogen production via electrolysis. Int J Hydrogen Energy 2015;40:11457–64. doi:10.1016/j.ijhydene.2015.01.097.

[208] Olah GA. Beyond Oil and Gas: The Methanol Economy. Angew Chemie - Int Ed 2005;44:2636–9. doi:10.1002/9783527627806.

[209] Rivera-Tinoco R, Farran M, Bouallou C, Auprêtre F, Valentin S, Millet P, et al. Investigation of power-to-methanol processes coupling electrolytic hydrogen production and catalytic CO2 reduction. Int J Hydrogen Energy 2016;41:4546–59. doi:10.1016/j.ijhydene.2016.01.059.

[210] Bozzano G, Manenti F. Efficient methanol synthesis: Perspectives, technologies and optimization strategies. Prog Energy Combust Sci 2016;56:71–105. doi:10.1016/j.pecs.2016.06.001.

[211] Ganesh I. Conversion of carbon dioxide into methanol - A potential liquid fuel: Fundamental challenges and opportunities (a review). Renew Sustain Energy Rev 2014;31:221–57. doi:10.1016/j.rser.2013.11.045.

[212] Olah GA, Goeppert A, Prakash GKS. Chemical recycling of carbon dioxide to methanol and dimethyl ether: From greenhouse gas to renewable, environmentally carbon neutral fuels and synthetic hydrocarbons. J Org Chem 2009;74:487–98. doi:10.1021/jo801260f.

[213] Albo J, Alvarez-Guerra M, Castaño P, Irabien A. Towards the electrochemical conversion of carbon dioxide into methanol. Green Chem 2015;17:2304–24. doi:10.1039/c4gc02453b.

[214] Jadhav SG, Vaidya PD, Bhanage BM, Joshi JB. Catalytic carbon dioxide hydrogenation to methanol: A review of recent studies. Chem Eng Res Des 2014;92:2557–67. doi:10.1016/j.cherd.2014.03.005.

[215] Albo J, Alvarez-Guerra M, Castaño P, Irabien A. Towards the electrochemical conversion of carbon dioxide into methanol. Green Chem 2015;17:2304–24. doi:10.1039/C4GC02453B.

[216] Matzen M, Mahdi A, Demirei Y. Technoeconomics and Sustainability of Renewable Methanol and Ammonia Productions Using Wind Power-based Hydrogen. J Adv Chem Eng 2015;5. doi:10.4172/2090-4568.1000128.

[217] Pérez-Fortes M, Schöneberger JC, Boulamanti A, Tzimas E. Methanol synthesis using captured CO2 as raw material: Techno-economic and environmental assessment. Appl Energy 2016;161:718–32. doi:10.1016/j.apenergy.2015.07.067.

[218] Atsonios K, Panopoulos KD, Kakaras E. Investigation of technical and economic aspects for methanol production through CO2 hydrogenation. Int J Hydrogen Energy 2016;41:2202–14.

doi:10.1016/j.ijhydene.2015.12.074.

[219] Bellotti D, Rivarolo M, Magistri L, Massardo AF. Feasibility study of methanol production plant from hydrogen and captured carbon dioxide. J CO2 Util 2017;21:132–8. doi:10.1016/j.jcou.2017.07.001.

[220] Methanol Institute. Methanol Safe Handling Manual 2013.

[221] Soares C. Gas turbines in simple cycle & combined cycle applications. Gas Turbines A Handb. Land, Sea Air Appl. 2nd ed., Oxford, UK: Butterworth-Heinemann Elsevier Inc.; 2014. doi:10.1016/C2012-0-05971-6.

[222] Wärtsilä. Gas Turbine for Power Generation 2017. http://www.wartsila.com/energy/learning-center/technical-comparisons/gas-turbine-for-power-generation-introduction (accessed January 3, 2017).

[223] General Electric. Power Generation Products 2017. https://powergen.gepower.com/products.html (accessed January 3, 2017).

[224] Siemens AG. Siemens Gas Turbines 2017.

[225] do Nascimento MAR, Rodrigues LDO, E. C. Dos Santos EEBG, Dias FLG, Velásques EIG, Carrillo R a. M. Micro Gas Turbine Engine: A Review 2014:107–42. doi:10.5772/54444 13.

[226] Capstone Turbine Corporation. Product specification: Models C600, C800, and C1000 2009:1–16.

[227] Vyncke-Wilson D. Advantages of aero-derivative gas turbines: technical, operational considerations on equipment selection. 20th Symp. Ind. Appl. Gas Turbines Comm., Banff, Alberta, Canada: 2013, p. 1–15.

[228] Olson A, Nick S, Kush P, Gabe K. Capital Cost Review of Power Generation Technologies: Recommendations for WECC's 10- and 20-Year Studies 2014:1–105.

[229] Guandalini G, Campanari S, Romano MC. Power-to-gas plants and gas turbines for improved wind energy dispatchability: Energy and economic assessment. Appl Energy 2015;147:117–30. doi:10.1016/j.apenergy.2015.02.055.

[230] U.S. Department of Energy. Combined Heat and Power Technology Fact Sheet Series - Microturbines 2016:1–4. doi:DOE/EE-1329.

[231] Doom TR. Aeroderivative Gas Turbines. Am Energy Innov Counc Publ 2013.

[232] Capstone Turbine Corporation. Shale Gas Utilization: A Distributed Generation Case Study 2014:1–40.

[233] Sevan Marine. Sevan Power Plant – an environmentally friendly and flexible energy producer 2007.

[234] Hetland J, Kvamsdal HM, Haugen G, Major F, Kårstad V, Tjellander G. Integrating a full carbon capture scheme onto a 450 MWe NGCC electric power generation hub for offshore operations: Presenting the Sevan GTW concept. Appl Energy 2009;86:2298–307. doi:10.1016/j.apenergy.2009.03.019.

[235] Fine LG. The SWOT Analysis: Using your Strength to overcome Weaknesses, Using Opportunities to overcome Threats. North Charleston, USA: Kick It, LLC; 2010.

[236] Cinelli M, Coles SR, Kirwan K. Analysis of the potentials of multi criteria decision analysis methods to conduct sustainability assessment. Ecol Indic 2014;46:138–48.

doi:10.1016/j.ecolind.2014.06.011.

[237] World Commission on Environment and Development (WCED). Our Common Future. New York, USA: Oxford University Press; 1987. doi:978-0192820808.

[238] EOLSS. Conceptual Framework. Oxford, UK: Encyclopedia of Life Support Systems (EOLSS) Publishers; 1998.

[239] Elkington J. Cannibals with Forks: The Triple Bottom Line of 21st Century Business. Oxford, UK: Capstone; 1997.

[240] Dincer I, Rosen MA. Exergy: Energy, Environment and Sustainable Development. 2nd ed. Oxford, UK: Elsevier; 2013.

[241] Strantzali E, Aravossis K. Decision making in renewable energy investments: A review. Renew Sustain Energy Rev 2016;55:885–98. doi:10.1016/j.rser.2015.11.021.

[242] Martín-Gamboa M, Iribarren D, García-Gusano D, Dufour J. A review of life-cycle approaches coupled with data envelopment analysis within multi-criteria decision analysis for sustainability assessment of energy systems. J Clean Prod 2017;150:164–74. doi:10.1016/j.jclepro.2017.03.017.

[243] Abu-Rayash A, Dincer I. Sustainability assessment of energy systems: A novel integrated model. J Clean Prod 2019;212:1098–116. doi:10.1016/j.jclepro.2018.12.090.

[244] Munda G. "Measuring sustainability": A multi-criterion framework. Environ Dev Sustain 2005;7:117–34. doi:10.1007/s10668-003-4713-0.

[245] Marttunen M, Lienert J, Belton V. Structuring problems for Multi-Criteria Decision Analysis in practice: A literature review of method combinations. Eur J Oper Res 2017;263:1–17. doi:10.1016/j.ejor.2017.04.041.

[246] Wang JJ, Jing YY, Zhang CF, Zhao JH. Review on multi-criteria decision analysis aid in sustainable energy decision-making. Renew Sustain Energy Rev 2009;13:2263–78. doi:10.1016/j.rser.2009.06.021.

[247] Rowley H V., Peters GM, Lundie S, Moore SJ. Aggregating sustainability indicators: Beyond the weighted sum. J Environ Manage 2012;111:24–33. doi:10.1016/j.jenvman.2012.05.004.

[248] Raza SS, Janajreh I, Ghenai C. Sustainability index approach as a selection criteria for energy storage system of an intermittent renewable energy source. Appl Energy 2014;136:909–20. doi:10.1016/j.apenergy.2014.04.080.

[249] Atilgan B, Azapagic A. An integrated life cycle sustainability assessment of electricity generation in Turkey. Energy Policy 2016;93:168–86. doi:10.1016/j.enpol.2016.02.055.

[250] Santoyo-Castelazo E, Azapagic A. Sustainability assessment of energy systems: Integrating environmental, economic and social aspects. J Clean Prod 2014;80:119–38. doi:10.1016/j.jclepro.2014.05.061.

[251] Cartelle Barros JJ, Lara Coira M, de la Cruz López MP, del Caño Gochi A. Assessing the global sustainability of different electricity generation systems. Energy 2015;89:473–89. doi:10.1016/j.energy.2015.05.110.

[252] Wang J-J, Jing Y-Y, Zhang C-F. Weighting methodologies in multi-criteria evaluations of combined heat and power systems. Int J Energy Res 2009;33:1023–39. doi:10.1002/er.1527.

[253] Pilavachi PA, Roumpeas CP, Minett S, Afgan NH. Multi-criteria evaluation for CHP system

options. Energy Convers Manag 2006;47:3519–29. doi:10.1016/j.enconman.2006.03.004.

[254] Lipošćak M, Afgan NH, Duić N, da Graça Carvalho M. Sustainability assessment of cogeneration sector development in Croatia. Energy 2006;31:2276–84. doi:10.1016/j.energy.2006.01.024.

[255] Dinca C, Badea A, Rousseaux P, Apostol T. A multi-criteria approach to evaluate the natural gas energy systems. Energy Policy 2007;35:5754–65. doi:10.1016/j.enpol.2007.06.024.

[256] Rojas-Zerpa JC, Yusta JM. Application of multicriteria decision methods for electric supply planning in rural and remote areas. Renew Sustain Energy Rev 2015;52:557–71. doi:10.1016/j.rser.2015.07.139.

[257] Rovere EL La, Soares JB, Oliveira LB, Lauria T. Sustainable expansion of electricity sector: Sustainability indicators as an instrument to support decision making. Renew Sustain Energy Rev 2010;14:422–9. doi:10.1016/j.rser.2009.07.033.

[258] Mainali B, Silveira S. Using a sustainability index to assess energy technologies for rural electrification. Renew Sustain Energy Rev 2015;41:1351–65. doi:10.1016/j.rser.2014.09.018.

[259] Kaya T, Kahraman C. Multicriteria renewable energy planning using an integrated fuzzy VIKOR & AHP methodology: The case of Istanbul. Energy 2010;35:2517–27. doi:10.1016/j.energy.2010.02.051.

[260] Gamboa G, Munda G. The problem of windfarm location: A social multi-criteria evaluation framework. Energy Policy 2007;35:1564–83. doi:10.1016/j.enpol.2006.04.021.

[261] Dincer I, Acar C. A review on clean energy solutions for better sustainability. Int J Energy Res 2015;39:585–606. doi:10.1002/er.

[262] Haurant P, Oberti P, Muselli M. Multicriteria selection aiding related to photovoltaic plants on farming fields on Corsica island: A real case study using the ELECTRE outranking framework. Energy Policy 2011;39:676–88. doi:10.1016/j.enpol.2010.10.040.

[263] Aragonés-Beltrán P, Chaparro-González F, Pastor-Ferrando JP, Pla-Rubio A. An AHP (Analytic Hierarchy Process)/ANP (Analytic Network Process)-based multi-criteria decision approach for the selection of solar-thermal power plant investment projects. Energy 2014;66:222–38. doi:10.1016/j.energy.2013.12.016.

[264] Hacatoglu K, Dincer I, Rosen MA. Sustainability assessment of a hybrid energy system with hydrogen-based storage. Int J Hydrogen Energy 2015;40:1559–68. doi:10.1016/j.ijhydene.2014.11.079.

[265] Montignac F, Noirot I, Chaudourne S. Multi-criteria evaluation of on-board hydrogen storage technologies using the MACBETH approach. Int J Hydrogen Energy 2009;34:4561–8. doi:10.1016/j.ijhydene.2008.09.098.

[266] McDowall W, Eames M. Towards a sustainable hydrogen economy: A multi-criteria sustainability appraisal of competing hydrogen futures. Int J Hydrogen Energy 2007;32:4611–26. doi:10.1016/j.ijhydene.2007.06.020.

[267] Afgan NH, Carvalho MG. Sustainability assessment of hydrogen energy systems. Int J Hydrogen Energy 2004;29:1327–42. doi:10.1016/j.ijhydene.2004.01.005.

[268] Gnanapragasam N V., Reddy B V., Rosen MA. A Methodology for assessing the sustainability of hydrogen production from solid fuels. Sustainability 2010;2:1472–91. doi:10.3390/su2061472.

[269] Pilavachi PA, Stephanidis SD, Pappas VA, Afgan NH. Multi-criteria evaluation of hydrogen and natural gas fuelled power plant technologies. Appl Therm Eng 2009;29:2228–34. doi:10.1016/j.applthermaleng.2008.11.014.

[270] Bojesen M, Boerboom L, Skov-Petersen H. Towards a sustainable capacity expansion of the Danish biogas sector. Land Use Policy 2015;42:264–77. doi:10.1016/j.landusepol.2014.07.022.

[271] Nzila C, Dewulf J, Spanjers H, Tuigong D, Kiriamiti H, van Langenhove H. Multi criteria sustainability assessment of biogas production in Kenya. Appl Energy 2012;93:496–506. doi:10.1016/j.apenergy.2011.12.020.

[272] Bai Z, Liu Q, Lei J, Li H, Jin H. A polygeneration system for the methanol production and the power generation with the solar-biomass thermal gasification. Energy Convers Manag 2015;102:190–201. doi:10.1016/j.enconman.2015.02.031.

[273] Tugnoli A, Santarelli F, Cozzani V. Implementation of Sustainability Drivers in the Design of Industrial Chemical Processes. AIChE J 2011;57:3063–84.

[274] Serna J, Díaz Martinez EN, Narváez Rincón PC, Camargo M, Gálvez D, Orjuela Á. Multi-criteria decision analysis for the selection of sustainable chemical process routes during early design stages. Chem Eng Res Des 2016;113:28–49. doi:10.1016/j.cherd.2016.07.001.

[275] Jia X, Li Z, Wang F, Qian Y. Integrated sustainability assessment for chemical processes. Clean Technol Environ Policy 2016;18:1295–306. doi:10.1007/s10098-015-1075-x.

[276] Turcksin L, Macharis C, Lebeau K, Boureima F, Van Mierlo J, Bram S, et al. A multi-actor multi-criteria framework to assess the stakeholder support for different biofuel options: The case of Belgium. Energy Policy 2011;39:200–14. doi:10.1016/j.enpol.2010.09.033.

[277] Kahraman C, Kaya I. A fuzzy multicriteria methodology for selection among energy alternatives. Expert Syst Appl 2010;37:6270–81. doi:10.1016/j.eswa.2010.02.095.

[278] May JR, Brennan DJ. Sustainability assessment of Australian electricity generation. Process Saf Environ Prot 2006;84:131–42. doi:10.1205/psep.04265.

[279] Klein SJW, Whalley S. Comparing the sustainability of U.S. electricity options through multi-criteria decision analysis. Energy Policy 2015;79:127–49. doi:10.1016/j.enpol.2015.01.007.

[280] Gumus AT, Yesim Yayla A, Çelik E, Yildiz A. A combined fuzzy-AHP and fuzzy-GRA methodology for hydrogen energy storage method selection in Turkey. Energies 2013;6:3017–32. doi:10.3390/en6063017.

[281] Tsoutsos T, Drandaki M, Frantzeskaki N, Iosifidis E, Kiosses I. Sustainable energy planning by using multi-criteria analysis application in the island of Crete. Energy Policy 2009;37:1587–600. doi:10.1016/j.enpol.2008.12.011.

[282] Shmelev SE, Van Den Bergh JCJM. Optimal diversity of renewable energy alternatives under multiple criteria: An application to the UK. Renew Sustain Energy Rev 2016;60:679–91. doi:10.1016/j.rser.2016.01.100.

[283] Roinioti A, Koroneos C. Integrated life cycle sustainability assessment of the Greek interconnected electricity system. Sustain Energy Technol Assessments 2019;32:29–46. doi:10.1016/j.seta.2019.01.003.

[284] Stagl S. Multicriteria evaluation and public participation: The case of UK energy policy. Land Use Policy 2006;23:53–62. doi:10.1016/j.landusepol.2004.08.007.

[285] Jayaraman R, Colapinto C, La Torre D, Malik T. Multi-criteria model for sustainable development using goal programming applied to the United Arab Emirates. Energy Policy 2015;87:447–54. doi:10.1016/j.enpol.2015.09.027.

[286] Rahman MM, Paatero J V., Lahdelma R, Wahid MA. Multicriteria-based decision aiding technique for assessing energy policy elements-demonstration to a case in Bangladesh. Appl Energy 2016;164:237–44. doi:10.1016/j.apenergy.2015.11.091.

[287] Ribeiro F, Ferreira P, Araújo M. Evaluating future scenarios for the power generation sector using a Multi-Criteria Decision Analysis (MCDA) tool: The Portuguese case. Energy 2013;52:126–36. doi:10.1016/j.energy.2012.12.036.

[288] Afgan NH, Carvalho MG, Hovanov N V. Energy system assessment with sustainability indicators. Energy Policy 2000;28:603–12. doi:10.1016/S0301-4215(00)00045-8.

[289] Claudia Roldán M, Martínez M, Peña R. Scenarios for a hierarchical assessment of the global sustainability of electric power plants in México. Renew Sustain Energy Rev 2014;33:154–60. doi:10.1016/j.rser.2014.02.007.

[290] Dombi M, Kuti I, Balogh P. Sustainability assessment of renewable power and heat generation technologies. Energy Policy 2014;67:264–71. doi:10.1016/j.enpol.2013.12.032.

[291] Doukas HC, Andreas BM, Psarras JE. Multi-criteria decision aid for the formulation of sustainable technological energy priorities using linguistic variables. Eur J Oper Res 2007;182:844–55. doi:10.1016/j.ejor.2006.08.037.

[292] Goldrath T, Ayalon O, Shechter M. A combined sustainability index for electricity efficiency measures. Energy Policy 2015;86:574–84. doi:10.1016/j.enpol.2015.08.013.

[293] Jovanović M, Afgan N, Bakic V. An analytical method for the measurement of energy systems sustainability in urban areas. Energy 2010;35:3909–20. doi:10.1016/j.energy.2010.06.010.

[294] Jovanovic M, Turanjanin V, Bakic V, Pezo M, Vucicevic B. Sustainability estimation of energy system options that use gas and renewable resources for domestic hot water production. Energy 2011;36:2169–75. doi:10.1016/j.energy.2010.08.042.

[295] Kaya T, Kahraman C. Multicriteria decision making in energy planning using a modified fuzzy TOPSIS methodology. Expert Syst Appl 2011;38:6577–85. doi:10.1016/j.eswa.2010.11.081.

[296] Kurka T. Application of the analytic hierarchy process to evaluate the regional sustainability of bioenergy developments. Energy 2013;62:393–402. doi:10.1016/j.energy.2013.09.053.

[297] Mattiussi A, Rosano M, Simeoni P. A decision support system for sustainable energy supply combining multi-objective and multi-attribute analysis: An Australian case study. Decis Support Syst 2014;57:150–9. doi:10.1016/j.dss.2013.08.013.

[298] Maxim A. Sustainability assessment of electricity generation technologies using weighted multi-criteria decision analysis. Energy Policy 2014;65:284–97. doi:10.1016/j.enpol.2013.09.059.

[299] Mikučionienė R, Martinaitis V, Keras E. Evaluation of energy efficiency measures sustainability by decision tree method. Energy Build 2014;76:64–71. doi:10.1016/j.enbuild.2014.02.048.

[300] Štreimikiene D, Šliogeriene J, Turskis Z. Multi-criteria analysis of electricity generation technologies in Lithuania. Renew Energy 2016;85:148–56. doi:10.1016/j.renene.2015.06.032.

[301] Zhao H, Li N. Evaluating the performance of thermal power enterprises using sustainability

balanced scorecard, fuzzy Delphic and hybrid multi-criteria decision making approaches for sustainability. J Clean Prod 2015;108:569–82. doi:10.1016/j.jclepro.2015.07.141.

[302] Evans A, Strezov V, Evans TJ. Assessment of sustainability indicators for renewable energy technologies. Renew Sustain Energy Rev 2009;13:1082–8. doi:10.1016/j.rser.2008.03.008.

[303] Begić F, Afgan NH. Sustainability assessment tool for the decision making in selection of energy system-Bosnian case. Energy 2007;32:1979–85. doi:10.1016/j.energy.2007.02.006.

[304] Liu G. Development of a general sustainability indicator for renewable energy systems: A review. Renew Sustain Energy Rev 2014;31:611–21. doi:10.1016/j.rser.2013.12.038.

[305] Pilavachi PA, Chatzipanagi AI, Spyropoulou AI. Evaluation of hydrogen production methods using the Analytic Hierarchy Process. Int J Hydrogen Energy 2009;34:5294–303. doi:10.1016/j.ijhydene.2009.04.026.

[306] Afgan NH, Carvalho MG. Multi-criteria assessment of new and renewable energy power plants. Energy 2002;27:739–55. doi:10.1016/S0360-5442(02)00019-1.

[307] Afgan NH, Carvalho MG. Sustainability assessment of a hybrid energy system. Energy Policy 2008;36:2893–900. doi:10.1016/j.enpol.2008.03.040.

[308] Shaaban M, Scheffran J. Selection of sustainable development indicators for the assessment of electricity production in Egypt. Sustain Energy Technol Assessments 2017;22:65–73. doi:10.1016/j.seta.2017.07.003.

[309] Upadhyay S, Sharma MP. A review on configurations, control and sizing methodologies of hybrid energy systems. Renew Sustain Energy Rev 2014;38:47–63. doi:10.1016/j.rser.2014.05.057.

[310] Barin A, Canha LN, Da Rosa Abaide A, Magnago KF. Selection of storage energy technologies in a power quality scenario - The AHP and the fuzzy logic. IECON Proc (Industrial Electron Conf 2009:3615–20. doi:10.1109/IECON.2009.5415150.

[311] Genoud S, Lesourd JB. Characterization of sustainable development indicators for various power generation technologies. Int J Green Energy 2009;6:257–67. doi:10.1080/15435070902880943.

[312] Gujba H, Mulugetta Y, Azapagic A. Environmental and economic appraisal of power generation capacity expansion plan in Nigeria. Energy Policy 2010;38:5636–52. doi:10.1016/j.enpol.2010.05.011.

[313] Wang JJ, Jing YY, Zhang CF, Shi GH, Zhang XT. A fuzzy multi-criteria decision-making model for trigeneration system. Energy Policy 2008;36:3823–32. doi:10.1016/j.enpol.2008.07.002.

[314] Beccali M, Cellura M, Mistretta M. Decision-making in energy planning . Application of the Electre method at regional level for the diffusion of renewable energy technology. Renew Energy 2003;28:2063–87. doi:10.1016/S0960-1481(03)00102-2.

[315] Varun, Prakash R, Bhat IK. Energy, economics and environmental impacts of renewable energy systems. Renew Sustain Energy Rev 2009;13:2716–21. doi:10.1016/j.rser.2009.05.007.

[316] Burton J, Hubacek K. Is small beautiful? A multicriteria assessment of small-scale energy technology applications in local governments. Energy Policy 2007;35:6402–12. doi:10.1016/j.enpol.2007.08.002.

[317] Rahman MM, Paatero J V., Lahdelma R. Evaluation of choices for sustainable rural electrification in developing countries: A multicriteria approach. Energy Policy 2013;59:589–99. doi:10.1016/j.enpol.2013.04.017.

[318] Stamford L, Azapagic A. Life cycle sustainability assessmnent of electricity options in UK. Int J Energy Res 2012;36:1263–90. doi:10.1002/er.2962.

[319] Borzoni M, Rizzi F, Frey M. Geothermal power in Italy: A social multi-criteria evaluation. Renew Energy 2014;69:60–73. doi:10.1016/j.renene.2014.03.026.

[320] Infante CEDDC, Mendonça FM De, Purcidonio PM, Valle R. Triple bottom line analysis of oil and gas industry with multicriteria decision making. J Clean Prod 2013;52:289–300. doi:10.1016/j.jclepro.2013.02.037.

[321] Troldborg M, Heslop S, Hough RL. Assessing the sustainability of renewable energy technologies using multi-criteria analysis: Suitability of approach for national-scale assessments and associated uncertainties. Renew Sustain Energy Rev 2014;39:1173–84. doi:10.1016/j.rser.2014.07.160.

[322] Cavallaro F, Ciraolo L. A multicriteria approach to evaluate wind energy plants on an Italian island. Energy Policy 2005;33:235–44. doi:10.1016/S0301-4215(03)00228-3.

[323] Chou JS, Ongkowijoyo CS. Risk-based group decision making regarding renewable energy schemes using a stochastic graphical matrix model. Autom Constr 2014;37:98–109. doi:10.1016/j.autcon.2013.10.010.

[324] Arroyo P, Tommelein ID, Ballard G, Rumsey P. Choosing by advantages: A case study for selecting an HVAC system for a net zero energy museum. Energy Build 2016;111:26–36. doi:10.1016/j.enbuild.2015.10.023.

[325] Kontu K, Rinne S, Olkkonen V, Lahdelma R, Salminen P. Multicriteria evaluation of heating choices for a new sustainable residential area. Energy Build 2015;93:169–79. doi:10.1016/j.enbuild.2015.02.003.

[326] Schenler W, Hirschberg S, Burgherr P, Makowski M, Granat J. Final report on sustainability assessment of advanced electricity supply options. Energy 2009;6.

[327] Hirschberg S, Dones R, Heck T, Burgherr P, Schenler W, Bauer C. Sustainability of Electricity Supply Technologies under German Conditions : A Comparative Evaluation. 2004.

[328] Jovanović M, Afgan N, Radovanović P, Stevanović V. Sustainable development of the Belgrade energy system. Energy 2009;34:532–9. doi:10.1016/j.energy.2008.01.013.

[329] Phdungsilp A. Integrated energy and carbon modeling with a decision support system: Policy scenarios for low-carbon city development in Bangkok. Energy Policy 2010;38:4808–17. doi:10.1016/j.enpol.2009.10.026.

[330] Carvalho A, Gani R, Matos H. Design of sustainable chemical processes: Systematic retrofit analysis generation and evaluation of alternatives. Process Saf Environ Prot 2008;86:328–46. doi:10.1016/j.psep.2007.11.003.

[331] Cobuloglu HI, Büyüktahtakin IE. A stochastic multi-criteria decision analysis for sustainable biomass crop selection. Expert Syst Appl 2015;42:6065–74. doi:10.1016/j.eswa.2015.04.006.

[332] Choudhary D, Shankar R. An STEEP-fuzzy AHP-TOPSIS framework for evaluation and selection of thermal power plant location: A case study from India. Energy 2012;42:510–21. doi:10.1016/j.energy.2012.03.010.

[333] Kowalski K, Stagl S, Madlener R, Omann I. Sustainable energy futures: Methodological challenges in combining scenarios and participatory multi-criteria analysis. Eur J Oper Res 2009;197:1063–74. doi:10.1016/j.ejor.2007.12.049.

[334] Diakoulaki D, Karangelis F. Multi-criteria decision analysis and cost-benefit analysis of alternative scenarios for the power generation sector in Greece. Renew Sustain Energy Rev 2007;11:716–27. doi:10.1016/j.rser.2005.06.007.

[335] Ghafghazi S, Sowlati T, Sokhansanj S, Melin S. A multicriteria approach to evaluate district heating system options. Appl Energy 2010;87:1134–40. doi:10.1016/j.apenergy.2009.06.021.

[336] Ren J, Lützen M. Fuzzy multi-criteria decision-making method for technology selection for emissions reduction from shipping under uncertainties. Transp Res Part D Transp Environ 2015;40:43–60. doi:10.1016/j.trd.2015.07.012.

[337] Chong YT, Teo KM, Tang LC. A lifecycle-based sustainability indicator framework for waste-to-energy systems and a proposed metric of sustainability. Renew Sustain Energy Rev 2016;56:797–809. doi:10.1016/j.rser.2015.11.036.

[338] Chatzimouratidis AI, Pilavachi PA. Multicriteria evaluation of power plants impact on the living standard using the analytic hierarchy process. Energy Policy 2008;36:1074–89. doi:10.1016/j.enpol.2007.11.028.

[339] Atilgan B, Azapagic A. An integrated life cycle sustainability assessment of electricity generation in Turkey. Energy Policy 2016;93:168–86. doi:10.1016/j.enpol.2016.02.055.

[340] Browne D, O'Regan B, Moles R. Use of multi-criteria decision analysis to explore alternative domestic energy and electricity policy scenarios in an Irish city-region. Energy 2010;35:518–28. doi:10.1016/j.energy.2009.10.020.

[341] Lehtveer M, Makowski M, Hedenus F, McCollum D, Strubegger M. Multi-criteria analysis of nuclear power in the global energy system: Assessing trade-offs between simultaneously attainable economic, environmental and social goals. Energy Strateg Rev 2015;8:45–55. doi:10.1016/j.esr.2015.09.004.

[342] Neves AR, Leal V, Lourenço JC. A methodology for sustainable and inclusive local energy planning. Sustain Cities Soc 2015;17:110–21. doi:10.1016/j.scs.2015.04.005.

[343] Gallego Carrera D, Mack A. Sustainability assessment of energy technologies via social indicators: Results of a survey among European energy experts. Energy Policy 2010;38:1030–9. doi:10.1016/j.enpol.2009.10.055.

[344] Onat NC, Kucukvar M, Tatari O, Zheng QP. Combined application of multi-criteria optimization and life-cycle sustainability assessment for optimal distribution of alternative passenger cars in U.S. J Clean Prod 2016;112:291–307. doi:10.1016/j.jclepro.2015.09.021.

[345] Guo S, Zhao H. Optimal site selection of electric vehicle charging station by using fuzzy TOPSIS based on sustainability perspective. Appl Energy 2015;158:390–402. doi:10.1016/j.apenergy.2015.08.082.

[346] Kühmaier M, Kanzian C, Stampfer K. Identification of potential energy wood terminal locations using a spatial multicriteria decision analysis. Biomass and Bioenergy 2014;66:337–47. doi:10.1016/j.biombioe.2014.03.048.

[347] Scarpellini S, Valero A, Llera E, Aranda A. Multicriteria analysis for the assessment of energy innovations in the transport sector. Energy 2013;57:160–8. doi:10.1016/j.energy.2012.12.004.

[348] Jeswani HK, Gujba H, Azapagic A. Assessing options for electricity generation from biomass on a life cycle basis: Environmental and economic evaluation. Waste and Biomass Valorization 2011;2:33–42. doi:10.1007/s12649-010-9057-z.

[349] Madlener R, Kowalski K, Stagl S. New ways for the integrated appraisal of national energy scenarios: The case of renewable energy use in Austria. Energy Policy 2007;35:6060–74. doi:10.1016/j.enpol.2007.08.015.

[350] Løken E, Botterud A, Holen AT. Use of the equivalent attribute technique in multi-criteria planning of local energy systems. Eur J Oper Res 2009;197:1075–83. doi:10.1016/j.ejor.2007.12.050.

[351] Haralambopoulos DA, Polatidis H. Renewable energy projects: Structuring a multi-criteria group decision-making framework. Renew Energy 2003;28:961–73. doi:10.1016/S0960-1481(02)00072-1.

[352] Papadopoulos A, Karagiannidis A. Application of the multi-criteria analysis method Electre III for the optimisation of decentralised energy systems. Omega 2008;36:766–76. doi:10.1016/j.omega.2006.01.004.

[353] Heinrich G, Basson L, Cohen B, Howells M, Petrie J. Ranking and selection of power expansion alternatives for multiple objectives under uncertainty. Energy 2007;32:2350–69. doi:10.1016/j.energy.2007.06.001.

[354] Dorini G, Kapelan Z, Azapagic A. Managing uncertainty in multiple-criteria decision making related to sustainability assessment. Clean Technol Environ Policy 2011;13:133–9. doi:10.1007/s10098-010-0291-7.

[355] Chatzimouratidis AI, Pilavachi PA. Sensitivity analysis of technological, economic and sustainability evaluation of power plants using the analytic hierarchy process. Energy Policy 2009;37:788–98. doi:10.1016/j.enpol.2008.11.021.

[356] Alanne K, Salo A, Saari A, Gustafsson SI. Multi-criteria evaluation of residential energy supply systems. Energy Build 2007;39:1218–26. doi:10.1016/j.enbuild.2007.01.009.

[357] Stamford L, Azapagic A. Life cycle sustainability assessment of electricity options for the UK. Int J Energy Res 2012;36:1263–90. doi:10.1002/er.2962.

[358] Cherni JA, Dyner I, Henao F, Jaramillo P, Smith R, Font RO. Energy supply for sustainable rural livelihoods. A multi-criteria decision-support system. Energy Policy 2007;35:1493–504. doi:10.1016/j.enpol.2006.03.026.

[359] Dombi M, Kuti I, Balogh P. Sustainability assessment of renewable power and heat generation technologies. Energy Policy 2014;67:264–71. doi:10.1016/j.enpol.2013.12.032.

[360] Çengel YA, Boles MA. Thermodynamics: An Engineering Approach. 8th ed. New York, USA: McGraw-Hill Education; 2011.

[361] Seider WD, Seader JD, Lewin DR, Widagolo S. Product and Process Design Principles - Synthesis, Analysis, and Evaluation. 3rd ed. United States of America: John Wiley & Sons, Inc.; 2009.

[362] Mikučioniene R, Martinaitis V, Keras E. Evaluation of energy efficiency measures sustainability by decision tree method. Energy Build 2014;76:64–71. doi:10.1016/j.enbuild.2014.02.048.

[363] Guinée JB. Handbook on Life Cycle Assessment: Operation Guide to the ISO Standards. 1st

ed. New York, USA: Kluwer Academic Publishers; 2002. doi:10.1007/0-306-48055-7.

[364] Dincer I, Rosen MA. Exergy - Energy, Environment and Sustainable Development. 2nd ed. Oxford, UK: Elsevier; 2013.

[365] Lenzen M. Double-counting in life cycle calculations. J Ind Ecol 2008;12. doi:10.1111/j.1530-9290.2008.00067.x.

[366] Bare JC, Hofstetter P, Pennington DW, de Haes HAU. Midpoints versus endpoints: The sacrifices and benefits. Int J Life Cycle Assess 2000;5:319–26. doi:10.1007/bf02978665.

[367] Mcphate AJ, Zerafa M, Venkataraman G, Popat N. Design Safety Lessons Learned From Major Offshore E&P Projects. SPE Int. Conf. Heal. Saf. Environ. Oil Gas Explor. Prod., Rio de Janeiro, Brazil: Society of Petroleum Engineers (SPE); 2010, p. 1–7.

[368] Randall SW. Managing risk and uncertainty provides competitive advantage. Oil Gas Financ J Digit Mag 2010.

[369] Kletz TA. Inherent Safer Chemical Processes: A Life Cycle Approach. 2nd ed. Hoboken, New Jersey, USA: American Institute of Chemical Engineers (AIChE), John Wiley & Sons, Inc.; 2009.

[370] Ruiz-Femenia R, Fernández-Torres MJ, Salcedo-Díaz R, Gómez-Rico MF, Caballero JA. Systematic Tools for the Conceptual Design of Inherently Safer Chemical Processes. Ind Eng Chem Res 2017;56:7301–13. doi:10.1021/acs.iecr.7b00901.

[371] Kidam K, Sahak HA, Hassim MH, Shahlan SS, Hurme M. Inherently safer design review and their timing during chemical process development and design. J Loss Prev Process Ind 2016;42:47–58. doi:10.1016/j.jlp.2015.09.016.

[372] Khan FI, Sadiq R, Husain T. Risk-based process safety assessment and control measures design for offshore process facilities. J Hazard Mater 2002;94:1–36. doi:10.1016/S0304-3894(02)00004-3.

[373] Oakden MM, Eades M. The application of inherently safer design principles to the design of a new offshore gas processing platform. Proc. 9th Int. Conf. Heal. Saf. Environ. Oil Gas Explor. Prod., Nice, France: Society of Petroleum Engineers (SPE); 2008, p. 1–10. doi:10.2118/111670-MS.

[374] De Galvez N, Marsot J, Martin P, Siadat A, Etienne A, Godot X. Design for Safety: Proposition of a Model to Detect Hazards through Energy Flows Analysis. Procedia CIRP 2016;41:1107–12. doi:10.1016/j.procir.2015.12.052.

[375] Kletz TA. What you don't have, can't leak. Chem Ind 1978;6:287–92.

[376] Kletz TA. Inherently safer plants. Plant/Operation Prog 1985;4:164–6.

[377] Kletz TA. Plant Design For Safety: A User - Friendly Approach. New York: Hemisphere - Taylor & Francis; 1991.

[378] Kletz TA, Amyotte P. Process plants: A handbook for inherent safer design. 2nd ed. Boca Raton, Florida, USA: CRC Press Taylor & Francis; 2010.

[379] Hendershot DC. Inherently Safer Chemical Process Design. J Loss Prev Process Ind 1997;10:151–7.

[380] Bollinger RE, Clark DG, Dowell AMI, Ewbank RM, Hendershot DC, Lutz WK, et al. Inherently safer chemical processes: A life cycle approach. 2nd ed. New York, USA: John

Wiley & Sons, Ltd.; 2009.

[381] Hurme M, Rahman M. Implementing inherent safety throughout process lifecycle. J Loss Prev Process Ind 2005;18:238–244.

[382] Khan FI, Amyotte PR. How to make inherent safety practice a reality. Process Saf Prog 2003;22:83–97.

[383] Zimmerman JB, Anastas PT. Design through the 12 principles of green engineering. Environ Sci Technol 2003;37:99(A)-101(A).

[384] Gonzalez MA, Smith R, Martin W, King L. A methodology to evaluate process sustainability. Environ Prog Sustain Energy 2003;22:269–76.

[385] Hassim MH, Hurme M. Inherent occupational health assessment during process research and development stage. J Loss Prev Process Ind 2010;23:127–38. doi:10.1016/j.jlp.2009.06.009.

[386] Sikdar SK. Journey Towards Sustainable Development: A Role for Chemical Engineers. Environ Prog 2003;22:227–32.

[387] Khan FI, Amyotte PR. Inherent safety in offshore oil and gas activities: A review of the present status and future directions. J Loss Prev Process Ind 2002;15:279–89. doi:10.1016/S0950-4230(02)00009-8.

[388] Zainal Abidin M, Rusli R, Buang A, Mohd Shariff A, Khan FI. Resolving inherent safety conflict using quantitative and qualitative technique. J Loss Prev Process Ind 2016;44:95–111. doi:10.1016/j.jlp.2016.08.018.

[389] Øien K, Utne IB, Tinmannsvik RK, Massaiu S. Building Safety indicators: Part 2 - Application, practices and results. Saf Sci 2011;49:162–71. doi:10.1016/j.ssci.2010.05.015.

[390] Skogdalen JE, Utne IB, Vinnem JE. Developing safety indicators for preventing offshore oil and gas deepwater drilling blowouts. Saf Sci 2011;49:1187–99. doi:10.1016/j.ssci.2011.03.012.

[391] Reiman T, Pietikäinen E. Leading indicators of system safety - Monitoring and driving the organizational safety potential. Saf Sci 2012;50:1993–2000. doi:10.1016/j.ssci.2011.07.015.

[392] Srinivasan R, Natarajan S. Developments in inherent safety: A review of the progress during 2001-2011 and opportunities ahead. Process Saf Environ Prot 2012;90:389–403. doi:10.1016/j.psep.2012.06.001.

[393] Swuste P, Theunissen J, Schmitz P, Reniers G, Blokland P. Process safety indicators, a review of literature. J Loss Prev Process Ind 2016;40:162–73. doi:10.1016/j.jlp.2015.12.020.

[394] Tang KHD, Md Dawal SZ, Olugu EU. A review of the offshore oil and gas safety indices. Saf Sci 2018;109:344–52. doi:10.1016/j.ssci.2018.06.018.

[395] Edwards DW, Lawrence DW. Assessing the inherent safety of chemical process routes: is there a relation between plant costs and inherent safety? Trans IChemE 1993;71:252–8.

[396] Cave SR, Edwards DW. Chemical process route selection based on assessment of inherent environmental hazard. Comput Chem Eng 1997;21:S965–70. doi:10.1016/S0098-1354(97)87627-2.

[397] Heikkilä A-M. Inherent safety in process plant design. Espoo, Finland: VTT Publications n384; 1999.

[398] Gentile M, Rogers WJ, Mannan MS. Development of an inherent safety index based on fuzzy

logic. AIChE J 2003;49:959–68. doi:10.1002/aic.690490413.

[399] Mansfield D, Clark J, Malmén Y, Schabel J, Rogers R, Suokas E, et al. The INSET toolkit INherent SHE Evaluation Tool. 2001.

[400] Palaniappan C, Srinivasan R, Tan R. Expert System for the Design of Inherently Safer Processes. 1- Route Selection Stage. Ind Eng Chem Res 2002;41:6698–710.

[401] Palaniappan C, Srinivasan R, Tan RB. Expert System for the Design of Inherently Safer Processes. 2-Flowsheet Development Stage. Ind Eng Chem Res 2002;41:6711–22.

[402] Edwards DW, Lawrence DW. Assessing the inherent safety of chemical process routes: is there a relation between plant cost and inherent safety? Trans IChemE 1993;71:252–8.

[403] Koller G, Fischer U, Hungerbu K. Assessing Safety, Health, and Environmental Impact Early during Process Development. Ind Eng Chem Res 2000;39:960–72.

[404] AIChE. Dow's Fire and Explosion Index Classification Guide. 7th ed. New York: The American Institute of Chemical Engineers; 1994.

[405] AIChE. Dow's Chemical Exposure Index Guide. New York: The American Institute of Chemical Engineers; 1994.

[406] Doran P, Greig TR. The Mond Index: how to identify, assess and minimise potential hazards on chemical plant units for new and existing processes. 2nd ed. Northwich, UK: Imperial Chemical Industries PLC; 1993.

[407] Khan FI, Abbasi SA. Multivariate Hazard Identification and Ranking System. Process Saf Prog 1998;17:157–70. doi:10.1002/prs.680170303.

[408] Khan FI, Husain T, Abbasi SA. Safety Weighted Hazard Index (SWeHI). Process Saf Environ Prot 2001;79:65–80. doi:10.1205/09575820151095157.

[409] Khan FI, Amyotte PR. Integrated inherent safety index (I2SI): A tool for inherent safety evaluation. Process Saf Prog 2004;23:136–48. doi:10.1002/prs.10015.

[410] Khan FI, Amyotte PR. I2SI: A comprehensive quantitative tool for inherent safety and cost evaluation. J Loss Prev Process Ind 2005;18:310–26.

[411] Tugnoli A, Khan F, Amyotte P, Cozzani V. Safety assessment in plant layout design using indexing approach: Implementing inherent safety perspective. Part 1 - Guideword applicability and method description. J Hazard Mater 2008;160:100–9. doi:10.1016/j.jhazmat.2008.02.089.

[412] Tugnoli A, Khan F, Amyotte P, Cozzani V. Safety assessment in plant layout design using indexing approach: Implementing inherent safety perspective. Part 2-Domino Hazard Index and case study. J Hazard Mater 2008;160:110–21. doi:10.1016/j.jhazmat.2008.02.091.

[413] Mohd Shariff A, Rusli R, Leong CT, Radhakrishnan VR, Buang A. Inherent safety tool for explosion consequences study. J Loss Prev Process Ind 2006;19:409–18. doi:10.1016/j.jlp.2005.10.008.

[414] Leong CT, Shariff AM. Inherent safety index module (ISIM) to assess inherent safety level during preliminary design stage. Process Saf Environ Prot 2008;86:113–9. doi:10.1016/j.psep.2007.10.016.

[415] Heikkilä AM. Inherent safety in process plant design. An index-based approach. VTT Publ 1999.

[416] Leong CT, Shariff AM. Process route index (PRI) to assess level of explosiveness for inherent

safety quantification. J Loss Prev Process Ind 2009;22:216–21. doi:10.1016/j.jlp.2008.12.008.

[417] Shariff AM, Leong CT, Zaini D. Using process stream index (PSI) to assess inherent safety level during preliminary design stage. Saf Sci 2012;50:1098–103. doi:10.1016/j.ssci.2011.11.015.

[418] Li X, Zanwar A, Jayswal A, Lou HH, Huang Y. Incorporating exergy analysis and inherent safety analysis for sustainability assessment of biofuels. Ind Eng Chem Res 2011;50:2981–93. doi:10.1021/ie101660q.

[419] Gangadharan P, Singh R, Cheng F, Lou HH. Novel Methodology for Inherent Safety Assessment in the Process Design Stage. Ind Eng Chem Res 2013;52:5921–33. doi:10.1021/ie303163y.

[420] Srinivasan R, Nhan NT. A statistical approach for evaluating inherent benign-ness of chemical process routes in early design stages. Process Saf Environ Prot 2008;86:163–74. doi:10.1016/j.psep.2007.10.011.

[421] Jiao W, Shuguang X. Quantitative Safety and Health Assessment Based on Fuzzy Inference and AHP at Preliminary Design Stage. Iran J Chem Chem Eng 2016;35:153–65.

[422] Ahmad SI, Hashim H, Hassim MH. Numerical Descriptive Inherent Safety Technique (NuDIST) for inherent safety assessment in petrochemical industry. Process Saf Environ Prot 2014;92:379–89. doi:10.1016/j.psep.2014.03.009.

[423] Ahmad SI, Hashim H, Hassim MH. A graphical method for assessing inherent safety during research and development phase of process design. J Loss Prev Process Ind 2016;42:59–69. doi:10.1016/j.jlp.2015.09.018.

[424] Ahmad SI, Hashim H, Hassim MH. Inherent safety assessment technique for preliminary design stage. Chem Eng Trans 2017;56:1345–50. doi:10.3303/CET1756225.

[425] Tugnoli A, Cozzani V, Landucci G. A Consequence Based Approach to the Quantitative Assessment of Inherent Safety. AIChE J 2007;53:3171–82.

[426] Tugnoli A, Landucci G, Salzano E, Cozzani V. Supporting the selection of process and plant design options by Inherent Safety KPIs. J Loss Prev Process Ind 2012;25:830–42. doi:10.1016/j.jlp.2012.03.008.

[427] Rusli R, Shariff AM, Khan FI. Evaluating hazard conflicts using inherently safer design concept. Saf Sci 2013;53:61–72. doi:10.1016/j.ssci.2012.09.002.

[428] Rathnayaka S, Khan F, Amyotte P. Risk-based process plant design considering inherent safety. Saf Sci 2014;70:438–64. doi:10.1016/j.ssci.2014.06.004.

[429] Gentile M, Rogers WJ, Mannan MS. Development of a fuzzy logic-based inherent safety index. Process Saf Environ Prot 2003;81:444–56.

[430] Doran P, Greig TR. The Mond Index: How to Identify, Assess and Minimise Potential Hazards on Chemical Plants Units for New and Existing Processes. 2nd ed. Northwich, UK: Imperial Chemical Industries (ICI) PLC; 1993.

[431] Cozzani V, Tugnoli A, Salzano E. The development of an inherent safety approach to the prevention of domino accidents. Accid Anal Prev 2009;41:1216–27.

[432] Xin P, Khan F, Ahmed S. Layout Optimization of a Floating Liquefied Natural Gas Facility Using Inherent Safety Principles. J Offshore Mech Arct Eng 2016;138:041602. doi:10.1115/1.4033076.

[433] Crivellari A, Tugnoli A, Macini P, Cozzani V. Multi-criteria Indicators for the Inherent Safety Profile of Off-shore Oil & Gas Facilities. Proc. 13th Offshore Mediterr. Conf. Exhib., Ravenna, Italy: Offshore Mediterranean Conference (OMC); 2017.

[434] Crivellari A, Tugnoli A, Cozzani V, Macini P. Systematic methodology for inherent safety indicators assessment of early design stages of offshore oil & gas projects. Chem Eng Trans 2018;67:691–6. doi:10.3303/CET1867116.

[435] Wallace BP, Brosnan T, McLamb D, Rowles T, Ruder E, Schroeder B, et al. Effects of the Deepwater Horizon oil spill on protected marine species. Endanger Species Res 2017;33:1–7. doi:10.3354/esr00789.

[436] Beyer J, Trannum HC, Bakke T, Hodson P V., Collier TK. Environmental effects of the Deepwater Horizon oil spill: A review. Mar Pollut Bull 2016;110:28–51. doi:10.1016/j.marpolbul.2016.06.027.

[437] Clough JS, Blancher EC, Park RA, Milroy SP, Graham WM, Rakocinski CF, et al. Establishing nearshore marine injuries for the Deepwater Horizon natural resource damage assessment using AQUATOX. Ecol Modell 2017;359:258–68. doi:10.1016/j.ecolmodel.2017.05.028.

[438] Stout SA, Rouhani S, Liu B, Oehrig J, Ricker RW, Baker G, et al. Assessing the footprint and volume of oil deposited in deep-sea sediments following the Deepwater Horizon oil spill. Mar Pollut Bull 2017;114:327–42. doi:10.1016/j.marpolbul.2016.09.046.

[439] Guterman L. Exxon Valdez Turns 20. Science (80-) 2009;323:1558–9. doi:10.1126/science.323.5921.1558.

[440] Peterson CH, Rice SD, Short JW, Esler D, Bodkin JL, Ballachey BE, et al. Long-Term Ecosystem Response to the Exxon Valdez Oil Spill. Science (80-) 2003;302:2082–6. doi:10.1126/science.1084282.

[441] Reddy CM, Eglinton TI, Hounshell A, White HK, Xu L, Gaines RB, et al. The West Falmouth oil spill after thirty years: The persistence of petroleum hydrocarbons in marsh sediments. Environ Sci Technol 2002;36:4754–60. doi:10.1021/es020656n.

[442] White HK, Xu L, Lima ALC, Eglinton TI, Reddy CM. Abundance, composition, and vertical transport of PAHs in marsh sediments. Environ Sci Technol 2005;39:8273–80. doi:10.1021/es050475w.

[443] Culbertson JB, Valiela I, Peacock EE, Reddy CM, Carter A, VanderKruik R. Long-term biological effects of petroleum residues on fiddler crabs in salt marshes. Mar Pollut Bull 2007;54:955–62. doi:10.1016/j.marpolbul.2007.02.015.

[444] Culbertson JB, Valiela I, Pickart M, Peacock EE, Reddy CM. Long-term consequences of residual petroleum on salt marsh grass. J Appl Ecol 2008;45:1284–92. doi:10.1111/j.1365-2664.2008.01477.x.

[445] Culbertson JB, Valiela I, Olsen YS, Reddy CM. Effect of field exposure to 38-year-old residual petroleum hydrocarbons on growth, condition index, and filtration rate of the ribbed mussel, Geukensia demissa. Environ Pollut 2008;154:312–9. doi:10.1016/j.envpol.2007.10.008.

[446] Neuparth T, Moreira SM, Santos MM, Reis-Henriques MA. Review of oil and HNS accidental spills in Europe: Identifying major environmental monitoring gaps and drawing priorities. Mar Pollut Bull 2012;64:1085–95. doi:10.1016/j.marpolbul.2012.03.016.

[447] IMO, ITOPF, Cedre E. Are HNS Spills More Dangerous than Oil Spills? A White Paper for the Interspill 2009 Conference and the 4th IMO R&D Forum 2010:1–81.

[448] Law RJ, Kelly C, Matthiessen P, Aldridge J. The loss of the chemical tanker Ievoli Sun in the English Channel, October 2000. Mar Pollut Bull 2003;46:254–7. doi:10.1016/S0025-326X(02)00222-9.

[449] Häkkinen JM, Posti AI. Overview of maritime accidents involving chemicals worldwide and in the Baltic sea. Mar Navig Saf Sea Transp Marit Transp Shipp 2013:15–25.

[450] ISO. ISO 31000 Risk Management - Guidelines 2018.

[451] ITOPF. Fate of Marine Oil Spills. vol. Technical. London, UK: The International Tankers Owners Pollution Federation (ITOPF); 2011.

[452] Mamaca E, Girin M, Floch S le, Zir R el. Review of chemical spills at sea and lessons learnt. Interspill Conf 4th IMO R&D Forum 2009:40.

[453] Kleissen F, Arentz L, Reed M, Johansen O. Marine environmental risk assessment system: conceptual design and preliminary demonstration for he Dutch Continental Shelf. 2007. doi:10.1016/0001-4575(69)90002-5.

[454] Astiaso Garcia D, Bruschi D, Cumo F, Gugliermetti F. The Oil Spill Hazard Index (OSHI) elaboration. An oil spill hazard assessment concerning Italian hydrocarbons maritime traffic. Ocean Coast Manag 2013;80:1–11. doi:10.1016/j.ocecoaman.2013.03.016.

[455] Dongdong L, Bin L, Chenguang B, Minghui M, Yan X, Chunyan Y. Marine oil spill risk mapping for accidental pollution and its application in a coastal city. Mar Pollut Bull 2015;96:220–5. doi:10.1016/j.marpolbul.2015.05.023.

[456] Olita A, Cucco A, Simeone S, Ribotti A, Fazioli L, Sorgente B, et al. Oil spill hazard and risk assessment for the shorelines of a Mediterranean coastal archipelago. Ocean Coast Manag 2012;57:44–52. doi:10.1016/j.ocecoaman.2011.11.006.

[457] Liubartseva S, De Dominicis M, Oddo P, Coppini G, Pinardi N, Greggio N. Oil spill hazard from dispersal of oil along shipping lanes in the Southern Adriatic and Northern Ionian Seas. Mar Pollut Bull 2015;90:259–72. doi:10.1016/j.marpolbul.2014.10.039.

[458] Al Shami A, Harik G, Alameddine I, Bruschi D, Garcia DA, El-Fadel M. Risk assessment of oil spills along the Mediterranean coast: A sensitivity analysis of the choice of hazard quantification. Sci Total Environ 2017;574:234–45. doi:10.1016/j.scitotenv.2016.09.064.

[459] Marignani M, Bruschi D, Astiaso Garcia D, Frondoni R, Carli E, Pinna MS, et al. Identification and prioritization of areas with high environmental risk in Mediterranean coastal areas: A flexible approach. Sci Total Environ 2017;590–591:566–78. doi:10.1016/j.scitotenv.2017.02.221.

[460] Sepp Neves AA, Pinardi N, Martins F, Janeiro J, Samaras A, Zodiatis G, et al. Towards a common oil spill risk assessment framework - Adapting ISO 31000 and addressing uncertainties. J Environ Manage 2015;159:158–68. doi:10.1016/j.jenvman.2015.04.044.

[461] Melaku Canu D, Solidoro C, Bandelj V, Quattrocchi G, Sorgente R, Olita A, et al. Assessment of oil slick hazard and risk at vulnerable coastal sites. Mar Pollut Bull 2015;94:84–95. doi:10.1016/j.marpolbul.2015.03.006.

[462] Guo W. Development of a statistical oil spill model for risk assessment. Environ Pollut 2017;230:945–53. doi:10.1016/j.envpol.2017.07.051.

[463] Azevedo A, Fortunato AB, Epifânio B, den Boer S, Oliveira ER, Alves FL, et al. An oil risk management system based on high-resolution hazard and vulnerability calculations. Ocean

Coast Manag 2017;136:1–18. doi:10.1016/j.ocecoaman.2016.11.014.

[464] Gunasekera MY, Edwards DW. Chemical process route selection based upon the potential toxic impact on the aquatic, terrestrial and atmospheric environments. J Loss Prev Process Ind 2006;19:60–9. doi:10.1016/j.jlp.2005.06.002.

[465] DETR. Management of Harm to the Environment: Criteria for the Management of Unplanned Releases to the Environment: Criteria for Management. London, UK: Department of Environment, Transport and the Regions; 1998.

[466] DETR. Guidance on the Interpretation of Major Accident to the Environment for the Purposes of the COMAH Regulations. London, UK: Crown; 1999.

[467] Wilday AJ, Ali MW, Wu Y. Index method for cost-effective assessment of risk to the environment from accidental releases. Inst Chem Eng Symp Ser 1998:475–88.

[468] Johnsen S, Frost TK, Hjelsvold M, Utvik TR. The environmental impact factor - A proposed tool for produced water impact reduction, management and regulation. SPE Int. Conf. Heal. Saf. Environ. Oil Gas Explor. Prod., Stavanger, Norway: 2000.

[469] Rye H, Reed M, Durgut I, Kristin M. Documentation report for the revised DREAM model. Trondheim, Norway: 2006.

[470] Sabeur ZA, Tyler AO. Validation and application of the PROTEUS model for the physical dispersion, geochemistry and biological impacts of produced waters. Environ Model Softw 2004;19:717–26. doi:10.1016/j.envsoft.2003.08.006.

[471] Thatcher M, Robson M, Henriquez LR, Karman CC, Payne G. CHARM Chemical Hazard Assessment and Risk Management - User guide for the evaluation of chemicals used and discharged offshore 2005.

[472] Passenko J, Lessin G, Erichsen AC, Raudsepp U. Validation of hydrostatic and non-hydrostatic versions of the hydrodynamical model MIKE 3 applied for the Baltic Sea. Est J Eng 2008;14:255–70. doi:10.3176/eng.2008.3.05.

[473] Vries P De, Karman CC. Environmental Risk Assessment of Produced Water Discharges on the Dutch Continental Shelf. Amsterdam, The Netherlands: Institute for Marine Resources and Ecosystem Studies (IMARES); 2009.

[474] Boyce MP. An Overview of Gas Turbines. Gas Turbine Eng. Handb. 4th ed., Oxford, United Kingdom: Butterworth-Heinemann Elsevier Inc.; 2012. doi:10.1016/C2009-0-64242-2.

[475] Castello P, Tzimas E, Moretto P, Peteves SD. Techno-economic assessment of Hydrogen transmission & distribution systems in Europe in the medium and long term 2005.

[476] GPSA. Engineering Data Book. 11th ed. Gas Processors Suppliers Association (GPSA), Gas Processors Association; 1998.

[477] Babicz J. Wärtsilä Encyclopedia of Ship Technology. 2nd ed. Wartsila Corporation; 2015. doi:10.1007/978-1-4614-9610-6.

[478] Seider WD, Seader JD, Lewin DR, Widagolo S. Product and Process Design Principles - Synthesis, Analysis, and Evaluation. 3rd ed. Hoboken, New Jersey, USA: John Wiley & Sons, Inc.; 2009.

[479] Access Intelligence. The Chemical Engineering Plant Cost Index 2019. https://www.chemengonline.com/pci-home (accessed March 16, 2019).

[480] Eurostat. Handbook on industrial producer price indices (PPI). Luxembourg: Publications Office of the European Union; 2012. doi:10.2785/33730.

[481] The Crown Estate, Offshore Renewable Energy Catapult. Guide to an offshore wind farm - Updated and extended 2019.

[482] O'Connor M, Lewis T, Dalton G. Operational expenditure costs for wave energy projects and impacts on financial returns. Renew Energy 2013;50:1119–31. doi:10.1016/j.renene.2012.08.059.

[483] Szargut J. Appendix 1. Standard chemical exergy. Egzergia Porad. obliczania i Stosow., Gliwice, Poland: Wydawnictwo Politechniki Śląskiej; 2007. doi:https://doi.org/10.1017/CBO9780511976049.

[484] Belton V, Stewart T. Multiple criteria decision analysis: an integrated approach. Boston: Kluwer Academic Publishers; 2002.

[485] Rowley H V., Peters GM, Lundie S, Moore SJ. Aggregating sustainability indicators: Beyond the weighted sum. J Environ Manage 2012;111:24–33. doi:10.1016/j.jenvman.2012.05.004.

[486] Saaty TL. The analytic hierarchy process. New York: McGraw-Hill International Book Co; 1980.

[487] Hacatoglu K. A Systems Approach to Assessing the Sustainability of Hybrid Community Energy Systems. University of Ontario Institute of Technology, 2014.

[488] Abu-Rayash A, Dincer I. Sustainability assessment of energy systems: A novel integrated model. J Clean Prod 2019;212:1098–116. doi:10.1016/j.jclepro.2018.12.090.

[489] Talukder B, Hipel KW, vanLoon GW. Developing composite indicators for agricultural sustainability assessment: Effect of normalization and aggregation techniques. Resources 2017;6. doi:10.3390/resources6040066.

[490] Krejčí J, Stoklasa J. Aggregation in the analytic hierarchy process: Why weighted geometric mean should be used instead of weighted arithmetic mean. Expert Syst Appl 2018;114:97–106. doi:10.1016/j.eswa.2018.06.060.

[491] Fiigueira J, Mousseau V, Roy B. ELECTRE methods. Multi Criteria Decis. Anal. State Art Surv., New York, USA: Springer-Verlag New York; 2005, p. 113–62. doi:10.1007/b100605.

[492] J. P. Brans, Vincke P. A Preference Ranking Organisation Method: (The PROMETHEE Method for Multiple Criteria Decision-Making). Manage Sci 1985;31:647–56. doi:10.1017/CBO9781107415324.004.

[493] Roy B. Multicriteria Methodology for Decision Aiding. 1st ed. USA: Springer; 1996. doi:10.1007/978-1-4757-2500-1.

[494] Brans JP, De Smet Y. PROMETHEE methods. In: Greco S, Ehrgott M, Figueira JR, editors. Mult. Criteria Decis. Anal. State Art Surv. 2nd ed., New York, USA: Springer; 2005, p. 163–86. doi:10.1007/978-1-4939-3094-4_6.

[495] Figueira JR, Greco S, Roy B, Slowinski R. An overview of ELECTRE methods and their recent extensions. J Multi-Criteria Decis Anal 2013;20:61–85. doi:10.1002/mcda.1482.

[496] Roy B, Figueira JR, Almeida-Dias J. Discriminating thresholds as a tool to cope with imperfect knowledge in multiple criteria decision aiding: Theoretical results and practical issues. Omega (United Kingdom) 2014;43:9–20. doi:10.1016/j.omega.2013.05.003.

[497] Mareschal B. Visual PROMETHEE 1.4 2014. http://www.promethee-gaia.net/software.html (accessed November 10, 2018).

[498] Figueira J, Roy B. Determining the weights of criteria in the ELECTRE type methods with a revised Simos' procedure. Eur J Oper Res 2002;139:317–26. doi:10.1016/S0377-2217(01)00370-8.

[499] Reikard G. Integrating wave energy into the power grid: Simulation and forecasting. Ocean Eng 2013;73:168–78. doi:10.1016/j.oceaneng.2013.08.005.

[500] Kubik ML, Coker PJ, Hunt C. Using Meteorological Wind Data to Estimate Turbine Generation Output: A Sensitivity Analysis. Proc. World Renew. Energy Congr., vol. 57, Linköping, Sweden: 2011, p. 4074–81. doi:10.3384/ecp110574074.

[501] Danish Wind Industry Association. Roughness Classes and Roughness Length 2003. http://drømstørre.dk/wp-content/wind/miller/windpower web/en/stat/unitsw.htm#roughness (accessed August 26, 2019).

[502] ORECCA. ORECCA Project 2011. http://www.orecca.eu (accessed September 30, 2019).

[503] Morgan EC, Lackner M, Vogel RM, Baise LG. Probability distributions for offshore wind speeds. Energy Convers Manag 2011;52:15–26. doi:10.1016/j.enconman.2010.06.015.

[504] Indhumathy D, Seshaiah C V, Sukkiramathi K. Estimation of Weibull Parameters for wind speed calculation at Kanyakumari in India. Int J Innov Res Sci Eng Technol 2014;3:8340–5.

[505] L. Serri, T. Pontes, J. Murphy KL. Resource Data and GIS Tool For Offshore Renewable Energy Projects in Europe. 2012.

[506] Pecher A. Performance Evaluation of Wave Energy Converters 2012. doi:10.13052/rp-9788792982278.

[507] Chang W-Y. A Literature Review of Wind Forecasting Methods. J Power Energy Eng 2014;02:161–8. doi:10.4236/jpee.2014.24023.

[508] Mackenzie H, Dyson J. Short Term Forecasting of Wind Power Plant Generation for System Stability and Provision of Ancillary Services. 16th Int. Work. Large-Scale Integr. Wind Power into Power Syst. as well as Transm. Networks Offshore Wind Power Plants, Berlin, Germany: 2017.

[509] Reikard G, Robertson B, Bidlot JR. Wave energy worldwide: Simulating wave farms, forecasting, and calculating reserves. Int J Mar Energy 2017;17:156–85. doi:10.1016/j.ijome.2017.01.004.

[510] Reikard G, Robertson B, Bidlot JR. Combining wave energy with wind and solar: Short-term forecasting. Renew Energy 2015;81:442–56. doi:10.1016/j.renene.2015.03.032.

[511] Reikard G, Pinson P, Bidlot JR. Forecasting ocean wave energy: The ECMWF wave model and time series methods. Ocean Eng 2011;38:1089–99. doi:10.1016/j.oceaneng.2011.04.009.

[512] Pinson P, Reikard G, Bidlot JR. Probabilistic forecasting of the wave energy flux. Appl Energy 2012;93:364–70. doi:10.1016/j.apenergy.2011.12.040.

[513] International Electrotechnical Commission (IEC). Wind turbines - Part 1: Design requirements. 3rd ed. Geneva, Switzerland: 2008.

[514] Arrambide I, Zubia I, Madariaga A. Critical review of offshore wind turbine energy production and site potential assessment. Electr Power Syst Res 2019;167:39–47.

doi:10.1016/j.epsr.2018.10.016.

[515] Sohoni V, Gupta SC, Nema RK. A Critical Review on Wind Turbine Power Curve Modelling Techniques and Their Applications in Wind Based Energy Systems. J Energy 2016;2016:1–18. doi:10.1155/2016/8519785.

[516] Sedaghat A, Alkhatib F, Eilaghi A, Sabati M, Borvayeh L, Mostafaeipour A. A new strategy for wind turbine selection using optimization based on rated wind speed. Energy Procedia 2019;160:582–9. doi:10.1016/j.egypro.2019.02.209.

[517] PelaFlow Consulting. WindPower Program 2019. http://www.wind-power-program.com/ (accessed August 27, 2019).

[518] Babarit A, Hals J, Muliawan MJ, Kurniawan A, Moan T, Krokstad J. Numerical benchmarking study of a selection of wave energy converters. Renew Energy 2012;41:44–63. doi:10.1016/j.renene.2011.10.002.

[519] Silva D, Rusu E, Soares CG. Evaluation of various technologies for wave energy conversion in the portuguese nearshore. Energies 2013;6:1344–64. doi:10.3390/en6031344.

[520] Chozsa JF, Kofoed JP, Jensen NEH. User guide – COE Calculation tool for Wave Energy Converters 2014.

[521] Zanuttigh B, Angelelli E, Bellotti G, Romano A, Krontira Y, Troianos D, et al. Boosting blue growth in a mild sea: Analysis of the synergies produced by a multi-purpose offshore installation in the Northern Adriatic, Italy. Sustainability 2015;7:6804–53. doi:10.3390/su7066804.

[522] Petersen H. Simplified Laws of Similarity for Wind Turbine Rotors 1984.

[523] Van Treuren KW, Burdett TA. Experimental Testing of Wind Turbines Using Wind Tunnels With an Emphasis on Small-Scale Wind Turbines Under Low Reynolds Numbers. WIT Trans. State Art Sci. Eng., vol. 81, Ashurst, UK: WIT Press; 2014, p. 67–110. doi:10.2495/978-1-78466-004-8/004.

[524] Sieros G, Chaviaropoulos P, Sørensen JD, Bulder BH, Jamieson P. Upscaling wind turbines: theoretical and practical aspects and their impact on the cost of energy. Wind Energy 2012;15:3–17. doi:10.1002/we.527.

[525] Hughes SA. Advanced Series on Ocean Engineering: Volume 7 - Physical Models and Laboratory Techniques in Coastal Engineering. World Scientific Publishing Co Pte Ltd; 1993. doi:10.1142/asoe10.1142/2154.

[526] de Andres A, Maillet J, Todalshaug JH, Möller P, Bould D, Jeffrey H. Techno-economic related metrics for a wave energy converters feasibility assessment. Sustain 2016;8. doi:10.3390/su8111109.

[527] O'Connor M, Lewis T, Dalton G. Techno-economic performance of the Pelamis P1 and Wavestar at different ratings and various locations in Europe. Renew Energy 2013;50:889–900. doi:10.1016/j.renene.2012.08.009.

[528] Grueger F, Möhrke F, Robinius M, Stolten D. Early power to gas applications: Reducing wind farm forecast errors and providing secondary control reserve. Appl Energy 2017;192:551–62. doi:10.1016/j.apenergy.2016.06.131.

[529] MathWave Technologies. EasyFit software 2014. http://www.mathwave.com/ (accessed August 26, 2019).

[530] Capstone Turbine Corporation. Capstone microturbines 2019. https://www.capstoneturbine.com/ (accessed August 24, 2019).

[531] Barelli L, Ottaviano A. Supercharged gas turbine combined cycle: An improvement in plant flexibility and efficiency. Energy 2015;81:615–26. doi:10.1016/j.energy.2015.01.004.

[532] Liu Z, Karimi IA. Simulation and optimization of a combined cycle gas turbine power plant under part-load operation. Comput Aided Chem Eng 2018;44:2401–6. doi:10.1016/B978-0-444-64241-7.50395-5.

[533] Trapani K, Millar DL. Proposing offshore photovoltaic (PV) technology to the energy mix of the Maltese islands. Energy Convers Manag 2013;67:18–26. doi:10.1016/j.enconman.2012.10.022.

[534] Kim TS. Comparative analysis on the part load performance of combined cycle plants considering design performance and power control strategy. Energy 2004;29:71–85. doi:10.1016/S0360-5442(03)00157-9.

[535] Li Y, Zhang G, Bai Z, Song X, Wang L, Yang Y. Backpressure adjustable gas turbine cycle: A method to improve part-load efficiency. Energy Convers Manag 2018;174:739–54. doi:10.1016/j.enconman.2018.07.077.

[536] U.S. Environmental Protection Agency. Greenhouse Gas (GHG) Verification Guideline Series: Natural Gas-Fired Microturbine Electrical Generators 2002.

[537] U.S. Department of Energy. Combined Heat and Power Technology Factsheet Series: Gas Turbines 2016:1–4.

[538] World Bank Group. Report of the High-Level Commission on Carbon Prices 2017:1–69.

[539] World Bank, Ecofys. State and Trends of Carbon Pricing 2018. Washington DC, USA: International Bank for Reconstruction and Development - The World Bank; 2018. doi:10.1596/978-1-4648-1292-7.

[540] IEA, NEA. Projected Costs of Generating Electricity 2015:1–215.

[541] Morris M, Miles A, Cooper J. Quantification of escalation effects in offshore quantitative risk assessment. J Loss Prev Process Ind 1994;7:337–44.

[542] Vinnem J-E. Offshore Risk Assessment - Principles, modelling and application of QRA studies. vol. 2. 3rd ed. London, United Kingdom: Springer Series in Reliability Engineering; 2014.

[543] British Petroleum (BP). Environmental & Socio-economic Impact Assessment. 2002.

[544] ITOPF. Effects of oil pollution on the marine environment 2011:1–12.

[545] IPIECA. Biological impacts of oil pollution: sedimentary shores. IPIECA Rep Ser 1999;9:1–24.

[546] IPIECA-IOGP. Impacts of oil spills on shorelines. vol. IOGP Repor. London, UK: International Petroleum Industry Environmental Conservation Association (IPIECA), International Association of Oil & Gas Producers (IOGP); 2016.

[547] The Netherlands Organization of Applied Scientific Research (TNO). Methods for the determination of possible damage to people and objects resulting from releases of hazardous materials (Green Book). Voorburg, The Netherlands: 1992.

[548] Christou M, Amendola A, Smeder M. The control of major accident hazards: The land-use

planning issue. J Hazard Mater 1999;65:151–78.

[549] Mannan S. Lees' Loss Prevention in the Process Industries. 3rd ed. Oxford, UK: Elsevier; 2005.

[550] Planas E, Arnaldos J, Silvetti B, Vallée A, Casal J. A Risk Severity Index for industrial plants and sites. J Hazard Mater 2006;130:242–50.

[551] Cozzani V, Gubinelli G, Salzano E. Escalation thresholds in the assessment of domino accidental events. J Hazard Mater 2006;129:1–21. doi:10.1016/j.jhazmat.2005.08.012.

[552] Cozzani V, Tugnoli A, Salzano E. Prevention of domino effect: From active and passive strategies to inherently safer design. J Hazard Mater 2007;139:209–19. doi:10.1016/j.jhazmat.2006.06.041.

[553] American Petroleum Institute (API). Recommended Practice for the Design of Offshore Facilities Against Fire and Blast Loading. 2006.

[554] Norwegian Oil and Gas Association. EIF Computanional Guidelines - A Manual for Standardised Modelling and Determination of the Environmental Impact Factor (EIF). 2003.

[555] French-McCay D. State-of-the-Art and Research Needs for Oil Spill Impact Assessment Modeling. 32nd AMOP Tech. Semin. Environ. Contam. Response, Ottawa, Canada: 2009, p. 601–53.

[556] European Parliament and the Council of the European Union. Directive establishing a framework for community action in the field of marine environmental policy (Marine Strategy Framework Directive). 2008.

[557] Law R, Hanke G, Batty J, Bignert A, Dachs J, Davies I, et al. Marine Strategy Framework Directive Task Group 8 Report Contaminants and pollutions effects. 2010. doi:10.2788/85887.

[558] Petroleum Safety Authority Norway. Regulations relating to health, safety and the environment in the petroleum activities and at certain onshore facilities (the framework regulations). 2016.

[559] UK Government. Petroleum Act 1987 Chapter 12. 1987.

[560] Step Change in Safety. Marine Operations: 500 m Safety Zone. 2017.

[561] Spouge J. A Guide To Quantitative Risk Assessment for Offshore Installations Principal Author. Cebtre for Marine and Petroleum Technology (CMPT); 1999.

[562] International Organization for Standardization (ISO). Petroleum and Natural Gas Industries - Offshore Production Installations - Guidelines on Tools and Techniques for Hazard Identification and Risk Assessments. ISO Stand 2000.

[563] American Petroleum Institute (API). Recommended Practice for Design and Hazards Analysis for Offshore Production Facilities 2001.

[564] American Petroleum Institute (API). Recommended Practice for Development of a Safety and Environmental Management Program for Offshore Operations and Facilities 2004.

[565] Health and Safety Executive (HSE). Guidance on Risk Assessment for Offshore Installations. 2006.

[566] American Petroleum Institute (API). Risk-based inspection base resource document 2000.

[567] Delvosalle C, Fievez C, Pipart A, Debray B. ARAMIS project: A comprehensive methodology

for the identification of reference accident scenarios in process industries. J Hazard Mater 2006;130:200–19. doi:10.1016/j.jhazmat.2005.07.005.

[568] Uijt de Haag PAM, Ale BJM. Guidelines for quantitative risk assessment (purple book). 1rst ed. The Hague, Netherlands: Commitee for the Prevention of Disasters; 2005.

[569] Lees F. Lees' Loss Prevention in the Process Industries. 4th ed. Oxford, UK: Butterworth-Heinemann; 2012.

[570] Advanced Mechanics & Engineering (AME). PARLOC 92 The update of loss of containment data for offshore pipelines. 1993.

[571] Holand P. Blowout and Well Release Characteristics and Frequencies. Trondheim, Norway: 2006. doi:10.1017/CBO9781107415324.004.

[572] Health and Safety Executive (HSE). Failure rate and event data for use within risk assessments. Health & Safety Executive Offshore Safety Division; 2012.

[573] Det Norske Veritas (DNV) AS. Failure frequency guidance - Process equipment leak frequency data for use in QRA. 2013.

[574] OREDA Participants. Offshore and Onshore Reliability Data - Vol. 1 Topside equipment. 6th ed. Høvik, Norway: Det Norske Veritas AS; 2015.

[575] OREDA Participants. Offshore and Onshore Reliability Data - Vol. 2 Subsea equipment. 6th ed. Høvik, Norway: Det Norske Veritas AS; 2015.

[576] International Association of Oil & Gas Producers (IOGP). Blowout frequencies. 2010.

[577] International Association of Oil & Gas Producers (IOGP). Process Release Frequencies. 2010.

[578] International Association of Oil & Gas Producers (IOGP). Storage incident frequencies. 2010.

[579] International Association of Oil & Gas Producers (IOGP). Riser & pipeline release frequencies. 2010.

[580] Milgram JH, Burgess JJ. Measurements of the surface flow above round bubble plumes. Appl Ocean Res 1984;6:40–4.

[581] Olsen JE, Skjetne P. Current understanding of subsea gas release: A review. Can J Chem Eng 2016;94:209–19. doi:10.1002/cjce.22345.

[582] van den Bosch CJH, Weterings RAPM. Methods for the calculation of physical effects due to releases of hazardous materials (liquids and gases) (yellow book). 3rd ed. The Hague, Netherlands: Commitee for the Prevention of Disasters; 2005.

[583] Fanneløp TK, Ryhming IL. Massive Release of Gas from Long Pipelines. J Energy 1982;6:132–40.

[584] Bettelini MSG, Fannelep TK. Underwater plume from an instantaneously started source. Appl Ocean Res 1993;15:195–206.

[585] Rew PJ, Gallagher P, Deaves DM. Dispersion of subsea releases - Review of Prediction Methodologies. 1995.

[586] Johansen Ø. DeepBlow ± a Lagrangian Plume Model for Deep Water Blowouts. Spill Sci Technol Bull 2000;6:103–11.

[587] Chen FH, Yapa PD. A model for simulating deepwater oil and gas blowouts - Part II: Comparison of numerical simulations with "deepspill" field experiments. J Hydraul Res

2003;41(4):353–65. doi:10.1080/00221680309499981.

[588] Nazir M, Khan F, Amyotte P, Sadiq R. Subsea Release of Oil from a Riser: An Ecological Risk Assessment. Risk Anal 2008;28:1173–95. doi:10.1111/j.1539-6924.2008.01136.x.

[589] Dasanayaka LK, Yapa PD. Role of plume dynamics phase in a deepwater oil and gas release model. J Hydro-Environment Res 2009;2:243–53. doi:10.1016/j.jher.2009.01.004.

[590] Abubakr-bibilazu A, Andrawus J a, Adom E, Steel J a, Brikinns T. Numerical Modelling of Subsea Multiphase Plumes : An Eularian Integral Approach. Engineering 2010;II:2–6.

[591] Zhao L, Boufadel MC, Socolofsky SA, Adams E, King T, Lee K. Evolution of droplets in subsea oil and gas blowouts : Development and validation of the numerical model VDROP-J. Mar Pollut Bull 2014;83:58–69. doi:10.1016/j.marpolbul.2014.04.020.

[592] DNV GL. Process hazard analysis software (PHAST) 2019. https://www.dnvgl.com/services/process-hazard-analysis-software-phast-1675 (accessed September 4, 2019).

[593] EPA. ALOHA Software 2019. https://www.epa.gov/cameo/aloha-software (accessed September 4, 2019).

[594] NOAA. Automated Data Inquiry for Oil Spills (ADIOS) Software 2019. https://response.restoration.noaa.gov/oil-and-chemical-spills/oil-spills/response-tools/adios.html (accessed September 4, 2019).

[595] NOAA. General NOAA Operational Modeling Environment (GNOME) Software 2019. https://response.restoration.noaa.gov/oil-and-chemical-spills/oil-spills/response-tools/gnome.html (accessed September 4, 2019).

[596] SINTEF. Oil Spill Contingency and Response (OSCAR) 2019. https://www.sintef.no/en/software/oscar/ (accessed September 4, 2019).

[597] SINTEF. Oil Weathering Model (OWM) User's Manual, version 10.0.0 2019.

[598] European Commission. Annex G: Technology readiness levels (TRL). 2014.

[599] Smith R. Chemical Process Design and Integration. Chichester, UK: John Wiley & Sons, Ltd; 2005.

[600] Shilling RL, Bernhagen PM, Goldschmidt VM, Hrnjak PS, Johnson D, Timmerhaus KD. Heat-Transfer Equipment. Perry's Chem. Eng. Handb. 8th ed., The McGraw-Hil Companies; 2008. doi:10.1036/0071511342.

[601] Doherty MF, Fidkowski ZT, Malone MF, Taylor R. Distillation. Perry's Chem. Eng. Handb. 8th ed., The McGraw-Hil Companies; 2008. doi:10.1036/0071511369.

[602] Reay D, Ramshaw C, Harvey A. Process Intensification - Engineering for Efficiency, Sustainability and Flexibility. 2nd ed. Oxford, UK: Elsevier Butterworth-Heinemann; 2013.

[603] Tian Y, Demirel SE, Hasan MMF, Pistikopoulos EN. An overview of process systems engineering approaches for process intensification: State of the art. Chem Eng Process - Process Intensif 2018;133:160–210. doi:10.1016/j.cep.2018.07.014.

[604] Douglas JM. Conceptual design of chemical processes. 1st ed. Singapore, Malaysia: McGraw-Hill Book Company; 1988.

[605] Aspen Technology. AspenTech tool products 2019. https://www.aspentech.com/en/products/engineering/engineering (accessed September 7,

2019).

[606] Chemstations. Chemcad software 2019. https://www.chemstations.com/CHEMCAD/ (accessed September 7, 2019).

[607] Aveva. PRO/II Process Engineering software 2019. https://sw.aveva.com/engineer-procure-construct/process-engineering-and-simulation (accessed September 7, 2019).

[608] Perry RH, Green DW. Perry´s Chemical Engineers´Handbook. 2008. doi:10.1036/0071511334.

[609] Kern DQ. Process Heat Transfer. Tokyo, Japan: McGraw-Hill International Book Company; 1965.

[610] R. K. Sinnott. Chemical Engineering Design. Coulson Richardson's Chem. Eng., vol. 6. 4th ed., Oxford, UK: Elsevier Butterworth-Heinemann; 2005.

[611] Ulrich GD. A Guide to Chemical Engineering Process Design and Economics. Hoboken, New Jersey, USA: John Wiley & Sons; 1984.

[612] Zlokarnik M. Scale-up in chemical engineering. 2nd ed. Weinheim, Germany: Wiley-VCH Verlag GmbH & Co. KGaA; 2006.

[613] Nauman EB. Chemical Reactor Design, Optimization, and Scaleup. 2nd ed. Hoboken, New Jersey, USA: John Wiley & Sons; 2008. doi:10.1002/9780470282076.

[614] Sulaymon AH, Abbar AH. Scale-Up of Electrochemical Reactors. Electrolysis, Rijeka, Croatia: InTech; 2012. doi:10.5772/48728.

[615] Lim MT, Shah Zulkifli AZ, Jayapalan KK, Chin O. Development of a dimensionless parameter for characterization of dielectric barrier discharge devices with respect to geometrical features. Plasma Sci Technol 2017;19. doi:10.1088/2058-6272/aa7382.

[616] Mukherjee PS, Ray AK. Major challenges in the design of a large-scale photocatalytic reactor for water treatment. Chem Eng Technol 1999;22:253–60. doi:10.1002/(SICI)1521-4125(199903)22:3<253::AID-CEAT253>3.0.CO;2-X.

[617] Stankiewicz AI, Moulijn JA. Process intensification: Transforming chemical engineering. Chem Eng Prog 2000;96:22–33.

[618] Siddiqui O, Dincer I. Analysis and performance assessment of a new solar-based multigeneration system integrated with ammonia fuel cell and solid oxide fuel cell-gas turbine combined cycle. J Power Sources 2017;370:138–54. doi:10.1016/j.jpowsour.2017.10.008.

[619] Ahmadi P, Dincer I. Exergoeconomics. Compr. Energy Syst. 1rst ed., Amsterdam, Netherlands: Elsevier Inc.; 2018, p. 340–76. doi:10.1016/B978-0-12-809597-3.00107-3.

[620] Chitsaz A, Mehr AS, Mahmoudi SMS. Exergoeconomic analysis of a trigeneration system driven by a solid oxide fuel cell. Energy Convers Manag 2015;106:921–31. doi:10.1016/j.enconman.2015.10.009.

[621] Ozbilen A, Dincer I, Rosen MA. Development of a four-step Cu-Cl cycle for hydrogen production - Part I: Exergoeconomic and exergoenvironmental analyses. Int J Hydrogen Energy 2016;41:7814–25. doi:10.1016/j.ijhydene.2015.12.184.

[622] Blumberg T, Lee YD, Morosuk T, Tsatsaronis G. Exergoenvironmental analysis of methanol production by steam reforming and autothermal reforming of natural gas. Energy 2019;181:1273–84. doi:10.1016/j.energy.2019.05.171.

[623] D. M. Hamby. A Review of Techniques for Parameter Sensitivity Analysis of Environmental Models. Environ Monit Assess 1994;32:135–54.

[624] Heijungs R, Kleijn R. Numerical approaches towards life cycle interpretation. Int J Life Cycle Assess 2001;6:141–8.

[625] Metropolis N, Ulam S. The Monte Carlo Method. J Am Stat Assoc 1949;44:335–41.

[626] Norwegian Petroleum. The oil and gas pipeline system 2019. https://www.norskpetroleum.no/en/production-and-exports/the-oil-and-gas-pipeline-system/ (accessed April 20, 2019).

[627] Gassco. Langeled pipeline 2019. https://www.gassco.no/en/our-activities/pipelines-and-platforms/langeled/ (accessed April 20, 2019).

[628] Equinor ASA. Hywind 2019. https://www.equinor.com/en/what-we-do/hywind-where-the-wind-takes-us.html (accessed April 20, 2019).

[629] Myhr A, Bjerkseter C, Ågotnes A, Nygaard TA. Levelised cost of energy for offshore floating wind turbines in a lifecycle perspective. Renew Energy 2014;66:714–28. doi:10.1016/j.renene.2014.01.017.

[630] Eurostat. Wholesale price of natural gas 2019. http://ec.europa.eu/eurostat/statistics-explained/index.php/Natural_gas_price_statistics (accessed April 20, 2019).

[631] Tractebel, Hinicio. Study on Early Business Cases for H2 in Energy Storage and More Broadly Power To H2 Applications 2017.

[632] Methanex Corporation. Wholesale price of methanol 2019. http://www.methanex.com/ (accessed April 20, 2019).

[633] OfGem. Non-Domestic RHI tariff table n.d.

[634] Worl Bank Group, Ecofys. State and Trends of Carbon Pricing 2018. Washington DC: 2018. doi:10.1596/978-1-4648-1292-7.

[635] Fraile D, Torres A, Rangel A, Barth F, Lanoix J-C, Vanhoudt W. Generic estimation scenarios of market penetration and demand forecast for “premium” green hydrogen in short, mid and long term 2016.

[636] Siemens. SILYZER 200 High-pressure efficiency in the megawatt range 2019.

[637] OfGem. Renewable Obligation 2019. https://www.ofgem.gov.uk/ro (accessed April 20, 2019).

[638] OfGem. Guidance for generators that receive or would like to receive support under the Renewables Obligation (RO) scheme 2019.

[639] OfGem. Wholesale Market Indicators 2019. https://www.ofgem.gov.uk/data-portal/wholesale-market-indicators (accessed April 20, 2019).

[640] OfGem. Renewables Obligation Late Payment Distribution 2017-2018 2019. https://www.ofgem.gov.uk/publications-and-updates/renewables-obligation-late-payment-distribution-2017-2018 (accessed April 20, 2019).

[641] Mathworks. MATLAB R2019b 2019. https://uk.mathworks.com/ (accessed September 13, 2019).

[642] Dal Pozzo A, Guglielmi D, Antonioni G, Tugnoli A. Sustainability analysis of dry treatment technologies for acid gas removal in waste-to-energy plants. J Clean Prod 2017;162:1061–74.

doi:10.1016/j.jclepro.2017.05.203.

[643] Lee B, Heo J, Heon N, Moon C, Moon S, Lim H. Economic evaluation with uncertainty analysis using a Monte-Carlo simulation method for hydrogen production from high pressure PEM water electrolysis in Korea. Int J Hydrogen Energy 2017;42:24612–9. doi:10.1016/j.ijhydene.2017.08.033.

[644] James R, Ros MC. Floating Offshore Wind: Market and Technology Review. 2015.

[645] Ruijgrok ECM, Druten EJ van, Bulder BH. Cost Evaluation of North Sea Offshore Wind Post 2030. 2019.

[646] OfGem. Non-Domestic RHI tariff table n.d. https://www.ofgem.gov.uk/publications-and-updates/non-domestic-rhi-tariff-table (accessed July 10, 2019).

[647] Lee B, Chae H, Choi NH, Moon C, Moon S, Lim H. Economic evaluation with sensitivity and profitability analysis for hydrogen production from water electrolysis in Korea. Int J Hydrogen Energy 2017;42:6462–71. doi:10.1016/j.ijhydene.2016.12.153.

[648] DGS-UNMIG. Italian Ministry of Economic Development - Georesources Office 2019. https://unmig.mise.gov.it/index.php/it/ (accessed September 27, 2019).

[649] Terna. Italian Transmission System Operator Terna 2019. https://www.terna.it/en (accessed September 27, 2019).

[650] Justus CG, Hargraves WR, Mikhail A, Graber D. Methods for estimating wind speed frequency distributions. J Appl Meteorol 1978;17:350–3.

[651] ECMWF. ERA5 Dataset Copernicus 2019. https://cds.climate.copernicus.eu/ (accessed September 27, 2019).

[652] ECMWF. ERA5 data Documentation 2019. https://confluence.ecmwf.int/display/CKB/ERA5+data+documentation (accessed September 27, 2019).

[653] Nordex SE. Nordex N90/2500 Offshore Datasheet 2019. http://www.nordex-online.com/en/produkte-service/wind-turbines/n90-25-mw/product-data-sheet-n90-25mw.html?no_cache=1 (accessed September 27, 2019).

[654] AEEG. Allegato A Condizioni per l'erogazione del pubblico servizio di dispacciamento dell'energia elettrica sul territorio nazionale per l'approvigionamento delle relative risorse su base di merito economico, ai sensi degli Articoli 3 e 5 del Decreto Legislati 2019:1–123.

[655] Ministero dello Sviluppo Economico. Decreto 23 Giugno 2016 Incentivazione dell'energia elettrica prodotta da fonti rinnovabii diverse dal fotovoltaico. 2016.

[656] GSE. Italian Energy Services Operator GSE n.d. https://www.gse.it/ (accessed September 30, 2019).

[657] Siemens. Gas Turbines from 4 to 567 MW Datasheets 2019.

[658] Olson A, Nick S, Kush P, Gabe K. Capital Cost Review of Power Generation Technologies 2014:1–105.

[659] OECD. Yearly producer price indices (total market) 2018. https://data.oecd.org/price/producer-price-indices-ppi.htm (accessed April 18, 2019).

[660] IRENA. Renewable Power Generation Costs in 2018. Abu Dhabi, UAE: International Renewable Energy Agency (IRENA); 2019.

[661] EIA. Levelized Cost and Levelized Avoided Cost of New Generation Resources in the Annual Energy Outlook 2019 2019:1–25.

[662] Camilla Thomson, Harrison GP. Life Cycle Costs and Carbon Emissions of Offshore Wind Power 2015.

[663] Mansfield D, Poulter L, Kletz TA. Improving Inherent Safety. vol. OTH96 521. London, UK: Health & Safety Executive; 1996. doi:ISBN 0-7176-1307-0.

[664] Khan FI, Amyotte PR. Inherent safety in offshore oil and gas activities: A review of the present status and future directions. J Loss Prev Process Ind 2002;15:279–89. doi:10.1016/S0950-4230(02)00009-8.

[665] Katalinić M, Ćorak M, Parunov J. Analysis of wave heights and wind speeds in the Adriatic Sea. In: Guedes Soares S, Santos TA, editors. Marit. Technol. Eng. Vol. 1, London, UK: CRC Press Taylor & Francis Group; 2015, p. 1389–94.

[666] Russo A, Carniel S, Sclavo M, Krzelj M. Climatology of the Northern-Central Adriatic Sea. In: Wang S-Y, editor. Mod. Climatol., InTech; 2012, p. 177–212.

[667] DNV GL. Process hazard analysis software (PHAST) 2019.

[668] Schacher GE, Speil DE, Davidson KL, Fairall CW. Comparison of Overwater Stability Classification Schemes with Measured Wind Direction Variability. Monterey, California, USA: 1982.

[669] Kinsella KG. A rapid assessment methodlogy for the prediction of vapour cloud explosion overpressure. Int. Conf. Exhib. Safety, Heal. Loss Prev. Oil, Chem. Process Ind. Singapore 15-19 Febr., Butterworth-Heinemann; 1993, p. 200–11.

[670] Raman R, Grillo P. Minimizing uncertainty in vapour cloud explosion modelling. Process Saf Environ Prot 2005;83:298–306. doi:10.1205/psep.05028.

[671] Centers for Disease Control and Prevention. CDC NIOSH Website 2019. https://www.cdc.gov/niosh/ (accessed September 17, 2019).

[672] Chakraborty S, Yeh C-H. A Simulation Based Comparative Study of Normalization Procedures in Multiattribute Decision Making. Proc. 6th WSEAS Int. Conf. Artif. Intell. Knowl. Eng. Data Bases, Corfu Island, Greece: 2007, p. 102–9.

[673] Zakaria Z, Kamarudin SK. Direct conversion technologies of methane to methanol: An overview. Renew Sustain Energy Rev 2016;65:250–61. doi:10.1016/j.rser.2016.05.082.

[674] Albo J, Sáez A, Solla-Gullón J, Montiel V, Irabien A. Production of methanol from CO2 electroreduction at Cu2O and Cu2O/ZnO-based electrodes in aqueous solution. Appl Catal B Environ 2015;176–177:709–17. doi:10.1016/j.apcatb.2015.04.055.

[675] Yarlagadda PS, Morton LA, Hunter NR, Gesser HD. Direct conversion of methane to methanol in a flow reactor. Ind Eng Chem Res 1988;27:252–6. doi:10.1021/ie00074a008.

[676] Xu J, Armstrong RD, Shaw G, Dummer NF, Freakley SJ, Taylor SH, et al. Continuous selective oxidation of methane to methanol over Cu- and Fe-modified ZSM-5 catalysts in a flow reactor. Catal Today 2016;270:93–100. doi:10.1016/j.cattod.2015.09.011.

[677] Williams GR. Liquid phase catalytic partial oxidation of methane. University of Bath, 2002.

[678] Ghaz-Jahanian MA, Khoshfetrat AB, Hosseinian Rostami M, Haghighi M. An innovative bioprocess for methane conversion to methanol using an efficient methane transfer chamber

coupled with an airlift bioreactor. Chem Eng Res Des 2018;134:80–9. doi:10.1016/j.cherd.2018.03.039.

[679] Mahammadunnisa S, Krushnamurty K, Subrahmanyam C. Catalytic nonthermal plasma assisted co-processing of methane and nitrous oxide for methanol production. Catal Today 2015;256:102–7. doi:10.1016/j.cattod.2015.03.011.

[680] Villa K, Murcia-lópez S, Andreu T, Ramón J. Mesoporous WO3 photocatalyst for the partial oxidation of methane to methanol using electron scavengers. Appl Catal B, Environ 2015;163:150–5. doi:10.1016/j.apcatb.2014.07.055.

[681] Lee JH, Foster NR. Direct partial oxidation of methane to methanol in supercritical water. J Supercrit Fluids 1996;9:99–105. doi:10.1016/S0896-8446(96)90004-2.

[682] Lee B, Hibino T. Efficient and selective formation of methanol from methane in a fuel cell-type reactor. J Catal 2011;279:233–40. doi:10.1016/j.jcat.2010.12.020.

[683] Rocha RS, Reis RM, Lanza MR V, Bertazzoli R. Electrosynthesis of methanol from methane: The role of V2O 5 in the reaction selectivity for methanol of a TiO 2/RuO2/V2O5 gas diffusion electrode. Electrochim Acta 2013;87:606–10. doi:10.1016/j.electacta.2012.09.113.

[684] Aspen Technology. AspenTech tool products 2019.

[685] Toth AJ, Mizsey P. Methanol removal from aqueous mixture with organophilic pervaporation: Experiments and modelling. Chem Eng Res Des 2015;98:123–35. doi:10.1016/j.cherd.2015.04.031.

[686] Guerreri G, Rase HF. Progettazione di impianti industriali chimici e alimentari - Volume primo. 2nd ed. Santarcangelo Di Romagna, Italy: Maggioli S.p.A.; 2007.

[687] Advanced Plasma Solutions. Dielectric barrier discharge (DBD) power supply 2019. https://www.advancedplasmasolutions.com/products/ dielectric-barrier-discharge-dbd-pulsed-power-system/ (accessed September 23, 2019).

[688] Access Intelligence. 2019 Chemical Engineering Plant Cost Index (CEPCI) updates 2019. https://www.chemengonline.com/2019-cepci-updates-june-prelim-and-may-final/ (accessed September 25, 2019).

[689] IEAGHG. Techno-Economic Evaluation of HYCO Plant Integrated to Ammonia/Urea or Methanol Production with CCS. vol. 03. IEA Environmental Projects (IEAGHG); 2017.

[690] Access Intelligence. The Chemical Engineering Plant Cost Index 2019. https://www.chemengonline.com/ (accessed May 3, 2019).

[691] ExxonMobil Canada. Offshore Sable Project 2018. http://soep.com/ (accessed November 10, 2018).

[692] Crivellari A, Cozzani V, Dincer I. Exergetic and exergoeconomic analyses of novel methanol synthesis processes driven by offshore renewable energies. Energy 2019;187:1–13. doi:10.1016/j.energy.2019.115947.

[693] NREL, HOMER Energy. Homer Pro Software 2018. https://www.homerenergy.com/products/pro/index.html (accessed December 1, 2018).

[694] NREL. SAM Software 2018. https://sam.nrel.gov/ (accessed December 1, 2018).

[695] Wagner MJ, Gilman P, Wagner MJ, Gilman P. Technical Manual for the SAM Physical Trough Model. 2011.

[696] Lazzaretto A, Tsatsaronis G. SPECO: A systematic and general methodology for calculating efficiencies and costs in thermal systems. Energy 2006;31:1257–89. doi:10.1016/j.energy.2005.03.011.

[697] Lenntech. Seawater desalination units - Large capacity packages Datasheet 2018.

[698] Siemens. Silyzer 300 Datasheet 2018.

[699] Bellotti D, Rivarolo M, Magistri L, Massardo AF. Feasibility study of methanol production plant from hydrogen and captured carbon dioxide. J CO2 Util 2017;21:132–8. doi:10.1016/j.jcou.2017.07.001.

[700] FCH JU. Commercialisation of energy storage in Europe. 2015.

[701] Yang C, Ogden J. Determining the lowest-cost hydrogen delivery mode. Int J Hydrogen Energy 2007;32:268–86. doi:10.1016/j.ijhydene.2006.05.009.

[702] André J, Auray S, De Wolf D, Memmah MM, Simonnet A. Time development of new hydrogen transmission pipeline networks for France. Int J Hydrogen Energy 2014;39:10323–37. doi:10.1016/j.ijhydene.2014.04.190.

[703] ENGIE. A World of Energy 2016 Edition 2016.

[704] Knoope MMJ, Guijt W, Ramírez A, Faaij APC. Improved cost models for optimizing CO2 pipeline configuration for point-to-point pipelines and simple networks. Int J Greenh Gas Control 2014;22:25–46. doi:10.1016/j.ijggc.2013.12.016.

[705] IEA GHG. Transmission of CO2 and energy. 2002.

[706] Knoope MMJ, Ramírez A, Faaij APC. A state-of-the-art review of techno-economic models predicting the costs of CO2 pipeline transport. Int J Greenh Gas Control 2013;16:241–70. doi:10.1016/j.ijggc.2013.01.005.

[707] Atsonios K, Panopoulos KD, Kakaras E. Investigation of technical and economic aspects for methanol production through CO2hydrogenation. Int J Hydrogen Energy 2016;41:2202–14. doi:10.1016/j.ijhydene.2015.12.074.

[708] De Saint Jean M, Baurens P, Bouallou C, Couturier K. Economic assessment of a power-to-substitute-natural-gas process including high-temperature steam electrolysis. Int J Hydrogen Energy 2015;40:6487–500. doi:10.1016/j.ijhydene.2015.03.066.

[709] Apostolakou AA, Kookos IK, Marazioti C, Angelopoulos KC. Techno-economic analysis of a biodiesel production process from vegetable oils. Fuel Process Technol 2009;90:1023–31. doi:10.1016/j.fuproc.2009.04.017.

[710] Daleel. Hire Rate of Platform Supply Vessels 2015. http://www.scmdaleel.com/category/platform-supply-vessel-psv/174 (accessed April 20, 2019).

[711] TERNA. Hourly aggregated zonal unbalance values and sign 2019. https://myterna.terna.it/SunSet/Public/%0A (accessed September 30, 2019).

[712] GME. Hourly prices of the supply offers accepted in the day-ahead market (MGP) 2019. https://www.mercatoelettrico.org/it/Esiti/MGP/EsitiMGP.aspx (accessed September 30, 2019).

[713] TERNA. Average prices of bids and supply offers accepted in the market of ancillary services in real-time balance (MB) 2019. https://www.terna.it/it/sistema-elettrico/mercato-

elettrico/mercato-servizi-dispacciamento (accessed September 30, 2019).

[714] Energy Press. Carbon dioxide price in European market 2019. https://energypress.eu/co2-prices-seen-rising-further-in-2019-icis-analyst-projects/ (accessed August 4, 2019).

[715] Global Petrol Prices. Methane prices around the world 2019. https://www.globalpetrolprices.com/methane_prices/ (accessed August 4, 2019).

[716] The Linde Group. Industrial gases price list 2019.

[717] Kearney D, Kelly B, Cable R, Potrovitza N, Herrmann U, Nava P, et al. Overview on use of a Molten Salt HTF in a Trough Solar Field. NREL Parabol. Trough Therm. Energy Storage Work., Golden, Colorado, USA: 2003.

[718] Kutsuna S, Chen L, Ohno K, Tokuhashi K, Sekiya A. Henry's law constants and hydrolysis rate constants of 2,2, 2-trifluoroethyl acetate and methyl trifluoroacetate. Atmos Environ 2004;38:725–32. doi:10.1016/j.atmosenv.2003.10.019.

[719] Chen L, Zhang XW, Huang L, Lei LC. Partial oxidation of methane with air for methanol production in a post-plasma catalytic system. Chem Eng Process Process Intensif 2009;48:1333–40. doi:10.1016/j.cep.2009.06.007.

[720] Villa K, Murcia-López S, Andreu T, Morante JR. Mesoporous WO3photocatalyst for the partial oxidation of methane to methanol using electron scavengers. Appl Catal B Environ 2015;163:150–5. doi:10.1016/j.apcatb.2014.07.055.

[721] Rocha RS, Reis RM, Lanza MR V, Bertazzoli R. Electrosynthesis of methanol from methane: The role of V2O 5 in the reaction selectivity for methanol of a TiO 2/RuO2/V2O5 gas diffusion electrode. Electrochim Acta 2013;87:606–10. doi:10.1016/j.electacta.2012.09.113.

Nomenclature

a_g	gravitational acceleration (m/s^2)	Equation (4.22)
A_{vuln}	vulnerability area of a given target (m^2)	Equation (4.64)
A_{rot}	swept area of rotor of the wind turbine (m^2)	Equation (4.21)
A_{oil-sl}	surface area of the oil slick (m^2)	Equations (4.56)-(4.57), (4.60)-(4.61)
A_{oil-th}	surface area of the oil thick slick (m^2)	Equations (4.58)-(4.59), (4.62)-(4.63)
AEP	gross annual energy production (MWh/y)	Equations (4.25), (4.27)
AHI	inherent hazard index addressing assets target (m^2/y)	Equation (4.45)
API	potential hazard index addressing assets target (m^2)	Equation (4.44)
ASI	aggregated sustainability index	Equations (4.18)-(4.19)
AV	availability	Equation (4.25), (4.27)
B	annual production of final product (MWh/y)	Equation (4.9)
c	scale factor of Weibull distribution	Equation (4.24)
$\dot{C}$	cost rate ($/h)	
C	cost (units of currency)	Equation (4.36)
C_{bm}	bare-module cost from Guthrie method ($)	
C_p	power coefficient of wind turbine	Equation (4.26)
C_{prod}	total production cost ($/y)	
C_{tci}	capital investment cost ($)	
cf	credit factor (1/y)	Equations (4.43), (4.45), (4.47), (4.49), (4.51), (4.53), (4.55), (4.57), (4.59), (4.61), (4.63)
CI	consistency index	Equation (4.14)
CR	consistency ratio	Equation (4.15)
d	damage distance for human target (m)	Equations (4.42)-(4.43)
D	diameter of rotor of the wind turbine (m)	
DNI	direct normal irradiance (W/m^2)	
e	damage distance for assets target (m)	Equations (4.44)-(4.45)
e_{GHG}	greenhouse gas emissions (kg_{CO2eq}/h)	Equations (4.11)-(4.41)
EHI	inherent hazard index addressing environment target (tons/y or tons·d/y or km^2/y or km^2·d/y)	Equations (4.47), (4.49), (4.51), (4.53), (4.55), (4.57), (4.59), (4.61), (4.63)

EPI	potential hazard index addressing environment target (tons)	Equations (4.46), (4.48), (4.50), (4.52), (4.54), (4.56), (4.58), (4.60)
ex	specific exergy (kJ/kg)	Equation (4.3)
$\dot{E}x$	exergy rate (kW)	Equation (4.3)
Exc	annual average exchange rate	Equation (4.1)
f	exergoeconomic factor	
F	total sub-indicators in each aspect of sustainability	Equations (4.16)-(4.17)
g	damage parameter for water column target (m)	Equations (4.46)-(4.47)
H_s	wave significant height (m)	Equation (4.22)
h	specific enthalpy (kJ/kg)	Equation (4.7)
HHI	inherent hazard index addressing the human target (m^2/y)	Equation (4.43)
HHV	higher heating value (kJ/kg)	
HPI	potential hazard index addressing the human target (m^2)	Equation (4.42)
I	general indicator	
In	Incentive (€/MWh)	Equation (5.1)
L	characteristic length of wave converter (m)	Equation (4.27)
LCOP	levelized cost of product (units of currency per MWh)	Equation (4.9)
LCOE	levelized cost of product (units of currency per MWh)	Equation (4.35)
LGHG	levelized greenhouse gas emissions (kg_{CO2eq}/MWh)	Equations (4.11), (4.41)
LHV	lower heating value (kJ/kg)	
LVOP	levelized value of product (units of currency per MWh)	Equation (4.10)
LVOE	levelized value of energy (units of currency per MWh)	Equation (4.36)
k	shape factor in Weibull distribution	Equation (4.24)
m	number of hours in the evaluated period	Equations (4.35)-(4.36)
m_I	number of indicators in the evaluation matrix	Equation (4.14)
$\dot{m}$	mass flowrate (kg/s)	Equations (4.2), (4.3), (4.11)
$m_{oil-rel}$	released oil mass (tons)	Equations (4.48)-(4.49)
m_{oil-sl}	oil mass in the slick (tons)	Equations (4.50)-(4.51)
m_{oil-th}	oil mass in the thick slick (tons)	Equations (4.54)-(4.55)

mw	molecular weight (kg/kmol)	Equation (4.8)
n_{year}	number of hours per year of converter's operation	Equations (4.25), (4.27)-(4.28)
N	total number of units/technologies	
NPV	net present value (units of currency)	Equation (4.20)
p	frequency occurrence	Equations (4.24), (4.27)
P	power (W or W/m)	Equations (4.21)-(4.22), (4.26), (4.32)-(4.33)
P_0	reference environment pressure (Pa)	
P_d	dispatched power (W)	Equation (4.31)
P_f	forecast power (W)	Equation (4.30)
P_r	real power (W)	Equations (4.30)-(4.31)
$Prob_d$	probability of correct dispatching	
PEC	purchased equipment cost	
Pr	price index	Equation (4.1)
PrIS	process intensification screening indicator	Equations (4.71)-(4.72)
$\dot{Q}$	heat rate (kW)	Equation (4.1)
r	discount rate	Equations (4.9), (4.10)
R	revenue (units of currency per year)	Equations (4.10), (4.36)
RI	random index	Equation (4.11)
s	specific entropy (kJ/kg-K)	Equation (4.7)
t_{lim}	limit time imposed from simulation tool	
T	total years in economic lifetime	Equations (4.9)-(4.10)
T_0	reference environment temperature (K)	
$T_{b,red}$	reduced base tariff for incentive (€/MWh)	Equation (5.1)
T_m	mean wave period (s)	Equation (4.22)
T_p	peak wave period (s)	
T_{prem}	Premium tariff (€/MWh)	Equation (5.1)
T_s	absolute temperature of the boundary (K)	
v	speed (m/s)	Equation (4.21)
w	weight factor	Equations (4.16)-(4.19)
$\dot{W}$	work rate (kW)	Equation (4.2)
x_c	molar fraction of compound	Equation (4.8)
X_I	general normalized indicator	Equation (4.12)
z	height of hub of the turbine (m)	Equations (4.21), (4.23)

z_0	roughness length (m)	Equation (4.23)
z_r	generic height (m)	Equation (4.23)
$\dot{Z}$	annual levelized total cost rate ($/h)	

Greek letters

η	energy efficiency	Equations (4.2), (4.34)
η_{GT}	part-load efficiency of gas turbine	Equations (4.32)-(4.33)
λ	scaling factor	
λ_{max}	principal eigen value	Equation (4.14)
ξ	absolute prediction error (W)	Equation (4.30)
ξ_d	absolute dispatching error (W)	Equation (4.31)
ρ	density (kg/m^3)	Equations (4.21)-(4.22)
Φ	net outranking flow	
ψ	exergy efficiency	Equation (4.3)

Subscripts

0	dead state
act	actual
ass	assets target
avail	available
c	aspect of sustainability
ch	chemical
conv	conventional
curr	currency
d	destruction
eff	effective
el	electrical
econ	economic category
env	environment target/category
f	sub-indicator in each aspect of sustainability
fac	facility
gen	generator
hum	human target
i	reference release mode
j	accident scenario
k	unit of the scheme
l	assets category
max	maximum
nom	nominal
ov	overall
ph	physical
ref	reference
renew	renewable

s	sea state
sell	selling
t	year or hour of the economic lifetime
tech	technical category
tot	total
unb+	positive power unbalance
unb-	negative power unbalance

Acronyms

ADIOS	automated data inquiry for oil spills
AHP	analytic hierarchy process
BC	business case
CAPEX	capital expenditure
CCS	carbon capture and sequestration
CCU	carbon capture and utilization
CDF	cumulative density function
CEI	chemical exposure index
CEPCI	chemical engineering plant cost index
CF	capacity factor
CHU	chemical hazard unit
CISI	comprehensive inherent safety index
COP	coefficient of performance
CSP	concentrating solar power
DBD	dielectric barrier discharge
DHI	domino hazard index
DREAM	dose related risk and effect assessment model
EHI	environmental hazard index
EHS	environment, health and safety
EIF	environmental impact factor
EISI	enhanced inherent safety index
ELECTRE	elimination and et choice translating reality
ETS	emission trading scheme
F&EI	fire & explosion index
FETI	fire, explosion and toxicity index
FIT	feed-in tariff
FLSI	fuzzy logic-based inherent safety index
FSO	floating storage and offloading
G2P	gas-to-power
GDE	gas diffusion electrode
GHG	greenhouse gas
GNOME	general NOAA operational modeling environment
GRAND	graphical descriptive technique for inherent safety assessment
GT	gas turbine
HENG	hydrogen enriched natural gas

HI	Inherent hazard index
HIRA	hazard identification and ranking
HOMER	hybrid optimization model for multiple energy resources
HP	high pressure
HVAC	high voltage alternating current
HVDC	high voltage direct current
I2SI	integrated inherent safety index
IBI	inherent benign-ness indicator
IPI	inherent preference index
iRET	integrated risk estimation tool
IRDI	inherent risk of design index
IS	inherent safety
ISAPEDS	inherent safety assessment for preliminary engineering design stage
ISI	inherent safety index
ISIM	inherent safety index module
KPI	key performance indicator
LCA	life cycle analysis
LIHC	likelihood index of hazard conflicts
LP	low pressure
MCDA	multi-criteria decision analysis
MP	medium pressure
NTP	non-thermal plasma
NuDIST	numerical descriptive inherent safety technique
O&M	operation and maintenance
OPEX	operational expenditure
OSCAR	oil spill contingency and response
OWM	oil weathering model
OWT	offshore wind turbine
P2G	power-to-gas
P2L	power-to-liquid
PDF	probability density function
PEC	predicted environmental concentration
PI	potential hazard index
PIIS	prototype-index for inherent safety
PNEC	predicted no effect concentration
PPI	producer price index
PRI	process route index
PrI	process intensification
PROMETHEE	preference ranking organization method for enrichment evaluation
PSI	process stream index
PTO	power take-off
PV	photovoltaics

RiskBD	risk for base design
RO	renewable obligation
ROC	renewable obligation certificate
SAM	system advisor model
SC	scenario
SNG	synthetic natural gas
SPECO	specific exergy costing method
SWeHI	safety weighted hazard index
SWHI	specific water hazard index
SWOT	strengths, weaknesses, opportunties, threats
TDI	target domino hazard index
TEC	tidal energy converter
TEG	triethylene glycol
TRL	technology readiness level
TSO	transmission system operator
UDI	unit domino hazard index
VCE	vapour cloud explosion
WAM	weighted arithmetic mean
WEC	wave energy converter
WGM	weighted geometric mean

List of Figures

List of Tables

Appendix A.

Technical, economic and environmental data for P2G/P2L options

A.1. Introduction

In the following the six alternative P2G and P2L strategies considered in case-study 1 are described, including definition of the process scheme assumed in the analysis, details of components and their operating conditions. Moreover, costs and emissions data, as well as calculations of CAPEX, OPEX, specific electrical power required and GHG emissions are presented for each component.

A.2. Data for assessment of Option 1

A.2.1. Definition of reference process scheme

The process stages and related technologies considered in the reference process scheme of Option 1 illustrated in Figure 4.3 are tabulated in Table A.1. This tables reports also the components assumed for each technology including their main features and operating conditions.

Table A.1. Features and operating conditions of components considered in the reference process scheme of Option 1.

Step	Process stage	Technology	Components	Main features	Operating conditions
Input supply	Desalination of seawater	Reverse osmosis	Lenntech LennRO [697]	2000 L/h stack capacity, 45% recovery, 95% salt rejection at 25°C	15°C, 75 bar (permeate stream)
First conversion	H_2 production	Proton exchange membrane electrolysis	Siemens Silyzer 200 [698]	1.25 MW stacked capacity, 225 Nm^3/h H_2 under nominal load, 1.5 L/Nm^3 H_2 fresh H_2O demand, 80000 h lifetime	80°C, 30 bar
First conditioning	H_2 compression	Centrifugal compression	Compressor [118]	75% isentropic efficiency, 95% driver efficiency, pressure ratio 5:1 per stage	80°C, 30-150 bar
Transportation	H_2 delivery in natural gas mixture	Subsea gas pipeline	Existing gas pipeline	10% by volume of H_2 in natural gas mixture, 10-1000 km length	50-150 r

A.2.2. CAPEX and OPEX calculations

CAPEX of electrolysis is calculated for each component by using the following cost function [699]:

$$CAPEX = 1500000 \cdot (\dot{W}_{el})^{0.85} \quad \text{(A.1)}$$

where $\dot{W}_{el}$ represents the installed power of electrolyzers in kW. The cost is in € referred to year 2015, thus price indices reported in Table A.5 are used for application of Equation (4.1). Annual OPEX of electrolysis takes into account the O&M costs which is assumed as 3.5% of CAPEX and also the costs

for replacement of the stack which are considered as approximately 35% of CAPEX every 40000 h of operations [116,700], for a total contribution of 11% of CAPEX.

CAPEX associated to reverse osmosis is estimated by multiplying the cost of a single integrated system which includes pre-treatment installation, cartridge filtration, high pressure pump and the LennRO module (31000 € referred to year 2017) [137] for the number of components required based on the H_2O needs of the electrolyzers. In addition, the costs for further operations, such as a second desalination process to remove salts towards 300 ppm by means of Lennetch module for brackish H_2O and a post-treatment through ion exchange polishing to ensure H_2O quality reaches values lower than 1 uS/cm, are considered in total as 17000 € referred to year 2017 per each component [137]. To convert the costs into € referred to year 2018, price indices reported in the Table A.5 are used for application of Equation (4.1). As reported by IEA and IRENA [164], annual OPEX associated to reverse osmosis desalination can be accounted for 2% of CAPEX.

The compression CAPEX is estimated as follows [701]:

$$CAPEX = 15000 \cdot \left(\frac{\dot{W}_{comp}}{10}\right)^{0.9} \tag{A.2}$$

where $\dot{W}_{comp}$ is the electrical power required for compression in kW. The cost value is in $ referred to year 2006, thus average exchange rate and price indices reported in Table A.5 are used for application of Equation (4.1). $\dot{W}_{comp}$ is evaluated by considering the adiabatic (isentropic) compression, i.e. the process is assumed to take place without any heat exchange between the compressed gas and the environment, and with no variations of entropy. The fluid power can be divided by the isentropic efficiency of compressor in order to obtain the shaft power and by the driver efficiency to account for the electrical motors driving the compressor [702]:

$$\dot{W}_{comp} = \frac{\dot{m}}{3600 \cdot 1000} \cdot Z \cdot T \cdot R_u \cdot \frac{N_{st} \cdot \gamma}{\gamma - 1} \cdot \left(\left(\frac{p_{out}}{p_{in}}\right)^{\frac{\gamma-1}{N_{st} \cdot \gamma}} - 1\right) / (\eta_{iso}\, \eta_{drv}) \tag{A.3}$$

where $\dot{m}$ is the mass flowrate of the fluid in kg/h, Z is the compressibility factor (assumed equal to 1 as an approximation for H_2 in this study), T is the inlet temperature of the compressor in K, R_u is the specific gas constant in J/kg-K (assumed equal to 4124 J/kg-K for H_2 in the present study), N_{st} is the number of stages, γ is the diatomic ratio of specific heats (assumed equal to 1.41 for H_2), p_{in} is the inlet pressure of the compressor in bar, p_{out} is the outlet pressure of the compressor in bar, η_{iso} and η_{drv} are the isentropic and driver efficiency whose values are reported in Table A.1. Annual OPEX associated to compression is evaluated as 4% of CAPEX [701].

The HENG mixture transportation is supposed to occur via existing gas pipeline to the onshore gas terminal, thus CAPEX calculation is disregarded. Whereas, OPEX is considered approximately equal to the costs for the international offshore natural gas pipeline according to the ENGIE's energy overview [703], i.e. 0.0008 $/(km-MMBTu) referred to year 2014, where MMBTu stands for millions british thermal units. To calculate the OPEX value, the volumetric flowrate of the fluid in MMBtu/h is used based on the conversion 1 Sm^3/h = 0.03955 MMBTu/h. To convert the cost into € referred to year 2018, average exchange rates and price indices reported in Table A.5 are used for application of Equation (4.1).

A.2.3. Specific electrical power and GHG emissions calculations

The specific electrical power of the commercial Siemens Silyzer 200 stack associated to electrolyzer (5.25 kWh/Nm^3) and to utilities and losses by rectification (0.60 kWh/Nm^3) [158] is used for the required electrical power calculation. To convert the specific consumption from kWh/Nm^3 into kWh/kg, the H_2 density at normal temperature and pressure equal to 0.08375 kg/m_3 is considered. On the other hand, a value of specific GHG emissions of 0.60 kg_{CO2e}/kg_{H2} is retrieved from the literature [162] for the GHG emissions calculation. Both specific electrical powers and specific GHG emissions are then multiplied for the H_2 mass flowrate produced from the component to obtain electrical power in kW and GHG emissions in kg_{CO2eq}/y.

For reverse osmosis desalination, a value of 6.7 kWh/m^3_{H2O} and 0.024 kg_{CO2eq}/kWh are used as specific electrical power and specific GHG emissions, respectively, as suggested in Lai et al. [173] for reverse osmosis driven by wind energy. The final electrical power in kW and GHG emissions in kg_{CO2eq}/y associated to this technology are estimated similarly to electrolysis.

The electrical power required for the compression corresponds to the power calculated by means of Equation (A.3). GHG emissions from this component are disregarded, given the assumption of wind energy-driven electrical motors.

A.3. Data for assessment of Option 2

A.3.1. Definition of reference process scheme

Except the transportation stage, components of the other process stages considered for the reference scheme of Option 2 (illustrated in Figure 4.3) can be found in Table A.1 including their features and operating conditions.

A dedicated pipeline for H_2 transportation is designed by assuming a steady-state isothermal flow, which is a common approximation for relatively long pipeline operating in stable conditions [475]. The

Weymouth equation can be used for compressible fluid in turbulent flow, long pipelines pipe and pressure drop greater than 40% of the upstream pressure [476]:

$$\dot{V}_s = 18.0625 \cdot \frac{T_s}{P_s} \cdot E \cdot \left(\frac{{p_{up}}^2 - {p_{down}}^2}{S \cdot Z \cdot T \cdot l}\right)^{0.5} \cdot {d_p}^{2.6667} \quad \text{(A.4)}$$

where $\dot{V}_s$ is the volumetric gas flowrate in ft^3/h at standard conditions, E is the efficiency factor (equal to 1.0 for new pipe), p_{up} is the upstream pressure in psia, p_{down} is the downstream pressure in psia, S is the specific gravity of gas relative to air, Z is the gas compressibility, T is the inlet temperature of the gas in °R, T_s and P_s are the temperature and pressure at standard conditions (520 °R, 14.73 psia) respectively, l is the pipeline length in miles, d_p is the internal pipe diameter in inch.

By applying Equation (A.4) inversely, the internal pipe diameter d_p can be calculated in function of the pipe length l (100-1000 km range) and upstream pressure p_{up} (50-150 bar range) by assuming proper values of the other parameters. In particular, $\dot{V}_s$ is set as 20000 Sm^3/h considering that 80 stacks of Siemens Silyzer 200 (100 MW nominal capacity) can produce 18000 Nm^3/h. For a given p_{up}, the downstream pressure p_{down} is calculated by setting a pressure drop equal to the minimum limit for application of the Weymouth equation. The inlet temperature T is approximated to H_2 outlet temperature from the electrolyzers. S and Z are assumed as 0.0696 and 1, respectively.

It should be noted that pipe diameters are expected to be smaller than pipeline delivering natural gas or admixture as in case of Option 1, due to the low density of pure H_2. An example of recommended diameters obtained from application of the general flow equation based on Bernoulli law for a range of volumetric flowrate of H_2 is reported in Table A.2. These data derived from a recent study [180] considers an upstream pressure from about 30 to 75 bar, a downstream pressure of 24 bar (gauge) and pipeline length of 100 km.

Table A.2. Example of diameters of pipeline delivering pure H_2 for different throughputs [180].

Volumetric flowrate (Nm^3/h)	Pipeline diameter $\boldsymbol{d_p}$ (mm)
12000	100-150
40000	150-250
80000	200-300
120000	250-400

A.3.2. CAPEX and OPEX calculations

The details of the data used for CAPEX and OPEX calculations of H_2 production, seawater desalination and H_2 compression are reported in Section A.2 presented for Option 1.

Concerning the CAPEX of H_2 pipeline, André et al. [702] developed a method for designing and dimensioning onshore H_2 pipeline which may be adopted to approximate investment costs per unit of length for offshore transmissions since it disregards licensing costs. Under this assumption, the CAPEX per unit of pipeline length is calculated as follows:

$$CAPEX = 418869 + 762.8 \cdot d_p + 2.306 \cdot d_p^2 \quad \text{(A.5)}$$

where d_p is the inlet pipe diameter in mm. The cost value is in \$/km referred to year 2004, thus average exchange rates and price indices reported in Table A.5 are used for application of Equation (4.1). It should be noted that this cost does not include the installation of specific coatings and/or other protections which may be required in offshore environment, thus representing a relatively rough estimation. As suggested by André et al. [702], annual OPEX associated to H_2 transportation in Option 2 is considered as 2% of CAPEX.

A.3.3. Specific electrical power and GHG emissions calculations

Equal data reported above for Option 1 are applied to the H_2 production, seawater desalination and H_2 compression stages of Option 2. It is supposed that no electrical consumptions and GHG emissions are present in case of H_2 transportation.

A.4. Data for assessment of Options 3a and 3b

A.4.1. Definition of reference process scheme

The components and related features and operating conditions considered for the process stages of the reference process scheme of Options 3a and 3b illustrated in Figure 4.3 are shown in Table A.3, except H_2 production and seawater desalination whose details are summarized in Table A.1.

Table A.3. Features and operating conditions of some components considered in the reference process scheme of Options 3a and 3b.

Step	Process stage	Technology	Components	Main features	Operating conditions
Input supply (Option 3a)	CO_2 capture from raw gas	Membrane separation	2-stage membrane cascade with retentate recycle [195]	9.5% CO_2 by volume in feed stream (60°C, 90°C, $7 \cdot 10^5$), 2% CO_2 by volume in retentate stream of the first stage, 90% CO_2 by volume in permeate stream of second stage, 81% CO_2 recovery	50°C, 1 bar (permeate stream of the second stage)
Input supply (Option 3b)	CO_2 delivery from onshore market	Gas transportation	Existing gas pipeline	10-1000 km length	4°C and 26 bar (delivery conditions) [206]
First conditioning	H_2 storage	Pressurized tank	Tank	48 h storage capacity	30 bar
	CO_2 compression	Centrifugal compression	Compressor [704]	80% isentropic efficiency, 99% driver efficiency, pressure ratio 2.04:1 per stage	4-50°C, 1-30 bar
Second conversion	SNG production	Catalytic methanation	Fixed bed reactor [122]	85% energy efficiency (MWh_{HH} of outlet SNG per MWh_{HHV} of inlet H_2), molar H_2:CO_2 ratio = 4:1	250°C, 30 bar
Second conditioning	SNG compression	Centrifugal compression	Compressor [118]	75% isentropic efficiency, 95% driver efficiency, pressure ratio 5:1 per stage	250°C, 30-150 bar
Transportation	SNG delivery	Gas transportation	Existing gas pipeline	10-1000 km length	50-150 bar (delivery pressure)

A.4.2. CAPEX and OPEX calculations

In the following, CAPEX and OPEX calculation of components tabulated in Table A.3 are described, referring the description of costs data of H_2 production and seawater desalination to Section A.2 dedicated to Option 1.

CAPEX of H_2 storage is calculated by using the following cost function [190]:

$$CAPEX = 80 \cdot 2500 \cdot (V_{st}/2500)^{0.75} \quad \text{(A.6)}$$

where V_{st} is the storage volume in Nm^3 required to store the produced H_2 in tanks with storage capacity reported in Table A.3. The cost is in € referred to year 2006, thus price indices reported in Table A.5 are used for application of Equation (4.1). Annual OPEX associated to H_2 storage are estimated as 2% of CAPEX [190].

CAPEX associated to SNG production includes the reactor cost, assumed as 300 $/kW referred to year 2016 [124], and the balance of the plants (heat exchanger, separators, etc.) cost, assumed as 350 $/kW referred to year 2016 [124]. High heating value of 14.5 kWh/kg is considered to convert the produced SNG mass flowrate produced in the reactor through stoichiometric reaction into its corresponding energy content for calculation of total CAPEX costs. Then, average exchange rates and price indices reported in Table A.5 are used for application of Equation (4.1). OPEX calculation is performed by considering a contribution of 6.25% of CAPEX associated to methanation reactor and of 6.5% of CAPEX associated to balance of plant [124], thus leading to an overall fraction of 9.75% of total CAPEX.

Concerning CAPEX of the membrane separation technology in Option 3a, the cost value is approximated by re-scaling the literature cost of $1.41 \cdot 10^7$ $ for a unit producing $6.24 \cdot 10^4$ kg/h of CO_2 in the permeate stream based on the actual CO_2 flowrate required for the methanation reaction. In this calculation, a scaling factor equal to 1 is assumed. Since such a cost value refers to year 2008, average exchange rates and price indices reported in Table A.5 are used for application of Equation (4.1). A fraction of 18% of CAPEX is adopted for OPEX associated to membrane separation, as suggested in [191].

For Option 3b, CO_2 source is considered to be purchased at a desired pressure from the onshore market with a fixed price of 6.5 €/t [209]. Since CO_2 is supposed to be delivered from the landfall terminal via an existing gas pipeline, CAPEX of CO_2 pipeline is disregarded. On the other hand, annual OPEX associated to offshore CO_2 transportation is calculated by converting the offshore pipeline OPEX proposed for survey vessel, repair vessel and intelligent pigging by IEA [705], as follows:

$$OPEX = \left(\frac{14000}{6} \cdot l + 70000 \cdot 19.8 \cdot l\right) + \left(\frac{98000}{10} \cdot l\right) + (700 \cdot \frac{2.5}{10} \cdot l + 120000) \quad \text{(A.7)}$$

where l is the pipeline length in km. To derive Equation (A.7), survey vessel is supposed to operate once a year [706], repair vessel once every 10 years and intelligent pigging once every 4 years; the survey vessel speed is set as 6 km/d as suggested in the IEA report [705]. The cost is in $/km/y referred to year 2000, thus average exchange rates and price indices reported in Table A.5 are used for application of Equation (4.1). The downstream pressure is approximated to the upstream pressure reported in Table A.3, since negligible pressure drops are derived by considering the delivery along a hypothetic pipeline with 36 inch diameter, 150 bar design pressure and variable length between 100 and 1000 km.

CAPEX of CO_2 compressor is calculated as follows [704]:

$$CAPEX = 14800000 \cdot \left(\frac{\dot{W}_{comp} \cdot 10^{-3}}{13}\right)^{0.67} \quad \text{(A.8)}$$

where $\dot{W}_{comp}$ is the power required for compression in kW. The cost value is in $ referred to year 2002, thus average exchange rates and price indices reported in Table A.5 are used for application of Equation

(4.1). $\dot{W}_{comp}$ is evaluated by approximating adiabatic (isentropic) compression and applying Equation (A.3). In this latter equation, the values tabulated in Table A.3 for isentropic and driver efficiencies and for temperature are considered; Z, γ and R_u are assumed equal to 0.94, 1.28 and 188.9 J/kg-K respectively. Annual OPEX associated to compression is evaluated as 5% of CAPEX [707].

For SNG compression, the following cost function is used [708]:

$$CAPEX = 267000 \cdot \left(\frac{\dot{W}_{comp} \cdot 10^{-3}}{445}\right)^{0.67} \quad \text{(A.9)}$$

where $\dot{W}_{comp}$ is the power required for compression in kW. The cost value is in € referred to year 2012, thus price indices reported in Table A.5 are used for application of Equation (4.1). $\dot{W}_{comp}$ is evaluated by approximating adiabatic (isentropic) compression and applying Equation (A.3). In this latter equation, the values tabulated in Table A.3 for isentropic and driver efficiencies and for temperature are considered; Z, γ and R_u are assumed equal to 1, 1.32 and 518.3 J/kg-K respectively. Annual OPEX associated to compression is evaluated as 6% of CAPEX [116].

Since existing gas pipeline is supposed for SNG transportation, CAPEX associated to this step is disregarded while OPEX per unit of pipeline length is calculated by applying the costs of international offshore natural gas pipeline reported in the ENGIE's energy overview [703], i.e. 0.0008 $/(km-MMBTu) referred to year 2014, where MMBTu stands for millions british thermal units. To calculate the OPEX value, the volumetric flowrate of the fluid in MMBtu/h is used based on the conversion 1 Sm^3/h = 0.03955 MMBTu/h. To convert the cost in € referred to year 2018, average exchange rates and price indices reported in Table A.5 are used for application of Equation (4.1).

A.4.3. Specific electrical power and GHG emissions calculations

Calculations performed for required electrical power and GHG emissions of H_2 production and seawater desalination steps are reported in Section A.2. Data used for other components of Options 3a and 3b are described in the following.

For CO_2 capture from raw gas in Option 3a, original values tabulated for a membrane separation unit producing $6.24 \cdot 10^4$ kg/h of CO_2 in the permeate stream (i.e. $7.53 \cdot 10^3$ kW and $7.80 \cdot 10^3$ for compression and capture duty, respectively [195]) are re-scaled based on the actual CO_2 flowrate produced in the methanation reactor through stoichiometric reaction. The electrical power required for CO_2 compression and SNG compression correspond to the power calculated by means of Equation (A.3) for these process stages. GHG emissions from all these components are disregarded, given the supply of renewable electricity from the wind farm.

On the other hand, specific electrical power and GHG emissions associated to methanation driven by wind energy are estimated as 0.33 kWh/kg_{SNG} and 0.30 kg_{CO2eq}/kg_{SNG} [162], respectively, thus the final values in kW and kg_{CO2eq}/y associated to this technology are estimated by multiplying for the produced SNG mass flowrate.

No electrical power and GHG emissions are supposed in case of H_2 storage and SNG transportation.

A.5. Data for assessment of Options 4a and 4b

A.5.1. Definition of reference process scheme

The components and related features and operating conditions considered for the process stages of the reference process scheme of Options 4a and 4b illustrated in Figure 4.3 are shown in Table A.4, except the details of H_2 production and seawater desalination summarized in Table A.1 and the information of CO_2 input supply and H_2 storage and CO_2 compression reported in Table A.3.

Table A.4. Features and operating conditions of some components considered in the reference process scheme of Options 4a and 4b.

Step	Process stage	Technology	Components	Main features	Operating conditions
First conditioning	H_2 + CO_2 compression	Centrifugal compression	Compressor [118]	75% isentropic efficiency, 95% driver efficiency, maximum pressure ratio 5:1 per stage	4-50°C, 30-80 bar
Second conversion	CH_3OH production	Catalytic hydrogenation	Multi-tubular reactor [219]	96% conversion efficiency, molar H_2:CO_2 ratio = 3:1	240°C, 80 bar
Second conditioning	CH_3OH storage	Atmospheric tank	Tank	4 weeks storage capacity	Ambient condition
Transportation	CH_3OH delivery	Liquid transportation	Supply vessel	10-1000 km voyage	Ambient condition

A.5.2. CAPEX and OPEX calculations

CAPEX and OPEX calculation of components tabulated in Table A.4 are presented in the following, referring the description of costs data of other components of the reference scheme to Section A.2 presented for Option 1 and Section A.4 for Options 3a and 3b.

CAPEX of CH_3OH production is calculated by using the following cost function [219]:

$$CAPEX = 14200000 \cdot (\dot{m}/54000)^{0.65} \quad \text{(A.10)}$$

where $\dot{m}$ is the CH_3OH mass flowrate in kg/h produced in the reactor through stoichiometric reaction. The cost is in € referred to year 2015, thus price indices reported in Table A.5 are used for application of Equation (4.1). Annual OPEX associated to CH_3OH production is estimated as 1.04% of CAPEX [219].

CAPEX associated to H_2 + CO_2 compression is estimated as follows [218]:

$$CAPEX = 12080000 \cdot \left(\frac{\dot{W}_{comp} \cdot 10^{-3}}{10}\right)^{0.67} \quad \text{(A.11)}$$

where $\dot{W}_{comp}$ is the power required for compression in kW, calculated through Equation (A.3) assuming adiabatic (isentropic) compression, mass flowrate ṁ in kg/h equal to the inlet mixture composed of H_2 and CO_2 at stoichiometric molar ratio 3:1, compressibility factor Z equal to 1, temperature T in K equal to the mixture temperature (i.e. weighted value with the mass flowrates of two fluids), specific gas constant R_u equal to 661 J/kg-K (i.e. weighted value with the mass fractions of two fluids in the mixture), p_{in} equal to 30 bar, p_{out} equal to the reactor working pressure of 80 bar, η_{iso} and η_{drv} equal to values reported in Table A.4. The constant γ is estimated as the ratio between the specific heat of the mixture $c_{p,mix}$ (i.e. weighted value of single specific heats with the mass fractions of two fluids in the mixture) and the quantity ($c_{p,mix} - R_u$). The number of stage, N_{st}, is assumed as 1, considering the maximum pressure ratio per stage in Table A.4. CAPEX in Equation (A.11) is in € referred to year 2006, thus price indices reported in Table A.5 are used for application of Equation (4.1). Annual OPEX associated to this compression step is evaluated as 5% of CAPEX [218].

For CH_3OH storage, CAPEX of storage tanks is estimated by using the following cost function [709]:

$$CAPEX = 250000 + 94.2 \cdot V_{st} \quad \text{(A.12)}$$

where V_{st} is the volume of the tank in m^3. Equation (A.12) can be applied for volumes between 2000 and 50000 m^3. Otherwise, for smaller tanks, CAPEX can be calculated as follows [709]:

$$CAPEX = 65000 + 158.7 \cdot V_{st} \quad \text{(A.13)}$$

V_{st} is obtained by assuming the availability of storage facilities to support production and product storage at the offshore platforms for 4 weeks (i.e. 28 days) and using a CH_3OH mass density of 790 kg/m^3 to convert the produced mass flowrate into volumetric flowrate. The cost values proposed in Equations (A.12) and (A.13) are in $ referred to year 2008, thus average exchange rates and price indices reported in Table A.5 are used for application of Equation (4.1). Annual OPEX associated to CH_3OH storage is considered as 2% of CAPEX.

Platform supply vessels are ships commonly used to support offshore activities when needed, transporting cargo, equipment and personnel [477]. A main cost driver of such vessels is the cargo capacity, expressed in terms of clear deck area (i.e. the space available to place cargo on deck) and deadweight tonnage (i.e.

the cargo carrying capacity). Daily rates reported for a vessel with deck areas between 300 and 600 m^2 and tonnage capacity between 1000 and 2000 t are from 6000 to 12000 $ referred to year 2015 [710]. By applying a time charter, which is the typical contract method used for oil & gas operations, the vessel owner responsibilities cover the vessel, crewing, maintenance and insurance, while the charterer responsibilities lie for port charges, cargo loading and discharge and bunkers. Moreover, the payment is calculated based on daily hire rate. In this case-study, a single supply vessel is supposed to be hired for CH_3OH transportation at a fixed rate of 9000 $/d. Average exchange rates and price indices reported in Table A.5 are used to obtain daily hire rate in €/d referred to year 2018. The service speed of the vessel is considered as 80% of the average speed of a platform supply vessel (typically comprising between 14 and 16 knots [477]), i.e. 20.4 km/h, and used to estimate the number of days required for total round trip along a given distance between the harbour and the offshore platform. Round trip time is divided into sailing time (40% of round trip time), loading time at the harbour (25% of round trip time) and unloading time at the platform (35% of the round trip time) [477]. Sailing time is first estimated as twice the distance between the harbour and the platform divided by the assumed vessel speed, then loading and unloading times are derived by applying the mentioned proportions. By supposing regular voyages of the supply vessel per year, annual costs for CH_3OH transportation are obtained based on the distance between the onshore harbour and the offshore platform.

A.5.3. Specific electrical power and GHG emissions calculations

Calculations performed for the required electrical power and GHG emissions of components of the process stages reported in Table A.4 are described in the following. Data used for the other steps of Options 4a and 4b are described in Section A.2 dedicated to Option 1 and Section A.4 to Options 3a and 3b.

The electrical power for H_2 + CO_2 compression is considered as the power calculated by means of Equation (A.3) under the assumptions described above, while GHG emissions from the component of this process stage are disregarded, given the supply of renewable electricity from the wind farm.

On the other hand, specific electrical power and GHG emissions associated to CH_3OH production are estimated as 0.402 kWh/kg_{CH3OH} and 0.269 kg_{CO2eq}/kg_{CH3OH} [216], respectively, thus the final values in kW and kg_{CO2eq}/y associated to this technology are estimated by multiplying for the produced CH_3OH mass flowrate.

No electrical power and GHG emissions are supposed in case of CH_3OH storage and CH_3OH transportation stages.

A.6. Definition of conversion rates and price indices for actualization

The values of conversion rates and price indices considered for application of Equation (4.1) in case-study 1 are summarized in Table A.5.

Table A.5. Values of currency conversion rates and price indices assumed for the application of Equation (4.1).

Year	$\boldsymbol{Exc}_{\$,\mathbf{t}\rightarrow€,\mathbf{t}}$ [174]	$\boldsymbol{Exc}_{£,\mathbf{t}\rightarrow€,\mathbf{t}}$ [174]	EU-28 PPI index (total market) [659]
2018	0.85	1.13	104.2
2017	0.89	1.14	102.0
2016	0.90	1.22	99.1
2015	0.90	1.38	100.0
2014	0.75	1.24	101.6
2013	0.75	1.18	103.0
2012	0.78	1.23	103.1
2011	0.72	1.15	100.8
2010	0.75	1.17	96.2
2009	0.72	1.12	93.4
2008	0.68	1.26	96.3
2007	0.73	1.46	92.6
2006	0.80	1.47	90.5
2005	0.80	1.46	88.1
2004	0.80	1.47	85.7
2003	0.88	1.44	83.9
2002	1.06	1.59	83.8
2001	1.12	1.61	83.9
2000	1.09	1.64	83.0

Appendix B.

Technical, economic and environmental data for OWTs farm and G2P options

B.1. Introduction

In the following, hourly technical, economic and environmental data calculated for the G2P offshore hybrid energy system in the four scenarios (SCs) introduced in case-study 2 are presented in detail.

B.2. Technical and environmental data for the alternative systems

Tables B.1, B.2, B.3, B.4 illustrates the technical and environmental data obtained for SC1, SC2, SC3 and SC4, respectively, over the interval of three days selected for the analysis in case-study 2. Each table contains the hourly available wind power ($P_{wind,avail}$) and the electrical produced power (P_r) from the OWT farm. Moreover, they include the hourly power which should be provided by the GT park to satisfy the defined dispatching plan ($P_{GT,eff}$), the number of operating GTs (N_{GT}) at the considered hour estimated by applying the approach described in Section 4.3, the resulting hourly electrical power produced from the GTs (P_{GT}), the efficiency of the park at part-load obtained by applying Equation (4.32). The tables report also the hourly fuel input power (P_{fuel}) resulting from the fuel (natural gas) combustion in GTs, estimated by means of P_{GT} and η_{GT} values, and the associated hourly GHG emissions ($e_{GHG,GT}$) evaluated from P_{fuel} values estimated at the same hours by assuming a typical emission factor per unit of fuel (natural gas) power (i.e. 202 kg/MWh$_{fuel}$ [229]).

Table B.1. Hourly power data of OWT farm, and hourly power, fuel consumption, GHG emissions of GT park for SC1 (3 h forecast horizon, 80% probability of correct dispatching).

Date	Time	$P_{wind,avail}$ (MW)	P_r (MW)	$P_{GT,eff}$ (MW)	N_{GT}	P_{GT} (MW)	η_{GT}	P_{fuel} (MW)	$e_{GHG,GT}$ (kg_{CO2eq})	Date	Time	$P_{wind,avail}$ (MW)	P_r (MW)	$P_{GT,eff}$ (MW)	N_{GT}	P_{GT} (MW)	η_{GT}	P_{fuel} (MW)	$e_{GHG,GT}$ (kg_{CO2eq})
26/02	0.00	12.76	5.82	0.0	-	0.0	-	0.0	0.0	27/02	12.00	21.88	10.48	0.0	-	0.0	-	0.0	0.0
26/02	1.00	6.69	2.22	0.0	-	0.0	-	0.0	0.0	27/02	13.00	11.00	4.78	4.1	1	4.1	10%	42.8	8640.3
26/02	2.00	8.06	3.01	0.0	-	0.0	-	0.0	0.0	27/02	14.00	0.39	0.00	9.8	2	9.8	15%	64.5	13027.3
26/02	3.00	7.88	2.91	0.0	-	0.0	-	0.0	0.0	27/02	15.00	0.09	0.00	10.3	2	10.3	16%	65.8	13293.1
26/02	4.00	13.01	5.96	0.0	-	0.0	-	0.0	0.0	27/02	16.00	0.30	0.00	10.8	2	10.8	16%	67.1	13552.0
26/02	5.00	8.06	3.01	0.0	-	0.0	-	0.0	0.0	27/02	17.00	0.72	0.00	11.9	3	11.9	17%	70.0	14134.6
26/02	6.00	7.97	2.96	0.0	-	0.0	-	0.0	0.0	27/02	18.00	9.11	3.56	8.9	2	8.9	14%	61.7	12469.3
26/02	7.00	4.02	0.68	3.0	1	3.0	8%	36.0	7278.7	27/02	19.00	17.44	8.30	4.8	1	4.8	10%	46.1	9306.0
26/02	8.00	0.24	0.00	5.24	2	6.9	13%	55.0	11109.9	27/02	20.00	34.54	16.23	0.0	-	0.0	-	0.0	0.0
26/02	9.00	0.65	0.00	8.7	2	8.7	14%	61.0	12329.0	27/02	21.00	68.59	30.61	0.0	-	0.0	-	0.0	0.0
26/02	10.00	2.63	0.25	7.6	2	7.6	13%	57.6	11629.4	27/02	22.00	82.30	35.36	0.0	-	0.0	-	0.0	0.0
26/02	11.00	6.77	2.27	3.9	1	3.9	9%	41.8	8437.0	27/02	23.00	110.74	43.29	0.0	-	0.0	-	0.0	0.0
26/02	12.00	9.92	4.09	1.3	0	0.0	-	0.0	0.0	28/02	0.00	108.15	42.68	0.0	-	0.0	-	0.0	0.0
26/02	13.00	6.22	1.92	2.8	0	0.0	-	0.0	0.0	28/02	1.00	88.44	37.30	0.0	-	0.0	-	0.0	0.0
26/02	14.00	4.08	0.70	2.7	0	0.0	-	0.0	0.0	28/02	2.00	75.24	33.01	0.0	-	0.0	-	0.0	0.0
26/02	15.00	6.22	1.92	0.8	0	0.0	-	0.0	0.0	28/02	3.00	63.06	28.47	0.0	-	0.0	-	0.0	0.0
26/02	16.00	7.10	2.47	0.0	-	0.0	-	0.0	0.0	28/02	4.00	82.30	35.36	0.0	-	0.0	-	0.0	0.0
26/02	17.00	6.86	2.32	0.0	-	0.0	-	0.0	0.0	28/02	5.00	74.43	32.74	0.0	-	0.0	-	0.0	0.0
26/02	18.00	5.08	1.13	0.0	-	0.0	-	0.0	0.0	28/02	6.00	81.02	34.95	0.0	-	0.0	-	0.0	0.0
26/02	19.00	6.00	1.77	0.0	-	0.0	-	0.0	0.0	28/02	7.00	57.50	26.19	0.0	-	0.0	-	0.0	0.0
26/02	20.00	10.45	4.44	0.0	-	0.0	-	0.0	0.0	28/02	8.00	42.25	19.68	0.0	-	0.0	-	0.0	0.0
26/02	21.00	14.98	7.00	0.0	-	0.0	-	0.0	0.0	28/02	9.00	36.49	17.03	0.0	-	0.0	-	0.0	0.0
26/02	22.00	27.21	12.93	0.0	-	0.0	-	0.0	0.0	28/02	10.00	74.43	32.74	0.0	-	0.0	-	0.0	0.0
26/02	23.00	29.96	14.23	0.0	-	0.0	-	0.0	0.0	28/02	11.00	57.84	26.34	0.0	-	0.0	-	0.0	0.0
27/02	0.00	29.10	13.83	0.0	-	0.0	-	0.0	0.0	28/02	12.00	65.24	29.33	0.0	-	0.0	-	0.0	0.0
27/02	1.00	38.52	17.90	0.0	-	0.0	-	0.0	0.0	28/02	13.00	87.99	37.16	0.0	-	0.0	-	0.0	0.0
27/02	2.00	21.35	10.24	0.0	-	0.0	-	0.0	0.0	28/02	14.00	81.02	34.95	0.0	-	0.0	-	0.0	0.0
27/02	3.00	18.06	8.62	0.0	-	0.0	-	0.0	0.0	28/02	15.00	118.20	45.02	0.0	-	0.0	-	0.0	0.0
27/02	4.00	12.28	5.55	0.0	-	0.0	-	0.0	0.0	28/02	16.00	55.18	25.20	16.2	3	16.2	20%	80.5	16266.2
27/02	5.00	31.07	14.73	0.0	-	0.0	-	0.0	0.0	28/02	17.00	44.20	20.57	22.8	4	22.8	24%	95.3	19244.7
27/02	6.00	11.57	5.13	0.0	-	0.0	-	0.0	0.0	28/02	18.00	71.28	31.60	12.0	3	12.0	17%	70.3	14193.0
27/02	7.00	17.14	8.14	0.0	-	0.0	-	0.0	0.0	28/02	19.00	72.45	32.03	11.7	3	11.7	17%	69.6	14054.6
27/02	8.00	35.26	16.53	0.0	-	0.0	-	0.0	0.0	28/02	20.00	137.10	47.64	0.0	-	0.0	-	0.0	0.0
27/02	9.00	85.33	36.33	0.0	-	0.0	-	0.0	0.0	28/02	21.00	223.49	49.95	0.0	-	0.0	-	0.0	0.0
27/02	10.00	41.43	19.30	0.0	-	0.0	-	0.0	0.0	28/02	22.00	76.05	33.29	10.6	2	10.6	16%	66.5	13442.7
27/02	11.00	39.30	18.28	0.0	-	0.0	-	0.0	0.0	28/02	23.00	58.18	26.48	17.3	3	17.3	21%	82.9	16738.5

Table B.2. Hourly power data of OWT farm, and hourly power, fuel consumption, GHG emissions of GT park for SC2 (3 h forecast horizon, 90% probability of correct dispatching).

Date	Time	$P_{wind,avail}$ (MW)	P_r (MW)	$P_{GT,eff}$ (MW)	N_{GT}	P_{GT} (MW)	η_{GT}	P_{fuel} (MW)	$e_{GHG,GT}$ (kg_{CO2eq})	Date	Time	$P_{wind,avail}$ (MW)	P_r (MW)	$P_{GT,eff}$ (MW)	N_{GT}	P_{GT} (MW)	η_{GT}	P_{fuel} (MW)	$e_{GHG,GT}$ (kg_{CO2eq})
26/02	0.00	12.76	5.82	0.0	-	0.0	-	0.0	0.0	27/02	12.00	21.88	10.48	0.0	-	0.0	-	0.0	0.0
26/02	1.00	6.69	2.22	0.0	-	0.0	-	0.0	0.0	27/02	13.00	11.00	4.78	0.0	-	0.0	-	0.0	0.0
26/02	2.00	8.06	3.01	0.0	-	0.0	-	0.0	0.0	27/02	14.00	0.39	0.00	1.9	-	0.0	-	0.0	0.0
26/02	3.00	7.88	2.91	0.0	-	0.0	-	0.0	0.0	27/02	15.00	0.09	0.00	2.4	-	0.0	-	0.0	0.0
26/02	4.00	13.01	5.96	0.0	-	0.0	-	0.0	0.0	27/02	16.00	0.30	0.00	2.9	-	0.0	-	0.0	0.0
26/02	5.00	8.06	3.01	0.0	-	0.0	-	0.0	0.0	27/02	17.00	0.72	0.00	4.0	1	4.0	10%	41.8	8444.3
26/02	6.00	7.97	2.96	0.0	-	0.0	-	0.0	0.0	27/02	18.00	9.11	3.56	1.0	-	0.0	-	0.0	0.0
26/02	7.00	4.02	0.68	0.0	-	0.0	-	0.0	0.0	27/02	19.00	17.44	8.30	0.0	-	0.0	-	0.0	0.0
26/02	8.00	0.24	0.00	0.0	-	0.0	-	0.0	0.0	27/02	20.00	34.54	16.23	0.0	-	0.0	-	0.0	0.0
26/02	9.00	0.65	0.00	0.8	0	0.0	-	0.0	0.0	27/02	21.00	68.59	30.61	0.0	-	0.0	-	0.0	0.0
26/02	10.00	2.63	0.25	0.0	-	0.0	-	0.0	0.0	27/02	22.00	82.30	35.36	0.0	-	0.0	-	0.0	0.0
26/02	11.00	6.77	2.27	0.0	-	0.0	-	0.0	0.0	27/02	23.00	110.74	43.29	0.0	-	0.0	-	0.0	0.0
26/02	12.00	9.92	4.09	0.0	-	0.0	-	0.0	0.0	28/02	0.00	108.15	42.68	0.0	-	0.0	-	0.0	0.0
26/02	13.00	6.22	1.92	0.0	-	0.0	-	0.0	0.0	28/02	1.00	88.44	37.30	0.0	-	0.0	-	0.0	0.0
26/02	14.00	4.08	0.70	0.0	-	0.0	-	0.0	0.0	28/02	2.00	75.24	33.01	0.0	-	0.0	-	0.0	0.0
26/02	15.00	6.22	1.92	0.0	-	0.0	-	0.0	0.0	28/02	3.00	63.06	28.47	0.0	-	0.0	-	0.0	0.0
26/02	16.00	7.10	2.47	0.0	-	0.0	-	0.0	0.0	28/02	4.00	82.30	35.36	0.0	-	0.0	-	0.0	0.0
26/02	17.00	6.86	2.32	0.0	-	0.0	-	0.0	0.0	28/02	5.00	74.43	32.74	0.0	-	0.0	-	0.0	0.0
26/02	18.00	5.08	1.13	0.0	-	0.0	-	0.0	0.0	28/02	6.00	81.02	34.95	0.0	-	0.0	-	0.0	0.0
26/02	19.00	6.00	1.77	0.0	-	0.0	-	0.0	0.0	28/02	7.00	57.50	26.19	0.0	-	0.0	-	0.0	0.0
26/02	20.00	10.45	4.44	0.0	-	0.0	-	0.0	0.0	28/02	8.00	42.25	19.68	0.0	-	0.0	-	0.0	0.0
26/02	21.00	14.98	7.00	0.0	-	0.0	-	0.0	0.0	28/02	9.00	36.49	17.03	0.0	-	0.0	-	0.0	0.0
26/02	22.00	27.21	12.93	0.0	-	0.0	-	0.0	0.0	28/02	10.00	74.43	32.74	0.0	-	0.0	-	0.0	0.0
26/02	23.00	29.96	14.23	0.0	-	0.0	-	0.0	0.0	28/02	11.00	57.84	26.34	0.0	-	0.0	-	0.0	0.0
27/02	0.00	29.10	13.83	0.0	-	0.0	-	0.0	0.0	28/02	12.00	65.24	29.33	0.0	-	0.0	-	0.0	0.0
27/02	1.00	38.52	17.90	0.0	-	0.0	-	0.0	0.0	28/02	13.00	87.99	37.16	0.0	-	0.0	-	0.0	0.0
27/02	2.00	21.35	10.24	0.0	-	0.0	-	0.0	0.0	28/02	14.00	81.02	34.95	0.0	-	0.0	-	0.0	0.0
27/02	3.00	18.06	8.62	0.0	-	0.0	-	0.0	0.0	28/02	15.00	118.20	45.02	0.0	-	0.0	-	0.0	0.0
27/02	4.00	12.28	5.55	0.0	-	0.0	-	0.0	0.0	28/02	16.00	55.18	25.20	8.3	2	8.3	14%	59.9	12104.2
27/02	5.00	31.07	14.73	0.0	-	0.0	-	0.0	0.0	28/02	17.00	44.20	20.57	14.9	3	14.9	19%	77.4	15635.0
27/02	6.00	11.57	5.13	0.0	-	0.0	-	0.0	0.0	28/02	18.00	71.28	31.60	4.1	1	4.1	10%	42.4	8572.2
27/02	7.00	17.14	8.14	0.0	-	0.0	-	0.0	0.0	28/02	19.00	72.45	32.03	3.8	1	3.8	9%	40.9	8265.2
27/02	8.00	35.26	16.53	0.0	-	0.0	-	0.0	0.0	28/02	20.00	137.10	47.64	0.0	-	0.0	-	0.0	0.0
27/02	9.00	85.33	36.33	0.0	-	0.0	-	0.0	0.0	28/02	21.00	223.49	49.95	0.0	-	0.0	-	0.0	0.0
27/02	10.00	41.43	19.30	0.0	-	0.0	-	0.0	0.0	28/02	22.00	76.05	33.29	2.7	-	0.0	-	0.0	0.0
27/02	11.00	39.30	18.28	0.0	-	0.0	-	0.0	0.0	28/02	23.00	58.18	26.48	9.4	2	9.4	15%	63.1	12736.8

Table B.3. Hourly power data of OWT farm, and hourly power, fuel consumption, GHG emissions of GT park for SC3 (6 h forecast horizon, 80% probability of correct dispatching).

Date	Time	$P_{wind,avail}$ (MW)	P_r (MW)	$P_{GT,eff}$ (MW)	N_{GT}	P_{GT} (MW)	η_{GT}	P_{fuel} (MW)	$e_{GHG,GT}$ (kg_{CO2eq})	Date	Time	$P_{wind,avail}$ (MW)	P_r (MW)	$P_{GT,eff}$ (MW)	N_{GT}	P_{GT} (MW)	η_{GT}	P_{fuel} (MW)	$e_{GHG,GT}$ (kg_{CO2eq})
26/02	0.00	12.76	5.82	0.0	-	0.0	-	0.0	0.0	27/02	12.00	21.88	10.48	0.0	-	0.0	-	0.0	0.0
26/02	1.00	6.69	2.22	0.5	0	0.0	-	0.0	0.0	27/02	13.00	11.00	4.78	0.0	-	0.0	-	0.0	0.0
26/02	2.00	8.06	3.01	0.8	0	0.0	-	0.0	0.0	27/02	14.00	0.39	0.00	9.9	2	9.9	15%	64.6	13050.3
26/02	3.00	7.88	2.91	1.4	0	0.0	-	0.0	0.0	27/02	15.00	0.09	0.00	14.2	3	14.2	19%	75.8	15315.8
26/02	4.00	13.01	5.96	0.0	-	0.0	-	0.0	0.0	27/02	16.00	0.30	0.00	19.1	4	19.1	22%	87.0	17573.0
26/02	5.00	8.06	3.01	3.0	1	3.0	8%	35.6	7181.8	27/02	17.00	0.72	0.00	28.7	5	28.7	26%	108.3	21877.6
26/02	6.00	7.97	2.96	3.6	1	3.6	9%	39.5	7980.2	27/02	18.00	9.11	3.56	29.4	6	29.4	27%	110.1	22232.2
26/02	7.00	4.02	0.68	6.4	2	6.4	12%	53.2	10744.9	27/02	19.00	17.44	8.30	28.5	5	28.5	26%	107.9	21795.5
26/02	8.00	0.24	0.00	8.5	2	8.5	14%	60.4	12197.6	27/02	20.00	34.54	16.23	22.6	4	22.6	24%	94.7	19130.0
26/02	9.00	0.65	0.00	9.2	2	9.2	15%	62.5	12627.7	27/02	21.00	68.59	30.61	8.7	2	8.7	14%	61.1	12350.0
26/02	10.00	2.63	0.25	9.6	2	9.6	15%	63.8	12893.0	27/02	22.00	82.30	35.36	4.1	1	4.1	10%	42.8	8638.7
26/02	11.00	6.77	2.27	9.0	2	9.0	15%	62.0	12515.6	27/02	23.00	110.74	43.29	0.0	-	0.0	-	0.0	0.0
26/02	12.00	9.92	4.09	7.9	2	7.9	13%	58.4	11796.3	28/02	0.00	108.15	42.68	0.0	-	0.0	-	0.0	0.0
26/02	13.00	6.22	1.92	10.3	2	10.3	16%	65.9	13303.5	28/02	1.00	88.44	37.30	2.5	0	0.0	-	0.0	0.0
26/02	14.00	4.08	0.70	12.2	3	12.2	17%	70.7	14288.5	28/02	2.00	75.24	33.01	6.5	2	6.5	12%	53.6	10823.8
26/02	15.00	6.22	1.92	11.3	2	11.3	16%	68.3	13806.5	28/02	3.00	63.06	28.47	10.9	2	10.9	16%	67.5	13632.9
26/02	16.00	7.10	2.47	11.0	2	11.0	16%	67.7	13677.9	28/02	4.00	82.30	35.36	3.6	1	3.6	9%	39.8	8032.8
26/02	17.00	6.86	2.32	11.8	3	11.8	17%	69.7	14082.7	28/02	5.00	74.43	32.74	4.6	1	4.6	10%	45.3	9140.9
26/02	18.00	5.08	1.13	13.3	3	13.3	18%	73.6	14860.3	28/02	6.00	81.02	34.95	0.3	0	0.0	-	0.0	0.0
26/02	19.00	6.00	1.77	13.0	3	13.0	18%	72.8	14710.6	28/02	7.00	57.50	26.19	5.2	1	5.2	11%	48.0	9692.8
26/02	20.00	10.45	4.44	11.0	2	11.0	16%	67.8	13686.6	28/02	8.00	42.25	19.68	3.1	1	3.1	8%	36.2	7313.1
26/02	21.00	14.98	7.00	8.8	2	8.8	14%	61.4	12406.3	28/02	9.00	36.49	17.03	1.2	0	0.0	-	0.0	0.0
26/02	22.00	27.21	12.93	3.2	1	3.2	9%	37.3	7536.7	28/02	10.00	74.43	32.74	0.0	-	0.0	-	0.0	0.0
26/02	23.00	29.96	14.23	2.6	0	0.0	-	0.0	0.0	28/02	11.00	57.84	26.34	0.0	-	0.0	-	0.0	0.0
27/02	0.00	29.10	13.83	3.4	1	3.4	9%	38.2	7712.3	28/02	12.00	65.24	29.33	0.0	-	0.0	-	0.0	0.0
27/02	1.00	38.52	17.90	0.0	-	0.0	-	0.0	0.0	28/02	13.00	87.99	37.16	0.0	-	0.0	-	0.0	0.0
27/02	2.00	21.35	10.24	2.9	0	0.0	-	0.0	0.0	28/02	14.00	81.02	34.95	0.0	-	0.0	-	0.0	0.0
27/02	3.00	18.06	8.62	3.2	1	3.2	9%	37.4	7548.5	28/02	15.00	118.20	45.02	0.0	-	0.0	-	0.0	0.0
27/02	4.00	12.28	5.55	5.1	1	5.1	11%	47.5	9595.8	28/02	16.00	55.18	25.20	0.0	-	0.0	-	0.0	0.0
27/02	5.00	31.07	14.73	0.0	-	0.0	-	0.0	0.0	28/02	17.00	44.20	20.57	0.0	-	0.0	-	0.0	0.0
27/02	6.00	11.57	5.13	1.8	0	0.0	-	0.0	0.0	28/02	18.00	71.28	31.60	0.0	-	0.0	-	0.0	0.0
27/02	7.00	17.14	8.14	0.0	-	0.0	-	0.0	0.0	28/02	19.00	72.45	32.03	0.0	-	0.0	-	0.0	0.0
27/02	8.00	35.26	16.53	0.0	-	0.0	-	0.0	0.0	28/02	20.00	137.10	47.64	0.0	-	0.0	-	0.0	0.0
27/02	9.00	85.33	36.33	0.0	-	0.0	-	0.0	0.0	28/02	21.00	223.49	49.95	0.0	-	0.0	-	0.0	0.0
27/02	10.00	41.43	19.30	0.0	-	0.0	-	0.0	0.0	28/02	22.00	76.05	33.29	0.0	-	0.0	-	0.0	0.0
27/02	11.00	39.30	18.28	0.0	-	0.0	-	0.0	0.0	28/02	23.00	58.18	26.48	0.0	-	0.0	-	0.0	0.0

Table B.4. Hourly power data of OWT farm, and hourly power, fuel consumption, GHG emissions of GT park for SC4 (6 h forecast horizon, 90% probability of correct dispatching).

Date	Time	$P_{wind,avail}$ (MW)	P_r (MW)	$P_{GT,eff}$ (MW)	N_{GT}	P_{GT} (MW)	η_{GT}	P_{fuel} (MW)	$e_{GHG,GT}$ (kg_{CO2eq})	Date	Time	$P_{wind,avail}$ (MW)	P_r (MW)	$P_{GT,eff}$ (MW)	N_{GT}	P_{GT} (MW)	η_{GT}	P_{fuel} (MW)	$e_{GHG,GT}$ (kg_{CO2eq})
26/02	0.00	12.76	5.82	0.0	-	0.0	-	0.0	0.0	27/02	12.00	21.88	10.48	0.0	-	0.0	-	0.0	0.0
26/02	1.00	6.69	2.22	0.0	-	0.0	-	0.0	0.0	27/02	13.00	11.00	4.78	0.0	-	0.0	-	0.0	0.0
26/02	2.00	8.06	3.01	0.0	-	0.0	-	0.0	0.0	27/02	14.00	0.39	0.00	2.3	0	0.0	-	0.0	0.0
26/02	3.00	7.88	2.91	0.0	-	0.0	-	0.0	0.0	27/02	15.00	0.09	0.00	6.6	2	6.6	12%	54.1	10933.9
26/02	4.00	13.01	5.96	0.0	-	0.0	-	0.0	0.0	27/02	16.00	0.30	0.00	11.5	2	11.5	17%	69.0	13946.0
26/02	5.00	8.06	3.01	0.0	-	0.0	-	0.0	0.0	27/02	17.00	0.72	0.00	21.1	4	21.1	23%	91.4	18453.2
26/02	6.00	7.97	2.96	0.0	-	0.0	-	0.0	0.0	27/02	18.00	9.11	3.56	21.8	4	21.8	23%	93.1	18801.1
26/02	7.00	4.02	0.68	0.0	-	0.0	-	0.0	0.0	27/02	19.00	17.44	8.30	20.9	4	20.9	23%	91.0	18372.4
26/02	8.00	0.24	0.00	0.9	0	0.0	-	0.0	0.0	27/02	20.00	34.54	16.23	15.0	3	15.0	19%	77.6	15670.4
26/02	9.00	0.65	0.00	1.6	0	0.0	-	0.0	0.0	27/02	21.00	68.59	30.61	1.1	0	0.0	-	0.0	0.0
26/02	10.00	2.63	0.25	2.0	0	0.0	-	0.0	0.0	27/02	22.00	82.30	35.36	0.0	-	0.0	-	0.0	0.0
26/02	11.00	6.77	2.27	1.4	0	0.0	-	0.0	0.0	27/02	23.00	110.74	43.29	0.0	-	0.0	-	0.0	0.0
26/02	12.00	9.92	4.09	0.3	0	0.0	-	0.0	0.0	28/02	0.00	108.15	42.68	0.0	-	0.0	-	0.0	0.0
26/02	13.00	6.22	1.92	2.7	0	0.0	-	0.0	0.0	28/02	1.00	88.44	37.30	0.0	-	0.0	-	0.0	0.0
26/02	14.00	4.08	0.70	4.6	1	4.6	10%	45.2	9124.6	28/02	2.00	75.24	33.01	0.0	-	0.0	-	0.0	0.0
26/02	15.00	6.22	1.92	3.7	1	3.7	9%	40.1	8097.4	28/02	3.00	63.06	28.47	3.3	1	3.3	9%	38.1	7689.1
26/02	16.00	7.10	2.47	3.4	1	3.4	9%	38.6	7797.2	28/02	4.00	82.30	35.36	0.0	-	0.0	-	0.0	0.0
26/02	17.00	6.86	2.32	4.2	1	4.2	10%	43.1	8703.6	28/02	5.00	74.43	32.74	0.0	-	0.0	-	0.0	0.0
26/02	18.00	5.08	1.13	5.7	1	5.7	11%	50.4	10183.4	28/02	6.00	81.02	34.95	0.0	-	0.0	-	0.0	0.0
26/02	19.00	6.00	1.77	5.4	1	5.4	11%	49.1	9920.2	28/02	7.00	57.50	26.19	0.0	-	0.0	-	0.0	0.0
26/02	20.00	10.45	4.44	3.4	1	3.4	11%	38.7	7817.8	28/02	8.00	42.25	19.68	0.0	-	0.0	-	0.0	0.0
26/02	21.00	14.98	7.00	1.2	0	0.0	9%	0.0	0.0	28/02	9.00	36.49	17.03	0.0	-	0.0	-	0.0	0.0
26/02	22.00	27.21	12.93	0.0	-	0.0	-	0.0	0.0	28/02	10.00	74.43	32.74	0.0	-	0.0	-	0.0	0.0
26/02	23.00	29.96	14.23	0.0	-	0.0	-	0.0	0.0	28/02	11.00	57.84	26.34	0.0	-	0.0	-	0.0	0.0
27/02	0.00	29.10	13.83	0.0	-	0.0	-	0.0	0.0	28/02	12.00	65.24	29.33	0.0	-	0.0	-	0.0	0.0
27/02	1.00	38.52	17.90	0.0	-	0.0	-	0.0	0.0	28/02	13.00	87.99	37.16	0.0	-	0.0	-	0.0	0.0
27/02	2.00	21.35	10.24	0.0	-	0.0	-	0.0	0.0	28/02	14.00	81.02	34.95	0.0	-	0.0	-	0.0	0.0
27/02	3.00	18.06	8.62	0.0	-	0.0	-	0.0	0.0	28/02	15.00	118.20	45.02	0.0	-	0.0	-	0.0	0.0
27/02	4.00	12.28	5.55	0.0	-	0.0	-	0.0	0.0	28/02	16.00	55.18	25.20	0.0	-	0.0	-	0.0	0.0
27/02	5.00	31.07	14.73	0.0	-	0.0	-	0.0	0.0	28/02	17.00	44.20	20.57	0.0	-	0.0	-	0.0	0.0
27/02	6.00	11.57	5.13	0.0	0	0.0	-	0.0	0.0	28/02	18.00	71.28	31.60	0.0	-	0.0	-	0.0	0.0
27/02	7.00	17.14	8.14	0.0	-	0.0	-	0.0	0.0	28/02	19.00	72.45	32.03	0.0	-	0.0	-	0.0	0.0
27/02	8.00	35.26	16.53	0.0	-	0.0	-	0.0	0.0	28/02	20.00	137.10	47.64	0.0	-	0.0	-	0.0	0.0
27/02	9.00	85.33	36.33	0.0	-	0.0	-	0.0	0.0	28/02	21.00	223.49	49.95	0.0	-	0.0	-	0.0	0.0
27/02	10.00	41.43	19.30	0.0	-	0.0	-	0.0	0.0	28/02	22.00	76.05	33.29	0.0	-	0.0	-	0.0	0.0
27/02	11.00	39.30	18.28	0.0	-	0.0	-	0.0	0.0	28/02	23.00	58.18	26.48	0.0	-	0.0	-	0.0	0.0

B.3. Economic performance data for the alternative systems

Some economic performance data associated to the power unbalances with respect to the declared power to grid operator are summarized in Tables B.5, B.6, B.7 and B.8 for SC1, SC2, SC3 and SC4, respectively, over the interval of three days selected for the analysis in case-study 2. Each table includes the hourly positive power unbalance (P_{unb+}) occurring when real power P_r is greater than the dispatched power P_d estimated once defined the dispatching plan, the hourly negative power unbalance (P_{unb-}) occurring when P_r is lower than P_d and gas turbines cannot operate due to technical minimum load limit. Moreover, the following information published by Italian TSO TERNA and "Gestore dei Mercati Energetici" (GME) is summarized: the sign of the hourly aggregated zonal unbalance associated the macro area where the point of dispatching is located (North Italy) [711], the hourly prices of the accepted supply offers ($Price_{MGP}$) in the day-ahead market (MGP) in the macro area where the point of dispatching is located (North Italy) [712], the average prices of the bids ($Price_{MB\downarrow}$) and supply offers ($Price_{MB\uparrow}$) accepted in the market of ancillary services in real-time balance (MB), weighted by volume, in the macro area where the dispatching point belongs (North Italy) [713]. These data are used to estimate revenues received by TERNA for positive unbalances (R_{unb+}) and costs paid to TERNA for negative unbalances (C_{unb-}), according to the single pricing mechanism defined in Table 5.10. Hourly R_{unb+} and C_{unb-} results are reported in Tables B.5-B.8.

Tables B.9, B.10, B.11 and B.12 show the details of the economic data about revenues due to electricity selling to the grid obtained for SC1, SC2, SC3 and SC4, respectively, over the interval of three days selected for the analysis in case-study 2. The hourly MGP prices for conventional electricity ($Price_{MGP}$) by GME as well as the hourly financial incentives for offshore wind power integrated into the grid (In_{OWT}), estimated according to the pull mechanism described in case-study 2 are reported in the tables. The revenues from the selling of conventional electricity produced from gas turbines ($R_{sell,GT}$) are derived by combining MGP prices with P_{GT} values (in Tables B.1-B.4), while the revenues from the selling of renewable electricity produced from OWTs ($R_{sell,OWT}$) are estimated by combining the sum of MGP prices and In_{OWT} with P_r values (in Tables B.1-B.4). The total revenues (R_{sell}) are then the summation of $R_{sell,GT}$ and $R_{sell,OWT}$. All the results are summarized in Table B.9-B.12. Other information reported in these tables is the costs associated to GHG emissions from the system ($C_{e_{GHG}}$) from the combination of $e_{GHG,GT}$ (in Tables B.1-B.4) and the EU ETS carbon allowance price of 15 €/t_{CO2eq} [229], as well as the discounted $OPEX_{GT}$ values estimated based on the data shown in Table 5.14 and economic assumptions (8% interest rate, 72 h economic period).

Table B.5. Hourly positive and negative power unbalances and associated revenues and costs for SC1 (3 h forecast horizon, 80% probability of correct dispatching).

Date	Time	P_{unb+} (MW)	P_{unb-} (MW)	Zonal unbal.	$Price_{MGP}$ (€/MWh)	$Price_{MB\downarrow}$ (€/MWh)	$Price_{MB\uparrow}$ (€/MWh)	R_{unb+} (€)	C_{unb-} (€)	Date	Time	P_{unb+} (MW)	P_{unb-} (MW)	Zonal unbal.	$Price_{MGP}$ (€/MWh)	$Price_{MB\downarrow}$ (€/MWh)	$Price_{MB\uparrow}$ (€/MWh)	R_{unb+} (€)	C_{unb-} (€)
26/02	0.00	5.8	-	Sign -	34.86	21.23	-	203	-	27/02	12.00	2.0	-	Sign +	33		72.1	67	-
26/02	1.00	2.2	-	Sign -	32	15.73	-	71	-	27/02	13.00	-	-	Sign +	30.72		72.97	-	-
26/02	2.00	3.0	-	Sign -	27.85	19.28	68	205	-	27/02	14.00	-	-	Sign +	28.89	25	70.1	-	-
26/02	3.00	2.9	-	Sign -	26.25	19.28	70.94	207	-	27/02	15.00	-	-	Sign +	28.55	24.9	70.04	-	-
26/02	4.00	6.0	-	Sign -	26.15	19.43	70.9	423	-	27/02	16.00	-	-	Sign +	29.65	25	70.04	-	-
26/02	5.00	2.2	-	Sign -	26.25	20	66.42	144	-	27/02	17.00	-	-	Sign -	33	23.83	-	-	-
26/02	6.00	0.7	-	Sign +	30.5	19.51	75.5	14	-	27/02	18.00	-	-	Sign -	38.2	24.64	-	-	-
26/02	7.00	-	-	Sign +	26	22.27	75.5	-	-	27/02	19.00	-	-	Sign -	46.45	24.26	-	-	-
26/02	8.00	-	-	Sign +	38.97	-	76.39	-	-	27/02	20.00	2.0	-	Sign -	46	25.93	-	2	-
26/02	9.00	-	-	Sign +	45	30.18	76.7	-	-	27/02	21.00	2.0	-	Sign -	40.01	24.45	-	16	-
26/02	10.00	-	-	Sign +	45.5	32.65	79.23	-	-	27/02	22.00	15.8	-	Sign -	35	22.82	-	22	-
26/02	11.00	-	-	Sign +	43.56	34.4	85.11	-	-	27/02	23.00	21.8	-	Sign -	31.39	20.07	-	32	-
26/02	12.00	-	1.3	Sign +	39	-	76.32	-	52	28/02	0.00	32.3	-	Sign -	25	2.38	66.26	33	-
26/02	13.00	-	2.8	Sign +	36	24	75.92	-	68	28/02	1.00	32.8	-	Sign -	26.17	2.27	75.24	28	-
26/02	14.00	-	2.7	Sign +	36	27.38	75.5	-	75	28/02	2.00	28.4	-	Sign -	21.9	-	61.25	26	-
26/02	15.00	-	0.8	Sign +	37.42	-	77.35	-	32	28/02	3.00	26.2	-	Sign -	19.15	-	61.25	23	-
26/02	16.00	0.4	-	Sign +	37.55	-	76.12	14	-	28/02	4.00	22.7	-	Sign -	17.73	-	66.74	30	-
26/02	17.00	1.5	-	Sign -	37.5	-	76.58	115	-	28/02	5.00	30.5	-	Sign -	17.31	-	61.25	30	-
26/02	18.00	0.9	-	Sign -	43.8	28.99	75.5	66	-	28/02	6.00	29.5	-	Sign +	17.46	-	61.25	33	-
26/02	19.00	1.8	-	Sign -	49.51	28.09	75.5	134	-	28/02	7.00	32.6	-	Sign +	20.4	-	51.99	25	-
26/02	20.00	4.4	-	Sign -	46.44	-	80.12	356	-	28/02	8.00	24.7	-	Sign +	20.27	-	55.5	20	-
26/02	21.00	7.0	-	Sign -	44	35	76.75	538	-	28/02	9.00	19.6	-	Sign -	24.65	0.52	52.37	17	-
26/02	22.00	12.9	-	Sign -	41.08	30.55	-	531	-	28/02	10.00	17.0	-	Sign +	27.38	4.11	-	30	-
26/02	23.00	14.2	-	Sign -	35.55	-	67.84	965	-	28/02	11.00	30.3	-	Sign -	36	7.49	-	16	-
27/02	0.00	13.8	-	Sign -	28.16	17.37	74.46	1030	-	28/02	12.00	16.2	-	Sign +	37	8.67	-	14	-
27/02	1.00	17.5	-	Sign -	33.78	16.33	99.95	1753	-	28/02	13.00	14.0	-	Sign +	34.38	4.74	82.32	16	-
27/02	2.00	8.9	-	Sign -	31.52	15.23	-	280	-	28/02	14.00	16.2	-	Sign +	30.55	5.12	-	2	-
27/02	3.00	6.7	-	Sign -	30.4	17.99	-	204	-	28/02	15.00	2.1	-	Sign +	30.4	4.4	82.32	7	-
27/02	4.00	3.1	-	Sign -	31.36	13.59	-	96	-	28/02	16.00	-	-	Sign -	30.86	3.44	84.75	-	-
27/02	5.00	11.1	-	Sign -	31.31	13.59	-	349	-	28/02	17.00	-	-	Sign -	30	0.31	81.8	-	-
27/02	6.00	1.0	-	Sign +	31.53	12.72	-	12	-	28/02	18.00	-	-	Sign -	32	8.4	84.75	-	-
27/02	7.00	3.4	-	Sign +	33	15.55	-	53	-	28/02	19.00	-	-	Sign -	36.68	11.6	-	-	-
27/02	8.00	10.6	-	Sign +	33.53	16.53	-	176	-	28/02	20.00	3.8	-	Sign -	37.5	11.13	-	141	-
27/02	9.00	29.8	-	Sign +	36	20.62	-	614	-	28/02	21.00	6.1	-	Sign -	36.68	11.08	73.34	46	-
27/02	10.00	12.3	-	Sign +	34	-	82.32	417	-	28/02	22.00	-	-	Sign -	34.83	7.61	-	-	-
27/02	11.00	10.3	-	Sign +	34.99	-	-	361	-	28/02	23.00	-	-	Sign -	30.4	6.95	-	-	-

Table B.6. Hourly positive and negative power unbalances and associated revenues and costs for SC2 (3 h forecast horizon, 90% probability of correct dispatching).

Date	Time	P_{unb+} (MW)	P_{unb-} (MW)	Zonal unbal.	$Price_{MGP}$ (€/MWh)	$Price_{MP\downarrow}$ (€/MWh)	$Price_{MP\uparrow}$ (€/MWh)	R_{unb+} (€)	$C_{unb\cdot}$ (€)	Date	Time	P_{unb+} (MW)	P_{unb-} (MW)	Zonal unbal.	$Price_{MGP}$ (€/MWh)	$Price_{MP\downarrow}$ (€/MWh)	$Price_{MP\uparrow}$ (€/MWh)	R_{unb+} (€)	$C_{unb\cdot}$ (€)
26/02	0.00	5.8	-	Sign -	34.86	21.23	-	203	-	27/02	12.00	10.0	-	Sign +	33		72.1	329	-
26/02	1.00	2.2	-	Sign -	32	15.73	-	71	-	27/02	13.00	3.8	-	Sign +	30.72		72.97	116	-
26/02	2.00	3.0	-	Sign -	27.85	19.28	68	205	-	27/02	14.00	-	1.9	Sign +	28.89	25	70.1	-	48
26/02	3.00	2.9	-	Sign -	26.25	19.28	70.94	207	-	27/02	15.00	-	2.4	Sign +	28.55	24.9	70.04	-	60
26/02	4.00	6.0	-	Sign -	26.15	19.43	70.9	423	-	27/02	16.00	-	2.9	Sign +	29.65	25	70.04	-	72
26/02	5.00	3.0	-	Sign -	26.25	20	66.42	200	-	27/02	17.00	-	-	Sign -	33	23.83	-	-	-
26/02	6.00	3.0	-	Sign +	30.5	19.51	75.5	58	-	27/02	18.00	-	1.0	Sign -	38.2	24.64	-	-	38
26/02	7.00	0.7	-	Sign +	26	22.27	75.5	15	-	27/02	19.00	3.2	-	Sign -	46.45	24.26	-	147	-
26/02	8.00	-	-	Sign +	38.97	-	76.39	-	-	27/02	20.00	9.9	-	Sign -	46	25.93	-	455	-
26/02	9.00	-	0.8	Sign +	45	30.18	76.7	-	23	27/02	21.00	23.7	-	Sign -	40.01	24.45	-	948	-
26/02	10.00	0.2	-	Sign +	45.5	32.65	79.23	8	-	27/02	22.00	29.8	-	Sign -	35	22.82	-	1042	-
26/02	11.00	2.3	-	Sign +	43.56	34.4	85.11	78	-	27/02	23.00	40.3	-	Sign -	31.39	20.07	-	1264	-
26/02	12.00	4.1	-	Sign +	39	-	76.32	160	-	28/02	0.00	40.7	-	Sign -	25	2.38	66.26	2696	-
26/02	13.00	1.9	-	Sign +	36	24	75.92	46	-	28/02	1.00	36.3	-	Sign -	26.17	2.27	75.24	2735	-
26/02	14.00	0.7	-	Sign +	36	27.38	75.5	19	-	28/02	2.00	33.0	-	Sign -	21.9	-	61.25	2022	-
26/02	15.00	1.9	-	Sign +	37.42	-	77.35	72	-	28/02	3.00	28.5	-	Sign -	19.15	-	61.25	1744	-
26/02	16.00	2.5	-	Sign +	37.55	-	76.12	93	-	28/02	4.00	35.4	-	Sign -	17.73	-	66.74	2360	-
26/02	17.00	2.3	-	Sign -	37.5	-	76.58	178	-	28/02	5.00	32.7	-	Sign -	17.31	-	61.25	2005	-
26/02	18.00	1.1	-	Sign -	43.8	28.99	75.5	85	-	28/02	6.00	34.9	-	Sign +	17.46	-	61.25	610	-
26/02	19.00	1.8	-	Sign -	49.51	28.09	75.5	134	-	28/02	7.00	26.2	-	Sign +	20.4	-	51.99	534	-
26/02	20.00	4.4	-	Sign -	46.44	-	80.12	356	-	28/02	8.00	19.7	-	Sign +	20.27	-	55.5	399	-
26/02	21.00	7.0	-	Sign -	44	35	76.75	538	-	28/02	9.00	17.0	-	Sign -	24.65	0.52	52.37	892	-
26/02	22.00	12.9	-	Sign -	41.08	30.55	-	531	-	28/02	10.00	32.7	-	Sign +	27.38	4.11	-	135	-
26/02	23.00	14.2	-	Sign -	35.55	-	67.84	965	-	28/02	11.00	24.1	-	Sign -	36	7.49	-	867	-
27/02	0.00	13.8	-	Sign -	28.16	17.37	74.46	1030	-	28/02	12.00	21.9	-	Sign +	37	8.67	-	190	-
27/02	1.00	17.9	-	Sign -	33.78	16.33	99.95	1789	-	28/02	13.00	24.1	-	Sign +	34.38	4.74	82.32	114	-
27/02	2.00	10.2	-	Sign -	31.52	15.23	-	323	-	28/02	14.00	10.0	-	Sign +	30.55	5.12	-	51	-
27/02	3.00	8.6	-	Sign -	30.4	17.99	-	262	-	28/02	15.00	14.7	-	Sign +	30.4	4.4	82.32	65	-
27/02	4.00	5.5	-	Sign -	31.36	13.59	-	174	-	28/02	16.00	-	-	Sign -	30.86	3.44	84.75	-	-
27/02	5.00	14.7	-	Sign -	31.31	13.59	-	461	-	28/02	17.00	-	-	Sign -	30	0.31	81.8	-	-
27/02	6.00	5.1	-	Sign +	31.53	12.72	-	65	-	28/02	18.00	-	-	Sign -	32	8.4	84.75	-	-
27/02	7.00	8.1	-	Sign +	33	15.55	-	127	-	28/02	19.00	-	-	Sign -	36.68	11.6	-	-	-
27/02	8.00	16.5	-	Sign +	33.53	16.53	-	273	-	28/02	20.00	11.7	-	Sign -	37.5	11.13	-	438	-
27/02	9.00	36.3	-	Sign +	36	20.62	-	749	-	28/02	21.00	14.0	-	Sign -	36.68	11.08	73.34	1027	-
27/02	10.00	19.3	-	Sign +	34	-	82.32	656	-	28/02	22.00	-	2.7	Sign -	34.83	7.61	-	-	92
27/02	11.00	18.2	-	Sign +	34.99	-	-	638	-	28/02	23.00	-	-	Sign -	30.4	6.95	-	-	-

Table B.7. Hourly positive and negative power unbalances and associated revenues and costs for SC3 (6 h forecast horizon, 80% probability of correct dispatching).

Date	Time	P_{unb+} (MW)	P_{unb-} (MW)	Zonal unbal.	$Price_{MGP}$ (€/MWh)	$Price_{MP\downarrow}$ (€/MWh)	$Price_{MP\uparrow}$ (€/MWh)	R_{unb+} (€)	C_{unb-} (€)	Date	Time	P_{unb+} (MW)	P_{unb-} (MW)	Zonal unbal.	$Price_{MGP}$ (€/MWh)	$Price_{MP\downarrow}$ (€/MWh)	$Price_{MP\uparrow}$ (€/MWh)	R_{unb+} (€)	C_{unb-} (€)
26/02	0.00	3.7	-	Sign -	34.86	21.23	-	128	-	27/02	12.00	10.5	-	Sign +	33		72.1	346	-
26/02	1.00	-	0.5	Sign -	32	15.73	-	-	15	27/02	13.00	2.3	-	Sign +	30.72		72.97	72	-
26/02	2.00	-	0.8	Sign -	27.85	19.28	68	-	53	27/02	14.00	-	-	Sign +	28.89	25	70.1	-	-
26/02	3.00	-	1.4	Sign -	26.25	19.28	70.94	-	101	27/02	15.00	-	-	Sign +	28.55	24.9	70.04	-	-
26/02	4.00	1.1	-	Sign -	26.15	19.43	70.9	76	-	27/02	16.00	-	-	Sign +	29.65	25	70.04	-	-
26/02	5.00	-	-	Sign -	26.25	20	66.42	-	-	27/02	17.00	-	-	Sign -	33	23.83	-	-	-
26/02	6.00	-	-	Sign +	30.5	19.51	75.5	-	-	27/02	18.00	-	-	Sign -	38.2	24.64	-	-	-
26/02	7.00	-	-	Sign +	26	22.27	75.5	-	-	27/02	19.00	-	-	Sign -	46.45	24.26	-	-	-
26/02	8.00	-	-	Sign +	38.97	-	76.39	-	-	27/02	20.00	-	-	Sign -	46	25.93	-	-	-
26/02	9.00	-	-	Sign +	45	30.18	76.7	-	-	27/02	21.00	-	-	Sign -	40.01	24.45	-	-	-
26/02	10.00	-	-	Sign +	45.5	32.65	79.23	-	-	27/02	22.00	-	-	Sign -	35	22.82	-	-	-
26/02	11.00	-	-	Sign +	43.56	34.4	85.11	-	-	27/02	23.00	3.5	-	Sign -	31.39	20.07	-	111	-
26/02	12.00	-	-	Sign +	39	-	76.32	-	-	28/02	0.00	2.9	-	Sign -	25	2.38	66.26	190	-
26/02	13.00	-	-	Sign +	36	24	75.92	-	-	28/02	1.00	-	2.5	Sign -	26.17	2.27	75.24	-	185
26/02	14.00	-	-	Sign +	36	27.38	75.5	-	-	28/02	2.00	-	-	Sign -	21.9	-	61.25	-	-
26/02	15.00	-	-	Sign +	37.42	-	77.35	-	-	28/02	3.00	-	-	Sign -	19.15	-	61.25	-	-
26/02	16.00	-	-	Sign +	37.55	-	76.12	-	-	28/02	4.00	-	-	Sign -	17.73	-	66.74	-	-
26/02	17.00	-	-	Sign -	37.5	-	76.58	-	-	28/02	5.00	-	-	Sign -	17.31	-	61.25	-	-
26/02	18.00	-	-	Sign -	43.8	28.99	75.5	-	-	28/02	6.00	-	0.3	Sign +	17.46	-	61.25	-	-
26/02	19.00	-	-	Sign -	49.51	28.09	75.5	-	-	28/02	7.00	-	-	Sign +	20.4	-	51.99	-	-
26/02	20.00	-	-	Sign -	46.44	-	80.12	-	-	28/02	8.00	-	-	Sign +	20.27	-	55.5	-	-
26/02	21.00	-	-	Sign -	44	35	76.75	-	-	28/02	9.00	-	1.2	Sign -	24.65	0.52	52.37	-	63
26/02	22.00	-	-	Sign -	41.08	30.55	-	-	-	28/02	10.00	20.4	-	Sign +	27.38	4.11	-	78	-
26/02	23.00	-	2.6	Sign -	35.55	-	67.84	-	177	28/02	11.00	26.6	-	Sign -	36	7.49	-	734	-
27/02	0.00	-	-	Sign -	28.16	17.37	74.46	-	-	28/02	12.00	35.8	-	Sign +	37	8.67	-	230	-
27/02	1.00	2.1	-	Sign -	33.78	16.33	99.95	212	-	28/02	13.00	34.9	-	Sign +	34.38	4.74	82.32	170	-
27/02	2.00	-	2.9	Sign -	31.52	15.23	-	-	90	28/02	14.00	45.0	-	Sign +	30.55	5.12	-	179	-
27/02	3.00	-	-	Sign -	30.4	17.99	-	-	-	28/02	15.00	25.2	-	Sign +	30.4	4.4	82.32	198	-
27/02	4.00	-	-	Sign -	31.36	13.59	-	-	-	28/02	16.00	20.6	-	Sign -	30.86	3.44	84.75	2136	-
27/02	5.00	6.6	-	Sign -	31.31	13.59	-	207	-	28/02	17.00	31.6	-	Sign -	30	0.31	81.8	1682	-
27/02	6.00	-	1.8	Sign +	31.53	12.72	-	-	23	28/02	18.00	32.0	-	Sign -	32	8.4	84.75	2678	-
27/02	7.00	2.2	-	Sign +	33	15.55	-	34	-	28/02	19.00	47.6	-	Sign -	36.68	11.6	-	1175	-
27/02	8.00	12.6	-	Sign +	33.53	16.53	-	208	-	28/02	20.00	50.0	-	Sign -	37.5	11.13	-	1787	-
27/02	9.00	33.4	-	Sign +	36	20.62	-	688	-	28/02	21.00	33.3	-	Sign -	36.68	11.08	73.34	3664	-
27/02	10.00	17.3	-	Sign +	34	-	82.32	589	-	28/02	22.00	26.5	-	Sign -	34.83	7.61	-	1159	92
27/02	11.00	18.0	-	Sign +	34.99	-	-	629	-	28/02	23.00	20.4	-	Sign -	30.4	6.95	-	805	-

Table B.8. Hourly positive and negative power unbalances and associated revenues and costs for SC4 (6 h forecast horizon, 90% probability of correct dispatching).

Date	Time	P_{unb+} (MW)	P_{unb-} (MW)	Zonal unbal.	$Price_{MGP}$ (€/MWh)	$Price_{MP\downarrow}$ (€/MWh)	$Price_{MP\uparrow}$ (€/MWh)	R_{unb+} (€)	$C_{unb\cdot}$ (€)	Date	Time	P_{unb+} (MW)	P_{unb-} (MW)	Zonal unbal.	$Price_{MGP}$ (€/MWh)	$Price_{MP\downarrow}$ (€/MWh)	$Price_{MP\uparrow}$ (€/MWh)	R_{unb+} (€)	$C_{unb\cdot}$ (€)
26/02	0.00	5.8	-	Sign -	34.86	21.23	-	203	-	27/02	12.00	10.5	-	Sign +	33		72.1	346	-
26/02	1.00	2.2	-	Sign -	32	15.73	-	71	-	27/02	13.00	4.8	-	Sign +	30.72		72.97	147	-
26/02	2.00	3.0	-	Sign -	27.85	19.28	68	205	-	27/02	14.00	-	2.3	Sign +	28.89	25	70.1	-	57
26/02	3.00	2.9	-	Sign -	26.25	19.28	70.94	207	-	27/02	15.00	-	-	Sign +	28.55	24.9	70.04	-	-
26/02	4.00	6.0	-	Sign -	26.15	19.43	70.9	423	-	27/02	16.00	-	-	Sign +	29.65	25	70.04	-	-
26/02	5.00	3.0	-	Sign -	26.25	20	66.42	200	-	27/02	17.00	-	-	Sign -	33	23.83	-	-	-
26/02	6.00	3.0	-	Sign +	30.5	19.51	75.5	58	-	27/02	18.00	-	-	Sign -	38.2	24.64	-	-	-
26/02	7.00	0.7	-	Sign +	26	22.27	75.5	15	-	27/02	19.00	-	-	Sign -	46.45	24.26	-	-	-
26/02	8.00	-	0.9	Sign +	38.97	-	76.39	-	35	27/02	20.00	-	-	Sign -	46	25.93	-	-	-
26/02	9.00	-	1.6	Sign +	45	30.18	76.7	-	48	27/02	21.00	-	1.1	Sign -	40.01	24.45	-	-	45
26/02	10.00	-	2.0	Sign +	45.5	32.65	79.23	-	66	27/02	22.00	3.5	-	Sign -	35	22.82	-	121	-
26/02	11.00	-	1.4	Sign +	43.56	34.4	85.11	-	48	27/02	23.00	11.1	-	Sign -	31.39	20.07	-	349	-
26/02	12.00	-	0.3	Sign +	39	-	76.32	-	11	28/02	0.00	10.5	-	Sign -	25	2.38	66.26	693	-
26/02	13.00	-	2.7	Sign +	36	24	75.92	-	66	28/02	1.00	5.1	-	Sign -	26.17	2.27	75.24	386	-
26/02	14.00	-	-	Sign +	36	27.38	75.5	-	-	28/02	2.00	1.1	-	Sign -	21.9	-	61.25	66	-
26/02	15.00	-	-	Sign +	37.42	-	77.35	-	-	28/02	3.00	-	-	Sign -	19.15	-	61.25	-	-
26/02	16.00	-	-	Sign +	37.55	-	76.12	-	-	28/02	4.00	4.0	-	Sign -	17.73	-	66.74	266	-
26/02	17.00	-	-	Sign -	37.5	-	76.58	-	-	28/02	5.00	3.0	-	Sign -	17.31	-	61.25	183	-
26/02	18.00	-	-	Sign -	43.8	28.99	75.5	-	-	28/02	6.00	7.3	-	Sign +	17.46	-	61.25	127	-
26/02	19.00	-	-	Sign -	49.51	28.09	75.5	-	-	28/02	7.00	2.4	-	Sign +	20.4	-	51.99	49	-
26/02	20.00	-	-	Sign -	46.44	-	80.12	-	-	28/02	8.00	4.5	-	Sign +	20.27	-	55.5	92	-
26/02	21.00	-	1.2	Sign -	44	35	76.75	-	93	28/02	9.00	6.4	-	Sign -	24.65	0.52	52.37	335	-
26/02	22.00	4.4	-	Sign -	41.08	30.55	-	179	-	28/02	10.00	26.6	-	Sign +	27.38	4.11	-	109	-
26/02	23.00	5.0	-	Sign -	35.55	-	67.84	338	-	28/02	11.00	26.3	-	Sign -	36	7.49	-	948	-
27/02	0.00	4.2	-	Sign -	28.16	17.37	74.46	315	-	28/02	12.00	29.3	-	Sign +	37	8.67	-	254	-
27/02	1.00	9.7	-	Sign -	33.78	16.33	99.95	970	-	28/02	13.00	37.2	-	Sign +	34.38	4.74	82.32	176	-
27/02	2.00	4.7	-	Sign -	31.52	15.23	-	149	-	28/02	14.00	34.9	-	Sign +	30.55	5.12	-	179	-
27/02	3.00	4.4	-	Sign -	30.4	17.99	-	132	-	28/02	15.00	45.0	-	Sign +	30.4	4.4	82.32	198	-
27/02	4.00	2.5	-	Sign -	31.36	13.59	-	79	-	28/02	16.00	25.2	-	Sign -	30.86	3.44	84.75	2136	-
27/02	5.00	14.2	-	Sign -	31.31	13.59	-	445	-	28/02	17.00	20.6	-	Sign -	30	0.31	81.8	1682	-
27/02	6.00	5.1	-	Sign +	31.53	12.72	-	65	-	28/02	18.00	31.6	-	Sign -	32	8.4	84.75	2678	-
27/02	7.00	8.1	-	Sign +	33	15.55	-	127	-	28/02	19.00	32.0	-	Sign -	36.68	11.6	-	1175	-
27/02	8.00	16.5	-	Sign +	33.53	16.53	-	273	-	28/02	20.00	47.6	-	Sign -	37.5	11.13	-	1787	-
27/02	9.00	36.3	-	Sign +	36	20.62	-	749	-	28/02	21.00	50.0	-	Sign -	36.68	11.08	73.34	3664	-
27/02	10.00	19.3	-	Sign +	34	-	82.32	656	-	28/02	22.00	33.3	-	Sign -	34.83	7.61	-	1159	-
27/02	11.00	18.3	-	Sign +	34.99	-	-	640	-	28/02	23.00	26.5	-	Sign -	30.4	6.95	-	805	-

Table B.9. Hourly revenues from electricity selling, GHG emissions costs and OPEX of the GT park for SC1 (3 h forecast horizon, 80% probability of correct dispatching).

Date	Time	$Price_{MGP}$ (€/MWh)	In_{OWT} (€/MWh)	$R_{sell,GT}$ (€)	$R_{sell,OWT}$ (€)	R_{sell} (€)	$C_{e_{GHG}}$ (€)	$OPEX_{GT}$ (€)	Date	Time	$Price_{MGP}$ (€/MWh)	In_{OWT} (€/MWh)	$R_{sell,GT}$ (€)	$R_{sell,OWT}$ (€)	R_{sell} (€)	$C_{e_{GHG}}$ (€)	$OPEX_{GT}$ (€)
26/02	0.00	34.9	135.5	0	992	992	-	-	27/02	12.00	33.0	137.4	0	1786	1786	-	-
26/02	1.00	32.0	138.4	0	378	378	-	-	27/02	13.00	30.7	139.6	127	815	942	130	11
26/02	2.00	27.9	142.5	0	513	513	-	-	27/02	14.00	28.9	141.5	284	0	284	195	26
26/02	3.00	26.3	144.1	0	497	497	-	-	27/02	15.00	28.6	141.8	294	0	294	199	27
26/02	4.00	26.2	144.2	0	1016	1016	-	-	27/02	16.00	29.7	140.7	320	0	320	203	29
26/02	5.00	26.3	144.1	0	513	513	-	-	27/02	17.00	33.0	137.4	392	0	392	212	32
26/02	6.00	30.5	139.9	0	505	505	-	-	27/02	18.00	38.2	132.2	340	606	947	187	24
26/02	7.00	36.0	134.4	109	116	225	109	8	27/02	19.00	46.5	123.9	221	1414	1635	140	13
26/02	8.00	39.0	131.4	268	0	268	167	18	27/02	20.00	46.0	124.4	0	2764	2764	-	-
26/02	9.00	45.0	125.4	391	0	391	185	23	27/02	21.00	40.0	130.3	0	5214	5214	-	-
26/02	10.00	45.5	124.9	346	42	389	174	20	27/02	22.00	35.0	135.4	0	6024	6024	-	-
26/02	11.00	43.6	126.8	172	387	559	127	11	27/02	23.00	31.4	139.0	0	7375	7375	-	-
26/02	12.00	39.0	131.4	0	697	697	109	8	28/02	0.00	25.0	145.4	0	7270	7270	-	-
26/02	13.00	36.0	134.4	0	328	328	-	-	28/02	1.00	26.2	144.2	0	6354	6354	-	-
26/02	14.00	36.0	134.4	0	119	119	-	-	28/02	2.00	21.9	148.5	0	5624	5624	-	-
26/02	15.00	37.4	132.9	0	328	328	-	-	28/02	3.00	19.2	151.2	0	4850	4850	-	-
26/02	16.00	37.6	132.8	0	420	420	-	-	28/02	4.00	17.7	152.6	0	6024	6024	-	-
26/02	17.00	37.5	132.9	0	395	395	-	-	28/02	5.00	17.3	153.0	0	5577	5577	-	-
26/02	18.00	43.8	126.6	0	192	192	-	-	28/02	6.00	17.5	152.9	0	5954	5954	-	-
26/02	19.00	49.5	120.8	0	302	302	-	-	28/02	7.00	20.4	150.0	0	4462	4462	-	-
26/02	20.00	46.4	123.9	0	756	756	-	-	28/02	8.00	20.3	150.1	0	3352	3352	-	-
26/02	21.00	44.0	126.4	0	1193	1193	-	-	28/02	9.00	24.7	145.7	0	2900	2900	-	-
26/02	22.00	41.1	129.3	0	2202	2202	-	-	28/02	10.00	27.4	143.0	0	5577	5577	-	-
26/02	23.00	35.6	134.8	0	2424	2424	-	-	28/02	11.00	36.0	134.4	0	4486	4486	-	-
27/02	0.00	28.2	142.2	0	2356	2356	-	-	28/02	12.00	37.0	133.4	0	4996	4996	-	-
27/02	1.00	33.8	136.6	0	3049	3049	-	-	28/02	13.00	34.4	136.0	0	6331	6331	-	-
27/02	2.00	31.5	138.8	0	1744	1744	-	-	28/02	14.00	30.6	139.8	0	5954	5954	-	-
27/02	3.00	30.4	140.0	0	1469	1469	-	-	28/02	15.00	30.4	140.0	0	7669	7669	-	-
27/02	4.00	31.4	139.0	0	945	945	-	-	28/02	16.00	30.9	139.5	501	4293	4794	244	43
27/02	5.00	31.3	139.0	0	2509	2509	-	-	28/02	17.00	30.0	140.4	685	3503	4188	289	61
27/02	6.00	31.5	138.8	0	874	874	-	-	28/02	18.00	32.0	138.4	384	5384	5767	213	32
27/02	7.00	33.0	137.4	0	1386	1386	-	-	28/02	19.00	36.7	133.7	430	5456	5886	211	31
27/02	8.00	33.5	136.8	0	2815	2815	-	-	28/02	20.00	37.5	132.9	0	8116	8116	-	-
27/02	9.00	36.0	134.4	0	6189	6189	-	-	28/02	21.00	36.7	133.7	0	8510	8510	-	-
27/02	10.00	34.0	136.4	0	3287	3287	-	-	28/02	22.00	34.8	135.5	369	5671	6039	202	28
27/02	11.00	35.0	135.4	0	3114	3114	-	-	28/02	23.00	30.4	140.0	525	4511	5036	251	46

Table B.10. Hourly revenues from electricity selling, GHG emissions costs and OPEX of the GT park for SC2 (3 h forecast horizon, 90% probability of correct dispatching).

Date	Time	$Price_{MGP}$ (€/MWh)	In_{OWT} (€/MWh)	$R_{sell,GT}$ (€)	$R_{sell,OWT}$ (€)	R_{sell} (€)	$C_{e_{GHG}}$ (€)	$OPEX_{GT}$ (€)	Date	Time	$Price_{MGP}$ (€/MWh)	In_{OWT} (€/MWh)	$R_{sell,GT}$ (€)	$R_{sell,OWT}$ (€)	R_{sell} (€)	$C_{e_{GHG}}$ (€)	$OPEX_{GT}$ (€)
26/02	0.00	34.9	135.5	0	992	992	-	-	27/02	12.00	33.0	137.4	0	1786	1786	-	
26/02	1.00	32.0	138.4	0	378	378	-	-	27/02	13.00	30.7	139.6	0	815	815	-	
26/02	2.00	27.9	142.5	0	513	513	-	-	27/02	14.00	28.9	141.5	0	0	-	-	
26/02	3.00	26.3	144.1	0	497	497	-	-	27/02	15.00	28.6	141.8	190	0	-	-	
26/02	4.00	26.2	144.2	0	1016	1016	-	-	27/02	16.00	29.7	140.7	341	0	-	-	
26/02	5.00	26.3	144.1	0	513	513	-	-	27/02	17.00	33.0	137.4	695	0	131	127	11
26/02	6.00	30.5	139.9	0	505	505	-	-	27/02	18.00	38.2	132.2	834	606	606	-	
26/02	7.00	36.0	134.4	0	116	116	-	-	27/02	19.00	46.5	123.9	970	1414	1414	-	
26/02	8.00	39.0	131.4	0	0	0	-	-	27/02	20.00	46.0	124.4	689	2764	2764	-	
26/02	9.00	45.0	125.4	0	0	0	-	-	27/02	21.00	40.0	130.3	0	5214	5214	-	
26/02	10.00	45.5	124.9	0	42	42	-	-	27/02	22.00	35.0	135.4	0	6024	6024	-	
26/02	11.00	43.6	126.8	0	387	387	-	-	27/02	23.00	31.4	139.0	0	7375	7375	-	
26/02	12.00	39.0	131.4	0	697	697	-	-	28/02	0.00	25.0	145.4	0	7270	7270	-	
26/02	13.00	36.0	134.4	0	328	328	-	-	28/02	1.00	26.2	144.2	0	6354	6354	-	
26/02	14.00	36.0	134.4	165	119	119	-	-	28/02	2.00	21.9	148.5	0	5624	5624	-	
26/02	15.00	37.4	132.9	137	328	328	-	-	28/02	3.00	19.2	151.2	64	4850	4850	-	
26/02	16.00	37.6	132.8	129	420	420	-	-	28/02	4.00	17.7	152.6	0	6024	6024	-	
26/02	17.00	37.5	132.9	157	395	395	-	-	28/02	5.00	17.3	153.0	0	5577	5577	-	
26/02	18.00	43.8	126.6	250	192	192	-	-	28/02	6.00	17.5	152.9	0	5954	5954	-	
26/02	19.00	49.5	120.8	268	302	302	-	-	28/02	7.00	20.4	150.0	0	4462	4462	-	
26/02	20.00	46.4	123.9	160	756	756	-	-	28/02	8.00	20.3	150.1	0	3352	3352	-	
26/02	21.00	44.0	126.4	0	1193	1193	-	-	28/02	9.00	24.7	145.7	0	2900	2900	-	
26/02	22.00	41.1	129.3	0	2202	2202	-	-	28/02	10.00	27.4	143.0	0	5577	5577	-	
26/02	23.00	35.6	134.8	0	2424	2424	-	-	28/02	11.00	36.0	134.4	0	4486	4486	-	
27/02	0.00	28.2	142.2	0	2356	2356	-	-	28/02	12.00	37.0	133.4	0	4996	4996	-	
27/02	1.00	33.8	136.6	0	3049	3049	-	-	28/02	13.00	34.4	136.0	0	6331	6331	-	
27/02	2.00	31.5	138.8	0	1744	1744	-	-	28/02	14.00	30.6	139.8	0	5954	5954	-	
27/02	3.00	30.4	140.0	0	1469	1469	-	-	28/02	15.00	30.4	140.0	0	7669	7669	-	
27/02	4.00	31.4	139.0	0	945	945	-	-	28/02	16.00	30.9	139.5	0	4293	4550	182	22
27/02	5.00	31.3	139.0	0	2509	2509	-	-	28/02	17.00	30.0	140.4	0	3503	3951	235	40
27/02	6.00	31.5	138.8	0	874	874	-	-	28/02	18.00	32.0	138.4	0	5384	5514	129	11
27/02	7.00	33.0	137.4	0	1386	1386	-	-	28/02	19.00	36.7	133.7	0	5456	5596	124	10
27/02	8.00	33.5	136.8	0	2815	2815	-	-	28/02	20.00	37.5	132.9	0	8116	8116	-	
27/02	9.00	36.0	134.4	0	6189	6189	-	-	28/02	21.00	36.7	133.7	0	8510	8510	-	
27/02	10.00	34.0	136.4	0	3287	3287	-	-	28/02	22.00	34.8	135.5	0	5671	5671	-	
27/02	11.00	35.0	135.4	0	3114	3114	-	-	28/02	23.00	30.4	140.0	0	4511	4795	191	25

Table B.11. Hourly revenues from electricity selling, GHG emissions costs and OPEX of the GT park for SC3 (6 h forecast horizon, 80% probability of correct dispatching).

Date	Time	$Price_{MGP}$ (€/MWh)	In_{OWT} (€/MWh)	$R_{sell,GT}$ (€)	$R_{sell,OWT}$ (€)	R_{sell} (€)	$C_{e_{GHG}}$ (€)	$OPEX_{GT}$ (€)	Date	Time	$Price_{MGP}$ (€/MWh)	In_{OWT} (€/MWh)	$R_{sell,GT}$ (€)	$R_{sell,OWT}$ (€)	R_{sell} (€)	$C_{e_{GHG}}$ (€)	$OPEX_{GT}$ (€)
26/02	0.00	34.9	135.5	0	992	992	-	-	27/02	12.00	33.0	137.4	0	1786	1786	-	-
26/02	1.00	32.0	138.4	0	378	378	-	-	27/02	13.00	30.7	139.6	0	815	815	-	-
26/02	2.00	27.9	142.5	0	513	513	-	-	27/02	14.00	28.9	141.5	286	0	286	196	26
26/02	3.00	26.3	144.1	0	497	497	-	-	27/02	15.00	28.6	141.8	407	0	407	230	38
26/02	4.00	26.2	144.2	0	1016	1016	-	-	27/02	16.00	29.7	140.7	566	0	566	264	51
26/02	5.00	26.3	144.1	78	513	591	108	8	27/02	17.00	33.0	137.4	945	0	945	328	76
26/02	6.00	30.5	139.9	109	505	614	120	10	27/02	18.00	38.2	132.2	1124	606	1730	333	78
26/02	7.00	36.0	134.4	231	116	347	161	17	27/02	19.00	46.5	123.9	1322	1414	2736	327	76
26/02	8.00	39.0	131.4	330	0	330	183	23	27/02	20.00	46.0	124.4	1038	2764	3802	287	60
26/02	9.00	45.0	125.4	413	0	413	189	24	27/02	21.00	40.0	130.3	349	5214	5563	185	23
26/02	10.00	45.5	124.9	438	42	480	193	26	27/02	22.00	35.0	135.4	144	6024	6169	130	11
26/02	11.00	43.6	126.8	391	387	778	188	24	27/02	23.00	31.4	139.0	0	7375	7375	-	-
26/02	12.00	39.0	131.4	307	697	1003	177	21	28/02	0.00	25.0	145.4	0	7270	7270	-	-
26/02	13.00	36.0	134.4	372	328	700	200	28	28/02	1.00	26.2	144.2	0	6354	6354	-	-
26/02	14.00	36.0	134.4	438	119	557	214	32	28/02	2.00	21.9	148.5	142	5624	5766	162	17
26/02	15.00	37.4	132.9	421	328	749	207	30	28/02	3.00	19.2	151.2	209	4850	5060	204	29
26/02	16.00	37.6	132.8	414	420	834	205	29	28/02	4.00	17.7	152.6	64	6024	6088	120	10
26/02	17.00	37.5	132.9	442	395	837	211	31	28/02	5.00	17.3	153.0	80	5577	5656	137	12
26/02	18.00	43.8	126.6	583	192	775	223	35	28/02	6.00	17.5	152.9	0	5954	5954	-	0
26/02	19.00	49.5	120.8	644	302	946	221	35	28/02	7.00	20.4	150.0	105	4462	4568	145	14
26/02	20.00	46.4	123.9	512	756	1268	205	29	28/02	8.00	20.3	150.1	62	3352	3414	110	8
26/02	21.00	44.0	126.4	388	1193	1581	186	23	28/02	9.00	24.7	145.7	0	2900	2900	-	-
26/02	22.00	41.1	129.3	133	2202	2335	113	9	28/02	10.00	27.4	143.0	0	5577	5577	-	-
26/02	23.00	35.6	134.8	0	2424	2424	-	-	28/02	11.00	36.0	134.4	0	4486	4486	-	-
27/02	0.00	28.2	142.2	95	2356	2450	116	-	28/02	12.00	37.0	133.4	0	4996	4996	-	-
27/02	1.00	33.8	136.6	0	3049	3049	-	-	28/02	13.00	34.4	136.0	0	6331	6331	-	-
27/02	2.00	31.5	138.8	0	1744	1744	-	-	28/02	14.00	30.6	139.8	0	5954	5954	-	-
27/02	3.00	30.4	140.0	98	1469	1567	113	-	28/02	15.00	30.4	140.0	0	7669	7669	-	-
27/02	4.00	31.4	139.0	159	945	1104	144	13	28/02	16.00	30.9	139.5	0	4293	4293	-	-
27/02	5.00	31.3	139.0	0	2509	2509	-	-	28/02	17.00	30.0	140.4	0	3503	3503	-	-
27/02	6.00	31.5	138.8	0	874	874	-	-	28/02	18.00	32.0	138.4	0	5384	5384	-	-
27/02	7.00	33.0	137.4	0	1386	1386	-	-	28/02	19.00	36.7	133.7	0	5456	5456	-	-
27/02	8.00	33.5	136.8	0	2815	2815	-	-	28/02	20.00	37.5	132.9	0	8116	8116	-	-
27/02	9.00	36.0	134.4	0	6189	6189	-	-	28/02	21.00	36.7	133.7	0	8510	8510	-	-
27/02	10.00	34.0	136.4	0	3287	3287	-	-	28/02	22.00	34.8	135.5	0	5671	5671	-	-
27/02	11.00	35.0	135.4	0	3114	3114	-	-	28/02	23.00	30.4	140.0	0	4511	4795	-	-

Table B.12. Hourly revenues from electricity selling, GHG emissions costs and OPEX of the GT park for SC4 (6 h forecast horizon, 90% probability of correct dispatching).

Date	Time	$Price_{MGP}$ (€/MWh)	In_{OWT} (€/MWh)	$R_{sell,GT}$ (€)	$R_{sell,OWT}$ (€)	R_{sell} (€)	$C_{e_{GHG}}$ (€)	$OPEX_{GT}$ (€)	Date	Time	$Price_{MGP}$ (€/MWh)	In_{OWT} (€/MWh)	$R_{sell,GT}$ (€)	$R_{sell,OWT}$ (€)	R_{sell} (€)	$C_{e_{GHG}}$ (€)	$OPEX_{GT}$ (€)
26/02	0.00	34.9	135.5	0	992	992	-	-	27/02	12.00	33.0	137.4	0	1786	1786	-	-
26/02	1.00	32.0	138.4	0	378	378	-	-	27/02	13.00	30.7	139.6	0	815	815	-	-
26/02	2.00	27.9	142.5	0	513	513	-	-	27/02	14.00	28.9	141.5	0	0	0	-	-
26/02	3.00	26.3	144.1	0	497	497	-	-	27/02	15.00	28.6	141.8	190	0	190	164	18
26/02	4.00	26.2	144.2	0	1016	1016	-	-	27/02	16.00	29.7	140.7	341	0	341	209	31
26/02	5.00	26.3	144.1	0	513	513	-	-	27/02	17.00	33.0	137.4	695	0	695	277	56
26/02	6.00	30.5	139.9	0	505	505	-	-	27/02	18.00	38.2	132.2	834	606	1440	282	58
26/02	7.00	36.0	134.4	0	116	116	-	-	27/02	19.00	46.5	123.9	970	1414	2384	276	56
26/02	8.00	39.0	131.4	0	0	0	-	-	27/02	20.00	46.0	124.4	689	2764	3453	235	40
26/02	9.00	45.0	125.4	0	0	0	-	-	27/02	21.00	40.0	130.3	0	5214	5214	-	-
26/02	10.00	45.5	124.9	0	42	42	-	-	27/02	22.00	35.0	135.4	0	6024	6024	-	-
26/02	11.00	43.6	126.8	0	387	387	-	-	27/02	23.00	31.4	139.0	0	7375	7375	-	-
26/02	12.00	39.0	131.4	0	697	697	-	-	28/02	0.00	25.0	145.4	0	7270	7270	-	-
26/02	13.00	36.0	134.4	0	328	328	-	-	28/02	1.00	26.2	144.2	0	6354	6354	-	-
26/02	14.00	36.0	134.4	165	119	284	137	12	28/02	2.00	21.9	148.5	0	5624	5624	-	-
26/02	15.00	37.4	132.9	137	328	465	121	10	28/02	3.00	19.2	151.2	64	4850	4914	115	9
26/02	16.00	37.6	132.8	129	420	549	117	9	28/02	4.00	17.7	152.6	0	6024	6024	-	-
26/02	17.00	37.5	132.9	157	395	552	131	11	28/02	5.00	17.3	153.0	0	5577	5577	-	-
26/02	18.00	43.8	126.6	250	192	443	153	15	28/02	6.00	17.5	152.9	0	5954	5954	-	-
26/02	19.00	49.5	120.8	268	302	570	149	14	28/02	7.00	20.4	150.0	0	4462	4462	-	-
26/02	20.00	46.4	123.9	160	756	916	117	9	28/02	8.00	20.3	150.1	0	3352	3352	-	-
26/02	21.00	44.0	126.4	0	1193	1193	-	-	28/02	9.00	24.7	145.7	0	2900	2900	-	-
26/02	22.00	41.1	129.3	0	2202	2202	-	-	28/02	10.00	27.4	143.0	0	5577	5577	-	-
26/02	23.00	35.6	134.8	0	2424	2424	-	-	28/02	11.00	36.0	134.4	0	4486	4486	-	-
27/02	0.00	28.2	142.2	0	2356	2356	-	-	28/02	12.00	37.0	133.4	0	4996	4996	-	-
27/02	1.00	33.8	136.6	0	3049	3049	-	-	28/02	13.00	34.4	136.0	0	6331	6331	-	-
27/02	2.00	31.5	138.8	0	1744	1744	-	-	28/02	14.00	30.6	139.8	0	5954	5954	-	-
27/02	3.00	30.4	140.0	0	1469	1469	-	-	28/02	15.00	30.4	140.0	0	7669	7669	-	-
27/02	4.00	31.4	139.0	0	945	945	-	-	28/02	16.00	30.9	139.5	0	4293	4293	-	-
27/02	5.00	31.3	139.0	0	2509	2509	-	-	28/02	17.00	30.0	140.4	0	3503	3503	-	-
27/02	6.00	31.5	138.8	0	874	874	-	-	28/02	18.00	32.0	138.4	0	5384	5384	-	-
27/02	7.00	33.0	137.4	0	1386	1386	-	-	28/02	19.00	36.7	133.7	0	5456	5456	-	-
27/02	8.00	33.5	136.8	0	2815	2815	-	-	28/02	20.00	37.5	132.9	0	8116	8116	-	-
27/02	9.00	36.0	134.4	0	6189	6189	-	-	28/02	21.00	36.7	133.7	0	8510	8510	-	-
27/02	10.00	34.0	136.4	0	3287	3287	-	-	28/02	22.00	34.8	135.5	0	5671	5671	-	-
27/02	11.00	35.0	135.4	0	3114	3114	-	-	28/02	23.00	30.4	140.0	0	4511	4511	-	-

Appendix C.

Set of event trees for offshore oil & gas production operations

C.1. Introduction

The set of reference event trees developed in the inherent safety assessment methodology described in Section 4.5 and used in the application of the method to case-study 3 and case-study 5 are presented in the following. R1, R2, R3a and R3b are the reference release modes defined in Table 4.20. The letters a to l identify the reference event tree corresponding to the release. The codes marked with star (*) refer to a release below the sea surface level.

C.2. Set of event trees

	Reference release mode	Secondary critical event	Tertiary critical event	Accident scenario	Effect
a)	R1/R2 /R3b	Pool formation	Pool ignited	Pool fire	Thermal radiation
	Liquid		Gas dispersion	Toxic cloud	Toxic concentration
				VCE	Overpressure
			Slick formation on the sea surface	Flash fire	Thermal radiation
				Toxic cloud	Toxic concentration
			Dissolution in water column	Environmental damage	Ecotoxic thickness
				Environmental damage	Ecotoxic concentration
b)	R3a	Pool formation	Pool ignited	Pool fire	Thermal radiation
	Liquid		Gas dispersion	Toxic cloud	Toxic concentration
				VCE	Overpressure
			Slick formation on the sea surface	Flash fire	Thermal radiation
				Toxic cloud	Toxic concentration
			Dissolution in water column	Environmental damage	Ecotoxic thickness
				Environmental damage	Ecotoxic concentration
c)	R3a	Catastrophic rupture	Vessel burst	Overpressure generation	Overpressure
	Liquid	Pool formation	Pool ignited	Pool fire	Thermal radiation
			Gas dispersion	Toxic cloud	Toxic concentration
				VCE	Overpressure
			Slick formation on the sea surface	Flash fire	Thermal radiation
				Toxic cloud	Toxic concentration
			Dissolution in water column	Environmental damage	Ecotoxic thickness
				Environmental damage	Ecotoxic concentration
d)	R1/R2/R3b	Gas jet	Gas jet ignited	Jet fire	Thermal radiation
	Gas		Gas dispersion	Toxic cloud	Toxic concentration
				VCE	Overpressure
				Flash fire	Thermal radiation
				Toxic cloud	Toxic concentration

e)

R3a	Gas puff	Gas puff ignited	Toxic cloud	Toxic concentration
Gas		Gas dispersion	VCE	Overpressure
			Flash fire	Thermal radiation
			Toxic cloud	Toxic concentration

f)

R3a	Catastrophic rupture	Vessel burst	BLEVE	Overpressure
Gas	Gas puff	Gas puff ignited	Fireball	Thermal radiation
			Toxic cloud	Toxic concentration
		Gas dispersion	VCE	Overpressure
			Flash fire	Thermal radiation
			Toxic cloud	Toxic concentration

g)

R1/R2/R3b	Pool formation	Pool ignited	Pool fire	Thermal radiation
Liquid-Gas			Toxic cloud	Toxic concentration
		Gas dispersion	VCE	Overpressure
			Flash fire	Thermal radiation
			Toxic cloud	Toxic concentration
		Slick formation on the sea surface	Environmental damage	Ecotoxic thickness
		Dissolution in water column	Environmental damage	Ecotoxic concentration
	Two-phase jet	Two-jet ignited	Jet fire	Thermal radiation
			Toxic cloud	Toxic concentration
		Gas dispersion	VCE	Overpressure
			Flash fire	Thermal radiation
			Toxic cloud	Toxic concentration

h)

R3a	Pool formation	Pool ignited	Pool fire	Thermal radiation
Liquid-Gas			Toxic cloud	Toxic concentration
		Gas dispersion	VCE	Overpressure
			Flashfire	Thermal radiation
			Toxic cloud	Toxic concentration
		Slick formation on sea surface	Environmental damage	Ecotoxic thickness
		Dissolution in water column	Environmental damage	Ecotoxic concentration
	Aerosol puff	Puff ignited	Toxic cloud	Toxic concentration
		Gas dispersion	VCE	Overpressure
			Flash fire	Thermal radiation
			Toxic cloud	Toxic concentration

i)	R3a	Catastrophic rupture	Vessel burst	BLEVE	Overpressure
	Liquid-Gas	Pool formation	Pool ignited	Pool fire	Thermal radiation
			Gas dispersion	Toxic cloud	Toxic concentration
				VCE	Overpressure
			Slick formation on sea surface	Flashfire	Thermal radiation
				Toxic cloud	Toxic concentration
				Environmental damage	Ecotoxic thickness
			Dissolution in water column	Environmental damage	Ecotoxic concentration
		Aerosol puff	Puff ignited	Fireball	Thermal radiation
			Gas dispersion	Toxic cloud	Toxic concentration
				VCE	Overpressure
				Flash fire	Thermal radiation
				Toxic cloud	Toxic concentration

l)*	R1/R2/R3b	Pool formation on sea surface	Pool ignited	Pool fire	Thermal radiation
	Liquid		Gas dispersion	Toxic cloud	Toxic concentration
				VCE	Overpressure
			Slick formation on sea surface	Flash fire	Thermal radiation
				Toxic cloud	Toxic concentration
				Environmental damage	Ecotoxic thickness
			Dissolution in water column	Environmental damage	Ecotoxic concentration
		Subsea liquid dispersion	Dissolution in water column	Environmental damage	Ecotoxic concentration

m)*	R1/R2/R3 b	Subsea gas dispersion up to the sea surface	Gas dispersion to the atmosphere	VCE	Overpressure
	Gas			Flash fire	Thermal radiation
				Toxic cloud	Toxic concentration

n)*	R1/R2/R3b	Pool formation and gas plume on the sea surface	Pool ignited	Pool fire	Thermal radiation
	Liquid-Gas		Gas dispersion	Toxic cloud	Toxic concentration
				VCE	Overpressure
			Slick formation on sea surface	Flash fire	Thermal radiation
				Toxic cloud	Toxic concentration
				Environmental damage	Ecotoxic thickness
			Dissolution in water column	Environmental damage	Ecotoxic concentration
		Subsea two-phase dispersion	Dissolution in water column	Environmental damage	Ecotoxic concentration

Appendix D.

Reference process schemes and intensified flowsheets of alternative CH_3OH production routes

D.1. Introduction

In the following, the eleven novel process routes for alternative CH_3OH production introduced in case-study 5 are described, including the details of the reference process schemes selected from the literature and the intensified process flowsheets simulated in Aspen HYSYS. Furthermore, geometric and economic data associated to two specific flowsheets are presented in view of the PrI screening assessment.

D.2. Data for CO_2-based processes

D.2.1. Data for catalytic hydrogenation of CO_2

D.2.1.1. Definition of reference process scheme

The thermo-catalytic plant designed and simulated by Matzen et al. [216] is adapted in the analysis of case-study 5 for CH_3OH synthesis by means of the catalytic hydrogenation of CO_2. The input materials are pure gaseous H_2 at 25 °C and 33 bar and liquid CO_2 at -25.6 °C and 16.4 bar. H_2 requires to be compressed and then mixed with the pumped stream of CO_2 and with a recycle stream previously compressed to reach the molar ratio of H_2 to CO_2 of 3:1. The resulting mixture is pre-heated and then fed to the multi-tubular catalytic reactor where the following scheme of reactions take place at continuous operation mode:

$$CO_2 + 3\,H_2 = CH_3OH + H_2O \qquad \Delta H°(298\ K) = -49.4\ kJ/mol \qquad (D.1)$$

$$CO + 2\,H_2 = CH_3OH \qquad \Delta H°(298\ K) = -90.55\ kJ/mol \qquad (D.2)$$

$$CO_2 + H_2 = H_2O + CO \qquad \Delta H°(298\ K) = 41.12\ kJ/mol \qquad (D.3)$$

where $\Delta H°$ is the standard enthalpy of reaction. The synthesis occurs at operating conditions of 235 °C bar and 50 bar, over the catalyst $Cu/ZnO/Al_2O_3$, according to the low-pressure isothermal Lurgy's system. At these conditions, the molar ratio H_2 to CO_2 is about 2.1 and molar conversion of CO_2 at the reactor is estimated about 47%. The gas stream from the reactor is then cooled down and expanded through a throttling valve to allow the atmospheric separation of CH_3OH and H_2O from the other compounds in the flash drum. The liquid obtained from the separation enters into the atmospheric distillation unit. Due to higher volatility, liquid CH_3OH is obtained in the distillate phase with composition of 99.7%wt (99.5%mol), while H_2O represents the waste stream of the unit with a composition of 98.3%wt (99.0%mol), both at 25°C and 1.01 bar [216]. The multi-tubular reactor designed by Matzen et al. has 15 tubes with a diameter 0.127 m and a length of 5 m, loaded with a total of 250 kg of catalyst. The distillation column has 20 stages with a feed stage 17 and partial top-condenser. Table D.1 summarizes the global material balance for the CH_3OH plant. The yield of CH_3OH in the distillate stream with respect to CO_2 in input is 98.9%.

Table D.1. Mass balance for the reference process scheme based on catalytic hydrogenation of CO_2.

Compound	Inlet flowrate		Outlet flowrate	
	kmol/h	t/h	kmol/h	t/h
CO_2	131.1	5.767	-	-
H_2	394.3	0.787	1.37	0.00274
CH_3OH	-	-	129.69	4.15
H_2O	-	-	130.44	2.35

D.2.1.2. Definition of intensified process flowsheet

Figure D.1 illustrates the intensified process flowsheet produced with Aspen HYSYS simulation for catalytic hydrogenation of CO_2. Data about the material streams in the flowsheet is summarized in Table D.2, while Table D.3 reports information on the energy streams and utilities related to the relevant components in the flowsheet.

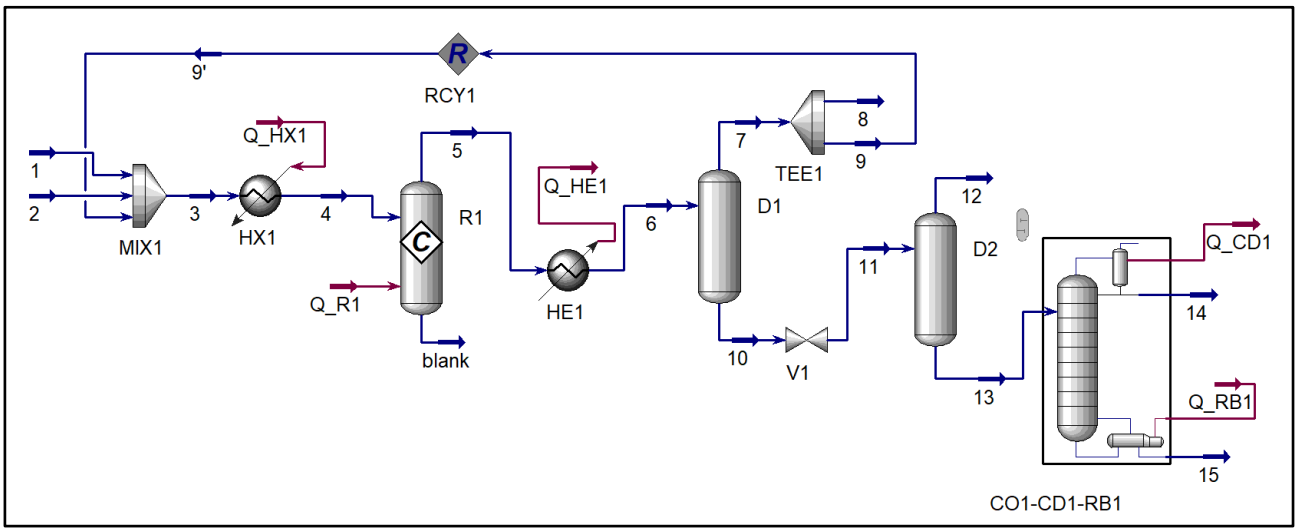

Figure D.1. Intensified process flowsheet for catalytic hydrogenation of CO_2 from Aspen HYSYS simulation.

As shown in Figure D.1, CO_2 (stream 1) and H_2 (stream 2) are mixed with gas recycle stream and then pre-heated in HX1 to reach the required temperature for reaction in R1. According to the reactions illustrated in Equations (D.1)-(D.3), the stoichiometry in R1 is set as -1, -2, +1, +1 for CO_2, H_2, H_2O, CH_3OH, respectively, while the conversion of CO_2 at the reactor is fixed as 47% as reported in the reference process scheme. The output stream from R1 is then cooled down in cooler HE1 and enters high-pressure flash drum D1 to separate gas and liquid phase. Gas outlet from D1 (stream 7) is then recycled, while liquid outlet (stream 10) is depressurized in V1 up to atmospheric conditions and then further separated into gas and liquid streams in flash drum D2. Liquid outlet from D2 (stream 13) finally feeds the distillation unit composed of column CO1, top-condenser CD1 and bottom-reboiler RB1. Distillate rate of 15.64 kmol/h, reflux ratio of 1.218 and number of stages as 12 (feed in stage 8) are set in CO1-CD1-RB1 unit.

Input flowrates of CO_2 and H_2 (streams 1 and 2 in Figure D.1) are adjusted in order to meet in the inlet of the reactor (stream 4 in Figure D.1) the molar ratio H_2 to CO_2 of 2.1 reported in the reference process scheme. As shown in Table D.3, the heat flow generated in R1 is used to produce steam at medium pressure (MP steam utility) which is further recovered to supply the required heat to RB1.

Table D.2. Data on material streams of the intensified process flowsheet illustrated in Figure D.1.

Stream	Vapor phase fraction	Temperature (°C)	Pressure (kPa)	Molar flowrate (kmol/h)	Molar fraction CO_2	Molar fraction H_2	Molar fraction H_2O	Molar fraction CH_3OH
1	1.00	25	5700	28.00	1.0000	0.0000	0.0000	0.0000
2	1.00	25	15600	80.00	0.0000	1.0000	0.0000	0.0000
3	0.98	73	5000	181.98	0.3096	0.6515	0.0097	0.0292
4	1.00	235	5000	181.98	0.3096	0.6515	0.0097	0.0292
5	1.00	235	5000	129.02	0.2314	0.3032	0.2190	0.2464
6	0.58	120	5000	129.02	0.2314	0.3032	0.2190	0.2464
7	1.00	120	5000	74.77	0.3829	0.5213	0.0239	0.0719
8	1.00	120	5000	0.07	0.3829	0.5213	0.0239	0.0719
9	1.00	120	5000	74.70	0.3829	0.5213	0.0239	0.0719
9’	1.00	120	5000	73.98	0.3831	0.5212	0.0240	0.0718
10	0.00	120	5000	54.25	0.0226	0.0026	0.4878	0.4870
11	0.14	77	101.3	54.25	0.0226	0.0026	0.4878	0.4870
12	1.00	77	101.3	7.55	0.1608	0.0189	0.1939	0.6264
13	0.00	77	101.3	46.69	0.0002	0.0000	0.5354	0.4644
14	0.00	63	101.3	15.64	0.0007	0.0000	0.0003	0.9990
15	0.00	94	101.3	31.05	0.0000	0.0000	0.8049	0.1951

Table D.3. Data on energy streams associated to components of the intensified process flowsheet in Figure D.1.

Stream	Heat flow (kW)	Utility	Pressure (kPa)	Inlet temperature (°C)	Outlet temperature (°C)	Utility mass flowrate (kg/h)
Q_R1	-462.40	MP steam generation	889.9	174	175	688.70
Q_HE1	691.89	Cooling water 1	250	30	40	57737.86
Q_CD1	365.63	Cooling water 1	250	30	40	30511.92
Q_RB1	379.07	MP steam	889.9	175	174	688.70
Q_HX1	317.61	HP steam	3913	250	249	671.36

MP: medium pressure, HP: high pressure

The performance of the CH_3OH production plant obtained with the proposed intensified process flowsheet is: relatively pure liquid CH_3OH in the distillate with the benchmark flowrate (stream 14) at 63°C and 1.01 bar, overall conversion of CO_2 of 99.9% and overall yield of CH_3OH with respect to input CO_2 of 55.80%.

D.2.1.3. Definition of final intensified process flowsheet

Table D.2 summarizes the information about the material streams of the final intensified process scheme for catalytic hydrogenation of CO_2 illustrated in Figure 5.30, as a result of step 2 of the methodology. The information about the energy streams is instead reported in Table D.3.

For each component in Figure 5.30, Table D.4 summarizes the main geometric data derived from the conceptual scale-up and design of process equipment in step 2 of the procedure, main factors considered for equipment costs, purchased cost and the final bare-module cost (C_{bm}) according to the Guthrie method. Equations proposed for cost estimation of process equipment [361] and CH_3OH synthesis reactor [219] are used in this case-study. To convert costs from $\$_{2006}$ into $€_{2019}$, CEPCI values of 500 (for 2006) and 613.3 (for 2019) [690] and exchange rate from $\$_{2019}$ to $€_{2019}$ of 0.8935 [174] are applied by means of Equation (4.1).

Table D.4. Geometric and economic data of the units in the final intensified process flowsheet illustrated in Figure 5.30.

Unit	Main geometric information	Design temper. and press.	Size factor for cost function	M/L/P factors for cost function	Main costs ($\$_{2006}$)	Purchased costs ($\$_{2006}$)	Bare-module factor	Bare-module cost $\mathbf{C_{bm}}$ ($€_{2019}$)
HX1	Horizontal, carbon steel, 60 tubes (6 passes, 2 m length), 365 mm shell diameter, 9.42 m^2 geometrical area	532°F, 1066 psig	Area:150 ft^2	M: 1, L: 1.25, P: 1.37	Base cost: 7379	$1.26 \cdot 10^4$	3.17	$4.38 \cdot 10^4$
R1	4 tubes (57 mm external diameter, 2 m length)	-	Inlet gas flowrate: 2920.6 kg/h	-	-	$2.50 \cdot 10^6$	4.30	$1.18 \cdot 10^7$
HE1	Horizontal, carbon steel, 42 tubes (6 passes, 2 m length), 316 mm shell diameter, 6.6 m^2 geometrical area	505°F, 1066 psig	Area: 150 ft^2	M: 1, L: 1.25, P: 1.37	Base cost: 7379	$1.26 \cdot 10^4$	3.17	$4.38 \cdot 10^4$
D1	Vertical, carbon steel, 508 mm diameter, 3.05 m height	298°F, 804 psig	Weight: 4200 lb, Diameter: 3 ft, Height: 12 ft	M: 1	Vessel: 25209, platform and ladders: 4722	$2.99 \cdot 10^4$	4.30	$1.41 \cdot 10^5$
V1	-	-	-	-	-	-	-	-
D2	Vertical, carbon steel, 508 mm diameter, 3.05 m height	221°F, 10 psig	Diameter: 3 ft, height: 12 ft	-	Platform and ladders: 4722	$4.72 \cdot 10^3$	4.30	$2.23 \cdot 10^4$
CO1	Vertical, diameter 390 mm, height 8 m, weight 243 kg, 12 trays, carbon steel	177°F, 10 psig	Weight: 9000 lb, diameter: 3 ft, height: 27 ft, no. of trays: 12	M: 1	Vessel: 51121, platform and ladders: 8471, installed trays: 10996	$7.04 \cdot 10^4$	3.	$3.33 \cdot 10^5$
CD1	Horizontal, carbon steel, 80 tubes (4 passes, 2 m length), 365 mm shell diameter, 12.6 m^2 geometrical area	196°F, 10 psig	Area: 150 ft^2	M: 1, L: 1.25, P: 0.98	Base cost: 7379	$9.06 \cdot 10^3$	3.17	$3.15 \cdot 10^4$
RB1	Vertical, carbon steel, 36 tubes (1 pass, 2 m length), 291 mm shell diameter, 7.2 m^2 geometrical area	307°F, 10 psig	Area: 150 ft^2	M: 1, L: 1.25, P: 0.98	Base cost: 7379	$9.06 \cdot 10^3$	3.17	$3.15 \cdot 10^4$

M: material, L: tube-length, P: shell-side pressure.

The method described in Seider et al. [361] for estimation of total capital investment cost (C_{tci}) and annual total production cost (C_{prod}) of an onshore chemical process plant is adopted for economic assessment of the process scheme. Table D.5 summarizes calculations, assumptions and values for the cost segments.

Table D.5. Cost segments of total capital investment and annual production costs for the scheme in Figure 5.30.

Cost segment	Calculation	Assumption	Cost value
Total bare-module for process equipment (C_{tbm})	Sum of C_{bm} values in Table C4	-	$1.24 \cdot 10^7$ €$_{2019}$
Site (C_{site})	15% C_{tbm}	Grass-roots onshore plant	$1.86 \cdot 10^6$ €$_{2019}$
Building (C_{build})	30% C_{tbm}	Process and non-process buildings in a grass-roots plant	$3.72 \cdot 10^6$ €$_{2019}$
Offsite facilities (C_{all})	820 \$ · $(Size_{steam})^{0.81}$	$Size_{steam}$ (HX1): 2000 lb/h	$2.50 \cdot 10^6$ €$_{2019}$
	1000 \$ · $(Size_{water})^{0.68}$	$Size_{water}$ (HE1+CD1): 1000 gpm	$1.20 \cdot 10^5$ €$_{2019}$
Total depreciable capital (C_{tdc})	1.18 · (C_{tbm} + C_{all} + C_{build} + C_{site})	Share of 3% contractor's fee and 15% contingency	$2.46 \cdot 10^7$ €$_{2019}$
Royalties (C_{roy})	2% C_{tdc}	Preliminary estimate	$4.92 \cdot 10^5$ €$_{2019}$
Start-up (C_{start})	30% C_{tdc}	Relatively new process	$7.38 \cdot 10^6$ €$_{2019}$
Total permanent investment (C_{dpi})	C_{tdc} + C_{roy} + C_{start}	-	$3.25 \cdot 10^7$ €$_{2019}$
Raw material (C_{raw})	H_2: 7 €/kg	Market price [631]	$6.80 \cdot 10^7$ €$_{2019}$/y
	CO_2: 0.025 €/kg	Market price [714]	$2.43 \cdot 10^5$ €$_{2019}$/y
Utility (C_{util})	HP steam: 0.0145 \$/kg	Typical cost [361]	$6.86 \cdot 10^4$ €$_{2019}$/y
	H_2O for MP steam generation: 0.5 \$/m^3	Typical cost [361]	$2.55 \cdot 10^3$ €$_{2019}$/y
	Cooling water: 0.02 \$/m^3	Typical cost [361]	$1.24 \cdot 10^4$ €$_{2019}$/y
Direct wages and benefits ($C_{dw\&b}$)	5 shifts · operators/shift · 2080 h/y · 35 \$/y	3 sections (reaction, vapor recovery, liquid separation), 1 operator per section, continuous operations fluids processing in medium plant	$9.76 \cdot 10^5$ €$_{2019}$/y
Directs salaries and benefits ($C_{sal,o}$)	15% $C_{dw\&b}$	-	$1.46 \cdot 10^5$ €$_{2019}$/y
Operating supplies (C_{suppl})	6% $C_{dw\&b}$	-	$5.85 \cdot 10^4$ €$_{2019}$/y
Technical assistance (C_{assist})	60000\$ · operators/shift	-	$1.61 \cdot 10^5$ €$_{2019}$/y
Control laboratory (C_{lab})	65000\$ · operators/shift	-	$1.74 \cdot 10^5$ €$_{2019}$/y
Labor-related operations (C_O)	$C_{dw\&b}$ + $C_{sal,o}$ + C_{suppl} + C_{assist} + C_{lab}	-	$1.52 \cdot 10^6$ €$_{2019}$/y
Maintenance wages and benefits ($C_{mw\&b}$)	3.5% C_{tdc}	Fluid handling process	$8.61 \cdot 10^5$ €$_{2019}$/y
Salaries and benefits ($C_{sal,m}$)	25% $C_{mw\&b}$	-	$2.15 \cdot 10^5$ €$_{2019}$/y
Material and services (C_{serv})	100% $C_{mw\&b}$	-	$8.61 \cdot 10^5$ €$_{2019}$/y
Maintenance overhead ($C_{over,m}$)	5% $C_{mw\&b}$	-	$4.31 \cdot 10^4$ €$_{2019}$/y
Maintenance (C_M)	$C_{mw\&b}$ + $C_{sal,m}$ + C_{serv} + $C_{over,m}$	-	$1.98 \cdot 10^6$ €$_{2019}$/y
Operating overhead ($C_{over,o}$)	0.228 · ($C_{dw\&b}$ + $C_{sal,o}$ + $C_{mw\&b}$ + $C_{sal,m}$)		$5.01 \cdot 10^5$ €$_{2019}$/y
Property tax and insurance (C_{tax})	2% C_{tdc}	Process of low risk located away from a heavily populated area	$4.92 \cdot 10^5$ €$_{2019}$/y
Direct plant depreciation ($C_{d,dir}$)	8% (C_{tdc} – 1.18 C_{all})	-	$1.70 \cdot 10^6$ €$_{2019}$/y
Allocated plant depreciation ($C_{d,all}$)	6% (1.18 C_{all})	-	$2.20 \cdot 10^5$ €$_{2019}$/y
Sales (S)	CH_3OH: 0.350 €/kg	Market price [632]	$1.38 \cdot 10^6$ €$_{2019}$/y
Licensing fee	2% S	Preliminary estimate	$4.15 \cdot 10^4$ €$_{2019}$/y
Cost of manufacture (C_{COM})	C_{raw} + C_{util} + C_O + C_M + $C_{over,o}$ + C_{tax} + $C_{d,dir}$ + $C_{d,all}$ + C_{lic}	-	$7.48 \cdot 10^7$ €$_{2019}$/y
General expenses (C_{gen})	11.55% S	-	$1.60 \cdot 10^5$ €$_{2019}$/y
Total production cost (C_{prod})	C_{COM} + C_{prod}	-	$7.49 \cdot 10^7$ €$_{2019}$/y
Working capital cost (C_{wc})	18.58% S + 8.33% C_{raw}	30 days for cash reserves, 7 days for liquid inventory, 30 days for accounts receivable and payable	$1.21 \cdot 10^7$ €$_{2019}$
Total capital investment (C_{tci})	C_{dpi} + C_{wc}	-	$4.45 \cdot 10^7$ €$_{2019}$

D.2.2. Data for electrochemical reduction of CO_2

D.2.2.1. Definition of reference process scheme

At an electrochemical cell, the reduction reaction of CO_2 at the cathode is combined with an oxidation reaction consisting in the H_2O electrolysis (or H_2 evolution reaction) at the anode to give the overall reaction of CH_3OH. The semi-reactions and overall reaction under standard conditions and continuous operation mode are [213]:

$$CO_2 + 6\,H^+ + 6\,e^- \rightarrow CH_3OH + H_2O \qquad E^\circ(298\ K) = -0.22\ V\ (vs.\ SCE) \qquad (D.4)$$

$$3\,H_2O \rightarrow 1.5\,O_2 + 6\,H^+ + 6\,e^- \qquad E^\circ(298\ K) = 0.99\ V\ (vs.\ SCE) \qquad (D.5)$$

$$CO_2 + 2\,H_2O + 6\,e^- = CH_3OH + 1.5\,O_2 \qquad E^\circ(298\ K) = 1.21\ V \qquad (D.6)$$

where E° is the standard electrode potential and SCE is saturated calomel electrode. These reactions generally occur at ambient conditions in an aqueous solution electrolyte and with a given catalyst material at the electrodes. The operating mode is typically continuous in a two-compartment electrochemical cell or undivided three-electrode electrochemical cell. In order to achieve high selectivity of the reaction for the production of CH_3OH (i.e. the faradic efficiency) and high production rates of CH_3OH, the selection of the suitable electrode material is crucial in order to avoid that energy consumption from the H_2 evolution reaction and thus promote the CO_2 reduction. Among the materials widely investigated for this process, Cu and Cu-based metals are very active leading to high values of current density (33 mA/cm) and faradaic efficiency greater than 100%.

The study by Albo et al. [674] investigating the performance of electrodes based on Cu_2O and Cu_2O-ZnO mixtures in a filter-press electrochemical cell towards CO_2 electroreduction to CH_3OH is assumed as reference process scheme for case-study 5. The cell is a standard three-electrode configuration composed of a cathode compartment and anode compartment separated by a Nafion 117 cation exchange membrane. The dimensions are height of 120 mm, width of 70 mm, length greater than 33 mm. A platinised titanium electrode is used as the anode and Ag/AgCl (saturated KCl) as reference electrode. The Cu_2O and Cu_2O/ZnO-catalyzed carbon papers are instead adopted as the working electrodes. The superficial area of each electrode is 10 cm^2, the electrode gap ranges from 0.7 to 8 mm with standard value of 4 mm. A CO_2 saturated 0.5 M $KHCO_3$ aqueous solution is used as both catholyte and anolyte. After the initial CO_2 bubbling in the aqueous solution, CO_2 is bubbled continuously in the catholyte during the experiment time of 90 min at constant voltage of -1.3 V vs. Ag/AgCl, in order to maintain the required CO_2 concentration for CH_3OH formation.

From the set of experiments with flowrate of electrolyte per unit of cathode area of 2 mL/min-cm^2, the highest faradaic efficiency (i.e. 45.7%) and highest rate of CH_3OH production (i.e. $6.08 \cdot 10^{-5}$ mol/m^2-s) are obtained when Cu_2O-based electrode is used and contains 1 mg/cm^2 under current density is 6.93 mA/cm^2 [674]. However, stability of the Cu_2O-based electrodes is critical for the industrial development of the electrochemical conversion of CO_2 into CH_3OH. It is resulted that Cu_2O/ZnO-based electrodes show better stability than the Cu_2O-deposited carbon papers during CH_3OH synthesis. For this reason, the production data obtained by using electrodes of Cu_2O/ZnO mixture (1:1 weight ratio) are assumed for the analysis of case-study 5, i.e. production CH_3OH rate per unit of electrode area of $3.17 \cdot 10^{-5}$ mol/m^2-s with 17.7% faradaic efficiency by using an input flowrate of electrolyte per unit of cathode area of 2 mL/min-cm^2 [674].

From the information reported above, mass balance is made in the present analysis to estimate all the input and output flowrates and composition. Table D.6 summarizes these data. By considering the superficial area of the electrode of 10 cm^2, the flowrate of each electrolyte is derived from the ratio mentioned above. The composition of the anolyte is 4.89%wt $KHCO_3$ (0.92%mol) and 95.11%wt water (or 99.08%mol). The composition of the catholyte with saturated CO_2 is 4.88%wt $KHCO_3$ (0.92%mol) and 94.98%wt H_2O (or 99.14%mol), 0.14%wt CO_2 (0.06%mol). The CO_2 bubbled into the catholyte during the process is estimated by assuming that the minimum quantity required for CH_3OH formation is equal to the molar production rate of CH_3OH according to Equation (D.6). The composition of the saturated catholyte with bubbled CO_2 is thus 4.88%wt $KHCO_3$ (0.92%mol) and 94.95%wt H_2O (or 99.01%mol), 0.17%wt CO_2 (0.07%mol). Being one sole carbon product (CH_3OH), the extent rate of the overall reaction in Equation (C6) is equal to the molar production rate of CH_3OH. Thus, output flowrates of all compounds from the electrochemical cell can be derived from the scheme of the reactions. At these conditions, the molar conversion of CO_2 to CH_3OH at the cell is 0.246% and the yield of CH_3OH with respect to CO_2 is 0.25%. CH_3OH fraction catholyte outlet flowrate is 0.00030%wt (0.00017%mol).

Table D.6. Mass balance for the reference process scheme based on electroreduction of CO_2.

Compound	Inlet flowrate		Outlet flowrate	
	kmol/h	t/h	kmol/h	t/h
$KHCO_3/H_2O$ Anolyte	$6.55 \cdot 10^{-2}$	$1.23 \cdot 10^{-3}$	$6.55 \cdot 10^{-2}$	$1.23 \cdot 10^{-3}$
$KHCO_3/H_2O$ Catholyte	$6.54 \cdot 10^{-2}$	$1.23 \cdot 10^{-3}$	$6.54 \cdot 10^{-2}$	$1.23 \cdot 10^{-3}$
CO_2 Catholyte	$4.63 \cdot 10^{-5}$	$2.04 \cdot 10^{-6}$	$4.62 \cdot 10^{-5}$	$2.03 \cdot 10^{-6}$
CO_2 bubbling into the catholyte	$1.14 \cdot 10^{-7}$	$5.02 \cdot 10^{-9}$	$1.14 \cdot 10^{-7}$	$5.02 \cdot 10^{-9}$
CH_3OH Catholyte	-	-	$1.14 \cdot 10^{-7}$	$3.66 \cdot 10^{-9}$
O_2 Anolyte	-	-	$1.71 \cdot 10^{-7}$	$5.48 \cdot 10^{-9}$

D.2.2.2. Definition of intensified process flowsheet

Figure D.2 illustrates the intensified process flowsheet produced with Aspen HYSYS simulation for electroreduction of CO_2. Data about the material streams in the flowsheet are summarized in Table D.7, while Table D.8 reports information on the energy streams and utilities related to the relevant components in the flowsheet.

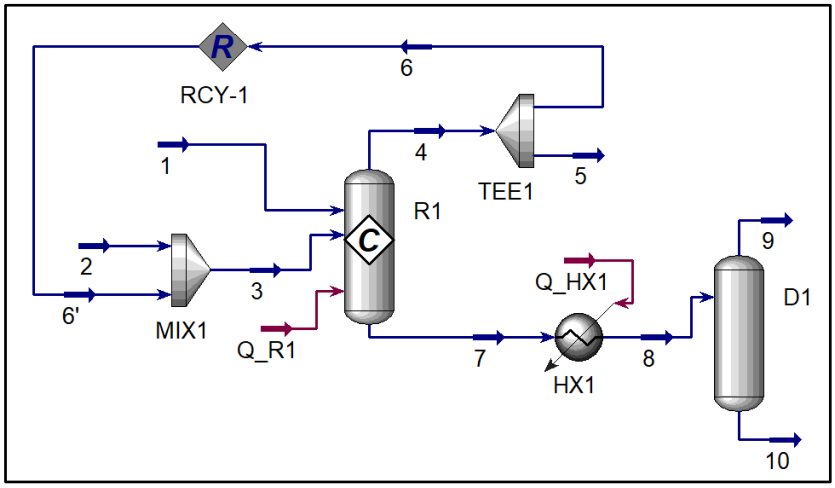

Figure D.2. Intensified process flowsheet for electroreduction of CO_2 from Aspen HYSYS simulation.

As shown in Figure D.2, CO_2 (stream 2), mixed with gas recycle stream, and liquid H_2O (stream 1) feed reactor R1. According to the global reaction illustrated in Equation (D.6), the stoichiometry in R1 is set as -2, -1, +1, +1.5 for H_2O, CO_2, CH_3OH, O_2, respectively, while the conversion of CO_2 at the reactor is fixed as 0.25% as reported in the reference process scheme. The gas output stream from R1 is then recycled, while the liquid output (stream 7) is heated in HX1 and enters atmospheric flash drum D1 to separate gas and liquid phase. No further separation operations of the liquid stream from D1 are included in the flowsheet since a merely fraction of CH_3OH is obtained in the stream (0.000175%mol).

Input flowrates of CO_2 and H_2O to the plant are adjusted in order to meet in inlet of R1 (streams 3 and 1 in Figure D.2) the molar ratio H_2O to CO_2 of 1396 reported in the reference process scheme with respect to the catholyte of the cell (Table D.6).

Even though incomplete, the performance of the CH_3OH production plant obtained with the proposed intensified process flowsheet are: highly diluted CH_3OH in H_2O in the liquid stream from D1 (stream 10) at 99.8°C and 1.01 bar, overall conversion of CO_2 of 98.08% and overall yield of CH_3OH with respect to input CO_2 of 4.92%.

Table D.7. Data on material streams of the intensified process flowsheet illustrated in Figure D.2.

Stream	Vapor phase fraction	Temperature (°C)	Pressure (kPa)	Molar flowrate (kmol/h)	Molar fraction CO_2	Molar fraction CH_3OH	Molar fraction H_2O	Molar fraction O_2
1	0.000	20.00	101.325	2825000.00	0.000	0.000	1.000	0.000
2	1.000	25.00	5700	100.00	1.000	0.000	0.000	0.000
3	1.000	24.85	101.325	27729.67	0.073	0.000	0.031	0.896
4	1.000	25.00	101.325	27629.25	0.070	0.000	0.031	0.899
5	1.000	25.00	101.325	27.63	0.070	0.000	0.031	0.899
6	1.000	25.00	101.325	27601.63	0.070	0.000	0.031	0.899
6’	1.000	25.00	101.325	27629.67	0.070	0.000	0.031	0.899
7	0.000	25.00	101.325	2825097.93	0.000	0.000	1.000	0.000
8	0.006	99.80	101.325	2825097.93	0.000	0.000	1.000	0.000
9	1.000	99.80	101.325	17873.03	0.005	0.000	0.994	0.000
10	0.000	99.80	101.325	2807224.90	0.000	0.0000018	0.9999973	0.000

Table D.8. Data on energy streams associated to components of the intensified process flowsheet in Figure D.2.

Stream	Heat flow (kW)
Q_R1	305915
Q_HX1	4791928

D.3. Data for CH_4-based processes

D.3.1. Data for homogeneous radical gas-phase reaction

D.3.1.1. Definition of reference process scheme

CH_3OH synthesis is based on partial oxidation of CH_4 in gas phase due to free radical mechanism at high temperature and pressure. To limit the formation of methyl radicals, initiators such as N_2 and sensitizers are used in the reaction mixture. The experiments performed by Yarlagadda et al. [675] is selected as reference source in the analysis of case-study 5 for CH_3OH production by means of homogeneous radical gas-phase reaction. The mechanism of reaction proposed is [675]:

$$CH_4 + O_2 \rightarrow CH_3^* + HO_2^* \quad \text{(D.7)}$$

$$CH_3^* + O_2 \rightarrow CH_3O_2^* \quad \text{(D.8)}$$

$$CH_3O_2^* \rightarrow CH_2O + OH^* \quad \text{(D.9)}$$

$$CH_3O_2^* + CH_4 \rightarrow CH_3O_2H^* + CH_3 \quad \text{(D.10)}$$

$$CH_3O_2H^* \rightarrow CH_3O^* + OH^* \quad \text{(D.11)}$$

$$CH_3O^* \rightarrow CH_2O + H^* \quad \text{(D.12)}$$

$$CH_3O^* + CH_4 \rightarrow CH_3OH + CH_3^* \quad \text{(D.13)}$$

$OH^* + CH_4 \rightarrow CH_3^* + H_2O$ (D.14)

$CH_3O^* \rightarrow CH_2O + H^*$ (D.15)

$CH_3O^* + CH_4 \rightarrow CH_3OH + CH_3^*$ (D.16)

$OH^* + CH_4 \rightarrow CH_3^* + H_2O$ (D.17)

$CH_3^* + CH_3^* \rightarrow C_2H_6$ (D.18)

$CH_3^* + CH_3O^* \rightarrow CH_3OCH_3$ (D.19)

$CH_2O + CH_3^* \rightarrow CH_4 + CHO^*$ (D.20)

$CHO^* + O_2 \rightarrow CO + HO_2^*$ (D.21)

$CH_2O + CH_3O^* \rightarrow CH_3OH + CHO^*$ (D.22)

$CHO^* + CH_3^* \rightarrow CO + CH_4$ (D.23)

Inlet gases mixture composed of 98%mol CH_4 and 2%mol N_2 is mixed with pure O_2 and routed to a tubular reactor of 0.36 cm internal diameter with an internal volume of 3.3 cm^3 or 5.7 m^3, mounted vertically in an electric furnace. The experiments occur in continuous mode during a period of 5-6 h. From the results obtained in several runs investigating the effect of temperature, pressure and O_2 concentration on conversion of CH_4 and CH_3OH selectivity, the test characterized by both higher values of conversion of CH_4 and selectivity of CH_3OH as well as less drastic operation conditions is selected for the case-study. Under reaction temperature of 451°C, pressure of 50 bar, flowrate of the inlet mixture in normal conditions of 31 mL/min ($7.66 \cdot 10^{-5}$ kmol/h) and 6.7%mol of O_2 concentration in the inlet gas stream, it is reported CH_4 molar conversion of 9.5%, CH_3OH molar selectivity of 76%, CO molar selectivity of 12.6%, CO_2 molar selectivity of 11.4% [675]. Besides the desired product CH_3OH, co-products are CO, CO_2 and H_2O. Known the compounds involving in the process, the following scheme of reactions in gas phase is derived:

$CH_4 + ½\ O_2 = CH_3OH$ (D.24)

$CH_4 + 3/2\ O_2 = CO + 2\ H_2O$ (D.25)

$CH_4 + 2\ O_2 = CO_2 + 2\ H_2O$ (D.26)

Based on this scheme and the information about inputs and reaction performance, output flowrates of all compounds from the reactor are estimated. Table D.9 summarizes the mass balance of the process. The yield of CH_3OH with respect to input CH_4 is 72.2%. CH_3OH fraction in the outlet stream from reactor is 11.51%wt (6.57%mol).

Table D.9. Mass balance for the reference process scheme based on homogeneous radical gas-phase reaction for CH_3OH production from CH_4.

Compound	Inlet flowrate		Outlet flowrate	
	kmol/h	t/h	kmol/h	t/h
CH_4	$7.00 \cdot 10^{-5}$	$1.12 \cdot 10^{-6}$	$6.34 \cdot 10^{-5}$	$1.01 \cdot 10^{-6}$
N_2	$1.43 \cdot 10^{-6}$	$4.00 \cdot 10^{-8}$	$1.43 \cdot 10^{-6}$	$4.00 \cdot 10^{-8}$
O_2	$5.13 \cdot 10^{-6}$	$1.64 \cdot 10^{-7}$	$2.36 \cdot 10^{-6}$	$7.54 \cdot 10^{-8}$
CH_3OH	-	-	$5.05 \cdot 10^{-6}$	$1.62 \cdot 10^{-7}$
CO_2	-	-	$7.58 \cdot 10^{-7}$	$3.34 \cdot 10^{-8}$
CO	-	-	$8.38 \cdot 10^{-7}$	$2.35 \cdot 10^{-8}$
H_2O	-	-	$3.19 \cdot 10^{-6}$	$5.75 \cdot 10^{-8}$

D.3.1.2. Definition of intensified process flowsheet

Figure D.3 illustrates the intensified process flowsheet produced with Aspen HYSYS simulation for homogeneous radical gas-phase reaction. Data about the material streams in the flowsheet are summarized in Table D.10, while Table D.11 reports information on the energy streams and utilities related to the relevant components in the flowsheet.

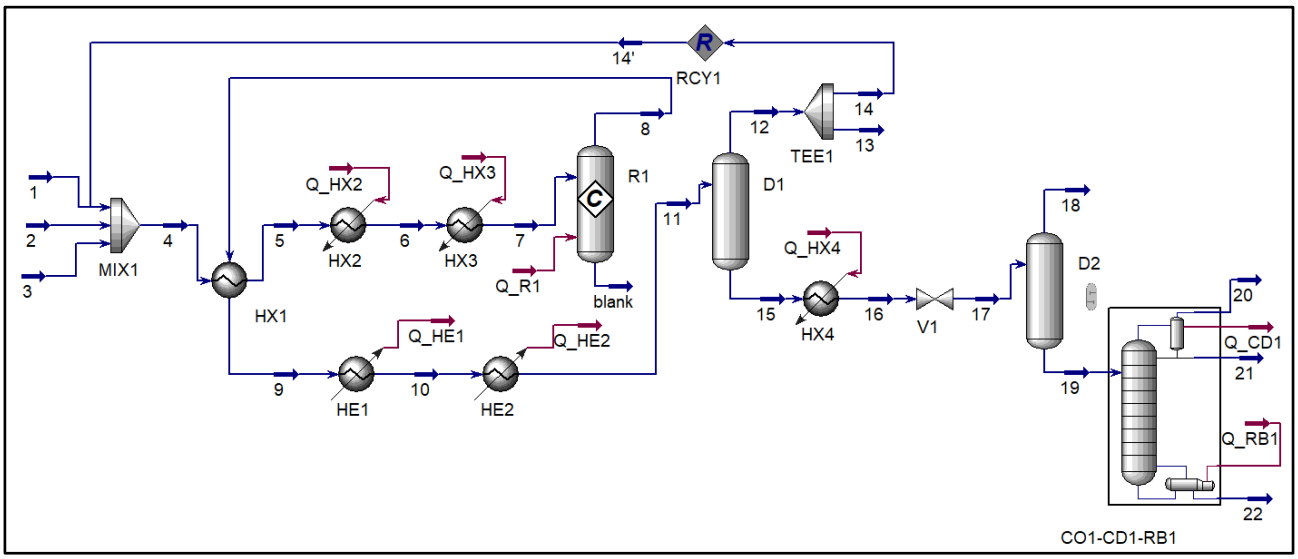

Figure D.3. Intensified process flowsheet for homogeneous radical gas-phase reaction from Aspen HYSYS simulation.

As shown in Figure D.3, CH_4 (stream 1) O2 (stream 2) and N_2 (stream 3) are mixed with gas recycle stream and then pre-heated in HX1, HX2 and HX3 to reach the required temperature for reaction in R1. According to the reactions illustrated in Equations (D.24)-(D.26), the stoichiometry in R1 is -3, -4, +1, +1, +1, +4 for CH_4, O_2, CH_3OH, CO, CO_2, H_2O, respectively; conversion of CH_4 at the reactor is fixed 9.5 % as reported in the reference process scheme. The output stream from R1 is then cooled down in coolers HE1 and HE2 and enters high-pressure flash drum D1 to separate gas and liquid phase. Gas outlet from D1 (stream 12) is then recycled, while liquid outlet (stream 15) is heated in HX4, depressurized in V1 up to atmospheric conditions and then further separated into gas and liquid streams in flash drum D2.

Liquid outlet from D2 (stream 19) finally feeds the distillation unit composed of column CO1, top-condenser CD1 and bottom-reboiler RB1. Distillate rate of 15.64 kmol/h, vent (stream 20) rate of 0.039 kmol/h, reflux ratio of 4.967 and number of stages as 18 (feed in stage 8) are set in CO1-CD1-RB1 unit.

Input flowrates of CH_4, O_2 and N_2 (streams 1, 2 and 3 in Figure D.3, respectively) are adjusted in order to meet in the inlet of the reactor (stream 7 in Figure D.3) the molar ratio O_2 to CH_4 of 0.0762 and N_2 to CH_4 of 0.0204 reported in the reference process scheme (Table D.9).

As illustrated in Figure D.3, hot gases from R1 are used as heating fluid in HX1. Moreover, as shown in Table D.11, the heat flow generated in R1 is used to produce steam at high pressure (HP steam utility) which is further recovered to supply the required heat to HX2.

Table D.10. Data on material streams of the intensified process flowsheet illustrated in Figure D.3.

Stream	Vapor phase fract.	Temper. (°C)	Press. (kPa)	Molar flowrate (kmol/h)	Molar fraction CH_4	Molar fraction N_2	Molar fraction CO	Molar fraction CO_2	Molar fraction CH_3OH	Molar fraction H_2O	Molar fraction O_2
1	1.000	25.00	13800	60.00	1.0000	0.0000	0.0000	0.0000	0.0000	0.0000	0.0000
2	1.000	25.00	15600	84.00	0.0000	0.0000	0.0000	0.0000	0.0000	0.0000	1.0000
3	1.000	25.00	15600	1.00	0.0000	1.0000	0.0000	0.0000	0.0000	0.0000	0.0000
4	1.000	-39.85	5000	23698.23	0.0465	0.0009	0.6666	0.2824	0.0000	0.0000	0.0035
5	1.000	199.34	5000	23698.23	0.0465	0.0009	0.6666	0.2824	0.0000	0.0000	0.0035
6	1.000	235.00	5000	23698.23	0.0465	0.0009	0.6666	0.2824	0.0000	0.0000	0.0035
7	1.000	451.00	5000	23698.23	0.0465	0.0009	0.6666	0.2824	0.0000	0.0000	0.0035
8	1.000	451.00	5000	23698.24	0.0439	0.0009	0.6675	0.2833	0.0009	0.0036	0.0000
9	1.000	210.76	5000	23698.24	0.0439	0.0009	0.6675	0.2833	0.0009	0.0036	0.0000
10	0.997	25.00	5000	23698.24	0.0439	0.0009	0.6675	0.2833	0.0009	0.0036	0.0000
11	0.995	-40.00	5000	23698.24	0.0439	0.0009	0.6675	0.2833	0.0009	0.0036	0.0000
12	1.000	-40.00	5000	23579.42	0.0441	0.0009	0.6708	0.2841	0.0000	0.0000	0.0000
13	1.000	-40.00	5000	23.58	0.0441	0.0009	0.6708	0.2841	0.0000	0.0000	0.0000
14	1.000	-40.00	5000	23555.84	0.0441	0.0009	0.6708	0.2841	0.0000	0.0000	0.0000
14’	1.000	-40.00	5000	23553.23	0.0443	0.0009	0.6707	0.2841	0.0000	0.0000	0.0000
15	0.000	-40.00	5000	118.82	0.0002	0.0000	0.0017	0.1144	0.1767	0.7070	0.0000
16	0.100	95.00	5000	118.82	0.0002	0.0000	0.0017	0.1144	0.1767	0.7070	0.0000
17	0.173	66.56	101.3	118.82	0.0002	0.0000	0.0017	0.1144	0.1767	0.7070	0.0000
18	1.000	66.56	101.3	20.62	0.0010	0.0001	0.0096	0.6577	0.1250	0.2067	0.0000
19	0.000	66.56	101.3	98.21	0.0000	0.0000	0.0000	0.0004	0.1876	0.8120	0.0000
20	1.000	58.27	101.3	0.04	0.0000	0.0000	0.0003	0.2945	0.7052	0.0000	0.0000
21	0.000	58.27	101.3	15.65	0.0000	0.0000	0.0000	0.0017	0.9981	0.0001	0.0000
22	0.000	99.20	101.3	82.52	0.0000	0.0000	0.0000	0.0000	0.0337	0.9663	0.0000

Table D.11. Data on energy streams associated to components of the intensified process flowsheet in Figure D.3.

Stream	Heat flow (kW)	Utility	Pressure (kPa)	Inlet temperature (°C)	Outlet temperature (°C)	Utility mass flowrate (kg/h)
Q_HE2	25820.9	Ammonia refrigerant	40	-50	-50	74113.2
Q_CD1	999.7	Cooling water 1	250	30	40	83438.3
Q_RB1	1079.0	LP steam	232	125	124	1768.0
Q_HX4	411.0	LP steam	232	125	124	673.6
Q_R1	-8444.5	HP steam generation	3913	249	250	17849.9
Q_HX3	52755.6	Molten salt	700	530	470	2079501.9
Q_HX2	8444.4	HP steam	3913	250	249	17370.0
Q_HE1	36864.7	Cooling water 1	250	30	40	3076330.7

LP: low pressure, HP: high pressure

The performance of the CH_3OH production plant obtained with the proposed intensified process flowsheet is: relatively pure liquid CH_3OH in the distillate with the benchmark flowrate (stream 21) at 58°C and 1.01 bar, overall conversion of CH_4 of 98.3% and overall yield of CH_3OH with respect to input CH_4 of 26.0%.

D.3.1.3. Definition of final intensified process flowsheet

Table D.12 summarizes the information about the material streams of the final intensified process scheme for homogeneous radical gas-phase reaction illustrated in Figure 5.31, as a result of step 2 of the methodology. The information about the energy streams is instead reported in Table D.13.

Table D.12. Data on material streams of the final intensified process flowsheet illustrated in Figure 5.31.

Stream	Temp. (°C)	Press. (kPa)	Molar flowrate (kmiol/h)	Stream in Figure D.3 for vapour phase fraction and composition	Stream	Temp. (°C)	Press. (kPa)	Molar flowrate (kmiol/h)	Stream in Figure D.3 for vapour phase fraction and composition
b1	25	13800	60	1	b29	451	5000	7899.6	8
b2	25	15600	83.5	2	b30	210.8	5000	7902.0	9
b3	25	15600	0.05	3	b31	210.8	5000	23701	9
b4	-39.9	5000	23701	4	b32	210.8	5000	7900.3	9
b5	-39.9	5000	7900	4	b33	55	5000	7900.3	10
b6	199.3	5000	7900	5	b34	210.8	5000	7900.3	9
b7	-39.9	5000	7900	4	b35	55	5000	7900.3	10
b8	199.3	5000	7900	5	b36	210.8	5000	7900.3	9
b9	-39.9	5000	7900	4	b37	55	5000	7900.3	10
b10	199.3	5000	7900	5	b38	55	5000	23701	10
b11	199.3	5000	23701	5	b39	55	5000	11851	10
b12	199.3	5000	11851	5	b40	-40	5000	11851	11
b13	234	5000	11851	6	b41	-40	5000	11851	10
b14	199.3	5000	11851	5	b42	-40	5000	11851	11
b15	234	5000	11851	6	b43	-40	5000	23701	11
b16	234	5000	23701	6	b44	-40	5000	23583	12
b17	234	5000	7900.3	6	b45	-40	5000	23.58	13
b18	451	5000	7900.3	7	b46	-40	5000	23557	14
b19	234	5000	7900.3	6	b46’	-40	5000	23559	14’
b20	451	5000	7900.3	7	b47	-40	5000	118.4	15
b21	234	5000	7900.3	6	b48’	95	5000	118.4	16
b22	451	5000	7900.3	7	b49	66.4	101.3	118.4	17
b23	451	5000	23701	7	b50	66.4	101.3	20.76	18
b24	451	5000	23701	8	b51	66.4	101.3	97.60	19
b25	451	5000	7899.6	8	b52	58.3	101.3	0.039	20
b26	210.8	5000	7899.6	9	b53	58.3	101.3	15.64	21
b27	451	5000	7899.6	8	b54	99.2	101.3	81.91	22
b28	210.8	5000	7899.6	9					

Table D.13. Data on energy streams associated to components of the final intensified process flowsheet in Figure 5.31.

Stream	Heat flow (kW)	Utility	Pressure (kPa)	Inlet temperature (°C)	Outlet temperature (°C)	Utility mass flowrate (kg/h)
Q_HE5	12907	Ammonia refrigerant	40	-50	-50	37056.6
Q_HE6	12907	Ammonia refrigerant	40	-50	-50	37056.6
Q_CD2	999.7	Cooling water 1	250	30	40	83438.3
Q_RB2	1079.0	LP steam	232	125	124	1768.0
Q_HX10	411.0	LP steam	232	125	124	673.6
Q_R2	-8444.5	HP steam generation	3913	249	250	17849.9
Q_HX7	17662.8	Molten salt	700	530	470	693167.3
Q_HX8	17662.8	Molten salt	700	530	470	693167.3
Q_HX9	17662.8	Molten salt	700	530	470	693167.3
Q_HX5	4108.4	HP steam	3913	250	249	8685
Q_HX6	4108.4	HP steam	3913	250	249	8685
Q_HE2	12289.3	Cooling water 1	250	30	40	37056.6
Q_HE3	1289.3	Cooling water 1	250	30	40	37056.6
Q_HE4	12289.3	Cooling water 1	250	30	40	37056.6

LP: low pressure, HP: high pressure

For each component in Figure 5.31, Table D.14 reports the main geometric information derived from the conceptual scale-up and design of process equipment (step 2 of the procedure), main factors considered for equipment costs, then purchased cost and the final bare-module cost according to the Guthrie method. Equations proposed for cost estimation of process equipment [361] and CH_3OH synthesis reactor [219] are used in this case-study.

The method described in Seider et al. [361] for estimation of total capital investment cost (C_{tci}) and annual total production cost (C_{prod}) of an onshore chemical process plant is adopted for economic assessment of the process scheme. Table D.15 summarizes calculations, assumptions and values for the cost segments. To convert costs from $\$_{2006}$ into $€_{2019}$, CEPCI values of 500 (for 2006) and 613.3 (for 2019) [690] and exchange rate from $\$_{2019}$ to $€_{2019}$ of 0.8935 [174] are applied through Equation (4.1).

Table D.14. Geometric and economic data of the units of the final intensified process flowsheet in Figure 5.31.

Unit	Main geometric information	Design temp. press.	Size factor for cost function	M/L/P factor for cost function	Main costs ($\$_{2006}$)	Purchased costs ($\$_{2006}$)	Bare-module factor	Bare-module cost ($€_{2019}$)
HX2 - HX3 - HX4	Horizontal, carbon steel, 548 tubes (4 passes, 6 m length), 1260 mm shell diameter, 394 m^2 geometrical area	894°F, 1066 psig	Area:4236 ft^2	M: 1, L: 1, P: 1.37	Base cost: 27598	$3.77 \cdot 10^4$	3.17	$1.31 \cdot 10^5$
HX5 - HX6	Horizontal, carbon steel, 257 tubes (2 passes, 4 m length), 1020 mm shell diameter, 205 m^2 geometrical area	532°F, 1066 psig	Area:2210 ft^2	M: 1, L: 1, P: 1.37	Base cost: 17961	$2.57 \cdot 10^4$	3.17	$8.95 \cdot 10^4$
HX7 - HX8 - HX9	Horizontal, carbon steel, 332 tubes (2 passes, 6 m length), 993 mm shell diameter, 238 m^2 geometrical area	1036°F, 1066 psig	Heat rate: 60003188 BTU/h	-	-	$1.17 \cdot 10^6$	3.17	$4.07 \cdot 10^6$
R2	1218 tubes (42.4 mm external diameter, 6 m length)	-	Inlet gas flowrate: 758020 kg/h	-	-	$9.26 \cdot 10^7$	4.30	$4.36 \cdot 10^8$
HE2 - HE3 - HE4	Horizontal, carbon steel, 1648 tubes (2 passes, 3 m length), 1239 mm shell diameter, 357 m^2 geometrical area	461°F, 1066 psig	Area: 3845 ft^2	M: 1, L: 1.12, P: 1.37	Base cost: 25753	$3.94 \cdot 10^4$	3.17	$1.37 \cdot 10^5$
HE5 - HE6	Vertical, carbon steel, 500 tubes (1 passe, 2 m length), 993 mm shell diameter, 100 m^2 geometrical area	181°F, 1066 psig	Area: 1081 ft^2	M: 1, L: 1.25, P: 1.37	Base cost: 12336	$2.11 \cdot 10^4$	3.17	$7.31 \cdot 10^4$
D3	Vertical, carbon steel, 508 mm diameter, 3.05 m height	10°F, 804 psig	Weight: 4200 lb, Diameter: 3 ft, Height: 12 ft	M: 1	Vessel: 32773, platform and ladders: 4722	$3.75 \cdot 10^4$	4.30	$1.77 \cdot 10^5$
HX10	Horizontal, carbon steel, 36 tubes (6 passes, 3 m length), 297 mm shell diameter, 8.4 m^2 geometrical area	307°F, 1066 psig	Area: 150 ft^2	M: 1, L: 1.12, P: 1.37	Base cost: 6419	$9.82 \cdot 10^3$	3.17	$3.41 \cdot 10^4$
V2	-	-	-	-	-	-	-	-
D4	Vertical, carbon steel, 508 mm diameter, 3.05 m height	202°F, 10 psig	Diameter: 3 ft, height: 12 ft	-	Platform and ladders: 4722	$4.72 \cdot 10^3$	4.30	$2.23 \cdot 10^4$
CO2	Vertical, 620 mm diameter, 11 m height, 526 kg weight, 18 trays, carbon steel	230°F, 10 psig	Weight: 9000 lb, diameter: 3 ft, height: 36 ft, no. of trays: 18	M: 1	Vessel: 51121, platform and ladders: 10687, Installed trays: 13007	$7.48 \cdot 10^4$	4.30	$3.53 \cdot 10^5$
CD2	Horizontal, carbon steel, 224 tubes (4 passes, length 2 m), 573 mm shell diameter, 52.8 m^2 geometrical area	196°F, 10 psig	Area: 568 ft^2	M: 1, L: 1.25, P: 0.98	Base cost: 9588	$1.18 \cdot 10^4$	3.17	$4.09 \cdot 10^4$
RB2	Vertical, carbon steel, 102 tubes (1 pass, length 2 m), 473 mm shell diameter, 20.5 m^2 geometrical area	307°F, 10 psig	Area: 221 ft^2	M: 1, L: 1.25, P: 0.98	Base cost: 7680	$9.43 \cdot 10^3$	3.17	$3.28 \cdot 10^4$

M: material, L: tube-length, P: shell-side pressure.

Table D.15. Cost segments of total capital investment and annual production costs for the scheme in Figure 5.31.

Cost segment	Calculation	Assumption	Cost value
Total bare-module for process equipment (C_{tbm})	Sum of C_{bm} values in Table D.11	-	$4.50 \cdot 10^8$ €$_{2019}$
Site (C_{site})	15% C_{tbm}	Grass-roots onshore plant	$6.75 \cdot 10^7$ €$_{2019}$
Building (C_{build})	30% C_{tbm}	Process and non-process buildings in a grass-roots plant	$1.35 \cdot 10^8$ €$_{2019}$
Offsite facilities (C_{all})	820 \$ · $(Size_{steam})^{0.81}$	$Size_{steam}$ (HX10+RB2): 5384 lb/h	$9.46 \cdot 10^5$ €$_{2019}$
	1000 \$ · $(Size_{water})^{0.68}$	$Size_{water}$ (HE2+HE3+HE4+CD2): 13928 gpm	$7.21 \cdot 10^5$ €$_{2019}$
	$Size_{refrig}$ /1000 · 11000 \$ · $(1000)^{0.77}$	$Size_{refrig}$ (HE5+HE6): 7342 t	$1.81 \cdot 10^7$ €$_{2019}$
Total depreciable capital (C_{tdc})	1.18 · (C_{tbm} + C_{all} + C_{build} + C_{site})	Share of 3% contractor's fee and 15% contingency	$8.20 \cdot 10^8$ €$_{2019}$
Royalties (C_{roy})	2% C_{tdc}	Preliminary estimate	$1.64 \cdot 10^7$ €$_{2019}$
Start-up (C_{start})	30% C_{tdc}	Relatively new process	$2.46 \cdot 10^8$ €$_{2019}$
Total permanent investment (C_{dpi})	C_{tdc} + C_{roy} + C_{start}	-	$1.08 \cdot 10^9$ €$_{2019}$
Raw material (C_{raw})	CH_4: 0.89 \$/L	Market price [715]	$5.43 \cdot 10^7$ €$_{2019}$/y
	O_2: 0.54 \$/L	Market price [716]	$6.03 \cdot 10^7$ €$_{2019}$/y
	N_2: 0.62 \$/L	Market price [716]	$4.59 \cdot 10^4$ €$_{2019}$/y
Utility (C_{util})	LP steam: 0.0066 \$/kg	Typical cost [361]	$1.14 \cdot 10^5$ €$_{2019}$/y
	H_2O for HP steam generation: 0.5 \$/m^3	Typical cost [361]	$7.71 \cdot 10^4$ €$_{2019}$/y
	Refrigeration -30°F: 2.4 \$/t-d	Typical cost [361]	$5.17 \cdot 10^6$ €$_{2019}$/y
	Cooling water: 0.02 \$/m^3	Typical cost [361]	$4.46 \cdot 10^5$ €$_{2019}$/y
	Molten salt: 0.93 \$/kg	Market price [717]	$1.36 \cdot 10^{10}$ €$_{2019}$/y
Direct wages and benefits ($C_{dw\&b}$)	5 shifts · operators/shift · 2080 h/y · 35 \$/y	3 sections (reaction, vapor recovery, liquid separation), 1 operator per section, continuous operations fluids processing in medium plant	$9.76 \cdot 10^5$ €$_{2019}$/y
Directs salaries and benefits ($C_{sal,o}$)	15% $C_{dw\&b}$	-	$1.46 \cdot 10^5$ €$_{2019}$/y
Operating supplies (C_{suppl})	6% $C_{dw\&b}$	-	$5.85 \cdot 10^4$ €$_{2019}$/y
Technical assistance (C_{assist})	60000 \$ · operators/shift	-	$1.61 \cdot 10^5$ €$_{2019}$/y
Control laboratory (C_{lab})	65000 \$ · operators/shift	-	$1.74 \cdot 10^5$ €$_{2019}$/y
Labor-related operations (C_O)	$C_{dw\&b}$ + $C_{sal,o}$ + C_{suppl} + C_{assist} + C_{lab}	-	$1.52 \cdot 10^6$ €$_{2019}$/y
Maintenance wages and benefits ($C_{mw\&b}$)	3.5% C_{tdc}	Fluid handling process	$2.87 \cdot 10^7$ €$_{2019}$/y
Salaries and benefits ($C_{sal,m}$)	25% $C_{mw\&b}$	-	$7.18 \cdot 10^6$ €$_{2019}$/y
Material and services (C_{serv})	100% $C_{mw\&b}$	-	$2.87 \cdot 10^7$ €$_{2019}$/y
Maintenance overhead ($C_{over,m}$)	5% $C_{mw\&b}$	-	$1.44 \cdot 10^6$ €$_{2019}$/y
Maintenance (C_M)	$C_{mw\&b}$ + $C_{sal,m}$ + C_{serv} + $C_{over,m}$	-	$6.60 \cdot 10^7$ €$_{2019}$/y
Operating overhead ($C_{over,o}$)	0.228 · ($C_{dw\&b}$ + $C_{sal,o}$ + $C_{mw\&b}$ + $C_{sal,m}$)	-	$8.44 \cdot 10^6$ €$_{2019}$/y
Property tax and insurance (C_{tax})	2% C_{tdc}	Process of low risk located away from a heavily populated area	$1.64 \cdot 10^7$ €$_{2019}$/y
Direct plant depreciation ($C_{d,dir}$)	8% (C_{tdc} – 1.18 C_{all})	-	$6.16 \cdot 10^7$ €$_{2019}$/y
Allocated plant depreciation ($C_{d,all}$)	6% (1.18 C_{all})	-	$2.99 \cdot 10^6$ €$_{2019}$/y
Sales (S)	CH_3OH: 0.350 €/kg	Market price [632]	$1.38 \cdot 10^6$ €$_{2019}$/y
Licensing fee	2% S	Preliminary estimate	$4.15 \cdot 10^4$ €$_{2019}$/y
Cost of manufacture (C_{COM})	C_{raw} + C_{util} + C_O + C_M + $C_{over,o}$ + C_{tax} + $C_{d,dir}$ + $C_{d,all}$ + C_{lic}	-	$7.48 \cdot 10^7$ €$_{2019}$/y
General expenses (C_{gen})	11.55% S	-	$1.60 \cdot 10^5$ €$_{2019}$/y
Total production cost (C_{prod})	C_{COM} + C_{prod}	-	$1.39 \cdot 10^{10}$ €$_{2019}$/y
Working capital cost (C_{wc})	18.58% S + 8.33% C_{raw}	30 days for cash reserves, 7 days for liquid inventory, 30 days for accounts receivable and payable	$1.17 \cdot 10^9$ €$_{2019}$
Total capital investment (C_{tci})	C_{dpi} + C_{wc}	-	$2.25 \cdot 10^9$ €$_{2019}$

D.3.2. Data for low temperature heterogeneous catalysis

D.3.2.1. Definition of reference process scheme

Compared to the homogeneous radical gas-phase reaction, the adoption of a solid catalyst and liquid oxidant allows to moderate operating conditions of the partial oxidation of CH_4, i.e. reducing temperature and pressure. Among the investigated catalysts for low temperature heterogeneous catalysis, Co-ZSM-5 zeolite modified with Fe and Cu in a continuous flow reactor proposed by Xu et al. [676] is adapted in the analysis of case-study 5 for CH_3OH synthesis based on this process.

Reported tests conditions are 1.5 g catalyst, partial pressure and inlet flowrate of CH_4 of 20 bar and 10 mL/min, respectively, 0.123 M H_2O_2/H_2O oxidant with inlet flowrate of 0.25 mL/min, temperature of 50°C. A stainless steel reactor 13 cm length, 1.6 cm internal diameter) in continuous operating mode is employed. Liquid and gas products are then separated in a high-pressure separator with total volume of 18 mL and collected periodically for analysis over a 5 h period [676].

From different combinations of catalysts tested, the experiment which uses 1.5%Fe 1.5%Cu/ZSM-5 catalyst results in the highest CH_3OH selectivity (i.e. 92.2%) and only one co-product (i.e. CO_2 with selectivity 7.8%), thus it is selected for case-study 5. CH_4 conversion of 0.5%, H_2O_2 conversion of 92.9% are reported for such a test [676]. Given the compounds involving in the process, the following scheme of reactions is derived:

$$CH_4 + 4\ H_2O_2 = CO_2 + 6\ H_2O \quad \text{(D.27)}$$

$$CH_4 + H_2O_2 = CH_3OH + H_2O \quad \text{(D.28)}$$

Based on this scheme and the information about inputs and reaction performance, output flowrates of all compounds from the reactor are estimated. Extent rate of reactions in Equations (D.27) and (D.28) are $1.80 \cdot 10^{-7}$ kmol/h and $2.13 \cdot 10^{-6}$ kmol/h, respectively. Table D.16 summarizes the mass balance of the process. The yield of CH_3OH with respect to input CH_4 is 46.1%. CH_3OH fraction in the outlet aqueous solution is 0.46%wt (0.26%mol).

Table D.16. Mass balance for the reference process scheme based on low temperature heterogenous catalysis for CH_3OH production from CH_4.

Compound	Inlet flowrate		Outlet flowrate	
	kmol/h	t/h	kmol/h	t/h
CH_4	$4.61 \cdot 10^{-4}$	$7.38 \cdot 10^{-6}$	$4.59 \cdot 10^{-4}$	$7.35 \cdot 10^{-6}$
H_2O_2/H_2O solution	$8.19 \cdot 10^{-4}$	$1.38 \cdot 10^{-5}$	$8.19 \cdot 10^{-4}$	$1.47 \cdot 10^{-5}$
CH_3OH	-	-	$2.13 \cdot 10^{-6}$	$6.81 \cdot 10^{-8}$
CO_2	-	-	$1.80 \cdot 10^{-7}$	$7.92 \cdot 10^{-9}$

D.3.2.2. Definition of intensified process flowsheet

Figure D.4 illustrates the intensified process flowsheet produced with Aspen HYSYS simulation for low temperature heterogeneous catalysis. Data about the material streams in the flowsheet are summarized in Table D.17, while Table D.18 reports information on the energy streams and utilities related to the relevant components in the flowsheet.

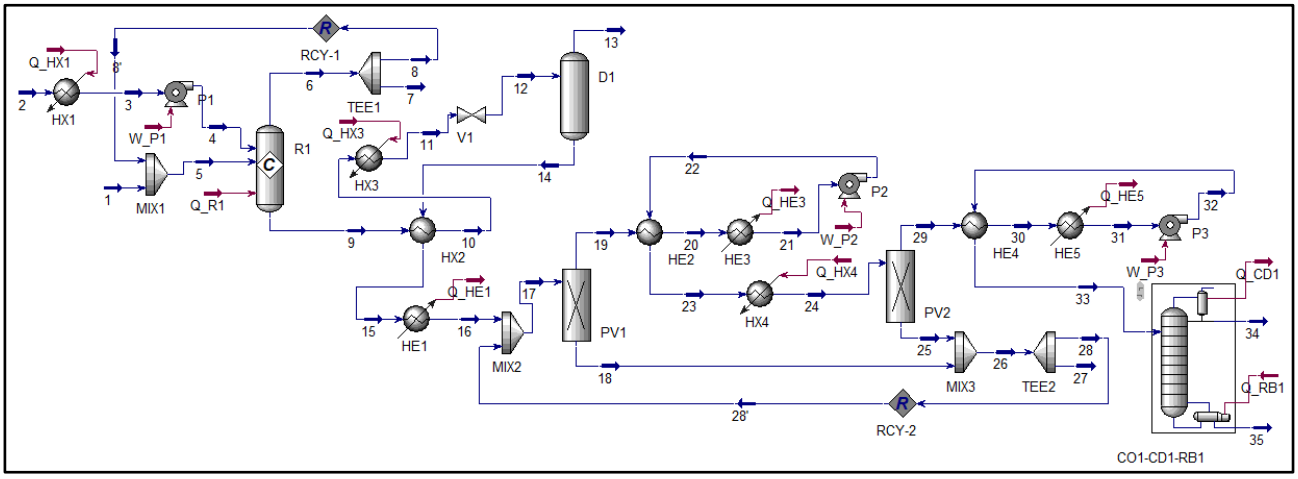

Figure D.4. Intensified process flowsheet for low temperature heterogeneous catalysis from Aspen HYSYS simulation.

As shown in Figure D.4, CH_4 (stream 1), mixed with gas recycle stream, and H_2O_2/H_2O solution (stream 2), heated in HX1 and pumped by means of P1, feed reactor R1. In R1, two reaction in series are introduced: the first one with the stoichiometry of Equation (D.27) and conversion of CH_4 of 0.039%, the second one with the stoichiometry of Equation (D.28) and conversion of CH_4 of 0.461%, which correspond to the overall conversion of CH_4 of 0.5% reported in the reference process scheme. The gas output stream from R1 is then recycled, while the liquid output (stream 9) is heated in HX2 and HX3, depressurized in V1 and separated into gas and liquid streams in atmospheric flash drum D1 to separate gas and liquid phase. The liquid stream from D1 (stream 14) is cooled down in HX2 and HE1 to the optimal temperature required for pervaporation based on PERVAP 4060 membrane (i.e. 70°C) [685]. The resulting stream (stream 16) is mixed with liquid recycle stream and enters the pervaporation membrane unit PV1. Permeate stream in vapor phase and under vacuum (stream 19) is then cooled to reach liquid conditions in HE2 and HE3 and pumped in P2 to atmospheric pressure. The resulting liquid stream is then re-heated to 70°C through HE2 and HX4 for another pervaporation stage composed of membrane PV2, coolers HE4 and HE5, pump P3. The resulting permeate from these components is heated in HE4 and routed for final separation to distillation unit, composed of column CO1, top-condenser CD1 and bottom-reboiler RB1. Retentate from PV1 (stream 18) and PV2 (stream 25) is recycled to the inlet of the first stage of pervaporation.

Distillate rate of 15.64 kmol/h, reflux ratio of 18.27 and number of stages of 24 (feed in stage 10) are set in CO1-CD1-RB1 unit. According to experimental data on PERVAP 4060 membrane [685], pressures of permeate and retentate in PV1 and PV2 are set to 0.2670 kPa and 101.3 kPa, respectively, both at 70°C; splits are fixed as feed fraction to product: in PV1 0.0002395 for CH_3OH and 0.00003687 for H_2O, in PV2 0.0001871 for CH_3OH and 0.00004423 for H_2O.

Input flowrates of CH_4 and H_2O_2/H_2O to the plant are adjusted in order to meet in the inlet of the reactor (streams 4 and 5 in Figure D.4) the molar ratio H_2O_2 to CH_4 of 0.00664 reported in the reference process scheme (Table D.16). As illustrated in Figure D.4, material process streams are used to supply heat in HX2 or absorb heat in HE2 and HE4. Moreover, as shown in Table D.18, a part of the heat flow to be removed in CD1 is used in HX1.

Table D.17. Data on material streams of the intensified process flowsheet illustrated in Figure D.4.

Stream	Vapor phase	Temp. (°C)	Press. (kPa)	Molar flowrate (kmol/h)	Molar fraction CH_4	Molar fraction CO_2	Molar fraction CH_3OH	Molar fraction H_2O	Molar fraction H_2O_2
1	1	25.0	13800	15.8	1.000	0.000	0.000	0.000	0.000
2	0	25.0	101.3	4735.8	0.000	0.000	0.000	0.996	0.004
3	0	50.0	101.3	4735.8	0.000	0.000	0.000	0.996	0.004
4	0	50.2	2000	4735.8	0.000	0.000	0.000	0.996	0.004
5	1	49.7	2000	2796.1	0.957	0.036	0.000	0.007	0.000
6	1	50.0	2000	2782.9	0.957	0.036	0.000	0.007	0.000
7	1	50.0	2000	2.8	0.957	0.036	0.000	0.007	0.000
8	1	50.0	2000	2780.1	0.957	0.036	0.000	0.007	0.000
8’	1	50.0	2000	2780.3	0.957	0.036	0.000	0.007	0.000
9	0	50.0	2000	4751.2	0.000	0.000	0.003	0.997	0.000
10	0	68.6	2000	4751.2	0.000	0.000	0.003	0.997	0.000
11	0	100.0	2000	4751.2	0.000	0.000	0.003	0.997	0.000
12	1.00	77	101.3	7.55	0.1608	0.0189	0.1939	0.6264	0.000
13	0.00	77	101.3	46.69	0.0002	0.0000	0.5354	0.4644	0.000
14	0.00	63	101.3	15.64	0.0007	0.0000	0.0003	0.9990	0.000
15	0.00	94	101.3	31.05	0.0000	0.0000	0.8049	0.1951	0.000
16	0	70.0	101.3	4732.9	0.000	0.000	0.003	0.997	0.000
17	0	70.0	101.3	162198719127	0.000	0.000	0.003	0.997	0.000
18	0	70.0	101.3	162192655283	0.000	0.000	0.003	0.997	0.000
19	1	70.0	0.267	6063843.5	0.000	0.000	0.017	0.983	0.000
20	1	25.0	0.267	6063843.5	0.000	0.000	0.017	0.983	0.000
21	0	-10.3	0.267	6063843.5	0.000	0.000	0.017	0.983	0.000
22	0	-10.0	101.3	6063843.5	0.000	0.000	0.017	0.983	0.000
23	0	9.3	101.3	6063843.5	0.000	0.000	0.017	0.983	0.000
24	0	70.0	101.3	6063843.5	0.000	0.000	0.017	0.983	0.000
25	0	70.0	101.3	6063560.9	0.000	0.000	0.017	0.983	0.000
26	0	70.0	101.3	162198718844	0.000	0.000	0.003	0.997	0.000
27	0	70.0	101.3	4055.0	0.000	0.000	0.003	0.997	0.000
28	0	70.0	101.3	162198714789	0.000	0.000	0.003	0.997	0.000
28’	0	70.0	101.3	162198714394	0.000	0.000	0.003	0.997	0.000
29	1	70.0	0.267	282.6	0.000	0.000	0.067	0.933	0.000
30	1	21.0	0.267	282.6	0.000	0.000	0.067	0.933	0.000
31	0	-10.5	0.267	282.6	0.000	0.000	0.067	0.933	0.000
32	0	-10.2	101.3	282.6	0.000	0.000	0.067	0.933	0.000
33	0	10.5	101.3	282.6	0.000	0.000	0.067	0.933	0.000
34	0	66.9	101.3	15.6	0.000	0.000	1.000	0.000	0.000
35	0	99.7	101.3	267.0	0.000	0.000	0.012	0.988	0.000

Table D.18. Data on energy streams associated to components of the intensified process flowsheet in Figure D.4.

Stream	Heat/Power flow (kW)	Utility	Pressure (kPa)	Inlet temp. (°C)	Outlet temp. (°C)	Utility mass flowrate (kg/h)
Q_R1	-1301	Cooling water 1	250	30	40	108607
Q_HX3	3263	LP steam	232	125	124	5348
Q_HE1	1032	Cooling water 1	250	30	40	86135
Q_HE3	79600703	Ammonia refrigerant	151.8	-25	-25	272238972
W_P2	4038	-	3913	250	249	671.36
Q_HX4	8049077	LP steam	232	125	124	13192805
W_P3	0.20	-	-	-	-	-
Q_HE5	3724	Ammonia refrigerant	151.8	-25	-25	12738
Q_CD1	3141	Cooling water 1 for 882 kW (Q_HX1 for remaining kW)	250	30	40	73599
Q_RB1	3726.58	LP steam	232	125	124	6108
W_P1	60.80	-	-	-	-	-
Q_HX1	2558.73	Process fluid (H_2O_2/H_2O)	1.01	25	50	85600

LP: low pressure

The performance of the CH_3OH production plant obtained with the proposed intensified process flowsheet is: relatively pure liquid CH_3OH in the distillate with the benchmark flowrate (stream 34) at 66.9°C and 1.01 bar, overall conversion of CH_4 of 83.1% and overall yield of CH_3OH with respect to input CH_4 of 98.99%.

D.3.3. Data for homogeneous catalysis in solution

D.3.3.1. Definition of reference process scheme

Another alternative to the gas-phase reaction at high operating conditions, the conversion of CH_4 into CH_3OH can be performed through homogeneous catalyst in solution under low temperature. Several studies investigating the performance of homogeneous catalysts can be retrieved in literature, even though in batch reactors. The experimental set-up employing a semi-continuous porous tube reactor proposed for liquid phase catalytic partial oxidation of CH_4 to CH_3OH derivative [677] is preferred in the analysis of case-study 5.

CH_4, O_2 and co-reductant CO constitute the gas mixture supplied continuously to the tubular reactor (400 mL volume) where they enter contact with the liquid phase through an alumina-based porous ceramic tube. The liquid consists of mixture of 3:1 trifluoroacetic acid CF_3COOH (TFA) and H_2O, while the catalytic system is a bimetallic catalyst of $Pd(CH_3CO_2)_2$ and $CuCl_2$. The metal first catalyses water gas shift reaction involving the oxidation of CO to CO_2 and H_2, then the catalytic combination of H_2 with O_2 yields in situ H_2O_2, and the metal-catalysed oxidation of CH_4 yields CH_3OH by means of H_2O_2. The CH_3OH derivative, CF_3COOCH_3(MTFA), is finally produced through esterification of CH_3OH with CF_3COOH (TFA) in the liquid phase. The overall reaction can be represented by the following equation:

$$CH_4 + CO + O_2 + CF_3COOH(TFA) = CF_3COOCH_3(MTFA) + CO_2 + H_2O \quad (D.29)$$

After the reactor, the gases are disengaged from the liquid phase in a hold-up vessel (600 mL volume) and vented. The liquid phase is continuously re-circulated via the air-lift effect which eliminated the need for high-pressurized pumping [677].

Experiments are carried out with CH_4 at partial pressure of 62 bar and flowrate of 1.8 L/min (at 0°C), CO at partial pressure of 14 bar and normal flowrate of 0.34 L/min (at 0°C), O_2 at partial pressure 7 bar and flowrate of 0.17 L/min (at 0°C), a volume of 300 mL of liquid (75 mL of H_2O and 225 mL of TFA) at 20°C. Thus, the total pressure of the system is 83 bar. From different runs investigating the effect of temperature, time course and catalyst concentrations, the best performance in terms of MTFA productivity is reported at 85°C temperature, 120 min time, 0.66 mol/m^3 Pd^{2+} and 4.9 mol/m^3 $CuCl_2$: MTFA concentration of 50 mol/m^3 in the liquid phase , i.e. 0.015 mol in 300 mL liquid volume [677]. 0.015 mol in 120 min of the run is also the extent rate of the reaction illustrated in Equation (D.29). Material balance can be thus completed, as summarized in Table D.19. Molar conversion of CH_4 is estimated as 0.181%.

Table D.19. Mass balance for the reference process scheme based on homogeneous catalysis in solution for CH_3OH derivative production from CH_4.

Compound	Inlet flowrate		Outlet flowrate	
	kmol/h	t/h	kmol/h	t/h
CH_4	$8.28 \cdot 10^{-3}$	$1.32 \cdot 10^{-4}$	$8.27 \cdot 10^{-3}$	$1.32 \cdot 10^{-4}$
CO	$4.14 \cdot 10^{-3}$	$5.24 \cdot 10^{-5}$	$1.85 \cdot 10^{-3}$	$5.19 \cdot 10^{-5}$
O_2	$3.53 \cdot 10^{-3}$	$2.99 \cdot 10^{-5}$	$9.20 \cdot 10^{-4}$	$2.94 \cdot 10^{-5}$
H2O	$4.15 \cdot 10^{-3}$	$7.47 \cdot 10^{-5}$	$4.17 \cdot 10^{-3}$	$7.50 \cdot 10^{-5}$
TFA	$2.94 \cdot 10^{-3}$	$3.35 \cdot 10^{-4}$	$2.92 \cdot 10^{-3}$	$3.33 \cdot 10^{-4}$
MTFA	-	-	$1.50 \cdot 10^{-5}$	$1.92 \cdot 10^{-6}$
CO_2	-	-	$1.50 \cdot 10^{-5}$	$6.60 \cdot 10^{-7}$

Hypothetically, pure CH_3OH can be obtained considering the opposite reaction of the esterification involving the liquid product from Equation (D.29), i.e. hydrolysis of MTFA, as follows:

$$CF_3COOCH_3(MTFA) + H_2O = CF_3COOH(TFA) + CH_3OH \quad (D.30)$$

All the molar amount of MTFA can be ideally converted into CH_3OH, while TFA and H_2O may be recycled to the inlet of the reactor.

D.3.3.2. Definition of intensified process flowsheet

Figure D.5 illustrates the intensified process flowsheet produced with Aspen HYSYS simulation for homogeneous catalysis in solution. Data about the material streams in the flowsheet are summarized in Table D.20, while Table D.21 reports information on the energy streams and utilities related to the relevant components in the flowsheet.

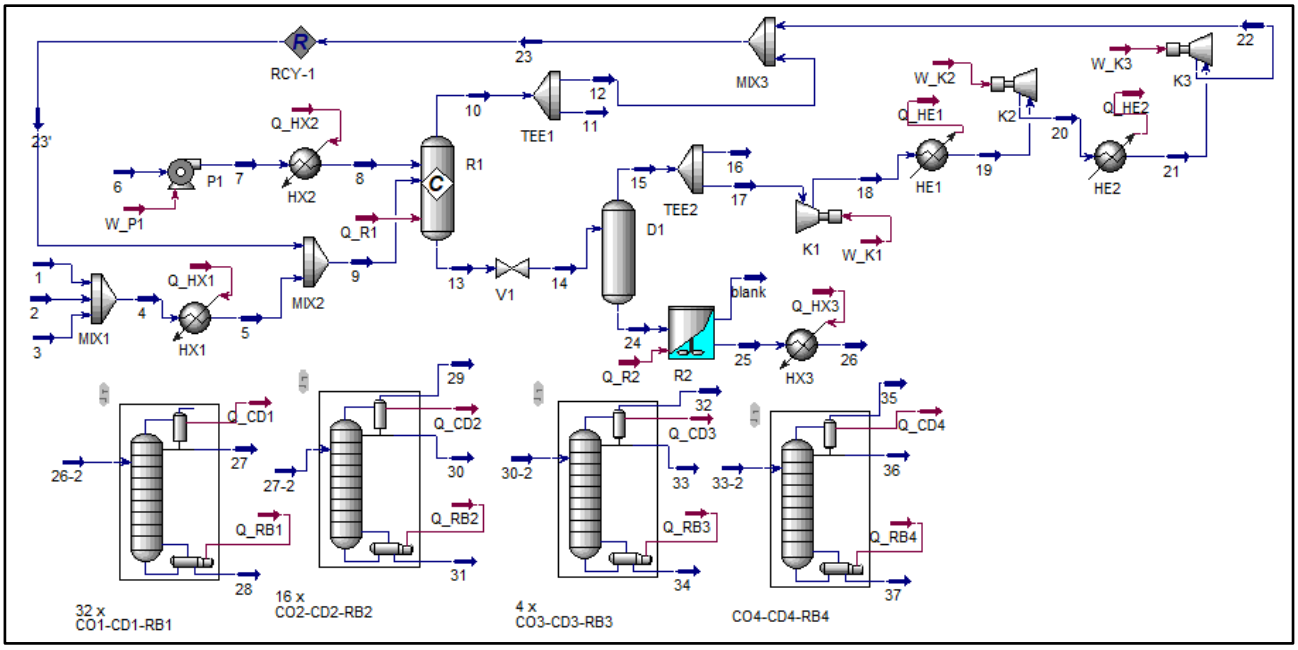

Figure D.5. Intensified process flowsheet for homogeneous catalysis in solution from Aspen HYSYS simulation.

As shown in Figure D.5, CH_4 (stream 1), CO (stream 2) and O_2 (stream 3) are pre-heated in HX1 to the reaction temperature and mixed with gas recycle stream. The resulting gas mixture and TFA/H_2O solution (stream 2), pumped by means of P1 and heated in HX2, feed the reactor R1. In R1, stoichiometry of reaction in Equation (D.29) and conversion of CH_4 of 0.181%, reported in the reference process scheme, are set. The gas output stream from R1 is then recycled, while the liquid output (stream 13) is depressurized to atmospheric conditions in V1 and separated into gas and liquid streams in flash drum D1. The gas outlet from D1 is first compressed in K1 and then undergoes two stages of compression-cooling in order to be recycled in inlet to the R1. The liquid phase from D1 (stream 24) enters reactor R2 where reaction illustrated in Equation (D.30) is simulated as kinetic reaction in Aspen CSTR reactor. Stoichiometry in Equation (D.30) and experimental data about forward kinetic constant of the hydrolysis reaction of MTFA as a function of temperature [718] are set. This latter information is energy activation (E_a) of 42151 kJ/kmol and pre-exponential factor (A) of 199526 1/s. Moreover, the volume of R2 in vertical configuration and cylindrical shape is fixed in order to obtain conversion of MTFA as higher as possible (i.e. 99.10%). The liquid outlet from R2 containing a mixture of H_2O-TFA-CH_3OH is then heated to feed four distillation stages in series. The first stage in CO1-CD1-RB1 consists of separation of TFA-CH_3OH from H_2O where distillate rate of 143 kmol/h, reflux ratio of 2.82 and number of stages of 20 (feed in stage 12) are set. The distillate stream from this unit is then routes to the following stages aiming at the separation of CH_3OH from TFA in order to obtain relatively pure CH_3OH as distillate. Bottom rate of 266 kmol/h, vent rate (stream 29) of 0.7 kmol/h, reflux ratio of 110.9, number of stages of 40 (feed in stage 10) are set in CO2-CD2-RB2 unit. Distillate rate of 13.87 kmol/h, vent rate (stream 32) of 0.78 kmol/h, reflux ratio of 65.32, number of stages of 40 (feed in stage 10) are set in CO3-CD3-RB3 unit.

Finally, distillate rate of 15.64 kmol/h, vent rate (stream 35) of 0.32 kmol/h, reflux ratio of 20.98, number of stages of 40 (feed in stage 11) are set in CO4-CD4-RB4 unit. As shown in Figure D.5, to obtain the benchmark CH_3OH, 32 units in parallel of CO1-CD1-RB1, 16 units in parallel of CO2-CD2-RB2, 4 units in parallel of CO3-CD3-RB3 are needed. Input flowrates of CH_4, CO, O_2 and TFA/H_2O to the plant are adjusted in order to meet in the inlet of the reactor R1 (streams 8 and 9 in Figure D.5) the molar ratio TFA to CH_4 of 0.355, CO to CH_4 of 0.226, O_2 to CH_4 0.113, reported in the reference process scheme (Table D.19). As illustrated in Figure D.5, hot gases in HE1 and HE2 are used to supply a part of the heat in HX2.

Table D.20. Data on material streams of the intensified process flowsheet illustrated in Figure D.5.

Stream	Vapor phase fract.	Temp. (°C)	Press. (kPa)	Molar flowrate (kmol/h)	Molar fract. CH_4	Molar fract. CH_3OH	Molar fract. CO_2	Molar fract. CO	Molar fract. H_2O	Molar fract. TFA	Molar fract. MTFA	Molar fract. O_2
1	1	25.0	13800	600.00	1.000	0.000	0.000	0.000	0.000	0.000	0.000	0.000
2	1	25.0	15000	430.00	0.000	0.000	0.000	1.000	0.000	0.000	0.000	0.000
3	1	25.0	15600	399.50	0.000	0.000	0.000	0.000	0.000	0.000	0.000	1.000
4	1	25.0	13800	1429.50	0.420	0.000	0.000	0.301	0.000	0.000	0.000	0.279
5	1	85.0	13800	1429.50	0.420	0.000	0.000	0.301	0.000	0.000	0.000	0.279
6	0	25.0	101.3	154000	0.000	0.000	0.000	0.000	0.585	0.415	0.000	0.000
7	0	28.2	8300	154000	0.000	0.000	0.000	0.000	0.585	0.415	0.000	0.000
8	0	85.0	8300	154000	0.000	0.000	0.000	0.000	0.585	0.415	0.000	0.000
9	0.99	102.6	8300	510450	0.412	0.000	0.413	0.096	0.011	0.022	0.000	0.045
10	1	85.0	8300	483313	0.428	0.000	0.412	0.100	0.004	0.009	0.000	0.047
11	1	85.0	8300	483.31	0.428	0.000	0.412	0.100	0.004	0.009	0.000	0.047
12	1	85.0	8300	482830	0.428	0.000	0.412	0.100	0.004	0.009	0.000	0.047
13	0	85.0	8300	180756	0.018	0.000	0.067	0.001	0.520	0.390	0.003	0.001
14	0.15	60.5	101.3	180756	0.018	0.000	0.067	0.001	0.520	0.390	0.003	0.001
15	1	60.5	101.3	26211	0.122	0.000	0.458	0.010	0.133	0.269	0.003	0.005
16	1	60.5	101.3	26.21	0.122	0.000	0.458	0.010	0.133	0.269	0.003	0.005
17	1	60.5	101.3	26186	0.122	0.000	0.458	0.010	0.133	0.269	0.003	0.005
18	1	250.0	1353	26186	0.122	0.000	0.458	0.010	0.133	0.269	0.003	0.005
19	1	133.7	1353	26186	0.122	0.000	0.458	0.010	0.133	0.269	0.003	0.005
20	1	250.0	5937	26186	0.122	0.000	0.458	0.010	0.133	0.269	0.003	0.005
21	1	193.8	5937	26186	0.122	0.000	0.458	0.010	0.133	0.269	0.003	0.005
22	1	221.4	8300	26186	0.122	0.000	0.458	0.010	0.133	0.269	0.003	0.005
23	0.99	102.6	8300	509016.	0.412	0.000	0.415	0.096	0.011	0.022	0.000	0.044
23’	0.99	102.6	8300	509021	0.412	0.000	0.415	0.096	0.011	0.022	0.000	0.044
24	0	60.5	101.3	154543	0.000	0.000	0.001	0.000	0.586	0.411	0.002	0.000
25	0	15.0	101.3	154543	0.000	0.002	0.001	0.000	0.583	0.413	0.000	0.000
26	0	50.0	101.3	154543	0.000	0.002	0.001	0.000	0.583	0.413	0.000	0.000
26-2	0	50.0	101.3	346.17	0.000	0.002	0.001	0.000	0.583	0.413	0.000	0.000
27	0	61.2	101.3	143.00	0.000	0.006	0.003	0.000	0.001	0.991	0.000	0.000
27-2	0	61.2	101.3	286.00	0.000	0.006	0.003	0.000	0.001	0.991	0.000	0.000
28	0	99.2	101.3	203.17	0.000	0.000	0.000	0.000	0.993	0.007	0.000	0.000
29	1	26.5	101.3	0.70	0.055	0.011	0.824	0.001	0.000	0.107	0.000	0.001
30	0	26.5	101.3	19.30	0.000	0.071	0.010	0.000	0.000	0.918	0.001	0.000
30-2	0	26.5	101.3	77.20	0.000	0.071	0.010	0.000	0.000	0.918	0.001	0.000
31	0	72.7	101.3	266.00	0.000	0.001	0.000	0.000	0.001	0.998	0.000	0.000
32	1	24.2	101.3	0.78	0.023	0.057	0.858	0.000	0.000	0.061	0.001	0.000
33	0	24.2	101.3	13.87	0.000	0.382	0.005	0.000	0.000	0.609	0.004	0.000
33-2	0	24.2	101.3	55.48	0.000	0.382	0.005	0.000	0.000	0.609	0.004	0.000
34	0	72.7	101.3	62.55	0.000	0.003	0.000	0.000	0.000	0.997	0.000	0.000
35	1	24.1	101.3	0.32	0.008	0.159	0.832	0.000	0.000	0.000	0.000	0.000
36	0	24.1	101.3	15.64	0.000	0.998	0.001	0.000	0.000	0.001	0.000	0.000
37	0	71.9	101.3	39.52	0.000	0.140	0.000	0.000	0.000	0.854	0.006	0.000

Table D.21. Data on energy streams associated to components of the intensified process flowsheet in Figure D.5.

Stream	Heat/Power flow (kW)	Utility	Pressure (kPa)	Inlet temp. (°C)	Outlet temp. (°C)	Utility mass flowrate (kg/h)
Q_R2	-228047	Cooling water 1	250	30	40	20951548
Q_R1	-251069	Cooling water 2	250	5	15	19030352
Q_CD1	5507	Cooling water 1	250	30	40	459555
Q_RB1	5800	LP steam	232	125	124	9506
Q_CD2	26152	Cooling water 2	250	5	15	2180336
Q_RB2	26279	LP steam	232	125	124	43072
W_P1	19460	-	-	-	-	-
Q_HX2	291570	LP steam for 225363 kW (hot gases in HE1 and HE2)	232	125	124	369380
Q_HX1	777	LP steam	232	125	124	1274
W_K1	84333	-	-	-	-	-
Q_HE1	53866	Process fluid (TFA/H_2O) in HX2	8300	28.2	85	1645097
W_K2	53589	-	-	-	-	-
Q_HE2	26916	Process fluid (TFA/H_2O) in HX2	8300	28.2	85	822124
W_K3	12850	-	-	-	-	-
Q_CD3	11239	Cooling water 2	250	5	15	937059
Q_RB3	11386	LP steam	232	125	124	18662
Q_CD4	3898	Cooling water 2	250	5	15	324996
Q_RB4	3988	LP steam	232	125	124	6537
Q_HX3	176758	LP steam	232	125	124	289715

LP: low pressure.

The performance of the CH_3OH production plant obtained with the proposed intensified process flowsheet is: relatively pure liquid CH_3OH in the distillate with the benchmark flowrate (stream 34) at 66.9°C and 1.01 bar, overall conversion of CH_4 of 83.1% and overall yield of CH_3OH with respect to input CH_4 of 98.99%.

D.3.4. Data for membrane-based biocatalysis

D.3.4.1. Definition of reference process scheme

Biosynthesis of CH_3OH from CH_4 is a biological conversion which uses a group of enzymes called methane monooxygenases (MMOs) in methanotrophic bacteria at ambient conditions and may employ a membrane inside the bioreactor to facilitate the separation of compounds. The bioprocess investigated by Ghaz-Jahanian et al. [678] is considered as reference source in the analysis of case-study 5 for CH_3OH production through biocatalysis.

A bench-scale external loop airlift bioreactor with 1 L working volume (3.2 cm internal diameter and 35 cm height) is proposed allowing inlet CH_4 and O_2 from air to dissolve according to stoichiometric ratios for bacterial consumption and CH_3OH synthesis in Equation (D.24), i.e. CH_4-to-air ratio of 1:20. A cylindrical settler (8 cm diameter and 4 cm height) is employed at the top of bioreactor to separate biomass from the medium and provide recycle of precipitated cells. CH_4 is continuously dissolved into the culture

by means of a hydraulic transfer chamber (11 cm diameter and 18.5 cm height) and such methane-enriched medium is then conducted to the airlift bioreactor. Inlet flowrate of air to the reactor is 0.4 L/min, while recycle flowrate of enriched medium is 0.1 L/min. Batch runs of about 4 h in airlift bioreactor using isolated methanotroph strain stabilized at the temperature of 28°C result in a peak of 1600 mg/L of CH_3OH during the first 3:30 h of single batch. At the end of the batch, aeration is stopped for 2 h and about 75% of medium is replaced by new one in order to start a new batch; CH_3OH is measured in the collected medium [678].

By assuming two batches per day (i.e. at maximum 12 h including loading, production, unloading and aeration stopping for collection), the inlet flowrates are estimated. To evaluate the CH_3OH flowrate, first the medium volume in the airlift reactor is estimated as 85% of the bioreactor volume and 75% of this latter one is considered as the collected medium volume for CH_3OH concentration measurement (i.e. 0.638 L). Thus, considering this volume and the two batches per day, the output CH_3OH is calculated, which coincides with the extent rate of the reaction in Equation (D.24) since CH_3OH is the only one carbon product. Material balance is then applied quantifying all the output flowrates. Table D.22 summarizes the data for this process. Molar conversion of CH_4 is derived equal to 10.36%, which represents also the yield of CH_3OH. CH_3OH fraction in the outlet medium is 0.16%wt (0.09%mol).

Table D.22. Mass balance for the reference process scheme based on biocatalysis for CH_3OH production from CH_4.

Compound	Inlet flowrate		Outlet flowrate	
	kmol/h	t/h	kmol/h	t/h
CH_4	$2.66 \cdot 10^{-6}$	$4.10 \cdot 10^{-7}$	$2.30 \cdot 10^{-5}$	$3.68 \cdot 10^{-7}$
Air	$2.83 \cdot 10^{-4}$	$8.20 \cdot 10^{-6}$	$2.16 \cdot 10^{-4}$	$6.26 \cdot 10^{-6}$
Liquid medium	$2.95 \cdot 10^{-3}$	$5.1 \cdot 10^{-5}$	$2.95 \cdot 10^{-3}$	$5.31 \cdot 10^{-5}$
CH_3OH	-	-	$2.66 \cdot 10^{-6}$	$8.50 \cdot 10^{-8}$

D.3.4.2. Definition of intensified process flowsheet

Figure D.6 illustrates the intensified process flowsheet produced with Aspen HYSYS simulation for biocatalysis. Data about the material streams in the flowsheet are summarized in Table D.23, while Table D.24 reports information on the energy streams and utilities related to the relevant components in the flowsheet.

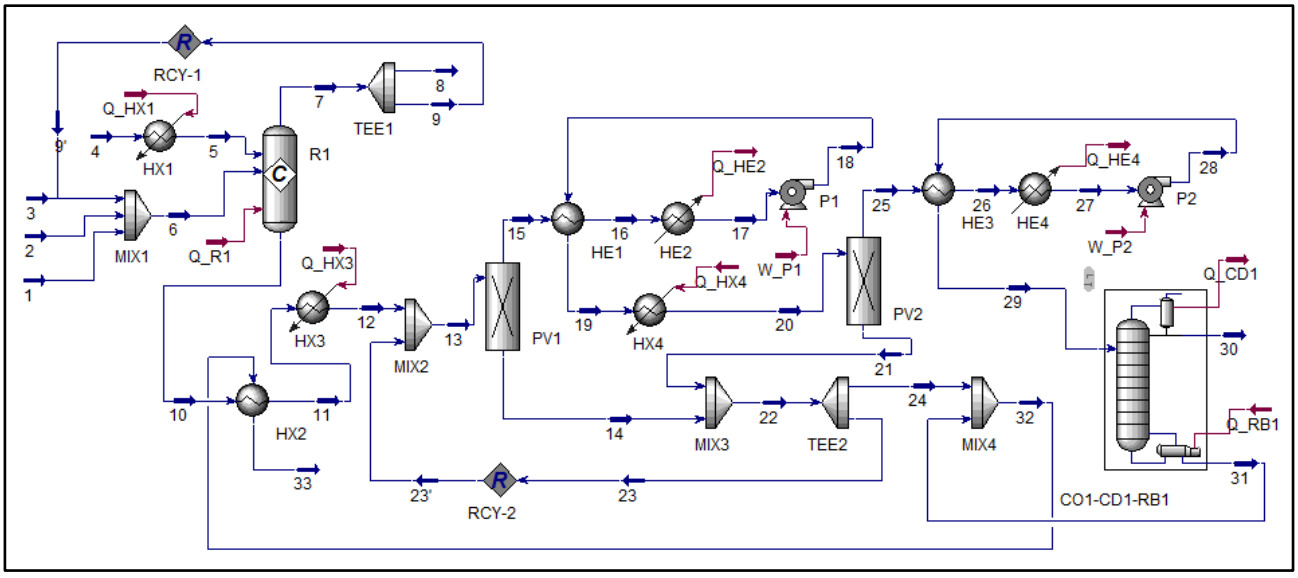

Figure D.6. Intensified process flowsheet for biocatalysis from Aspen HYSYS simulation.

As shown in Figure D.6, gases CH_4 (stream 1), N_2 (stream 2) and O_2 (stream 3), mixed with gas recycle stream, and H_2O_2/H_2O solution (stream 4), heated in HX1, enter reactor R1. According to Equation (D.24), the stoichiometry in R1 is -1, -0.5, +1 for CH_4, O_2, CH_3OH, respectively; conversion of CH_4 at the reactor is fixed 10.36 % as reported in the reference process scheme. The gas output stream from R1 is then recycled, while the liquid output (stream 10) is heated in HX2 and HX3, depressurized in V1 and separated into gas and liquid streams in atmospheric flash drum D1 to separate gas and liquid phase. The liquid stream from D1 (stream 14) is cooled down in HX2 and HE1 to the optimal temperature required for pervaporation based on PERVAP 4060 membrane (i.e. 70°C) [685]. The resulting stream (stream 13) is mixed with liquid recycle stream and enters the pervaporation membrane unit PV1. Permeate stream in vapor phase and under vacuum (stream 15) is then cooled to reach liquid conditions in HE1 and HE2 and pumped in P1 to atmospheric pressure. The resulting liquid stream is then re-heated to 70°C through HE1 and HX4 for another pervaporation stage composed of membrane PV2, coolers HE3 and HE4, pump P2. The resulting permeate from these components is routed for final separation to the distillation unit, composed of column CO1, top-condenser CD1 and bottom-reboiler RB1. A part of retentate from PV1 (stream 14) and PV2 (stream 21) are recycled to the inlet of the first stage of pervaporation. The other part is mixed with the waste stream of CO1-CD1-RB1 unit and used as heating fluid in HX2.

Distillate rate of 15.64 kmol/h, reflux ratio of 39.77 and number of stages of 26 (feed in stage 10) are set in CO1-CD1-RB1 unit.

According to experimental data on PERVAP 4060 membrane [685], pressures of permeate and retentate in PV1 and PV2 are set to 0.2670 kPa and 101.3 kPa, respectively, both at 70°C; splits are fixed as feed

fraction to product: in PV1 0.0002504 for CH_3OH and 0.00003559 for H_2O, in PV2 0.0002285 for CH_3OH and 0.00003791 for H_2O.

Input flowrates to the plant are adjusted in order to meet in the inlet of the reactor (streams 5 and 6 in Figure D.6) the molar ratio H_2O to CH_4 of 115.1, N_2 to CH_4 of 8.72, H_2O to CH_4 of 2.225 reported in the reference process scheme (Table D.22).

As illustrated in Figure D.6, material process streams are used to supply heat in HX2 or absorb heat in HE1 and HE3. Moreover, as shown in Table D.24, a part of the heat flow to be removed from CD1 is used in HX1.

Table D.23. Data on material streams of the intensified process flowsheet illustrated in Figure D.6.

Stream	Vapor phase fract.	Temp. (°C)	Press. (kPa)	Molar flowrate (kmol/h)	Molar fraction CH_4	Molar fraction CH_3OH	Molar fraction H_2O	Molar fraction N_2	Molar fraction O_2
1	1	25.0	13800	16.5	1.0000	0.0000	0.0000	0.0000	0.0000
2	1	25.0	800	1.8	0.0000	0.0000	0.0000	1.0000	0.0000
3	1	25.0	800	8.6	0.0000	0.0000	0.0000	0.0000	1.0000
4	0	25.0	101.3	18040.4	0.0000	0.0000	1.0000	0.0000	0.0000
5	0	28.0	101.3	18040.4	0.0000	0.0000	1.0000	0.0000	0.0000
6	1	27.7	101.3	1956.1	0.0806	0.0000	0.0366	0.7035	0.1793
7	1	28.0	101.3	1931.5	0.0731	0.0000	0.0371	0.7123	0.1774
8	1	28.0	101.3	2.1	0.0731	0.0000	0.0371	0.7123	0.1774
9	1	28.0	101.3	1929.4	0.0731	0.0000	0.0371	0.7123	0.1774
9’	1	28.0	101.3	1929.3	0.0731	0.0000	0.0371	0.7123	0.1774
10	0	28.0	101.3	18056.8	0.0000	0.0009	0.9991	0.0000	0.0000
11	0	43.0	101.3	18056.8	0.0000	0.0009	0.9991	0.0000	0.0000
12	0	70.0	101.3	18056.8	0.0000	0.0009	0.9991	0.0000	0.0000
13	0	70.0	101.3	331884266383	0.0000	0.0009	0.9991	0.0000	0.0000
14	0	70.0	101.3	331872390796	0.0000	0.0009	0.9991	0.0000	0.0000
15	1	70.0	0.267	11875587.4	0.0000	0.0063	0.9937	0.0000	0.0000
16	1	25.0	0.267	11875587.4	0.0000	0.0063	0.9937	0.0000	0.0000
17	0	-10.3	0.267	11875587.4	0.0000	0.0063	0.9937	0.0000	0.0000
18	0	-10.1	101.3	11875587.4	0.0000	0.0063	0.9937	0.0000	0.0000
19	0	9.4	101.3	11875587.4	0.0000	0.0063	0.9937	0.0000	0.0000
20	0	70.0	101.3	11875587.4	0.0000	0.0063	0.9937	0.0000	0.0000
21	0	70.0	101.3	11875123.0	0.0000	0.0063	0.9937	0.0000	0.0000
22	0	70.0	101.3	331884265919	0.0000	0.0009	0.9991	0.0000	0.0000
23	0	70.0	101.3	331884249324	0.0000	0.0009	0.9991	0.0000	0.0000
23’	0	70.0	101.3	331884248326	0.0000	0.0009	0.9991	0.0000	0.0000
24	0	70.0	101.3	16594.2	0.0000	0.0009	0.9991	0.0000	0.0000
25	1	70.0	0.267	464.4	0.0000	0.0366	0.9634	0.0000	0.0000
26	1	21.0	0.267	464.4	0.0000	0.0366	0.9634	0.0000	0.0000
27	0	-10.3	0.267	464.4	0.0000	0.0366	0.9634	0.0000	0.0000
28	0	-10.1	101.3	464.4	0.0000	0.0366	0.9634	0.0000	0.0000
29	0	10.8	101.3	464.4	0.0000	0.0366	0.9634	0.0000	0.0000
30	0	66.9	101.3	15.6	0.0000	0.9987	0.0013	0.0000	0.0000
31	0	99.9	101.3	448.7	0.0000	0.0031	0.9969	0.0000	0.0000
32	0	70.8	101.3	17043.0	0.0000	0.0010	0.9990	0.0000	0.0000
33	0	55.0	101.3	17043.0	0.0000	0.0010	0.9990	0.0000	0.0000

Table D.24. Data on energy streams associated to components of the intensified process flowsheet in Figure D.6.

Stream	Heat/Power flow (kW)	Utility	Pressure (kPa)	Inlet temp. (°C)	Outlet temp. (°C)	Utility mass flowrate (kg/h)
Q_R1	-787.2	Cooling water 2	250	5	15	65632
Q_HX4	15644478	LP steam	232	125	124	25644178
W_P1	7808.8	-	-	-	-	-
Q_HE4	6096.7	Ammonia refrigerant	151.8	-25	-25	20850
W_P2	0.3	-	-	-	-	-
Q_CD1	6647.1	Cooling water 1 for 5479 kW (Q_HX1 for remaining kW)	250	30	40	457200
Q_RB1	7584.3	LP steam	232	125	124	12431
Q_HE2	155658775	Ammonia refrigerant	151.8	-25	-25	532319329
Q_HX3	10565.2	LP steam	232	125	124	73599
Q_HX1	1168.2	Process fluid (H_2O)	1.01	25	28	325000

LP: low pressure.

The performance of the CH_3OH production plant obtained with the proposed intensified process flowsheet is: relatively pure liquid CH_3OH in the distillate with the benchmark flowrate (stream 30) at 66.9°C and 1.01 bar, overall conversion of CH_4 of 99.06% and overall yield of CH_3OH with respect to input CH_4 of 94.66%.

D.3.5. Data for plasma technology

D.3.5.1. Definition of reference process scheme

Decomposition of CH_4 using nonthermal plasma (NTP) at room temperature and atmospheric pressure represents an alternative to the thermo-catalytic techniques described above. In NTP, the majority of the electrical energy is used to produce energetic electrons which can break the C-H bonds of CH_4 rather than to heat the gas, thus by the bulk gas temperature remains under ambient conditions. NTP can be generated by different electrical discharges. In dielectric-barrier discharge (DBD), micro-discharges are distributed throughout the discharge volume by means of the dielectric barrier, thus the chemical reactions involving ions, radicals and activated molecules are initiated [719]. To increase the selectivity of the desired products, addition of heterogeneous catalyst to plasma reactor appears to be useful. The study by Sk. Mahammadunnisa et al. [679] investigating the catalytic NTP assisted co-processing of N_2O and CH_4 for CH_3OH formation is considered as reference process in the analysis of case-study 5.

The DBD reactor is composed of a cylindrical quartz tube (20 mm inner diameter, 21 mm outer diameter, 250 mm length) containing a stainless rod acting as inner electrode and rolled from a copper wire acting as outer electrode. The inner electrode is connected to HVAC source, while the outer electrode is grounded. The gap between the quartz tube and the outer ground electrode is 1 mm. Discharge length is 15 mm and discharge gap is fixed at 3.5 mm. The area of the Lissajous diagram (charge, i.e. time integrated current, versus voltage across the capacitor connected in series with the outer electrode)

characterizes the energy dissipated in the discharge during one period of the voltage. The average power dissipated in the discharge can be calculated by multiplying the area with the frequency. Specific input energy of the discharge (in J/L) is derived as the ratio of the dissipated power (in W) to the inlet gas flowrate (in L/s). High pure CH_4 (10%mol diluted in Ar) and N_2O (10%mol diluted in Ar) are the input gases to the DBD reactor operating in continuous mode. Different catalysts (i.e. CuO/CeO_2, NiO/CeO_2 and Cu-Ni(5-5)/CeO_2) are tested for the conversion at a specific input energy of 6 kJ/L, gas input flowrate of 60 mL/min (fixed feed ratio CH_4:N_2O equal to 5:1) and operating conditions of 25°C and 1 bar. It is noticed that, besides the desired product CH_3OH, co-products are H_2, CH_2O, CO and CO_2 [679]. The results of the experiment using Cu-Ni(5-5)/CeO_2 catalyst and showing the highest selectivity of CH_3OH is assumed for the analysis of case-study 5: conversion of CH_4 and N_2O of 23% and 68%, respectively, selectivity of CH_3OH of 36%, selectivity of CH_2O of 13%, selectivity of H_2 of 45%, selectivity of CO of 1.5%, selectivity of CO_2 4.5% [679]. Given the compounds involving in the process, the following scheme of reactions in gas phase is derived:

$$CH_4 + N_2O = CH_3OH + N_2 \quad \text{(D.31)}$$

$$CH_4 + N_2O = CH_2O + H_2 + N_2 \quad \text{(D.32)}$$

$$CH_4 + N_2O = CO + 2\ H_2 + N_2 \quad \text{(D.33)}$$

$$CH_4 + 2\ N_2O = CO_2 + 2\ H_2 + 2\ N_2 \quad \text{(D.34)}$$

Based on this scheme and the information about inputs and reaction performance, output flowrates of all compounds from the reactor are estimated. Table D.25 summarizes the mass balance of the process. Extent rate of reaction in Equations (D.31), (D.32), (D.33), (D.34) are $1.05 \cdot 10^{-6}$ kmol/h, $3.79 \cdot 10^{-7}$ kmol/h, $4.38 \cdot 10^{-8}$ kmol/h, $1.31 \cdot 10^{-7}$ kmol/h, respectively. The yield of CH_3OH with respect to input CH_4 is 8.28%.

Table D.25. Mass balance for the reference process scheme based on plasma technology for CH_3OH production from CH_4.

Compound	Inlet flowrate		Outlet flowrate	
	kmol/h	t/h	kmol/h	t/h
CH_4	$1.27 \cdot 10^{-5}$	$2.03 \cdot 10^{-7}$	$1.11 \cdot 10^{-5}$	$1.77 \cdot 10^{-7}$
N_2O	$2.54 \cdot 10^{-6}$	$1.12 \cdot 10^{-7}$	$8.01 \cdot 10^{-7}$	$3.53 \cdot 10^{-8}$
Ar for CH_4	$1.14 \cdot 10^{-4}$	$4.56 \cdot 10^{-6}$	$1.14 \cdot 10^{-4}$	$4.56 \cdot 10^{-6}$
Ar for N_2O	$2.28 \cdot 10^{-5}$	$9.12 \cdot 10^{-7}$	$2.28 \cdot 10^{-5}$	$9.12 \cdot 10^{-7}$
CH_3OH	-	-	$1.05 \cdot 10^{-6}$	$3.36 \cdot 10^{-8}$
CH_2O	-	-	$3.79 \cdot 10^{-7}$	$1.14 \cdot 10^{-8}$
H_2	-	-	$7.30 \cdot 10^{-7}$	$1.46 \cdot 10^{-9}$
CO	-	-	$4.38 \cdot 10^{-8}$	$1.23 \cdot 10^{-9}$
CO_2	-	-	$1.31 \cdot 10^{-7}$	$5.78 \cdot 10^{-9}$
N_2	-	-	$1.74 \cdot 10^{-6}$	$4.86 \cdot 10^{-8}$

D.3.5.2. Definition of intensified process flowsheet

Figure D.7 illustrates the intensified process flowsheet produced with Aspen HYSYS simulation for plasma technology. Data about the material streams in the flowsheet are summarized in Table D.26, while Table D.27 reports information on the energy streams and utilities related to the relevant components in the flowsheet.

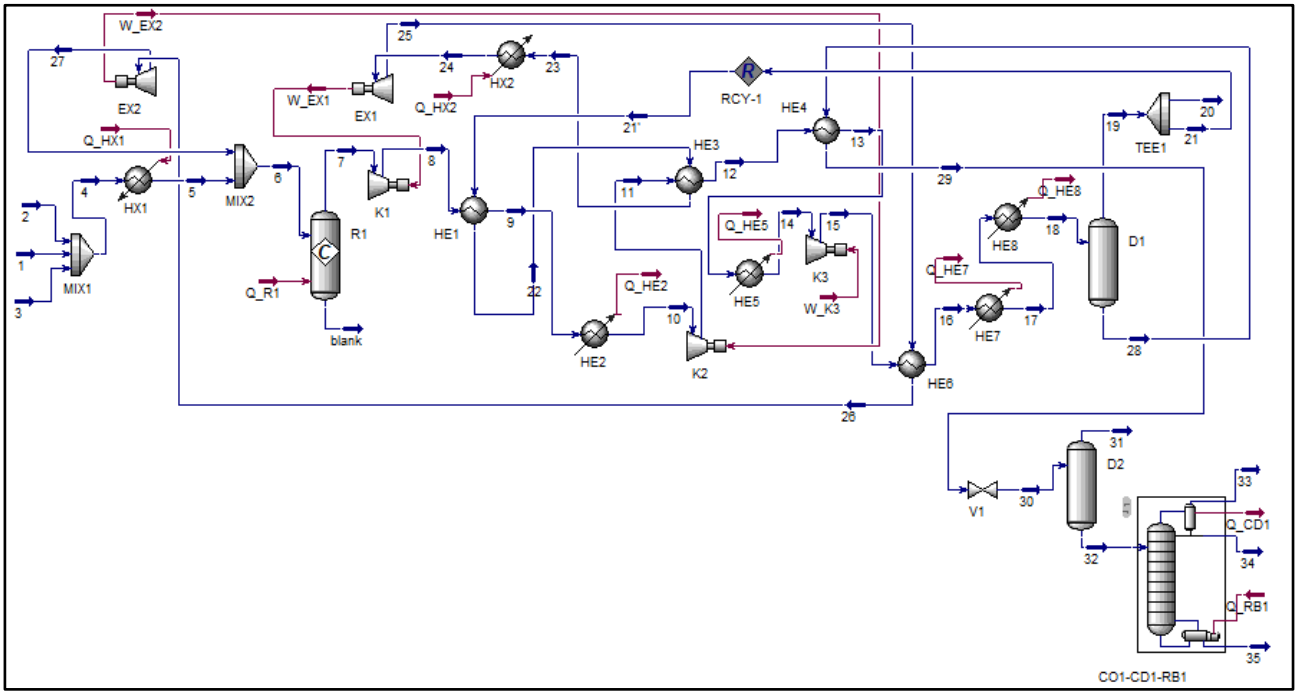

Figure D.7. Intensified process flowsheet for plasma technology from Aspen HYSYS simulation.

As shown in Figure D.7, CH_4 (stream 1), Ar (stream 2) and N_2O (stream 3) are pre-heated in HX1 to the reaction temperature and mixed with gas recycle stream. The resulting gas mixture feeds the reactor R1. In R1, four reactions in series are added: the first one with stoichiometry of reaction in Equation (D.31) and conversion of CH_4 of 8.28%, the second one with stoichiometry of reaction in Equation (D.32) and conversion of CH_4 of 2.99%, the third one with stoichiometry of reaction in Equation (D.33) and conversion of CH_4 of 0.35%, the fourth one with stoichiometry of reaction in Equation (D.34) and conversion of CH_4 of 1.04%, corresponding to the overall conversion of CH_4 of 23% reported in the reference process scheme. The gas output stream from R1 undergoes to three stages of compression-cooling: it is first compressed in K1 and cooled down in HE1 and HE2, then compressed in K2 and cooled down in HE3, HE4 and HE5, and finally compressed in K3 and cooled down in HE6, HE7 and HE8. The resulting mixture is separated in gas and liquid streams in flash drum D1. The gas outlet from D1 is partially recycled to the inlet of R1 while heating in HE1, HE3 and HX1, expansion in EX1, heating in HE6 and expansion in EX2. Liquid phase from D1, mainly containing CH_3OH and CH_2O, is heated in HE4, depressurized to ambient conditions in V1, degassed in D2 and finally separated in distillation unit

CO1-CD1-RB1. Molar CH_3OH fraction in bottom stream of 0.998, vent rate (stream 33) of 1.05 kmol/h, reflux ratio of 0.5, number of stages of 5 (feed in stage 3) are set in the distillation unit.

Input flowrates of CH_4, Ar and N_2O to the plant are adjusted in order to meet in the inlet of the reactor R1 (stream 6 in Figure D.7) the molar ratio Ar to CH_4 of 10.8, N_2O to CH_4 of 0.20, reported in the reference process scheme (Table D.25).

As illustrated in Figure D.7, material process streams at high temperature are re-used to absorb heat in HE1, HE3, HE4, HE6. Moreover, electrical power produced in EX1 and EX2 is used to supply K1 and K2, respectively.

Table D.26. Data on material streams of the intensified process flowsheet illustrated in Figure D.7.

Stream	Vapor phase fract.	Temp. (°C)	Press. (kPa)	Molar flowrate (kmol/h)	Molar fract. CH_4	Molar fract. CH_3OH	Molar fract. H_2	Molar fract. N_2	Molar fract. N_2O	Molar fract. Ar	Molar fract. CO	Molar fract. CO_2	Molar fract. CH_2O
1	1	25.0	13000	32.5	1.000	0.000	0.000	0.000	0.000	0.000	0.000	0.000	0.000
2	1	25.0	15600	46.0	0.000	0.000	0.000	0.000	0.000	1.000	0.000	0.000	0.000
3	1	50.0	5700	29.1	0.000	0.000	0.000	0.000	1.000	0.000	0.000	0.000	0.000
4	1	10.1	5700	107.6	0.302	0.000	0.000	0.000	0.270	0.428	0.000	0.000	0.000
5	1	25.0	5700	107.6	0.302	0.000	0.000	0.000	0.270	0.428	0.000	0.000	0.000
6	1	24.0	101.3	4578.8	0.046	0.000	0.123	0.291	0.009	0.491	0.007	0.019	0.012
7	1	25.0	101.3	4590.9	0.040	0.004	0.125	0.297	0.003	0.490	0.008	0.020	0.014
8	1	191.0	301.6	4590.9	0.040	0.004	0.125	0.297	0.003	0.490	0.008	0.020	0.014
9	1	100.0	301.6	4590.9	0.040	0.004	0.125	0.297	0.003	0.490	0.008	0.020	0.014
10	1	25.0	301.6	4590.9	0.040	0.004	0.125	0.297	0.003	0.490	0.008	0.020	0.014
11	1	129.1	621.8	4590.9	0.040	0.004	0.125	0.297	0.003	0.490	0.008	0.020	0.014
12	1	95.5	621.8	4590.9	0.040	0.004	0.125	0.297	0.003	0.490	0.008	0.020	0.014
13	1	92.5	622.8	4590.9	0.040	0.004	0.125	0.297	0.003	0.490	0.008	0.020	0.014
14	1	25.0	621.8	4590.9	0.040	0.004	0.125	0.297	0.003	0.490	0.008	0.020	0.014
15	1	250.8	2557	4590.9	0.040	0.004	0.125	0.297	0.003	0.490	0.008	0.020	0.014
16	1	181.9	2557	4590.9	0.040	0.004	0.125	0.297	0.003	0.490	0.008	0.020	0.014
17	1	25.0	2557	4590.9	0.040	0.004	0.125	0.297	0.003	0.490	0.008	0.020	0.014
18	0.99	-30.0	2557	4590.9	0.040	0.004	0.125	0.297	0.003	0.490	0.008	0.020	0.014
19	1	-30.0	2557	4567.9	0.040	0.000	0.126	0.298	0.003	0.492	0.008	0.020	0.013
20	1	-30.0	2557	91.4	0.040	0.000	0.126	0.298	0.003	0.492	0.008	0.020	0.013
21	1	-30.0	2557	4476.5	0.040	0.000	0.126	0.298	0.003	0.492	0.008	0.020	0.013
21’	1	-30.0	2557	4471.2	0.040	0.000	0.126	0.298	0.003	0.493	0.008	0.020	0.013
22	1	60.9	2557	4471.2	0.040	0.000	0.126	0.298	0.003	0.493	0.008	0.020	0.013
23	1	95.0	2557	4471.2	0.040	0.000	0.126	0.298	0.003	0.493	0.008	0.020	0.013
24	1	230.0	2557	4471.2	0.040	0.000	0.126	0.298	0.003	0.493	0.008	0.020	0.013
25	1	59.0	390.0	4471.2	0.040	0.000	0.126	0.298	0.003	0.493	0.008	0.020	0.013
26	1	132.6	390.0	4471.2	0.040	0.000	0.126	0.298	0.003	0.493	0.008	0.020	0.013
27	1	25.0	101.3	4471.2	0.040	0.000	0.126	0.298	0.003	0.493	0.008	0.020	0.013
28	0	-30.0	2557	23.0	0.001	0.755	0.000	0.003	0.003	0.008	0.000	0.012	0.218
29	0	82.0	2557	23.0	0.001	0.755	0.000	0.003	0.003	0.008	0.000	0.012	0.218
30	0.27	39.6	101.3	23.0	0.001	0.755	0.000	0.003	0.003	0.008	0.000	0.012	0.218
31	1	39.6	101.3	6.1	0.005	0.239	0.000	0.011	0.010	0.029	0.000	0.044	0.661
32	0	39.6	101.3	16.9	0.000	0.941	0.000	0.000	0.000	0.000	0.000	0.000	0.058
33	1	24.4	101.3	1.0	0.000	0.093	0.000	0.000	0.002	0.000	0.000	0.005	0.900
34	0	24.4	101.3	0.2	0.000	0.880	0.000	0.000	0.000	0.000	0.000	0.000	0.119
35	0	67.7	101.3	15.7	0.000	0.999	0.000	0.000	0.000	0.000	0.000	0.000	0.001

Table D.27. Data on energy streams associated to components of the intensified process flowsheet in Figure D.7.

Stream	Heat/Power flow (kW)	Utility	Pressure (kPa)	Inlet temp. (°C)	Outlet temp. (°C)	Utility mass flowrate (kg/h)
Q_HE5	2241.0	Cooling water 2	250	5	15	186835
Q_HX2	4469.1	HP steam	3913	250	249	9447
W_K3	7544.8	-	-	-	-	-
Q_HE7	5365.2	Cooling water 2	250	5	15	447304
Q_R1	-1500.7	Cooling water 2	250	5	15	125113
Q_HX1	16.9	LP steam	232	125	124	28
W_EX1	5508.7	-	-	-	-	-
Q_HE8	2172.6	Refrigerant 1	105.3	-39	-40	42755
W_EX2	3432.0	-	-	-	-	-
Q_HE2	2477.3	Cooling water 2	250	5	15	206540
Q_CD1	9.9	Cooling water 2	250	5	15	824.8
Q_RB1	35.8	LP steam	232	125	124	59

HP: high pressure, LP: low pressure

The performance of the CH_3OH production plant obtained with the proposed intensified process flowsheet is: relatively pure liquid CH_3OH in the distillate with the benchmark flowrate (stream 35) at 67.7°C and 1.01 bar, overall conversion of CH_4 of 88.73% and overall yield of CH_3OH with respect to input CH_4 of 48.13%.

D.3.6. Data for photocatalysis

D.3.6.1. Definition of reference process scheme

Photocatalysis is one of the methods allowing to convert CH_4 into CH_3OH by means of a suitable catalyst and light. Among the candidate catalyst, the study by Villa et al. [680] investigating an aqueous suspension containing ordered mesoporous WO_3 is chosen as the reference process for the analysis of case-study 5. A photochemical reactor (500 mL volume) with an immerged medium pressure lamp producing UVC-visible light irradiation is employed. The reaction temperature is kept constant at 55°C by using cold H_2O recirculation in the outer jacket of the lamp. Inlet gas mixture is composed of CH_4 (4.5 mL/min) and He (17.9 mL/min). In the experiment, 300 mL of H_2O containing 0.3 g of WO_3 is used [720]. The initial pH of the suspension is adjusted with 1 M H_2SO_4. After proper stirring of the suspension, the lamp is turned on. When the WO_3 slurry is irradiated with light energy higher than 2.7 eV, pairs of electrons in conduction band (e_{CB}^-) and holes in valence band (h_{VB}^+) are generated through Equation (D.35), then the holes h_{VB}^+ react with H_2O or hydroxide ions adsorbed on the surface to produce hydroxyl radicals by means of Equations (D.36) and (D.37), which react with CH_4 to produce CH_3OH as shown in Equations (D.38) and (D.39):

$$WO_3 \rightarrow e_{CB}^- + h_{VB}^+ \quad \text{(D.35)}$$

$$h_{VB}^+ + H_2O_{ads} \rightarrow HO^*_{ads} + H^+ \quad \text{(D.36)}$$

h_{VB}^{+} + HO^{-}_{ads} → HO^{*}_{ads} + H^{+} (D.37)

CH_4 + HO^{*}_{ads} → CH_3^{*} + H_2O (D.38)

CH_3^{*} + H_2O_{ads} → CH_3OH + ½ H_2 (D.39)

The addition of electrons scavengers allows to avoid the self-reduction process of WO_3 by photogenerated electrons leading to a reduction in photocatalytic activity and CH_3OH production. Among the chemical additives examined as electrons scavengers, it is noticed that the system WO_3/Fe^{3+} (1 mM) shows the best performance in terms of CH_3OH production per mass of catalyst (i.e. 67.5 µmol/h-g) for 2 hours of irradiation in continuous flow of input gas and dosage of WO_3 of 1 mg/L. Reported co-products are C_2H_6 (2.3 µmol/h-g) and CO_2 (4.3.3 µmol/h-g) [680].

Given the compounds involving in the process, the following scheme of reactions is derived:

$CH_4 + H_2O = CH_3OH + H_2$ (D.40)

$2\ CH_4 = C_2H_6 + H_2$ (D.41)

$CH_4 + 2\ H_2O = CO_2 + 4\ H_2$ (D.42)

By assuming four batches per day (i.e. at maximum 6 h including loading, lamp irradiation and unloading), the inlet flowrates are estimated. Based on the reactions scheme and the information about reaction performance, output flowrates of all compounds from the reactor are calculated. Table D.28 summarizes the material balance of the process. Extent rate of reaction in Equations (D.40), (D.41) and (D.42) are $6.75 \cdot 10^{-9}$ kmol/h, $2.30 \cdot 10^{-10}$ kmol/h, $4.33 \cdot 10^{-9}$ kmol/h, respectively. Molar conversion of CH_4 is estimated as 0.348%. The yield of CH_3OH with respect to input CH_4 is 0.20%. CH_3OH fraction in the aqueous solution from the reactor is 0.00041%wt (0.00025%mol).

Table D.28. Mass balance for the reference process scheme based on photocatalysis for CH_3OH production from CH_4.

Compound	Inlet flowrate		Outlet flowrate	
	kmol/h	t/h	kmol/h	t/h
CH_4	$3.31 \cdot 10^{-6}$	$5.30 \cdot 10^{-8}$	$3.30 \cdot 10^{-6}$	$5.28 \cdot 10^{-8}$
He	$1.31 \cdot 10^{-5}$	$5.25 \cdot 10^{-8}$	$1.31 \cdot 10^{-5}$	$5.25 \cdot 10^{-8}$
H_2SO_4/H_2O	$2.70 \cdot 10^{-3}$	$5.23 \cdot 10^{-5}$	$2.70 \cdot 10^{-3}$	$5.23 \cdot 10^{-5}$
CH_3OH	-	-	$6.75 \cdot 10^{-9}$	$2.16 \cdot 10^{-10}$
C_2H_6	-	-	$2.30 \cdot 10^{-10}$	$6.90 \cdot 10^{-12}$
CO_2	-	-	$4.33 \cdot 10^{-9}$	$1.91 \cdot 10^{-10}$

D.3.6.2. Definition of intensified process flowsheet

Figure D.8 illustrates the intensified process flowsheet produced with Aspen HYSYS simulation for photocatalysis. Data about the material streams in the flowsheet are summarized in Table D.29, while Table D.30 reports information on the energy streams related to the relevant components in the flowsheet.

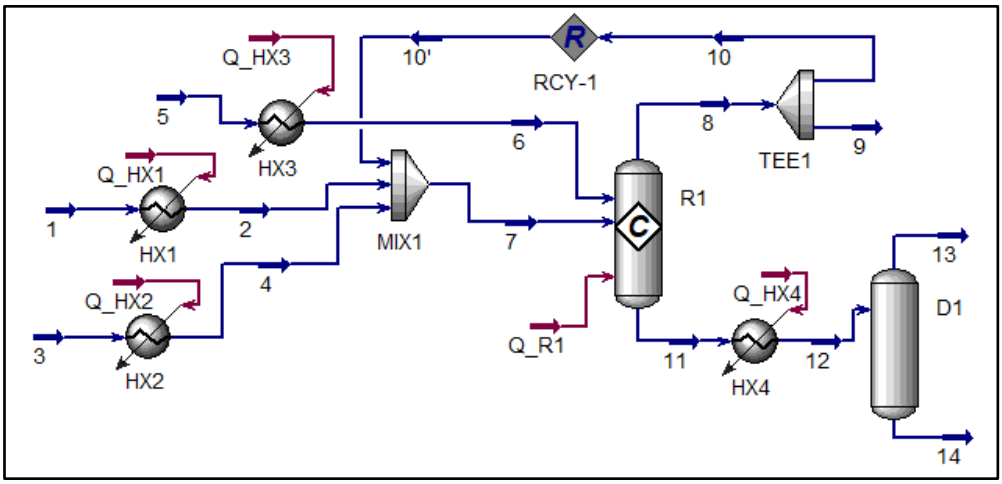

Figure D.8. Intensified process flowsheet for photocatalysis from Aspen HYSYS simulation.

As shown in Figure D.8, CH_4 (stream 1) and He (stream 3) are mixed with gas recycle stream. This mixture (stream 7) and liquid H_2O heated in HX1(stream 6) enter reactor R1. In R1, three reactions in series are introduced: the first one with the stoichiometry of Equation (D.40) and conversion of CH_4 of 0.204%, the second one with the stoichiometry of Equation (D.41) and conversion of CH_4 of 0.014%, the third one with stoichiometry of Equation (D.42) and conversion of CH_4 of 0.131%, which correspond to the overall conversion of CH_4 of 0.348% reported in the reference process scheme. The gas output stream from R1 is then recycled, while the liquid output (stream 11) is heated in HX4 and enters atmospheric flash drum D1 to separate gas and liquid phases. No further separation operations of the liquid stream from D1 are included in the flowsheet since a merely fraction of CH_3OH is obtained in the stream (0.00032%mol).

Input flowrates of CH_4, He and H_2O to the plant are adjusted in order to meet in inlet of R1 (streams 6 and 7 in Figure D.8) the molar ratio H_2O to CH_4 of 630.1 and He to CH_4 of 3.954 reported in the reference process scheme (Table D.28).

Even though incomplete, the performance of the CH_3OH production plant obtained with the proposed intensified process flowsheet are: highly diluted CH_3OH in H_2O in the liquid stream from D1 (stream 14) at 99.8°C and 1.01 bar, overall conversion of CH_4 of 77.8% and overall yield of CH_3OH with respect to input CH_4 of 45.3%.

Table D.29. Data on material streams of the intensified process flowsheet illustrated in Figure D.8.

Stream	Vapor phase	Temp. (°C)	Press. (kPa)	Molar flowrate (kmol/h)	Molar fraction CH_4	Molar fraction CO_2	Molar fraction CH_3OH	Molar fraction H_2O	Molar fraction H_2	Molar fraction C_2H_6	Molar fraction He
1	1	25.0	13800	50	1	0	0	0	0	0	0
2	1	55.0	13800	50	1	0	0	0	0	0	0
3	1	25.0	15600	86	0	0	0	0	0	0	1
4	1	55.0	15600	86	0	0	0	0	0	0	1
5	0	25.0	101.3	7000000	0	0	0	1	0	0	0
6	0	55.0	101.3	7000000	0	0	0	1	0	0	0
7	1	55.0	101.3	154429.3	0.072	0.007	0.000	0.155	0.476	0.005	0.285
8	1	55.0	101.3	154445.1	0.072	0.007	0.000	0.155	0.476	0.005	0.285
9	1	55.0	101.3	154.4451	0.072	0.007	0.000	0.155	0.476	0.005	0.285
10	1	55.0	101.3	154290.6	0.072	0.007	0.000	0.155	0.476	0.005	0.285
10’	1	55.0	101.3	154293.3	0.072	0.007	0.000	0.155	0.476	0.005	0.285
11	0	55.0	101.3	7000013	0.000	0.000	0.000	1.000	0.000	0.000	0.000
12	0	99.8	101.3	7000013	0.000	0.000	0.000	1.000	0.000	0.000	0.000
13	1	99.8	101.3	11323.01	0.000	0.001	0.000	0.994	0.001	0.000	0.004
14	0	99.8	101.3	6988690	0.000	0.000	0.000	1.000	0.000	0.000	0.000

Table D.30. Data on energy streams associated to components of the intensified process flowsheet in Figure D.8.

Stream	Heat flow (kW)
Q_R1	2308.5
Q_HX4	6963042.8
Q_HX3	4536603.5
Q_HX1	21.1
Q_HX2	15.0

D.3.7. Data for supercritical water oxidation technology

D.3.7.1. Definition of reference process scheme

The supercritical H_2O oxidation method uses H_2O at elevated temperatures and pressures above the critical point of the mixture as fluid medium to enhance the conversion of CH_4 into CH_3OH. Supercritical H_2O would facilitate the removal of heat as well as allows the reaction to occur in a single phase due to miscibility of CH_4, O_2 CH_3OH with supercritical H_2O. The process investigated by Lee et al. [681] is considered as reference in the analysis of case-study 5 for CH_3OH production by this method. A continuous laminar reactor is employed composed of coiled tube (730 mm length, 6.35 mm outside diameter, 4.58 mm internal diameter) immersed in a fluidized sand-bath for controlled temperature. Deionized H_2O, saturated with O_2, and CH_4 are routed to pre-heaters immersed in the sand-bath and then mixed to enter into the tubular reactor. To enhance the mixing, CH_4 is passed through a sparge which uses air. Different experiments are carried out in a temperature range of 400-450°C at 250 bar producing CO, CO_2, H_2 besides CH_3OH. The results of the test showing the highest yield of CH_3OH are used for the analysis of the case-study. At 410°C with inlet flowrate of CH_4 0.231 mol/L and O_2 0.0123 mol/L and ratio CH_4/H_2O equal to 0.007, it is reported CH_4 conversion of 4.5%, O_2 conversion greater than 99%,

CH_3OH selectivity of 29%, CO selectivity of 50%, CO_2 selectivity of 21%, H_2 selectivity of 9.2%, percentage of CO_2 produced via water gas shift reaction of 74.4% [681].

Given the compounds involving in the process, the following scheme of reactions is derived:

$$CH_4 + 1/2\ O_2 = CH_3OH \quad \text{(D.43)}$$

$$CH_4 + 2\ O_2 = CO_2 + 2\ H_2O \quad \text{(D.44)}$$

$$CH_4 + 3/2\ O_2 = CO + 2\ H_2O \quad \text{(D.45)}$$

$$CO + H_2O = CO_2 + H_2 \quad \text{(D.46)}$$

Based on this scheme and the information about inputs and reaction performance, output flowrates of all compounds from the reactor are estimated. Extent rate of reactions in Equations (D.43), (D.44), (D.45), (D.46) are $6.06 \cdot 10^{-6}$ kmol/h, $1.12 \cdot 10^{-6}$ kmol/h, $1.37 \cdot 10^{-5}$ kmol/h, $3.26 \cdot 10^{-6}$ kmol/h, respectively. Table D.31 summarizes the mass balance of the process. The yield of CH_3OH with respect to input CH_4 is 1.3%. CH_3OH fraction in the outlet stream from the reactor is 0.016%wt (0.009%mol).

Table D.31. Mass balance for the reference process scheme based on supercritical water technology for CH_3OH production from CH_4.

Compound	Inlet flowrate		Outlet flowrate	
	kmol/h	t/h	kmol/h	t/h
CH_4	$4.64 \cdot 10^{-4}$	$7.43 \cdot 10^{-6}$	$4.43 \cdot 10^{-4}$	$7.09 \cdot 10^{-6}$
N_2 in Air	$9.30 \cdot 10^{-5}$	$2.60 \cdot 10^{-6}$	$9.30 \cdot 10^{-5}$	$2.60 \cdot 10^{-6}$
O_2 in Air	$2.47 \cdot 10^{-5}$	$7.91 \cdot 10^{-7}$	$1.12 \cdot 10^{-6}$	$3.58 \cdot 10^{-8}$
O_2 for H_2O saturation	$6.53 \cdot 10^{-4}$	$2.09 \cdot 10^{-5}$	$6.53 \cdot 10^{-4}$	$2.09 \cdot 10^{-5}$
H_2O	$6.63 \cdot 10^{-2}$	$1.19 \cdot 10^{-3}$	$6.63 \cdot 10^{-2}$	$1.19 \cdot 10^{-3}$
CH_3OH	-	-	$6.06 \cdot 10^{-6}$	$1.94 \cdot 10^{-7}$
CO	-	-	$1.04 \cdot 10^{-5}$	$2.92 \cdot 10^{-7}$
CO_2	-	-	$4.39 \cdot 10^{-6}$	$1.93 \cdot 10^{-7}$
H2	-	-	$3.26 \cdot 10^{-6}$	$6.53 \cdot 10^{-6}$

D.3.7.2. Definition of intensified process flowsheet

Figure D.9 illustrates the intensified process flowsheet produced with Aspen HYSYS simulation for supercritical water technology. Data about the material streams in the flowsheet are summarized in Table D.32, while Table D.33 reports information on the energy streams related to the relevant components in the flowsheet.

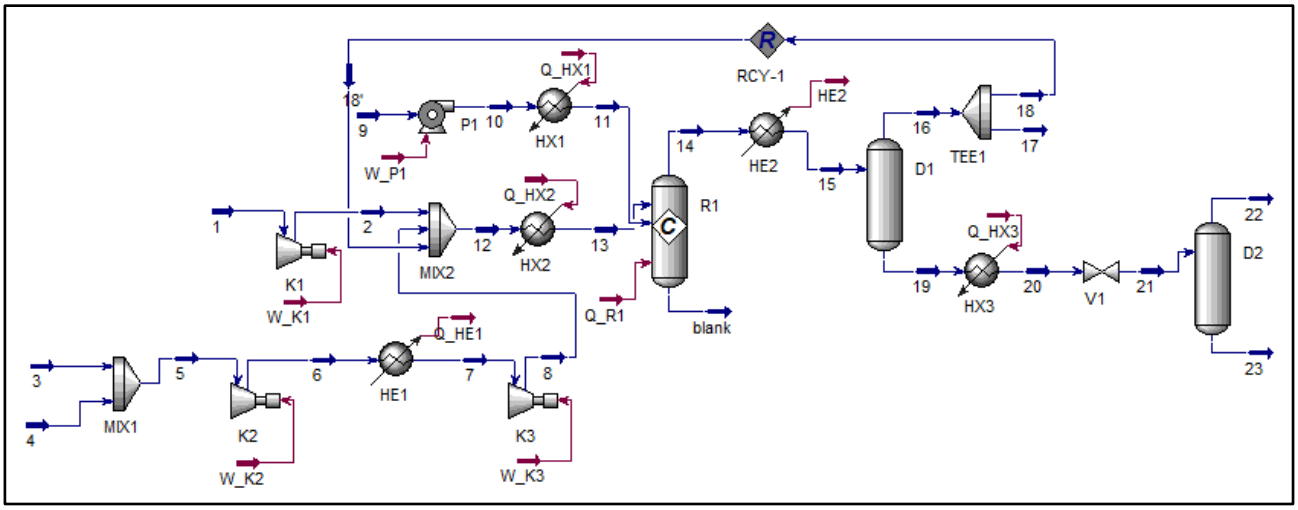

Figure D.9. Intensified process flowsheet for supercritical water technology from Aspen HYSYS simulation.

As shown in Figure D.9, CH_4 (stream 1) and O_2 and N_2 from air (streams 3 and 4) are properly compressed in K1, K2 and K3 to reach the required pressure for CH_3OH synthesis and then mixed with gas recycle stream and pre-heated in HX2 to the reaction temperature. The resulting mixture (stream 13) and liquid H_2O pumped in P1 and heated in HX1 (stream 11) enter reactor R1. In R1, four reactions in series are introduced: the first one with the stoichiometry of Equation (D.43) and conversion of CH_4 of 1.305%, the second one with the stoichiometry of Equation (D.42) and conversion of CH_4 of 0.242%, the third one with stoichiometry of Equation (D.43) and conversion of CH_4 of 2.953%, which correspond to the overall conversion of CH_4 of 4.5% reported in the reference process scheme. The fourth one is added with stoichiometry of Equation (D.44) and conversion of CO of 23.8%. The gas output stream from R1 is cooled down in HE2 and separated into gas and liquid streams in flash drum D1. The gas outlet is then recycled, while the liquid output (stream 19) is heated in HX3, depressurized to atmospheric conditions in V1 and enters atmospheric flash drum D2 to separate gas and liquid phases. No further separation operations of the liquid stream from D2 are included in the flowsheet since a small fraction of CH_3OH is obtained in the stream (0.01%mol).

Input flowrates of CH_4, Air and H_2O to the plant are adjusted in order to meet in inlet of R1 (streams 11 and 13 in Figure D.9) the molar ratio O_2 to CH_4 of 1.46, N_2 to CH_4 of 0.20, H_2O to CH_4 of 142.9 reported in the reference process scheme (Table D.31).

Even though incomplete, the performance of the CH_3OH production plant obtained with the proposed intensified process flowsheet are: highly diluted CH_3OH in H_2O in the liquid stream from D2 (stream 23) at 89.5°C and 1.01 bar, overall conversion of CH_4 of 70.15% and overall yield of CH_3OH with respect to input CH_4 of 20.4%.

Table D.32. Data on material streams of the intensified process flowsheet illustrated in Figure D.9.

Stream	Vapor phase fract.	Temp. (°C)	Press. (kPa)	Molar flowrate (kmol/h)	Mol. fract. CH_4	Mol. fract. CO_2	Mol. fract. CH_3OH	Mol. fract. H_2O	Mol. fract. H_2	Mol. fract. CO	Mol. fract. O_2	Mol. fract. N_2
1	1	25.0	13800	3000	1.000	0.000	0.0000	0.000	0.000	0.000	0.000	0.000
2	1	78.0	25000	3000	1.000	0.000	0.0000	0.000	0.000	0.000	0.000	0.000
3	1	25.0	800	4450	0.000	0.000	0.0000	0.000	0.000	0.000	1.000	0.000
4	1	25.0	800	1500	0.000	0.000	0.0000	0.000	0.000	0.000	0.000	1.000
5	1	25.0	800	5950	0.000	0.000	0.0000	0.000	0.000	0.000	0.748	0.252
6	1	250.0	4031	5950	0.000	0.000	0.0000	0.000	0.000	0.000	0.748	0.252
7	1	25.0	4023	5950	0.000	0.000	0.0000	0.000	0.000	0.000	0.748	0.252
8	1	286.8	25000	5950	0.000	0.000	0.0000	0.000	0.000	0.000	0.748	0.252
9	0	25.0	101.3	6690000	0.000	0.000	0.0000	1.000	0.000	0.000	0.000	0.000
10	0	27.2	25000	6690000	0.000	0.000	0.0000	1.000	0.000	0.000	0.000	0.000
11	1	410.0	25000	6690000	0.000	0.000	0.0000	1.000	0.000	0.000	0.000	0.000
12	1	0.3	25000	182268	0.257	0.002	0.0000	0.000	0.294	0.022	0.374	0.051
13	1	410.0	25000	182268	0.257	0.002	0.0000	0.000	0.294	0.022	0.374	0.051
14	1	410.0	25000	6872655	0.007	0.000	0.0001	0.974	0.008	0.001	0.010	0.001
15	0.026	-10.0	25000	6872655	0.007	0.000	0.0001	0.974	0.008	0.001	0.010	0.001
16	1	-10.0	25000	176906	0.253	0.002	0.0000	0.000	0.309	0.023	0.368	0.045
17	1	-10.0	25000	3538	0.253	0.002	0.0000	0.000	0.309	0.023	0.368	0.045
18	1	-10.0	25000	173368	0.253	0.002	0.0000	0.000	0.309	0.023	0.368	0.045
18’	1	-10.0	25000	173318	0.253	0.002	0.0000	0.000	0.309	0.023	0.367	0.045
19	0	-10.0	25000	6695749	0.000	0.000	0.0001	0.999	0.000	0.000	0.000	0.000
20	0	85.0	25000	6695749	0.000	0.000	0.0001	0.999	0.000	0.000	0.000	0.000
21	0.002	89.5	101.3	6695749	0.000	0.000	0.0001	0.999	0.000	0.000	0.000	0.000
22	1	89.5	101.3	10197	0.000	0.121	0.0001	0.680	0.018	0.002	0.042	0.137
23	0	89.5	101.3	6685552	0.000	0.000	0.0001	1.000	0.000	0.000	0.000	0.000

Table D.33. Data on energy streams associated to components of the intensified process flowsheet in Figure D.9.

Stream	Heat/power flow (kW)
Q_R1	1351174
HE2	95436720
Q_HX3	13682072
Q_HX2	776678
W_P1	1103318
Q_HX1	87653871
W_K1	1499
W_K2	11181
Q_HE1	11642
W_K3	13237

D.3.8. Data for fuel cells technology

D.3.8.1. Definition of reference process scheme

Direct oxidation of CH_4 into CH_3OH at low temperature can be performed by using a fuel-cell type reactor consisting of metal cathode and anode or metal oxide catalyst. The study by Lee and Hibino [682] investigating different metals and metal oxides impregnated on the surface of the support catalysts in fuel-cell reactor is selected in the analysis of case-study 5 for CH_3OH synthesis based on this technology. At the electrochemical cell, a mixture of CH_4 and H_2O vapor is supplied to the anode and air to the cathode

in order to produce CH_3OH at the anode. The semi-reactions and overall reaction under continuous operation mode are [682]:

$$CH_4 + H_2O \rightarrow CH_3OH + 2\ H^+ + 2\ e^- \quad (D.47)$$

$$O_2 + 4\ H^+ + 4\ e^- \rightarrow 2\ H_2O \quad (D.48)$$

$$CH_4 + ½\ O_2 = CH_3OH \quad (D.49)$$

For the experiments, anode and cathode with single superficial area of 0.5 cm^2 are arranged on opposite faces of a given electrolyte pellet. The anode and cathode chambers are supplied with a mixture of 10% CH_4, 1% H_2O (Ar balance) and air, respectively, at a flow rate of 30 mL/min. Reactions occur at constant current of 2 mA and temperature of 100°C. Pt/C cathode is adopted. From the tests using various non-platinum catalysts and non-carbon supports for the anode, the best performance is obtained with V_2O_5 catalyst and SnO_2 support: CH_3OH selectivity of 88.4%, CO_2 selectivity of 11.6%, CH_3OH molar fraction of 0.0306% and CO_2 molar fraction of 0.004%. These results are assumed for the case-study.

Given the compounds involving in the process, the following scheme of reactions is derived:

$$CH_4 + 1/2\ O_2 = CH_3OH \quad (D.50)$$

$$CH_4 + 2\ O_2 = CO_2 + 2\ H_2O \quad (D.51)$$

Based on this scheme and the information about inputs and reaction performance, output flowrates of all compounds from the reactor are estimated. Extent rate of reactions in Equations (D.50) and (D.51) are $3.80 \cdot 10^{-8}$ kmol/h and $4.97 \cdot 10^{-9}$ kmol/h, respectively. Table D.34 summarizes the mass balance of the process. Molar conversion of CH_4 is 0.69%. The yield of CH_3OH with respect to input CH_4 is 0.61%. CH_3OH fraction in the outlet stream from the anode is 0.05%wt (0.06%mol).

Table D.34. Mass balance for the reference process scheme based on fuel cell technology for CH_3OH production from CH_4.

Compound	Inlet flowrate		Outlet flowrate	
	kmol/h	t/h	kmol/h	t/h
CH_4 - Anode	$6.21 \cdot 10^{-6}$	$9.94 \cdot 10^{-8}$	$6.17 \cdot 10^{-6}$	$9.87 \cdot 10^{-8}$
H2O - Anode	$6.21 \cdot 10^{-7}$	$1.12 \cdot 10^{-8}$	$6.31 \cdot 10^{-7}$	$1.14 \cdot 10^{-8}$
Ar - Anode	$5.53 \cdot 10^{-5}$	$2.21 \cdot 10^{-6}$	$5.53 \cdot 10^{-5}$	$2.21 \cdot 10^{-6}$
N_2 in Air - Cathode	$4.90 \cdot 10^{-5}$	$1.37 \cdot 10^{-6}$	$4.90 \cdot 10^{-5}$	$1.37 \cdot 10^{-6}$
O_2 in Air - Cathode	$1.30 \cdot 10^{-5}$	$4.17 \cdot 10^{-7}$	$1.30 \cdot 10^{-6}$	$4.16 \cdot 10^{-7}$
CH_3OH	-	-	$3.80 \cdot 10^{-8}$	$1.22 \cdot 10^{-9}$
CO_2	-	-	$1.04 \cdot 10^{-5}$	$2.19 \cdot 10^{-10}$

D.3.8.2. Definition of intensified process flowsheet

Figure D.10 illustrates the intensified process flowsheet produced with Aspen HYSYS simulation for photocatalysis. Data about the material streams in the flowsheet are summarized in Table D.35, while Table D.36 reports information on the energy streams related to the relevant components in the flowsheet.

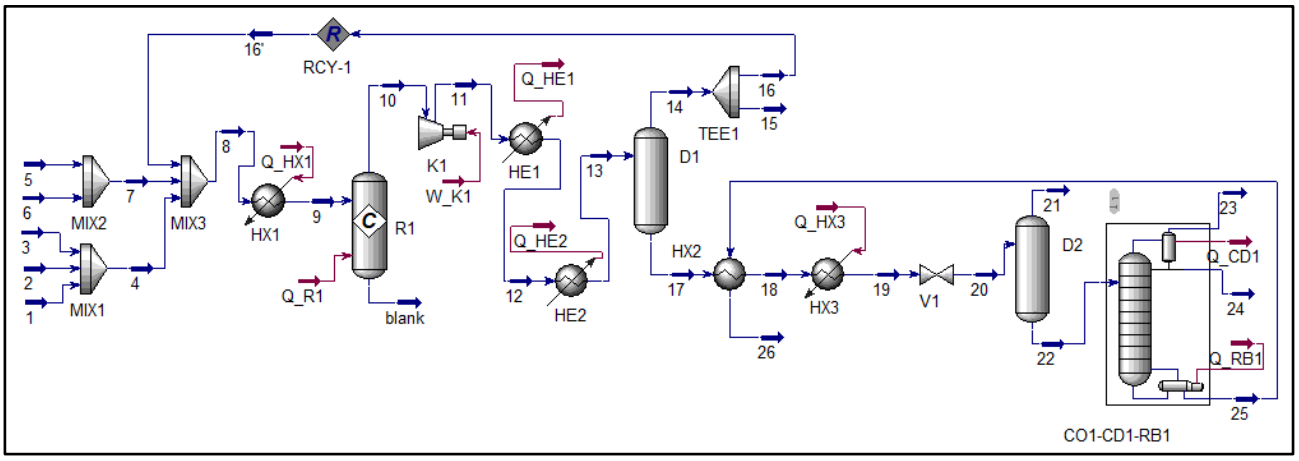

Figure D.10. Intensified process flowsheet for fuel cell technology from Aspen HYSYS simulation.

As shown in Figure D.10, CH_4 (stream 1), Ar (stream 2) and vapor H_2O (stream 3) are mixed with O_2 (stream 5) and N_2 (stream 6) from air and with recycled gas stream. The resulting mixture is pre-heated in HX1 to the reaction temperature and feeds the reactor R1. In R1, two reactions in series are added: the first one with stoichiometry of reaction in Equation (D.50) and conversion of CH_4 of 0.611%, the second one with stoichiometry of reaction in Equation (D.51) and conversion of CH_4 of 0.080%, corresponding to the overall conversion of CH_4 of 0.69% reported in the reference process scheme. The gas output stream from D1 is partially recycled to the inlet of R1, while liquid phase is heated in HX2 and HX3, depressurized to ambient conditions in V1, degassed in D2 and finally separated in distillation unit CO1-CD1-RB1. Distillate rate of 15.64 kmol/h, vent rate (stream 23) of 0.1 kmol/h, reflux ratio of 24.69, number of stages of 17 (feed in stage 9) are set in the distillation unit.

Input flowrates of CH_4, Ar, H_2O, O_2, N_2 to the plant are adjusted in order to meet in the inlet of the reactor R1 (stream 9 in Figure D.10) the molar ratio Ar to CH_4 of 8.9, H_2O to CH_4 of 0.1, O_2 to CH_4 of 2.096, N_2 to CH_4 of 7.885 reported in the reference process scheme (Table D.34). As illustrated in Figure D.10, material process stream from the bottom of CO1-CD1-RB1 is used as heating fluid in HX2.

The performance of the CH_3OH production plant obtained with the proposed intensified process flowsheet is: relatively pure liquid CH_3OH in the distillate with the benchmark flowrate (stream 24) at 62.7°C and 1.01 bar, overall conversion of CH_4 of 87.44% and overall yield of CH_3OH with respect to input CH_4 of 55.15%.

Table D.35. Data on material streams of the intensified process flowsheet illustrated in Figure D.10.

Stream	Vapor phase fract.	Temp. (°C)	Press. (kPa)	Molar flowrate (kmol/h)	Molar fract. CH_4	Molar fract. CH_3OH	Molar fract. H_2	Molar fract. N_2	Molar fract. N_2O	Molar fract. Ar	Molar fract. CO
1	1	25	13800	28.3	1.000	0.000	0.000	0.000	0.000	0.000	0.000
2	1	25	15600	45	0.000	0.000	1.000	0.000	0.000	0.000	0.000
3	1	120	101.3	340	0.000	1.000	0.000	0.000	0.000	0.000	0.000
4	1	97.1	101.3	413.3	0.069	0.823	0.109	0.000	0.000	0.000	0.000
5	1	25	800	34	0.000	0.000	0.000	0.000	0.000	0.000	1.000
6	1	25	800	32	0.000	0.000	0.000	0.000	0.000	1.000	0.000
7	1	25.0	800	66	0.000	0.000	0.000	0.000	0.000	0.485	0.515
8	0.998	-6.4	101.3	74954	0.048	0.006	0.435	0.000	0.037	0.376	0.098
9	1	100	101.3	74954	0.048	0.006	0.435	0.000	0.037	0.376	0.098
10	1	100	101.3	74943	0.047	0.006	0.435	0.000	0.037	0.376	0.098
11	1	258.5	250	74943	0.047	0.006	0.435	0.000	0.037	0.376	0.098
12	1	55	250	74943	0.047	0.006	0.435	0.000	0.037	0.376	0.098
13	0.995	-10.0	250	74943	0.047	0.006	0.435	0.000	0.037	0.376	0.098
14	1	-10.0	250	74576	0.048	0.001	0.437	0.000	0.037	0.378	0.099
15	1	-10.0	250	75	0.048	0.001	0.437	0.000	0.037	0.378	0.099
16	1	-10.0	250	74501	0.048	0.001	0.437	0.000	0.037	0.378	0.099
16’	1	-10.0	250	74475	0.048	0.001	0.437	0.000	0.037	0.378	0.099
17	0	-10.0	250	368	0.000	0.941	0.000	0.059	0.000	0.000	0.000
18	0	36.6	250	368	0.000	0.941	0.000	0.059	0.000	0.000	0.000
19	0	85.0	250	368	0.000	0.941	0.000	0.059	0.000	0.000	0.000
20	0	85.0	101.3	368	0.000	0.941	0.000	0.059	0.000	0.000	0.000
21	1	85.0	101.3	0	0.000	0.536	0.000	0.066	0.278	0.119	0.002
22	0	85.0	101.3	367	0.000	0.941	0.000	0.059	0.000	0.000	0.000
23	1	62.7	101.3	0	0.000	0.000	0.000	0.847	0.148	0.005	0.000
24	0	62.7	101.3	16	0.000	0.000	0.000	0.999	0.001	0.000	0.000
25	0	99.6	101.3	352	0.000	0.983	0.000	0.017	0.000	0.000	0.000
26	0	50.0	101.3	352	0.000	0.983	0.000	0.017	0.000	0.000	0.000
27	1	25.0	101.3	4471.2	0.040	0.000	0.126	0.298	0.003	0.493	0.008
28	0	-30.0	2557	23.0	0.001	0.755	0.000	0.003	0.003	0.008	0.000
29	0	82.0	2557	23.0	0.001	0.755	0.000	0.003	0.003	0.008	0.000
30	0.27	39.6	101.3	23.0	0.001	0.755	0.000	0.003	0.003	0.008	0.000
31	1	39.6	101.3	6.1	0.005	0.239	0.000	0.011	0.010	0.029	0.000
32	0	39.6	101.3	16.9	0.000	0.941	0.000	0.000	0.000	0.000	0.000
33	1	24.4	101.3	1.0	0.000	0.093	0.000	0.000	0.002	0.000	0.000
34	0	24.4	101.3	0.2	0.000	0.880	0.000	0.000	0.000	0.000	0.000
35	0	67.7	101.3	15.7	0.000	0.999	0.000	0.000	0.000	0.000	0.000

Table D.36. Data on energy streams associated to components of the intensified process flowsheet in Figure D.10.

Stream	Heat/Power flow (kW)	Utility	Pressure (kPa)	Inlet temp. (°C)	Outlet temp. (°C)	Utility mass flowrate (kg/h)
Q_HX3	402.9	LP steam	232	125	124	660
Q_R1	-1410.1	Cooling water 1	250	30	40	117676
Q_CD1	4266.5	Cooling water 1	250	30	40	355995
Q_RB1	4400.4	LP steam	232	125	124	7213
W_K1	89708.5	-	-	-	-	-
Q_HE2	40356.4	LP steam	232	125	124	129807
Q_HE1	114855.3	Cooling water 1	250	30	40	9584588
Q_HX1	60365.8	Refrigerant 1	105.3	-39	-40	98942

LP: low pressure.

D.3.9. Data for electrosynthesis

D.3.9.1. Definition of reference process scheme

Electrosynthesis of CH_3OH is the oxidative conversion of CH_4 in an electrochemical cell using gas diffusion electrode (GDEs) as anode which allows effectively the contact between gas reactant and liquid medium because of their porous structure. The study by Rocha et al. [721] investigating the electrosynthesis of CH_3OH using GDE composed of $TiO_2/RuO_2/V_2O_5$ hot-pressed with PTFE is considered as reference source in the analysis of case-study 5. The discharge of H_2O on the conductive oxide electrodes (titanium) generates hydroxyl electrodes which chemically adsorb on the oxide surface in forms of O_2 atoms, these O_2 atoms then oxidize CH_4 to CH_3OH. However, CH_4 is also oxidized by the redox cycle of RuO_2 to CH_3OH, HCOOH and CH_2O. The addition of V_2O_5 allows to suppress the formation of HCOOH and limit the formation of CH_2O.

A single-compartment three-electrode cell (one compartment 100 mL volume) is employed including the working electrode GDE placed at the bottom, a platinum foil as counter-electrode and SCE as reference electrode. The working electrode potential is controlled in the range of 1.3-2.3 V vs SCE and O_2 back-fed from air. The electrolyte used is 0.1 mol/L Na_2SO_4 aqueous solution with a volume of 100 mL. The experiment occurs in semi-batch mode for a duration of 1 h. It is reported that by applying a differential potential of 2.0 V the GDE reaches the highest current efficiency and thus selectivity for CH_3OH at 5.6% V_2O_5 in the powder. The results from this test is thus assumed in the case-study: faradaic efficiency of 57%, CH_3OH concentration of 297 mg/L and CH_2O concentration of 7 mg/L in the solution of 100 mL [721]. To estimate the O_2 flowrate consumed at the cathode, the current intensity is first calculated by using faradaic efficiency and molar quantity of produced CH_3OH and then the current is divided by Faraday constant and 4 electrons transferred per mol of O_2 reduction of O_2 to H_2O. Given the compounds involving in the process, the following scheme of reactions is derived:

$$CH_4 + H_2O = CH_3OH + H_2 \quad \text{(D.52)}$$

$$CH_4 + H_2O = CH_2O + 2\ H_2 \quad \text{(D.53)}$$

By assuming four batches per day (i.e. at maximum 6 h including loading, reaction and unloading), the inlet and carbon output flowrates are estimated. Based on this information and the reactions scheme, other outlet flowrates can be determined. Extent rate of the reactions in Equations (D.52)-(D.53) are $2.32 \cdot 10^{-7}$ kmol/h and $5.83 \cdot 10^{-9}$ kmol/h, respectively. Table D.37 summarizes the mass balance of the process. Molar conversion of CH_4 is 62.19%. The yield of CH_3OH with respect to input CH_4 is 60.66%. CH_3OH fraction in the solution is 0.0298%wt (0.0169%mol).

Table D.37. Mass balance for the reference process scheme based on electrosynthesis for CH_3OH production from CH_4.

Compound	Inlet flowrate		Outlet flowrate	
	kmol/h	t/h	kmol/h	t/h
CH_4	$3.83 \cdot 10^{-7}$	$6.12 \cdot 10^{-9}$	$9.64 \cdot 10^{-8}$	$3.09 \cdot 10^{-9}$
Na_2SO4/H_2O	$1.37 \cdot 10^{-3}$	$2.50 \cdot 10^{-5}$	$1.37 \cdot 10^{-3}$	$2.49 \cdot 10^{-5}$
CH_3OH	-	-	$2.32 \cdot 10^{-7}$	$7.43 \cdot 10^{-9}$
CH_2O	-	-	$5.83 \cdot 10^{-9}$	$1.75 \cdot 10^{-10}$
H_2	-	-	$2.44 \cdot 10^{-7}$	$4.87 \cdot 10^{-10}$

D.3.9.2. Definition of intensified process flowsheet

Figure D.11 illustrates the intensified process flowsheet produced with Aspen HYSYS simulation for photocatalysis. Data about the material streams in the flowsheet are summarized in Table D.38, while Table D.39 reports information on the energy streams related to the relevant components in the flowsheet.

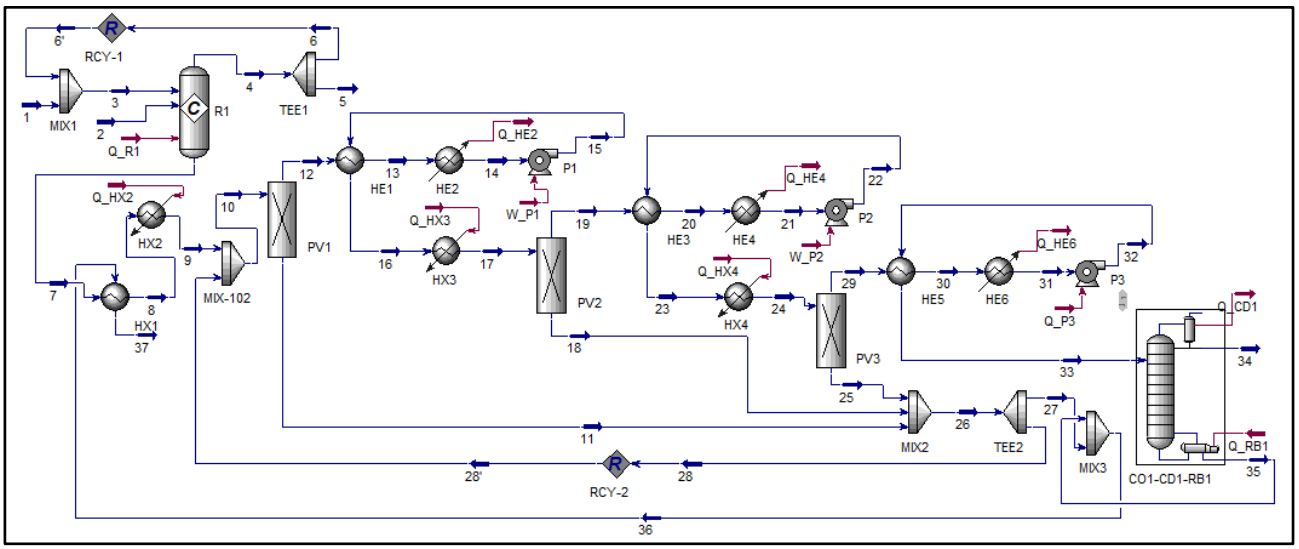

Figure D.11. Intensified process flowsheet for electrosynthesis from Aspen HYSYS simulation.

As shown in Figure D.11, CH_4 (stream 1) mixed with gas recycle stream, and H_2O (stream 2) enter reactor R1. In R1, two reactions in series are added: the first one with stoichiometry of reaction in Equation (D.52) and conversion of CH_4 of 97.55%, the second one with stoichiometry of reaction in Equation (D.53) and conversion of CH_4 of 2.45%, which correspond to the overall reaction of CH_4 of 62.19% reported in the reference process scheme. The gas output stream from R1 is then recycled, while the liquid output (stream 7) is heated in HX1 and HX2 to the optimal temperature required for pervaporation based on PERVAP 4060 membrane (i.e. 70°C) [685]. The resulting stream (stream 9) is mixed with liquid recycle stream and enters the pervaporation membrane unit PV1. Permeate stream in vapor phase and under vacuum (stream 12) is then cooled to reach liquid conditions in HE1 and HE2 and pumped in P1 to atmospheric pressure. The resulting liquid stream is then re-heated to 70°C through HE1 and HX3 for another two pervaporation stages composed of membrane PV2, coolers HE3 and HE4, pump P2 in the first one, and membrane PV3,

coolers HE5 and HE6, pump P3 in the second one. The resulting permeate from these components is routed for final separation to the distillation unit, composed of column CO1, top-condenser CD1 and bottom-reboiler RB1. A part of retentate from PV1, PV2 and PV3 (stream 28) is recycled to the inlet of the first stage of pervaporation. The other part is mixed with the waste stream of CO1-CD1-RB1 unit and used as heating fluid in HX1.

Table D.38. Data on material streams of the intensified process flowsheet illustrated in Figure D.11.

Stream	Vapor phase fract.	Temp. (°C)	Press. (kPa)	Molar flowrate (kmol/h)	Molar fract. CH_4	Molar fract. CH_2O	Molar fract. CH_3OH	Molar fract. H_2	Molar fract. H_2O
1	1	25.0	101.3	185218	0.000	0.014	0.000	0.956	0.031
2	0	25.0	101.3	54300	0.000	0.000	0.000	0.000	1.000
3	1	25.0	101.3	185217	0.000	0.014	0.000	0.956	0.031
4	1	25.0	101.3	185218	0.000	0.014	0.000	0.956	0.031
5	1	25.0	101.3	0	0.000	0.014	0.000	0.956	0.031
6	1	25.0	101.3	185217	0.000	0.014	0.000	0.956	0.031
6’	1	25.0	101.3	185200	0.000	0.014	0.000	0.956	0.031
7	0	25.0	101.3	54299	0.000	0.000	0.000	0.000	1.000
8	0	40.0	101.3	54299	0.000	0.000	0.000	0.000	1.000
9	0	70.0	101.3	54299	0.000	0.000	0.000	0.000	1.000
10	0	70.0	101.3	5319901265251550	0.000	0.000	0.000	0.000	1.000
11	0	70.0	101.3	5319713993394860	0.000	0.000	0.000	0.000	1.000
12	1	70.0	0.267	187271856691	0.000	0.000	0.002	0.000	0.998
13	1	25.0	0.267	187271856691	0.000	0.000	0.002	0.000	0.998
14	0	-10.4	0.267	187271856691	0.000	0.000	0.002	0.000	0.998
15	0	-10.1	101.3	187271856691	0.000	0.000	0.002	0.000	0.998
16	0	9.3	101.3	187271856691	0.000	0.000	0.002	0.000	0.998
17	0	70.0	101.3	187271856691	0.000	0.000	0.002	0.000	0.998
18	0	70.0	101.3	187265066050	0.000	0.000	0.002	0.000	0.998
19	1	70.0	0.267	6790641	0.000	0.000	0.015	0.000	0.985
20	1	25.0	0.267	6790641	0.000	0.000	0.015	0.000	0.985
21	0	-10.3	0.267	6790641	0.000	0.000	0.015	0.000	0.985
22	0	-10.1	101.3	6790641	0.000	0.000	0.015	0.000	0.985
23	0	9.3	101.3	6790641	0.000	0.000	0.015	0.000	0.985
24	0	70.0	101.3	6790641	0.000	0.000	0.015	0.000	0.985
25	0	70.0	101.3	6790356	0.000	0.000	0.015	0.000	0.985
26	0	70.0	101.3	5319901265251270	0.000	0.000	0.000	0.000	1.000
27	0	70.0	101.3	50539	0.000	0.000	0.000	0.000	1.000
28	0	70.0	101.3	5319901265200730	0.000	0.000	0.000	0.000	1.000
28’	0	70.0	101.3	5319901265197250	0.000	0.000	0.000	0.000	1.000
29	1	70.0	0.267	286	0.000	0.000	0.067	0.000	0.933
30	1	25.0	0.267	286	0.000	0.000	0.067	0.000	0.933
31	0	-10.5	0.267	286	0.000	0.000	0.067	0.000	0.933
32	0	-10.2	101.3	286	0.000	0.000	0.067	0.000	0.933
33	0	8.8	101.3	286	0.000	0.000	0.067	0.000	0.933
34	0	66.9	101.3	16	0.000	0.000	0.999	0.000	0.001
35	0	99.7	101.3	270	0.000	0.000	0.013	0.000	0.987
36	0	70.1	101.3	50809	0.000	0.000	0.000	0.000	1.000
37	0	54.2	101.3	50809	0.000	0.000	0.000	0.000	1.000

Table D.39. Data on energy streams associated to components of the intensified process flowsheet in Figure D.11.

Stream	Heat/Power flow (kW)	Utility	Pressure (kPa)	Inlet temp. (°C)	Outlet temp. (°C)	Utility mass flowrate (kg/h)
Q_R1	544	Cooling water 1	40	30	124	45373
Q_HX2	35275	LP steam	232	125	124	57818
Q_HX3	246063926956	LP stean	232	125	124	403310024150
Q_HE2	2453239531199	Ammonia refrigerant	151.8	-25	-25	8652635120233
W_P1	122518000	-	-	-	-	-
Q_HX4	9012486	LP steam	232	125	124	14771876
Q_HE4	89129187	Ammonia refrigerant	151.8	-25	-25	314382995
W_P2	4511	-	-	-	-	-
Q_HE6	3775	Ammonia refrigerant	151.8	-25	-25	13314
Q_P3	0	-				
Q_CD1	3106	Cooling water 1	30	40		259156
Q_RB1	3708	LP steam	232	125	124	6078

LP: low pressure.

Distillate rate of 15.64 kmol/h, reflux ratio of 18.05 and number of stages of 19 (feed in stage 10) are set in CO1-CD1-RB1 unit. According to experimental data on PERVAP 4060 membrane [685], pressures of permeate and retentate in PV1, PV2 and PV3 re set to 0.2670 kPa and 101.3 kPa, respectively, both at 70°C; splits are fixed as feed fraction to product: in PV1 0.0002758 for CH_3OH and 0.00003514 for H_2O, in PV2 0.0002490 for CH_3OH and 0.00003580 for H_2O, in PV3 0.0001915 for CH_3OH and 0.00003981 for H_2O.

Input flowrates to the plant are adjusted in order to meet in the inlet of the reactor (streams 2 and 3 in Figure D.11) the molar ratio H_2O to CH_4 of 3573 reported in the reference process scheme (Table D.37).

As illustrated in Figure D.11, material process streams are used to supply heat in HX1 or absorb heat in HE1, HE3 and HE5.

The performance of the CH_3OH production plant obtained with the proposed intensified process flowsheet is: relatively pure liquid CH_3OH in the distillate with the benchmark flowrate (stream 34) at 66.9°C and 1.01 bar, overall conversion of CH_4 of 100% and overall yield of CH_3OH with respect to input CH_4 of 93.04%.